An Introduction to Galaxies and Cosmology

Compiled by a team of experts from The Open University and other UK universities, this textbook has been designed for elementary university courses in astronomy and astrophysics. It starts with a detailed discussion of the structure and history of our own Galaxy, the Milky Way, and goes on to give a general introduction to normal and active galaxies including models for their formation and evolution. The second part of the book provides an overview of the wide range of cosmological models and discusses the big bang and the expansion of the Universe. Written in an accessible style that avoids complex mathematics, and illustrated in colour throughout, this book is suitable for self-study and will appeal to amateur astronomers as well as undergraduate students. It contains numerous helpful learning features such as boxed summaries, student exercises with full solutions, and a glossary of terms. The book is also supported by a website hosting further teaching materials **http://publishing.cambridge.org/9780521546232**

About the editors:

MARK JONES is a Staff Tutor in the Department of Physics and Astronomy at The Open University. He studied for his PhD in the X-ray astronomy group at the University of Leicester, before carrying out post-doctoral research in space-based infrared astronomy at Queen Mary and Westfield (University of London). He has a wide range of astronomical interests and has published papers on interplanetary dust, the interstellar medium, interacting binary stars and active galaxies. He has been a Fellow of the Royal Astronomical Society since 1991.

ROBERT LAMBOURNE is the Head of the Physics and Astronomy Department at The Open University. He obtained his PhD at Queen Mary College London, where he worked on the quantum theory of fundamental particles. His career in university teaching has spanned many areas of mathematics, physics and astronomy, with a particular emphasis on relativity and cosmology. He is also a very active popularizer of science. He is a Fellow of the Royal Astronomical Society and a Fellow of the Institute of Physics. In 2002 he was awarded the Bragg Medal of the Institute of Physics in recognition of his contributions to physics education.

Background image: A composite image of the galaxy M33 that combines optical data from the 0.9 m telescope at Kitt Peak National Observatory with radio data from the Very Large Array and the Westerbork Synthesis Radio Telescope. The optical data show stars (yellow/white) and regions of star formation (red), whereas the radio data (shown in blue/violet) map the distribution of cool hydrogen gas throughout the galaxy. M33 is a relatively nearby galaxy, being only about two million light years away from us. The field of view of this image is approximately one square degree. (T. A. Rector (NRAO/AUI/NSF and NOAO/AURA/NSF) and M. Hanna (NOAO/AURA/NSF))

Thumbnail images: (from left to right) Gravitational lensing in the cluster of galaxies Abell 2218 (Hubble Space Telescope). An X-ray image showing the jet in the Centaurus A radio galaxy (Chandra X-ray Observatory). The interacting galaxy pair NGC 4676, also known as the 'Mice' galaxies (Hubble Space Telescope). Fluctuations in the cosmic microwave background (BOOMERANG).

An Introduction to Galaxies and Cosmology

Edited by Mark H. Jones and Robert J. Lambourne

Authors:

David J. Adams

Alan Cayless

Anthony W. Jones

Barrie W. Jones

Mark H. Jones

Robert J. A. Lambourne

Lesley I. Onuora

Sean G. Ryan

Elizabeth Swinbank

Andrew N. Taylor

The Open University

CAMBRIDGE UNIVERSITY PRESS

PUBLISHED BY THE PRESS SYNDICATE OF THE UNIVERSITY OF CAMBRIDGE

The Pitt Building, Trumpington Street, Cambridge, United Kingdom

IN ASSOCIATION WITH

The Open University, Walton Hall, Milton Keynes, MK7 6AA

CAMBRIDGE UNIVERSITY PRESS

Cambridge, New York, Melbourne, Madrid, Cape Town, Singapore, São Paulo

Cambridge University Press

The Edinburgh Building, Cambridge CB2 8RU, UK

http://www.cambridge.org

Information on this title: www.cambridge.org/9780521546232

First published 2003.

This co-published edition first published 2004. Reprinted 2007.

Edited, designed and typeset by The Open University.

Printed in the United Kingdom by The University Press, Cambridge

This book forms part of an Open University course S282 *Astronomy*. Details of this and other Open University courses can be obtained from the Student Registration and Enquiry Service, The Open University, PO Box 197, Milton Keynes MK7 6BJ, United Kingdom: tel. +44 (0)870 333 4340, email general-enquiries@open.ac.uk

http://www.open.ac.uk

ISBN-10: 0 521 83738 3 hardback; ISBN-13: 978 0 521 83738 5 hardback

ISBN-10: 0 521 54623 0 paperback; ISBN-13: 978 0 521 54623 2 paperback

2.2

CONTENTS

INTRODUCTION

To the naked-eye, the night sky offers a quite misleading impression of the distribution of matter in the Universe around us. We see stars in every direction, and we could be excused for jumping to the erroneous conclusion that the cosmos is simply filled with a more-or-less uniform distribution of stars. We now recognize this view to be incorrect: stars are, in fact, distributed in vast stellar systems called galaxies, and we live within one such system – the Milky Way Galaxy. The starting point of this book is to study our own Galaxy, and then move on to consider galaxies in general. Equally importantly, we shall also discuss the astronomical techniques and the scientific reasoning that has led to our current view of galaxies. One finding of such studies is that the luminous output of the majority of galaxies is dominated by their stars, but there are exceptions to this rule: the so-called *active galaxies*, in which a huge luminosity is emitted from a region that is no bigger than our Solar System.

It took painstaking efforts by pioneering astronomers, most notably Edwin Hubble, to establish the existence of galaxies external to the Milky Way. However, once this leap had been made in the 1920s, the scene was set for an exploration of the Universe on ever larger scales. The picture that has emerged is that galaxies appear to be the 'building blocks' that make up the large-scale distribution of matter in the Universe. So, a question arises as to why the Universe is organized in this way – how, and why, do galaxies form? Although there are no simple answers to these questions, throughout this book we shall see how these problems are currently being tackled by astronomers.

Observations of galaxies play a key role in *cosmology* – the scientific study of the nature and evolution of the Universe as a whole. It was, again, Edwin Hubble who made the observations that revolutionized this field. His work led to the single most important result in cosmology: that the Universe is expanding – the distances between galaxies are increasing as time progresses. Once this idea is accepted, it is not difficult to deduce that in the past, galaxies must have been closer together. This idea is taken to its logical extreme in the idea of the *big bang* model: at some finite time in the past – about 14 billion years ago – the separation between objects in the Universe would have been extremely small, and ever since this time the Universe has been expanding. Later in this book we shall explore the reasoning behind, and the implications of, this model in much more detail. However, since the idea of the big bang plays such a fundamental role in modern astronomy and cosmology it is worth here highlighting a few of the key features of this model:

- The Universe has a finite age, which is currently estimated to be about 14 billion years.
- The Universe has been expanding since the very first instant of the big bang.
- The early stages of the evolution of the Universe were characterized by high temperatures and densities. Furthermore, at any given time, the density and temperature were highly, although not perfectly, uniform.
- Within the first few minutes of the big bang, nuclear reactions formed light nuclei. As a result, the fraction (by mass) of material in the Universe after these processes came to an end was about 76% hydrogen and 24% helium. A trace amount of lithium was also formed.

A surprising feature of modern astronomy is that much of cosmic history can be viewed directly. Light, and other forms of electromagnetic radiation, travels at the finite speed of $3 \times 10^8 \text{ m s}^{-1}$. It takes about two million years for light to reach us from the nearby Andromeda Galaxy – so the images we make today actually show the appearance of this galaxy as it was two million years ago. Two million years is a very short time by cosmic standards, but the same principle applies to observations of much more distant galaxies. Current observations using the most sensitive telescopes can view galaxies as they appeared over ten billion years ago. Such studies are now allowing astronomers to piece together a picture of the formation and evolution of galaxies over the history of the Universe. And this is not the limit of our vision – we can also detect background radiation that gives us a view of the Universe as it appeared when it was only about 400 000 years old. This information is now allowing cosmologists to test theories that describe the Universe during the first few fractions of a second of the big bang.

In this book, we shall explore the implications of the latest observational techniques for astronomy and cosmology. We hope that in doing so, we will share with you some of the sense of excitement that a scientific study of the Universe can bring.

Note: It is assumed that readers of this book already have an understanding of the fundamental aspects of stellar astronomy and the processes of stellar evolution. These topics are dealt with in detail in the companion volume to this book – *An Introduction to the Sun and Stars*.

CHAPTER 1
THE MILKY WAY – OUR GALAXY

1.1 Introduction

To the observer, the Milky Way is the faint band of diffuse light that arches across the night sky from horizon to horizon (Figure 1.1). This light comes mainly from a multitude of stars, although the unaided eye is unable to resolve these stars individually, hence the appearance of a 'band' of light. The stellar nature of the visible Milky Way was revealed about four hundred years ago when Galileo Galilei (1564–1642) made some of the earliest astronomical observations using a telescope.

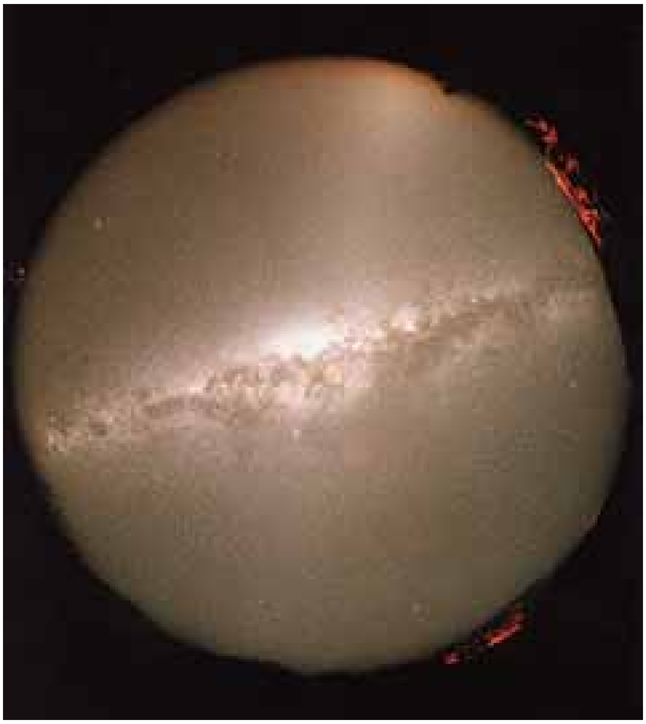

Figure 1.1 A photograph of one hemisphere of the night sky, showing the Milky Way stretching from horizon to horizon. The most prominent, central portion of the Milky Way is directly overhead in this image. The light comes mainly from the enormous number of stars that exist within our Galaxy; there are about 10^{11} in all, but many are too faint to see, or are obscured by the dust that is also part of the Galaxy. (D. di Cicco, Sky Publishing Corp.)

Although Galileo recognized the existence of huge numbers of stars in the Milky Way in around 1610, it was not until the 20th century that astronomers were able to deduce the distribution of those stars with any accuracy, and only over the past decade or two have they arrived at what is believed to be a true understanding of the nature of the Milky Way. We now know roughly how far the Milky Way extends in each direction in space, and that its light comes mostly from stars distributed in a flattened disc-like structure some 100 000 light-years (ly) across. We also know that, in addition to stars, the Milky Way contains gas and dust. Perhaps most astonishingly of all, the majority of astronomers have now become convinced that such familiar entities as stars, gas and dust account for no more than about 10% of the mass of the Milky Way. Most of the mass, a staggering 10^{12} times the mass of the Sun (i.e. $10^{12}M_\odot$, where $M_\odot \approx 2 \times 10^{30}$ kg), is now believed to be attributable to some kind of unidentified form of matter known, somewhat enigmatically, as 'dark matter'. The term **Milky Way** is now applied to this whole collection of entities – the system of stars, gas, dust, and dark matter – not just to the diffuse band of starlight resolved by Galileo.

Does anything exist beyond the boundary of the Milky Way? The answer is an emphatic 'yes'. At still greater distances, beyond the limits of the 100 000 light-year disc, astronomers have discovered other huge collections of stars, gas, dust and dark matter that, like the Milky Way, occupy relatively well-defined, and usually well-separated, volumes of space. These structures are called **galaxies**. Figure 1.2 shows one of these 'external' galaxies that is thought to be somewhat similar to the Milky Way in many respects. The Milky Way is simply *our* galaxy, the galaxy in which we have been born and have come of age. To emphasize this, the Milky Way is often referred to as 'the Galaxy', the capital 'G' distinguishing it from the billions of other galaxies in the observable Universe. In later chapters you will learn more about those other galaxies. Here in Chapter 1 we concentrate on the Milky Way.

Figure 1.2 An 'external' galaxy (NGC 2997) thought to be similar to the Milky Way. If this really represented the Milky Way, the Sun would be located about halfway between the centre and the edge of the flattened 'disc' of stars, gas and dust. This location, within a relatively thin disc, explains why we mainly see the Milky Way as a 'band' encircling the Earth. (D. Malin/AAO)

In the sections that follow you will learn a great deal about the Milky Way. Section 1.2 provides a general overview of the Milky Way as a galaxy, including its structure, size and composition. Section 1.3 is devoted to the mass of the Milky Way. Sections 1.4 and 1.5 discuss some of the main structural components of the Galaxy in detail, and Section 1.6 considers the formation and evolution of the Milky Way. As you study these sections you will also gain insight into the *process* of astronomical science. You will see, in outline at least, *how* the nature of the Galaxy has been uncovered, *how* the disc of the Milky Way has been shown to be about 100 000 light-years across, *how* the Milky Way's mass has been roughly determined to be about $10^{12}M_\odot$ and *how* astronomers have estimated the age of the Galaxy at between 12×10^9 and 15×10^9 yr. By examining the process of astronomy you will begin to understand how the making of careful observations, combined with the continuous review of their significance in the light of physical laws, enables findings and theories to be critically examined, refined and improved. Developing an understanding of this process is more important than learning any particular fact or figure.

1.2 An overview of the Milky Way

This section examines some of the general features of the Milky Way as a galaxy. It starts with an introduction to the main structural components of the Milky Way, and then goes on to examine the sizes of those components and their constituents. Particular emphasis is given to the stellar content of the Milky Way, since it is the study of the nature, distribution and movement of the stars in the Milky Way that

has provided the key to much of what has been learnt about the Galaxy. The discussion of stars in the Milky Way introduces the important concept of *stellar populations*, and the section ends with a brief discussion of the related issue of the chemical evolution of the Milky Way. Detailed discussion of the mass of the Milky Way is deferred to Section 1.3.

1.2.1 The structure of the Milky Way

When asked to describe the Galaxy, most people think of the huge numbers of stars gathered together to form a flattened disc. Indeed, this was the description we began with above. There are some 10^{11} stars in our Galaxy, most of them in the disc, and they dominate the visible light emitted from it, so this view is quite understandable. However, while stars are luminous and hence easily seen, they are only the visible tips of our Galactic iceberg. There is more to the Galaxy, *vastly* more, than meets the eye.

The modern view of the Galaxy is that its largest and most massive component is a huge, roughly spherical cloud consisting of some kind of non-luminous matter. Since this non-luminous matter has never been directly observed at any wavelength it is known as **dark matter**. The nature of dark matter is unknown at the time of writing. Its presence is revealed by the gravitational influence that it has on the more familiar forms of matter that can be directly observed. Despite knowing very little about dark matter, most astronomers have become convinced that the total mass of dark matter in the Milky Way is about ten times greater than the total mass of stars and about 100 times greater than the total mass of gas and dust. Furthermore, this appears to be the case for other galaxies too; as you will see later, the nature, distribution and significance of dark matter is a recurring theme of great importance in the study of galaxies and cosmology.

The huge cloud of dark matter that is believed to be the main structural component of the Milky Way is usually referred to as the **dark-matter halo**. The mass of this component is so great that it is the gravity of the dark matter, rather than the gravity of all of the stars, that is primarily responsible for holding the Galaxy together. The gravitational influence of dark matter on luminous material allows astronomers to infer the shape of the dark-matter halo. They have concluded that the dark-matter halo takes the form of a *spheroid* – the three-dimensional figure formed by rotating an ellipse about one of its axes. Spheroids themselves come in a variety of shapes; the dark-matter halo is thought to be an *oblate* spheroid, that is to say it resembles a sphere that has been flattened at its poles, with a shortest-to-longest axis ratio of about 0.8. The stars of the Milky Way, which provide most of the Galaxy's luminous output are located in the centre of this dark-matter halo.

Let's now consider in more detail how this luminous matter is distributed – and how it makes up the visible parts of the Galaxy. Most of the stars, including the Sun, occupy a flattened, disc-shaped volume. This is called the **Galactic disc**, or simply the **disc**, and is the second major structural component of the Galaxy. Its mass is about $10^{11} M_{\odot}$. In addition to stars, the Galactic disc contains a substantial mass of gas and dust in the space between the stars. The mid-plane of the disc defines the **Galactic plane**, which plays an important part in providing a system of coordinates for defining positions in the Milky Way (see Box 1.1). The Sun is located very close to the Galactic plane, about halfway between the centre of the disc and its outer edge.

BOX 1.1 GALACTIC COORDINATES

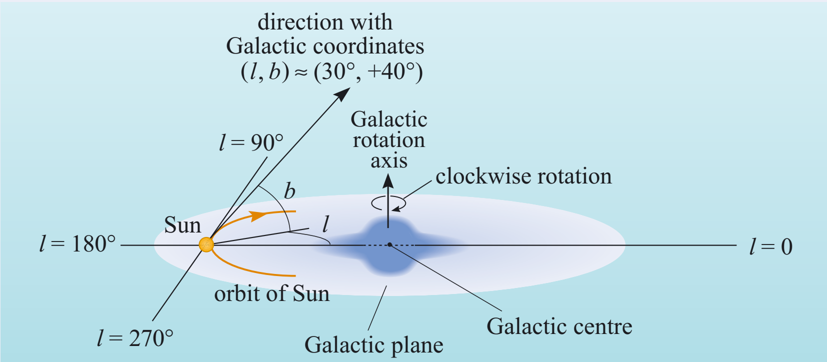

Figure 1.3 Galactic coordinates are centred on the Sun, and use the Galactic plane and the direction approximately towards the Galactic centre to define a frame of reference. A direction with $l \approx 30°$ and $b \approx +40°$ is shown.

Astronomers who study the Galaxy find it useful to define a coordinate system that reflects the Galaxy's symmetry about the Galactic plane as it is viewed from the Earth. In the system of **Galactic coordinates**, the direction of any object in the sky can be expressed in terms of its **Galactic latitude** (b) and **Galactic longitude** (l), both of which are angles normally expressed in degrees. Figure 1.3 shows how they are defined. The **Galactic equator** runs close to the mid-plane of the Milky Way's disc. The origin of the coordinate system, the point $l = 0°$ and $b = 0°$, is defined to be *nearly* – but not precisely – in the direction of the Galactic centre, which is in the direction of the constellation Sagittarius. (The convention is to show the Galaxy with the North Galactic Pole upwards.) Galactic latitudes are measured north (b positive) or south (b negative) of the Galactic equator, so they range between $b = +90°$ and $b = -90°$. Galactic longitude ranges from $l = 0°$ (roughly towards the Galactic centre), eastwards through $l = 90°$ (roughly in the direction of Galactic rotation), and on to $l = 360°$.

From our vantage point, we see the disc edge-on from within. It is our location that causes most of the other stars in the Milky Way's disc to appear concentrated within a band looping around us – the source of the diffuse band of light that Galileo resolved into stars.

If the disc could be viewed face-on, we would see a spiral pattern due to the presence of bright features called **spiral arms**. (Such arms are an obvious feature of many galaxies; the evidence for their existence in the Milky Way is described in Section 1.4.) Edge-on and almost face-on views of two galaxies that are thought to be broadly similar to the Milky Way are shown in Figure 1.4.

The overall spiral shape in Figure 1.4b is clear, but in detail the arms are fragmented and distorted. Although spiral arms are prominent, they stand out because they contain unusually hot, *luminous* stars, and not because they contain unduly large numbers of stars. The reasons why bright stars are concentrated in this way is discussed in detail in Section 1.4. Spiral arms suggest that galaxies are rotating. Sure enough, the Sun and its neighbouring stars in the disc orbit the Galactic centre at speeds of about 220 km s^{-1}. However, as you will see later in this chapter, the stars and the pattern of spiral arms generally travel at *different* speeds.

Figure 1.5 is a schematic diagram of the major structural components of the Galaxy that we are introducing in this section, including the dark-matter halo and disc that we have met already, as well as other components that are described shortly. Their approximate sizes, which we discuss in Section 1.2.2, are also given. This diagram should be compared with the edge-on and face-on images of galaxies in Figure 1.4, which are broadly similar to the Milky Way.

(a) (b)

Figure 1.4 (a) NGC 891, a spiral galaxy seen edge-on, observed in infrared light. (b) NGC 6744, a barred spiral galaxy seen almost face-on. These galaxies are thought to be similar in structure to the Milky Way. ((a) J. C. Barentine and G. A. Esquerdo, Kitt Peak, NOAO; (b) S. Lee, C. Tinney and D. Malin/AAO)

Towards the centre of the Galaxy the density of stars increases, and the Milky Way appears to be 'thicker' there than further out. This broad, central region is called the **bulge**, and is the third structural component of the Galaxy. An example of a bulge can be seen in the centre of the galaxy pictured in Figure 1.4a. The Milky Way's bulge has a mass of around $10^{10} M_{\odot}$. The central regions of the Galaxy are notoriously difficult to observe from our vantage point near the Sun, but there is evidence that the Milky Way's bulge is elongated, which makes the Milky Way a **barred spiral galaxy** like the one in Figure 1.4b. The Milky Way is far from being unique in this respect; observations of other spiral galaxies show that most have *some* trace of a central bar.

Surrounding the disc is a sparsely populated structural component called the **stellar halo**, or just the **halo**, the mass of which is only about $10^9 M_{\odot}$. Because the number of stars per unit volume is much lower in the halo than in the disc, the halo does not show up in the two images in Figure 1.4. Each clearly shows a disc and a bulge, but gives little indication of a stellar halo, which is only revealed by more detailed studies. This Galactic component is not flat like the disc, but rather has a spheroidal shape, with only slight flattening. For this reason, the halo (and often the bulge with it) is sometimes referred to as the **Galactic spheroid**, or simply the **spheroid**. The name 'stellar halo' suggests there are only stars, not gas, in this component. In fact there is some gas, but present only at a very low density. Furthermore, as we see in Section 1.6, some of the gas traditionally associated with the halo may not really belong to the Galaxy at all. This highlights the fact that the Galaxy is not as isolated in space as the introduction above may have suggested; rather the Galaxy is surrounded by an environment with which it interacts. More will be said about this *intergalactic medium* in later chapters, but we shall also see several other examples of the way the Galaxy interacts with its environment later in this chapter.

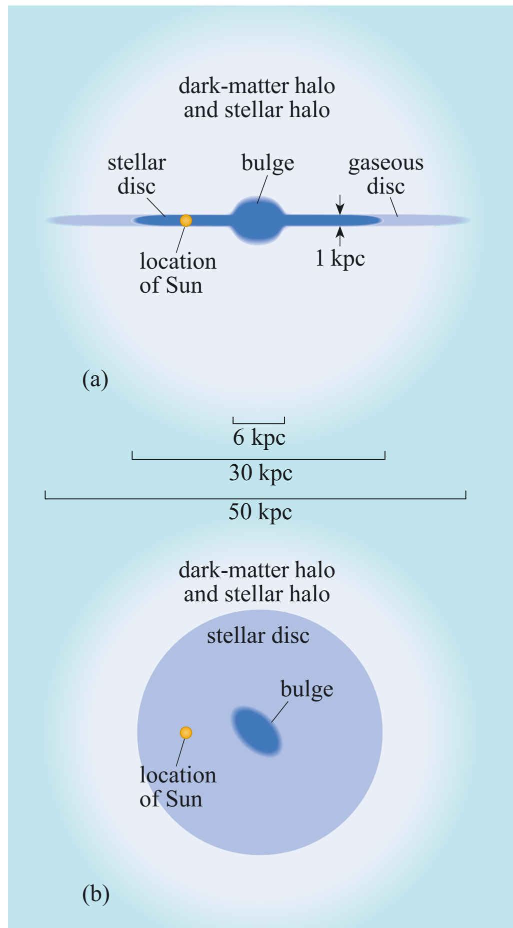

Figure 1.5 (a) Edge-on and (b) face-on schematic views of the four major structural components of the Milky Way: the dark-matter halo, the disc, the stellar halo and the bulge. The sizes indicated in this figure are expressed in kiloparsec (kpc), where 1 kpc ≈ 3260 ly.

In summary, the Galaxy's major component is the *dark-matter halo*. Embedded within this is the *Galactic disc*, which is where most of the stars, gas and dust are found. The central region of the Galaxy is thicker than the rest of the disc, and is called the *bulge*. Surrounding the disc is the sparsely populated *stellar halo*. The disc contains bright *spiral arms*, and the bulge is elongated into a *bar*; the Milky Way is therefore a *barred spiral galaxy*.

■ What are the shapes and approximate masses of each of the four main structural components of the Galaxy?

❑ The dark-matter halo and the stellar halo are both slightly flattened (oblate) spheroids. The disc has the flattened circular form its name implies, and the central bulge is elongated into a bar. Very roughly, the stellar halo has a mass of $10^9 M_\odot$, the bulge mass is $10^{10} M_\odot$, the mass of the disc is $10^{11} M_\odot$ and the dark-matter halo has a mass of $10^{12} M_\odot$, although this last value is particularly uncertain.

1.2.2 The size of the Milky Way

A table of frequently used conversion factors and physical constants is provided in the Appendix.

Having introduced the main structural components of the Galaxy, we now examine their sizes. Although the size of the disc was given above as 100 000 light-years, distances in the Galaxy are usually measured in units of **parsecs** (pc) or **kiloparsecs** (kpc), where 1 kpc = 1000 pc. One parsec is equal to about 3.26 light-years, or 3.09×10^{16} m.

So, how big is the Galaxy? The answer depends greatly on which component you measure. The dark-matter halo is the most extensive component, but it is also the most difficult to measure since its presence is deduced only from its gravitational influence. The size of the dark-matter halo can be assessed from its effect on the motions of neighbouring galaxies. The Magellanic Clouds are two small galaxies that are 50 to 60 kpc from the Milky Way, and the dark-matter halo apparently extends at least that far. So, in answer to the question: 'How big is the Galaxy?' you could cite the distance of the Magellanic Clouds as a lower limit on the radius of the dark-matter halo, implying a diameter of at least 100 to 120 kpc.

Since the dark-matter halo cannot be observed very easily, you may prefer to consider a different question: 'How big is the disc of the Galaxy?' It turns out that even this more carefully posed question requires a cautious response. In short, the answer depends on which constituent of the disc you measure: stars or gas. The stellar disc of the Milky Way has a radius of at least 15 kpc. Observations indicate that the Sun is about 8.5 kpc from the centre of the Milky Way, which places it around halfway out in the stellar disc. This disc is around 1 kpc thick, which means some stars travel up to about 500 pc from the mid-plane of the disc.

■ If the radius of the Galactic disc is 15 kpc, then its diameter is 30 kpc. How many light-years is 30 kpc?

❑ 1 pc = 3.26 ly, so 30 kpc = 30×10^3 pc $\times$ 3.26 ly pc^{-1} = 9.8×10^4 ly $\approx$ 100 000 ly.

In contrast to the stars, the *gas* and in particular the atomic hydrogen in the Galactic disc extends out to a radius of at least 25 kpc (although its density does fall considerably beyond 15 kpc). A clear example of the difference between the gaseous

and stellar discs in a spiral galaxy is given by the barred spiral galaxy NGC 6744, which we observe almost face on, and which we believe is similar to the Milky Way. This was the galaxy pictured in Figure 1.4b. Contours showing the atomic hydrogen gas density inferred from radio measurements of NGC 6744 are superimposed on the optical image in Figure 1.6. It has a gaseous disc that extends out to at least 1.5 times the radius of its stellar disc, maintaining the spiral structure seen in the visible image as it does so.

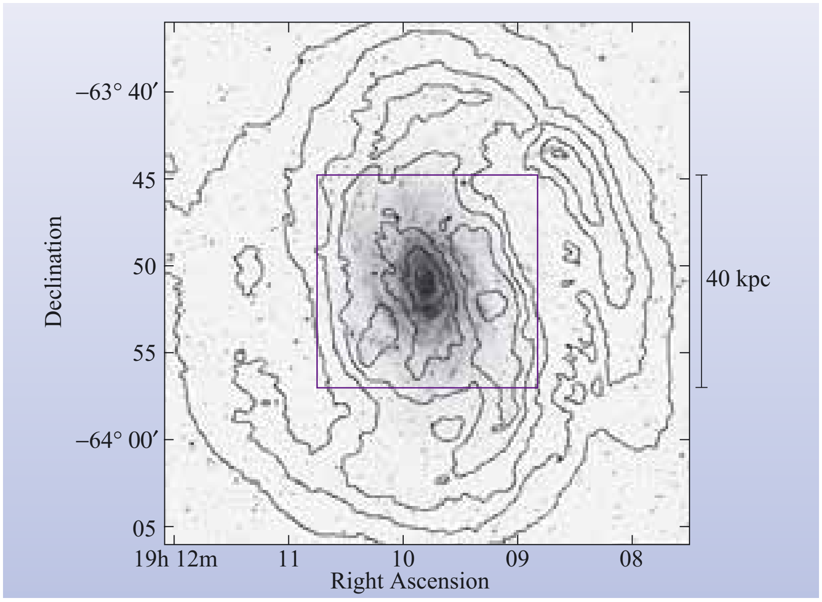

Figure 1.6 Contours of atomic hydrogen gas density in the barred spiral galaxy NGC 6744, based on radio observations, superimposed on an optical image from the Digitized Sky Survey. The central square corresponds to the image in Figure 1.4b, and measures approximately 40 kpc on each side. Note that the gas extends well beyond the stellar disc, and that the spiral pattern is visible out to the edge of the gas disc. This galaxy is believed to be similar to the Milky Way. (Ryder *et al.*, 1999)

■ Can you suggest why the stars in the Galactic disc are found only out to a radius of 15 kpc from the Galactic centre, even though the gaseous disc extends out to 25 kpc?

❑ Stars form from the gas, and they form preferentially where the gas density is higher. Even though the gas extends out to 25 kpc, its density falls considerably beyond 15 kpc. So a plausible explanation may be that star formation does not occur at the gas densities that occur at a radius greater than about 15 kpc.

As the stellar halo has no substantial gaseous component, its size is given by the distribution of stars. However, defining the edge of this distribution is difficult, because the density of stars falls off gradually with distance from the centre of the Galaxy. For now we simply state that the stellar halo extends further than the disc, well beyond 20 kpc.

The bulge of the Galaxy takes the form of an elongated bar. The longest axis of this bar is in the Galactic plane and stretches out to about 3 kpc either side of the Galactic centre. The cross-sectional diameter of the bar is roughly 2 kpc. The mass of the bulge is much greater than that of the stellar halo, but its small size means that it has little relevance to any discussion of the overall size of the Galaxy.

Although approximate sizes for each of the Galaxy's main structural components have now been quoted, you may have noticed that the exact size of our Galaxy has still not been specified. It is always possible to define the size of the Galaxy as the size of *one* of the components, but such a definition would be rather arbitrary. It is more useful to retain a broad knowledge of the nature and scale of each of the structural components that make up our Galaxy.

QUESTION 1.1

If the Sun is 8.5 kpc from the Galactic centre and moving in a circular orbit at 220 km s^{-1}, how long will it take to travel once around the Galaxy? Express your answer in both SI units (seconds) and years.

(Recall that the relationship between a body's speed, v, the distance travelled, d, and the time taken, t, is $v = d/t$, and that the circumference of a circle of radius R is $d = 2\pi R$.)

1.2.3 The major constituents of the Milky Way

The major structural components of the Milky Way – the dark-matter halo, disc, bulge and stellar halo – have now been introduced, and you have briefly encountered their constituents: dark matter, stars, gas, and dust. Now we look at these constituents more closely. We start with the dominant component, the dark matter.

Dark matter

Dark matter is detectable by its gravitational influence, but appears neither to emit nor absorb light nor any other form of electromagnetic radiation. The total mass of dark matter in the Milky Way seems to be about $10^{12}M_{\odot}$. However, at present we do not know the nature of this matter.

Everyday matter that we regularly encounter on Earth, and which constitutes the material in ordinary stars, is primarily made up of particles called **baryons**, the best known of which are protons and neutrons. Some of the dark matter may be dense, non-luminous, baryonic matter, but there is strong evidence (related to studies of the early Universe that are described later) indicating that much of the dark matter is non-baryonic. So, in addition to **baryonic dark matter**, which would be 'ordinary' matter that happened to be difficult to detect and about which we know very little, there is also a need for **non-baryonic dark matter**, about which we know even less.

Although the nature of non-baryonic dark matter is still a mystery, a number of proposals have been made regarding its possible composition. Most of these proposals assume that the non-baryonic dark matter consists of hypothetical fundamental particles of one kind or another. If any of these proposals is correct, then the dark-matter halo would simply be a vast cloud of these particles. Furthermore, since we are situated within this cloud, dark-matter particles should be detectable here on Earth. As we shall see in Chapter 8, experiments with this aim are underway or currently being developed.

Stars

There are about 10^{11} stars in the Galaxy, and, since the Sun's mass ($M_{\odot} \approx 2 \times 10^{30}$ kg) is typical, they have a combined mass of about $10^{11}M_{\odot}$, roughly one-tenth the total mass of dark matter. The vast majority of these stars occupy the disc.

Stars can differ from one another in their *mass*, their *age*, and their *chemical composition*; differences in these three fundamental parameters lead to differences in other properties, such as luminosity and temperature. The *spectral class* of a star is an important property that is closely related to its temperature. In order of

decreasing surface temperature, the spectral classes are O, B, A, F, G, K, M. Many of the brightest stars in the Milky Way are large, bright, blue–white stars belonging to classes O and B, but by far the most common are small, faint, red stars belonging to class M. Stars form from large clouds of gas, and spend the greater part of their luminous lives as *main sequence stars* that are powered by the conversion of hydrogen into helium in their cores. The subsequent evolution of a star depends on its mass (the greater the mass, the shorter the life), but in most cases it includes the eventual enlargement of the star to form a *giant*, and the conversion of helium into a range of heavier elements.

Do the stars in each of the three Galactic components that contain stars – the stellar halo, disc and bulge – have the same range of masses, ages and compositions? Observations show that they do not. It turns out that the stellar halo and bulge contain much older stars than the disc, and that stars in the halo contain few elements heavier than helium. These differences led to categories of stars called **stellar populations** being defined. The differences between the populations tell us much of what we know about the origin and evolution of the Milky Way. We examine the differences between the various stellar populations in Section 1.2.4, and we shall return to their evolutionary implications several times in this chapter.

Gas and dust

Most of the Milky Way's gas and dust lies in the disc, and is found within a vertical distance of 150 pc of the Galactic plane: it does not extend nearly so far from the mid-plane of the Galaxy as do the stars.

The gas is roughly 70% hydrogen and 28% helium (by mass). The remaining 2% is made up of the other elements – these are collectively referred to (by astronomers) as **metals**. The hydrogen can exist in various forms depending on the density, temperature, and flux of ultraviolet (UV) radiation in each locality. In high-density, low-temperature environments with a low UV flux, the hydrogen is mostly in the form of **molecular hydrogen** (H_2). In environments where the temperature and/or the UV flux is high enough to free the hydrogen atom's single electron, there is a likelihood of finding **ionized hydrogen** (H^+, usually written HII and pronounced 'H-two'), particularly where the density is low enough to reduce the chance of the liberated electrons recombining with the positive ions. **Atomic hydrogen** (H, often written HI and pronounced 'H-one') occurs where conditions lie between the other two extremes. The total mass of gas in the Galaxy is estimated to be about 10% of the stellar mass.

What astronomers call **dust** consists of tiny lumps of solid (condensed) compounds of carbon, oxygen, silicon and other metals. (The term 'metals' is used here, and throughout this book, in its astronomical sense.) Most of the bulk of a dust grain comprises either graphite or silicate compounds. The outside of the grain is often surrounded by a coating, or *mantle*, of more volatile compounds such as water-ice (H_2O), ammonia (NH_3) and carbon monoxide (CO). Dust particles are typically 10^{-7} to 10^{-6} m (0.1 μm to 1 μm) across, close in size to smoke particles on Earth. The total mass of dust in the Galaxy is about 0.1% of the stellar mass.

The size of dust particles is comparable to the wavelength of light, and thus makes them particularly effective at scattering light, as well as absorbing it. Since the dust is mainly concentrated within 150 pc of the mid-plane of the disc, its obscuring effect is especially evident when we look in directions close to the

Galactic plane, as indicated in Figures 1.1 and 1.4a. The presence of dust in the disc of the Milky Way severely limits our ability to make optical observations in certain directions (see Figure 1.7), and creates what is called the **zone of obscuration** or **zone of avoidance** on the sky – a band, extending to about 15° either side of the Galactic equator, within which very few galaxies are seen. Fortunately, technological developments over the last few decades have allowed astronomers to make observations at infrared and other wavelengths that are relatively unaffected by dust obscuration.

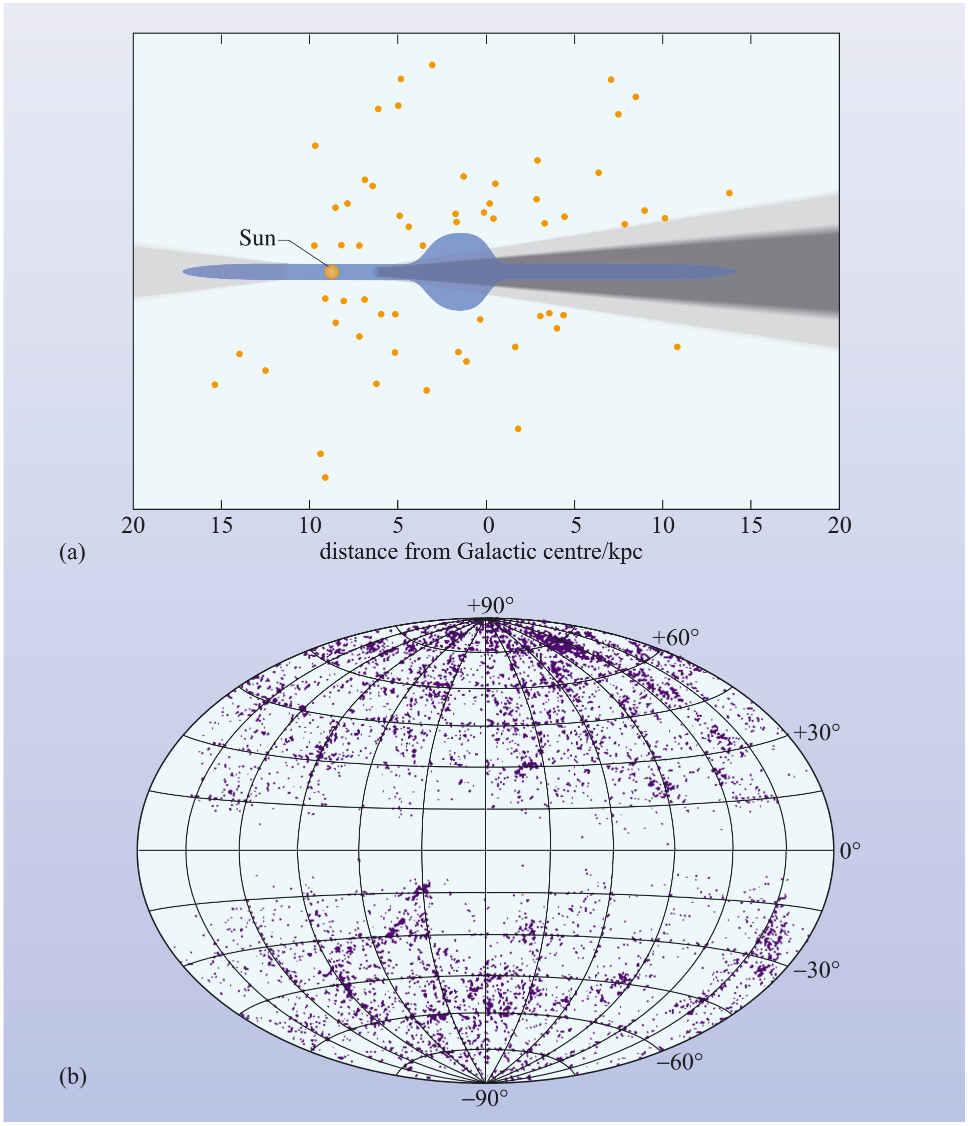

Figure 1.7 (a) Due to the presence of dust in the Milky Way's disc, optical observations in the regions shaded light grey are very difficult, and those in the dark grey region are essentially impossible, except for *very* bright objects within about 5 kpc. (b) An all-sky map in Galactic coordinates, in which the Galactic equator runs horizontally across the middle and the centre of the map corresponds to the direction directly *away* from the centre of the Galaxy ($l \approx 180°$, $b \approx 0°$). This map shows the positions of bright galaxies beyond the Milky Way. Dust in our Galaxy prevents us from seeing the light from other galaxies in directions close to the Galactic plane. This illustrates the effect of the zone of avoidance. ((b) Binney and Merrifield, 1998)

■ What is the total mass of gas in the Galaxy, in solar masses?

❑ The mass of gas is 10% of the stellar mass of the Galaxy, and the latter is about $10^{11}M_\odot$, so the mass of gas is

$$10\% \times 10^{11}M_\odot = (10/100) \times 10^{11}M_\odot = 10^{-1} \times 10^{11}M_\odot = 10^{10}M_\odot$$

■ What is the total mass of dust in the Galaxy, in solar masses?

❑ The mass of dust is 0.1% of the stellar mass of the Galaxy, and the latter is $10^{11}M_\odot$, so the mass of dust is

$$0.1\% \times 10^{11}M_\odot = (0.1/100) \times 10^{11}M_\odot = 10^{-3} \times 10^{11}M_\odot = 10^{8}M_\odot$$

The term **interstellar medium**, or **ISM**, is used to describe the gas and dust that occupies the space between the stars. On average the ISM contains about 10^6 particles per cubic metre, but the density and nature of the ISM varies greatly from one region to another, so this average does not have major significance. Almost half of the ISM (by mass) is contained in cool **dense clouds**, often called **molecular clouds** because they are rich in molecular hydrogen (H_2). These clouds occur with a wide range of masses, the most massive containing up to $10^7M_\odot$ of gas and dust. Molecular clouds are usually many thousands of times denser than the average ISM, with typical diameters of 10 to 100 pc. However, these clouds account for only 1% or so of the volume of the ISM, despite contributing nearly 50% of its mass. Another contribution to the ISM comes from localized clouds (typically a few parsecs across) of hot, ionized gas known as **HII regions**. These regions account for a few per cent or so of the ISM's mass and volume. The Orion Nebula (see Figure 1.8) is one of the best known of these regions.

Figure 1.8 The Orion Nebula (M42). A prominent HII region in which the hydrogen is ionized by the UV radiation from a group of bright young stars. The Orion Nebula is about 6 pc in diameter and contains hundreds of solar masses of gas. The nebula forms a sort of blister on the face of a giant molecular cloud. (NASA)

Much of the remaining volume of the ISM is occupied by an **intercloud medium** that may be hot or warm, depending on local conditions. Within the Galactic disc, the intercloud medium can be loosely regarded as a disc about 300 pc thick that is rich in atomic hydrogen (HI), and more or less uniformly distributed. However, this disc of intercloud medium, along with the thousands of individual clouds it contains, is embedded in a large body of hot intercloud medium that occupies at least part of the halo. There is still much uncertainty about the distribution of the intercloud medium, but the low density of this component of the ISM means that it contributes only a minor part of the ISM's mass, despite its large volume.

The ISM is intimately associated with star formation and stellar evolution: stars are born from cool dense molecular clouds, and they return matter to interstellar space in a variety of ways that gradually increase the proportion of heavy elements in the Galaxy. This process is known as *Galactic chemical enrichment*, and is discussed in greater detail in Section 1.2.5.

We have now completed our survey of the main Galactic components and their constituents. Having seen that the Galaxy is made of dark matter, stars, gas and dust, and how it is divided into the dark-matter halo, disc, stellar halo and bulge, we are in a position to start using observations of these entities to uncover the history of the Galaxy. We begin this process by looking more closely at the differences between populations of stars.

1.2.4 The stellar populations of the Milky Way

It was noted above that a star can be described by its mass, age and composition, and we foreshadowed the fact that significant differences in these parameters exist between the stars in each of the different Galactic components. In this section we explore the nature of those differences and what they tell us about the evolution of the Galaxy.

The first indication that there might be systematic variations in stellar properties between one region of the Milky Way and another came from a comparison of observations of our Galaxy with the nearby spiral galaxy M31 (the Andromeda Galaxy). However, before we attempt to describe and understand these differences it is necessary to know something about the spherical clusters of stars called **globular clusters** (see Figure 1.9). Globular clusters are compact, dense clusters of very old stars, typically containing 10^4 to 10^6 members in a spherical region of space less than about 50 pc in diameter. Around two-thirds of globular clusters belong to the stellar halo and one-third to the disc. While globular clusters are easy to recognize, they account for only about 1% of all stars in the stellar halo. The distribution of globular clusters in the Milky Way is shown in Figure 1.10, which gives a good indication of the shape of the stellar halo and how fundamentally it differs from the disc.

Figure 1.9 The globular cluster 47 Tuc. This globular cluster is one of the 150 or so globular clusters that are known to be associated with the Milky Way. (NASA/ESA)

The German–American astronomer Walter Baade (Figure 1.11) found that he could just detect the brightest O and B stars and red giants in M31 as single stars in his photographic observations, despite that galaxy being 750 kpc away. He noted a difference in colour between the stars in the disc and spheroid of M31. The disc stars were blue, while the spheroid stars were red. He named these two stellar types **Population I** (Pop. I, pronounced ‘pop one’) and **Population II** (Pop. II, pronounced ‘pop two’), respectively. Importantly, he noted that the colour difference meant that Pop. I stars resembled the brightest stars in the disc of the Milky Way, which are predominantly blue, while the Pop. II stars resembled the brightest stars in the Milky Way’s globular clusters, which are predominantly red.

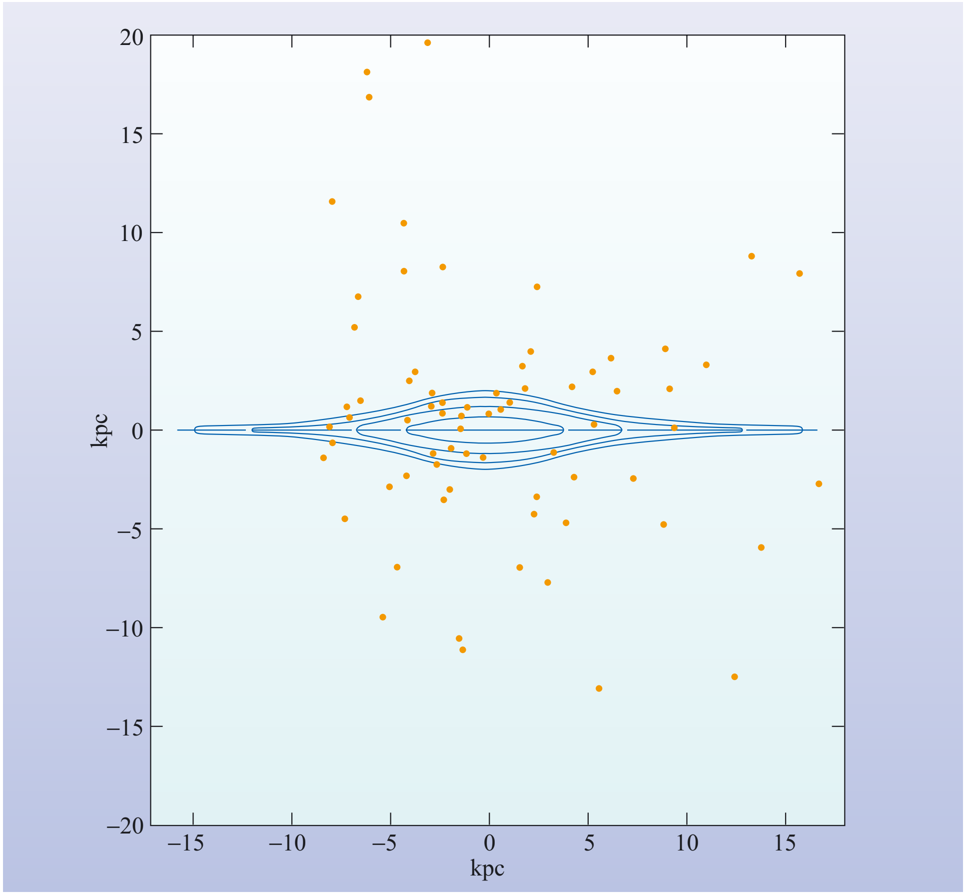

Figure 1.10 An edge-on projection of the Galaxy showing the locations of a sample of globular clusters. They are distributed approximately spherically about the centre of the Galaxy, in contrast to the highly flattened shape of the disc. The contours show curves of equal density of disc stars. The Sun is located 8.5 kpc from the Galactic centre (at the distance −8.5 kpc from the Galactic centre in this diagram). (Blaauw and Schmidt, 1965)

WALTER BAADE (1893–1960)

Walter Baade (Figure 1.11) was educated in Germany, at the universities of Münster and Göttingen. In 1931, after spending a number of years at the University of Hamburg, he moved to the USA where he worked successively at the Mount Wilson and Mount Palomar Observatories in California. It was during this period that Baade carried out the astronomical work for which he is best remembered. This includes his recognition of the existence of two distinct stellar populations, and the discovery that many of the measured distances to other galaxies were incorrect because two different populations of Cepheid variable (see Chapter 2) had been treated as a single uniform population. Baade also discovered a one-sided jet in the galaxy M87, and recognized the Crab Nebula as the remnant of a supernova that had been observed in 1054. Baade later returned to Germany to take up a post at Göttingen, and died there in 1960.

Figure 1.11 Walter Baade. (Mt. Wilson Observatory)

Following on from Baade's discovery, much effort has gone into studying the characteristics of the different populations. Advances in observational technology and astrophysical theory have made it possible to refine Baade's original idea, so that stellar populations can now be defined in terms of the age, metal content, and location of the stars. While this work has been extremely profitable in developing an understanding of the nature of the stars and the origins of the populations, the proliferation of alternative definitions of populations has not always been helpful. As a result, population descriptions are sometimes used loosely, often meaning different things to different astronomers. This problem has been exacerbated by correlations that often exist between the three key population parameters: age, metal content, and location. In this chapter we adopt one of the simpler classification schemes, concentrating on the two major population divisions that originated with Baade. We also note a third population, unknown to Baade and which has not yet been observed, but which almost certainly existed early in the history of the Universe.

- ■ The three key population parameters in current use are age, metal content, and location, but Baade observed colours and locations. Which of these key parameters corresponds to colour, and why?
- ❑ The colours of very luminous stars depend on their age: luminous blue stars are short lived so they are all young; luminous red stars are old, they are elderly red giants.

Before defining the three populations that are used in this book it is helpful to define a quantitative measure of a star's metal content. A useful definition, although by no means the only one possible, provides a measure of the fraction of the mass of an object that is accounted for by elements heavier than helium, that is, the metals. This is the **metallicity**, Z, defined by the following equation.

$$Z = \frac{\text{the mass of elements heavier than helium in the object}}{\text{the mass of all elements in the object}} \tag{1.1}$$

The metallicity of the Sun is $Z = 0.02$. That is, 2% of the Sun's mass comes from elements heavier than helium.

Having set out the key parameters for describing stellar populations, we now go on to see how these differ for the three populations of interest.

Population I

Pop. I, which Baade associated with the disc, includes many very young stars, some just a few million years old, but also includes some as old as 10^{10} yr. Their metallicities are mostly in the range $Z = 0.01$ to 0.04 (i.e. within a factor of two of the solar value) although some Pop. I stars with still lower metallicities exist. The stars of Pop. I move in essentially circular orbits (around the Galactic centre), which do not take them far above or below the plane of the Galaxy, and hence they are confined to the flat, circular structure that constitutes the Galactic disc. The answer to Question 1.1 shows that the Sun takes roughly 240 million years to move once around the Galaxy. This value is typical of other Pop. I stars near the Sun.

Population II

Pop. II stars occupy the spheroid – the stellar halo and bulge – and turn out to be the oldest stars known, with ages in the range (12 to 15) × 10^9 yr. Conspicuous examples are globular-cluster stars. Little or no interstellar gas is still associated with Pop. II stars, which is consistent with star formation in the spheroid ceasing long ago. Because this population is so old, only low-mass stars (which have long lifetimes) still shine as main sequence stars burning hydrogen in their cores. The more massive stars that formed at the same time as the surviving low-mass ones have already left the main sequence and are now red giants or white dwarfs.

For a long time it was thought that all Pop. II stars had much lower metallicities than do Pop. I stars, but it is now known that this applies only to the stellar halo, for which $Z < 0.002$, and where the lowest-metallicity stars detected so far have $Z \sim 2 \times 10^{-6}$. Some bulge stars, on the other hand, have the same metallicity as the Sun.

Unlike disc stars, Pop. II stars do not follow circular orbits, nor are they confined to the plane of the Galaxy. They move in eccentric orbits (see Figure 1.12), although still attracted to the Galactic centre, and may travel many kiloparsecs from the Galactic plane. This is of course consistent with Pop. II stars belonging to the spheroid, briefly passing through the disc as they move from one side of the Galactic plane to the other. Such fleeting visitors to the Galactic disc are known as **high-velocity stars** because of their high speed relative to the Pop. I stars that belong to the disc. In contrast to the disc, there is almost no net rotation of the halo, so almost half of all halo stars travel in **retrograde** orbits (i.e. in the opposite sense to the more orderly disc stars, which all orbit in the clockwise direction as viewed from the north Galactic pole).

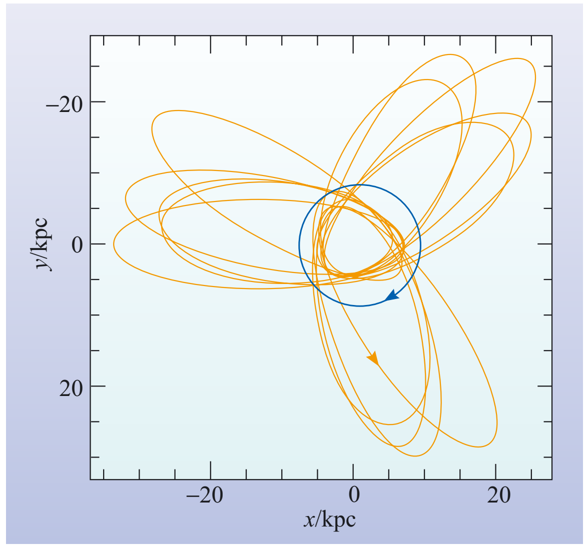

Figure 1.12 A face-on view of the Galaxy showing sample orbits for Pop. I (blue) and Pop. II (orange) stars. Shown is a clockwise, circular orbit for a Pop. I star 8.5 kpc from the Galactic centre, and an anticlockwise (retrograde), three-lobed orbit for a Pop. II star that takes it from 4 kpc to 35 kpc from the centre. This Pop. II star also travels up to 20 kpc above and below the disc, while the Pop. I star remains close to the Galactic plane. (S. Ryan (Open University))

Population III

The term Pop. III describes a theoretical population rather than one that has actually been observed. It encompasses stars that formed out of the unprocessed gas that would have been produced by the big bang. This material would have been almost entirely composed of hydrogen and helium. Even lithium, the next most abundant element in this gas, would only constitute one particle in a billion. Consequently the metallicity of these stars when they first formed ($Z \approx 10^{-9}$, see Example 1.1), would have been much lower than that of even the lowest metallicity stars of Population II ($Z \approx 2 \times 10^{-6}$). No Pop. III star has yet been observed, but theoretically they must have existed as the very first generation of stars in the Universe.

EXAMPLE 1.1

The lithium nuclei that were produced in the big bang account for only a tiny fraction of the total number of nuclei produced, around 1.6×10^{-10} of the total number. Given that each lithium nucleus has a mass seven times that of hydrogen, what was the metallicity of the gas from which Pop. III stars formed? (Only the lightest three elements, H, He and Li, were produced in the big bang. The fraction of helium produced by the big bang was 0.075 of the total number of nuclei, and each helium nucleus has a mass four times that of hydrogen.)

SOLUTION

Since there are only three elements (H, He and Li) produced in the big bang, we can begin with the definition for metallicity (Equation 1.1)

$$Z = \frac{\text{the mass of elements heavier than helium in the gas}}{\text{the mass of all elements in the gas}}$$

and rewrite it as

$$Z = \frac{\text{the mass of lithium in the gas}}{\text{the mass of all elements in the gas}}$$

We introduce the symbols N_X for the number of nuclei of element X, and M_X for the mass of each nucleus of element X, giving

$$Z = \frac{N_{\text{Li}} M_{\text{Li}}}{N_{\text{H}} M_{\text{H}} + N_{\text{He}} M_{\text{He}} + N_{\text{Li}} M_{\text{Li}}}$$

We don't know the total number of nuclei $N_{\text{tot}} = N_{\text{H}} + N_{\text{He}} + N_{\text{Li}}$ produced in the big bang, but that doesn't matter because we know what *fraction* of the total is accounted for by each type of nucleus. That is, we know the values $N_{\text{H}}/N_{\text{tot}}$, $N_{\text{He}}/N_{\text{tot}}$, and $N_{\text{Li}}/N_{\text{tot}}$. (These were given in the question, and come from astronomical observations.) To proceed, we divide the top and bottom lines by N_{tot}, and also by M_{H} for reasons that will become clear.

$$\begin{aligned} Z &= \frac{(N_{\text{Li}} M_{\text{Li}})/(N_{\text{tot}} M_{\text{H}})}{(N_{\text{H}} M_{\text{H}} + N_{\text{He}} M_{\text{He}} + N_{\text{Li}} M_{\text{Li}})/(N_{\text{tot}} M_{\text{H}})} \\ &= \frac{(N_{\text{Li}}/N_{\text{tot}})(M_{\text{Li}}/M_{\text{H}})}{(N_{\text{H}}/N_{\text{tot}})(M_{\text{H}}/M_{\text{H}}) + (N_{\text{He}}/N_{\text{tot}})(M_{\text{He}}/M_{\text{H}}) + (N_{\text{Li}}/N_{\text{tot}})(M_{\text{Li}}/M_{\text{H}})} \end{aligned}$$

This can now be evaluated, because all the ratios that appear in the equation are given in the question. Note that, since only H, He, and Li are produced in the big bang, the number of hydrogen nuclei is given by $N_{\text{H}} = N_{\text{tot}} - N_{\text{He}} - N_{\text{Li}}$, so $N_{\text{H}}/N_{\text{tot}} = 1 - (N_{\text{He}}/N_{\text{tot}}) - (N_{\text{Li}}/N_{\text{tot}})$, so

$$\begin{aligned} Z &= \frac{1.6 \times 10^{-10} \times 7}{(1 - 0.075 - 1.6 \times 10^{-10}) \times 1 + 0.075 \times 4 + 1.6 \times 10^{-10} \times 7} \\ &= \frac{1.12 \times 10^{-9}}{0.925 + 0.30 + 1.12 \times 10^{-9}} = 9.1 \times 10^{-10} \\ &\approx 10^{-9} \end{aligned}$$

That is, the metallicity of a Pop. III star is expected to have been $Z \sim 10^{-9}$.

QUESTION 1.2

(a) Describe Baade's observations of M31 and their implications for the Milky Way. (*Note*: Baade did not know the details of stellar evolution – those did not become clear until many years later – so your answer should *not* discuss stellar evolution.)

(b) From what you know about the evolution of stars, how would you interpret the differences between red and blue stars in Baade's observations?

QUESTION 1.3

Stellar populations differ in age, metallicity and location, but sometimes stellar motion is used as an alternative criterion to location. Why is this reasonable?

1.2.5 The chemical evolution of the Milky Way

We have seen that the stellar populations of the Galaxy have a range of ages, metallicities and locations. To understand why the different populations have different ranges of metallicity we have to consider where the metals come from.

The only metal produced in the big bang was lithium, all others result directly or indirectly from nuclear reactions occurring in stars. The metallicity of a main sequence star corresponds to the metallicity of the ISM at the time the star formed. The fact that each stellar population contains a range of metallicities, and that the younger stars in a population tend to have higher metallicities, therefore suggests the operation of some process that progressively enriches the ISM by increasing its metallicity. There are a number of routes by which metals that form inside a star can escape and enter the surrounding ISM, thereby bringing about the required chemical enrichment. These escape routes only become available during the late stages of a star's life (although these come relatively quickly for high-mass stars), and may include the emission of high-speed stellar winds, the ejection of shells of gas to form planetary nebulae, and, in some cases, disruption of the star in the explosive process known as a supernova. By whichever routes it happens, the transfer of chemically enriched material from a star to the ISM enriches the ISM and ensures that the next generation of main sequence stars to form in that region will have higher metallicity than its predecessor. Thus the chemical evolution of the Galaxy is a cyclic process involving star formation, element production within stars (nucleosynthesis), and the return of chemically enriched material to the ISM where it can form more stars. This process is sometimes called **cosmic recycling**, and is central to our understanding of the differences between Pop. I and Pop. II stars in terms of the way the Galaxy has evolved since its formation.

Although cosmic recycling will have taken place in each of the Galactic components (disc, bulge and stellar halo) that contain stars, it probably did not proceed at the same rate in each of them, nor does it necessarily continue at a significant rate in each of them today. The presence of various amounts of metals in stars of different ages allows astronomers to deduce the history of cosmic recycling in the various stellar populations, which in turn allows them to trace the star formation history of the Galaxy. We will explore this topic in more detail later, particularly in Section 1.6.2.

Before concluding this section we provide a few questions to encourage you to think about the link between the content of the Galaxy and its evolution.

QUESTION 1.4

Why would you expect surviving Pop. II main sequence stars to have lower metallicity than Pop. I main sequence stars?

QUESTION 1.5

Some people think that old stars have been undergoing nucleosynthesis for a long time, so when we observe Pop. II main sequence stars they should exhibit higher metallicity than the younger Pop. I stars because of the accumulated products of nucleosynthesis. Explain why this view is wrong.

1.3 The mass of the Milky Way

When the structural components of the Galaxy were introduced in Section 1.2.1, their masses were simply stated. At the time, did you ask yourself how astronomers might know these values, or how uncertain they might be? You may be surprised to learn that reasonable estimates can be obtained from some quite simple calculations based on the influence of gravity on the motions of objects, although determining the mass of the entire Galaxy accurately is a major challenge.

In answering Question 1.1, you learned that the Sun takes roughly 240 million years to complete one orbit of the Galactic centre. To perform this calculation you needed to know the speed at which the Sun travels in its orbit and its distance from the Galactic centre. The speed of the Sun was established in the 1920s, by Bertil Lindblad (1895–1965) and Jan Hendrik Oort (1900–1992), from the motion of Pop. I stars relative to Pop. II stars. As you saw in Section 1.2.4, Pop. II stars have little net rotation about the Galactic centre, and so provide a reference population relative to which the Sun's motion can be determined. Pop. I stars in our part of the Milky Way are streaming past the Pop. II stars at speeds that are typically $220\,\mathrm{km\,s^{-1}}$. We will soon use this information to calculate the mass of the inner part of the Galaxy, but before doing so we introduce a graphical tool that plays an important part in the characterization and analysis of rotating systems.

A plot of speed against distance from the centre for the various parts of a rotating system is called a **rotation curve**. The rotation curve for a rigid wheel 3 m in diameter, making one revolution per second, is displayed in Figure 1.13a. As the figure shows, the speed (usually expressed in metres per second; $\mathrm{m\,s^{-1}}$) of each part of the wheel increases in proportion to the distance from the centre. Note, however, that in the case of a rigid wheel the angular speed of each part about the centre – the angle that each part sweeps out per second, as viewed from the centre of the wheel – is the same. Finding that all parts of a body have the same angular speed is a characteristic of **rigid body rotation**.

Figure 1.13b shows the rotation curve of planets orbiting the Sun. Each planet takes a different length of time to complete one orbit, which means each travels at a different angular speed. This is characteristic of **differential rotation**, and is clearly different from rigid body rotation. As you can see, the rotation curve for such a system is *not* a straight line through the origin, so speed is *not* proportional to distance from the centre.

Figure 1.13c shows the rotation curve of the Milky Way. This has a different shape from Figure 1.13b, but it still shows that the speed is not proportional to distance from the centre, and therefore indicates differential rotation with a range of angular speeds. The difference between Figures 1.13b and 1.13c is due to the fact that there is no massive central body dominating the Milky Way, whereas the mass of the Sun dominates the Solar System.

1.3.1 Calculating the mass of a gravitating system

The equations describing the rotation curve of a system governed by the gravitational attraction of a single central body relate the orbital speed and orbital radius to the mass of the central body. This is very important in astronomy, as it allows us to calculate the mass of a gravitating body from the motions of particles orbiting it. For an object in a circular orbit of radius r about a single,

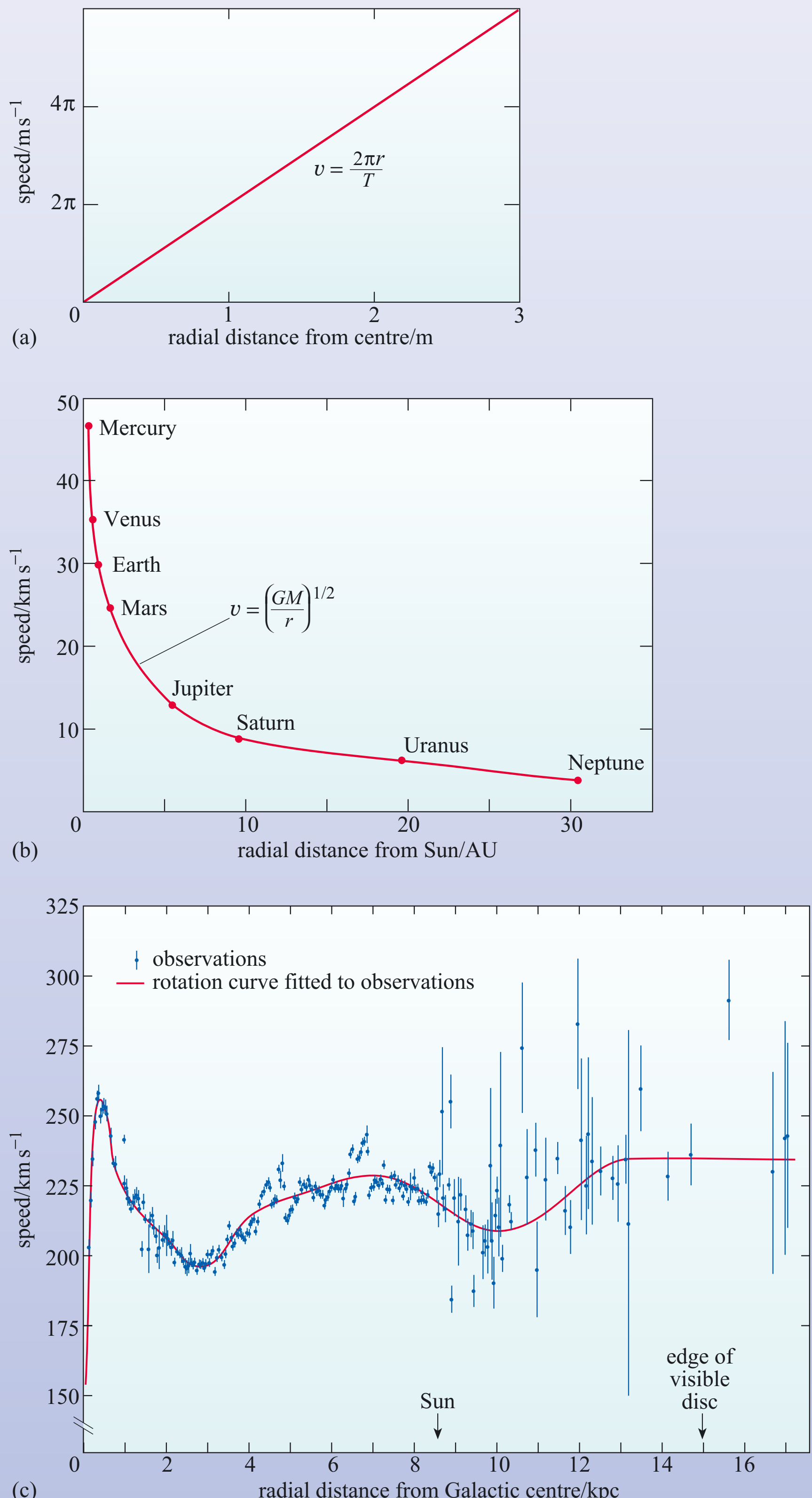

Figure 1.13 The rotation curves, showing speed v against radial distance r, of (a) a rigid wheel, 3 m in diameter, with a rotation period T of 1 s; (b) the planets of the Solar System; and (c) the Milky Way, based on Doppler-shift studies of gas clouds in the disc. Note that the rotation curve for the Galaxy is based on data that are subject to substantial observational uncertainties, and is therefore 'noisier' than the other two curves. This is because the observations are harder to make (especially for objects further from the Galactic centre than the Sun), and the analyses are plagued by additional complications, such as the non-uniform distribution of matter in the Galactic disc. ((c) Combes, 1991)

much more massive object of mass M, the equation describing the rotation curve (see Box 1.2) is

$$v = \left(\frac{GM}{r}\right)^{1/2}$$

The reciprocal of some quantity x is $1/x$.

The symbol $\propto$ means 'is proportional to'.

Note that $\sqrt{x} = x^{1/2}$

This equation indicates that the speed v is proportional to $1/r^{1/2}$, which means that the orbital speed falls as the radius increases, at a rate given by the reciprocal of the square root of the radius. We can write this in mathematical shorthand as $v \propto 1/r^{1/2}$. The curve plotted in Figure 1.13b has this functional form.

BOX 1.2 ROTATION CURVES FOR GRAVITATING SYSTEMS

According to Newton's second law of motion, the magnitude of the acceleration a_i of some body (labelled 'i') of mass m_i, due to a force of strength F, is

$$a_\mathrm{i} = F/m_\mathrm{i} \tag{1.2}$$

According to Newton's law of gravitation, the strength F_g of the gravitational force on each of two point-like bodies of masses m and M, when their centres are separated by a distance r, is

$$F_\mathrm{g} = GMm/r^2 \tag{1.3}$$

where G is the universal gravitational constant, $6.673 \times 10^{-11}\,\mathrm{N\,m^2\,kg^{-2}}$.

Substituting this expression for F_g into Equation 1.2 shows that, due to the gravitational attraction of the body of mass M, the body of mass m will have an acceleration of magnitude

$$a_{\mathrm{g},m} = \frac{GMm/r^2}{m} = GM/r^2$$

Similarly, due to the attraction of the body of mass m, the body of mass M will have an acceleration of magnitude

$$a_{\mathrm{g},M} = \frac{GMm/r^2}{M} = Gm/r^2$$

In cases where M greatly exceeds m, written $M \gg m$, we can also write $GM/r^2 \gg Gm/r^2$, implying that $a_{\mathrm{g},m} \gg a_{\mathrm{g},M}$. That is, the acceleration of the more massive body has a magnitude, $a_{\mathrm{g},M}$, that is much smaller than the magnitude of the acceleration of the less massive body, $a_{\mathrm{g},m}$. Therefore the more massive body barely moves, and we can regard it as being the stationary centre of motion for the less massive body. One particularly simple form that this motion might take is for the less massive body to move around the more massive body at constant speed in a circular orbit. This kind of motion is known as uniform circular motion.

Any body moving in uniform circular motion at speed v about some centre at a distance r must be accelerating at all times. This acceleration is called its centripetal acceleration; it is always directed towards the centre of the motion and its magnitude is

$$a_\mathrm{cen} = v^2/r$$

When this uniform circular motion is the result of the gravitational attraction between two bodies, the centripetal acceleration is provided by the gravitational acceleration, so for the less massive body in motion about the stationary, more massive one, we can write:

$$a_\mathrm{cen} = a_{\mathrm{g},m}$$

so $\quad v^2/r = GM/r^2$

and hence

$$v^2 = GM/r$$

This equation can be rearranged in two slightly different ways to give useful equations relating the orbital speed and the central mass of a two-body system:

$$v = (GM/r)^{1/2} \tag{1.4}$$

and

$$M = v^2r/G \tag{1.5}$$

Note that the orbital speed of the less massive body does not depend on its mass. Also notice that we can deduce the mass of the central body from the speed and radial separation of an orbiting body, without knowing the mass of that orbiting body.

QUESTION 1.6

(a) Calculate the circumference of the Earth's orbit around the Sun. (The Earth is 150 million kilometres from the Sun, to three significant figures.) Give your answer in SI units.

(b) Calculate the speed at which the Earth orbits the Sun. Give your answer in SI units.

(c) Use the formula for the rotation curve to calculate the mass of the Sun from the orbital speed of the Earth. Give your answer in SI units. (For the universal gravitational constant, use the value $G = 6.673 \times 10^{-11}\,\mathrm{N\,m^2\,kg^{-2}}$.)

(d) How many significant figures are there in your final answer, and why?

How does your answer to Question 1.6 compare with the modern value, $M_\odot = 1.9891 \times 10^{30}\,\mathrm{kg}$? Did you ever realize just how easy it would be to calculate the mass of the Sun? All you need to know is the speed and orbital radius of one small body in a circular orbit. You don't even need to know the smaller body's mass.

You could look up the orbital radii and periods of a few other planets to convince yourself that you get the same answer, but for now we have bigger fish to fry; let's calculate the mass of the inner part of the Galaxy!

Unlike the Solar System, the Milky Way does not have a single dominant mass at its centre. Rather, its constituents move under the gravitational influence of all the other constituents. This makes a detailed analysis very complicated, but it is still possible to make a simple estimate of the mass of the inner part of the Galaxy. The basis of this analysis is provided by the following result taken from Newtonian gravitation theory.

When the mass of a system is distributed in a spherically symmetrical manner about some central point, then the net gravitational force on a point-like object at some radius is due only to the mass *within* that radius. Furthermore, the net gravitational force is the same as if the mass inside that radius was all located at the centre.

In the case of the Milky Way, the distribution is not really spherically symmetrical, but mass outside a given radius has only a moderate effect, and a reasonable estimate of the mass can still be obtained using the method above. (Detailed calculations can be performed for more realistic mass distributions to confirm this.) If we adopt this procedure for the Galaxy, then the observed orbital speed at some radius r can be inserted into the rotation-curve equation to estimate the mass of the Galaxy enclosed within that radius from the Galactic centre. As this gives the mass within the radius r, rather than the total mass of the Galaxy, we denote that mass by $M(r)$.

QUESTION 1.7

(a) Following the technique used in Question 1.6c, calculate the mass of the Milky Way out to the distance of the Sun from the Galactic centre. Give your answer both in SI units and solar masses, assuming $M_\odot = 1.99 \times 10^{30}\,\mathrm{kg}$. (*Hint*: You know already that the Sun is 8.5 kpc from the Galactic centre, and that it moves at $220\,\mathrm{km\,s^{-1}}$ in a nearly circular orbit.)

(b) How many significant figures can you quote the result to, if you follow the usual mathematical rules? Is there any physical reason why you might deviate from this rule?

1.3.2 Using rotation curves

The answer to Question 1.7 shows that interior to the Sun's orbit at 8.5 kpc, the mass of the Galaxy is $10^{11}M_\odot$. If we want to find the *total* mass of the Milky Way, we have to study its outskirts, where the orbiting material encloses virtually all the mass of the Galaxy. This is difficult, not least because it is difficult to determine exactly where the Galaxy ends. Even if we think there is not much more *visible* matter beyond a certain radius, we cannot be sure that we have found the 'edge' of any dark matter that is associated with the Galaxy.

Plotting a rotation curve can throw light on the question: 'Where does the Galaxy end?' We have just seen in Question 1.7 how it is possible to compute the enclosed mass at some radius in the Galaxy by knowing the orbital speed there. From an observed rotation curve, it is possible to compute the enclosed mass $M(r)$ at a whole range of radii, and doing so shows how $M(r)$ increases with radius, which therefore gives the *distribution* of mass. By seeing how the mass distribution is changing in the outermost *measurable* parts of a Galaxy, it is possible to have some idea of whether the mass distribution is tailing off near the last measurement.

The usual procedure for deducing $M(r)$ for a galaxy is to take an educated guess at the distribution of matter and then work out the rotation curve that such a distribution would produce. The initial guess is then adjusted until the modelled rotation curve agrees with the observed one. To see how this process works, in the following example and question we compute the rotation curves for some simple, assumed mass distributions, and then use these results to interpret what has been measured for the Milky Way, which is shown in Figure 1.13c.

EXAMPLE 1.2

Use the rotation-curve equation to help you to sketch a rotation curve for the following distribution of matter: $M(r) = M$, a constant, indicating a central mass only.

SOLUTION

A rotation curve is a plot of speed versus radius, so the more useful form of the rotation-curve equation (see Box 1.2) is $v(r) = (GM(r)/r)^{1/2}$ (Equation 1.4). To sketch the rotation curve, we need to know how v varies with r.

Since in the example $M(r)$ is a constant, M, the equation for the speed becomes

$$v(r) = (GM/r)^{1/2} = \text{const} \times 1/r^{1/2}$$

Note that we have put the constant parts of this expression into one term called 'const', and have kept the variable parts separate.

This equation shows that the rotation curve falls with increasing radius as $1/\sqrt{r}$, so your sketch of the rotation curve in this case should decrease in speed as radius increases, and it should flatten out towards large radius. One example of a system dominated by a central mass is the Solar System, so the rotation curve should match Figure 1.13b.

Historically, it was Johannes Kepler (1571–1630) who first recognized that a relationship of this form describes the motion of planets in the Solar System. This is the origin of the term **Keplerian orbit** that astronomers now use to refer to the motion of a body under the gravitational influence of a much more massive body.

QUESTION 1.8

Following the example presented above, use the rotation-curve equation to help you to sketch a rotation curve for each of the following distributions of matter.

(a) $M(r) = kr$ (for some constant of proportionality k);

(b) a uniform-density sphere, i.e. where $M(r)$ = density × (volume of sphere of radius r) $= \rho \times \frac{4}{3}\pi r^3$

Figure 1.13c shows the measured rotation curve of the Milky Way. Some of the features of Figure 1.13c, such as the peak near the Galactic centre and the sharp dip that follows it, are more likely to be due to the inadequacy of the symmetry assumptions that underpin the analysis rather than real features of the rotation. However, the flatness of the rotation curve at large distances is thought to be real. It is flatness of this kind, extending well beyond the edge of the visible disc, which provides evidence for the presence of a substantial amount of non-luminous matter on the outskirts of the Milky Way – dark matter. If you compare all but the central parsec of the Milky Way's rotation curve (Figure 1.13c) with your answers to Question 1.8, you will see that it is similar to the flat curve for $M(r) = kr$. Note that a mass distribution of the form $M(r) \propto r$ thins out with increasing radius, so a flat rotation curve does not imply constant density.

If most of the mass of the Galaxy were well within the largest measured radius, the rotation curve would be expected to decline quite rapidly with increasing radial distance, as in the case $M(r)$ = constant in the solution to Example 1.2. The answer to the question: 'What is the mass of the Galaxy?' really depends on the answer to another question: 'Where does the rotation curve turn down?'

Several independent investigations have failed to show any sign of a decline in the rotation curve of the Milky Way out to a radius of 20 kpc, indicating a substantial amount of matter at least out to that radius. This matter has not been directly observed at any wavelength and is therefore some form of dark matter.

There are still many uncertainties about the distribution of mass in the Milky Way. Different assumptions about the radius of the Galaxy and the distribution of dark matter can easily provide estimates of the total Galactic mass that range from a conservative four times the mass of the stars, that is $4 \times 10^{11} M_\odot$, to a very substantial 60 times: $6 \times 10^{12} M_\odot$. The mass of the Galaxy can be assessed using the velocities of other objects besides disc gas, such as distant halo stars, globular clusters and nearby galaxies, but they too are based on specific assumptions and do not yet settle the question.

We noted at the beginning of this chapter that measuring the *size* of the Galaxy was not as simple a task as it might first sound. Astronomers Michel Fich and Scott Tremaine described the problem of measuring the *mass* of the Galaxy by attacking the question, in the following way:

> 'What is the mass of the Galaxy? The most important recent progress in addressing this question has been the recognition that it is not well-posed. … there is probably no natural definition of the mass of a giant galaxy like our own …'

- Could you calculate the mass of the wheel whose rotation curve is shown in Figure 1.13a, using the technique used in Question 1.7? Would it make any difference if most of the mass of the wheel were concentrated near the centre of rotation? Explain your answer.

- You could not determine the mass of the wheel; the rotation curve contains no information on its mass because rotation of the wheel is governed by non-gravitational forces. (The forces are electrostatic, and act between the many neighbouring particles in the rigid structures of the wheel.) You could calculate the centripetal acceleration of various parts of the wheel, but those accelerations would not be related to its mass distribution. This answer would not be any different if the mass were concentrated near the axle.

1.4 The disc of the Milky Way

The major components of the Galaxy have now been introduced, their chief constituents have been described, and, at least as far as its inner parts are concerned, the mass of the Galaxy has been estimated. In the remaining sections of this chapter we examine the disc, the stellar halo and the bulge in more detail, and we begin to uncover the evolutionary history of the Milky Way. We start in this section with a detailed account of the Galactic disc.

We have seen already that dark matter dominates the mass of the Galaxy as a whole, but if we consider the disc alone, we find that there the dark matter has less impact. The motion of stars perpendicular to the disc indicates that no more than 30–50% of the *disc's* mass is due to dark matter. Stars and gas are so abundant in the disc that visible matter dominates there.

The disc is important to our understanding of the Galaxy for two reasons: it is the component to which most of the visible matter – stars, gas and dust – belongs, and it is the main site of current star formation in the Milky Way. Most of that star forming

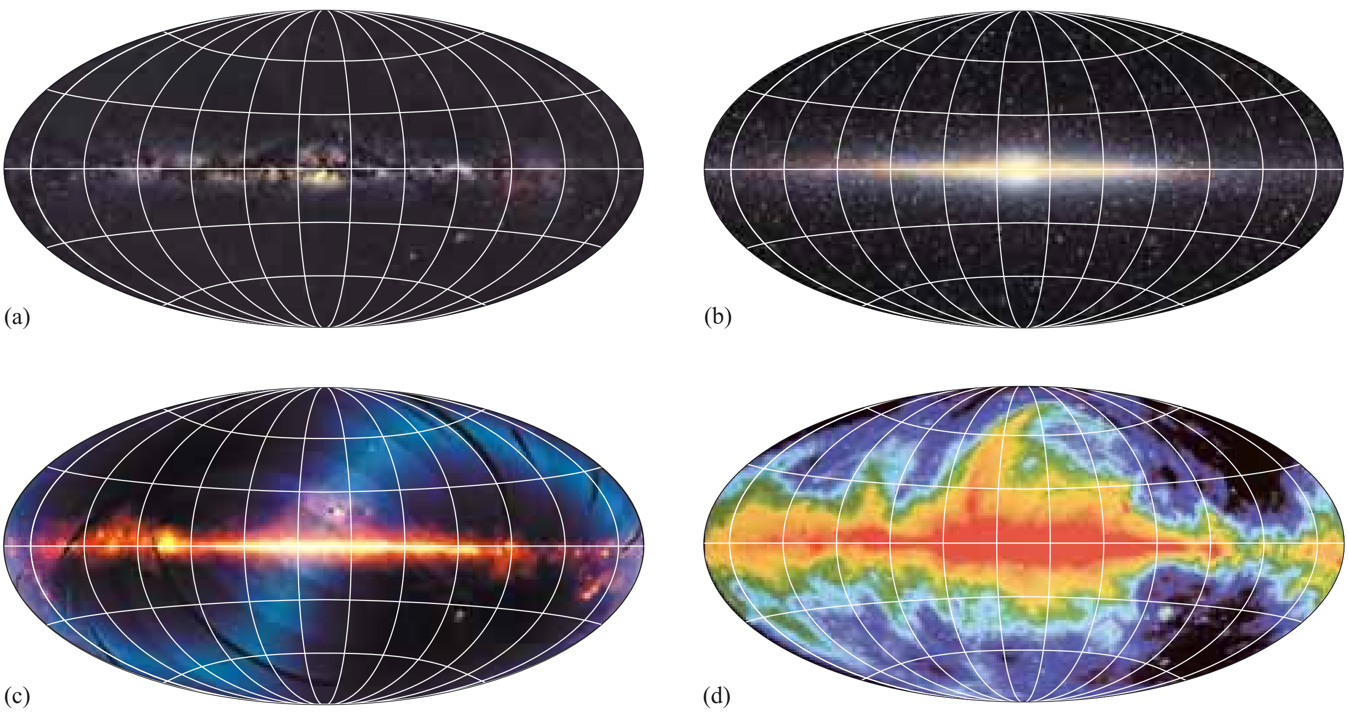

(a) (b) (c) (d)

Figure 1.14 All-sky views of the Milky Way at various wavelengths. The symmetry of the Galaxy and the proximity of the Sun to the mid-plane of the disc are emphasized in these views, which are presented in Galactic coordinates with the Galactic equator running horizontally across the middle. They are arranged with the Galactic centre ($l \approx 0°$, $b \approx 0°$) near the middle. (a) Optical light which is predominantly the thermal radiation from stars; (b) near-infrared emission dominated by thermal radiation from cool stars; (c) far-infrared emission dominated by thermal radiation from dust, especially that associated with star-forming regions; (d) 73.5 cm radio continuum emission. Note that the blue 'S'-shaped band in the far-infrared image (c) is due to hot dust within our Solar System. ((a) A. Mellinger (University of Potsdam, Germany); (b) N. Wright; (c) NASA/Goddard Space Flight Center; (d) G. Haslam *et al.*, (Max-Planck-Institut für Radioastronomie, Bonn))

activity occurs in the spiral arms, which would be a prominent feature of the disc if we could view it externally. Many of the characteristic features of the disc that we can observe, such as the presence of young, high-metallicity stars, dense molecular clouds and HII regions, are directly connected with star formation. A major aim of this section is to survey these observable features and to relate them to star formation and cosmic recycling.

The visual appearance of the Milky Way (Figure 1.14a) is dominated by luminous stars, mostly belonging to the disc, although in various directions the view is obscured by dark dust clouds. Viewed at the longer wavelengths of near-infrared radiation (Figure 1.14b), the dust clouds become transparent, allowing us a relatively clear line of sight towards the Galactic centre. At the still longer wavelengths of far-infrared radiation, the dust itself becomes a luminous source of radiation (Figure 1.14c), and at even longer radio wavelengths the Galactic gas that surrounds us becomes visible (Figure 1.14d), creating a view that is very different from that of the visible stars.

- ■ On the maps in Figure 1.14, where is the Galactic anti-centre, i.e. the direction directly away from the Galactic centre?
- ❑ It is the point that lies on the Galactic equator, 180° from the Galactic centre. This point appears both at the far left and far right ends of each map, where they 'wrap around'.

1.4.1 The stellar content of the disc

Stars are the most luminous constituent of the Milky Way, and most stars reside in the Galactic disc. Usually stars do not form alone, but instead begin their lives in clusters or associations. This is a consequence of stars forming from dense molecular clouds (see Section 1.2.3) that contain enough gas to create large numbers of stars. **Open clusters** occupy regions of space, typically 2–3 pc across, where the density of stars is enhanced locally by a group of a few tens to a few hundred stars that formed at the same time. The cluster members are bound together by their mutual gravitational attraction. There are thousands of open clusters in the Galactic disc. Some are sufficiently prominent to be visible to the naked eye, most notably the Pleiades (Figure 1.15).

Because of their concentration close to the plane of the Galaxy, open clusters used to be called *galactic clusters*. However, this term is potentially confusing ('galaxy clusters', which is a term sometimes used to describe clusters *of* galaxies, are quite different) and its use is discouraged.

Figure 1.15 The Pleiades is a very young open cluster with an age of only ~80 Myr. Massive hot, blue stars dominate its appearance. (D. Malin/Royal Observatory Edinburgh/Anglo-Australian Telescope Board)

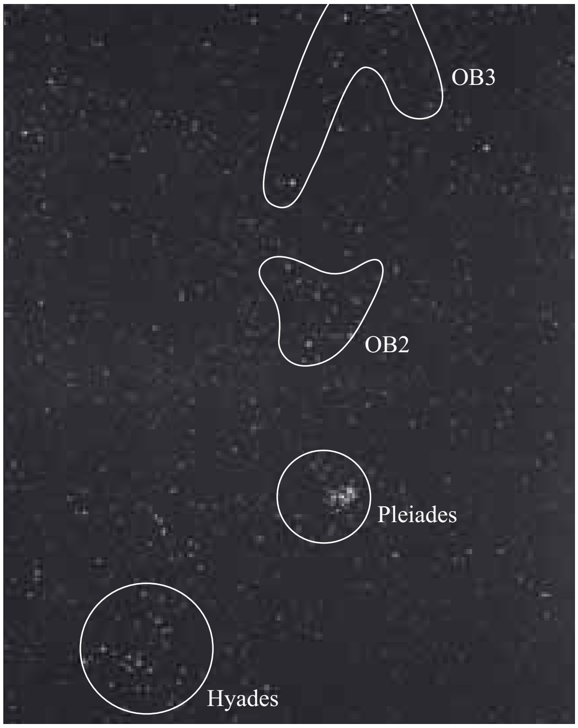

Figure 1.16 A portion of the Milky Way showing the Hyades and Pleiades open clusters, and OB associations in Taurus and Perseus.

Open clusters are believed to have relatively short lives. With very few exceptions no individual open cluster is expected to survive for more than 10^9 years. The smallest open clusters live for even shorter periods, just a few million years, so they are mainly found in the spiral arms, since this is where star formation mainly takes place. Why do the clusters disrupt and dissipate in a time that is much shorter than the lives of many of the stars they contain? There are three processes that aid this. First, a cluster moving in the disc might be torn apart by a gravitational encounter with some other object such as a giant molecular cloud or another cluster. Secondly, gravitational interactions between a cluster's members can give one star enough energy to escape; given long enough, this process, called **evaporation**, would disperse all clusters. A third process that disrupts clusters is differential rotation, which was described in Section 1.3. The stars in an open cluster, while moving around one another, are also orbiting the Galactic centre and hence are subject to the effects of differential rotation that will stretch, distort and eventually destroy the cluster. The concentration of open clusters in the spiral arms must mean that the clusters have relatively short lives, otherwise motion relative to the arms would relocate them to various positions in the disc.

Stellar aggregates of another kind found in the disc, particularly within the spiral arms, are the so-called **OB associations**. OB associations have diameters of 100 pc or so, and densities not much greater than their general surroundings, but contain an unusually high proportion of O- and B-class stars (Figure 1.16). Many OB associations have a very young open cluster at their centre. The presence of numerous O and B stars, which have very short main sequence lifetimes, is a sure sign that OB associations are young, no more than a few million years old. About 70 OB associations are known.

The stars of the disc are primarily Pop. I objects. They can be divided into a range of subpopulations, three of which are described below. Other schemes can be used too; the important thing is not to get hung up on these definitions, but rather to appreciate that a range of objects exists and that *sometimes* it is useful to make distinctions between them.

- *Pop. I, spiral-arm stars* are the youngest stars in the Galaxy, with ages less than about 0.1×10^9 yr, and are found in the spiral arms. They are associated with the spiral arms because that is where they have formed, and their short lives have not enabled them to move far from their birthplace. Examples include stars in young open clusters such as the Pleiades (Figure 1.15) and the Hyades (Figure 1.16), short-lived massive stars such as O and B stars, supergiant stars, and the pulsating giant stars called **classical Cepheids**. The young stellar objects known as **T Tauri stars** also belong to this subpopulation. The metallicities of Pop. I spiral-arm objects are typically solar or greater, i.e. $Z = 0.02$ to 0.04. Associated objects include glowing HII regions (see Section 1.2.3), which are produced where high-energy UV photons from O- and B-type stars ionize hydrogen gas in the interstellar medium.
- *Pop. I, thin-disc stars* are older than the spiral arm stars, with ages from (1 to almost 10) $\times 10^9$ yr, and their metallicities include some much lower values, $Z = 0.005$ to 0.04. These stars move in circular orbits, and have lived long

enough to escape from the spiral arms and spread themselves across the disc. The word 'thin' is included in the name because they are seldom found more than 500 pc from the mid-plane of the disc, so they occupy a **thin disc** with a relatively small cross-section. The significance of this will become clearer when we discuss the next subpopulation, the thick-disc stars.

- *Intermediate Population or thick-disc stars* have lower metallicities than thin-disc stars, typically $Z \approx 0.002$ to 0.01, and ages closer to the thin-disc maximum, 10×10^9 yr. Another distinguishing feature is that while their orbits are still basically circular, the thick-disc stars travel to greater distances from the Galactic plane. This last characteristic means they are not confined as close to the Galactic plane as normal thin-disc stars, so they occupy a **thick disc** with a greater cross-sectional area than the thin disc. Their typical locations and metallicities give these objects properties intermediate between those of the Pop. I and Pop. II stars discussed earlier, so they are also known as **Intermediate Population** stars.

In Section 1.2.5 we introduced the concept of cosmic recycling, and discussed the differences between Pop. I and Pop. II stars in terms of the chemical evolution of the Galaxy. The existence of the three subpopulations described above now emphasizes that there is also an evolutionary sequence within the disc, with thick-disc stars having formed 10×10^9 yr ago from low metallicity gas, and spiral-arm objects having formed much more recently, less than 0.1×10^9 yr ago, from gas with a much higher metallicity. The existence of stars with a range of ages, metallicities and motions provides clues to the evolutionary history of the disc, and indicates that it is continuing to evolve. We return to this topic in Section 1.6.

■ Why would you expect HII regions to be associated with the spiral arms?

❑ HII regions need the presence of O and B stars to provide ionizing UV photons, and O and B stars are themselves associated with the spiral arms because they are short-lived stars that do not survive long enough to move very far away from their sites of formation.

1.4.2 The gaseous content of the disc

The gaseous interstellar medium (ISM) is intimately associated with stellar evolution. Stars form from cool dense clouds in the ISM, and at the ends of their lives they return matter to the ISM in a variety of ways that gradually increase the metallicity of the Galaxy. Gas and dust are therefore important constituents of the disc, and we examine their composition and distribution in this section. Included in the discussion are descriptions of how the gas can be observed.

Interstellar gas

As you saw earlier, the total mass of gas in the disc amounts to about 10% of the stellar mass. The gas forms a disc about 300 pc thick that is surrounded by hotter gas, which stretches out into the halo. Much of the gas is in the form of *clouds*, of which there are many thousands, with a range of temperatures and densities. The individual clouds probably take the form of sheets or filaments of gas rather than some idealized spherical shape. Regions of the ISM not occupied by clouds constitute the extensive but low-density *intercloud medium*. There the hydrogen exists mainly in the form of neutral atoms (HI), which are easily observed due to their emission of radio waves at a wavelength of 21 cm (see Box 1.3).

BOX 1.3 THE 21 CENTIMETRE EMISSION LINE OF ATOMIC HYDROGEN

A major indicator of the distribution and line-of-sight velocity of neutral (atomic) hydrogen (HI) gas, not just in the Milky Way but other galaxies as well, is its emission line in the radio region of the spectrum at a wavelength of 21 cm. The origin of this **21 centimetre radiation** involves the relative *spins* of the electron and proton that constitute the hydrogen atom. These spins are illustrated in a classical (i.e. non-quantum) sense in Figure 1.17, where the proton and the electron are pictured as small spheres spinning at a fixed rate around axes through their centres. The quantum physics of the hydrogen atom ensures that the electron spin is always either parallel to that of the proton, as in Figure 1.17a, or anti-parallel (i.e. opposed to it), as in Figure 1.17b. There is a small energy difference between the states shown in Figure 1.17, and it is the transition from the higher energy state (a) to the lower energy state (b) that gives rise to the 21 cm emission line.

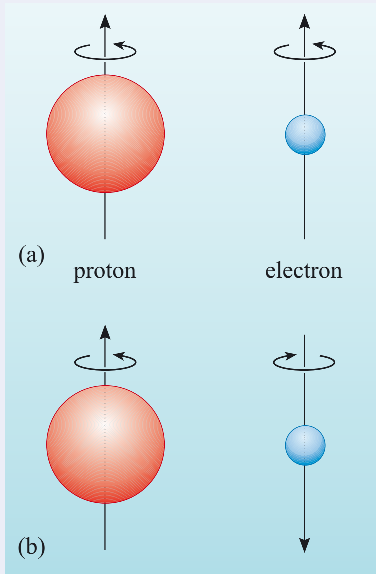

Figure 1.17 A classical view of the hydrogen atom, in which the proton and electron spins are (a) parallel or (b) anti-parallel.

- What is the energy difference between these two states, in SI units (joules) and electronvolts?

- The energy difference between the states is just the energy of the emitted photon. This is given by

$$\varepsilon = hf = hc/\lambda \tag{1.6}$$

Thus the energy difference between the two states associated with the 21 cm line is

$$\begin{aligned}\varepsilon &= hc/\lambda \\ &= 6.63 \times 10^{-34}\,\mathrm{J\,s} \times 3.00 \times 10^{8}\,\mathrm{m\,s^{-1}}/0.21\,\mathrm{m} \\ &= 9.5 \times 10^{-25}\,\mathrm{J}\end{aligned}$$

Since $1\,\mathrm{eV} = 1.60 \times 10^{-19}\,\mathrm{J}$, the energy difference can also be expressed as

$$\begin{aligned}\varepsilon &= 9.5 \times 10^{-25}\,\mathrm{J}/1.60 \times 10^{-19}\,\mathrm{J\,eV^{-1}} \\ &= 5.9 \times 10^{-6}\,\mathrm{eV}\end{aligned}$$

For us to observe this emission line, the hydrogen atoms must be in an environment where they can readily gain the energy required to raise them into the upper energy level at a reasonable rate compared with the rate at which they are reverting to the lower energy level by emitting radiation. One energy source is provided by collisions between hydrogen atoms as a result of their random thermal motion – this is an example of **collisional excitation**. For a reasonable proportion of such collisions to be sufficiently energetic, the average translational kinetic energy of an atom, e_k, must exceed the energy difference between levels, ε, such that $e_k \geq \varepsilon$. For thermal motion, the average translational kinetic energy is related to the temperature T of the gas particles via the equation $e_k = 3kT/2$, where k is the Boltzmann constant. Thus, by requiring $e_k \geq \varepsilon$, we get $3kT/2 \geq \varepsilon$ and hence $T \geq 2\varepsilon/3k$.

Putting in the value of ε, we get the requirement $T \geq 2 \times 9.5 \times 10^{-25}\,\mathrm{J}/(3 \times 1.38 \times 10^{-23}\,\mathrm{J\,K^{-1}}) = 0.046\,\mathrm{K}$. This condition is met everywhere in the ISM, so the 21 cm line is readily emitted wherever atomic hydrogen exists.

The radial velocity of a cloud of atomic hydrogen can be measured from the Doppler shift of the 21 cm emission line. In general, the radial velocity (i.e. the component of velocity along the line of sight) of an object that emits (or absorbs) radiation at a wavelength λ_{em} is given by

$$v_r = c(\lambda_{obs} - \lambda_{em})/\lambda_{em} \tag{1.7}$$

where λ_{obs} is the wavelength at which the radiation is observed and c is the speed of light. This relationship is valid provided that the radial velocity is much smaller than the speed of light, v_r must be less than about $0.1c$. Note also that the convention used in Equation 1.7, and throughout this book, is that an object moving *away* from the observer has a *positive* radial velocity.

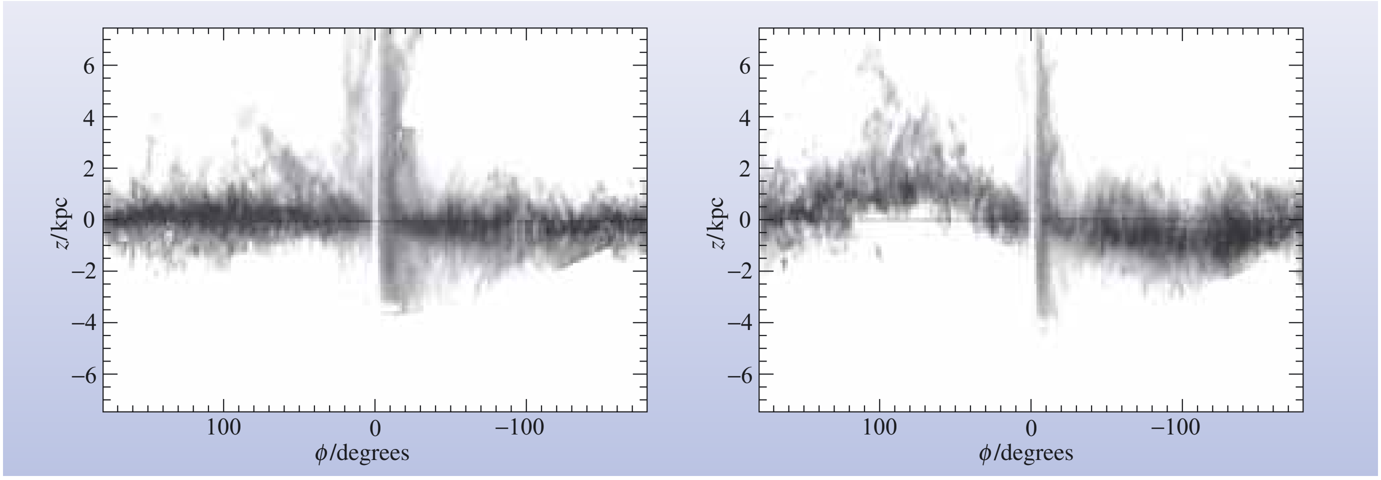

Figure 1.18 The Galactic HI density on cylindrical surfaces at (a) 12 kpc and (b) 16 kpc from the Galactic centre. Each map plots the distribution of gas at a vertical displacement, z, from the Galactic plane and an azimuthal angle, ϕ, measured in the Galactic plane. Each map is constructed as if viewed from the Galactic centre. The warping of the disc, which sets in around 16 kpc, is seen as a wave-like displacement of the gas from the equatorial plane, strongest around $\phi = \pm 90°$. (The vertical column of gas in the centre of each image is an artefact of the way the maps have been made.) (Binney and Merrifield, 1998; from data published in Burton, 1985; Hartmann and Burton, 1997; and Kerr *et al.*, 1986, courtesy of T. Voskes and B. Burton)

Although we have said that the gas forms a disc with a thickness of 300 pc, this disc is not completely flat. Its mid-plane is flat out to a radius of 12 kpc from the Galactic centre, but at greater distances it is warped (tilted). This can be seen in the two parts of Figure 1.18, which show the gas distribution at 12 kpc and 16 kpc from the Galactic centre, as it would be seen from the Galactic centre rather than from the location of the Solar System. The images are built up from measurements of the hydrogen 21 cm emission line. The figure shows that at a distance of 12 kpc, the gas distribution is centred about the Galactic plane, indicating that the disc is flat at this distance from the Galactic centre. However, at 16 kpc the gas rises above and falls below the Galactic plane (see Figure 1.19). This demonstrates the presence of a warp, which can be interpreted as a tilt of the gaseous disc at distances around 16 kpc. The tilt is also present beyond 16 kpc. The gas reaches an altitude (z) of 1 kpc to 2 kpc above the plane in one azimuthal direction ($\phi = +90°$), and a similar distance below the plane in the opposite direction, ($\phi = -90°$). Roughly one-quarter of galaxies have warped discs, and although various possible causes of warping have been explored, no compelling explanation has been developed.

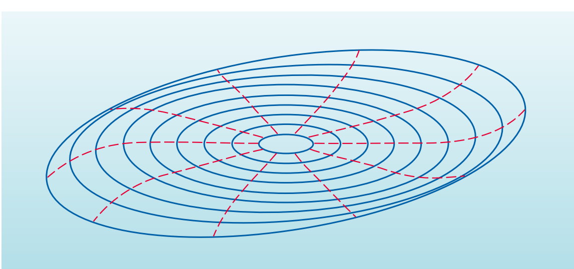

Figure 1.19 A schematic diagram of the warped disc of gas. Nine circular contours 2 kpc apart are shown. The inner six contours of the disc are in the same plane, but the outer three are progressively tilted by a few degrees. (S. Ryan (Open University))

Figure 1.20 Cool dense molecular clouds silhouetted against a bright HII region. This particular example is the Horsehead Nebula. (Anglo-Australian Telescope Board)

In the disc, about 50% of the mass of the hydrogen is molecular (H_2). A high molecular content is expected where: (i) the density is high, since this promotes the meeting of atoms; (ii) the temperatures are low, below 100 K, since this avoids the collisional disruption of molecules; and (iii) the UV flux is low, since this avoids the UV-induced disruption of molecules. These are the conditions within the cool dense clouds that are often referred to as molecular clouds (see Figure 1.20). These clouds are found throughout the disc, but are particularly numerous between about 4 and 7 kpc from the Galactic centre. In dense clouds, not only is the hydrogen present mainly as H_2, but similarly all of the chemically reactive elements are predominantly combined into molecules. A particularly important molecule is CO, which is vital for detecting the presence of cold molecular gas (see Box 1.4). There are also some quite large molecules, such as ethanol (CH_3CH_2OH, more often known as 'alcohol'). About 100 different molecules have been detected in dense clouds. In such an environment, only chemically unreactive elements, such as He and Ne, remain predominantly in atomic form.

The relatively small mass of ionized hydrogen (HII) in the ISM is contained in the intercloud media and, much more spectacularly, in HII regions (Figure 1.20). HII regions are frequently associated with dense clouds.

- Gas clouds cooler than about 100 K generally do not emit the 21 cm line; why not?
- At $T < 100$ K, hydrogen forms into H_2 molecules, so no atomic hydrogen remains.

- Why are hot HII regions often found in association with cool, dense clouds?
- New stars form within cool, dense clouds. Only very hot (and therefore massive) stars, particularly the short lived but highly luminous main sequence stars of spectral classes O and B, can ionize hydrogen in their vicinity and thus produce HII regions. As massive stars are short lived, they can be observed still in close association with the original dense clouds. Hence HII regions are found near the cool, dense clouds from which the O and B stars formed.

Interstellar dust

The nature of the soot-like dust grains that form a constituent of the interstellar medium was outlined in Section 1.2.3. The total mass of dust is about 0.1% of the stellar mass of the disc. Dust forms from atoms and molecules in the gaseous ISM that condense directly to solid particles; liquids do not form. The regions of the ISM that favour the formation of dust are those where the density is high and the temperature low. These conditions occur in the disc, where matter ejected from cool giants or supergiants in stellar winds moves away from the star and cools.

BOX 1.4 CARBON MONOXIDE (CO) AS A TRACER OF MOLECULAR GAS

The energy associated with the rotation of a molecule is quantized, analogous to the way that the energy of an electron in an atom is quantized. This means that there are only certain rotational energies that a molecule can have, and changes in the rotational energy of molecules are accompanied by the absorption or emission of a photon. The differences between rotational energy states are very small, and so only low-energy photons are involved; the spectral lines for transitions between two rotational energy states are generally found at radio wavelengths.

However, molecular hydrogen (H_2), and other diatomic molecules that consist of identical atoms (such as C_2, O_2, and N_2) do not emit radiation from rotational energy transitions, for reasons connected with their symmetry. Hence the huge amounts of H_2 in the Galaxy are essentially undetectable. (H_2 does produce some ultraviolet spectral lines, but conditions are seldom favourable for these to be observed.)

Most of the hydrogen in the ISM is in molecular rather than atomic form at temperatures below about 100 K. Consequently, the most abundant element in the Universe effectively becomes invisible at temperatures below 100 K.

However, the carbon monoxide (CO) molecule is composed of two dissimilar atoms, so its rotational transitions *can* be observed. This makes CO, which is reasonably abundant and believed to be distributed in the same way as H_2, an important tracer of cold molecular clouds in space. Carbon monoxide has strong radio emission lines at 1.3 and 2.6 mm that are used for this purpose.

Dust grains emit a continuous spectrum of radiation that is similar to the black-body spectrum. The spectrum of dust may therefore be used to deduce its temperature. If dust particles are heated too much they **sublimate**, that is, they change directly from being solid to being gaseous without melting to form a liquid. The temperature at which sublimation occurs depends on the precise composition of the dust, but even the least volatile compounds (those that are most resistant to evaporation) sublime at temperatures no greater than about 2000 K. In practice though, most interstellar dust grains are well below their sublimation temperature, nearer to 20 K than 2000 K, and are thus easily able to survive in the environment of space. The spectrum emitted by stars peaks in the visible part of the spectrum at wavelengths shorter than 2 μm, whereas the energy emitted by dust grains at a temperature of 20 K peaks around 100 μm (see Figure 1.21). At such a relatively long wavelength, the peak of the dust emission is in the far-infrared region of the spectrum. The distribution of dust can therefore be deduced from far-infrared images, such as Figure 1.14c.

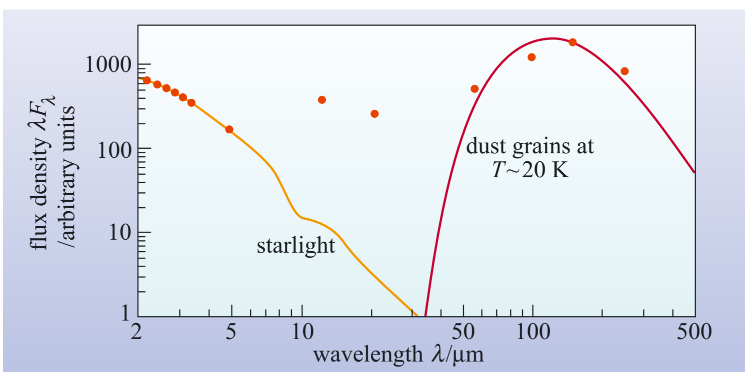

Figure 1.21 The infrared spectrum of radiation emitted by sources in the Galactic plane. The solid dots give the measured spectrum; the curves show the contributions due to starlight, which peaks at $\lambda < 2$ μm (in the visible part of the spectrum), and dust grains at 20 K, which peaks at $\lambda \sim 100$ μm (in the far-infrared). The additional flux around 10 μm to 20 μm comes from large carbon-rich molecules. (Note that this spectrum is shown as $\lambda \times F_\lambda$ against wavelength λ. A full discussion of this type of spectrum is given in Chapter 3.) (Based on data from Li and Draine, 2001)

1.4.3 A cross-section through the disc

In this section we examine the distribution of disc material above and below the Galactic plane. An important aim of this section is to describe the vertical distribution of Galactic components that have no definite boundary. We noted earlier that the

BOX 1.5 THE EXPONENTIAL FUNCTION

The **exponential function** makes use of an important mathematical constant, usually denoted e, which has the value 2.718 to four significant figures. Any mathematical function relates a given value of a variable, x say, to some other value that can be denoted $f(x)$. In the case of the exponential function, this value is given by $f(x) = e^x$ for any value of x. (This last statement is one of many ways of defining the exponential function.) So, if $x = 1$, the exponential function has the value $f(1) = e^1 = 2.718$ (to four significant figures); if $x = 2$ then $f(2) = e^2 = 7.389$; if $x = -1$ then $f(-1) = e^{-1} = 1/e = 0.3679$; and so on.

The exponential function is of great importance throughout physics and astronomy because many natural processes exhibit the phenomenon of *exponential growth* or *exponential decay*, and such processes are described by an equation of the form $y = y_0\,e^{bx}$, where y_0 and b are independent parameters, i.e. two fixed values that may be chosen to fit any particular case. As indicated in Figure 1.22, the chosen value of y_0 will be the value of y when $x = 0$, and the chosen value of b will determine how rapidly y increases or decreases as x changes. Note that positive values of b imply exponential growth, and negative values of b imply exponential decay.

Examples of exponential decay relevant to astronomy include the rate of decay of the radioactive nuclei ^{56}Ni and ^{56}Co which maintain the light output of supernovae, and the absorption of starlight as it passes through an absorbing gas cloud.

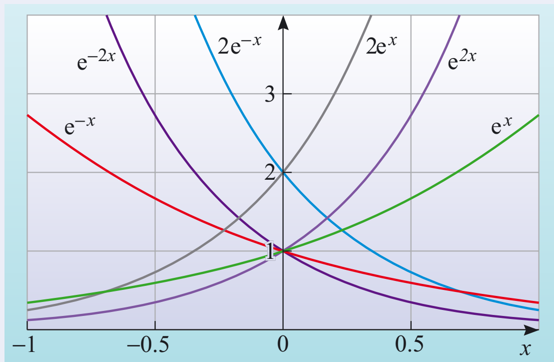

Figure 1.22 Exponential curves described by the equation $y = y_0\,e^{bx}$, for various values of y_0 and b. The value of y_0 is the value of y when $x = 0$, and the value of b determines how rapidly y increases or decreases as x changes.

density of stars declines with increasing distance from the mid-plane of the disc, making it difficult to interpret statements such as: 'the disc has a thickness of about 1 kpc'. Fortunately, the technique introduced here will clarify the meaning of such statements, and thereby allow us to develop a more satisfactory description of the size and structure of the disc. In order to achieve this we make use of a mathematical entity known as the *exponential function* (Box 1.5).

The vertical distribution of stars provides an example of exponential decay. More specifically, the **number density** of stars (i.e. the number of stars per unit volume), n, decreases with distance from the mid-plane, according to the equation:

$$n(z) = n_0\,e^{-|z|/h} \tag{1.8}$$

Here, the positive quantity $|z|$ represents the distance above or below the mid-plane; h is an important distance parameter called the **scale height** of the disc that characterizes the 'thickness' of the disc; n_0 is the number density of stars in the mid-plane; and $n(z)$ is the number density of stars at a displacement z from the mid-plane, with $z > 0$ for points above the mid-plane and $z < 0$ for points below the mid-plane. The symbol $|z|$ is often read as 'the absolute value of z' or 'the modulus of z', since the modulus sign, $|\;|$, indicates that only the magnitude (as opposed to the sign) of the enclosed quantity should be considered. That is, $|z|$ is always a positive quantity, irrespective of the value of z.

■ What is the ratio of the number density of stars at a distance h from the mid-plane, to the mid-plane number density?

❑ When $z = h$, Equation 1.8 becomes $n(h) = n_0\,e^{-|h|/h} = n_0\,e^{-1}$

You can evaluate e^{-1} using a calculator, or you can note that $e^{-1} = 1/e \approx 1/2.718$. Hence $n(h) \approx n_0 \times 1/2.718 \approx 0.37n_0$, and hence $n(h)/n_0 \approx 0.37$.

That is, at a distance of one scale height above the mid-plane, the number density of stars is a factor 1/e times the mid-plane density, that is, about 0.37 times the mid-plane number density. This illustrates the significance of the scale height, h.

The *scale height* of the disc is the distance over which the number density of disc stars decreases to 1/e times its mid-plane value.

The related ideas of exponential decay and scale height have been introduced in the context of the whole collection of disc stars, but observations indicate that these concepts can, at least approximately, be applied to the various subpopulations of stars in the disc, and even to other entities such as the ISM. Assigning scale heights to subpopulations of stars or classes of objects allows us to describe the vertical structure of the disc far more precisely than could be done by making crude statements about its 'thickness'. The scale height of a subpopulation doesn't say where that subpopulation ends, since there is no 'end', but it does indicate, in a precise way, the distance from the mid-plane at which the density of that subpopulation has significantly decreased. Below, we consider the scale height values for various constituents of the disc, and we comment on the significance of some of those values. We start with the stellar subpopulation belonging to the thin disc that was introduced in Section 1.4.1.

The thin disc

Observations show that the scale heights of stars belonging to the thin disc depend on their spectral classes. That is, thin-disc stars of different spectral types have different distributions above and below the mid-plane of the disc.

Main sequence stars with spectral types G, K or M belonging to the thin disc (including the Sun) are distributed with a scale height of around 300 pc.

■ By what factor does the density of thin-disc G-type main sequence stars change 1.0 kpc from the mid-plane, relative to the density in the mid-plane?

❑ The scale height h for Pop. I G-type main sequence stars is 300 pc. When $z = 1.0$ kpc and $h = 300$ pc, we can write Equation 1.8 as $n(1.0\,\text{kpc}) = n_0\,e^{-|1000\,\text{pc}|/300\,\text{pc}} \approx 0.036n_0$. That is, at 1.0 kpc from the mid-plane, the density of G-type main sequence stars drops to just under 4% of its mid-plane value. This indicates that very few G-type stars of Population I would be found more than 1 kpc from the mid-plane of the disc.

The O and B stars belonging to the thin disc have scale heights of only 50 pc to 60 pc.

Now, we know that O and B stars are very young, whereas the G, K and M stars of the thin disc are Pop. I objects that span the whole age range of that population. It follows that the older stars of the thin disc are likely to be found further from the mid-plane than the more recently formed stars. This observed variation of scale height with age is thought to indicate an evolutionary process that operates within the disc. It is believed most stars form near the mid-plane, but once they have formed they are gradually scattered to greater heights by interactions with giant molecular clouds, which may be as massive as $10^7 M_\odot$.

The thick disc

In Section 1.4.1, it was stated that the stars belonging to the thick disc travel to greater distances from the Galactic plane than the stars of the thin disc. This is reflected in the scale heights associated with this subpopulation.

> The G and K stars belonging to the thick disc have a scale height of approximately 1000 pc to 1300 pc. It is because this scale height is much larger than the scale height of thin-disc stars of similar spectral type (only 300 pc), that the 'thick' disc is so-named.

Thick-disc stars are far less common than thin-disc stars in the mid-plane of the Galaxy. However, the relatively large value of its scale height indicates that the number density of thick-disc stars declines much more slowly than that of thin-disc stars as the displacement from the mid-plane increases. Thus, the thick-disc stars become relatively more important as distance from the mid-plane increases.

It is currently uncertain why the thin disc and the thick disc differ in this way; it could reflect different origins of the two subpopulations, or could be due to some event during the formation of the disc (such as a collision with a dwarf galaxy that added energy to the stars' orbits). This is one issue bearing on the origin and evolution of the Milky Way for which we do not yet have a satisfactory explanation.

The ISM

So far we have compared the scale heights of different classes of stars, but now we consider the vertical distribution of the gas and dust of the ISM. In this case we continue to represent the scale height by h, but rather than consider the exponential decay of a number density of stars, n, we consider the (mass) density ρ of the ISM, measured in $\mathrm{kg\,m^{-3}}$ or some similar unit. Thus, the vertical distribution will be described by an equation of the kind $\rho(z) = \rho_0\,e^{-|z|/h}$.

> The ISM is more concentrated towards the Galactic plane than most G and K stars; it has a scale height around 150 pc.

The fact that the scale height of young O and B stars, 50 pc to 60 pc, is *less* than that of the gas from which they formed tells us about the star formation process. The rate at which stars are formed from the ISM is called the **star formation rate**, **SFR**, and may be measured in solar masses per year in any specified region (often the whole Galaxy). If the star formation rate were proportional to the local density of gas, that is, if SFR $\propto \rho$, then stars would be formed with the same height distribution as the gas. However, the O and B stars are *more* concentrated towards the mid-plane than is the gas. This indicates that the simple proportionality between

SFR and ρ cannot be correct. Since young stars are more concentrated towards the mid-plane than is the ISM, it must be the case that star formation is more effective when the ISM density is higher. (This implies that any simple 'power law' relating SFR to ρ must take the form SFR $\propto \rho^n$, where n is a number greater than 1.) We have thus used the vertical distribution of gas and young stars in the disc to infer something about how the star formation rate depends on the density of gas.

- Can you state the scale height for the Sun? Justify your answer.
- The concept of a scale height has no meaning for a *single* object; it characterizes how the density of a *class* of objects varies, so it cannot be applied to individual members of the class.

1.4.4 The spiral arms

So far in this section we have examined the constituents of the disc, their distribution and composition. We have also seen that the Milky Way has a thin stellar disc, and in this way resembles the spiral galaxies we observe beyond our Galaxy. So it is not surprising that we find evidence for spiral structure in the Milky Way. In this section we look at the structure of the spiral arms and their possible origin.

Tracing spiral structure

As indicated in Section 1.2.1, it is believed that spiral arms stand out mainly because they contain concentrations of *bright* objects associated with recent star formation rather than being strong concentrations of *mass*. O and B stars are so short lived that, when you see them, they cannot be far from where they were born, so it is usual to regard the spiral arms as the main locations of star formation in the Milky Way.

At optical wavelengths, dust makes it difficult to see stars in the disc of the Milky Way if they are more than a few kiloparsecs away. Consequently, the spiral structure of the Galaxy is more easily mapped by using a combination of optical and radio 21 cm observations, since the latter are unaffected by dust and permit the detection of neutral hydrogen to much greater distances. A range of objects has been observed that appear to map out spiral structure. Such objects include dense molecular clouds, HII regions, open clusters, and OB associations. Objects which are used to map the locations of the spiral arms are called **spiral-arm tracers**.

The map shown in Figure 1.23a (overleaf) indicates the distribution of bright HII regions, prominent clusters of young stars, and dense clouds. They seem to trace out three parallel strips near the Sun that can be interpreted as neighbouring spiral arms. An artist's conceptualization of this and other data (Figure 1.23b) shows the location of the Sun relative to the Galactic centre and the local spiral arms, named the **Sagittarius–Carina Arm**, the **Orion–Cygnus Arm** and the **Perseus Arm**. The Sun seems to be contained within the Orion arm, although it is unclear whether this is really a spiral arm in its own right or simply a 'side spur' belonging to some other arm; sometimes it is referred to as the **Orion Spur**. When looking at artists' conceptions of the Milky Way (e.g. Figure 1.23b) that include beautifully unbroken spiral arms, remember that scientific backing for such detailed views is almost entirely lacking. As noted in the introduction to this chapter, there is also evidence of a central bar in the Milky Way, which is rarely shown in older artistic pictures.

The winding dilemma

We have discussed how the spiral arms can be traced using objects associated with recent star formation. However, in the remaining parts of this section, you will see that it is difficult to explain *why* star formation occurs along these reasonably well-defined spiral tracks. It is also difficult to explain their persistence over long periods of time.

- How do we know that spiral arms last for long periods of time?
- Observations of the Milky Way do not tell us this. However, astronomers see many other spiral galaxies and are hence able to infer that spiral arms are not just transient (short-lived) structures.

In trying to account for the existence and persistence of spiral arms, one point must be kept clearly in mind: if the arms were composed of an *unchanging* set of stars, the differential rotation of the disc would cause the shape of the arms to alter with time, so an initially 'realistic' pattern of arms would soon cease to resemble any observed spiral arms. This is called the **winding dilemma**, and is explored further in Question 1.9.

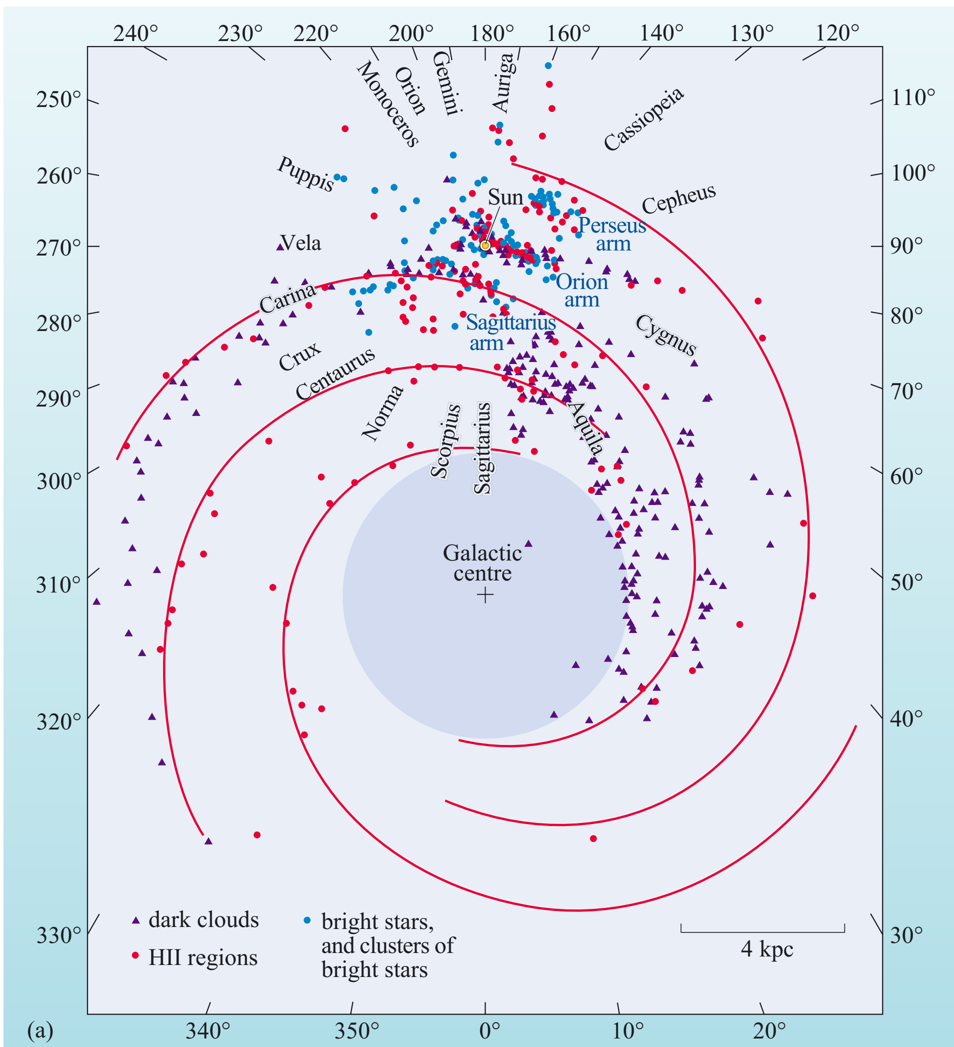

Figure 1.23 (a) The spiral arms of the Galaxy as mapped out by the distribution of dark clouds, HII regions and prominent clusters of young stars. This is a face-on view of the Galactic disc, with galactic longitude shown around the perimeter (note that the galactic coordinate system is centred on the Sun and *not* on the Galactic centre). (Composite of data from Georgelin and Georgelin, 1971, 1976; Grabelsky *et al*., 1988; and Binney and Merrifield, 1998, from data kindly provided by P. Solomon)

QUESTION 1.9

Imagine that all disc stars have the same rotation speed of 220 km s^{-1} for all radial distances from 4 to 10 kpc from the Galactic centre, and suppose that a pattern of spiral arms like that shown in Figure 1.23b already existed in the Galaxy 4.5×10^9 years ago, when the Sun formed.

(a) How many orbits of the Galactic centre would the inner end of one of the arms, located 4 kpc from the Galactic centre, have completed since the formation of the Sun?

(b) How many orbits would the outer end of one of the arms, located 10 kpc from the Galactic centre, have completed in the same time?

(c) If the spiral arms had been made of the same stars throughout the lifetime of the Sun, what would they look like now? How well does your answer correspond to the actual appearance of spiral arms?

Even allowing for its oversimplifications, the answer to Question 1.9 indicates that there is no permanent population of 'spiral arm' stars. This suggests that the bulk of the stars that are currently in spiral arms must be moving relative to those arms, and will not remain in them for long.

Although spiral arms may represent a persistent pattern, they cannot always be made of the same stars throughout their lifetime.

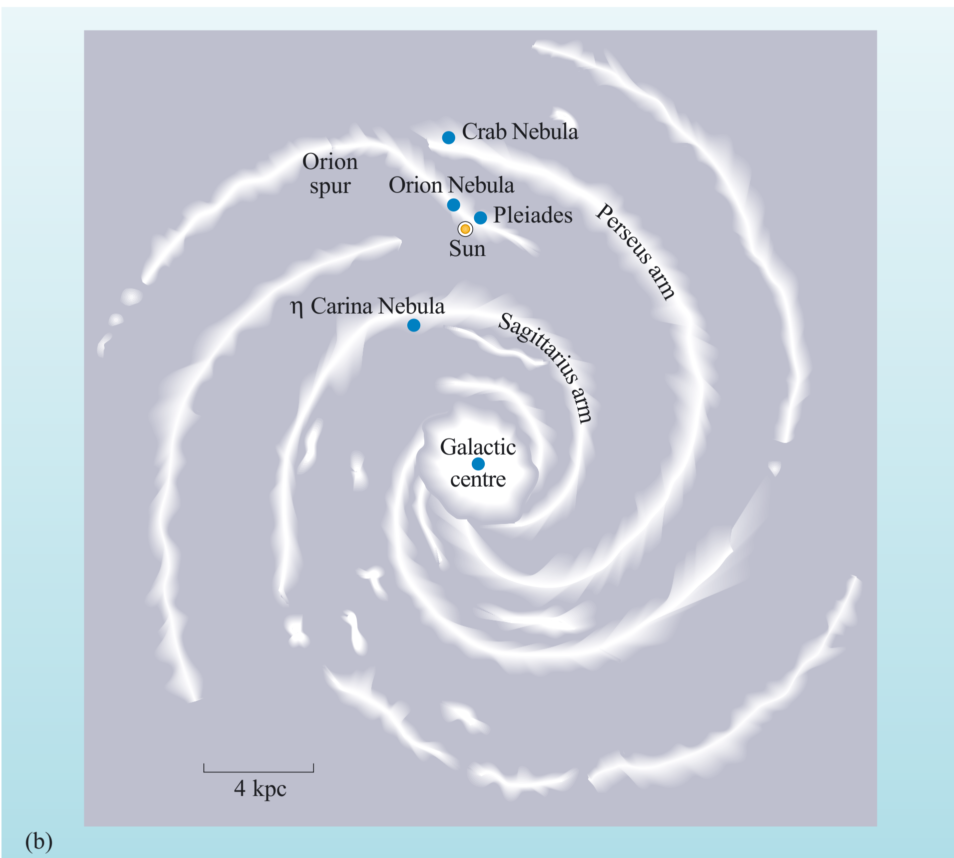

Figure 1.23 (b) Artist's schematic of the location of the Sun relative to the spiral arms. The bar/bulge is not shown in this highly schematic view.

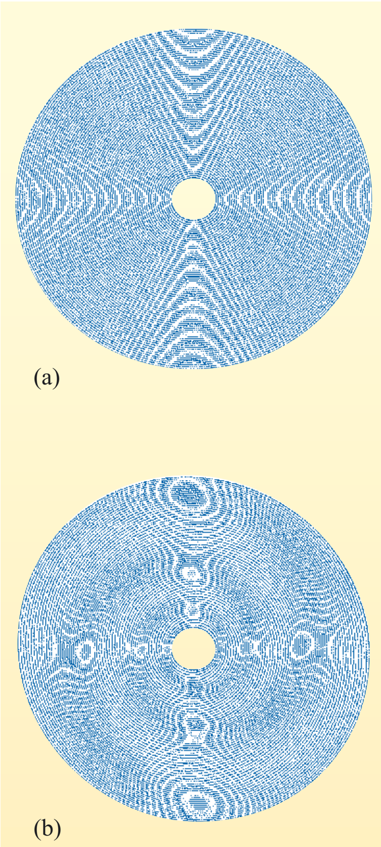

Figure 1.24 (a) Nested elliptical orbits with the long axes of the ellipses aligned in the same direction. (b) The same orbits as in (a), but with each ellipse rotated slightly relative to the adjacent one, giving rise to two spiral density waves, through which orbiting material can pass. (S. Ryan (Open University))

How is the persistence of spiral arms reconciled with the differential motion of the stars and clouds that trace them? Various answers have been proposed to this question. One idea is that the spiral arms represent the current location of 'waves' of star formation that are travelling through the disc. Such waves need not participate in the differential rotation of the disc any more than sound waves travelling through air have to travel at the speed of the wind. If the waves formed a spiral pattern, as might be natural in a differentially rotating disc, then a persistent pattern of spiral arms might be an expected feature of the Galaxy. Below we outline one specific proposal regarding the origin of such waves of star formation.

Density wave theory

The **density wave theory** was developed by C. C. Lin and Frank H. Shu in the 1960s. They treated the disc as an approximately smooth, axially symmetric distribution of matter in a state of steady differential rotation, but they assumed that such a disc would naturally develop regions in which the density was enhanced relative to the surrounding material. Lin and Shu argued that certain spiral patterns of density enhancement were especially favoured and could become self-perpetuating. Long-lived patterns of density enhancement of this kind are called **spiral density waves**.

Figure 1.24 provides a highly simplified view of a spiral density wave. A set of ellipses is shown in Figure 1.24a, representing orbiting stars and gas in the disc of the Galaxy. The long axes of all orbits in Figure 1.24a point in the same direction. However, if each successive orbit is rotated slightly, as in Figure 1.24b, then a spiral pattern emerges. If such a pattern of orbits could persist, then the disc would show a permanent pattern of density enhancements, even though the material responsible for that pattern would change continuously as orbiting material moved through the regions where the arms are seen. In practice, such a simple pattern of orbits would not persist, due to the gravitational interaction of material in neighbouring orbits. The challenge addressed by Lin and Shu was to show that some such pattern of spiral density enhancements could arise and persist in a more realistic differentially rotating disc.

A simple spiral density wave is expected to rotate about the Galactic centre, but to maintain its shape as it does so. That is, the pattern rotates *rigidly*, despite the fact that the material from which it is made rotates *differentially*. In fact, across most of the disc, the density wave moves more slowly than the matter in the disc. Only towards the outer edge of the pattern does the rotation speed of the density wave equal that of the disc. The radius at which this occurs is called the **co-rotation radius**. This means that throughout most of the disc, stars and gas approach the slowly moving density wave from behind, pass through it, and then move ahead of the wave's leading edge. Gas is compressed when it enters the density wave. For a giant molecular cloud on the verge of forming stars, this increase in density might be enough to trigger star formation and thus account for the presence of the young objects that trace the arm.

Despite the reasonableness of these ideas, density-wave theory could hardly be said to be well-confirmed. In particular, there is substantial doubt about the mechanism that produces and (at least temporarily) maintains the density wave. So, despite the great importance of spiral arms in the Milky Way's disc, their origin should still be regarded as uncertain at present.

QUESTION 1.10

Assuming that the co-rotation radius of the Milky Way is at 15 kpc from the Galactic centre, and using the Galactic rotation curve given in Figure 1.13c, draw the rotation curve of a spiral density wave and estimate the speed at which the Sun would approach such a wave.

1.5 The stellar halo and bulge of the Milky Way

We now turn our attention from the disc – which is a region of ongoing star formation – to the stellar halo and the bulge. These two regions, which together form the Galactic spheroid, are locations where star formation has long since ceased, and where the oldest stars in the Galaxy are found. It is by studying these regions that we might hope to find clues about the early evolution of the Galaxy. With this in mind, we now proceed to examine these components of our Galaxy.

The stellar halo consists mainly of very old Population II stars which have low metallicities and which move in roughly elliptical orbits (Figure 1.12) that are often highly inclined to the Galactic plane. Stars following such orbits plunge through the disc from time to time, but the spaces between stars, even in the disc, are so great that collisions are highly improbable.

- ■ Which spectral classes of main sequence star would you expect to be common in the stellar halo? What other kinds of star are likely to be abundant there?
- ❑ Only long-lived stars should be common. Apart from old main sequence stars of spectral classes K and M, there should be other, more highly evolved, stars such as red giants, horizontal branch stars, and stars belonging to the asymptotic giant branch of the H–R diagram. Even more highly evolved objects, such as white dwarfs, might also be expected.

Measurements indicate that the stellar halo is somewhat flatter than a perfect sphere. Shape determinations are based on counts of the number of halo stars in a plane surrounding the Sun that is perpendicular to the direction of the Galactic centre (see Figure 1.25). Stars in this particular plane at a given distance from the Sun will all be at a common distance from the Galactic centre, so counts of such stars can be used to assess the shape of a section through the stellar halo. Such measurements indicate that the ratio of the axes a and c, shown Figure 1.25, is $c/a \approx 0.8$, making the stellar halo an oblate spheroid.

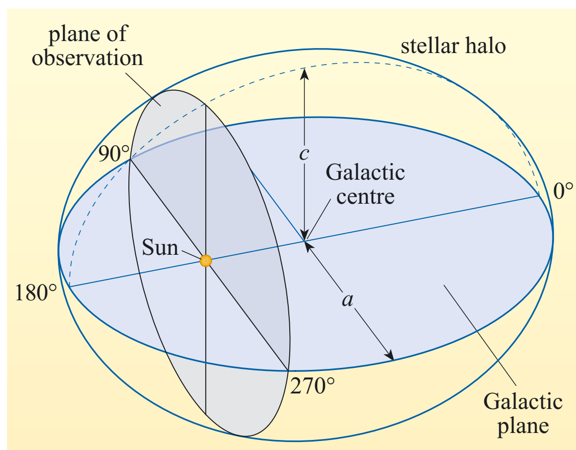

Figure 1.25 The shape of the stellar halo is determined by counting stars in a plane of observation cutting vertically through the Galaxy at the location of the Sun. Counts made at various Galactic latitudes determine the ratio of axes c/a (or axial ratio) of the stellar halo.

1.5.1 Globular clusters

Globular clusters were introduced in Section 1.2.4, where it was stated that about 1% of halo stars are found in these objects and that they typically contain 10^4 to 10^6 stars in a spherical region up to about 50 pc across. They are relatively prominent, and can easily be picked out and studied in unobscured regions of the sky. There are probably between 150 and 200 globular clusters in the Milky Way, about two-thirds of which are associated with the halo.

The stars in a globular cluster are most densely packed toward the centre. Because of this central concentration, the central regions of globular clusters are often overexposed in photographs. The number density of stars at the *centre* of a globular cluster is typically 10^4 pc^{-3}. This is approximately 10^5 times higher than the number density in the solar neighbourhood (~0.1 pc^{-3}), but it still leaves plenty of space between individual stars.

QUESTION 1.11

(a) What is the average separation of stars in the centre of a globular cluster? Give your answer in pc. (*Hint*: consider the average volume occupied by a single star.)

(b) How does this compare to the distance between the Sun and the stellar system of alpha Centauri, which is 1.31pc away?

The distribution of globular clusters

Globular clusters played a key role in developing our view of the size and shape of the Galaxy. Globular clusters are not distributed uniformly around the sky, but are concentrated in the direction of the constellation of Sagittarius. This was first recognized by Harlow Shapley, and is shown quite clearly in Figure 1.26a, which is a map of the positions of halo globular clusters on the sky. (This complements the side-on view of Figure 1.10.) In 1917, on the basis of his studies of globular clusters, Shapley asserted that the centre of the Milky Way was in the direction of the constellation of Sagittarius. Realizing that globular clusters were more numerous near the Galactic centre, he correctly reasoned that the centre of their distribution probably indicated the centre of the Galaxy.

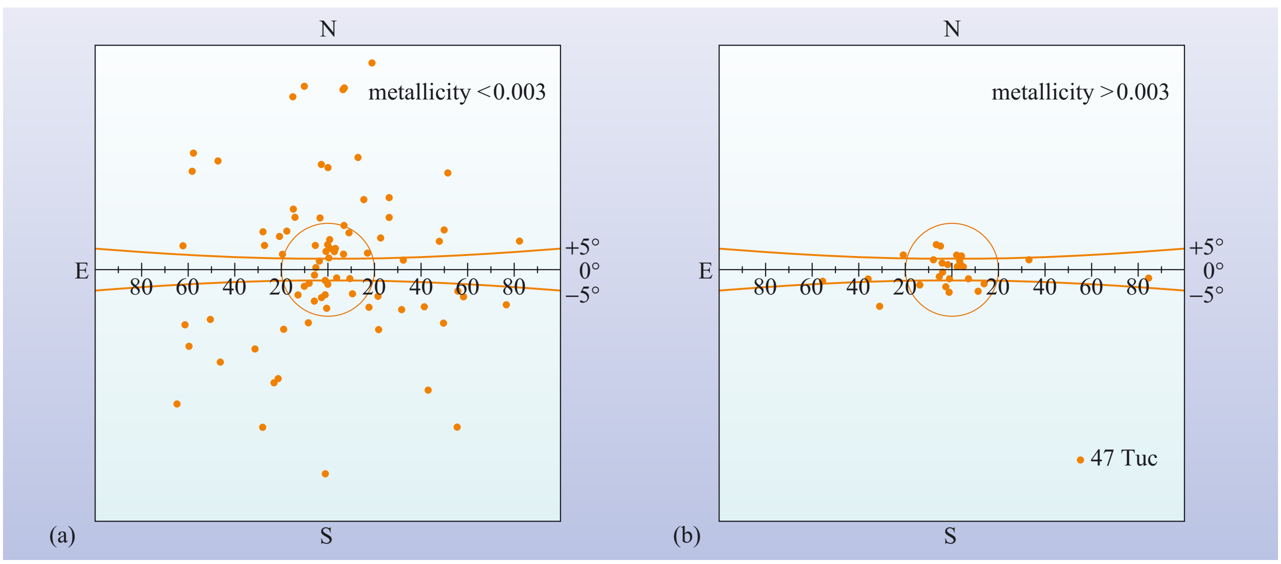

Figure 1.26 The locations of globular clusters on maps of the sky centred on the Galactic centre. The horizontal line is the Galactic plane, and the shallow curves mark Galactic latitudes ±5°. The circle has a radius of 20°, which corresponds to ≈3 kpc at the distance of the Galactic centre where the globular cluster distribution is centred. Map (a) shows globular clusters with very low metallicity $Z < 0.003$ (the halo globular clusters), while map (b) shows clusters with $Z > 0.003$ (the disc globular clusters). The latter are much more concentrated towards the Galactic centre and the Galactic plane. (Zinn, 1985)

HARLOW SHAPLEY (1885–1972)

Harlow Shapley (Figure 1.27), the son of a farmer, was born in Missouri, USA. After a limited education he began work as a crime reporter on a small Kansas newspaper. Further study led to the University of Missouri, where he planned to take a degree in journalism. However, the School of Journalism had not yet opened, so rather than waste a year he took an astronomy course and thereby began one of the most distinguished astronomical careers of the 20th century. He gained his PhD from Princeton in 1913, was a staff member at the Mount Wilson Observatory until 1921, and was then appointed Director of the Harvard College Observatory where he remained until 1952. Shapley began his studies of Cepheid variables in globular clusters while at Mount Wilson. Using the Cepheids as distance indicators (see Chapter 2) he found that the known globular clusters were concentrated about a location in the direction of Sagittarius that he identified as the centre of the Milky Way. Shapley overestimated the diameter of the Milky Way's disc by a factor of three, but he did comprehend its structure, and he recognized the off-centre location of the Sun. In a long and illustrious career, Shapley made many contributions to the study of the Milky Way and other galaxies.

Figure 1.27 Harlow Shapley. (Bachrach Portrait Studios)

Because globular clusters are so conspicuous, and hence can be recognized at great distances, they provide a potential means of determining the size of the stellar halo. Their distances can be derived from the brightness of their stars. Observations show that although there are many globular clusters within 20 kpc of the centre of the Galaxy, and a few beyond 37 kpc, there are none in between. Some astronomers treat the break at 20 kpc as a rough indication of the outer edge of the stellar halo, while others regard the more distant ones as indicating just how very extensive the stellar halo is! Unfortunately, the low number of globular clusters in the Galaxy – there are probably no more than about 200 – prevents any improvement in estimates based on globular clusters alone. In order to probe the outer part of the stellar halo, it is necessary to use the more numerous, but harder to recognize, non-cluster stars. Such objects are discussed in the next section.

Not all the globular clusters actually belong to the halo. Globular clusters with metallicity $Z > 0.003$ used to be regarded as halo objects, but are now recognized as belonging to the thick disc. They account for approximately one-third of all globular clusters in the Galaxy. Figure 1.26b shows the location of these relatively high-metallicity clusters. As you can see, they are mostly confined to the Galactic plane, as is appropriate for thick-disc objects.

Globular cluster ages

The halo stars are the oldest known stars. Those that are in globular clusters are particularly important because of the relative ease with which their ages can be determined. The globular clusters of the halo formed early in the evolution of the Milky Way, probably even before the Galaxy was a well-defined entity, so they can teach us something about the formation of the Milky Way. In addition, these oldest globular clusters provide a lower limit for the age of the Universe. Obviously, the Universe must be older than the oldest globular clusters it contains. There have been

times when the observationally determined globular cluster ages have exceeded the age of the Universe estimated from some cosmological arguments. Such conflicts have been a source of great controversy, and their resolution is a significant sign of progress.

The age of a globular cluster is determined by analysing its Hertzsprung–Russell or H–R diagram. In order to see how this is done, we need to consider how the H–R diagram is drawn. Box 1.6 provides a description of the different forms of the H–R diagram that we shall refer to.

BOX 1.6 H–R DIAGRAMS

Theoretical models of stars generally provide calculated surface temperatures and luminosities. The theoretical **H–R diagram** of a set of stars is therefore a plot of luminosity versus (surface) temperature. Such a plot is sometimes called a *temperature–luminosity diagram*. However, the temperatures and luminosities of real stars cannot be measured directly; they must be inferred from quantities that can be measured. It is quite common to plot the H–R diagram of real stars using the observed properties that correspond most closely to temperature and luminosity, which are *colour* and *brightness*.

■ Why does colour correspond to temperature?

❑ Stars behave similarly to black bodies, and the continuous spectra emitted by black bodies peak at shorter wavelengths the hotter they are, so hotter stars look bluer.

Instead of just saying that a star is blue or red, astronomers express colour in a quantitative way by comparing the amount of energy received in one part of the spectrum with the amount of energy in another. One common way of measuring colour is to compare the energy received in the blue (B) part of the spectrum with the energy received in the green part. Since the green part of the spectrum is where the human eye has maximum sensitivity, this part of the spectrum is called the visual (V) band. From the ratio of the energy between the blue and visual bands, astronomers define a value they call the **colour index**, $B - V$, (pronounced ‘B minus V’). For hot, white stars, $B - V \sim 0.0$, whereas for cool, red stars, $B - V \sim 1.0$. (You need not be concerned here about the details of how exactly the $B - V$ value is calculated from the observations.)

The brightness of a star is usually expressed using a magnitude scale, which describes its brightness relative to other stars. A difference of 2.5 magnitudes between two stars corresponds to a factor of 10 in brightness. (It could be considered as a *faintness* scale, as stars whose magnitudes are at the positive end of the magnitude range are the faintest ones, while the brightest stars are at the negative end!) Magnitude determinations are often restricted to a specified part of the spectrum, such as the visual (V) band. Within such a specified band, a star has two magnitudes that are of interest. The first of these is the easily determined **apparent visual magnitude** (m_V), which directly compares the apparent brightness of stars, even though those stars may be at very different distances. The other kind of magnitude is the **absolute visual magnitude** (M_V), which compares the brightness that the stars would have if they were all at the same distance. It is this latter quantity that is most directly related to their intrinsic luminosity, but it is also the harder to determine accurately. The two kinds of magnitude are defined in such a way that their values would be equal for a star that was 10 pc away.

The precise relationship between the apparent and absolute visual magnitudes of a star at a distance d is given by

$$M_V = m_V - 5 \log_{10} (d/\text{pc}) + 5 \tag{1.9}$$

where the distance is expressed in parsecs.

In contrast to the theoretical temperature–luminosity diagram, the observational version of the H–R diagram plots a colour index on the horizontal axis and a magnitude scale on the vertical axis. Sometimes a diagram of this type is called a *colour–magnitude diagram*. Stars map out similar patterns in both the theoretical and observed versions of the diagram, as the physical information captured in the H–R diagram is essentially the same even in these different forms, and we use the name H–R diagram to refer to all the different forms.

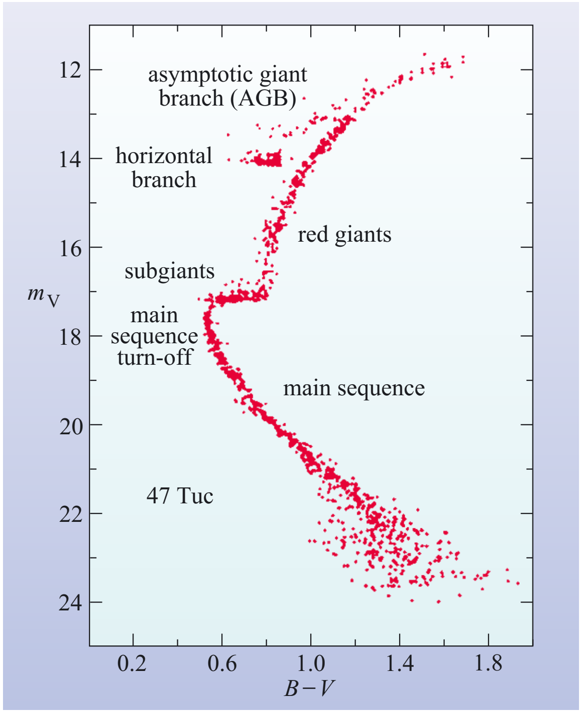

Figure 1.28 The H–R diagram of the globular cluster 47 Tuc. Some of the major features of the H–R diagram have been labelled. (Hesser *et al*., 1987)

Figure 1.28 shows the H–R diagram of the globular cluster 47 Tuc, which is broadly representative of most globular clusters. It is presumed that the stars comprising a cluster all formed at the same time and had the same composition. When it was still young, all the cluster's stars would have belonged to the main sequence and the cluster's H–R diagram would have looked something like that of NGC 2362 in Figure 1.29a. As the cluster aged, the more massive stars of high luminosity would have left the main sequence and evolved to become supergiants. The point on the cluster's H–R diagram corresponding to stars that are just reaching the end of their time on the main sequence is called the **main sequence turn-off**. This is clearly seen in the cluster H–R diagram of Praesepe (Figure 1.29b) – the main sequence turn-off in this case is at $B - V \approx 0.2$, $M_V \approx 1$. With the further passage of time, the main sequence would have become progressively depopulated of massive stars. The H–R diagram of a middle-aged cluster would have looked something like that of M67 (Figure 1.29c) – which begins to resemble the old-cluster diagram, Figure 1.28. The age of an individual star cluster can be gauged by making a calculation of the time required for the H–R diagram to evolve into the observed form.

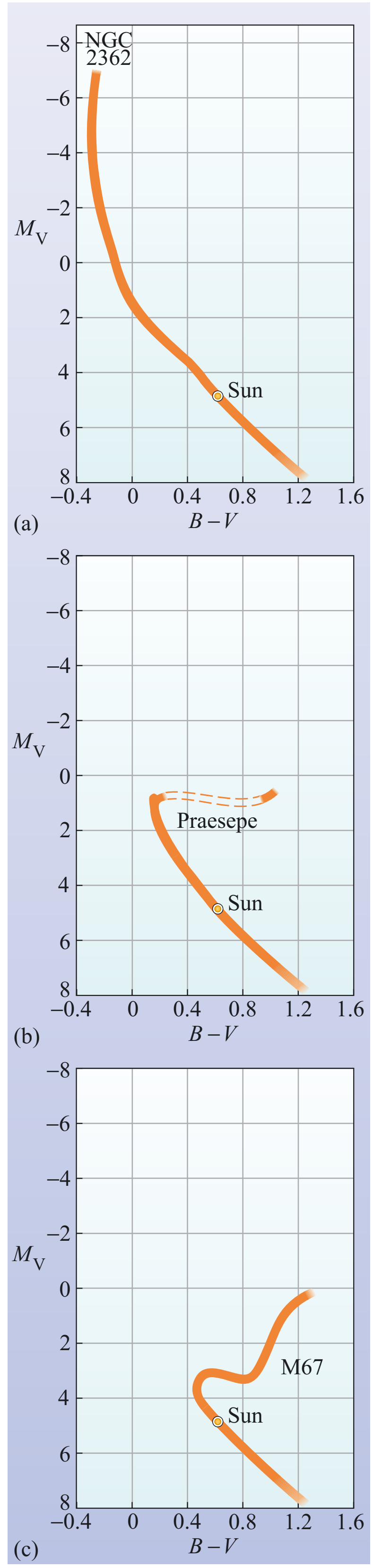

Figure 1.29 The H–R diagrams of three clusters of stars. (a) When the cluster is only a few million years old, as in the case of NGC 2362, essentially all its stars belong to the main sequence. (b) After a hundred million years, the age of the Praesepe cluster, all the high-mass stars will have left the main sequence. (c) After a few billion years, the age of M67, only low-mass main sequence stars remain. The surviving intermediate-mass stars will have evolved into red giants. All of these clusters are open clusters. As in the case of globular clusters, it is believed that all the stars in a given open cluster were formed at the same time from material of uniform composition. (Based on Arp, 1958)

The process of making a theoretical estimate of the time required for a cluster's H–R diagram to acquire a specific form involves the use of computer programs to model the evolution of the stars that make up the observed H–R diagram. Theoretical stellar models are much simpler than real stars, so they must be made as realistic as possible. Some aspects of stellar modelling are particularly difficult, notably the treatment of convection. Despite the difficulties, a good deal of effort has gone into the computation of theoretical cluster H–R diagrams. As a result of such calculations, it is possible to plot the theoretical positions on an H–R diagram of stars in a cluster for a particular age of that cluster. Such a plot defines a curve on the H–R diagram that is called an **isochrone**. The most age-sensitive feature of a set of isochrones of differing ages is the location of the main sequence turn-off, so it is this that is used to date the clusters. Figure 1.30 shows a comparison between the predicted forms of the turn-off and the observations for one particular cluster (M92). As you can see, the age indicated in this case is about 16×10^9 years, although there is clearly some uncertainty, more so in the models than in the observations. Improved calculations show that globular cluster ages are in the range (12 to 15) $\times 10^9$ yr.

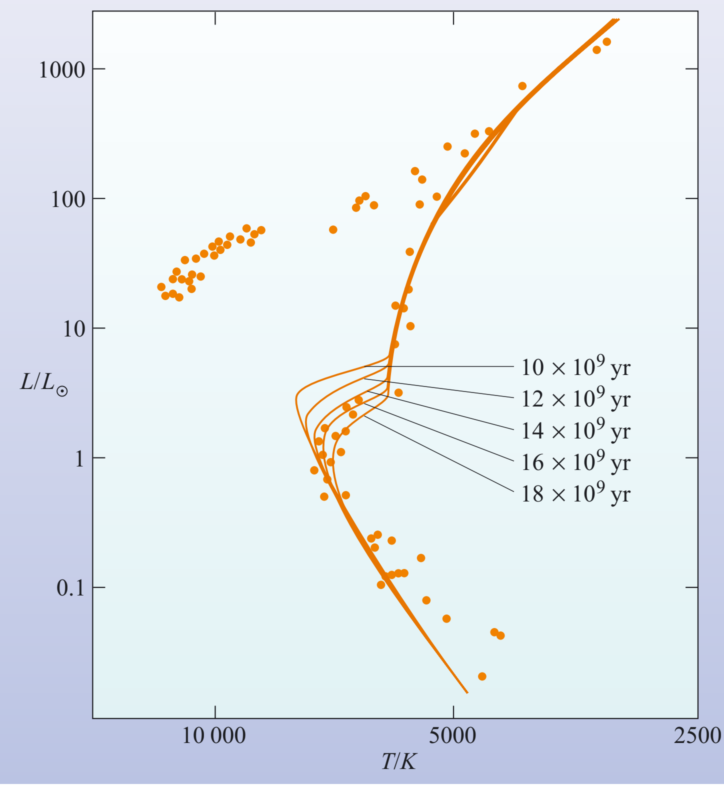

Figure 1.30 Theoretical isochrones showing predictions of the main sequence turn-off points in a globular cluster at various ages, compared with observational data for the globular cluster M92. (Mihalas and Binney, 1981)

Because of difficulties in finding precise *absolute* ages, there has been more progress with the question of the *relative* ages of different globular clusters. Studies indicate that some of the halo clusters are several billion years older than others. If this is correct, it indicates that the formation of the stellar halo was not, as was once thought, the result of the rapid collapse of a galaxy-sized gas cloud over just a few tens of million years. Either the collapse was a much more gradual process, or the stellar halo didn't form in a collapse at all, but rather by the coalescence of many different clouds. Under this second scheme, globular clusters formed either in these clouds or in collisions between them. In either case, the range of globular cluster ages indicates the timescale of the halo formation process.

1.5.2 RR Lyrae stars

The small number of globular clusters limits their usefulness as probes of the vast stellar halo. Fortunately, non-cluster stars belonging to the halo greatly outnumber globular clusters, and these stars can be used to probe the halo further. Members of a particular class of variable stars, known as **RR Lyrae stars**, are especially valuable for this purpose. These stars are named after the first star of their class to be studied, the star designated 'RR' in the constellation Lyra.

Low-metallicity, low-mass stars that have already been through the main sequence and red giant stages of evolution, and have become hot enough in their cores to burn helium, are called '**horizontal branch**' stars (see Figure 1.28). This name was given because all such stars have similar luminosities irrespective of their effective temperature, and they therefore form an almost horizontal band in the H–R diagram. RR Lyrae stars are a subset of the horizontal branch stars, and therefore have known absolute magnitudes.

Objects that, as a class, have known absolute magnitudes, are called '**standard candles**' because their known 'standard' light output allows the distance of any member of the class to be determined from a measurement of its apparent magnitude. (Uses for other standard candles in gauging the distances to other galaxies are discussed in Chapter 2.) Horizontal branch stars meet this criterion, which makes RR Lyrae stars excellent standard candles, *provided* they can be recognized. How do you recognize an RR Lyrae star? They are the subset of horizontal branch stars falling in a region of the H–R diagram within which the outer layers of stars are unstable and pulsate. This region of the H–R diagram is called the **instability strip**. It is the pulsational properties of RR Lyrae variables that make them recognizable.

■ Horizontal branch stars that do not lie within the instability strip also exist. Could these be used easily as standard candles too?

❏ The absolute magnitudes of non-variable horizontal branch stars are known, so they could in principle be used as standard candles. However, there is a practical difficulty: when you observe a non-variable star, it is not usually easy to tell whether it lies on the horizontal branch unless you already know its distance, in which case you don't need a standard candle. It is the distinctive variability of the RR Lyraes which identifies beyond doubt that they lie on the horizontal branch.

The known absolute magnitudes of RR Lyraes, and the relative ease with which they can be recognized, makes them useful for studying the distribution of matter in the halo.

QUESTION 1.12

The equation which relates the absolute and apparent magnitudes of an object to its distance d (in parsecs) (Equation 1.9) can be expressed as

$$m_V - M_V = 5\log_{10}(d/\mathrm{pc}) - 5$$

The absolute magnitudes of RR Lyrae variables are $M_V \approx +0.5$. Assuming a well-equipped telescope could detect stars down to an apparent magnitude $m_V \approx +20.5$, to what distance could they be seen?

As RR Lyrae stars can be seen out to distances of tens of kiloparsecs, they are very useful probes of the stellar halo. They show that the number density of stars in the halo (i.e. the number per unit volume) falls off with distance from the Galactic centre, r, roughly in proportion to $1/r^3$, at least out to about 30 kpc. This is compatible with the decrease in number density seen for the globular clusters. As the globular clusters and RR Lyrae stars share the same spatial distribution, age, and metal content, it is fair to assume they are part of the same population.

We saw above that globular clusters provided the basis of one of the first reliable measurements of the direction and distance to the Galactic centre. RR Lyrae stars are also valuable for this purpose. Astronomers can observe RR Lyrae stars in the direction of the Galactic centre, and calculate the distance of each one they see. By noting the distance at which the number density of RR Lyrae stars reaches a maximum, astronomers have inferred a distance to the Galactic centre of 8.7 ± 0.6 kpc. This is clearly consistent with the value 8.5 kpc that is often adopted.

We have seen previously that cosmic recycling leads to an increase in the metallicity of the Galaxy with time. Just as stars convert light elements into metals, they also convert hydrogen into helium, the second most abundant element in the Universe. So, due to cosmic recycling, there should be some change in the abundance of helium over time, and the old Pop. II stars of the halo might be expected to contain a smaller proportion of helium than younger Pop. I stars such as the Sun. The helium content of stars is generally very difficult to measure, but fortunately the pulsational properties of RR Lyraes depend on their helium content. Thanks to this, RR Lyrae stars made possible one of the earliest measurements of the helium content of Pop. II stars. In halo stars, the helium fraction in the stellar envelope appears to be around 0.24 to 0.25 by mass, meaning that a quarter of the mass of the stellar envelope is helium, whereas in the Sun it is slightly higher at 0.27 to 0.28. This provides evidence of how much star formation has occurred over the time between the formation of halo stars and the formation of the Sun.

1.5.3 The Galactic bulge

We have seen how the globular clusters and RR Lyrae stars occupy the relatively sparsely populated spheroid, and have provided much information about the structure, size and age of the Galaxy, but there is an equally old component in the Galaxy that has a much greater density. This is the bulge, which occupies the central few kiloparsecs of the Galaxy. In the remainder of this section we investigate the structure of the bulge and the very centre of the Galaxy.

Our view of the bulge is heavily obscured by dust, particularly the central region, which is the meeting place of the densest parts of the halo and the disc. However, it can be observed at infrared wavelengths (this was shown in Figure 1.14b) where it manifests itself as a concentration of brightness, and a thickening around the Galactic centre. The equatorial radius of the bulge is about 3 kpc.

While the majority of bulge stars are probably as old as the stellar halo, many of them have the same metallicity as the Sun. This combination of great age and high metallicity suggests that star formation proceeded very rapidly in the bulge, so that a large degree of cosmic recycling was achieved very quickly. This is consistent with the relatively high density of the bulge compared with the halo, since the star-formation rate, and hence the metal-enrichment rate, would be expected to be greater in a region of greater density.

Unlike the situation in the disc, where stars travel in almost circular orbits around the Galactic centre, the motions of stars in the bulge appear to be more diverse, with speeds in its outer regions around 100 km s^{-1}. Studies of the bulges of other galaxies, combined with available information about the Milky Way, have assessed whether the bulges of galaxies are oblate spheroids that are symmetric about the galaxy's rotation axis, or, alternatively, whether they have three axes of different length. For the Milky Way, the evidence points to the bulge being a triaxial bar. The first suggestion that the Milky Way might have a central bar was made by Gerard de Vaucouleurs (1918–1995) in 1964, based on the motion of HI gas in the inner regions of the Galaxy. The studies described below make use of more recent evidence.

The distribution of diffuse starlight

Infrared observations at a wavelength of 2.4 μm reveal diffuse starlight from an old population of stars towards the Galactic centre. They show an enhancement to one side of the centre, suggesting an asymmetry in the distribution of stars around the central region. This asymmetry can be interpreted as evidence of a bar-like distribution of stars, as indicated by the innermost central contour in Figure 1.31. Its discoverers associate this small bar with the central feature seen in the infrared image of the Galaxy (Figure 1.14b), which was obtained using the Diffuse Infrared Background Experiment (DIRBE) on the Cosmic Background Explorer (COBE) satellite.

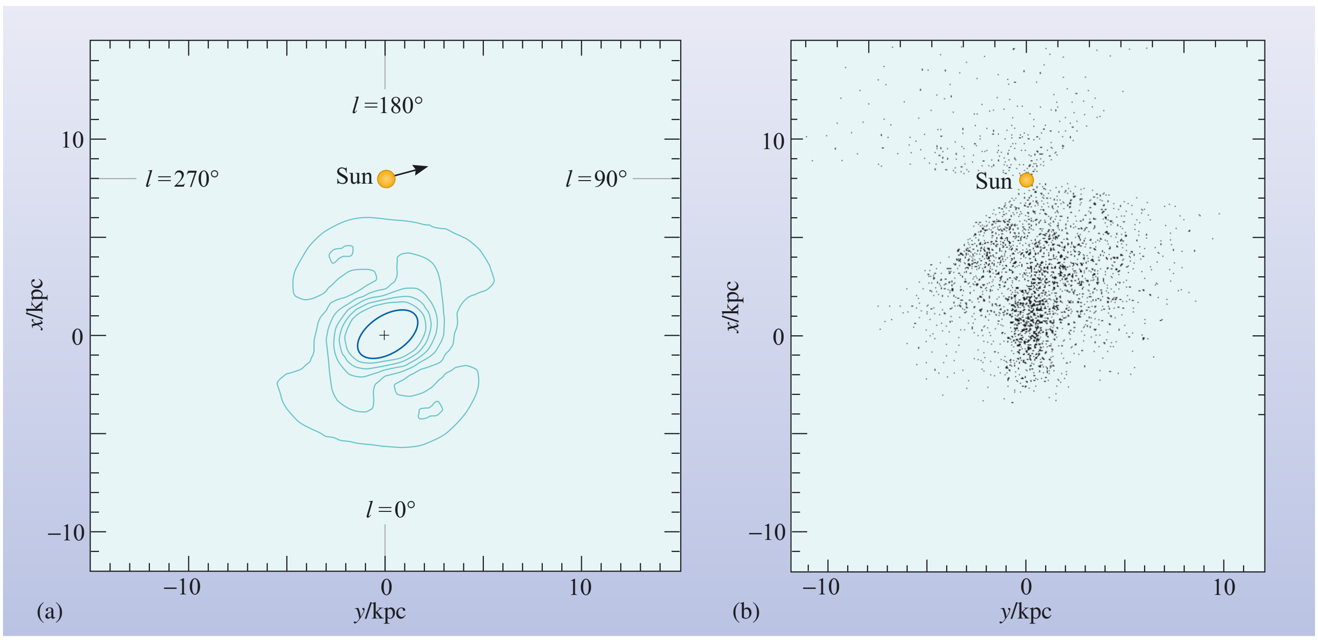

Figure 1.31 (a) Schematic view of the size and orientation of a small central bar approximately 3 kpc long, based on numerous observations. The location and motion of the Sun are also shown. The innermost contour shows the bar shape and orientation suggested by 2.4 μm observations of diffuse starlight. Contours further out, based on the space density of asymptotic giant branch (AGB) stars, show the bar extending out to a ring-like structure with a radius of approximately 5 kpc, which might be the densest, innermost portions of spiral arms. (b) The positions of about 5000 AGB stars observed with IRAS, showing the bar-shaped distribution of the stars. ((a) Based on data from Blitz and Spergel, 1991 and Weinberg, 1992; (b) Nikolaev and Weinberg, 1997)

The distribution of individual stars

High-metallicity red giants that are burning helium in their cores, and a group of asymptotic giant branch (AGB) stars (see Figure 1.28), have been observed towards the Galactic centre. The locations of about 5000 AGB stars are shown in Figure 1.31b, and contours of the number density of such stars are shown in Figure 1.31a. These stars have a bar-like distribution that is consistent with the 2.4 μm results included in Figure 1.31a. The distribution of AGB stars suggests the presence of three components: a non-circular central 'bulge', a bar-like structure (about 6 kpc in length) oriented at 36° to the line of sight, and a structure 5 kpc from the Galactic centre that might be inner portions of the spiral arms (the outer contour of Figure 1.31a).

■ Why don't the AGB stars show the spiral-arm structure as clearly as, say, the HII regions in Figure 1.23?

❑ The best tracers of spiral arms are short-lived objects that must still be close to the place they formed, such as O- and B-type stars. HII regions are used as tracers because they are excited by such stars. AGB stars are generally older objects that are only now reaching the ends of their lives. The AGB stars therefore cannot be expected to be good tracers of spiral arms.

Are bars unavoidable?

Once the existence of a bar is accepted, it prompts the question: 'Why does the bar exist?' Computer models of the motions of stars in galactic discs have shown that bars are very natural features. It turns out that discs without bars are difficult to produce, because a smooth disc dominated by rotational rather than random motion is unstable to the formation of a bar. That is, asymmetries in a disc can rapidly (within a few rotations of the galaxy) produce a bar structure; this behaviour of discs is called the **bar instability**. This suggests that there is no need to explain where the Galactic bar came from; the difficulty may be to explain why non-barred spirals do *not* have one.

1.5.4 The central black hole

We saw in Section 1.3 that it is possible to measure the mass of an object by its gravitational influence on other bodies that orbit it. We performed calculations for the mass of the Sun (for which we obtained the mass $M_\odot = 2 \times 10^{30}$ kg), and for the inner part of the Galaxy out to the radius of the Sun (for which we obtained $1 \times 10^{11} M_\odot$). In this section we examine another mass estimate, that for the compact object that has been found at the very centre of the Milky Way. Our findings have implications not only for the conditions in the Galactic centre, but also for the formation of our Galaxy and for many other galaxies – a topic that is discussed in subsequent chapters.

The central region of the Galaxy contains two features that are particularly prominent in radio continuum maps, named Sagittarius A (Sgr A) and Sagittarius B2 (sometimes written Sgr B_2). Sagittarius B2 is associated with a number of HII regions and is usually regarded as a star-forming region. One of the first signs that the Galactic centre is a particularly interesting location in the Galaxy was the discovery that Sagittarius A encloses an intense, unresolved radio source known as **Sagittarius A*** (pronounced 'Sagittarius A star' and often written Sgr A*); it is this latter object which is thought to mark the precise centre of the Milky Way. Within

0.04 pc (1 arcsec) of Sgr A* lies a star cluster whose members include hot, massive, and therefore young stars, whose age appears to be only 10^7 yr. This suggests that either a burst of star formation occurred that recently, or else collisions and mergers of stars have occurred in the dense stellar environment.

It is possible to estimate the mass enclosed within a certain volume by studying the motion of material around that volume, as we did in Section 1.3, provided the observed motion is the result of gravitational forces alone. In the case of the Galactic centre, observations have been performed of one particular star whose motion about the centre has been mapped over two-thirds of a complete orbit (Figure 1.32). The *velocity dispersion*, which measures the spread of orbital speeds obtained from the observations of a range of objects near the Galactic centre (Figure 1.33) is remarkably similar to the Keplerian $1/r^{1/2}$ decline (Figure 1.13b) seen in the Solar System, thus indicating that a highly concentrated mass dominates the environment.

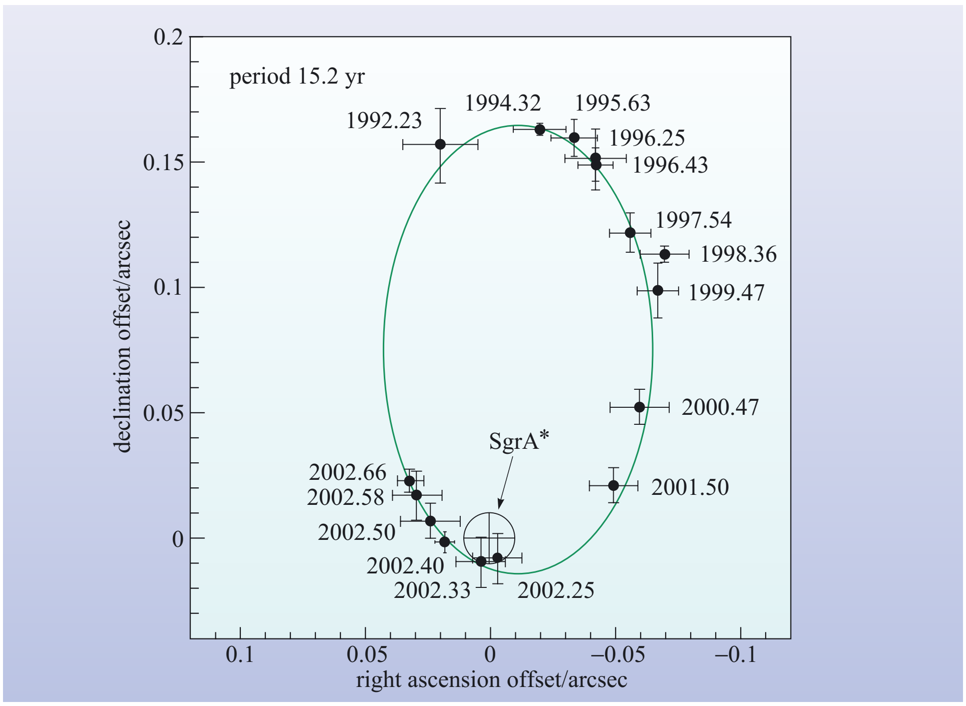

Figure 1.32 The motion of a star within the inner 0.008 pc (0.2 arcsec) of the Galaxy, observed over ten years of its 15-year orbit. (Schödel *et al*., 2002)

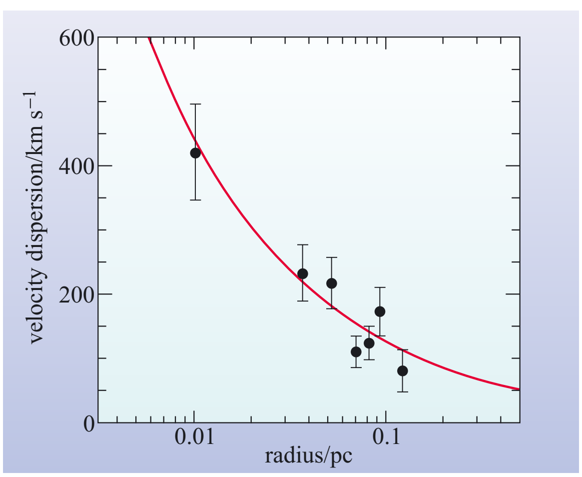

Figure 1.33 The velocity dispersion of objects near the Galactic centre, as a function of their distance from the centre. (Ghez *et al*., 1999)

The resulting limits on the enclosed mass within spherical regions of various radii, centred on the Galactic centre, are shown in Figure 1.34. The figure indicates that a mass of about $2.6 \times 10^6 M_\odot$ is contained within 0.001 pc of the centre. A highly probable explanation is that the enclosed mass takes the form of a *massive black hole* with a mass of $2.6 \times 10^6 M_\odot$ or so. Radio measurements of Sgr A* place an upper limit on its size, indicating that its radius can't be more than a few times the distance from the Earth to the Sun. Although only an upper limit, this is already sufficient to confirm that the central object is very compact as well as enormously massive.

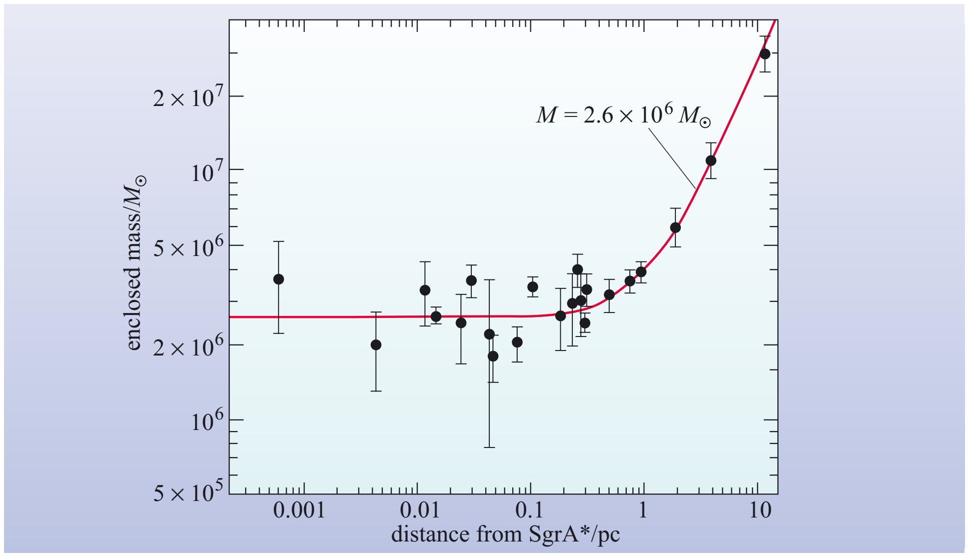

Figure 1.34 The mass $M(r)$ enclosed within spherical volumes of various radii r, centred on the Galactic centre. The enclosed mass tends to a limit $\approx 2.6 \times 10^6 M_\odot$ as r approaches zero, suggesting that this large mass is concentrated at the position of Sgr A*, perhaps as a black hole. (Schödel *et al.*, 2002)

What are the implications for the formation of the Galaxy of finding a massive black hole in its centre? You will see in Chapter 3 that black holes probably exist at the centres of many other galaxies, although those black holes cannot be studied in the same detail as the one in the centre of the Milky Way. From observations of the Milky Way and other galaxies, it appears that the presence of a massive central black hole may be connected with the existence of a spheroidal component. Much of this work is still in progress, so the picture is still emerging.

We have now completed our survey of the major components of the Galaxy, and have seen hints of the processes that link them together. The final section of this chapter brings these ideas together to look at the evolution of the Galaxy.

1.6 The formation and evolution of the Milky Way

At several points in this chapter we have seen the threads of a theory for the formation and evolution of the Galaxy. In this final section of Chapter 1 we pull these various pieces of evidence together to see what light they throw on the origin and evolution of our Galaxy.

In attempting to use observations of the Milky Way to illuminate its origin, we have to wind back the clock of star formation to see what the Galaxy would have been like at earlier times. We can hope for some success in doing this, because the Galaxy contains stars spanning a wide range of ages, and we can observe their different characteristics. Nevertheless, there is a limit to how much this process can reveal, since some information concerning the formation of the Galaxy has been erased, or

at least obscured, by subsequent events. Consequently, the observations must be united with theoretical models that work forwards in time rather than backwards. Some models, such as the model of cosmic recycling that was introduced in Section 1.2.5 and is elaborated below, consider the way that material in the ISM is processed through stars, chemically enriched and injected back into the ISM again. Other models, which are discussed in subsequent chapters, look at the way dark matter and normal matter interact to form the pool of gas from which the first Galactic stars formed. Yet another series of models looks at the way structure emerged in the early Universe, and how this allowed matter to form the kind of aggregates that developed into the groups and clusters of galaxies that surround us. As you will see later, understanding the formation and evolution of the Milky Way involves every part of this story, and every chapter in this book … and more. For that reason our objectives in this section are rather modest. Rather than trying to present a full account of the origin and evolution of the Milky Way, we content ourselves with surveying some relevant observations, raising some difficult questions, and preparing the way for wider ranging discussions of galaxy formation in later chapters.

1.6.1 The evolution of the interstellar medium

We now take a slightly more detailed look at the model for the chemical evolution of the Galaxy (i.e. cosmic recycling) that was introduced in Section 1.2.5. We begin with a schematic diagram (Figure 1.35) that sets out the flows of mass between different constituents and through different processes in the enrichment cycle.

The ISM is a key element of the evolutionary picture, because it is the birthplace of stars and it is the repository for material ejected from stars towards the end of their lives. Dense molecular clouds form from the low-density ISM, and these give rise to a new generation of stars in a star cluster. The stars go on to produce metals. The metals may be ejected back into the ISM at the end of a star's life, or they may be locked away in a dense stellar remnant such as a white dwarf, a neutron star or a

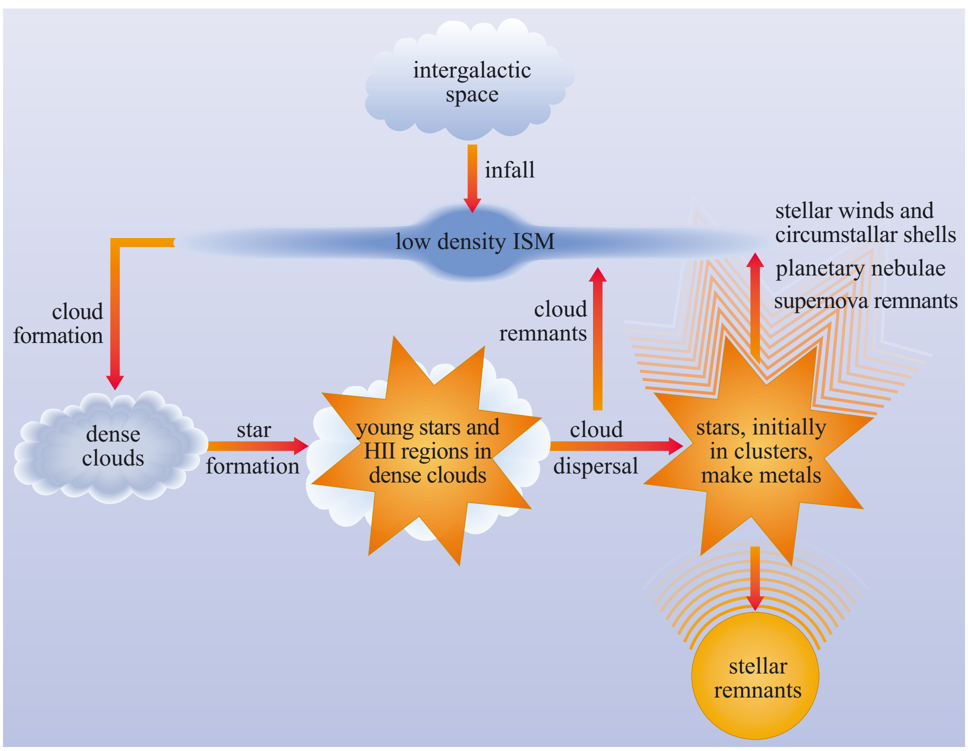

Figure 1.35 The evolution of the interstellar medium includes cycles, sources (infall from the intergalactic medium) and sinks (losses to stellar remnants).

black hole. Metals that are ejected enrich the low-density ISM, and allow the cycle of enrichment to continue.

The return of matter from stars to the ISM occurs in several ways, via:

- stellar winds from cool giants/supergiants;
- the ejection of planetary nebulae, which are the envelopes of intermediate mass stars – with initial masses less than about $11M_\odot$ – shed when the stars evolve to become white dwarfs;
- supernova ejecta containing most or all of a star's mass, some of which is enriched with metals.

A supernova produces an energetic shock wave that heats and ionizes a bubble of material in the ISM. Where large numbers of supernovae are occurring, such as in very active star-forming regions, these bubbles overlap, producing a very large cavity of hot, ionized gas called a **superbubble**. This hot material is restricted from expanding in the disc plane due to the pressure of the surrounding ISM, but it can expand vertically due to the much lower pressure of gas in the stellar halo. ISM material heated by supernovae may therefore enter the stellar halo via so-called **chimneys**, which are passages that open up where the hot, expanding material breaks out of the disc. Eventually, the hot material cools and probably returns in fragments to the disc. This mechanism has been termed a **Galactic fountain**, because of the motion of material squirted away from the disc and brought back again by gravity. It has been estimated that roughly $10M_\odot$ of material per year passes around this cycle.

Although the stellar halo now contains very little gas, almost none compared to the disc, there nevertheless exists a tenuous body of hot halo gas that is sometimes referred to as the **gaseous corona**. Figure 1.36 reveals the presence of this hot gas, which causes absorption lines in the ultraviolet (UV) spectra of distant stars. This coronal gas may be sustained by the Galactic fountain.

Is there any evidence for a returning flow of cooler gas? Possibly. Observations at wavelengths near 21 cm reveal the presence of clouds of atomic hydrogen, moving rapidly relative to the Sun. Many of these clouds have a significant velocity component *towards* the Sun. They are referred to as **high-velocity clouds**. It is difficult to determine the distance of these clouds, but they are known to be further

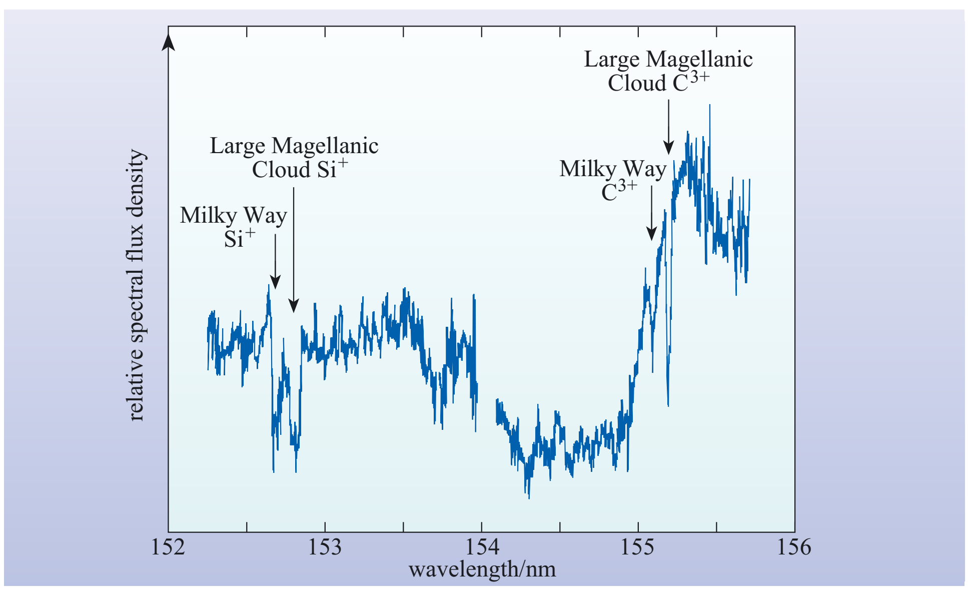

Figure 1.36 Part of the spectrum of the star HD 38282 which resides in a nearby galaxy, the Large Magellanic Cloud. Two pairs of absorption features are arrowed, one pair due to singly ionized silicon (Si^+), the other due to triply ionized carbon (C^{3+}). In each case, the shorter-wavelength member of the pair is due to absorption by gas in the gaseous corona of the Milky Way. The longer-wavelength member is due to similar absorption in the Large Magellanic Cloud, but is Doppler-shifted due to the relative motion of the two galaxies. (de Boer and Savage, 1982)

away than most disc stars. They are often *presumed* to be in the Galactic halo, in which case they could represent the returning flow of gas ejected by the Galactic fountain. However, it is also possible that at least some of them are much further away than that. The distances of some clouds have been estimated at 400 kpc to 1000 kpc, comparable to the 750 kpc distance of the spiral galaxy M31. This would make them intergalactic rather than merely interstellar. Their origin is still a mystery.

- How could the speed of such clouds, towards or away from the Sun, be determined?
- By looking for a shift in the wavelength (or frequency) of the 21 cm line, and assuming that it is a Doppler effect due to the motion of the cloud.

In addition to the return of material to the ISM, there is also the possibility of new matter entering the enrichment cycle, due to the infall of gas and dust from outside the Galaxy. This would come from the *intergalactic* medium, which consists of low-density gas that is found between galaxies. Although little is known about such material in the neighbourhood of the Milky Way, the high-velocity clouds may be examples of such material.

Once the various sources and sinks of gas are accounted for, what is the net rate of gain or loss of ISM gas today? The rate at which matter is entering the ISM is probably between $0.4M_\odot$ and $3M_\odot$ per year, of which no more than about $1.4M_\odot$ is infall from the intergalactic medium. The present rate at which mass is leaving the ISM, to form new stars, is probably somewhere between about $3M_\odot$ and $10M_\odot$ per year, and so it is likely that the rate of loss by the ISM is still exceeding its rate of gain.

The ISM evolves not only in the fraction of mass that it contains, but also in its composition. The metallicity of a main sequence star indicates the metallicity of the ISM at the time that star formed. As noted earlier, Pop. II stars in the stellar halo have a wide range of metallicities, from $Z = 2 \times 10^{-6}$ to 0.002. Stars of progressively higher metallicity record the chemical composition of the Galaxy as it was enriched by the ejecta of successive generations of stars and supernovae. Observations of very old stars and gas clouds whose metal content has not been enriched by nucleosynthesis suggest that, when the Galaxy formed, the relative *numbers* of nuclei of H : He : metals were 93 : 7 : 0. This ratio is not very different from the present one, which is something like 91 : 9 : 0.1. Thus, the ISM still consists mainly of hydrogen and helium. However, over the lifetime of the Milky Way, the metallicity, Z, has increased from 10^{-9} to 0.04.

1.6.2 The evolution of the stellar populations

The stellar content of the Milky Way evolves in a number of ways as a result of cosmic recycling. One way is the change in the average chemical composition of stars that has taken place over time. We have already seen that within the Galaxy the youngest disc stars are also those with the highest metallicity. This makes good sense in terms of the picture of cosmic recycling. A corresponding tendency for old stars to have low metallicities was noted when we discussed the halo. Recall that the halo contains some of the oldest stars in the Galaxy and these have the lowest metallicities (down to $Z = 2 \times 10^{-6}$ in some cases). This correlation between age and metallicity is known as the **age–metallicity relation**.

However, the correlation between age and metallicity is imperfect; bulge stars are also very old, but, as we have seen, some have similar metallicities to the Sun. This fact is attributed to the higher rate of star formation and cosmic recycling in the relatively

dense bulge. But the need to recognize this limitation on the age–metallicity relation provides a useful reminder that in a complicated galaxy like the Milky Way, star formation is unlikely to have a simple evolutionary history.

Besides the increase in metallicity with time, there has also been a change in the distribution of stars. Many stars in the old components of the Galaxy – the bulge and the stellar halo – follow orbits that take them far from the Galactic plane. On the other hand, disc stars are seldom found more than a few hundred parsecs from the mid-plane. The vertical distribution of the disc stars reflects that of the gas from which they formed, and the gas now has a scale height of only 150 pc. But what was it like in the past? The thick-disc stars have a larger scale height, greater ages, and lower metallicities. Does this indicate that the disc used to be thicker, and that it has collapsed closer towards the Galactic plane, or alternatively did the thick disc used to be thin and has it been fluffed up to its current size by some energetic process, such as the collision between the Milky Way and another galaxy? And what about the stellar halo? This has an even greater extent than the disc and bulge, extending out to tens of kiloparsecs, and it contains the oldest stars. Did the Galaxy form its first stars when it was still this large, postponing the majority until later when the gas had collapsed into the Galactic plane to form the disc, or did the halo stars join the Galaxy, ready made, from another source?

These are typical of the unanswered questions relating to star formation that underlie the developing model for the formation and evolution of the Galaxy.

QUESTION 1.13

By considering the processes in Figure 1.35, describe, in a couple of sentences, the amount and composition of the ISM that will exist in the Galaxy a *long* time in the future.

1.6.3 New arrivals

To conclude our discussion of the evolution of the Galaxy, we note that some of its stars are recent arrivals. Astronomers have speculated for several decades that galaxies would on occasions collide, and that these events would lead to some remarkable shapes for the affected galaxies, as well as triggering new bursts of star formation as gas clouds are compressed in the collisions. (Stars, in contrast to gas clouds, are very small and almost never collide with one another, so the evolution of gas and stars differ greatly in collisions.) There are many examples of galaxies that appear to have collided recently; examples of such events are discussed in Chapter 2. It has even been speculated that the Galactic halo was populated by the remnants of small galaxies that collided with the Milky Way, and were captured in the process. What astronomers didn't realize until 1994 was that the Milky Way is involved in a collision *right now*.

What was discovered in 1994 is that a small galaxy, subsequently named the **Sagittarius dwarf galaxy**, is colliding with our Galaxy, and being shredded in the process (Figure 1.37). This collision is taking place on the far side of the Galaxy, which is why it went unobserved for so long. Nonetheless, the collision is adding stars to the halo. But that's not all; several globular clusters that were previously believed to be ordinary members of the Milky Way are now recognized as having been captured from the Sagittarius dwarf. These observations emphasize that even though most of the stellar halo is very old, it is still a dynamic part of the Galaxy. The Milky Way continues to evolve!

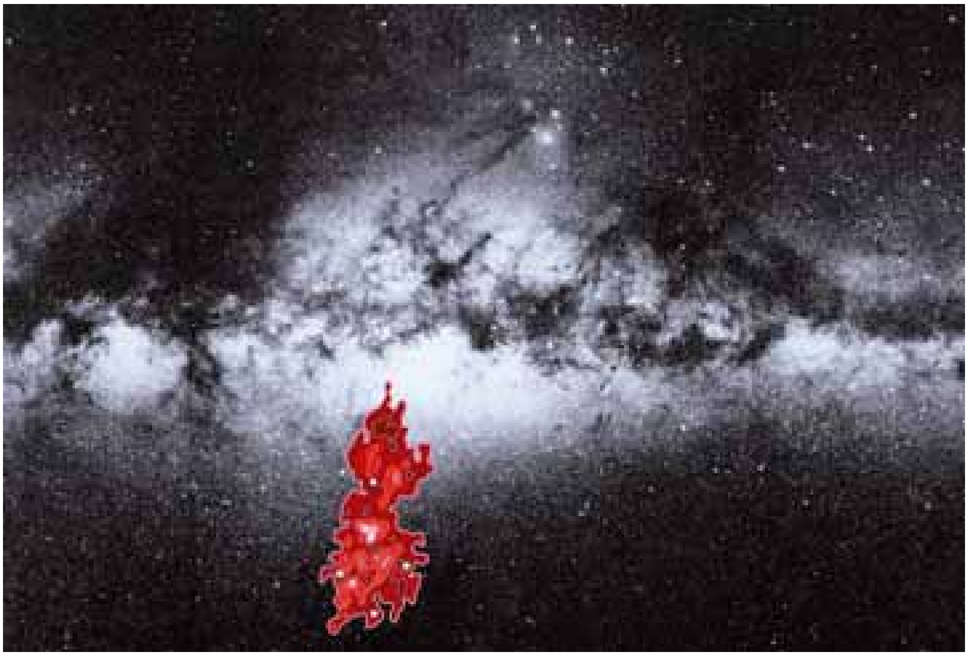

Figure 1.37 The collision of the Sagittarius dwarf galaxy with the Milky Way. The stars of the Sagittarius dwarf are very faint, so the dwarf galaxy is shown here as a red outline only. Astronomers have worked out that the Sagittarius dwarf is currently located on the far side of the Galaxy, almost in line with the Galactic centre (compare with Figure 1.1), and close to the southern side of the disc. (R. Ibata, R. Wyse and R. Sword/NASA)

1.7 Summary of Chapter 1

We conclude this chapter with a summary table of the major structural components of the Milky Way (Table 1.1), followed by a revision of key points.

Table 1.1 The major structural components of the Milky Way.

Component	Shape	Dimensions	Main forms of baryonic matter		Mass/$M_\odot$	Motion
			Stellar	Gaseous		
dark-matter halo	oblate spheroid?	>50 kpc?	?	?	$\sim 10^{12}$	?
disc	flat disc	radius ~15 kpc				
thin disc	spiral arms	thickness ~1 kpc	Pop. I $Z \sim 0.005$ to 0.04; O, B, stars in spiral arms	dense and diffuse clouds; intercloud medium, HII regions	stars $\sim 10^{11}$ gas $\sim 10^{10}$ dust $\sim 10^{8}$	circular differential rotation; confined to plane of disc
thick disc		thickness ~2 kpc	old; intermediate Pop; $Z \sim 0.004$	little or no gas	stars $\sim 10^{10}$	almost circular, scale height ~1 kpc
spheroid			Pop. II			
stellar halo	oblate spheroid $c/a \approx 0.8$	radius > 20 kpc	$Z < 0.002$	very little gas; high-velocity clouds?	stars $\sim 10^{9}$ gas negligible	elliptical orbits, often highly inclined to Galactic plane
nuclear bulge	triaxial ellipsoid (bar)	radius 3 kpc	$Z \approx 0.02$ $2.6 \times 10^{6} M_\odot$ black hole at centre		stars + gas $\sim 10^{10}$	
hot corona				tenuous hot gas		

Overview of the Milky Way

- The Milky Way – our Galaxy – is a barred spiral galaxy with four major structural components: a dark-matter halo which is only detected gravitationally, a disc, a stellar halo and a central bulge. The total mass is $\sim 10^{12} M_\odot$.
- The nature of the dark matter is unclear, but it may account for 90% of the total mass.
- The directly detectable matter consists mainly of stars (~90% by mass), gas (~10%) and dust (~0.1%).
- The disc is about 30 kpc in diameter and 1 kpc thick. The stellar halo is roughly spherical; its diameter is difficult to determine but estimates of more than 40 kpc are common. The nuclear bulge is a triaxial bar extending out to about 3 kpc from the centre.
- The stars of the Milky Way may be divided into a number of populations, each of which predominates in a particular region of the Galaxy. The very youngest stars are found mainly in the spiral arms. Population I stars reside in the disc. The oldest known stars, of Population II, are found mainly as individual stars of the stellar halo, and less commonly but more recognizably in globular clusters.
- The disc is in a state of differential rotation, with stars in the vicinity of the Sun taking about 2×10^8 yr to make a complete orbit of the Galactic centre.

The mass of the Milky Way

- The rotation curve that describes movement about the Galactic centre constrains the total mass of the Galaxy. Interior to the Sun's orbit, the mass is approximately $10^{11} M_\odot$. It is difficult to determine how much material resides beyond the Sun's orbit, and estimates for the total mass range from $4 \times 10^{11} M_\odot$ to $6 \times 10^{12} M_\odot$.

The disc

- There are about 10^{11} stars in all, with a total mass $\sim 10^{11} M_\odot$.
- Most stars and gas are approximately 70% hydrogen, 28% helium, and 2% heavier elements (metals) by mass.
- Hydrogen occurs in the form of molecules (H_2), atoms (HI) or ions (HII), according to local conditions. Molecular hydrogen is difficult to detect, however, so carbon monoxide (CO) is used as a tracer of H_2.
- Dust consists of μm-sized solid compounds, especially graphite and silicates with icy mantles, and accounts for about 1% of the ISM by mass.
- The (number) density of the disc's visible constituents, stars, gas and dust, falls off with distance from the mid-plane. In each case this is described by a scale height.
- The Sun is one of the Pop. I stars, located about 8.5 kpc from the centre of the Galaxy, close to the mid-plane of the disc. It is part of the thin-disc subpopulation that has a scale height of about 300 pc. There is also a thick disc subpopulation with a scale height of about 1000–1300 pc.
- The spiral arms are sites of active star formation. Attempts to trace the arms make use of young, short-lived objects in the disc such as bright HII regions, young open clusters, OB associations, dense clouds and clouds of neutral hydrogen gas.

- The spiral arm pattern might be caused by density waves – relatively slow-moving regions of density enhancement that rotate 'rigidly' around the Galactic centre. The compression of dense molecular clouds as they enter these regions might trigger the birth of the short-lived features that trace the spiral arms.

The stellar halo and bulge

- The stellar halo is roughly spherical but with polar flattening, resulting in an oblate spheroidal shape. Its radius is more than 20 kpc, although its density falls off with distance.
- The main constituents of the stellar halo are old, low-metallicity stars of Pop. II. The total mass of these stars is about $10^9 M_\odot$.
- About 1% of the halo stars are contained in globular clusters: spherical gatherings of stars, up to about 50 pc across, that contain 10^4 to 10^6 members with ages in the range $(12 \text{ to } 15) \times 10^9$ years.
- The stellar halo includes a corona of tenuous, hot ($\approx 10^6$ K) gas, thought to be heated by Galactic fountains that are powered by supernovae. The high-velocity clouds of atomic hydrogen may be located in the stellar halo or may belong to intergalactic space.
- The bulge seems to have the form of a triaxial bar extending out to 3 kpc from the Galactic centre. Its outer regions rotate at about 100 km s^{-1} and its total mass is around $10^{10} M_\odot$.
- The bulge mainly consists of old stars of the same age as the stellar halo, although their metallicities seem similar to that of the Sun's.
- Near the Galactic centre, the compact radio source Sagittarius A* lies at the heart of the Milky Way. From the motions of stars orbiting close to the Galactic centre, Sagittarius A* is believed to be a black hole of mass $2.6 \times 10^6 M_\odot$.

The formation and evolution of the Milky Way

- A process of Galactic chemical enrichment is at work, driven by cosmic recycling, in which some of the gas removed from the ISM to form stars is returned to the ISM by stellar winds, planetary nebulae, and supernovae, enriched in the heavy elements (metals) that are formed within stars.
- Observations indicate an increase in the metallicity of newly formed stars with time, but this increase has proceeded at different rates in different parts of the Galaxy. There is also evidence that the locations of stars have changed with time, but the implications of this are unclear.
- The composition of the ISM has also evolved over time, although it is still predominantly hydrogen and helium. In addition, various sources and sinks of gas are changing the total mass of gas in the Milky Way, causing the fraction of the Galaxy's mass that is composed of gas to evolve with time.
- The Sagittarius dwarf galaxy is currently merging with the Galaxy, contributing new stars and star clusters, and ensuring that evolution is a continuing process.

Questions

QUESTION 1.14

Why do high-velocity stars have lower metallicity than the Sun?

QUESTION 1.15

The Sun is 8.5 kpc from the Galactic centre, and is thought to be 4.5×10^9 years old. Use these data, and the rotation speed you can estimate from Figure 1.13c, to calculate the number of times the Sun has orbited the Galactic centre.

QUESTION 1.16

Assuming that optical views in the disc of the Milky Way are limited to a range of 5 kpc, estimate the fraction of the volume of the stellar disc that can be surveyed optically. What is the main cause of this limitation? (Assume that the thickness of the stellar disc is about 1 kpc.)

QUESTION 1.17

If the Sun was born in association with other stars, and originally formed part of an open cluster (which is not certain), why can we no longer see any evidence of that cluster?

QUESTION 1.18

How does density wave theory solve the winding dilemma?

QUESTION 1.19

Make a list of the kinds of astronomical objects that can be used in attempts to trace the spiral arms of the Milky Way.

QUESTION 1.20

What colour are the brightest stars in the Milky Way's globular clusters? Why?

QUESTION 1.21

'The Galaxy is not an unchanging body; rather, it continues to evolve.' Summarize the evidence for this assertion.

CHAPTER 2
NORMAL GALAXIES

2.1 Introduction

Despite its vast size, the Milky Way occupies only a tiny part of the visible Universe. This simple observation raises the question: 'What, if anything, lies beyond the boundaries of our own Galaxy?' Until the 1920s the answer was uncertain, but we now know that the correct response is: 'Other galaxies – thousands of millions of them'. These other galaxies, sometimes called *external galaxies* to emphasize the fact that they lie *beyond* the confines of the Milky Way, can be broadly divided into two classes. The majority of them belong to the class of **normal galaxies**, which have a more or less unvarying luminosity that is roughly accounted for by the stars and interstellar matter that they contain. A minority of external galaxies – perhaps 2%, although it is very difficult to be precise – belong to a different class, that of **active galaxies**, characterized by an unusually high (and sometimes variable) luminosity that appears to be largely non-stellar in origin. This chapter is concerned with normal external galaxies; the more specialized subject of active galaxies is explored in Chapter 3.

The text of this chapter is divided into four major sections. The first deals with the classification of galaxies according to their shape and certain other readily apparent characteristics. This subject was pioneered by the great American astronomer Edwin P. Hubble (Figure 2.1) in the 1920s, and it is a version of Hubble's classification scheme that provides the basis for our own discussion. The second section is concerned with the determination of a range of important properties of galaxies, including mass, luminosity and composition. The third section concentrates on the determination of the distances of galaxies. Distance determinations are difficult, but they are of great importance since they hold the key to many other issues, including the extent to which galaxies gather together into the sort of *groups* or *clusters* that will be discussed in Chapter 4. The fourth, and final, section concerns the origin and evolution of galaxies, a complex and perplexing field of study which is widely regarded as the greatest challenge facing the current generation of astronomers and astrophysicists.

Note on terminology

The term 'galactic astronomy' (as opposed to 'extra-galactic astronomy') is often used to refer to the astronomical study of the Milky Way, and thus excludes the study of other galaxies. Because of this usage, terms such as 'galactic distance' and 'galactic mass' have to be used with caution since some readers might interpret them as referring specifically to the Milky Way. To avoid this potential confusion some authors use the terms 'galaxian distance' and 'galaxian mass' when referring to galaxies other than the Milky Way. However, in common with most astronomical literature, we do not follow this convention. In this text the term 'galactic' should be taken to refer to galaxies in general. However, when specific reference to the Milky Way is intended we follow the convention of Chapter 1 by spelling Galactic with a capital G. Thus, the term 'galactic centre' refers to the centre of any galaxy under discussion, whereas 'Galactic centre' refers specifically to the centre of the Milky Way.

EDWIN P. HUBBLE (1889–1953)

Figure 2.1 Edwin P. Hubble. (Caltech)

Hubble came from Marshfield, Missouri, USA, and originally intended to follow his father's profession by training as a lawyer. He studied law at the University of Chicago, and as a Rhodes Scholar at Oxford University. His career in law was short: at Chicago he had developed an interest in astronomy, and in 1914 he returned there to begin astronomical research. His career was interrupted by the First World War – he served in the US Army and was wounded in France. But in 1919 he took up a post at the Mount Wilson Observatory in California, and it was there, with his assistant Milton Humason, that he made his most significant contributions to astronomy. His most famous discovery, now called Hubble's law (described in Section 4), provides a simple relationship between the redshift of a galaxy and its distance. Hubble's Law revolutionized the scientific view of the Universe, since it implies that the Universe is expanding and that it has a finite age.

As recognition of his outstanding contribution to astronomy, NASA and the European Space Agency named their major space-based optical observatory the Hubble Space Telescope in his honour.

2.2 The classification of galaxies

2.2.1 The Hubble classification

The meeting of the American National Academy of Sciences held at the Smithsonian Institute in Washington DC in April 1920 is widely regarded as a major event in the history of astronomy. This meeting was the scene of what has become known as 'Astronomy's Great Debate', in which Harlow Shapley (whose work on the distribution of globular clusters was described in Chapter 1) and Heber D. Curtis (1872–1942) took opposing views on two fundamental issues: the determination of the size of the Milky Way, and the existence of external galaxies beyond the Milky Way. Shapley believed that the Milky Way was very large and occupied more or less the entire Universe, whereas Curtis favoured the idea that it was just one galaxy among many.

By 1930 these two issues, which had so greatly perplexed the astronomers of 1920, had been settled. Shapley's method of working out the size of the Milky Way had been widely accepted (though the value it provided was substantially revised in the 1950s) and the existence of external galaxies had been definitively established by Edwin Hubble. Indeed, by that time so many external galaxies were known that it had already become customary to divide them into a number of different classes, according to their **morphology**, that is, their apparent shape and structure. One reason for classification is convenience: it provides a shorthand way of referring to galaxies that seem to have something in common. But galaxy classification expresses more than a desire for convenient labelling. If morphology reflects underlying physical properties – if galaxies that look different really are different – then it can be hoped that the detailed study of a few representative members of a given morphological class will provide insight into the nature of all the members of that class.

A classification scheme for galaxies was first introduced by Hubble, in 1926. A modified version of this **Hubble classification scheme** is given in Figure 2.2. Though alternative schemes are sometimes used, Hubble's scheme still provides the most common basis for the morphological classification of galaxies. As you can see, the scheme recognizes four major **Hubble classes** of galaxy: **elliptical**, **lenticular**, **spiral** and **irregular**, with both the lenticular and spiral classes being subdivided into **barred** and **unbarred** varieties. In addition, the various classes and subclasses are divided into a number of **Hubble types**, each of which is denoted by a combination of letters and numbers.

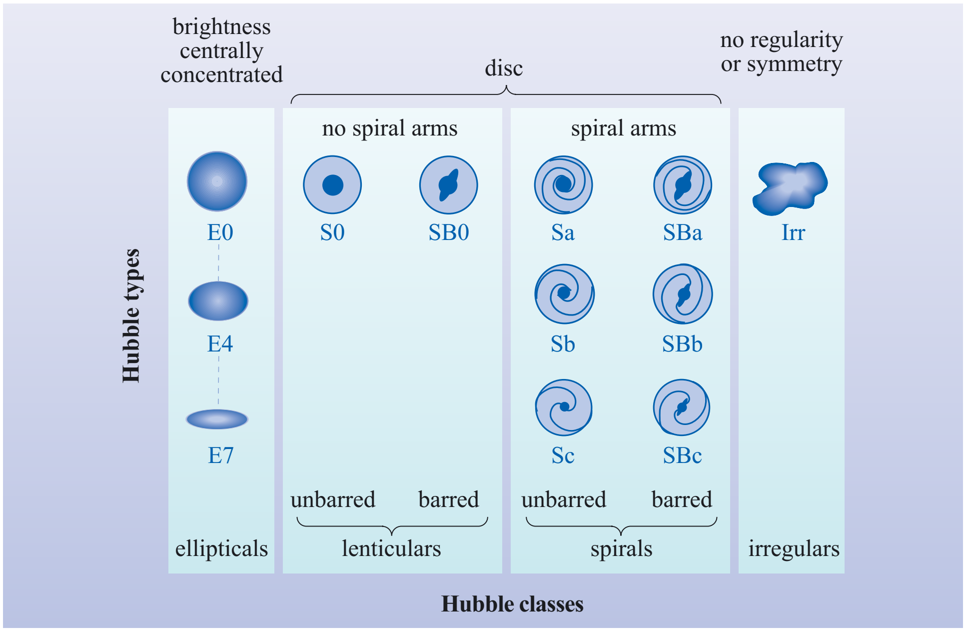

Figure 2.2 The Hubble classification scheme for galaxies.

The Hubble classification is of great importance in galactic astronomy, and there are indeed physical as well as morphological differences between the various types and classes. But how are the classes and types defined? There are several important questions to ask when determining the Hubble class of a galaxy.

- Is there any overall regularity or symmetry?
- Is the light concentrated in the centre?
- Is there a disc?
- Are there any spiral arms?

As discussed below, the answers to these questions puts a galaxy into one of the main Hubble classes. Other observational properties are then used to assign a galaxy to one of the types within its main class.

Elliptical galaxies

Elliptical galaxies are characterized by an overall elliptical outline when viewed in the sky, and a generally featureless appearance, combined with a light output that is highly concentrated in the galactic centre and decreases steadily with increasing distance from the centre. Galaxies in this class are divided into Hubble types that range from E0, for those that appear circular, to E7 for the most elongated (Figure 2.2). The whole number that follows the E in each type designation is determined by the relative size of the **semimajor axis**, a, and **semiminor axis**, b,

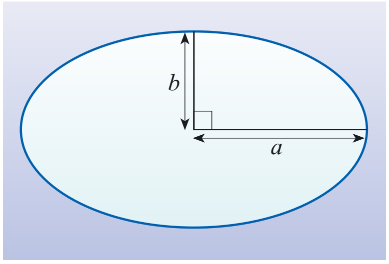

Figure 2.3 The semimajor axis, a, and the semiminor axis, b, of an ellipse.

of the observed ellipse (see Figure 2.3), and is obtained by multiplying the flattening factor $f = (a - b)/a$ by ten, and then rounding the result to the nearest whole number. The lack of elliptical galaxies with flattening factors greater than 0.7 probably indicates that such highly flattened ellipticals would be unstable.

Photographic images of various types of elliptical galaxy are shown in Figure 2.4. Note that elliptical galaxies are assigned a Hubble type according to their *visually observed* shape. The scheme takes no account of an elliptical galaxy's 'true' shape as a three-dimensional object. Nor does the appearance at non-visual wavelengths have any influence on the classification, even though it may differ from the visual appearance.

(a) (b) (c)

Figure 2.4 Elliptical galaxies of various Hubble types. (a) M89 or NGC 4552 (type E0), (b) M49 or NGC 4472 (type E4), (c) M5 or NGC 4621 (type E5). (*Note*: The prefix 'M' indicates that the galaxy is in the Messier catalogue that was published in 1784 by Charles Messier. 'NGC' stands for the New General Catalogue of Nebulae and Clusters (of stars), published in 1888 by Johan Dreyer. Most of the objects classified in the NGC are now known to be galaxies, but in 1888 the existence of galaxies beyond the Milky Way was unrecognized.) (NOAO)

Spiral galaxies

The light of spiral galaxies is much less centrally concentrated than is the case for ellipticals. Spiral galaxies are characterized by a circular disc and a nuclear bulge, and the disc contains spiral arms. The nearby galaxy M31, shown in Figure 2.5, is one such galaxy that exhibits these features. As with many spirals, the disc of M31 appears to be elliptical, but this is a result of M31's orientation. The elliptical appearance can be used to determine the angle of inclination between a line drawn at right angles to the disc and the line of sight from the Earth. This method allows spirals to be classified according to the shape they would have if viewed 'face-on' (with a 0° angle of inclination), in contrast to ellipticals.

Spiral galaxies are divided into two subclasses according to whether or not they have a central bar, and each subclass is further divided into the Hubble types Sa, Sb, Sc or, for those with central bars, SBa, SBb, SBc according to the openness of the arms and the relative size of the central bulge (Figure 2.2). Spirals of types Sa and SBa have tightly wound arms and a relatively large bulge; those of types Sc and SBc have loosely wound arms and a relatively small bulge. Spiral galaxies that cannot be unambiguously assigned to one type are classified as a combination of the two nearest

Figure 2.5 The M31 galaxy in Andromeda is classified as type Sb. Note the presence of two smaller elliptical galaxies that are satellites of M31. (B. Miller)

types, for example, a galaxy that is intermediate between Sa and Sb is denoted Sab. In some spirals the arms are long and continuous while in others they are broken or fragmented and, consequently, difficult to follow in detail despite an overall impression of spiral structure. It may well be that the Milky Way is of this latter sort.

Lenticular galaxies

As their name implies, these are lens-shaped galaxies. Like spirals, they have a disc and a central bulge – but no spiral arms. The bulge may be quite large in comparison with the disc (much more so, on average, than in the case of the Milky Way for instance), and may take the form of a spheroid, as in the S0 type, or may be elongated into a 'bar' to give the SB0 type. Lenticular galaxies are often seen as an intermediate class between ellipticals and spirals. Indeed, they are sometimes described as 'armless spirals', which is really a contradiction in terms but gives the right impression to readers who are already familiar with a spiral galaxy such as the Milky Way.

Photographic images of various types of lenticular and spiral galaxy are shown in Figure 2.6. It should be noted that although the diagrams in Figure 2.2 show spiral galaxies face-on and with two spiral arms apiece, the observed spirals are normally inclined relative to the observer and may have more than two arms. Note also that in many cases the arms may be fragmented (this is particularly the case for Sa galaxies).

On the basis of our (rather poor) estimate of the external appearance of our own galaxy, it has long been traditional to describe the Milky Way as a galaxy of Hubble type Sb or Sc (or Sbc, to indicate that it is intermediate between Sb and Sc).

Figure 2.6 Lenticular (S0, SB0) and spiral (S and SB) galaxies of various Hubble types.
(a) NGC 524 Hubble type S0,
(b) NGC 936 Hubble type SB0,
(c) NGC 7217 Hubble type Sab,
(d) NGC 4650 Hubble type SBa,
(e) M77 Hubble type Sb,
(f) M91 Hubble type SBb,
(g) M99 Hubble type Sc,
(h) NGC 1073 Hubble type SBc.
((a), (c) Sandage and Bedke, 1994;
(b) Sloan Digital Sky Survey;
(d), (e), (f) (g) NOAO/AURA/NSF;
(h) David and Christine Smith/
Adam Block/NOAO/AURA/NSF)

(a) NGC 524 Hubble type S0

(b) NGC 936 Hubble type SB0

(c) NGC 7217 Hubble type Sab

(d) NGC 4650 Hubble type SBa

(e) M77 Hubble type Sb

(f) M91 Hubble type SBb

(g) M99 Hubble type Sc

(h) NGC 1073 Hubble type SBc

However, as noted in Chapter 1, there is now strong evidence that we are actually living in a barred rather than an unbarred spiral.

- Given that the Milky Way is a barred spiral, how would you write its Hubble type?
- SBb or SBc (or SBbc – intermediate between SBb and SBc).

Irregular galaxies

As you would expect, these galaxies (class Irr) show little sign of symmetry or regularity. Some have bar-like structures and some show vague signs of spiral arms. Others are totally irregular. An example is the irregular galaxy IC5152 shown in Figure 2.7a, and further examples of this class are the Large and Small Magellanic Clouds that are near neighbours of the Milky Way (Figures 2.7b and c).

(a)

(b)

(c)

Figure 2.7 Examples of irregular galaxies: (a) IC5152 (the bright star slightly to the north of the galaxy is a foreground star that lies within the Milky Way), (b) The Large Magellanic Cloud, and (c) the Small Magellanic Cloud. (D. Malin/AAO)

Before leaving the topic of the Hubble scheme, it should be noted that classifying galaxies is not as unambiguous as it may seem from the above discussion and Figure 2.2. Some aspects are somewhat subjective, and different observers may classify the same object differently. In the case of galaxies with discs, it can be difficult to distinguish between lenticulars and various types of spiral when the angle of inclination is large and the galaxy is almost edge-on. A more serious problem is that, in optical images, the appearance of a galaxy may be affected by such things as exposure time. For example, a short-exposure image of an elliptical galaxy will show only the bright central parts, while a longer exposure will reveal the outer parts as well and give a different impression of the overall shape.

Most people's mental picture of a galaxy is probably of a spiral, since these are the most photogenic and tend to predominate in illustrated books on astronomy. However, faint **dwarf elliptical** galaxies, with masses around $10^6 M_\odot$, such as the galaxy Leo I that is shown in Figure 2.8, are in fact the most common type of galaxy. Over 60% of galaxies are elliptical, fewer than 30% are spiral, and fewer than 15% are irregular. These figures are subject to some variation according to how the sample being surveyed is selected: there are relatively more E, S0 and SB0 galaxies in regions where galaxies are more densely clustered together, and in the most densely clustered regions S, SB and Irr galaxies are almost totally absent. In any survey it is important to account for bias: if only the most easily observable galaxies are surveyed (i.e. those with the greatest apparent brightness), then the faint dwarf ellipticals will be under-represented, and the biased sample obtained will give the impression that there are relatively fewer ellipticals than is actually the case. While mentioning statistics, it is also worth noting that about 60% of spirals and lenticulars are barred.

Finally, it should be noted that about 1% of galaxies cannot be assigned to any of the Hubble classes shown in Figure 2.2, even when their shape is known. Some of these cases are discussed briefly at the end of this section.

Figure 2.8 The dwarf elliptical galaxy Leo I lies at a distance of about 250 kpc from the Sun. Dwarf elliptical galaxies are very numerous, but their low luminosities make them difficult to detect. (D. Malin/AAO)

2.2.2 The physical characteristics of the Hubble classes

It is interesting that, even though the range of galactic shapes is so limited, the great majority of galaxies can be assigned to membership of one or another of the Hubble classes. However, it would be even more interesting to know the physical significance of such membership. Surely galaxies that differ in shape as radically as an E3 and an SBc must also show differences in their physical properties. The exploration of these intrinsic physical differences (as opposed to mere shape) is the purpose of this section.

It has occasionally been suggested that the Hubble classification reveals an evolutionary sequence. In the past, some proponents of this idea believed that newly formed galaxies were elliptical and that they flattened and developed into spirals with the passage of time. Many authors introduce the Hubble classes using a diagram that almost invites this evolutionary interpretation, although we have deliberately tried to avoid this in Figure 2.2. Still, no matter how the Hubble classes are introduced, the view that they form an evolutionary sequence is now totally rejected. The current belief is that the Hubble class of a galaxy is mainly determined by the environment in which it formed. There may be some subsequent evolution (as will be described later) but even this is not thought to involve a steady progression through the Hubble classes.

Despite the lack of evolutionary progression through the Hubble classification, galaxies do have physical properties that show systematic variation with Hubble class or type. One such property relates to rotation. On the whole, the angular momentum per unit mass of elliptical and irregular galaxies is low, whereas it is relatively high for spirals and lenticulars. For spiral galaxies of a given mass, angular momentum increases through the types Sa, Sb, Sc (or SBa, SBb, SBc).

The angular momentum of a galaxy depends on the rate at which the various parts of the galaxy rotate about the centre, and its degree of compactness.

Another property correlated with Hubble class concerns the ratio of the mass of gas to the total mass of stars in a galaxy. More specifically, the ratio of the mass of gas that is in molecular or atomic form to the mass of stars, expressed as a percentage, varies considerably between Hubble classes. In the case of the Milky Way, this ratio is about 10% (see Chapter 1). For spiral types Sa to Sc (or SBa to SBc) this proportion is 5–15% (and increases in progressing from Sa to Sc or SBa to SBc), while the proportion is typically in the range 15–25% in irregulars. In contrast, many ellipticals and lenticulars have scarcely any molecular or atomic gas – the gas that is present in such galaxies is typically very hot (at temperatures exceeding 10^6 K) and is consequently highly ionized. The proportion of mass in the form of atomic or molecular gas is thus very low for ellipticals and lenticulars (1%, say). The presence or absence of molecular or atomic gas is related to a number of other important distinguishing features of the various Hubble classes.

QUESTION 2.1

Considering the variation of gas content with Hubble class, describe and explain any systematic variations you would expect to find between elliptical and spiral galaxies with regard to the following properties: presence of high-mass main sequence stars; proportion of stars in open clusters; prevalence of HII regions; abundance of Population I stars relative to Population II stars.

A number of other important galactic properties, such as mass, luminosity and diameter (the determination of which will be discussed later), show wide variation in value from one galaxy to another, even within a given class. Because of the individual variations, these properties cannot be simply correlated with Hubble class. However, the *range* of variation of each of these properties *can* be so correlated, at least loosely. In general terms, spiral galaxies have a fairly narrow range of mass, luminosity and diameter (masses, for example are usually in the range from about $10^9 M_\odot$ to a few times $10^{12} M_\odot$), while elliptical galaxies cover a much wider range (masses of ellipticals vary from about $10^5 M_\odot$ to somewhat over $10^{13} M_\odot$). Irregular galaxies exhibit an intermediate range of properties (roughly 10^7–$10^{10} M_\odot$ in mass – even the largest irregulars are less than a quarter of the mass of the Milky Way).

Another topic that merits discussion here is that of the true shape of elliptical galaxies. The fact that the Hubble types E0–E7 are based on 'apparent' (i.e. projected, two-dimensional) shape rather than 'true' (three-dimensional) shape raises a number of questions about elliptical galaxies. For instance, is it possible that all elliptical galaxies actually have the same three-dimensional shape, and that the apparent differences between the Hubble types from E0 to E7 are a result of viewing that single common shape from different directions?

Any three-dimensional shape that appears to be elliptical from all directions is called an **ellipsoid**. The shape of any particular ellipsoid is determined by the relative lengths of its three principal semi-axes, as indicated in Figure 2.9. If two of these semi-axes are of equal length the ellipsoid will have a circular cross-section perpendicular to its third principal semi-axis. An ellipsoid of this kind is called a *spheroid*, and may be classified as an **oblate spheroid** or a **prolate spheroid** depending on whether the third principal semi-axis is shorter or longer than the other two (see Figure 2.9). Ellipsoids with three unequal principal semi-axes do not appear circular from any direction, and are said to be **triaxial ellipsoids**.

Before the three-dimensional shapes of elliptical galaxies were properly investigated it was more or less tacitly assumed that every elliptical galaxy was an oblate spheroid (like Figure 2.9a). Furthermore, it was widely assumed that each elliptical galaxy rotated about the shortest axis and that the flattening was mainly due to this rotation – like the polar flattening of the Earth. However, detailed studies of elliptical galaxies now indicate that these assumptions are not always justified. In some cases the observed line-of-sight velocities of stars in elliptical galaxies are simply not consistent with a spheroidal distribution, and (particularly in the most luminous ellipticals) the rotations are often too slow to produce the observed flattenings. Moreover, some elliptical galaxies appear to be rotating about an axis other than the shortest axis, so their flattening is almost certainly *not* due to rotation.

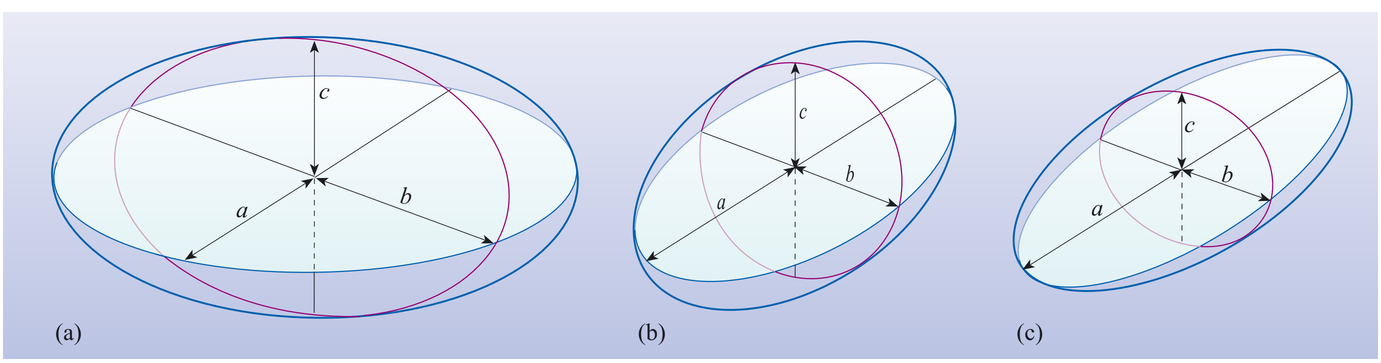

Figure 2.9 An ellipsoid is a three-dimensional body that appears to be elliptical from every direction. The shape of any particular ellipsoid can be specified by assigning lengths to the so-called principal semi-axes a, b and c shown in the diagram. (a) An oblate spheroid has $a = b > c$. (b) A prolate spheroid has $a > b = c$. (c) A triaxial ellipsoid has $a > b > c$.

Another peculiarity that besets some ellipticals is that the elliptical contours of equal surface brightness do not have a common major axis – there appears to be some sort of 'twist' in the heart of the galaxy. In view of these findings the simple spheroidal model of elliptical galaxies cannot be trusted, so the safest statement to make at the present time about the shapes of elliptical galaxies is that at least some are triaxial, although it is still quite possible that many are spheroidal.

Interestingly, it is now possible to use computer simulations to investigate the gradual changes that can occur within a galaxy due to the host of gravitational interactions between constituents that change stellar orbits and velocities. Such studies indicate that triaxial distributions of stars may evolve into oblate spheroids, and that the time taken for this evolution to occur increases with the size of the galaxy. However, it also appears that some triaxial distributions of stars are stable, provided the galactic rotation is fairly slow.

It would be remiss to end this section without some reference to those galaxies that cannot be fitted into the Hubble classes shown in Figure 2.2, and to others that can only be accommodated with difficulty. Various amendments and extensions to the Hubble scheme have been proposed that reflect more accurately the true range of galactic shapes, but rather than discuss these in detail we shall just mention some of the limitations and shortcomings of the basic scheme.

Many galaxies have a more or less readily apparent Hubble type apart from the presence of some kind of abnormal feature. A case in point is the giant elliptical galaxy M87 (in the constellation of Virgo). A medium exposure image of this galaxy shows an apparently ordinary elliptical galaxy of type E0 or possibly E1, similar to the galaxy shown in Figure 2.4a. However, a short exposure that emphasizes the central regions of the galaxy (Figure 2.10a) shows an unusual feature – a 'jet' of material apparently spurting out from the core. Because of the presence of this jet, M87 is said to be a **peculiar galaxy** and is usually classified as having Hubble type E0p; the final 'p' indicating the presence of the peculiarity. (As you will see in Chapter 3, M87 is, in fact, an *active galaxy*; jets are seen in many active galaxies.) A jet is not the only feature that can make a galaxy peculiar. Many peculiar galaxies appear to have been distorted in gravitational encounters with other galaxies: all interacting galaxies are peculiar. Some examples of interacting galaxies are included in parts (b) to (e) of Figure 2.10.

Another sort of galaxy that deserves a mention is a **cD galaxy**. The name comes from astronomical terminology that is no longer widely used – the 'c' indicates a supergiant system, while the 'D' indicates that the galaxy has a large, diffuse envelope. An example of a cD galaxy is NGC 4874 (Figure 2.11), a giant elliptical near the centre of a rich cluster of galaxies in the constellation of Coma. The densely packed centres of large clusters of galaxies often harbour cD galaxies, which are widely thought to result from the merger of several other galaxies. Detailed studies of some cD galaxies reveal the presence of several bright spots near the centre. These are sometimes interpreted as the nuclei of galaxies that have already been absorbed and are taken to be evidence in favour of the merger hypothesis.

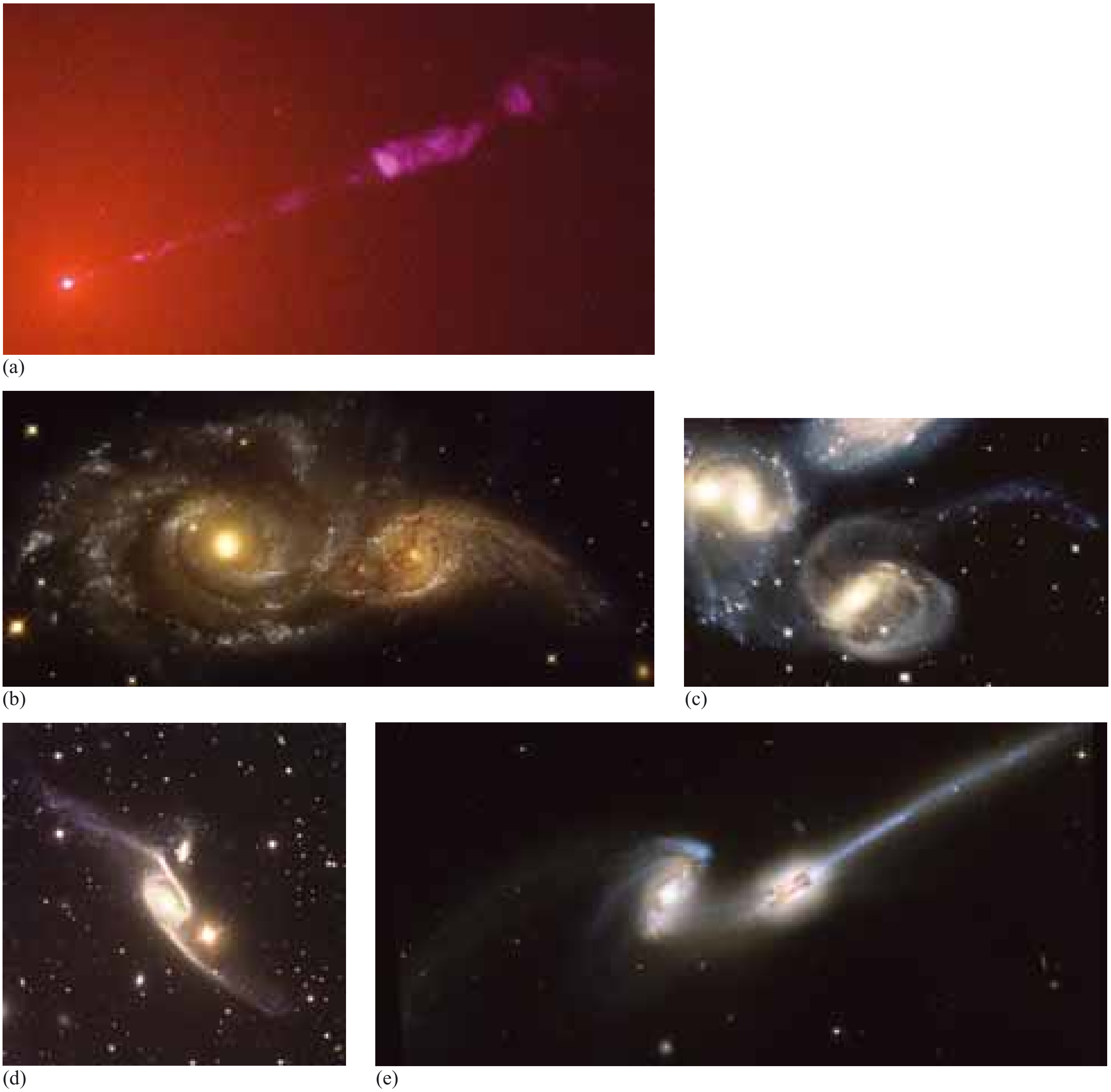

Figure 2.10 Some peculiar galaxies: (a) M87 a peculiar elliptical galaxy with a jet emerging from its core, (b) interacting galaxies NGC 2207 and IC 2163, (c) part of a group of interacting galaxies called Stephan's Quintet, (d) interacting galaxies NGC 6872 and IC 4970, and (e) NGC 4676. ((a) J. Biretta/STScI/Johns Hopkins University/NASA; (b) Hubble Heritage Team/STScI; (c) S. Gallagher (Pennsylvania State University); (d) ESO; (e) H. Ford/Johns Hopkins University/NASA)

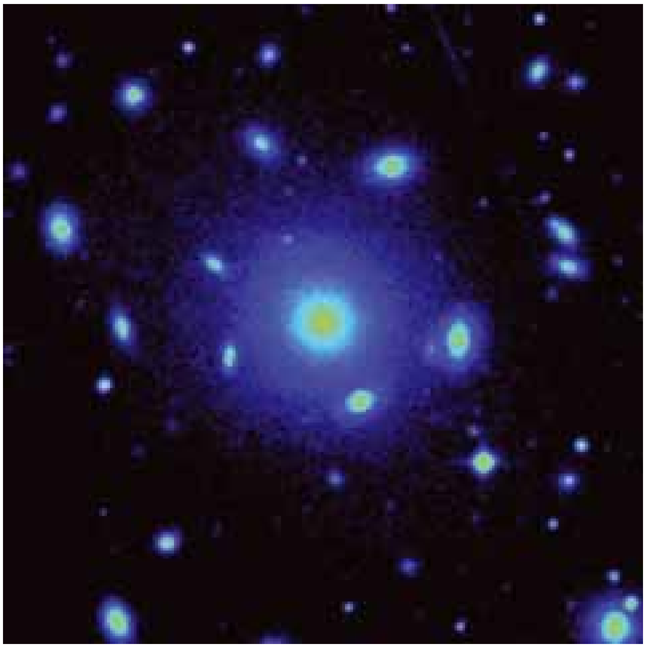

Figure 2.11 NGC 4874 (at the centre of this image) is a giant elliptical galaxy that is classified as a cD galaxy. This galaxy lies close to the centre of the Coma cluster of galaxies. Note that this optical image is displayed in false colours in order to simultaneously show regions of low and high surface brightness (shown as blue and yellow respectively). (Digitized Sky Survey/STScI)

QUESTION 2.2

Fill in the missing data in Table 2.1, which compares and contrasts various properties of three of the main classes of galaxy.

Table 2.1 A comparison of Hubble classes. (For use with Question 2.2)

Property	Ellipticals	Spirals	Irregulars
approximate proportion of all galaxies	$\gtrsim$60%	$\lesssim$30%	$\lesssim$15%
mass of molecular and atomic gas as % of mass of stars		5–15%	
stellar populations			Populations I and II
approximate mass range			
approximate luminosity range	a few times $10^5 L_\odot$ to $\sim 10^{11} L_\odot$	$\sim 10^9 L_\odot$ to a few times $10^{11} L_\odot$	$\sim 10^7 L_\odot$ to $10^{10} L_\odot$
approximate diameter range[a]	(0.01–5) $d_{\rm MW}$	(0.02–1.5) $d_{\rm MW}$	(0.05–0.25) $d_{\rm MW}$
angular momentum per unit mass			low

[a] $d_{\rm MW}$, diameter of Milky Way.

2.3 The determination of the properties of galaxies

In Section 2.2 various assertions were made about the physical characteristics of the different types of galaxy included in the Hubble classification scheme. Much of this information was summarized in Table 2.1, which indicates typical ranges for quantities such as luminosity, diameter, mass and composition without making any serious attempt to explain how such information was obtained. This section is concerned with just such determinations.

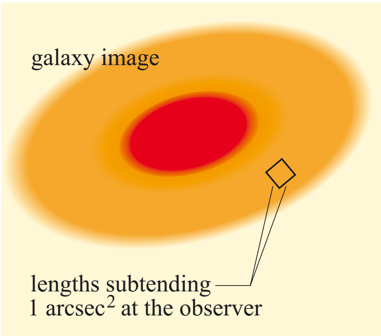

Figure 2.12 The apparent surface brightness of a galaxy provides a measure of the flux originating in an angular area of 1 arcsec^2 surrounding the point being observed.

2.3.1 Luminosities and sizes of galaxies

When viewed with a sufficiently powerful telescope, most galaxies are seen as faint, extended objects with a brightness that varies from point to point. In studying the energy received from such objects the quantity that is directly measured is the **apparent surface brightness** of the source. This quantity can be roughly thought of as the rate at which energy would reach a detector with a collecting area of 1 m^2 (i.e. the flux density) from a small region of angular area 1 arcsec^2 surrounding the point being observed (see Figure 2.12). Acceptable SI units of apparent surface brightness are W m^{-2} arcsec^{-2}. In practice, however, astronomers tend to express the observed flux density as an apparent magnitude and therefore quote the apparent surface brightness in units of magnitudes arcsec^{-2}. Also, since flux density measurements are usually restricted to a particular range (or band) of wavelengths, measurements of apparent surface brightness are usually made in a specified waveband, such as the widely used V-band.

The V-band covers a range of wavelengths in the yellow–green part of the spectrum, the range over which the eye is most sensitive. The band is centred on a wavelength of 545 nm and has a bandwidth of 88 nm.

Since the apparent surface brightness of a galaxy tends to decline smoothly from its centre, it is often useful to display images of galaxies using *isophotal contours*. An **isophote** is simply a closed curve connecting points of equal apparent surface brightness, in much the same way that a closed contour line can be used to show points of equal height on a map. Figure 2.13 shows an example of such an image – in this case of the elliptical galaxy NGC 4278. Like all galaxies, this particular example has no sharp boundary or edge. There is no isophotal contour that marks

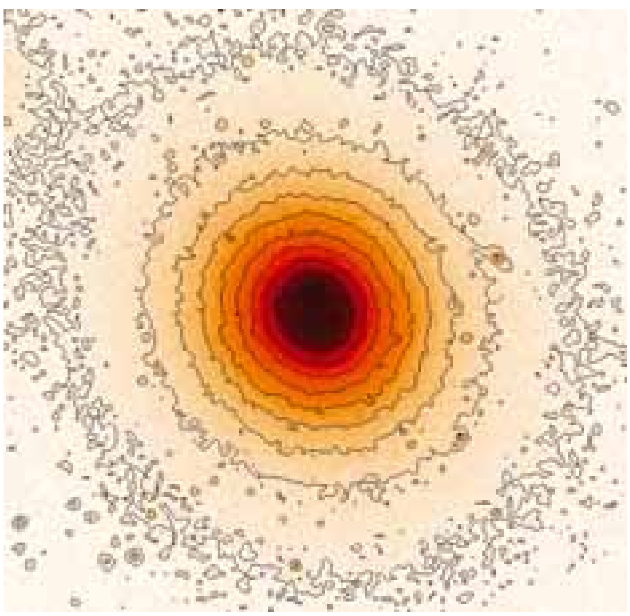

Figure 2.13 Isophotes of the giant elliptical galaxy NGC 4278. These isophotes correspond to measurements made in the red part of the visible spectrum. (Digitized Sky Survey/ STScI)

the edge of the galaxy – the isophote with the greatest radius in this image simply represents the lowest level that can be seen above instrumental noise, and does not necessarily mark the physical boundary of the galaxy.

This extended nature of galactic images is a source of difficulty for those engaged in measuring galactic luminosities – it is much easier to deal with point sources like stars. Because galaxies 'fade out' it is hard to know where to stop measuring. However, galaxies of similar type (morphology and luminosity) usually have a similar **surface brightness profile**; that is to say, the way in which the surface brightness changes with distance from the centre of the galaxy is similar in all galaxies of a given type. By measuring the apparent surface brightness of a galaxy over its brighter parts it is therefore possible to calculate its total flux density by assuming that the surface brightness over its unmeasured regions follows a standard surface brightness profile. Figure 2.14 shows an example of one of these surface brightness profiles, in this case for a spiral galaxy.

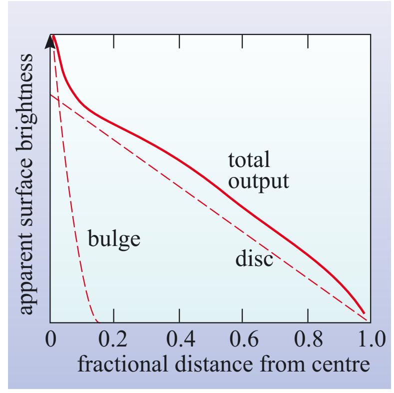

Figure 2.14 Apparent surface brightness as a function of fractional distance from the galactic centre for an averaged sample of face-on Sc galaxies. The dashed lines show the contributions from the nuclear bulge and from a smooth disc (as in an S0 galaxy). The solid line includes both contributions, together with the contribution from the spiral arms that augment the light output of the disc. Note that the vertical axis is logarithmic.

Even when the total flux density from a galaxy is known, determining the corresponding luminosity is not entirely straightforward. For example, in the case of spiral galaxies the orientation relative to the observer (see Figure 2.15) has an effect: because of its disc, a spiral galaxy will not radiate uniformly in all directions, and the orientation will also influence the extent to which radiation is scattered and absorbed by dust within the observed galaxy. Fortunately, the effects of orientation can be estimated from the ratio of major to minor axes in the observed galaxy (within a selected isophote). This observed ratio can then be used to compute standard corrections to the observed flux density that will account for the effects of orientation. The 'corrected' flux density F that emerges from such a calculation, together with the distance d of the galaxy, will then provide a value for the galactic luminosity L, after making due allowance for interstellar absorption within the Milky Way. Similarly, the angular diameter within a selected isophote can be used to estimate the angular diameter θ of the whole galaxy, which can in turn be used in conjunction with the distance of the galaxy to determine its linear diameter l. These procedures are subject to many uncertainties and assumptions, so they cannot possibly provide an absolutely precise value for any physical quantity. Rather, the aim is to approach the determination in a standardized way, so that comparisons between the luminosities and diameters of different galaxies are as meaningful as possible.

The luminosity is given by $L = 4\pi d^2 F$ where d and F are the distance and flux density of a source respectively. The linear diameter is given by $l = d \times (\theta/\text{radians})$.

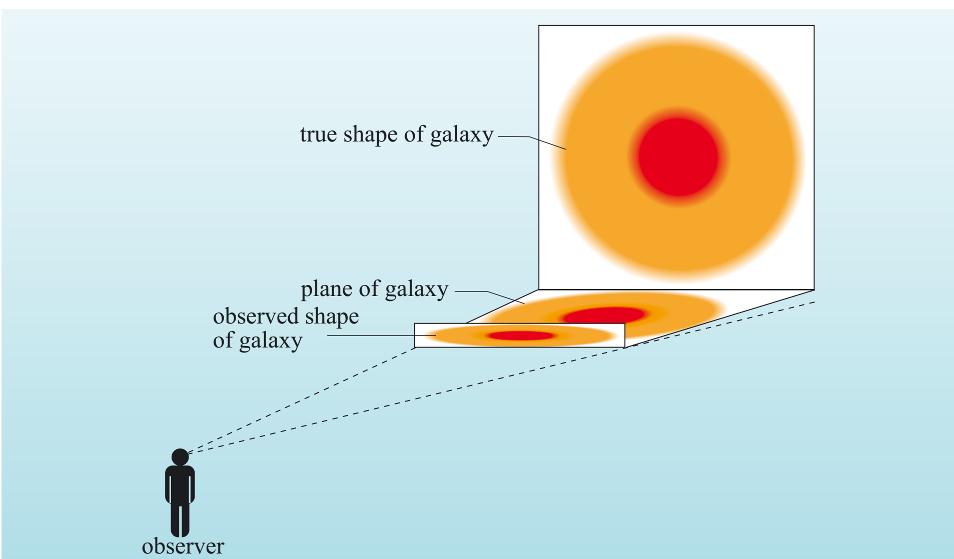

Figure 2.15 The observed shape of a galaxy arises from a combination of its true shape and its orientation relative to the observer.

The results of luminosity and diameter determinations have already been summarized in Table 2.1. Basically, ellipticals are the most diverse class with luminosities that range from a few times $10^5 L_\odot$ for dwarf elliptical galaxies to about $10^{11} L_\odot$ for giant ellipticals (and cD galaxies). Spirals, on the other hand, occupy a narrower range, from about 10^9 to a few times $10^{11} L_\odot$. Irregulars occupy a wider range than do spirals, but are generally less luminous. Diameters follow a similar pattern, as Table 2.1 shows.

2.3.2 Masses of galaxies

You will recall from Chapter 1 that a great deal of uncertainty still surrounds the mass of the Milky Way, mainly due to the problem of assessing how much dark matter is associated with our Galaxy and how it is distributed. Similar problems are associated with all galaxies. Thus, although three methods of determining galactic masses will be briefly described, you should not be surprised to learn that the results they provide are not fully consistent since they certainly differ in their sensitivity to dark matter and may also have other shortcomings.

Method 1: Rotation curves for spiral galaxies

The use of a *rotation curve* – a plot of rotational speed v against radial distance r from the galactic centre – to determine the mass of a spiral galaxy has already been described in Section 1.3. The basic principles are quite simple. The rotation curve of a galaxy is measured observationally and compared with the theoretical rotation curve predicted by a model of the galaxy in which mass is distributed in a plausible way, including that in the dark-matter halo. The theoretical mass distribution is then adjusted until there is reasonable agreement between the observed curve and the predicted curve. The total mass in the final model (including that of the dark matter) then represents the true mass of the galaxy. The method suffers from various drawbacks, including the fact that (owing to assumptions about symmetry on which the method relies) it is rather unsuitable for spirals that have strongly pronounced bars, and because it gives only a lower limit to the galactic mass. The method also depends on knowing the radial distance r, which in turn requires that the distance of the galaxy is known. Nonetheless, it is relatively straightforward and has been used extensively.

■ Why does the method only give a lower limit on the mass? (This limitation was discussed in Chapter 1.)

❏ The method provides insight only into the mass within the largest value of r for which the rotation curve has been measured (see Section 1.2.2).

In order to ensure that observations of rotation curves extend out to the greatest possible values of r, it is usual to base them on Doppler shifts of the 21 cm radiation emitted by neutral hydrogen. In nearby galaxies 21 cm emission can often be traced well beyond the optical limits of the disc (dark matter would extend still further). An example of the mapping of Doppler shifts is shown in a colour-coded form for the galaxy M81 in Figure 2.16. Of course, Doppler shift measurements only determine velocity components along the line of sight, so to derive a galaxy's rotation curve from the data shown in Figure 2.16 it is necessary to take into account the orientation of the galaxy relative to the observer. The rotation curve derived in this way for M81 and for several other galaxies is shown in Figure 2.17.

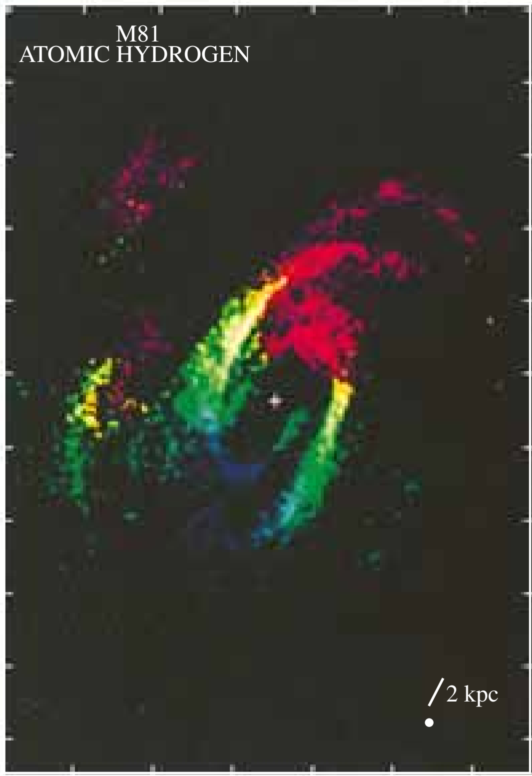

Figure 2.16 An image of the galaxy M81 that has been reconstructed from 21 cm radio observations. The intensity shows the strength of 21 cm emission, while the colour coding shows the extent to which the 21 cm line is Doppler shifted (red represents a high speed along the line of sight away from us, blue is a high speed towards Earth). The circle at the lower right of the map shows the angular resolution of the radio telescope used to make these observations. (Westerbork Synthesis Radio Telescope)

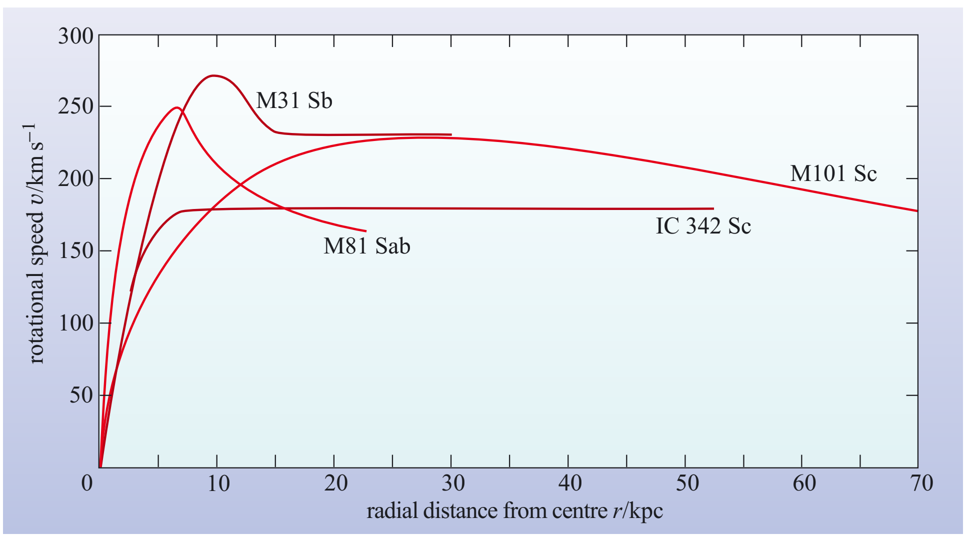

Figure 2.17 Schematic representations of the rotation curves for some nearby galaxies. Note that each curve is marked with the catalogue designation and Hubble type of the galaxy to which it refers. (Mihalas and Binney, 1981)

For more distant galaxies, the resolution of the 21 cm measurements may be too low to map Doppler shifts at different locations in the disc. In this case a different approach can be adopted whereby a spatially unresolved measurement is made of the 21 cm line. Because this line is the sum of 21 cm emission from gas in all parts of the galaxy, it will be broadened due to the different Doppler shifts of the various contributions. While it is not possible to determine the rotation curve from such measurements, the maximum rotation speed in the disc can be found, and, from this value, a mass estimate of the galaxy can be obtained.

Irrespective of their limitations, 21 cm measurements, rotation curves and the related mass determinations have been of great value in modern astronomy. They have provided evidence of galactic mass distributions that extend well beyond the limits of visible discs, and have thus played an important part in giving dark matter its current significance.

Method 2: Velocity dispersions for elliptical galaxies

Rotation (an orderly motion in one plane around the galactic centre) is relatively unimportant in elliptical galaxies, which are often regarded as simple 'star piles' – swarms of stars that have long since settled down into galactic orbits under one another's gravitational influence. If this view of generally settled stellar motions within an elliptical galaxy is correct, then it should be possible to predict the value of a quantity called the **velocity dispersion**, Δv, for a given elliptical galaxy. The velocity dispersion is a statistical quantity that provides a measure of the range of speeds of stars along a line of sight. In an elliptical galaxy of given shape, the velocity dispersion is expected to be proportional to the quantity $(M/R)^{1/2}$, where M is the mass of the galaxy and R is a scale length related to its size. This result, derived from what is known as the *virial theorem* (Box 2.1), may be applied to elliptical galaxies whose size R is known and for which Δv can be estimated from Doppler-shift measurements. This procedure seems to give reasonable values for M, though, once again, the mass obtained is only a lower limit since it is really that enclosed by the stellar orbits.

BOX 2.1 THE VIRIAL THEOREM

The **virial theorem** is a very useful result that relates the total gravitational potential energy of a galaxy to the sum of the kinetic energies of all of the individual components that make up that galaxy. We won't prove this theorem here, but simply quote the relationship and show why such a result is reasonable.

The virial theorem applies to any system consisting of bodies that interact solely by mutual gravitational interaction. Of course, galaxies are such systems, but the theorem also applies to smaller entities, such as globular clusters, as well as to larger ones such as clusters of galaxies.

Here let us consider an idealized galaxy which consists solely of stars (i.e. we will ignore any other components that might be present in a real galaxy). The total kinetic energy of the entire system (E_k) is simply the sum of the kinetic energies of all the stars that it contains.

Each star also has a gravitational potential energy which arises from the gravitational interaction of that star with all the other stars in the galaxy. This gravitational potential energy is equal to −1 times the energy required to remove the star from the galaxy.

The gravitational potential energy of each star is a negative quantity because, by convention, the gravitational potential energy of a star is taken to be zero when it is so far from the galaxy that it is effectively free of the gravitational pull of the galaxy. Since any star would have to be given a *positive* amount of energy to enable it to attain this zero energy state, it must be the case that each of the stars in the assembled galaxy has a *negative* gravitational potential energy.

The total gravitational potential energy (E_g) of a galaxy can be defined in a similar way. By convention, the total gravitational potential energy is taken to be zero when all the stars are so widely dispersed that each is effectively free of the gravitational influence of all the others. If you imagine a process in which stars are removed one by one from the galaxy, then it's easy to see that some positive amount of energy will be required to achieve the total disassembly that corresponds to the state of zero gravitational potential energy. The total gravitational potential energy of the assembled galaxy will be the negative of this 'disassembly' energy.

The virial theorem states that when a galaxy exists in a stable state, such that it is neither contracting nor expanding, the total kinetic energy and the total gravitational potential energy are related by

$$E_k = -\tfrac{1}{2} E_g \qquad (2.1)$$

The proof of this statement would be a lengthy diversion here, but it is useful to note two features of this relationship. First, the negative sign is expected because the total kinetic energy E_k will be positive, while the total gravitational potential energy E_g must be negative. The second point is that the kinetic energy of the stars is less than the energy that would be required to completely disassemble the galaxy. This also seems reasonable: if the total kinetic energy exceeded $-E_g$ (remember, $-E_g$ is a *positive* quantity) it could cause the stars to completely disperse and thus disrupt the galaxy.

The condition that the galaxy is in a stable state – neither contracting nor expanding – is vital. If this is not true then the virial theorem simply does not hold.

To illustrate this, consider a system of stars, distributed in such a way that they form a uniform spherical cloud. Furthermore, suppose that initially all the stars are stationary.

- What is the total kinetic energy of this system?
- Since the stars are all stationary, the total kinetic energy is zero.

In this case the virial theorem does not hold, but this is, of course, a highly unstable situation. Released from rest, the system starts to collapse as each star accelerates under the gravitational influence of all the other stars. Thus the total kinetic energy of the stars increases. Because they are relatively small and widely separated, the stars are unlikely to collide with one another, though some will pass sufficiently close to others for their paths to be deflected. In this way kinetic and gravitational potential energy can be interchanged, although the total energy of the system remains constant throughout the collapse. The system as a whole contracts somewhat from its initial size, and this decreases the gravitational potential energy of the system (i.e. it becomes more negative). However, as the gravitational potential energy decreases there is a corresponding increase in the kinetic energy of the stars. Eventually, the system can be expected to settle into a state in which it is neither expanding nor contracting. When this happens the total energy is divided between kinetic energy and gravitational energy in just the way described by Equation 2.1. The virial theorem then applies to the system, which can be said to be in a **virialized** state.

It should be noted that the virial theorem applies to *any* system of bodies that interact solely by gravity, provided the system has become virialized. So the theorem should be expected to apply to spiral as well as elliptical galaxies, provided they have virialized.

Method 3: X-ray halos of ellipticals

Some bright ellipticals have substantial halos of hot, diffuse gas with temperatures of several million kelvin. X-ray observations of such galaxies allow the extent, temperature and density of these gaseous halos to be determined. The mass measurement technique is based on the assumption that these hot, gaseous halos are gravitationally bound to their respective galaxies. Roughly speaking, a halo of a given extent and temperature implies that the galaxy has a certain mass: a very hot and extended halo would require the presence of a high-mass galaxy to prevent the gas from escaping. In practice, detailed X-ray measurements are compared with a theoretical model of the gaseous halo, and this allows the mass of the galaxy to be found. This method is becoming widely used for determining the mass of giant ellipticals, and as you will see in Chapter 4, is similar in principle to a method that is used to measure the mass of clusters of galaxies.

In passing, it is worth noting that X-ray measurements of elliptical galaxies also provide evidence for substantial amounts of matter (mainly hydrogen) occupying larger volumes than the matter that is emitting at visible wavelengths.

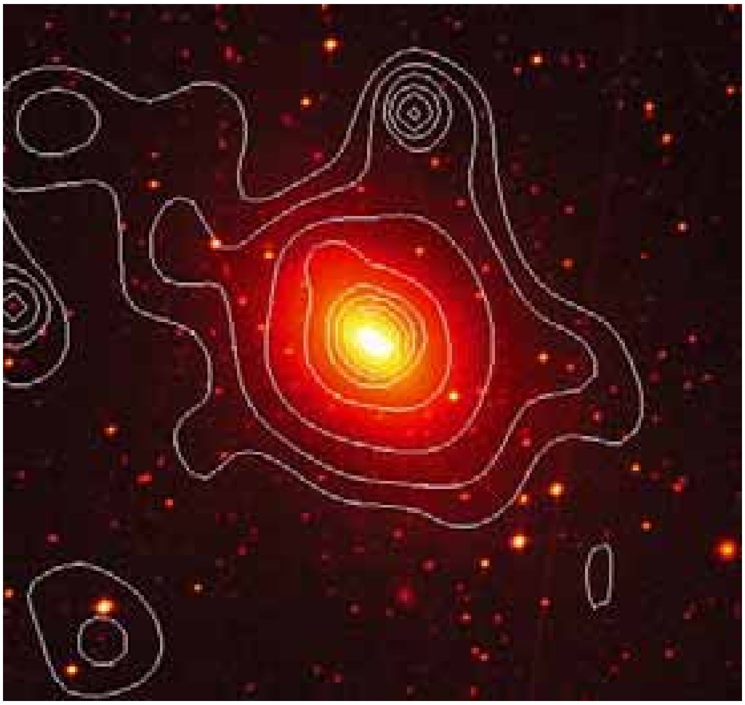

Figure 2.18 The elliptical galaxy NGC 3923. The optical image of the galaxy is shown overlaid with contours of X-ray emission. (Astrophysics and Space Research Group, University of Birmingham)

This is illustrated in Figure 2.18, which shows optical and X-ray images of the elliptical galaxy NGC 3923; the hot, diffuse gas is traced by the X-ray emission and can be seen to have a much greater extent than the optical image.

2.3.3 Compositions of galaxies

The answer to the question: 'What are galaxies made of?' should already be familiar to you. Broadly speaking, galaxies are made of dark matter, stars, and ordinary (baryonic) gas, together with various minor constituents such as dust. This section is concerned with the methods employed to determine the detailed compositions of individual galaxies. It aims to explain how we set about answering questions such as: 'How many stars are there in a galaxy?' or: 'What kind of stars predominate?' or: 'How much of the galaxy's mass is due to gas?'

The last of the above questions is one of the simplest to answer. At least, there is a relatively straightforward procedure for attaching a numerical value to the quantity $M_{\rm H}/M$, where $M_{\rm H}$ is the mass of atomic hydrogen in a galaxy and M is the 'total' mass of that galaxy estimated from its rotation curve or velocity dispersion. The determination of $M_{\rm H}$ can simply be based on the flux density of 21 cm radiation received from atomic hydrogen in the galaxy, although there is evidence that certain galaxies are dominated by H_2. Studies of the ratio $M_{\rm H}/M$ indicate a fairly systematic variation with Hubble class. Ellipticals have very little atomic hydrogen, spirals a few per cent and irregulars 15–25%. However, measurements of 21 cm line emission do not reveal anything about the presence of ionized hydrogen. You saw in the previous section that some giant elliptical galaxies have extensive halos of gas at a temperature of several million kelvin. At such temperatures hydrogen would be ionized. Detailed X-ray observations can be used to measure the mass of ionized hydrogen in such galaxies. It appears that the proportion of mass of gas in ionized form in giant elliptical galaxies is similar to the proportion of mass of gas in atomic or molecular form in spiral galaxies. In less massive ellipticals, the proportion of the mass of gas in ionized form seems to be somewhat lower than in giant elliptical galaxies.

Questions about the numbers and types of stars in a galaxy are really interconnected and are best answered together. In principle, a galaxy might be expected to contain representatives of all the stellar types that were discussed in Chapter 1. However, star formation requires the presence of relatively cold gas – gas that is in atomic or molecular form. Since atomic or molecular gas is rare in elliptical galaxies, we might reasonably expect that there is little ongoing star formation in such systems. It is thus reasonable to suppose that those types of stars that belong to Population I will be exceptional in elliptical galaxies, but to what extent do observations support that idea? The absence of bright star forming regions in elliptical galaxies is easily confirmed by direct observation, but such

observations are not able to provide an accurate picture of the relative abundances of the various stellar types, since only the brightest sorts of star are visible individually in even the nearest galaxies. Another technique is needed to investigate stellar contents, one that can be based on the properties of a galaxy treated as a whole.

The main method used to investigate the stellar contents of galaxies is a technique known as **population synthesis**. This technique may make use of a variety of galactic properties, including the mass M, luminosity L, and the mass-to-light ratio M/L, but its major ingredient is the spectrum of the entire galaxy, or at least some large region of the galaxy – the so-called **integrated spectrum**. A major problem of stellar population synthesis is that cool, low-mass stars that contribute much of the total mass do not emit much visible light, so it is best to include infrared as well as visual observations. An example of an integrated spectrum, that for the central regions of the elliptical galaxy NGC 1427, is shown in Figure 2.19.

The method of population synthesis starts by defining a number of different stellar categories – these are defined in terms of both stellar mass and metallicity. A plausible assumption is made about the relative numbers of stars in each category, and on this basis their contribution to the total mass and luminosity of the galaxy can be worked out. It is also possible to work out the integrated stellar spectrum that would be expected from such a combination of stars. The results of these various calculations are then compared with observations (including the observed spectrum), and the mix of stars adjusted to improve the agreement. Figure 2.19 shows the 'best fit' model spectrum as well as the spectra from each component in the synthesized population for NGC 1427. Another example of the results of population synthesis analysis is shown in Table 2.2 for the nuclear bulge of M31.

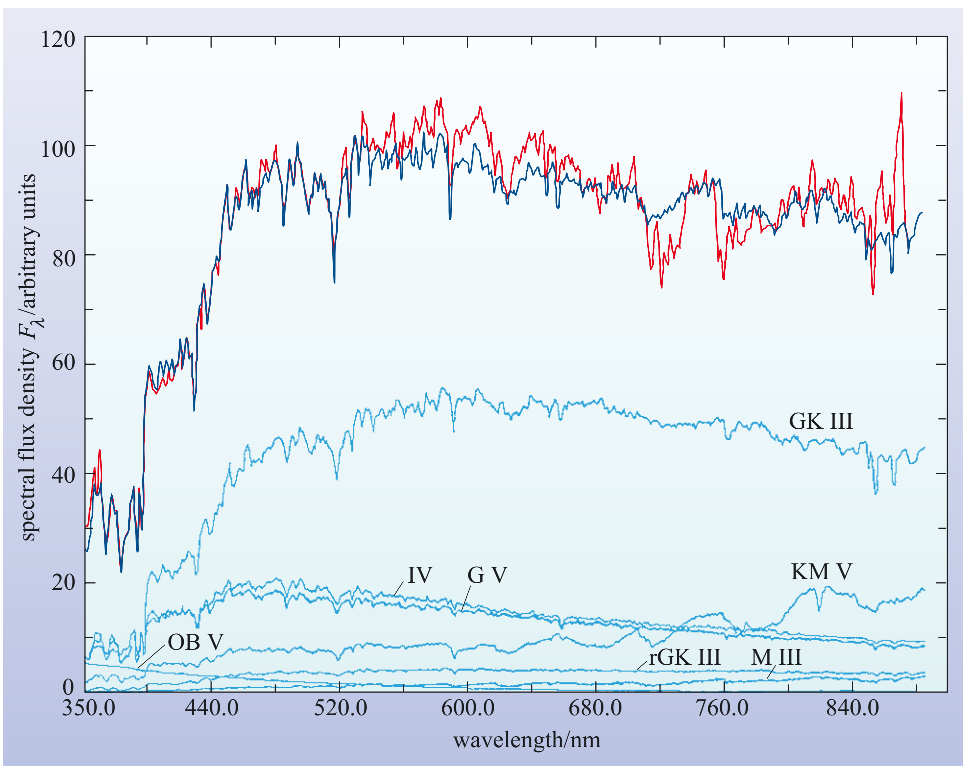

Figure 2.19 Population synthesis of the spectrum of the elliptical galaxy NGC 1427. The red line shows the observed composite spectrum of the galaxy, while the dark blue line shows the 'best fit' population synthesis model. The light blue traces show the components of this model due to different classes of stars. (*Note:* the prefix 'r' refers to metal-rich giants, and the spectrum labelled IV represents the contribution from subgiant stars). (Pickles, 1985)

Once a population model has been formulated, the known luminosity of each kind of star can be used in conjunction with the total luminosity of the galaxy to find the total number of stars in the galaxy. The relative importance of the various minor constituents can usually be deduced from observations made at a variety of wavelengths: for instance, far-infrared observations help to determine the dust content.

- Does the population synthesis analysis of the nuclear bulge of M31 (Table 2.2) support the view that the stellar component of the mass is predominantly in the form of low-mass stars?

- Yes. The dominant contribution to the mass of stars is from main sequence stars of spectral type M, and especially from type M7. These are low-mass stars.

Table 2.2 An example of a population model of M31's nuclear bulge. The letters SMR stand for 'super-metal-rich' and refer to a particular compositional feature.

Stellar category	Contribution to total mass/%	Contribution to (V-band) luminosity/%
Main sequence		
G0–G4	0.77	11.56
G5–K0	0.76	3.10
K1–K2	0.40	2.29
K3–K4	0.78	3.07
K5–K7	1.12	1.24
M0–M2	0.73	0.27
M3–M4	10.3	1.09
M5–M6	4.6	0.15
M7	69.4	1.74
Subgiants		
G0–G4	0.35	11.88
G5–G9	0.26	8.79
K0–K1 (SMR)	0.13	6.74
K2 (SMR)[a]	0.12	26.57
Giants		
K3 (SMR)	0.03	12.23
K4–K5 (SMR)	0.01	5.98
M5–M6 (SMR)	0.003	1.32

[a] Includes K2 (SMR) giants too.

2.4 The determination of the distances of galaxies

2.4.1 Introducing distance determinations

Measuring the distances to external galaxies is a task of crucial importance in modern astronomy. There are three main reasons for this. First, if we want to determine properties of galaxies we often need to know their actual, rather than their apparent, sizes. If the distance d to a galaxy is known, then its angular size θ can be used in the formula $l = d \times (\theta/\text{radians})$ to find the actual size (provided θ is small, which in practice it always will be). Secondly, galactic distances are crucial to mapping the layout of the Universe. It is easy to identify the directions of observable galaxies and clusters, but only when their distances are known can their arrangement throughout space be fully determined. The third reason is that galactic distances hold the key to working out the age, evolution and ultimate fate of the Universe – more will be said about these issues in Chapters 5–8. For the present it is sufficient to note that there are several different theoretical models of the Universe, and if galactic distances can be measured with sufficient accuracy then it may be possible to discount some of them.

So, the measurement of galactic distances is of great importance. But how is it done, and how reliable are the results? There are many methods of measuring galactic distances and new ones are being developed, or old ones revised and improved, all the time. We cannot hope to give an exhaustive account of this vast subject here, but we will outline the general principles and then examine a few methods in more detail, noting some of their limitations and shortcomings. Many of the methods for finding distances fall into a few broad categories.

Methods based on geometry

The basic idea behind the **geometrical methods** used to determine the distances to other galaxies is very simple: within an external galaxy, identify a feature of known linear diameter l, measure the angular diameter, θ, of that feature, then work out the feature's distance, d, by using the formula

$$d = l/(\theta/\text{radians})$$

(This is just a rearrangement of the formula $l = d(\theta/\text{radians})$ that was quoted earlier.) The main shortcoming of this method is equally simple – there are few features of 'known linear diameter' in external galaxies, and even those features that do exist are unlikely to have accurately measurable angular diameters in any external galaxies apart from those that are *very* close to the Milky Way.

A good example of the geometric approach is the method used to make what is thought to be an accurate determination of the distance to the Large Magellanic Cloud (LMC), one of the nearest external galaxies. The LMC was the site of a supernova (a massive stellar explosion) observed in February 1987. This event, known as SN 1987A, is shown in Figure 2.20. Three and a half years after the supernova occurred, radiation spreading outwards from the site of the explosion encountered a ring of gas that had been ejected from the supernova's progenitor star thousands of years earlier. As the radiation met the ring it caused the various parts of the ring to brighten, leading to the effect shown in Figure 2.21. It appears

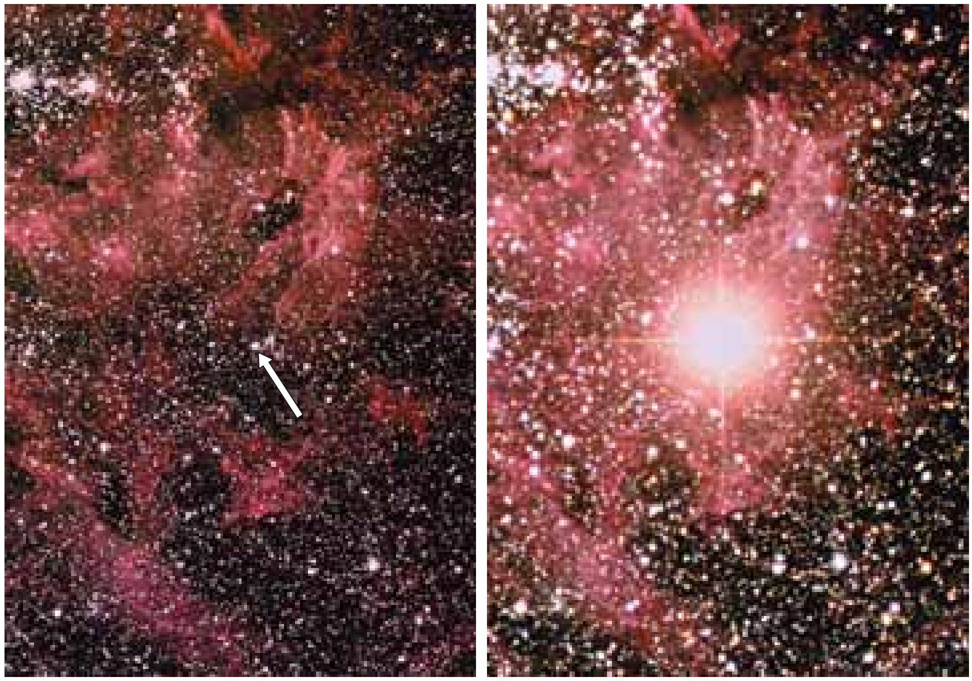

Figure 2.20 Supernova 1987A (a) The left-hand panel shows the progenitor to SN 1987A (arrowed), while the right-hand panel (b) shows the same region of sky after the supernova erupted. (D. Malin/AAO)

Figure 2.21 The ring observed three and a half years after the initial explosion consists of material that was expelled by the progenitor prior to the explosion and was subsequently illuminated by radiation from the supernova. (NASA/ESA)

from the figure that the supernova occurred at the centre of the ring, so it might be expected that each part of the ring would brighten at the same time. However, as seen from Earth, some parts of the ring were observed to brighten before others. The reason for this is easy to explain. The ring is inclined relative to the line of sight from Earth to the supernova, so some parts of the ring are closer to the Earth than others. Consequently there are time delays between the arrival of light signals that left different parts of the ring at the same time. Observations of the time delay between the brightening of the closest and furthest parts of the ring provide information that, together with other observations concerning the orientation of the ring, can be used to work out the ring's linear diameter. (Details of this calculation are indicated in Example 2.1.) Comparing this with the ring's observed angular diameter, the distance of the ring, and hence of the LMC itself, has been shown to be 52 ± 3 kpc. This result places the LMC just beyond the outskirts of the Milky Way, in good agreement with independent determinations of its distance by other methods.

EXAMPLE 2.1

Find an expression for the diameter of the ring around SN 1987A in terms of the time delay (Δt) between the brightening of the nearest and furthest parts of the ring, and the ratio (b/a) between the semiminor and semimajor axes of the ring as it appears to an observer at the Earth. Assume that the ring is actually circular.

SOLUTION

The circular ring around SN 1987A appears to be elliptical because the ring is inclined with respect to our line of sight to its centre. This geometry is shown in Figure 2.22. When viewed from Earth (Figure 2.22a), the ring appears as an ellipse with semimajor and semiminor axes a and b, respectively.

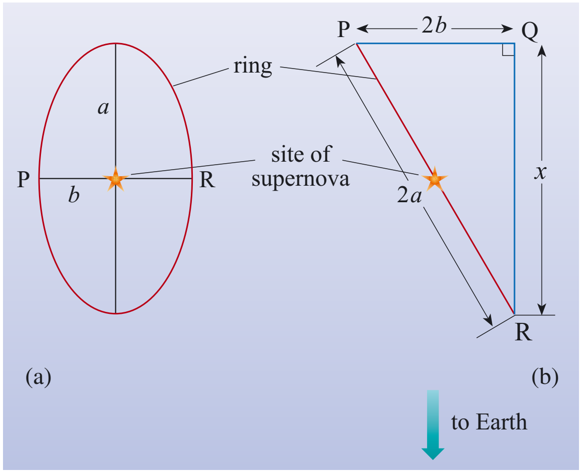

Figure 2.22 The geometry of the ring around SN 1987A. (a) A face-on view of the ring as seen from Earth. (b) A side view showing the relationship between points P and R on the ring.

A side view that cuts through the centre of the ring (Figure 2.22b) shows the relationship between a, b and the extra distance x ($= c \times \Delta t$) that light must travel if it is emitted from the far side of the ring (point P) compared with light that is emitted from the near side of the ring (point R). Pythagoras' theorem can be applied to the right-angled triangle PQR to obtain an expression for x in terms of a and b,

$$x^2 = (2a)^2 - (2b)^2$$

The aim is to find an expression for the diameter of the ring ($2a$) in terms of quantities that can be measured. One such quantity is x, which is related to the measured time delay. The other quantity that can also be determined from observations is the ratio b/a – the ratio of the semiminor and semimajor axes of the image of the ring. So the aim of the algebraic manipulation is to obtain an expression for the diameter of the ring in terms of x and b/a.

Dividing both sides of the equation for x^2 by a^2 gives

$$\left(\frac{x}{a}\right)^2 = (2)^2 - \left(2\frac{b}{a}\right)^2 = (2^2) \times \left(1 - \left(\frac{b}{a}\right)^2\right)$$

Taking the square root of both sides of this equation

$$\frac{x}{a} = 2\sqrt{\left(1 - \left(\frac{b}{a}\right)^2\right)}$$

This equation can be rearranged to give an expression for $2a$

$$2a = \frac{x}{\sqrt{\left(1 - \left(\frac{b}{a}\right)^2\right)}}$$

But $x = c \times \Delta t$ so the equation for the diameter ($2a$) can be written as

$$2a = \frac{c\Delta t}{\sqrt{\left(1 - \left(\frac{b}{a}\right)^2\right)}} \qquad (2.2)$$

This expresses the linear diameter of the ring in terms of observable quantities (Δt and b/a), as required.

QUESTION 2.3

In the case of SN 1987A, light from the far side of the ring took 340 days longer to get to us than did light from the near side, and the angular diameter of the ring was measured to be 1.66 arcsec.

(a) Use Equation 2.2 to calculate the diameter of the ring around SN 1987A. (The ratio (b/a) can be estimated from Figure 2.21.)

(b) Using your answer from part (a), calculate the distance to SN 1987A. Express your answer in kpc.

Methods involving a 'standard candle'

This category covers a wider range of methods and is much more important than the previous 'geometric'category, but the basic idea is just as simple. A standard candle is an object of known luminosity embedded in the object whose distance is to be determined. In Chapter 1 the kind of horizontal branch star known as an RR Lyrae star was spoken of as a standard candle for the purpose of determining the layout of the Milky Way's halo. In this chapter a range of stars and other objects will be used as standard candles for the purpose of determining galactic distances

Once a standard candle has been identified, its distance is found by comparing the flux density, F, that it provides to observers on Earth, with its (known) luminosity L.

$$d = \sqrt{\frac{L}{4\pi F}} \qquad (2.3)$$

Techniques that use this approach to measure distance are generically referred to as **standard candle methods**.

QUESTION 2.4

(a) Equation 2.3 expresses the relation between luminosity, flux density and distance in the absence of any absorption. What effect does absorption have on the observed flux density? Hence what is the effect of absorption on a distance estimate based on the observed flux density and Equation 2.3?

(b) In practice, it is not usually the flux density F over all wavelengths, but the flux density within a narrow wavelength range that is measured. Suppose that the V-band (i.e. the visual band) is used, and that in this band the observed flux density from a standard candle is F_V. What implication does this have for the use of that standard candle, and how should Equation 2.3 be modified to reflect this?

Standard candle methods have played an important role in the history of galactic distance determinations and have great potential for the future. The two fundamental questions that face every standard candle method are:

- Which astronomical sources are suitable to be standard candles?
- What is the luminosity of a selected standard candle?

Later in this section we examine several examples of standard candle techniques and see how these issues are addressed.

The redshift method

This is a very important method of measuring distances to galaxies, and one which is quite distinct from geometrical or standard candle methods. The method is based on a correlation between the measured distances of galaxies and the observed spectral red-shifts of those galaxies that was first recognized by Edwin Hubble in 1929. The details of this correlation and the precise definition of a quantity called the *redshift* (z) that characterizes the red-shifts of spectral lines will be treated in Section 2.4.7. However, it is worth noting here that, if the distance of a galaxy is represented by d and its redshift by z, then the correlation that forms the basis of Hubble's law is given by the simple proportionality

$$d \propto z$$

So, having deduced the existence of the redshift–distance relationship from the measured distances and redshifts of some galaxies, it is a relatively simple matter to use that relationship to infer the distances of other galaxies from measurements of their redshifts alone. The great advantage of this method is that the redshift z is easy to measure. The main disadvantage is that the redshift–distance correlation is only approximately true for any individual galaxy, so the value of d determined for a particular galaxy will only provide an approximate value for its distance. As you will see later, Hubble's discovery indicates that the Universe is expanding – one of the key observations in modern cosmology.

2.4.2 The distance ladder and its calibration

A major problem in distance measurement is that no single method spans the entire range of astronomical distances. Figure 2.23 lists some of the methods of measuring astronomical distances, and indicates the range of distances over which they have been used. (Note that the distance scale is logarithmic, and that the listing includes one method that is confined to the Milky Way.) Almost all methods of distance determination involve using distances found by one method to support another. The use of a chain of measurements, each relying on another, leads to the so-called **distance ladder** – a ladder in the sense that the accessibility of the upper steps depends on having appropriate steps, firmly in place, lower down.

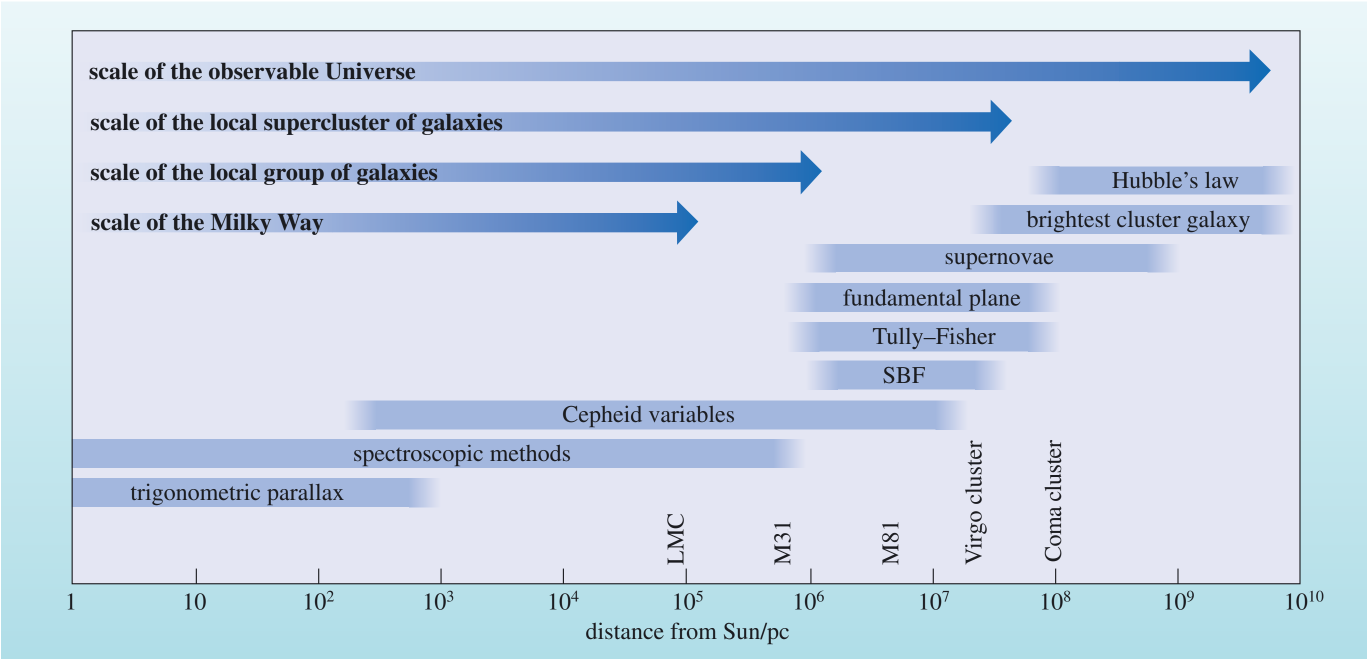

Figure 2.23 Some methods of measuring astronomical distances. Also included are various terms and size scales that will be explained later in this book. SBF stands for 'surface brightness fluctuations'.

1 Mpc (megaparsec) = 10^6 pc = 10^3 kpc.

Relating one step on the distance ladder to another involves a process of **calibration**, that is, the use of an established method of measurement to give absolute meaning to the relative measurements provided by some other method. For example, measuring the redshift of a galaxy's spectrum is fairly easy with modern equipment, so determining the redshifts of several different galaxies is straightforward, and this should give an indication of the *relative* distances of those galaxies. (According to Hubble's redshift–distance correlation, the greater the redshift of a galaxy, the greater its distance.) However, in order to use those redshifts to determine the *absolute* distance of each of the observed galaxies (i.e. the distance measured in well-defined distance units such as Mpc) it is necessary that the absolute distance to one or more of those galaxies should already have been determined using an established method of distance measurement, such as a well-checked standard candle method. Only by using the absolute distance measurements provided by one step on the distance ladder can the relative distances indicated by some other step be checked, refined and calibrated so that they too can be interpreted as absolute distances.

The great advantage of this procedure is that it allows an established method of distance measurement, with a limited range, to be used to calibrate a newer method with a greater range, and in this way permits the cosmic distance ladder to be extended out to the farthest reaches of space. The disadvantage, however, is that any errors or uncertainties in the established methods of distance measurement are carried over to the newer methods when they are calibrated. Until recently this was a very serious problem that was a source of great uncertainty in the measurement of distances to remote galaxies. Happily, the 1990s saw a significant improvement in the calibration of the distance scale, with the result that astronomers are now able to measure distances to remote galaxies (>100 Mpc, say) with an uncertainty of only about 15%.

The following sections examine some of the methods of distance determination in more detail. This is by no means a comprehensive review of distance measurement methods, but it does highlight some of the more important techniques that have been applied in calibrating the distance ladder in recent years.

2.4.3 The Cepheid variable method

Cepheids are giant or supergiant stars with a variable light output that can change by as much as a factor of ten over a period that may be anything from about a day to about 100 days. The name 'Cepheid' is derived from δ Cephei, which was the first star of this class to be described. Cepheids have quite high average luminosities, so they are visible at large distances. A **light curve** showing the variation with time of the apparent visual magnitude of one particular Cepheid is given in Figure 2.24. The recognition that such highly individual stars could be used as standard candles was the outcome of the collective efforts of three astronomers, Henrietta Leavitt (1868–1921), Ejnar Hertzsprung (1873–1967) and Harlow Shapley.

In 1907, while examining variables in one of our nearest neighbouring galaxies, the Small Magellanic Cloud (SMC), Leavitt discovered a correlation between the period (i.e. the time between successive peaks in the light curve) of a certain kind of variable star and its average apparent magnitude. Since all the stars in the SMC are at roughly the same distance from the Sun, it followed from Leavitt's discovery that there must also be a correlation between the period of such a variable and its average luminosity. The existence of this **period–luminosity relationship** implied that for any variable belonging to the same class as those studied by Leavitt, the average luminosity could be deduced from the (easily observed) period of variation. Of course, before the period–luminosity relationship could be used in this way it was first necessary to *calibrate* the relationship by using some established technique to determine the average luminosity of at least one variable star of the appropriate type. This was Hertzsprung's particular contribution – and it was no easy matter.

Hertzsprung's first achievement was recognizing that Leavitt's variables were in fact Cepheids. This insight reduced the calibration problem to that of measuring the average luminosity of a Cepheid, but the task was still not simple. There were many known Cepheids within the Milky Way, but none of them was close enough for its distance to be measured by the method of trigonometric parallax; consequently none of them had a reliably determined average luminosity. So Hertzsprung was forced to use more complicated and less reliable methods in order to obtain the average luminosity of a Cepheid. This he eventually did, although for various reasons, including a serious underestimate of the effects of interstellar absorption, his calibration was inaccurate and the resulting value for the distance of the SMC quite wrong.

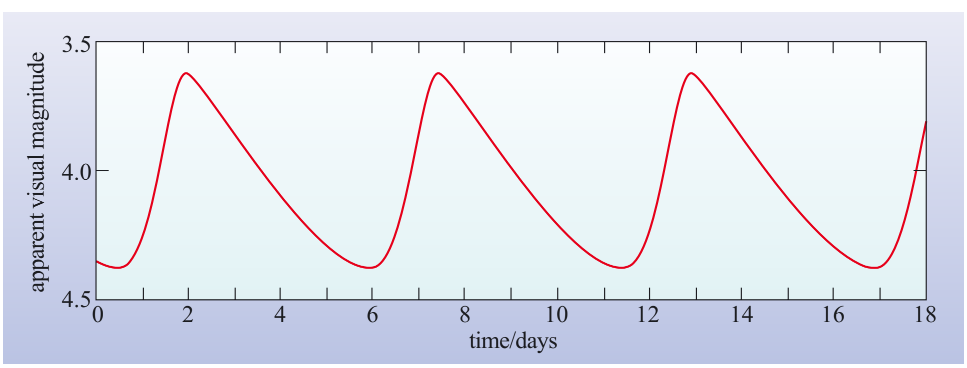

Figure 2.24 The light curve of the variable star δ Cephei, which gives its name to the class of Cepheid variables. The period of such a star is the time between successive peaks of the light curve, and is about 5.4 days in this case. (Bok and Bok, 1974)

Modern versions of the Cepheid period–luminosity relationship have, of course, been re-calibrated. Although there is still some debate about the accuracy, it is now accepted that this method can yield the distance to any given Cepheid with an uncertainty of just 15%. A recent version of the period–luminosity relationship is shown in Figure 2.25. There are three points about this that should be noted. First, despite its name, the period–luminosity relationship is usually presented as a relationship between period and average absolute magnitude (i.e. the average magnitude an object would have if viewed from a distance of 10 pc). Secondly, the absolute magnitude of a Cepheid will vary with time, but the average absolute magnitude will not, since it corresponds to the mean luminosity of the Cepheid over its full period of variation. Third, the magnitude used is usually restricted to one or other of the standard wavelength bands used by astronomers, in the case of Figure 2.25 the V (or visual) band has been chosen.

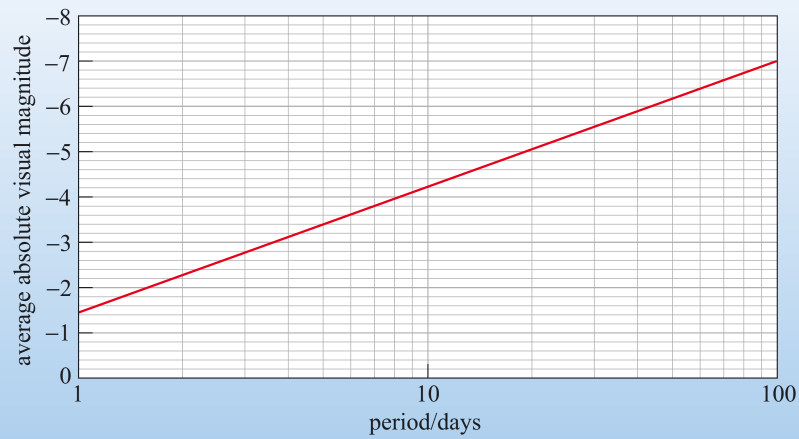

Figure 2.25 The period–luminosity relationship for Cepheid variables. Note that, in accordance with convention, the average luminosity is represented by an average absolute visual magnitude (which is calculated from the mean luminosity over a full period). The period–luminosity relation shown here is for Type I (classical) Cepheids. Type II Cepheids have lower luminosity than Type I Cepheids of comparable period.

QUESTION 2.5

A certain Cepheid is observed to have a period of 10 days. What is the average absolute visual magnitude (corresponding to the mean luminosity) of the Cepheid expected to be?

The **Cepheid variable method** has played an important part in the history of astronomical distance measurements. It was employed, somewhat erroneously, by Harlow Shapley, who developed his own independent version of the method during his studies of the distribution of globular clusters, and it was used by Hubble to determine the distance of the spiral galaxy M31 (Figure 2.5). It was this latter measurement, announced in 1924, that convinced the majority of astronomers that there were galaxies external to the Milky Way and it thus ushered in the era of *extra-galactic astronomy*. Figure 2.26 shows the photographic plate that Hubble was studying when he realized that what he had thought was a nova was in fact a Cepheid that held the key to M31's distance.

The sensitivity and high spatial resolution of the Hubble Space Telescope have allowed astronomers to use the Cepheid variable method to measure the distances of galaxies that are up to about 30 Mpc from the Milky Way. While this is not a very large distance in cosmic terms, it is sufficient to allow the calibration of several other distance estimation methods (discussed below), which cannot easily be

Figure 2.26 The photographic plate of M31 on which Hubble discovered a Cepheid. Note that the N (for nova) at the top right has been crossed out and VAR (for variable) written in its place. (Berendzen *et al.*, 1976)

calibrated by any other means. Thus the Cepheid variable method is a key step in building up the cosmic distance ladder.

It is also worth noting that, although the period–luminosity relationship was discovered empirically, there seems to be a good underlying physical explanation for it. The variation in luminosity of a Cepheid is thought to arise because the envelope of the star is pulsating (i.e. expanding and contracting regularly) with a period that depends on the mass of the star. The more massive the star, the larger and hotter (and thus more luminous) it is, and hence there is a relation between period and luminosity.

2.4.4 Supernova methods

Figure 2.27 shows a supernova in an external galaxy. As you can see, the supernova is very bright compared with the rest of its host galaxy and is easily discerned. Supernovae are classified as Type I or II mainly on the basis of their spectra (Box 2.2). Members of a subclass of Type I, **Type Ia supernovae**, appear to have approximately the same peak luminosity, and can therefore be used as standard candles. Type II supernovae are less uniform than those of Type Ia, but still provide the basis for a different technique of distance measurement.

Figure 2.27 The galaxy NGC 3368 during the eruption of the Type Ia supernova 1998 BU. The location of the supernova is indicated. (N. Suntzeff, CTIO)

BOX 2.2 CLASSIFICATION OF SUPERNOVAE

Supernovae are classified into two broad groups depending on whether or not their spectra show hydrogen lines: Type I supernovae do not show hydrogen lines, whereas Type II supernovae do. Type II supernovae result from the core collapse of a supergiant star that has a significant amount of hydrogen in its envelope. This gives rise to a spectrum that contains hydrogen spectral lines.

The Type I class is subdivided according to the presence of silicon absorption lines in the spectrum. Those with silicon lines are classed as Type Ia, whereas those that lack silicon lines are classed as Type Ib or Type Ic. Very massive supergiants (with initial masses exceeding about $30M_{\odot}$) are thought to lose their hydrogen envelopes in intense stellar winds, and the core collapse of these stars gives rise to Type Ib and Ic supernovae.

Type Ia supernovae arise from a different mechanism to core collapse. It is believed that they occur in interacting binary star systems in which one star is losing mass by Roche lobe overflow. (Roche lobe overflow is a mechanism whereby an evolved star can lose matter to a companion.)

The star that gathers the overflowing material is a white dwarf that is close to the maximum mass that such a star can have. This mass is called the *Chandrasekhar limit* and has a value of about $1.4M_{\odot}$ (the exact value depends on the composition of the white dwarf). The white dwarf accretes material from its companion until it exceeds this mass limit, at which point the elements (usually carbon and oxygen) that make up the bulk of the white dwarf undergo rapid thermonuclear burning. This results in an energetic explosion that is seen as a supernova.

Type Ia supernova methods

Over the past 40 years or so, three galaxies have each been observed to host two Type Ia supernovae, and in each of these three galaxies the two supernovae have had almost the same maximum apparent brightness, suggesting that all Type Ia supernovae might have the same peak luminosity. Thus, Type Ia supernovae have the potential of being good standard candles. There is actually a good physical reason to suppose that Type Ia supernovae might be reliable standard candles. As described in Box 2.2, Type Ia supernovae are produced by the thermonuclear explosion of a white dwarf that is at the Chandrasekhar limit. Since this critical mass is similar for all white dwarfs, it is reasonable to suppose that they should all have similar luminosities.

Having identified Type Ia supernovae as possible standard candles, the next requirement is calibration. This requires that the peak luminosity of at least one Type Ia supernova should be determined from an observation of its apparent magnitude and a measurement of its distance based on an established method. (The theoretical understanding of Type Ia supernovae has improved enormously over just the past few years, but it is still not good enough to allow predictions of peak luminosity to replace measurements based on established methods of distance determination.) Fortunately, there are observations that can contribute to the

calibration process, most notably the study of Cepheids in galaxies that have also contained a Type Ia supernova.

QUESTION 2.6

Type Ia supernovae have been observed in three nearby galaxies. List the items of information concerning these supernovae and their host galaxies that you would need in order to calibrate the Type Ia supernova method. Briefly explain how you would use the items in your list.

Studies of the sort outlined in the answer to Question 2.6 indicate that the peak luminosity of a typical Type Ia supernova is about $5.5 \times 10^9 L_\odot$. On this basis, astronomers have used Type Ia supernovae to determine the distances of remote galaxies. These studies have led to such important and startling results that the reliability of the method has become a very significant issue that has been intensively investigated. The results obtained using Type Ia supernovae, and the refinements to the basic method that must be used in the most precise work, will be discussed in Chapters 5 and 7, respectively. For the present we simply note that, despite some remaining concerns about reliability, the Type Ia supernova method has proved to be a technique of great value and importance.

Type II supernova methods

Type II supernovae provide another means of determining galactic distances. The technique is based on the relationship between the radius R, temperature T and luminosity L of a spherical black body.

$$L = 4\pi R^2 \sigma T^4 \tag{2.4}$$

Here, $\sigma = 5.67 \times 10^{-8}\ \mathrm{W\ m^{-2}\ K^{-4}}$ is the Stefan–Boltzmann constant, one of the fundamental constants of radiation physics. In simple terms, the main idea in this approach is to treat the exploding supernova as a spherical black body and, at some particular time, to determine both its temperature and its radius from directly observable quantities. Equation 2.4 can then be used to determine the luminosity at that time, enabling the Type II supernova to play the role of a standard candle.

The temperature of the supernova changes with time, but can be determined at any particular time from the directly observable spectrum of the supernova. Determining the radius is more problematic. It is not currently possible to measure the radius by direct observation since the photosphere of the supernova cannot be resolved by any existing telescope. However, the radius can be inferred in the following way. Suppose the temperature and the flux of radiation from the supernova are measured at two different times, denoted by the subscripts 0 and 1, respectively. If the supernova acts as a spherical black body at both these times, then the relationship between the observed flux, temperature and radius at those two times can be shown to be (see Question 2.7, below):

$$\frac{F_1}{F_0} = \frac{R_1^2 T_1^4}{R_0^2 T_0^4} \tag{2.5}$$

This can be rearranged to give

$$\frac{R_1}{R_0} = \left(\frac{F_1}{F_0}\right)^{1/2}\left(\frac{T_0}{T_1}\right)^2 \tag{2.6}$$

However the supernova is expanding, and Doppler shifts in spectral lines can be used to measure the speed (v) of its outer layers. Given a time interval Δt between the observations, and assuming a uniform rate of expansion, the radius of the supernova at the later time is related to the radius at the earlier time by

$$R_1 = R_0 + v\Delta t$$

- Substitute the expression for R_1 into Equation 2.6. Of the quantities in the resulting equation, how many are measured, and how many are unknown?

- The resulting equation is

$$\frac{R_0 + v\Delta t}{R_0} = \left(\frac{F_1}{F_0}\right)^{1/2}\left(\frac{T_0}{T_1}\right)^2 \tag{2.7}$$

Of the quantities in this expression, F_0, T_0, F_1, T_1, v and Δt have been measured, and only R_0 is unknown.

Equation 2.7 can be rearranged to provide an expression for the unknown quantity R_0 in terms of quantities that can be measured.

$$R_0 = \frac{v\Delta t}{\left(\left(\frac{F_1}{F_0}\right)^{1/2}\left(\frac{T_0}{T_1}\right) - 1\right)} \tag{2.8}$$

Using this value of the radius, together with the corresponding value of the temperature (T_0), the luminosity can be determined using Equation 2.4. That luminosity can be compared with the apparent magnitude (measured at the same time) to determine the distance of the supernova.

In principle, this approach could be used for any type of supernova. However, the expanding shell of a supernova does not behave exactly as a black body, and in order to refine the technique astronomers need to use theoretical models of supernova explosions. At present, such models are only well developed for Type II supernovae, and thus the technique can only be applied to supernovae of that type.

One of the potential advantages of this method is that the luminosity of the standard candle could, in principle, be determined without reference to other steps on the distance ladder. While there is some controversy over the reliability of the theoretical models that are used in this approach, this method seems to produce distance estimates that are in good agreement with the Cepheid method.

QUESTION 2.7

Show that if a supernova can be considered as a black-body source then the relationship between measured flux, temperature and the radius of the supernova at two different times, is as shown by Equation 2.5.

2.4.5 Surface brightness fluctuations in galaxies

Even when a galaxy is too distant for its individual stars to be resolved, the fact that stars are discrete objects that are not distributed perfectly uniformly gives rise to spatial fluctuations in the surface brightness of the galaxy. The size of this fluctuation provides another method of measuring the distance of a galaxy.

The principle behind the technique can be appreciated by considering a very simplified model of a galaxy in which identical stars are distributed randomly across the face of the galaxy. There would be no concentration of stars towards the centre of the galaxy. Suppose that two such simplified galaxies are observed at different distances from the Earth, and that their images are recorded using a camera fitted with a CCD detector. Each pixel (picture element) will correspond to a certain angular extent, so any features in the image that are smaller than the pixel size will be unresolved.

CCD (charge-coupled device) cameras work on similar principles to domestic digital cameras except that they are extremely sensitive. The vast majority of optical astronomical observations are made using CCD cameras of one sort or another.

These two recorded images are shown in Figure 2.28. In case (a) the galaxy is relatively close, and each pixel contains a relatively small number of stars; in case (b) the galaxy is further away, so there are more stars in each pixel. This, in itself, does not help at all in finding the distance to the galaxy – in fact, the number of stars in each element increases with distance in a way that exactly matches the decrease in flux density from each star with distance, and hence the surface brightness of the galaxy is independent of its distance from us. The key to measuring its distance lies in the fact that stars are discrete objects, hence there will be a statistical fluctuation in the number of stars that fall within each pixel.

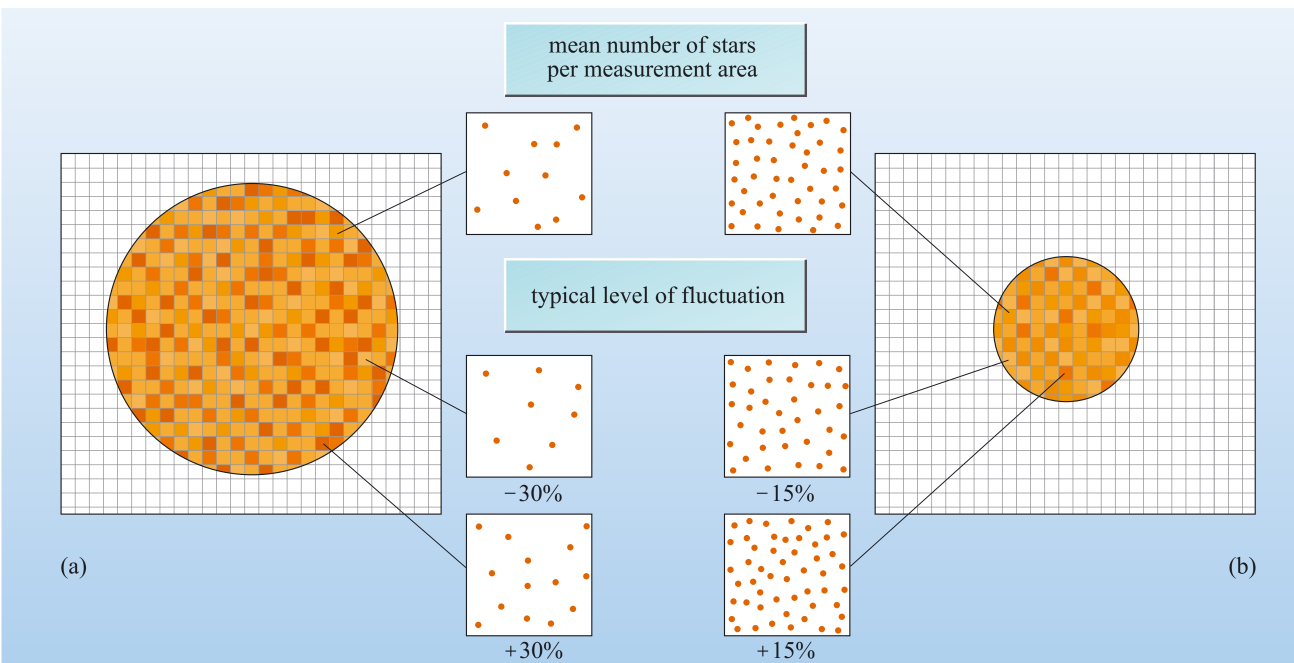

Figure 2.28 A simplified model of a galaxy that shows how surface brightness fluctuations decrease with distance. In both cases the galaxy is observed at the same angular resolution – the grid over the galaxy represents pixels in the camera that are *unresolved*. In this schematic diagram, the stellar content of some of the pixels are shown, illustrating the mean number of stars and the typical level of fluctuation. In case (a) the galaxy is relatively close, there are few stars per pixel and the surface brightness fluctuations are relatively large; in case (b) the distance to the galaxy is twice that in case (a) and the average number of stars in each pixel is 4 (i.e. 2×2) times greater and the surface brightness fluctuations are relatively small. Note that this figure is highly schematic – in practice the level of fluctuation may be as little as 1%.

When the number of stars within a pixel is small, the relative fluctuation is high (as is indicated for case (a) in Figure 2.28), and as the number of stars within the pixel increases the relative fluctuation becomes smaller (case (b)). Thus the relative level of fluctuation decreases with distance and provides a mechanism for measuring distance. In practice, real galaxies are not as simple as the model that has been described here, and surface brightness fluctuations are much smaller than indicated in the example shown in Figure 2.28 – the variation in flux per unit area may be less than 1%. However, by making somewhat more realistic assumptions about the stellar populations of galaxies, and by making very sensitive measurements, it has been possible to apply this technique to galaxies at distances of 50 Mpc or more.

2.4.6 Galaxies as standard candles

The luminous output of an entire galaxy is potentially a very useful type of standard candle. However, as you saw in Section 2.2, there is a vast range in the luminosities of galaxies, and so efforts to adopt them as standard candles depend on the identification of sets of galaxies which, by their nature or situation, might reasonably be expected to have a common luminosity. One approach that has been used with some degree of success is based on a statistical argument, according to which the third brightest galaxies in a cluster of galaxies should have approximately the same intrinsic luminosity as the third brightest galaxy in any similar cluster.

Another type of argument is based on the assumption that the amount of luminous matter in a galaxy is related to its total mass, and this, in turn, determines some kinematic property of the galaxy. Thus we might expect, for instance, that an elliptical galaxy with a high value of velocity dispersion would have a high mass and hence a high luminosity. Since the motions of stars within spirals and ellipticals are quite different in nature, it is perhaps not surprising that there are distinct methods for relating kinematic properties to luminosity for these different types of galaxy. It is these two techniques that we shall concentrate on in this section.

Spiral galaxies: The Tully–Fisher relation

In 1977 Brent Tully and Richard Fisher discovered that there is a correlation between the luminosity of a spiral galaxy and its maximum rotation speed (as indicated by the Doppler broadened width of the 21 cm emission line in the galaxy's radio spectrum). The existence of this **Tully–Fisher relation** accords with the idea that more massive (and, by assumption, more luminous) galaxies should be rotating more rapidly. (It was shown in Chapter 1 that orbital speed depends on the mass enclosed by the orbit.) The 21 cm line emitted by a massive spiral galaxy should therefore be expected to include contributions from hydrogen clouds travelling with a greater range of speeds along the line of sight (including a greater maximum speed), than the 21 cm line emitted by a less massive spiral. Consequently, the measured width of the 21 cm line should be greater for more luminous spiral galaxies. According to the Tully–Fisher relation, the luminosity of a spiral increases roughly in proportion to the fourth power of the maximum rotational speed V_{max}, so approximately

$$L \propto (V_{\text{max}})^4 \tag{2.9}$$

Tully and Fisher established and calibrated this relation using a sample of ten nearby spirals, the distances (and hence luminosities) of which had been determined using the Cepheid variable method. In using the relationship to find unknown galactic distances, account must be taken of the orientation of the galaxy being observed

(since this plays a role in determining the link between its measured 21 cm line width and the inferred value of V_{max}) and any absorption/scattering that occurs along the light path. When the method is applied in its most sophisticated form (and assuming that it has been perfectly calibrated!) it is believed that the distance of an individual galaxy can be determined to within ±15%.

Elliptical galaxies: The Faber–Jackson relation and the fundamental plane relation

For elliptical galaxies the analogue of the Tully–Fisher relation is called the **Faber–Jackson relation** (after Sandra M. Faber and R. E. Jackson who discovered it in 1976). Elliptical galaxies show little rotation; the kinematics of their stars is dominated by random motions. As you saw in Section 2.3.2 the range of these motions can be characterized by a quantity called the velocity dispersion Δv. The Faber–Jackson relation states that the luminosity of an elliptical galaxy is approximately related to the velocity dispersion by

$$L \propto (\Delta v)^4 \tag{2.10}$$

In practice, this relation is hard to calibrate because of the difficulties in measuring the total flux from an elliptical galaxy in an unambiguous way (see Section 2.3.1). Thus the relation is usually converted into a form that relates quantities that can be more easily determined, such as the diameter of an isophote at which a certain level of surface brightness is reached.

It should also be noted that the Faber–Jackson relation is rather approximate, and that there exists a somewhat better relationship between velocity dispersion, the radius of an isophote and the surface brightness at that isophote. This is called the *fundamental plane relation*, and is the usual way in which kinematic information about an elliptical galaxy is used to infer its luminosity. Using this method, the distance to an elliptical galaxy can be determined with an uncertainty similar to that involved in measurements based on the Tully–Fisher relation.

QUESTION 2.8

If two elliptical galaxies differ in their velocity dispersions by a factor of 1.2:

(a) What is the ratio of the luminosities of these galaxies? (Assume that the Faber–Jackson relation applies.)

(b) What is the ratio of their masses, if their radii are the same?

2.4.7 Hubble's law

Establishing Hubble's law

The terms 'red-shift' and 'blue-shift' refer respectively to displacements of identifiable spectral features, such as spectral lines, towards longer or shorter wavelengths than those at which they would normally be observed under standard laboratory conditions. One way that such shifts can arise is as a consequence of the Doppler effect, caused by the motion of the source of radiation relative to the observer. In such cases the shift can be used to determine the speed at which the emitter is receding from, or approaching, the observer. However, there are other possible causes of red-shift and blue-shift.

The spectra of distant galaxies exhibit red-shifts. As you will see later, these red-shifts are not simply the result of the Doppler effect, though they do arise from a change with time of the separation between us and the galaxies. A red-shift corresponds to an increasing separation. A schematic example of a red-shifted galactic spectrum is shown in Figure 2.29. In this case, which is typical of distant galaxies, the extent to which any of the spectral lines is red-shifted can be characterized by a single numerical value z that is said to be the **redshift** of the line. (Note that the term redshift, meaning the numerical parameter z, is conventionally written without hyphenation.)

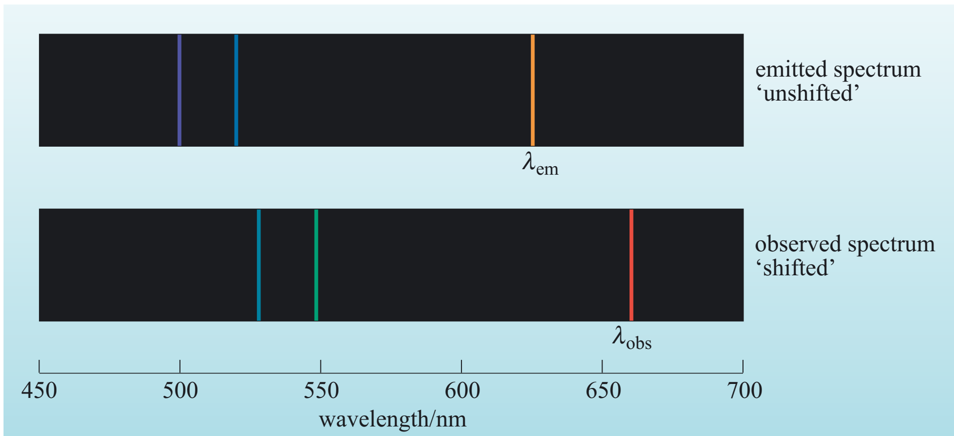

Figure 2.29 As a result of red-shift, a spectral line emitted at a wavelength λ_{em} is seen by observers at a wavelength λ_{obs}.

To evaluate the redshift z in a specific case, all that is needed is a value for the observed wavelength (λ_{obs}) of a spectral line that has a known wavelength (λ_{em}) at the point of emission. The value of z can then be obtained from the definition

$$z = \frac{\lambda_{obs} - \lambda_{em}}{\lambda_{em}} = \frac{\lambda_{obs}}{\lambda_{em}} - 1 \tag{2.11}$$

Generally speaking, all the spectral lines originating in a distant galaxy will be red-shifted to the same extent, so the redshift of any particular line in that galaxy's spectrum will also be the redshift of the galaxy itself. In the few cases where the spectrum of a galaxy shows a blue-shift rather than a red-shift, Equation 2.11 will give a negative value for z. Throughout this chapter we speak exclusively of redshifts, with the tacit understanding that a blue-shifted spectrum is characterized by a negative redshift.

■ Oxygen emits a spectral line at an 'unshifted' wavelength of 500.9 nm. Suppose that this line is observed in the spectrum of a galaxy at a wavelength of 596.1 nm. What is the redshift of the galaxy from which the line was emitted?

❏ $$z = \frac{(596.1 - 500.9)\,\text{nm}}{500.9\,\text{nm}} = 0.190$$

In the late 1920s, when many astronomical measurements were a good deal harder to perform than they are now, only a few galaxies had their redshifts measured. Nonetheless, as Hubble followed up his determination of the distance to M31 with

various other galactic distance determinations, he was able to compare distances with redshifts for a growing sample of galaxies. By 1929, using a sample of just 24 galaxies, he presented the first convincing evidence of a linear relationship between the redshifts and distances of galaxies. The basis of this relationship was introduced in Section 2.4.1; in modern notation the complete relationship is usually written as:

$$z = \frac{H_0}{c} d \tag{2.12}$$

where c is the speed of light (3.00×10^8 m s^{-1}) and H_0 is a constant of proportionality known as the **Hubble constant**.

There are two important aspects of the redshift–distance relation that need to be emphasized. The first is that Equation 2.12 only applies over a relatively small range of redshifts – up to about 0.2. At higher redshifts the relationship between redshift and distance becomes more complicated. It would be a lengthy diversion to explore this here, but a more detailed discussion is provided in Chapter 5.

Secondly, even at low redshifts, the linear relationship between z and d is not a perfect one, as you can see from Figure 2.30. Nonetheless, Equation 2.12, idealized though it may be, does sum up the general trend of a great deal of data and is one of the standard ways of expressing what is now known as **Hubble's law**.

Hubble's law is usually interpreted as showing that the Universe as a whole is expanding. We will return to this in Chapter 5, but it is useful at this stage to illustrate how this interpretation arises. Equation 2.12 can be rewritten as $cz = H_0 d$. We have already noted that it is not generally correct to attribute galaxy red-shifts to the Doppler effect. However, they can be interpreted in this way provided the redshift is sufficiently small, in which case the quantity cz can be identified as the speed of recession v of a galaxy. Equation 2.12 can then be expressed as

$$v = H_0 d \tag{2.13}$$

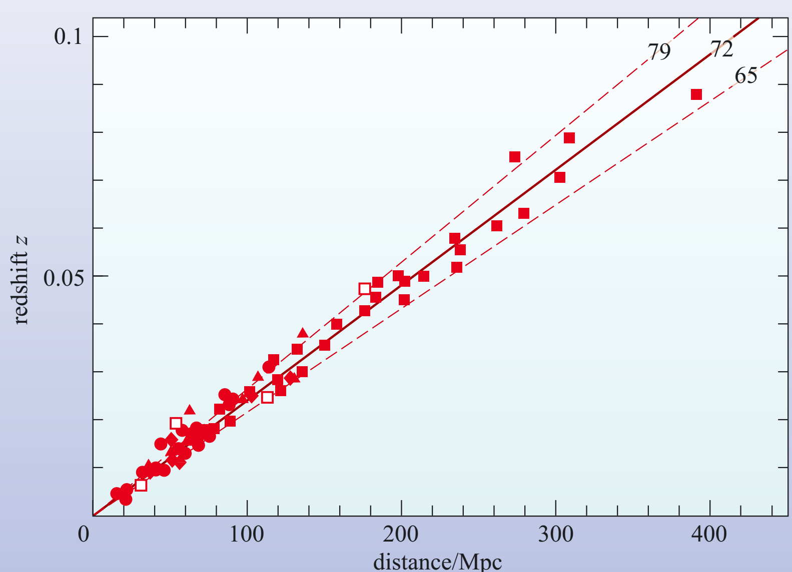

Figure 2.30 A plot of redshift against distance for some galaxies and clusters of galaxies. The different symbols represent different techniques that were used to measure the distances independently of the redshift. (We will discuss this further in Chapter 7.) The solid straight line shows the expected relationship between redshift and distance for a Hubble constant of 72 km s^{-1} Mpc^{-1}. The dotted lines show the expected relationship for H_0 values of 79 and 65 km s^{-1} Mpc^{-1} respectively. (Freedman *et al*., 2001)

Thus, in this interpretation, the speed of recession of a galaxy is proportional to its distance from us. This is just what would be expected in a Universe that was undergoing a uniform expansion. Every point would move away from every other point, and the speed of one point relative to another would be proportional to the distance between them. In such a uniformly expanding Universe, Hubble's constant would be very significant, since it would provide a measure of the rate of cosmic expansion. Note that although galaxies are generally seen to be moving away from the Earth, this does not imply that the Earth occupies any particularly special place in the Universe. In a uniformly expanding Universe *every* point moves away from *every* other point.

The distance–velocity relationship (Equation 2.13) is often quoted in books, and is sometimes confusingly also referred to as Hubble's law. In this book we adopt the convention that Hubble's law is a relationship between redshift and distance, as given in Equation 2.12.

You should note that it is also fairly common practice for astronomers to quote the inferred recession speed (using the relationship $v = cz$) instead of the observed redshift z. We will avoid this practice.

Using Hubble's law

Clearly, despite some deviations from the linear relationship, Hubble's law has great potential as a method of determining the distances of galaxies. Now that redshifts can be measured with relative ease, it would appear to be a simple matter to determine the distance of any galaxy if we know the value of the Hubble constant H_0. Evaluating H_0 is, of course, nothing other than the calibration problem for this method of determining distances. The determination of the Hubble constant has been one of the major problems in astronomy since the discovery of Hubble's law.

- In what SI units would you express H_0 if you knew its value?
- z is a ratio of similar quantities (wavelengths) so it has no units. Thus, H_0 should have the same units as c/d. If we use SI units, then c (which is a speed) is measured in $\mathrm{m\,s^{-1}}$ and d (which is a distance) in m, with the consequence that H_0 could be measured in $\mathrm{s^{-1}}$.

Given that astronomy is littered with unconventional units, you may not be too surprised to learn that astronomers tend not to express H_0 in terms of SI units. Instead, H_0 is usually given in terms of $\mathrm{km\,s^{-1}\,Mpc^{-1}}$. Of course, since these units express a speed per unit distance, they are a valid alternative to the SI units of $\mathrm{s^{-1}}$.

It has already been mentioned that H_0 is an important quantity in cosmology, and for that reason we postpone a detailed discussion of how it has been established until Chapter 7, where it is considered along with other key quantities that describe properties of the Universe as a whole. For the present discussion it is sufficient to note that the value of H_0 is about $72\,\mathrm{km\,s^{-1}\,Mpc^{-1}}$ and that this value is believed to be correct within an experimental uncertainty of less than 10%.

QUESTION 2.9

Using a value for H_0 of $72\,\mathrm{km\,s^{-1}\,Mpc^{-1}}$ calculate the distance of a galaxy that has a redshift of $z = 0.048$. Check your calculation by referring to Figure 2.30.

QUESTION 2.10

If H_0 has the value 72 km s^{-1} Mpc^{-1}, what is its corresponding value in SI units (i.e. expressed in units of s^{-1})?

The origin of the scatter in the relationship between redshift and distance is an important consideration when using Hubble's law.

- What would be the effect on the plot of redshift against distance if, in addition to the relationship described by Hubble's law, galaxies also had some random motion?
- Random motions would give rise to Doppler shifts which would result in positive and negative contributions to the total redshift. Thus the effect of random motions would be to introduce some scatter into the relationship between distance and redshift.

The random motion of individual galaxies, sometimes referred to as a **peculiar motion** in this context, seems to be the explanation for the scatter in the relationship between distance and redshift shown in Figure 2.30. Galaxies close to our own, where the effect of the Hubble expansion of the Universe is negligible, seem to have motions through space of a few hundred km s^{-1}. (In fact, these motions are often the result of galaxies being attracted, under the influence of gravity, towards over-dense regions of the Universe.) When applying Hubble's law it is useful to know the typical distance at which the redshift due to the Hubble expansion is likely to exceed the redshift due to random motions. This is the topic of the following question.

QUESTION 2.11

If it is assumed that galaxies have random velocities of typically 300 km s^{-1}:

(a) Calculate the typical redshift that would be expected for nearby galaxies (i.e. galaxies that are so close that the systematic redshifts predicted by Hubble's law can be ignored). Would this redshift necessarily be positive?

(b) At what distance does the redshift predicted by Hubble's law dominate over the spread in redshift calculated in part (a)? Assume that Hubble's law dominates when the Hubble redshift is a factor of ten greater than the typical redshift due to the random motion of galaxies, and that H_0 = 72 km s^{-1} Mpc^{-1}.

The answer to Question 2.11 indicates that Hubble's law is likely to be unreliable for measuring distances when the redshifts are less than 0.01 – this corresponds to a distance of about 40 Mpc (assuming H_0 = 72 km s^{-1} Mpc^{-1}).

2.5 The formation and evolution of galaxies

Some of the questions that relate to the existence of galaxies are as follows.

- How do galaxies form?
- When did galaxies form?
- What are the important factors that determine a galaxy's morphological type?
- What is the relationship between the formation of stars and the formation of a galaxy?

Definitive answers to these questions do not exist. However, these and related areas are the subject of intense research effort, and some answers are beginning to emerge on the topic of galaxy formation and evolution.

There are two lines of attack in studying issues of galaxy formation and evolution. One approach is to use observations of the properties of galaxies and attempt to 'work backwards' to see what inferences can be drawn about how galaxies have evolved, and possibly even how they were formed. As we see later, some of the most distant galaxies that can be observed are so far away that the light we see now was emitted when the Universe was only 10% of its current age. Thus we are in the remarkable position of being able to look back and see galaxies over a large fraction of cosmic history. Of course, we only have rather limited information about very distant, and hence very faint, galaxies, but such data are invaluable in studying the evolution of galaxies.

The alternative approach to 'looking backwards' is to consider how conditions in the early Universe are likely to have given rise to the structures we observe. This is possible because conditions in the early Universe were remarkably uniform and predictable. The seemingly complex structures of galaxies we observe in the present-day Universe have evolved from these simple conditions through a range of physical processes. As we shall see, the success of this approach depends on how well these physical processes can be modelled.

These two approaches are complementary. The aim of the theory of galaxy formation is to describe how galaxies arose from the conditions of the early Universe. Observations that look back from the present day over a significant fraction of the age of Universe provide the data against which such models must be tested.

In this section we begin with a brief introduction to the early Universe and then give an overview of the major theoretical ideas about how galaxies could have formed. We will introduce some cosmological concepts that are dealt with in more detail in Chapters 5 to 8. The observational approach is introduced by considering how isolated galaxies evolve, and then considering the role that interactions and mergers may have played in galactic evolution. The section concludes with a review of how deep surveys are starting to yield some answers about the formation and evolution of galaxies.

2.5.1 The early Universe

Any investigation of galaxy formation must be considered within the cosmological framework of the origin and evolution of the Universe as a whole. A detailed discussion of current ideas in cosmology is developed in Chapters 5 to 8 of this book. However in order to develop an understanding of galaxy formation, it is

necessary here to introduce some key ideas about the history of the Universe. The most important concept is the widely accepted paradigm for describing the origin and evolution of the Universe called the **hot big bang** theory. The following points describe those features or consequences of the theory that are important in understanding galaxy formation.

- The Universe has a finite age, which is currently estimated to be about 14 billion years.
- The cosmic expansion that we see today, as implied by Hubble's law, has persisted since the earliest times, although the rate of expansion has not always had its current value.
- The physical conditions in the Universe at early times were characterized by extremely high temperatures and densities. However at any given instant, the density and temperature of matter throughout the Universe were highly, but not perfectly, uniform.
- As the Universe expanded and cooled, protons and neutrons (i.e. particles of 'ordinary' baryonic matter) formed from more fundamental particles (quarks). The number of protons exactly balances the number of electrons, which results in there being a net electric charge of zero on matter in the Universe.
- Within the first few minutes after the big bang, nuclear reactions resulted in the formation of helium nuclei. As a result of these reactions about 24% of the mass of baryonic matter was in the form of helium nuclei and about 76% in the form of hydrogen nuclei. Only very small traces of other light elements would have been produced.
- The matter that filled the early Universe also contained particles of non-baryonic matter. These account for the non-baryonic dark matter that now appears to be the dominant form of matter in galaxies.
- There has always been mutual gravitational attraction between all forms of matter (baryonic and non-baryonic) in the Universe.
- Despite its high degree of uniformity, the cosmic gas of baryonic and non-baryonic matter that filled the early Universe was subject to slight density fluctuations. In other words, there were regions of the early Universe where the actual density of matter departed slightly from the average.

2.5.2 The origin of galaxies

The basic idea of galaxy formation is that the slight density fluctuations which were present in the early Universe have grown under the influence of gravity. As the Universe expanded the average density of the cosmic gas would have declined. However, against this background of a declining average density, some density enhancements of sufficient size, such as those shown in Figure 2.31, became more pronounced, thanks to their own gravitational attraction. These attracted matter from surrounding regions, increasing still further the lumpiness of the Universe that evolved from the highly (but not perfectly) uniform distribution of matter in the early Universe. This process, known as **gravitational instability**, was therefore responsible for the production of localized regions in which clouds of cosmic gas collapsed despite the general background of expansion. It is these collapsing clouds which are supposed to have been the 'seeds' of the galaxies and clusters of galaxies that surround us now.

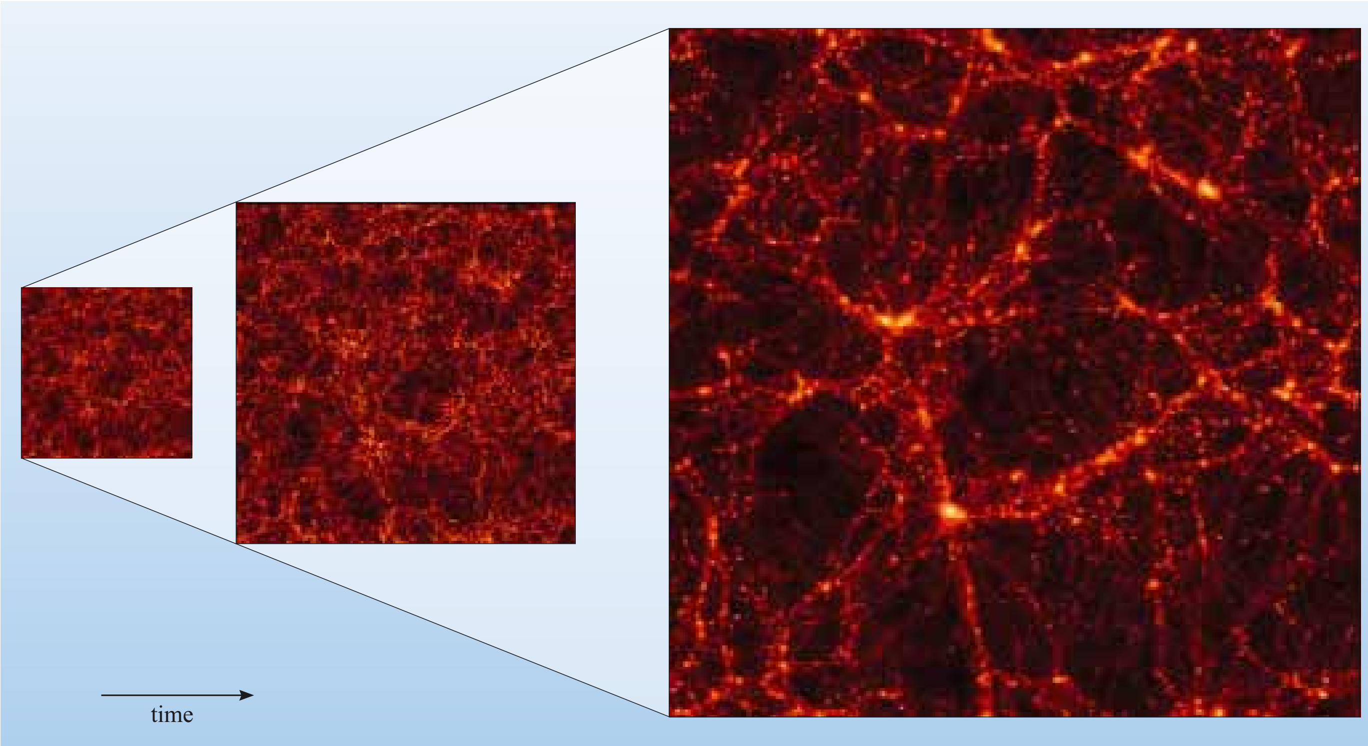

Figure 2.31 The effect of gravitational instabilities in a region of the expanding Universe dominated by dark matter. Regions of enhanced density tend to grow along with the general cosmic expansion, but if sufficiently dense they may eventually defy the expansion and collapse. In each case the number of particles in the region shown is the same and the particles themselves are a mix of baryons and dark matter particles. (Virgo Consortium)

So how did these collapsing clouds give rise to the galaxies that we see today? The simplest scenario for galaxy formation is that the collapse of a single over-dense region gives rise to a single galaxy. The mass contained in such a region would therefore correspond to the mass of the resulting galaxy. The mass would be mainly due to (non-baryonic) dark matter, but the region would also contain some baryonic matter, and this too would contribute to the galaxy. This baryonic matter would radiate away energy in ways that dark matter could not. Consequently, the baryonic matter settles into the centre of the dark matter halo, where it forms the visible part of the galaxy. This type of formation process is often referred to as a **monolithic collapse** scenario. As we see later this scenario has some attractive features, but at this point it is instructive to consider how the process of gravitational collapse is studied from a theoretical point of view, as this highlights other ways in which galaxies may have formed.

Since the way in which gravitational collapse proceeds depends on the distribution of mass, it is evident that the most dominant form of matter in the Universe – the dark matter – should play the key role in this process. The lack of knowledge about the nature of dark matter is essentially the largest uncertainty in understanding how gravitational collapse may have proceeded.

Astrophysicists have tackled this obstacle by making specific assumptions about the dynamical behaviour of the dark matter, and then investigating how a Universe that is dominated by this assumed form of dark matter would evolve. We return to discuss candidates for dark matter in Chapter 8, but we note here that it seems likely that the majority of the dark matter is in the form of fundamental particles that have yet to be detected. As you will see later, there are very good reasons for believing that the dark matter cannot consist of normal baryonic particles (protons, neutrons etc.).

At this point we consider the two extremes for the dynamical behaviour of dark matter as it affects the growth of gravitational instabilities. In one, dark matter consists of slow moving, massive particles. This kind of dark matter is referred to as **cold dark matter** (CDM). The term 'cold' refers to the fact that the hypothetical dark matter particles have random speeds that are small compared with the speed of light, and this condition has applied throughout most of the history of the Universe. Computer-based simulations of the progress of gravitational collapse, in a Universe dominated by CDM, reveal that the first structures to form have masses of order $10^6 M_\odot$ – lower than those typically found for galaxies (typically $10^{11} M_\odot$) in the present-day Universe. As time progresses, larger scale features develop by further collapse and by the merger of the lower mass structures that were formed previously. The overall picture is one in which proto-galactic fragments form early in the history of the Universe and many of the galaxies we see today are the result of mergers. This type of process is termed an **hierarchical scenario** or a **bottom-up scenario**, since galaxies are generally formed by the amalgamation of smaller entities.

The other extreme of behaviour is one in which the dark matter particles are rapidly moving, and goes by the name of **hot dark matter** (HDM). The term 'hot' refers to the condition that the dark matter particles have speeds that are comparable to the speed of light. One effect of these high speeds is to wash out small scale density fluctuations, leading to a distinctly different outcome from CDM models. A typical prediction of HDM models is that the first entities to form in the Universe would have much greater masses than individual galaxies. Structures with masses similar to present-day galaxies would form by the fragmentation of these larger entities. This type of process is called a **top-down scenario**. As we see in Chapter 4, there *is* structure on larger scales than individual galaxies – many galaxies exist within gravitationally bound clusters and within even more widely distributed large-scale structure. The major problem with HDM models is that in order to produce structures with masses that are typical of galaxies in the present-day Universe, they predict more structure on very large scales than is actually seen. Also, the notion that large-scale structure is formed before galaxies seems contrary to observation.

The currently favoured theory is that structure in the Universe formed in a bottom-up scenario under the influence of CDM. In such a scenario it is expected that the first objects formed might be very high-mass stars, followed by structures on the scale of globular clusters. Galaxies would form by the merging of these smaller components.

On large scales, the behaviour of matter is dominated by the effects of gravity – essentially, density enhancements grow by gravitational instability – and this behaviour can be modelled well in computer simulations. The greatest challenge in developing a theory of galaxy formation is to incorporate the physical effects that arise once star formation starts in the Universe.

■ Apart from gravitational attraction, name three processes associated with massive stars that have an influence on the environment around these stars. What sort of effects do these processes have?

❏ Massive stars emit high-energy photons that are capable of ionizing any neutral gas nearby. Strong stellar winds from supergiants, and the supernovae that end the lives of some supergiants, have dynamical effects on any nearby material. Supernovae also result in a dramatic heating of the local interstellar medium as well as causing chemical enrichment.

The processes that occur on the scale of individual stars are believed to have an important effect on how galaxies form, but these effects are, as yet, very poorly understood and difficult to incorporate into computer simulations. For instance, shock waves from early supernovae could compress gas clouds and trigger further star formation. On the other hand, the kinetic energy released by many supernova explosions could also have the effect of removing interstellar gas from proto-galaxies, and this could inhibit further star formation. Predictions of what would happen in this kind of complicated situation could, in principle, be made by a computer simulation that follows gas flows and individual stars within a galaxy. Unfortunately such a level of detail is far beyond the capabilities of even the most powerful computers available at present. Despite this limitation, some progress has been made by carrying out numerical simulations in which the overall effects of such processes are estimated. Such work seems to reproduce some of the gross features of galaxies that we see in the present-day Universe, but is far from being able to offer a complete description of the process of galaxy formation.

At present, models of galaxy formation cannot predict morphological types. There are, however, some general principles that are believed to hold. Simulations show that when a galaxy is formed by a merger, then the morphology and the distribution of stellar velocities is as expected for an elliptical galaxy. This, then, seems to fit well with the hierarchical scenario of galaxy formation.

The formation of spiral galaxies is much more problematic within a hierarchical scenario. To appreciate why this is so, it is useful to consider the monolithic collapse scenario in more detail. This scenario, in which a single cloud collapses to form a galaxy, provides a plausible account of the formation of spiral galaxies. If we consider an over-dense region that has acquired angular momentum from interactions with its neighbours, then collapse in the central parts would occur very rapidly to form a spheroidal distribution of stars that corresponds to the halo of the galaxy. However, in the outer parts of the collapsing region the orbits of gas clouds would intersect in the plane of rotation of the entire system. Collisions of such clouds would dissipate energy, leaving a thin rotating disc of gas.

This mechanism for forming a disc does not arise naturally in the scenario in which galaxies are formed purely by hierarchical growth. It has already been noted that the outcome of a merger between two or more galaxies is likely to be an elliptical galaxy. This is the case even if both the galaxies involved in a merger are spirals.

One solution that has been proposed to this problem is a scenario which combines elements of both the hierarchical growth and the monolithic collapse models. As in the hierarchical scenario, mergers produce elliptical galaxies of ever increasing mass. However, there is also a long-term in-fall of gas from the environment surrounding these galaxies. If this gas has sufficient angular momentum, it forms discs around what were previously elliptical galaxies, thus transforming them into lenticular or spiral galaxies. Of course, at any time any two galaxies may undergo a merger, and thus form a new elliptical galaxy. An attractive feature of this scenario is that it provides a plausible explanation for the similarity of the elliptical galaxies and nuclear bulges of spiral galaxies – they are essentially the same structures, but in the case of a spiral a disc has grown around the nuclear bulge. The essence of this scheme is summed up in Figure 2.32, which shows a schematic history of a giant elliptical galaxy. Such a diagram, which illustrates how a galaxy is formed from the coalescence of many smaller galaxies, is termed a **merger tree**. At the time when this sequence starts – at the top of the tree – there are many low-mass

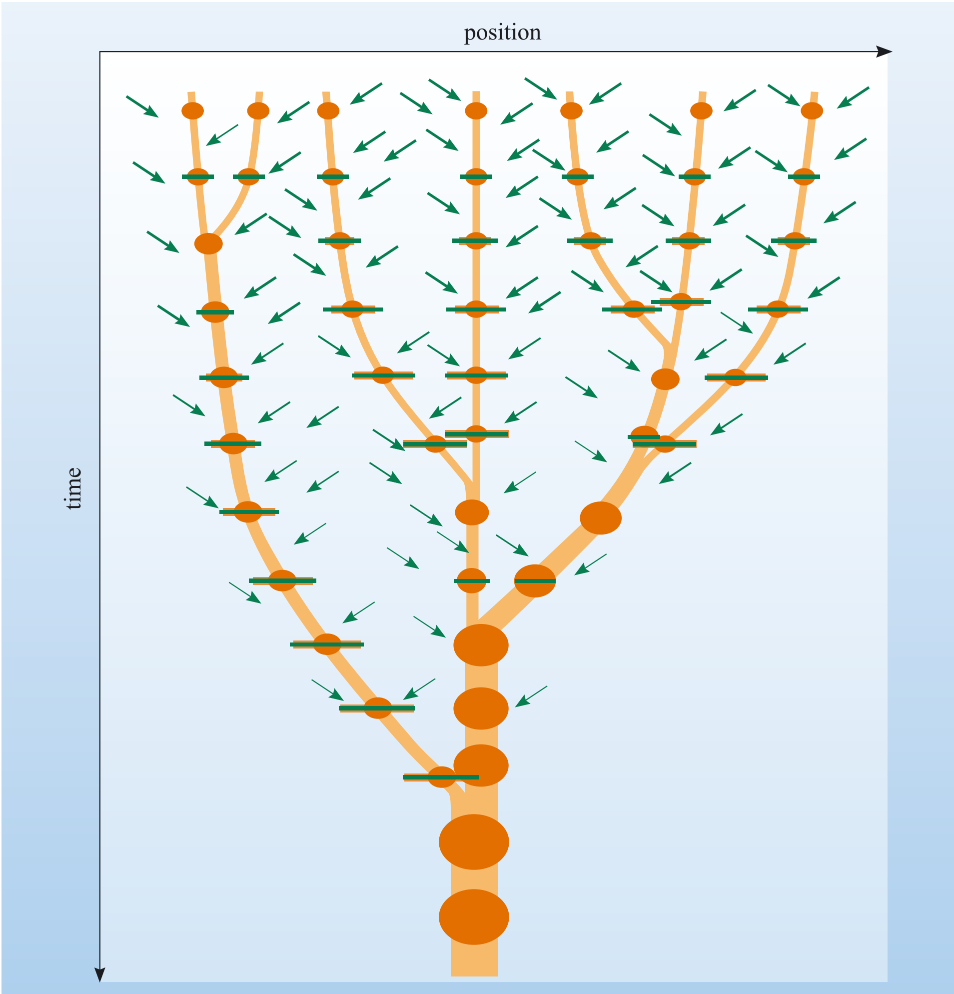

Figure 2.32 A 'merger tree' that shows the schematic history of the formation of a single giant elliptical galaxy by the merger of many smaller galaxies. The stellar content of galaxies is shown in dark orange and neutral gas is indicated in green. The result of every merger event is an elliptical galaxy. The longer an individual galaxy goes without a merger (those on the longest 'branches') the more substantial is the disc that develops by in-fall of intergalactic gas. Note also that as time passes, the density of intergalactic gas decreases, so discs grow more slowly at later times. (M. Merrifield (University of Nottingham))

elliptical galaxies in an environment that has a relatively high gas density. As time progresses, two types of process occur: there is a gradual in-fall of gas that forms discs, and there is a series of rapid merger events. The diagram indicates how the development of a disc depends on the time between merger events – a galaxy that has not undergone a merger for a long time is likely to develop a substantial disc. When a merger event occurs, an elliptical galaxy forms and all traces of the discs are wiped out. Furthermore, as time passes, the gas that originally surrounded these galaxies ends up within the galaxies. Thus the density of the intergalactic gas drops and so the rate at which discs form becomes slower with time. This view of galaxy formation clearly has some attractive features, but is should be stressed that it is currently regarded as a plausible scenario rather than a fully accepted theory.

In this subsection we have concentrated on the ideas of how galaxies may have formed from an initially almost completely smooth distribution of matter, and we have found that progress towards a full understanding of galaxy formation is hampered by a lack of understanding of the process and effects of star formation. In the remainder of this section we discuss how studies of the evolution of observable galaxies may allow astronomers to 'wind back the clock' and hence shed some light on the process of galaxy formation.

2.5.3 The evolution of isolated galaxies

The hierarchical scenario of galaxy formation suggests that interactions and mergers of structures smaller than galaxies must have occurred in the past. Hence the evolution of galaxies will depend both on those changes that are due to interactions and on those that are intrinsic to the galaxy itself. Since evolution of isolated galaxies and merger events are likely to have quite distinct observational consequences, we treat these two topics separately. Here we consider how an isolated galaxy might evolve with time, while interactions are the topic of the next section.

Cosmic rays are high-energy particles, probably accelerated by supernovae and other such energetic processes.

Consider a hypothetical galaxy that has already formed and exists as a vast collection of stars, suffused by gas, dust, magnetic fields, cosmic rays and radiation, all embedded in an overwhelming amount of dark matter. How would such a galaxy evolve?

There are at least two important ways in which an isolated galaxy evolves. The study of each has become a specialized sub-field of galactic astronomy. Each is briefly described below.

Evolution of luminosity and spectra

Since the luminous output of galaxies is essentially the sum of the luminous output from its stars, the way in which the luminosity of a galaxy varies with time depends on two factors.

1 The star formation rate (SFR), which is usually quoted as mass of stars formed per year.

2 The luminosity evolution of the stars that are formed within the galaxy.

It is usually assumed that when stars form, the distribution of their masses follows a pattern that is similar for all galaxies. Although the exact distribution of masses remains an area of active research, its approximate form is reasonably well known. Since the evolution of stars of different masses is well understood, it would be possible to calculate the luminous output of a galaxy if the total rate at which stars were formed throughout the history of the galaxy was known.

■ From the information given in Section 2.2, do you think that the star formation rate would be the same for elliptical and spiral galaxies?

❏ No. Spiral galaxies have a relatively high gas content and are sites of ongoing star formation. Elliptical galaxies are devoid of cold gas and show little sign of recent star formation, so their stars must have formed early in their evolution.

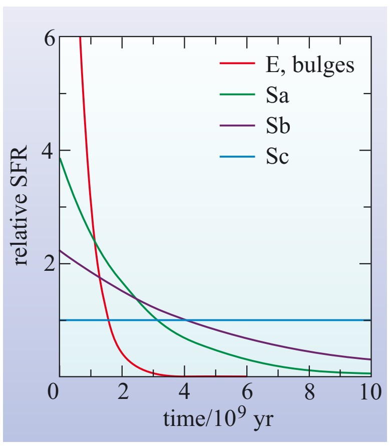

Figure 2.33 A schematic illustration of the star formation rate (SFR) as a function of age for galaxies of different types. Note that the time elapsed is the time since the event that formed the galaxy. The curve that represents the star formation rate in elliptical galaxies and the bulges of spiral galaxies is rather uncertain – the curve shown here should simply be taken as an indication that star formation in such systems took place as a rapid burst. (Kennicutt, 1998)

This qualitative difference in star formation rates between spiral and elliptical galaxies is borne out by more detailed studies. Figure 2.33 shows estimates of the star formation rates in ellipticals (and the bulge regions of spirals), and in the discs of spirals of types Sa, Sb and Sc. From this diagram it can be seen that the star formation rate in ellipticals (and bulges of spirals) was initially very high, but that it declined very rapidly. In fact, because star formation has effectively ended in elliptical galaxies, observational data concerning the star formation rate in such systems are very scarce.

The curve shown in Figure 2.33 for elliptical galaxies and bulges should be treated with some caution. It is clear that star formation has essentially stopped in such systems, and it is likely that there was a rapid burst of star formation at the time that the galaxy formed. It is this burst of star formation that is shown in Figure 2.33. However, if ellipticals are formed as the result of mergers, then it is likely that many stars in such galaxies would have been formed prior to the merger event. Thus it may be expected that the history of star formation in elliptical galaxies may be quite complicated, and the only definitive statement that can be made is that no new stars are being formed in these galaxies.

In contrast to ellipticals, the star formation rate in the discs of spiral galaxies declines much more slowly after the formation of the galaxy. There is also a clear progression for different morphological types in that the star formation rate drops relatively quickly for type Sa galaxies, but is essentially constant for type Sc galaxies. Sb galaxies show intermediate evolution in star formation rate. Note that no curve is shown for irregular galaxies since the star formation rate in these systems is difficult to ascertain. However, it should be noted that at the present epoch many irregular galaxies do have high star formation rates.

Except for the discs of Sc galaxies (and perhaps irregulars), the star formation rate of any galaxy will fall with time after the formation of that galaxy. Thus young galaxies might well have been highly luminous and were probably rather blue.

■ Why might you expect a galaxy filled with young stars to be blue?

❑ The luminosity of a youthful population is usually dominated by the luminous blue stars at the upper end of the main sequence.

This expectation is borne out by the so-called **Butcher–Oemler effect**. When very distant clusters of galaxies (where we are observing light that was emitted when the Universe was much younger than its present age) are compared with those nearby, and the effects of red-shift are taken into account, the distant clusters have a higher proportion of blue galaxies.

QUESTION 2.12

If all the stars in an elliptical galaxy formed in a single massive burst of star formation when the galaxy was very young, how would you expect the luminosity and colour of the galaxy to evolve subsequently?

In order to carry out a proper analysis of the evolution of the luminosity of a galaxy, it is necessary to model the rate at which stars of various types formed and died throughout the history of that galaxy. Then, using theoretical models of the evolution of each type, it is possible to calculate how the luminosity and the spectrum of the entire galaxy would evolve with time. Comparing these calculations with observations allows models of galactic formation and evolution to be tested and refined.

■ When comparing evolutionary predictions with the properties of observed galaxies, is it ever possible to observe the evolution of a single galaxy? If not, how can such comparisons be handled?

❑ Galaxies evolve too slowly for changes in any one galaxy to be seen. By looking at many galaxies it may be possible, as in the case of stars, to observe similar individuals at different stages in their evolution.

Although this approach has led to some advances in understanding the evolution of galaxies, the interpretation of observational data is far from straightforward. In particular, there is very little information to help astronomers to put these ‘snapshots’ of individual galaxies into an evolutionary sequence.

Chemical evolution

The first stars, formed from the cosmic gas that filled the early Universe, should have consisted almost entirely of hydrogen and helium (in the terms used in Chapter 1, these would have been stars belonging to Population III). As these stars burnt themselves out, some would have exploded in supernovae, enriching their surroundings with the products of nuclear fusion. This enriched material would have contributed to the formation of later generations of stars which would, consequently, have had a higher metallicity than the earliest stars. As this process continued, both the interstellar matter in a galaxy and the stars that were embedded in it would gradually change their chemical composition. The abundance of hydrogen would slowly decrease over time, whereas the abundances of helium and heavy elements would gradually increase.

■ Apart from supernovae, what other processes would you expect to contribute to the chemical enrichment of the interstellar medium?

❑ Apart from supernovae, all the other processes that cause stars to expel matter might be of relevance: stellar winds, the formation of planetary nebulae, and novae.

The study of chemical evolution is another highly technical field, particularly for spiral galaxies such as the Milky Way, where rates of star formation, and hence (presumably) of chemical enrichment, vary from one region to another. On the basis of chemical evidence it is possible to derive models for the changing rate of star formation, at least for the solar neighbourhood. These models depend on the extent to which matter from outside the Milky Way may have settled into the disc over time. This type of study may eventually help to establish whether it is likely that the discs of spiral galaxies developed from the gradual in-fall of material as outlined in Section 2.5.2.

2.5.4 The role of interactions and mergers in galaxy evolution

We have already seen that the favoured scenario for the formation of galaxies is one in which mergers and interactions play an important role, and here we look in detail at the observational consequences of such events. The numbers of galaxies that currently seem to be undergoing interactions is rather low – only a few per cent of bright ($L > 10^{10} L_\odot$) galaxies. However, observational interest in these galaxies was heightened by the discovery that they tend to be sites of intense star formation.

Theoretical work on interactions began in the 1970s, when two Estonian brothers working in America, Alar and Juri Toomre, published the results of various simulations of **interacting galaxies**. The Toomres were soon followed by others, and a new field of research quickly developed, aided by the availability of ever-larger computers. Some frames from one particular Toomre simulation are shown in Figure 2.34b (overleaf), and the corresponding astronomical object – the so-called 'Antennae galaxies' (NGC 4038 and NGC 4039) – are shown in Figure 2.34a. As you can see, the relevance of the simulation to the real world seems apparent and undeniable. Other peculiar systems have also been modelled with great success.

The widespread recognition that interactions might be of much more general importance followed the 1983 discovery, by the Infrared Astronomical Satellite (IRAS), that many galaxies shine more brightly at infrared wavelengths than they do at visible wavelengths. Enhanced infrared emission is frequently associated with interacting galaxies. It is believed that the interactions promote star formation. This gives rise to a population of high luminosity O and B type stars and hence HII regions. The ultraviolet radiation from the hot stars is absorbed by dust in the interstellar medium, which then re-radiates this energy in the infrared. A schematic illustration of this is shown in Figure 2.35. Galaxies that show evidence for very high current rates of star formation are termed **starburst galaxies**, and many of these systems appear to be galaxies that are undergoing or have recently undergone some type of interaction or merger.

Figure 2.36 shows the results of an observation of the Antennae galaxies made using the Infrared Space Observatory (ISO). Contours of infrared emission (at 15 μm) are shown overlaid on a Hubble Space Telescope image of the central regions of the interacting pair (a larger scale optical image of the galaxies, with their tails, is inset at the top right of the figure). One of the surprising features is that the peak of the infrared emission occurs at a different location from the maximum optical emission. In fact, about half of the entire luminosity of this system is radiated in the infrared from the region that appears dark on the optical image. This shows that not only is the UV light from young stars reprocessed by dust, but that the dust completely shrouds the intense star forming regions.

The reprocessing of stellar UV radiation by interstellar dust has dramatic consequences for the observation of galaxies in which intense bursts of star formation are going on. The dust absorbs UV and visible light from stars but it re-radiates all this energy as far-infrared radiation. So observations of interacting galaxies at the present time suggest that bursts of star formation may result in galaxies that appear to be very strong sources in the far-infrared, and may not be particularly strong sources in the UV and visible bands.

It has already been noted in Section 2.5.2 that numerical simulations suggest the outcome of a merger between two galaxies will be an elliptical galaxy, but to what extent is this borne out by observations? Of course, galactic mergers occur over a very long timescale, typically taking tens to hundreds of millions of years, so there is no possibility of observing an individual galaxy changing as a result of a collision. However there are galaxies that show evidence of collisions that took place in the past, and these provide key evidence to support the idea that ellipticals can be formed by mergers.

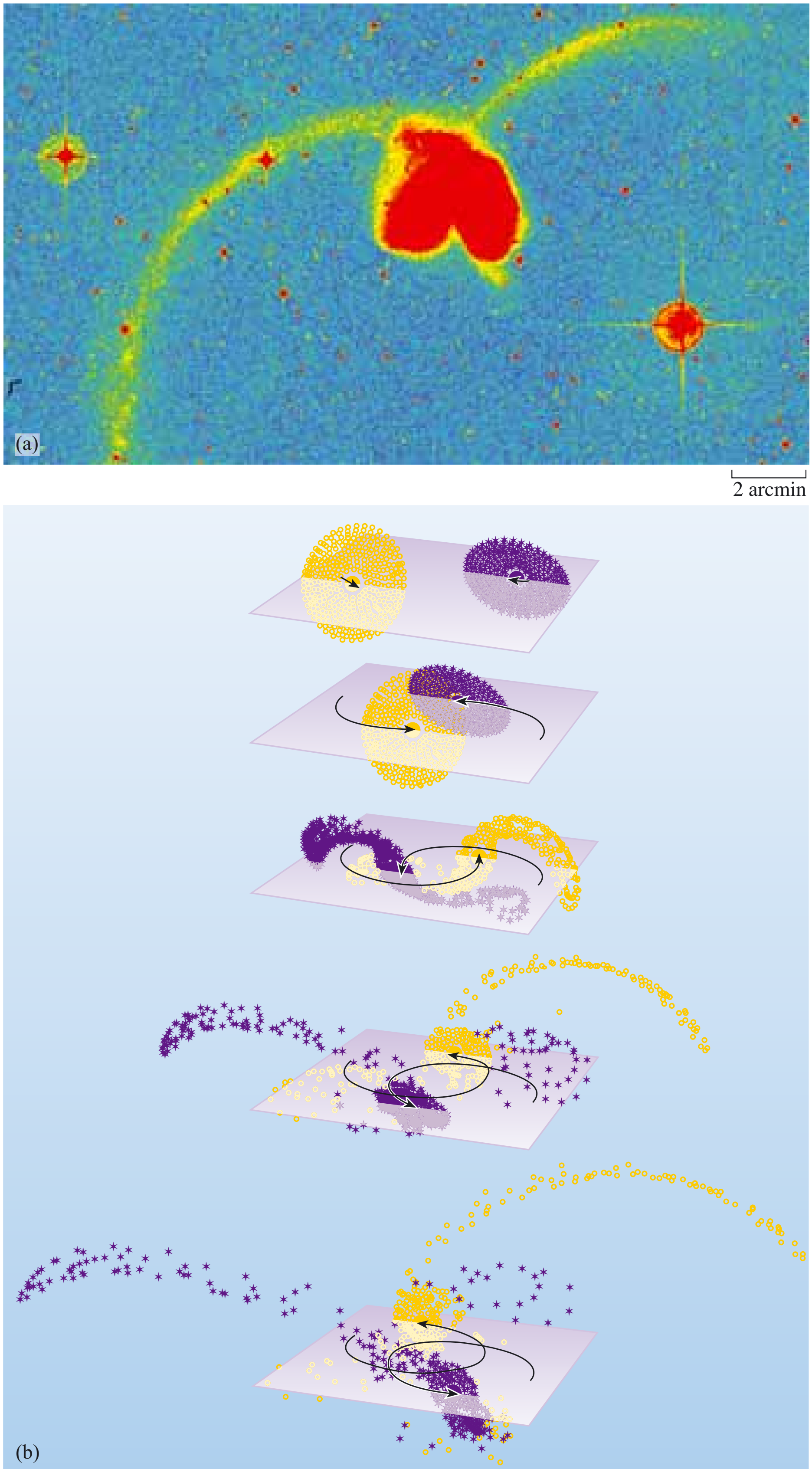

Figure 2.34 (a) The galaxies NGC 4038 and NGC 4039 are a colliding pair that go under the name of the Antennae galaxies. (b) A sequence of 'snapshots' from the pioneering numerical simulation carried out by Alar and Juri Toomre that successfully reproduces the main features of the Antennae galaxies. In the simulation, the colliding galaxies are represented by discs of stars, with each star interacting gravitationally with all the other stars in the simulated galaxies. The gravitational interaction of the two galaxies produces the 'tidal tails' of stars that account for the 'antennae' of NGC 4038 and NGC 4039. ((b) A. Toomre (MIT) and J. Toomre (University of Colorado))

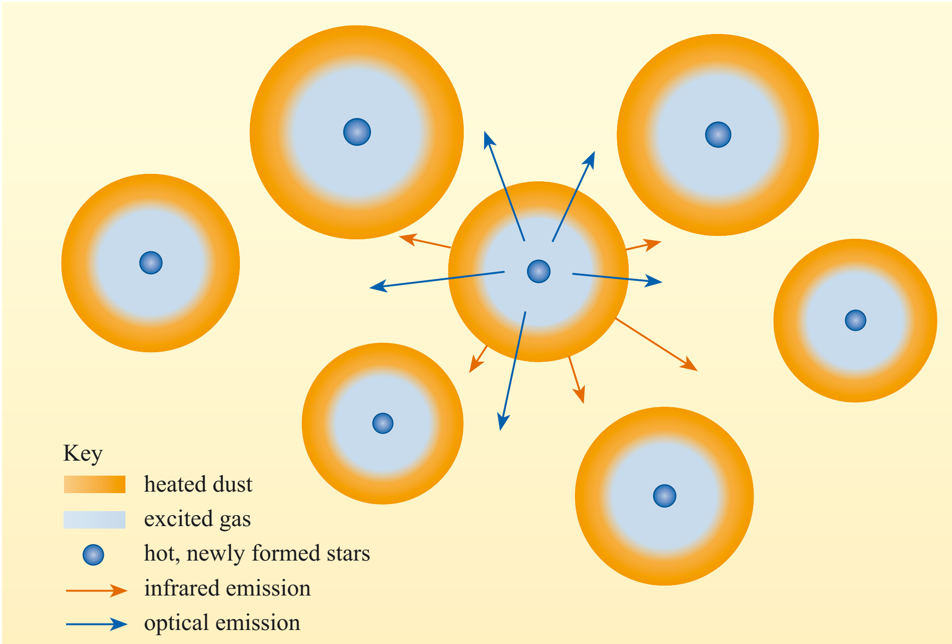

Figure 2.35 A schematic diagram of HII regions and dust in a starburst galaxy.

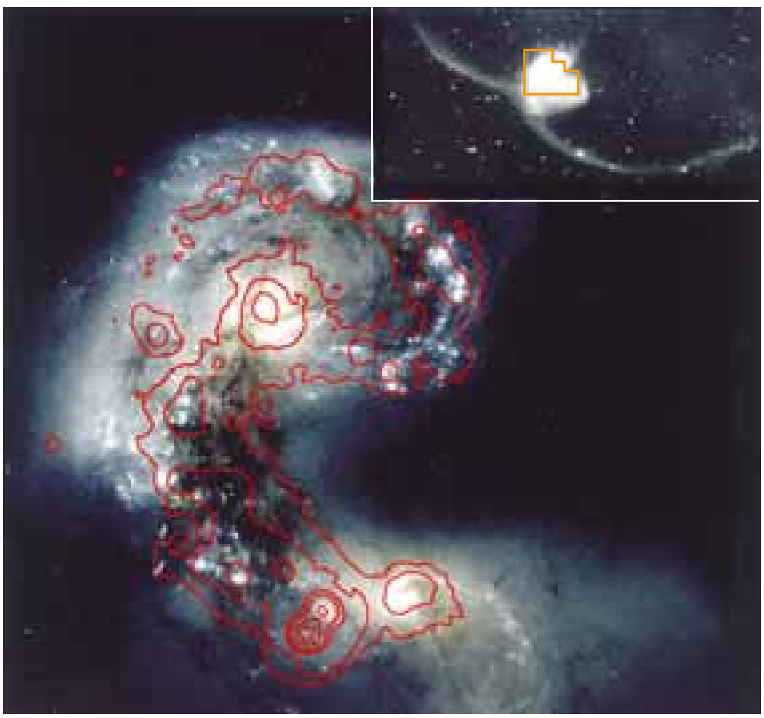

Figure 2.36 The Antennae galaxies, NGC 4038 and NGC 4039. The main image shows the infrared emission at 15 μm (as measured using the Infrared Space Observatory) as red contours that are overlaid on optical image (obtained with the Hubble Space Telescope). The inset image at the top right is a large-scale optical image that shows the full extent of these interacting galaxies and their distinctive tails. The orange outline in the inset image shows the field of view of the Hubble Space Telescope that is shown in the main image. (Mirabel *et al*., 1998)

A galaxy that appears to have undergone a merger event in the past is NGC 7252. On the basis of a short exposure image it might be classified as an elliptical galaxy (Figure 2.37a). However a longer observation reveals different picture: the low surface brightness parts of the galaxy show evidence of peculiar structure in this galaxy. In particular, there are long tails which are a tell-tale sign of a past collision (Figure 2.37b). Detailed studies of NGC 7252 reveal that the collision was between two spiral galaxies, and suggest that it is in the process of becoming an elliptical galaxy.

Historically, it was only morphologically peculiar galaxies that could easily be identified as systems that had undergone interactions and mergers. In the 1990s, however, developments in instrumentation opened up the possibility of detecting the aftermath of interactions in galaxies with apparently normal morphologies. The principle behind such studies lies in the fact that the stars from two interacting galaxies often retain distinctly different kinematic properties. In order to carry out such studies, a special type of instrument is used to map the spectrum at hundreds of locations over the face of a galaxy.

An example of a galaxy that has undergone a merger event, but shows no structural trace of interaction, is the galaxy NGC 4365. Figure 2.38a shows the surface brightness distribution of the galaxy, which appears to be a normal elliptical of type E3. By measuring the spectrum over the face of the galaxy a map can be formed that shows stellar velocities. This map is shown in Figure 2.38b; the blue areas represent regions in which stars are moving towards us and the red areas are where stars are moving away from us. In the outer part of the galaxy it appears as though the system is rotating around the long axis of the galaxy. However, in the inner parts of the galaxy the stars are rotating around the short axis. This strongly suggests that the galaxy was formed by the merger of two systems that had axes of rotation that were roughly perpendicular to one another. The map of spectra can also be used to study the stars that make up these two components, and it is found that the stars in both parts of the galaxy appear to have the same age, which is estimated to be in excess of 12×10^9 years. The inference drawn from this is that an ancient merger event caused a burst of star formation throughout the entire galaxy. While individual cases cannot prove that all elliptical galaxies formed by mergers, studies of this kind do lend support to the view that galaxy formation is the result of a hierarchical process.

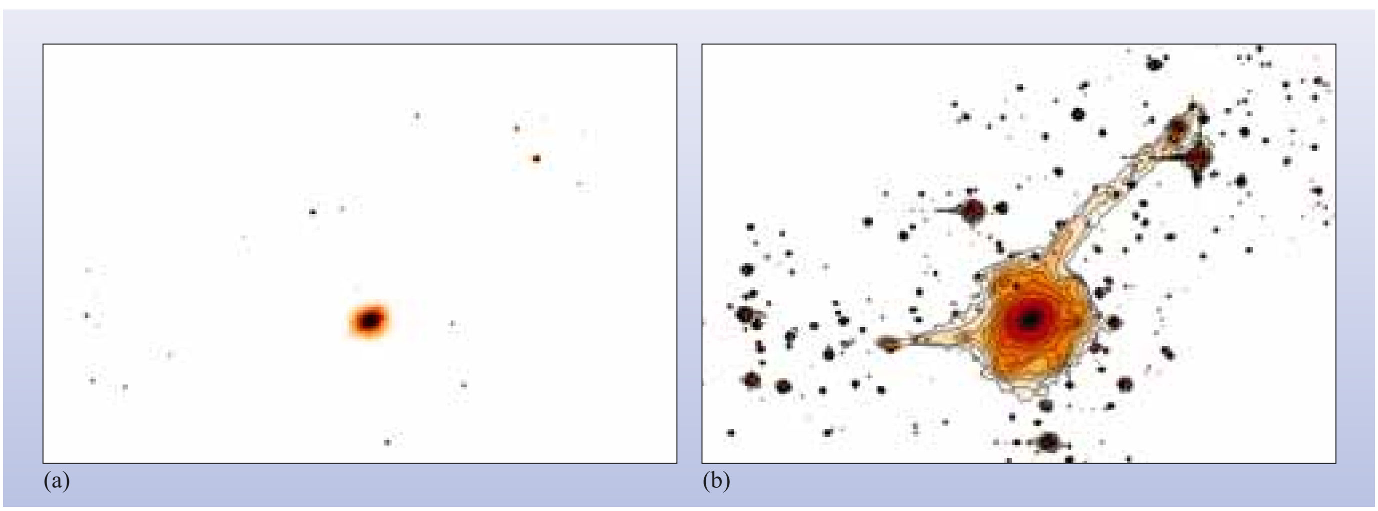

(a) (b)

Figure 2.37 The merger galaxy NGC 7252. Both images show the same field of view, but are sensitive to different levels of surface brightness. (a) Shows the brightest features of the galaxy (this is equivalent to taking a relatively short exposure photograph). In this image the galaxy appears as an elliptical. (b) Shows features at very low surface brightnesses (this corresponds to taking a relatively long exposure photograph). The features visible at low surface brightness show that the galaxy has undergone a merger event. (Data provided by NASA/IPAC Extragalactic Database from the observations of Hibbard *et al*., 1994)

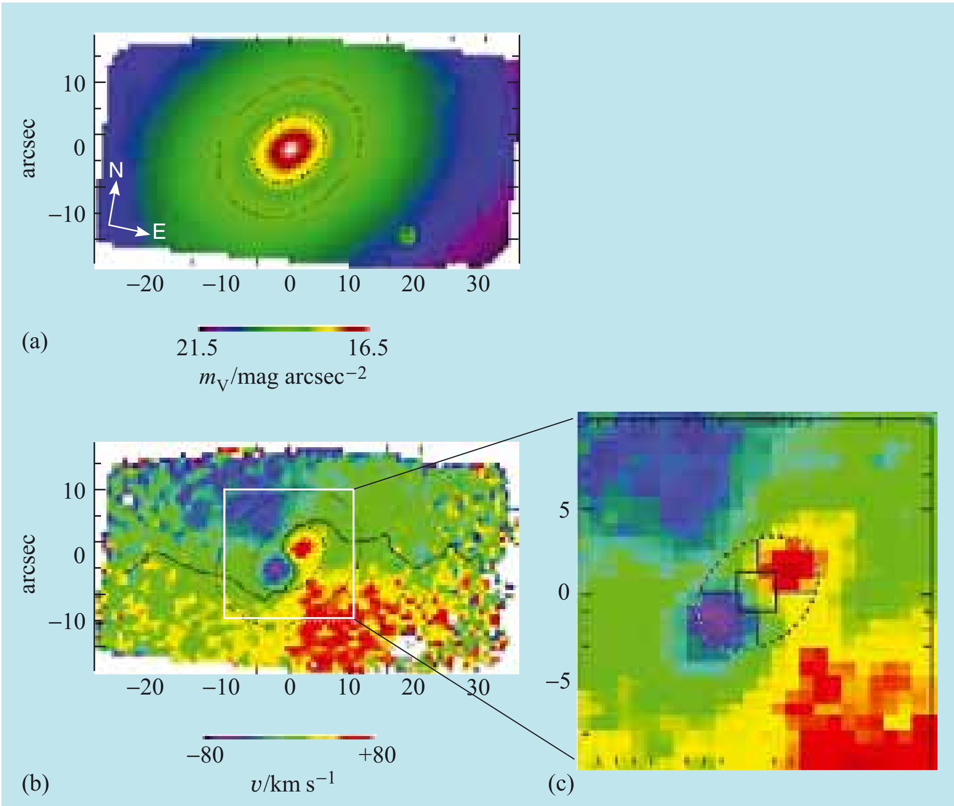

Figure 2.38 Observations of the galaxy NGC 4365. (a) The surface brightness distribution. (b) A velocity map of the same area as shown in (a), blue represents motion towards the observer and red is motion away from the observer. The colours indicate that the outer part of the galaxy is rotating around its long axis, while the inner region is rotating around an axis that is almost perpendicular to the long axis. (c) An enlarged view of the centre of the field of (b). (Davies *et al*., 2001)

2.5.5 Observations of galaxy evolution by deep surveys

The most direct test of ideas of galaxy evolution is to make the most sensitive survey possible of a patch of sky well away from the plane of the Milky Way. If the field chosen is relatively free from any bright foreground stars or nearby galaxies then such a survey should detect galaxies over a range of redshifts. Sensitive surveys of this kind that include galaxies with large redshifts are known as **deep surveys**. You have already seen (Equation 2.12) that the redshift of a galaxy is related to its distance. The larger the redshift of a galaxy, the more distant it is, and hence the longer it has taken for the light that we observe to get to Earth. So the higher the redshift of a galaxy the earlier in the history of the Universe its light was emitted. The relationship between the time at which light was emitted by an object and its redshift depends on the way in which cosmic expansion has proceeded, and this in turn depends on factors such as the average density of matter in the Universe. As you will see in Chapter 7, there remains some uncertainty in the determination of such factors (or *cosmological parameters*), but it is thought that the time of emission of light and the observed redshift should be related by a curve similar to that shown in Figure 2.39. Note that in this diagram the time of emission $t(z)$ is expressed as a fraction of the current age of the Universe t_0, that is, the age of the Universe at the time of emission divided by the age of the Universe at present. Thus it can be seen that a galaxy with a redshift $z \approx 1$ corresponds to emission at a time when the Universe was only about 40% of its current age.

One of the best-known deep surveys was conducted using the Hubble Space Telescope, and goes by the name of the Hubble Deep Field (HDF). The HDF actually consists of two fields, one in the northern hemisphere (HDF-N) and

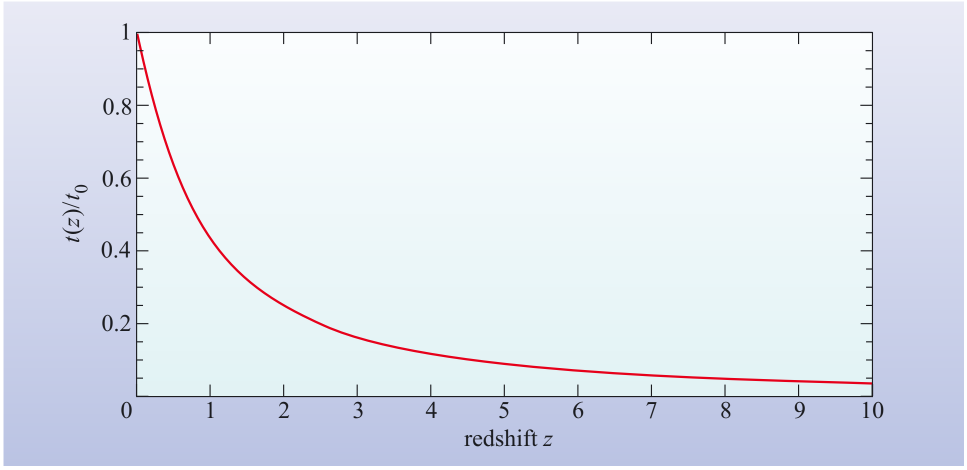

Figure 2.39 The relationship between the redshift, z of a galaxy and the time $t(z)$ at which the light now being observed from that galaxy was emitted. Note that the time of emission is expressed as a fraction of the current age of the Universe, t_0. Also note that there is some uncertainty in this relationship, but the curve shown is believed to be approximately correct.

another in the south (HDF-S). Both fields were first observed in the mid to late 1990s and will continue to be observed as new instruments are fitted to the Hubble Space Telescope. The image obtained for HDF-N is shown in Figure 2.40; it shows only some of the thousands of galaxies that were detected.

The HDF surveys include many galaxies with redshifts between 1 and 3, and there are a few galaxies detected in the field that have redshifts greater than 5.

Figure 2.40 The northern Hubble Deep Field (HDF-N). The field is located in the constellation of Ursa Major. The field of view is about 2.5 arc minutes across. (R. Williams and the HDF team (STScI)/NASA)

- What, approximately, was the fractional age of the Universe when light was emitted from galaxies that are now observed with a redshift of 5?
- From Figure 2.39, a redshift of 5 corresponds to fractional age of 0.1, that is, a time when the age of the Universe was just 10% of its current age.

Thus the HDF surveys provide a window back over cosmic history. The data from these surveys should provide information about various aspects of the way in which galaxies have evolved over the history of the Universe.

While the principle behind the observations is essentially simple – the observations are long exposures of seemingly blank fields – the interpretation of the image data is not at all straightforward. There are many difficulties in dealing with data from such surveys: not because the observations or instruments are flawed, but because the observations are at the limit of what can be achieved with current technology. One difficulty is that many of the observed sources have very low flux densities. As a result, most of galaxies in the HDF are too faint for their spectra to be measured, even using the largest available telescopes. This has meant that astronomers have had to develop techniques by which the redshift of a galaxy can be estimated from its broadband colours. A second major problem is that even though the Hubble Space Telescope has excellent angular resolution, many galaxies are only just resolved, so the task of determining their morphological class is very difficult.

Another type of problem arises because of the high redshifts of the galaxies that are observed in the HDF. The relationship between the observed and emitted wavelengths and the redshift z of a galaxy is given by Equation 2.11. This can be rearranged to give

$$\lambda_{\text{em}} = \frac{\lambda_{\text{obs}}}{(1+z)} \tag{2.14}$$

- A galaxy with $z = 1$ is observed at a visual wavelength of 500 nm. At what wavelength was this light emitted? In what part of the spectrum is this?
- Using Equation 2.14, the emitted wavelength was $\lambda_{\text{em}} = 500\,\text{nm}/(1+1) = 250\,\text{nm}$. This corresponds to the ultraviolet part of the electromagnetic spectrum.

Thus the observed visual images of many galaxies in the HDF actually correspond to their appearance in the ultraviolet. This effect – that the observed image corresponds to emission at a quite different wavelength – is often referred to as **band-shifting**. Ultraviolet emissions from galaxies tend to be dominated by the radiation from massive, short-lived stars. So basing the morphological classification of a high redshift galaxy on a visual image can result in the galaxy being assigned to an inappropriate morphological class.

Despite these and other difficulties in interpreting the Hubble Space Telescope data, some results are beginning to be accepted by the wider astronomical community. Here we concentrate on two results from the HDF.

Morphological change with redshift

A well-accepted result from the Hubble Deep Field survey is a confirmation of the explanation of the Butcher–Oemler effect that was mentioned in Section 2.5.3. At high redshifts, clusters of galaxies do seem to contain a much higher proportion of blue galaxies (which turn out to be spirals) than do clusters in the nearby Universe.

One of the more controversial results from the HDF observations is that the proportion of galaxies that are irregular or peculiar was much higher in the past than it is in the present-day Universe. Although the percentage of all galaxies that are irregular at the present epoch is quite high (maybe as much as 15%, see Table 2.1), the majority of these irregulars have low luminosities. The proportion of bright galaxies – those with a luminosity similar to that of the Milky Way – that are irregular or peculiar at the current epoch is only a few per cent and certainly less than 7%. The HDF reveals a fraction of luminous irregular and peculiar galaxies that appears to be in excess of 25%. Although it is possible that this result has arisen because of the problem of band-shifting described above, another interpretation is that we are observing the Universe at a time when mergers and interactions were far more frequent than they are at present. This would be expected if hierarchical merging had an important role in galaxy evolution. However, at the time of writing, a detailed understanding of these observations is far from complete, and they continue to be an area of active research.

The star formation history of the Universe

Deep surveys provide a way of investigating how the star formation rate within galaxies has varied over the history of the Universe. We have already seen that bursts of star formation result in the creation of stars across a wide range of masses. The luminous output from a star forming region is dominated by the emission from high-mass stars. Thus the ultraviolet luminosity of a galaxy may be used to provide a measure of its star formation rate. If a survey is made of star formation rates of galaxies as a function of their measured redshift, then it is possible, in principle, to determine how the rate of star formation has varied with cosmic history. This type of work was in progress prior to the HDF observations, but surveys with the Hubble Space Telescope provided vital information for extending such work to high redshift. The results from such studies are shown in Figure 2.41, which plots the star formation rate (as determined by UV luminosities of galaxies) against redshift (and fractional age of the Universe as described by Figure 2.39).

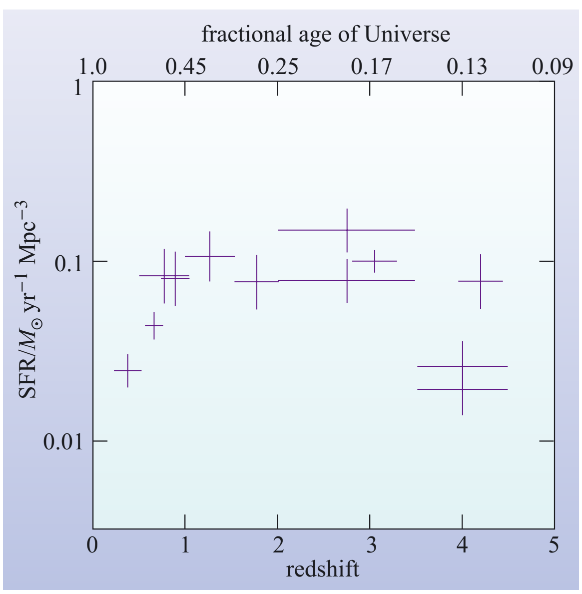

Figure 2.41 The star formation rate as a function of redshift *z* (lower axis) and the fractional age of the Universe (upper axis). The star formation rate is defined as the mass of stars that are formed per year in a volume that is currently 1 Mpc^3. Because of the expansion of the Universe, a volume that currently encloses 1 Mpc^3 would have been smaller in the past: the star formation rate shown here takes this change in volume into account. The diagram shows results from different types of measurement, and it should be noted that different techniques can give quite different estimates of the star formation rate at a given epoch. The bars drawn through each data point indicate estimated uncertainties. Such a diagram is often referred to as a 'Madau plot' after the astronomer Pierro Madau who first suggested its use. (Adapted from Ferguson *et al*., 2000)

- What is the potential problem in determining star formation rate from the UV luminosities in galaxies?

- The UV luminosity may not be a good tracer of the star formation rate. We know from studies of starburst galaxies in the local Universe that intense bursts of star formation are often shrouded in dust. Consequently, when observing regions where the star formation rate is high, much of the emerging radiation may be in the far-infrared.

Attempts have been made by researchers to account for the effects of dust in star forming galaxies in generating diagrams such as Figure 2.41, although it should be noted that the effects of dust in star forming galaxies are an issue of contentious debate in the astronomical community.

There are two key features of Figure 2.41. First, the current ($z = 0$) rate of star formation is substantially lower than it was in the past. At the present epoch, the star formation rate is about ten times lower than it was at redshift $z \sim 1$. Although Figure 2.41 seems to indicate that the star formation rate was at a maximum between $z = 1$ and 3, it should be noted that the high redshift data points are very sensitive to assumptions made about the effects of dust, and it may well be that the peak star formation rate occurred at redshifts greater than 3.

Secondly, this diagram potentially gives information about the formation rate of galaxies with cosmic history. We saw in Section 2.5.3 that the evolution of star formation rates in different types of galaxies is approximately known (Figure 2.33). Astronomers are therefore able to model the star formation rate in the Universe over cosmic history by making assumptions about the times of formation, and relative proportion, of different types of galaxy. The results of such modelling show that the star formation history of the Universe is consistent with galaxies being formed by interactions and mergers over a long spread of time. One scenario that seems to be ruled out is the idea that galaxies were formed at one single time in the history of the Universe. Thus the results of studies of the star formation rate in the Universe also seem to support the hierarchical model of galaxy formation.

2.6 Summary of Chapter 2

Morphology

- Mainly according to their shape, most galaxies can be assigned to one of four different classes: elliptical, lenticular, spiral or irregular.
- In the modified form of the Hubble classification scheme, shown in Figure 2.2, the spirals and lenticulars can be subdivided into barred and unbarred subclasses. The spirals can be further divided into a number of Hubble types. The ellipticals are also divided into a number of Hubble types.
- Irregular galaxies are generally chaotic and asymmetric, although some exhibit a bar and others show some traces of spiral structure.
- Over 60% of galaxies are elliptical, fewer than 30% are spiral, and fewer than 15% irregular. Dwarf ellipticals are the most common type.

Physical properties of morphological classes

- Elliptical galaxies are essentially ellipsoidal distributions of old (Population II) stars, almost devoid of cold gas and dust. Their three-dimensional shape is difficult to determine, but some at least appear to be triaxial ellipsoids with very little rotation. Some of the smaller ellipticals may be oblate spheroids.
- Lenticular galaxies appear to be an intermediate class between the most flattened of elliptical galaxies and the most tightly wound spirals. They show clear signs of a disc and a central bulge, but they have no spiral arms and little cold interstellar gas.
- Spiral galaxies have a disc, a central bulge and often a central bar. Within this class, spiral arms may be more or less tightly wound and the bulge may be more or less prominent in relation to the disc. (The Milky Way is a spiral galaxy and was traditionally described as being of Hubble type Sb or Sc, but it is now known to have a bar and is probably best described as type SBbc.)
- The largest normal galaxies are the cD galaxies – giant ellipticals which may have been formed in mergers and which are often found close to the centres of clusters of galaxies.

The measurement of the physical properties of galaxies

- The surface brightness of galaxies varies from point to point. Continuous lines passing through points of equal surface brightness are called isophotes. As it is often difficult to determine the edge of a galaxy, observations of galaxies are often confined to the region within some specified isophote.
- Empirical relations obtained from observations of nearby galaxies are used to estimate quantities such as the luminosity and angular size of a distant galaxy, on the basis of its flux density within a given isophote.
- Galactic masses are generally hard to measure. However, the methods that may be used to determine them include the use of rotation curves for spirals, velocity dispersions and X-ray halos for ellipticals, and velocity dispersions for clusters of galaxies.
- The masses of clusters of galaxies are of the order of ten times greater than the estimated masses of the matter that has been detected via electromagnetic radiation, indicating that they contain substantial amounts of dark matter.
- The stellar content of galaxies can be estimated through the process of population synthesis. Direct observations at various wavelengths can be used to establish the importance of gas and dust in a galaxy.

The distance scale

- Determining the distances of galaxies is of great importance in astronomy. Distance information can be crucial to the determination of other galactic properties, and it plays a vital part in investigations of the large-scale distribution of galaxies.
- There are many different methods of distance determination. Those applicable to galaxies include geometrical methods, standard candle methods and the redshift method based on Hubble's law.
- The various methods, taken together, form a galactic distance ladder in which the calibration process that most steps require is usually dependent on the accuracy of other steps lower down the ladder. This means that uncertainties tend to increase as the ladder is climbed.

- The distances of remote galaxies may be determined using Hubble's law, which relates distance to redshift. The calibration of this method (i.e. the process of determining the Hubble constant) is such that distances can be determined with an uncertainty of about 10%.

The formation and evolution of galaxies

- Galaxies are thought to have formed as a result of the gravitational instability of the expanding gas of baryonic and non-baryonic matter produced by the big bang.
- Galaxy formation can be studied theoretically using numerical techniques that extrapolate forward in time from the conditions of the early Universe. The major difficulty in such an approach lies in incorporating the effects of star formation.
- The most likely scenario for galaxy formation is of a bottom-up process in which cold dark matter played a vital role. A feature of this scenario is that interactions and mergers play an important role in galaxy formation.
- Interacting galaxies at the present epoch may be sites of intense star formation.
- Galaxy evolution can be studied observationally by performing deep surveys that sample a large fraction of cosmic history. Such studies can reveal how the distribution of galaxies between different morphological types has changed with time, and can give information about the evolution of the star-formation rate in the Universe.
- The results of deep surveys are generally in accord with a hierarchical scenario of galaxy formation.

Questions

QUESTION 2.13

If the ellipse shown in Figure 2.3 represented the outline of an elliptical galaxy, what would be its Hubble type?

QUESTION 2.14

Figure 2.42 shows three different galaxies. On the basis of these images alone, what would you expect the Hubble types of the three galaxies to be?

(a) (b) (c)

Figure 2.42 Three optical images of galaxies (for use with Question 2.14). (NOAO)

QUESTION 2.15

Why does the fact that elliptical galaxies have elliptical outlines imply that their stars occupy an ellipsoidal volume of space?

QUESTION 2.16

List some of the shortcomings of standard candle methods for finding distances.

QUESTION 2.17

Sketch some typical isophotal contours of (a) an E4 galaxy, and (b) a face-on S0 galaxy.

QUESTION 2.18

Why is it not possible to use the rotation curve method to determine the masses of elliptical galaxies?

QUESTION 2.19

(a) Why does it make good sense to model the population of the central bulge of M31 separately from that of its disc?

(b) If asked to carry out a population synthesis of an E2 galaxy, which of the stellar categories listed below would you expect to be well represented? Explain your answer.

(i) Lower main sequence stars
(ii) Red giants
(iii) Upper main sequence stars
(iv) Cepheid variables

QUESTION 2.20

Figure 2.43 shows a sort of Hertzsprung–Russell (H–R) diagram which has been divided into cells corresponding to various ranges of temperature and luminosity. Within some of the cells a block has been drawn. The size of each block is proportional to the number of stars in a certain galaxy that fall within the given range of temperature and luminosity. The three parts of Figure 2.43 (a, b and c) represent, in a random order, population models for various stages in the evolution of a galaxy that formed all its stars in one huge burst of star formation. Write down the correct chronological sequence of the diagrams and explain the effects that such evolution would have on the appearance of the galaxy.

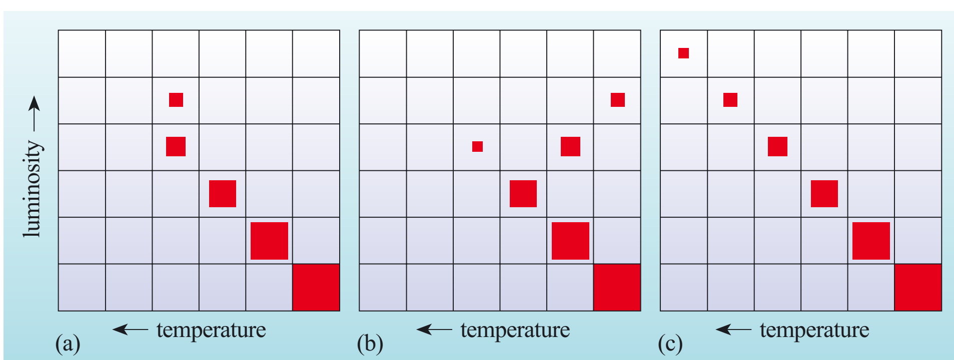

Figure 2.43 Galactic populations on a cellular H–R diagram. Note that these are not in chronological sequence.

CHAPTER 3
ACTIVE GALAXIES

3.1 Introduction

Even in images taken with the most modern equipment on a large telescope, it can be difficult to pick out the galaxies now known as 'active' from the other more normal galaxies. But if your telescope were equipped to examine the *spectra* of the galaxies, then the active galaxies would stand out. Normal galaxies contain stars that are generally similar to those in our own Galaxy; and spiral galaxies have additional similarities to the Milky Way in their gas and dust content. Active galaxies show extra emission of radiation, and this is most apparent from the spectra.

Active galaxies come in a variety of types, including Seyfert galaxies, quasars, radio galaxies and blazars. These types were discovered separately and at first seemed quite different, but they all have some form of spectral peculiarity. There is also evidence in each case that a very large amount of energy is being released in a region that is *tiny* compared with the size of the galaxy, and so they are classified together. It is usually found that the tiny source region can be traced to the nucleus of the galaxy, so the origin of the excess radiation is attributed to the **active galactic nucleus** or **AGN**. An active galaxy may be regarded as a normal galaxy *plus* an AGN with its attendant effects.

Active galaxies seem to be quite rare in the nearby Universe. Whether every galaxy goes through an active phase in its lifetime, or whether active galaxies are a separate class of object is not clear. We have been aware of these objects only since the 1940s, and the galaxies have been around for at least 10^{10} years. So the fact that we observe a small percentage of galaxies in an active phase could mean that every galaxy becomes active for the same small percentage of its lifetime, but it could also mean that a small proportion of galaxies become active for a longer time. At present we cannot tell which of these scenarios may be correct. A further complication is that some nearby galaxies, including our own, show evidence of a low level of activity in their nuclei, but we shall concentrate in this chapter on the prominent and powerful active galaxies.

The **engine** that powers the AGN, the tiny nucleus of the active galaxy, is a great mystery. It has to produce 10^{11} or more times the power of our own Sun, but it has to do this in a region little larger than the Solar System. To explain this remarkable phenomenon, a remarkable explanation is required. This has proved to be within the imaginative powers of astronomers, who have proposed that the engine consists of an *accreting supermassive black hole*, around which gravitational energy is converted into electromagnetic radiation.

In Section 3.2 you will learn how spectroscopy can be used to distinguish different kinds of galaxy and to measure their properties. Section 3.3 then introduces the four main classes of active galaxies and describes how they can be recognized. Section 3.4 examines the evidence for the existence of black holes at the centres of active galaxies, and in Section 3.5 you will study a simple model that attempts to explain the key characteristics of active galaxies in an illuminating way. Finally, in Section 3.6, we consider some of the outstanding questions about the origin and evolution of active galaxies.

We begin by looking at the spectra of galaxies.

3.2 The spectra of galaxies

This section reviews what you have already encountered about the spectra of galaxies. The topic will be further developed to equip you to appreciate the spectra of active galaxies.

- ■ List the four main constituents of a galaxy.
- ❑ Dark matter, stars, gas and dust.

Congratulations if you remembered dark matter! But even though it is the main constituent of a galaxy, dark matter does not contribute to the spectrum of the galaxy so we need not consider it any further. The spectrum of a galaxy contains contributions from stars, gas and (sometimes) dust.

The spectrum of a *star* normally consists of a continuous thermal spectrum with absorption lines cut into it (Figure 3.1). As you probably know, it is possible to learn a lot about the star from a study of these absorption lines.

- ■ List what can be learned about a star from its absorption lines, briefly indicating the measurements which would need to be made on the lines.
- ❑ The strengths and widths of the absorption lines contain information about the star's chemical composition, surface temperature and luminosity. By looking for Doppler shifts in the lines you can measure radial velocity and, if the Doppler shifts are periodic in time, you can detect the binary nature of a star.

The *gas* in a galaxy is partly visible in the form of hot clouds known as HII regions, which you came across in Chapter 1. Such regions are usually only seen where there is ongoing star formation, and so are prominent in spiral and irregular galaxies. The optical spectrum of an HII region consists of just a few emission lines, as can be seen in Figure 3.2. HII regions can make a substantial contribution to the spectra of galaxies because they are very bright. The only other gaseous objects in a normal galaxy to emit at optical wavelengths are supernova remnants and planetary nebulae, and these are faint compared with HII regions.

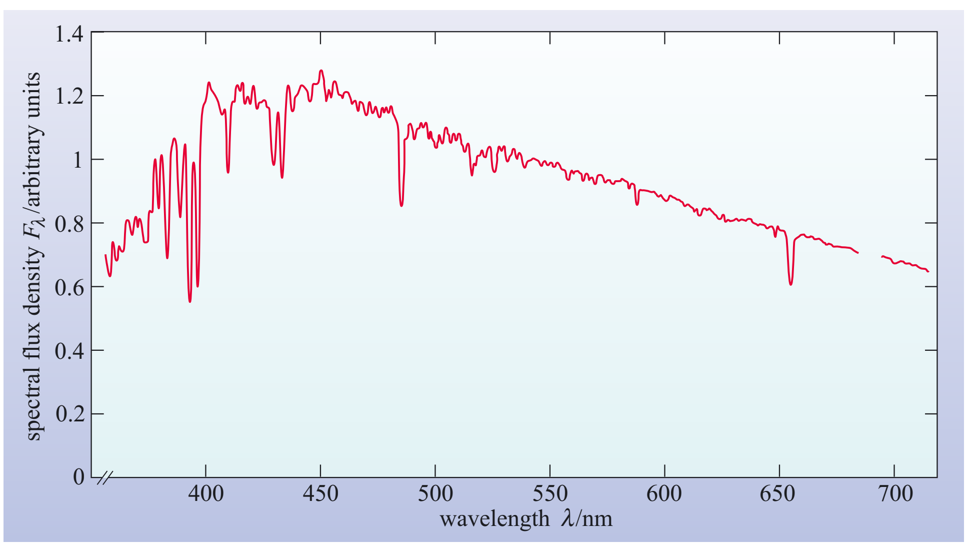

Figure 3.1 The optical spectrum of a star – in this case of spectral type F5 – shown as the spectral flux density, F_λ, plotted against wavelength. (From data described in Silva and Cornell, 1992)

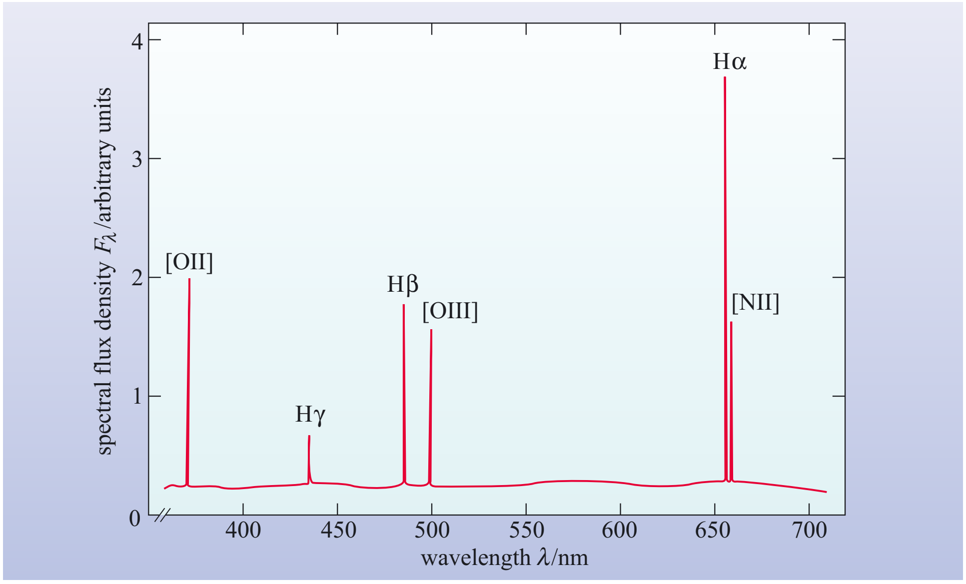

Figure 3.2 The schematic spectrum of a typical HII region, showing emission lines. HII denotes a singly ionized hydrogen atom, NII represents a singly ionized nitrogen atom, and OII and OIII denote singly and doubly ionized oxygen atoms. [NII], [OIII] and [OII] denote particular electronic transitions in these ions – the meaning of the square brackets is explained in Section 3.2.1. Hα, Hβ and Hγ are the first three Balmer lines of hydrogen.

The *dust* component of a galaxy, being relatively cool, does not lead to any emission features in the optical spectrum of a galaxy. The main effect of dust at optical wavelengths is to absorb starlight. However, as you saw in Chapter 1, dust can emit strongly at far-infrared wavelengths (λ of about 100 μm).

As a rule, optical absorption lines result from stars, and optical emission lines result from hot gas.

The spectra of stars and HII regions extend far beyond the optical region. The Sun, for example, radiates throughout the ultraviolet, X-ray, infrared and radio regions of the electromagnetic spectrum. The majority of the Sun's radiation is concentrated into the optical part of its spectrum but, as you will shortly see, this is not the case for active galaxies, for which it is necessary to consider all the observed wavelength ranges. We shall call this the **broadband spectrum** to distinguish it from the narrower optical spectrum. You will recall that the word *optical* means visible wavelengths plus the near ultraviolet and near infrared wavelengths that can be observed from the ground, and extends from 300 to 900 nm. The optical spectrum is just one part of the broadband spectrum albeit an important part. The spectrum of a normal galaxy is the composite spectrum of the stars and gas that make up the galaxy. Some of the absorption lines of the stars and some of the emission lines of the gas can be discerned in the galaxy's spectrum. As well as being able to work out the mix of stars that make up the galaxy, astronomers can measure the Doppler shifts of these spectral lines and so work out the motions within the galaxy as well as the speed of the galaxy through space.

In the case of active galaxies, the spectrum shows features *in addition* to those of normal galaxies, and it is from these features that the active nucleus of the galaxy can be detected.

3.2.1 Optical spectra

Normal galaxies

Normal galaxies are made up of stars and (in the case of spiral and irregular galaxies) gas and dust. Their spectra consist of the sum of the spectra of these components.

The optical spectra of normal stars are continuous spectra overlaid by absorption lines (Figure 3.1). There are two factors to consider when adding up the spectra of a number of stars to produce the spectrum of a galaxy. First, different types of star have different absorption lines in their spectra. When the spectra are added together, the absorption lines are 'diluted' because a line in the spectrum of one type of star may not appear in the spectra of other types. Second, Doppler shifts can affect all spectral lines. All lines from a galaxy share the red-shift of the galaxy, but Doppler shifts can also arise from motions of objects within the galaxy. As a result, the absorption lines become broader and shallower. Box 3.1 explains how this Doppler broadening comes about.

HII regions in spiral and irregular galaxies (though not, of course, ellipticals) shine brightly and contribute significantly to the spectrum of the galaxy. The optical spectrum of an HII region consists mainly of emission lines, as in Figure 3.2. When the spectra of the HII regions and the stars of a galaxy are added together, the emission lines from the HII regions tend to remain as prominent features in the spectrum unless a line coincides with a stellar absorption line. There are Doppler shift effects, however, as described for stellar absorption lines, and hence emission lines too are broadened because of the motion of HII regions within a galaxy.

BOX 3.1 DOPPLER BROADENING

The Doppler effect causes wavelengths to be lengthened when the source is moving away from the observer (*red-shifted*) and shortened when the source is moving towards the observer (*blue-shifted*).

Light from an astrophysical source is the sum of many photons emitted by individual atoms. Each of these atoms is in motion and so their photons will be seen as blue- or red-shifted according to the relative speeds of the atom and the observer. For example, even though all hydrogen atoms emit Hα photons of precisely the same wavelength, an observer will see the photons arrive with a spread of wavelengths: the effect is to broaden the Hα spectral line – called **Doppler broadening**.

In general, if the emitting atoms are in motion with a range of speeds Δv along the line of sight to the observer (the *velocity dispersion*) then the Doppler broadening is given by

$$\Delta\lambda/\lambda \approx \Delta v/c \tag{3.1}$$

where c is the speed of light, and λ is the central wavelength of the spectral line.

Why would the atoms be in motion? An obvious reason is that they are 'hot'. Atoms in a hot gas, for example, will be moving randomly with a range of speeds related to the temperature of the gas. For a gas of atoms of mass m at a temperature T, the velocity dispersion is given by

$$\Delta v \approx \left(\frac{2kT}{m}\right)^{1/2} \tag{3.2}$$

where k is the Boltzmann constant ($1.38 \times 10^{-23}\,\mathrm{J\,K^{-1}}$).

QUESTION 3.1

Calculate the velocity dispersion for hydrogen atoms in the solar photosphere (temperature $\sim 6 \times 10^3\,\mathrm{K}$). Then work out the width in nanometres of the Hα line (656.3 nm) due to thermal Doppler broadening.

It is very common for Doppler broadening to be expressed as a speed rather than $\Delta\lambda$ or even $\Delta\lambda/\lambda$. So astronomers would say that the width of the solar Hα line is about $10\,\mathrm{km\,s^{-1}}$.

You can also see that thermal Doppler broadening depends on the mass of the atom so, for the same temperature, hydrogen lines will be wider than iron lines.

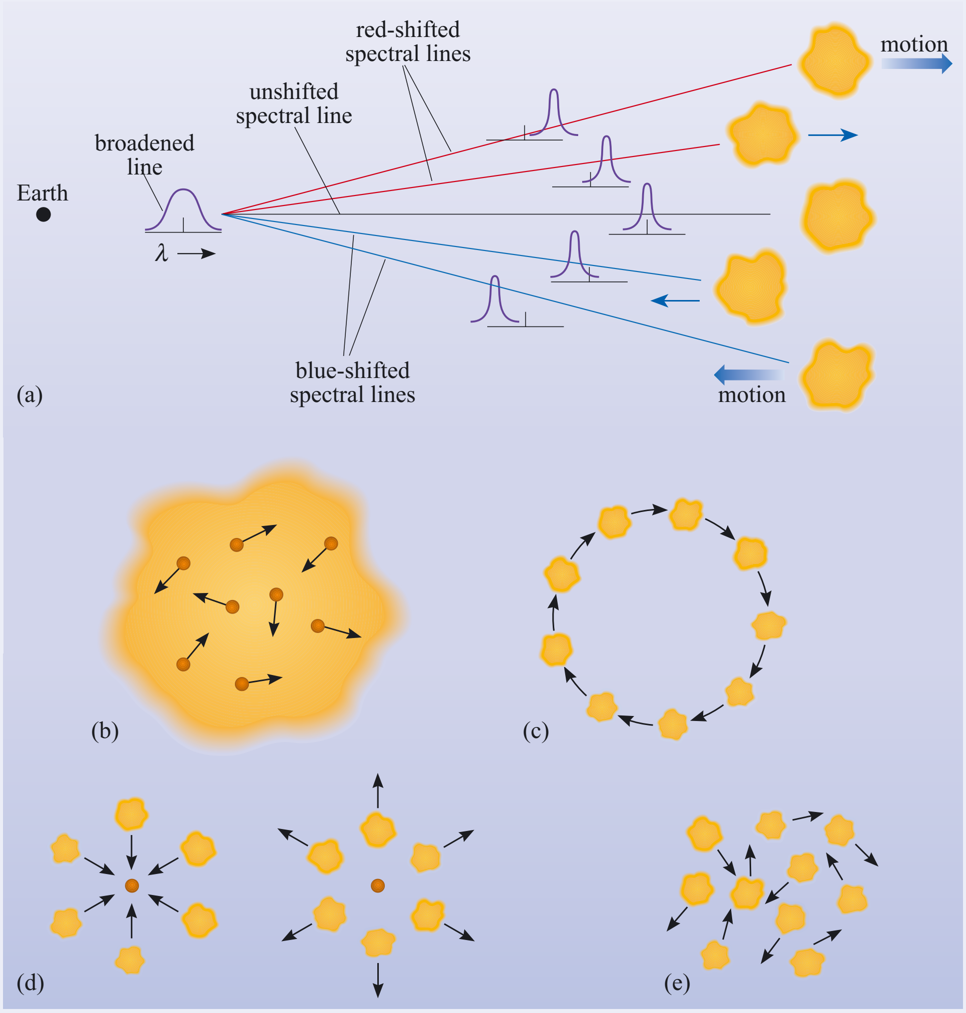

Figure 3.3 Doppler broadening arises when the source of a spectral line contains atoms moving at different speeds along the line of sight (a). This can be due to (b) thermal motion of atoms in a gas, (c) rotational motion of a galaxy, (d) inflow or outflow of gas from a centre, (e) chaotic motion in a gas cloud.

Thermal motion is not the only way in which a velocity dispersion can arise. Bulk movements of material can also broaden spectral lines.

■ What kinds of bulk motions could give rise to Doppler broadening?

❑ For a line to be broadened, the emitting atoms must be moving at different speeds along the line of sight. This could occur where a gas cloud is rotating, where gas is flowing inwards or outwards from a centre, or where gas is in turbulent or chaotic motion.

So a galaxy rotating about its centre will produce a spectrum in which the lines are broadened. Normal galaxies have Δv values of between 100 and 300 km s^{-1}, which you can see is far higher than thermal motions in a hot gas such as the Sun's photosphere. Whether the bulk motion is a rotation, an infall, an outflow, or just turbulence makes no difference; the net effect will be a broadened line whose width is proportional to the range of velocities present.

■ How might you distinguish thermal broadening in a spectrum from broadening due to bulk motions?

❑ Thermal broadening depends on the mass of the individual emitting atoms (heavy atoms move more slowly) so lines from different elements will have different values of $\Delta\lambda/\lambda$. Broadening from bulk motion will affect all spectral lines equally, they will have the same value of $\Delta\lambda/\lambda$.

Doppler broadening applies equally to emission and absorption lines. The broadening is due to the motion of the emitting or absorbing atoms (Figure 3.3).

QUESTION 3.2

From the Galactic rotation curve in Figure 1.13, estimate the broadening of lines from our own Galaxy in km s^{-1} if it were observed edge-on by an astronomer situated in a distant cluster of galaxies. (Assume that our Galaxy is not spatially resolved in such observations.)

The term ‘forbidden line’ arose from quantum theory. The permitted lines all obey a certain set of rules in that theory, whereas the forbidden lines break these rules.

One more feature of emission lines from HII regions needs to be mentioned, and that is the presence of so-called **forbidden lines**, as opposed to the others, which are called permitted lines. Most spectral lines that are seen astronomically can be produced in regions of either high or low gas density. Forbidden lines are produced only in regions of very low density; this is because the excited states responsible for their production are so long-lived that, at higher densities, the atom or ion is likely to be de-excited by collision with another particle before a photon can be emitted spontaneously. Such low densities cannot be achieved on Earth which is why these lines are not observed in the laboratory. When they are observed astronomically, we can be sure that they have been produced in a region of extremely low density. They are prominent in the spectra of active galaxies and are denoted by square brackets [ ]. Strong forbidden lines seen in HII regions include [NII] at 655 nm and [OIII] at 501 nm (see Figure 3.2).

So what will the spectrum from a normal galaxy look like? It depends what kind of galaxy it is. The optical spectrum of an *elliptical galaxy* is a continuous spectrum with absorption lines. You saw an example of such a spectrum in Chapter 2, when we considered the spectrum of the normal elliptical galaxy NGC 1427 (Figure 2.19). Sensitive observations of elliptical galaxies typically reveal the presence of many absorption lines, although these lines are somewhat broader and shallower than those seen in individual stellar spectra. There are no emission lines, because elliptical galaxies have no HII regions. The overall shape of the spectrum looks like that of a K-type (fairly cool) star because cool giant stars dominate the luminous output of the galaxy.

The optical spectrum of a *spiral galaxy* consists of the continuous spectrum from starlight with a few shallow absorption lines from stars, plus a few rather weak

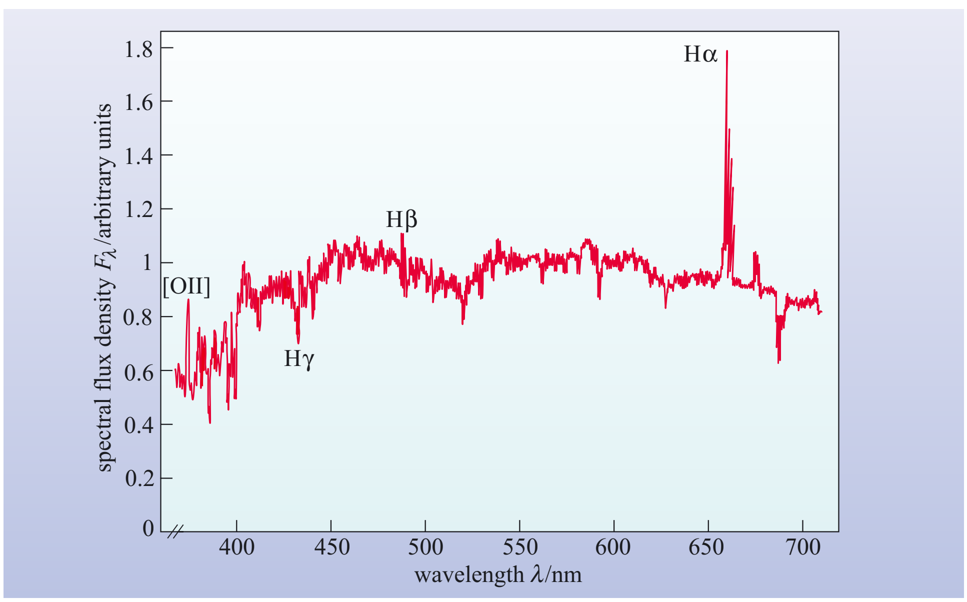

Figure 3.4 The optical spectrum of the normal spiral galaxy NGC 4750. It shows absorption lines and some emission lines. (Note that because of the Doppler shift caused by the motion of the galaxy, a particular spectral line is not necessarily at the same wavelength in all the figures in which it appears. Also note that this is a real, and not a schematic spectrum. Consequently this trace is more erratic than a schematic spectrum because of the presence of many faint absorption lines and the effect of instrumental noise.) (Kennicutt, 1992)

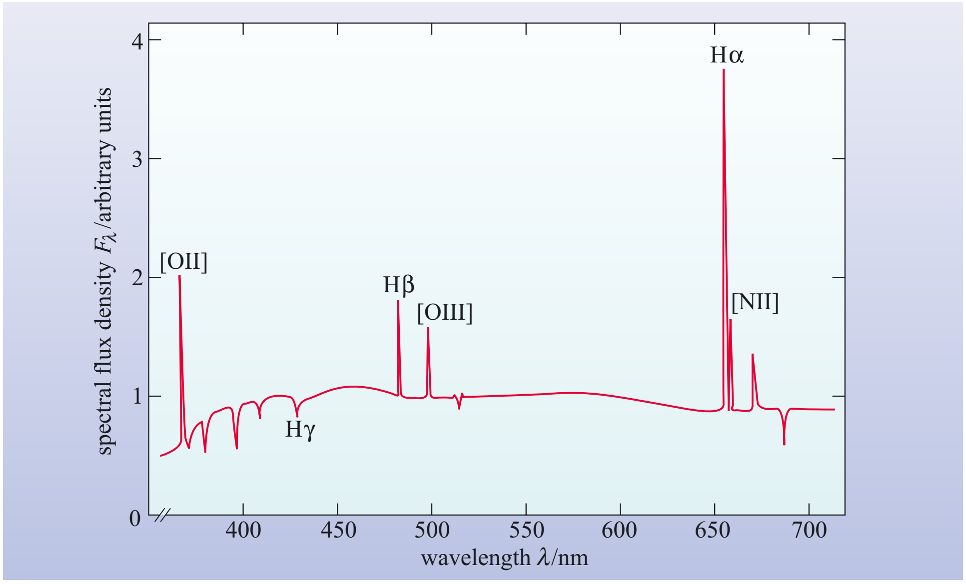

Figure 3.5 Spectrum of a mystery galaxy shown schematically. Note the strong emission lines, which have approximately the same width as those in normal spiral galaxies.

emission lines from the HII regions. Figure 3.4 shows an example. Note that the Hα line in this spectrum is a result of both absorption from stars and emission from HII regions.

- Why has there been no mention of dust so far?
- Because we are only discussing optical spectra. Other than dimming the starlight, dust has no emission or absorption lines in the optical region.

Before moving on to consider the spectrum of active galaxies, look at the spectrum in Figure 3.5.

- How does the spectrum of the mystery galaxy in Figure 3.5 compare with those in Figures 3.2 and 3.4? How would you interpret the difference?
- The spectrum in Figure 3.5 shows very strong emission lines, similar to the spectrum of an HII region in Figure 3.2. Although the stellar absorption spectrum is present, the line spectrum is dominated by HII regions rather than stars. It looks like a galaxy with more HII regions than normal.

In fact, Figure 3.5 is the spectrum of a *starburst galaxy*. In Chapter 2 you saw that starburst galaxies are otherwise normal galaxies that are undergoing an intense episode of star formation. They contain many HII regions illuminated by hot, young stars, and the emission lines show up clearly in the optical spectrum. We mention starburst galaxies here because, as you will see, their spectra have a resemblance to active galaxies, and it is important to be able to distinguish them.

Active galaxies

Figure 3.6 (overleaf) shows a schematic optical spectrum of an active galaxy. It is immediately apparent that the emission lines are stronger and broader than in the spectrum of a normal galaxy shown in Figure 3.4. They are also broader than in the spectrum of the starburst galaxy in Figure 3.5. It is as if a component producing strong and *broad* emission lines had been added to the spectrum of Figure 3.4.

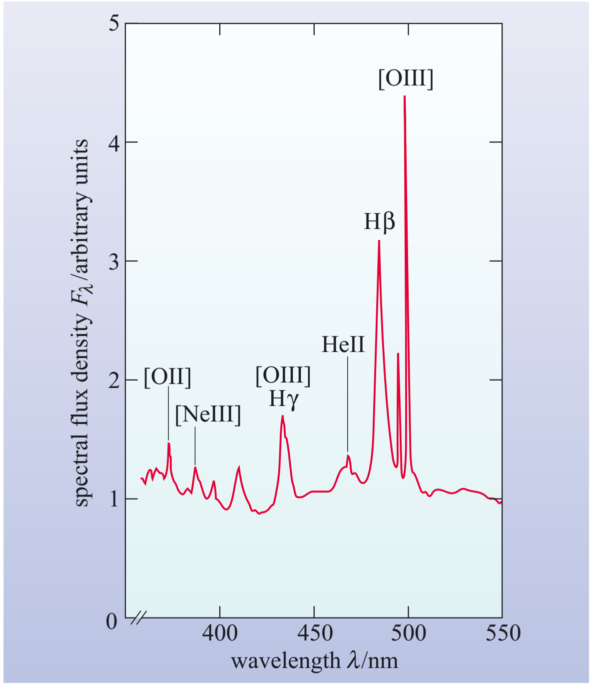

Figure 3.6 The schematic optical spectrum of an active galaxy. Note the strong and broad emission lines, especially the two hydrogen lines Hβ and Hγ. The forbidden lines remain narrow ([OIII] at $\lambda = 436\,\text{nm}$ is almost coincident with Hγ).

- From what you have learned so far, what might be the nature of this component?
- The strong emission lines suggest that the galaxy contains hot gas similar to an HII region. The broad lines imply that the gas must be either extremely hot or in rapid motion.

Now answer Question 3.3, which will help you decide which of these two possibilities is the more likely.

QUESTION 3.3

Measure the wavelength and width of the Hβ line in Figure 3.6 (at half the height of the peak above the background) and so make a rough calculation of the velocity dispersion of the gas that gave rise to it. If the line widths are due to thermal Doppler broadening, estimate the temperature of the gas.

The answer to Question 3.3 is quite surprising. Not only is the implied temperature higher than the *core* temperatures of all but the most massive stars, it is also inconsistent with the process by which Hβ emission occurs, since at such temperatures any hydrogen would be completely ionized. In fact, the relative strengths of various emission lines can be used to estimate the temperature of the gas, and this is found to be only about 10^4 K. So the broadening cannot be thermal. The alternative explanation is *bulk* motions of several thousand kilometres per

second. These are very large velocities indeed, and imply that large amounts of kinetic energy are tied up in the gas motions. We shall return to the nature of these motions later in this chapter.

3.2.2 Broadband spectra

The broadband spectrum is the spectrum over all the observed wavelength ranges. To plot the broadband spectrum of any object it is necessary to choose logarithmic axes.

- Why is it necessary to use logarithmic axes?
- Because both the spectral flux density, F_λ, and the wavelength vary by many powers of 10.

Figure 3.7 shows the broadband spectrum of the Sun: it has a strong peak at optical wavelengths with very small contributions at X-ray and radio wavelengths.

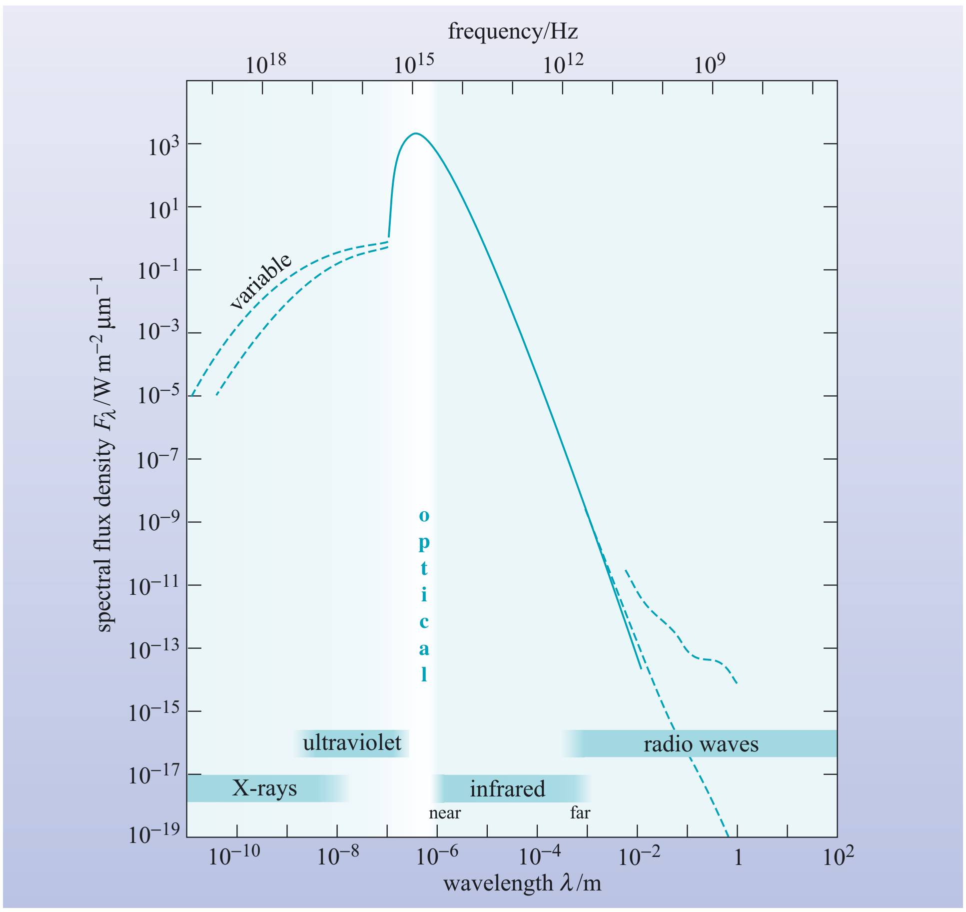

Figure 3.7 The broadband spectrum of the Sun. The dashed lines indicate the maximum and minimum in regions where the flux density varies. (Adapted from Nicolson, 1982)

Normal galaxies

Figure 3.8 shows schematically the broadband spectrum of a normal spiral galaxy. It resembles that of the Sun, although the peak occurs at a slightly longer wavelength and there are relatively greater spectral flux densities at X-ray, infrared and radio wavelengths.

- List the objects in a normal galaxy that emit at (a) X-ray, (b) infrared and (c) radio wavelengths.

- (a) X-rays are emitted by X-ray binary stars, supernova remnants and the hot interstellar medium.

  (b) Infrared radiation comes predominantly from cool stars, dust clouds, and dust surrounding HII regions.

  (c) Radio waves are emitted by supernova remnants, atomic hydrogen and molecules such as CO.

From Figure 3.8 you would conclude that the spectrum peaks in the optical, but there is a subtlety in the definition of F_λ which needs to be addressed.

- Look again at the broadband spectrum in Figure 3.8. Is this galaxy brighter in X-rays or in the far-infrared ($\lambda \sim 100\ \mu m$)?

- The F_λ curve is higher in the X-ray region, so the galaxy appears to be brighter in X-rays than in the far-infrared (far-IR).

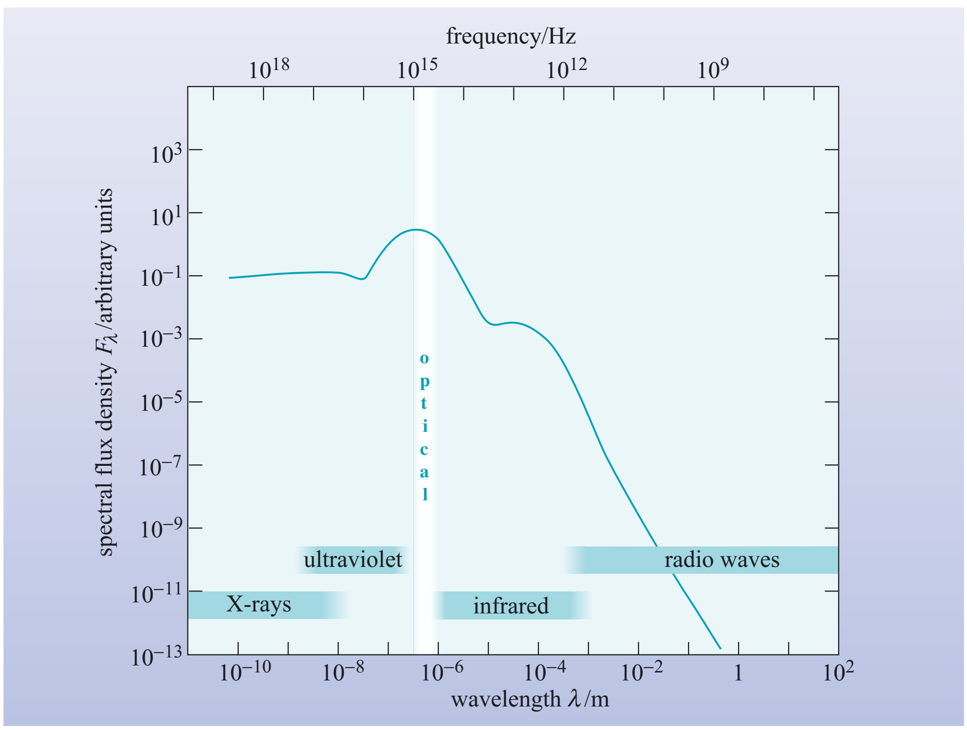

Figure 3.8 Schematic broadband spectrum of a normal spiral galaxy.

Obvious, isn't it? Well, appearances can be misleading. The spectral flux density F_λ is defined as the flux density received over a 1-μm bandwidth (see Box 3.2 overleaf). At far-IR and radio wavelengths that bandwidth is a tiny fraction of the spectrum. But at shorter wavelengths, 1 μm covers the entire X-ray, UV and visible regions of the spectrum! So F_λ will underestimate the energy emitted by a galaxy in the far-IR (and radio wavelengths) and exaggerate the energy emitted in X-rays.

To correct this bias in F_λ spectra, astronomers often plot the quantity λF_λ instead. $\boldsymbol{\lambda F_\lambda}$, pronounced 'lambda eff lambda', (with units of W m^{-2}) is a useful quantity when we are comparing widely separated parts of a broadband spectrum. If the spectrum in its normal form of F_λ against λ is replotted in the form of λF_λ against λ, (still on logarithmic axes) then the highest points of λF_λ will indicate the wavelength regions of maximum power received from the source. A broadband spectrum plotted in this way is known as a **spectral energy distribution** (or **SED**) because the height of the curve is a measure of the energy emitted at each point in the spectrum.

In Figure 3.9, λF_λ has been plotted against λ for the normal galaxy spectrum of Figure 3.8, and it can be clearly seen that this curve has a peak at optical wavelengths, confirming what was suspected. But it also shows that more energy is being radiated at far-IR wavelengths than in X-rays, the opposite of the impression given by Figure 3.8. From now on in this chapter broadband spectra will be plotted as SEDs with λF_λ against λ on logarithmic axes.

You may have found the concept of λF_λ difficult to grasp. If so, don't worry about the justification, but just accept that a λF_λ plot allows you to compare widely differing wavelengths fairly, whereas a conventional F_λ plot does not.

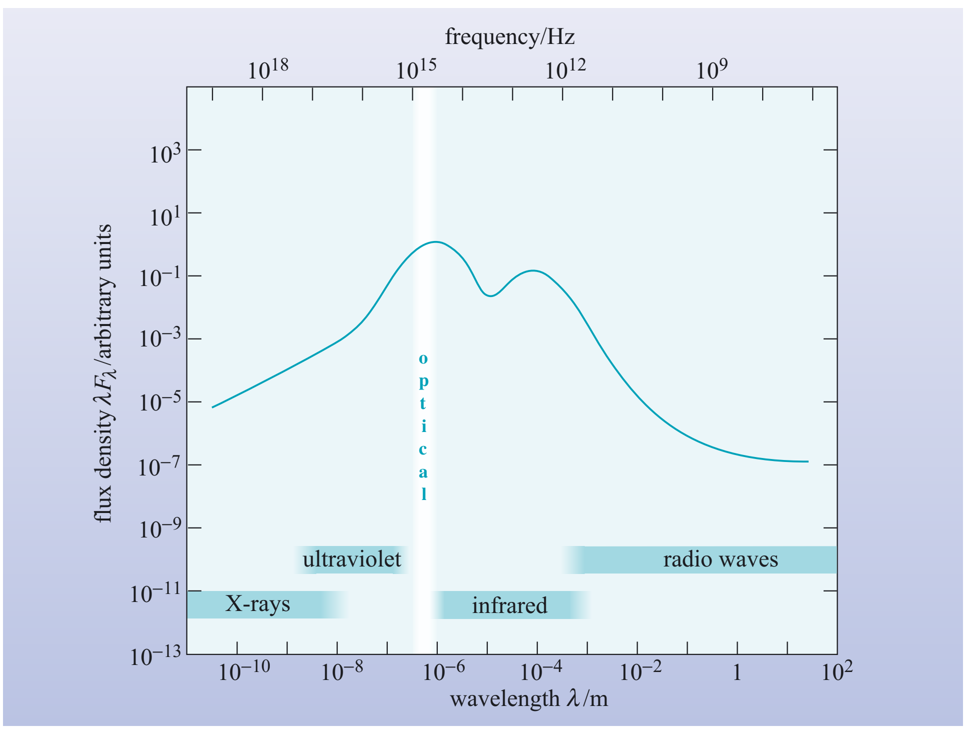

Figure 3.9 The spectral energy distribution (SED) of the galaxy in Figure 3.8. The vertical axis is now λF_λ instead of F_λ.

BOX 3.2 FLUX UNITS

Astronomers use several different units to measure the electromagnetic radiation received from an object.

Flux density, F, is the power received per square metre of telescope collecting area. It is measured in watts per square metre, $W\,m^{-2}$.

Spectral flux density is the flux density measured in a small range of bandwidth. As bandwidth can be expressed either in terms of wavelength (λ) or frequency (ν) there are two kinds of spectral flux density in common use. F_λ is measured in watts per square metre per micrometre ($W\,m^{-2}\,\mu m^{-1}$) and F_ν is measured in watts per square metre per hertz ($W\,m^{-2}\,Hz^{-1}$). The former is preferred by optical and infrared astronomers (who work in wavelengths) and the latter by radio astronomers (who work in frequencies). The special unit, the *jansky* (Jy), is given to a spectral flux density of $10^{-26}\,W\,m^{-2}\,Hz^{-1}$, in honour of the US engineer Karl Jansky (1905–1950) who made pioneering observations of the radio sky in the early 1930s.

Both flux density and spectral flux density are commonly (though inaccurately) referred to as *flux*.

Note that the symbol ν (Greek letter 'nu') is commonly used to denote the frequency of electromagnetic radiation. In this book, the convention is to use f to denote frequency.

QUESTION 3.4

Astronomers observe two galaxies at the same distance. Both have broad, smooth spectra. Galaxy A is seen at optical wavelengths (around 500 nm), and yields a spectral flux density $F_\lambda = 10^{-29}\,W\,m^{-2}\,\mu m^{-1}$; it is not detected in the far infrared at around 100 μm (the upper limit to the measured flux density is $F_\lambda < 10^{-32}\,W\,m^{-2}\,\mu m^{-1}$). Galaxy B appears fainter in the optical and gives $F_\lambda = 10^{-30}\,W\,m^{-2}\,\mu m^{-1}$ around 500 nm, and the same value at around 100 μm. Which (on these data) is the more luminous galaxy?

Active galaxies

Figure 3.10 shows the spectral energy distribution of an active galaxy.

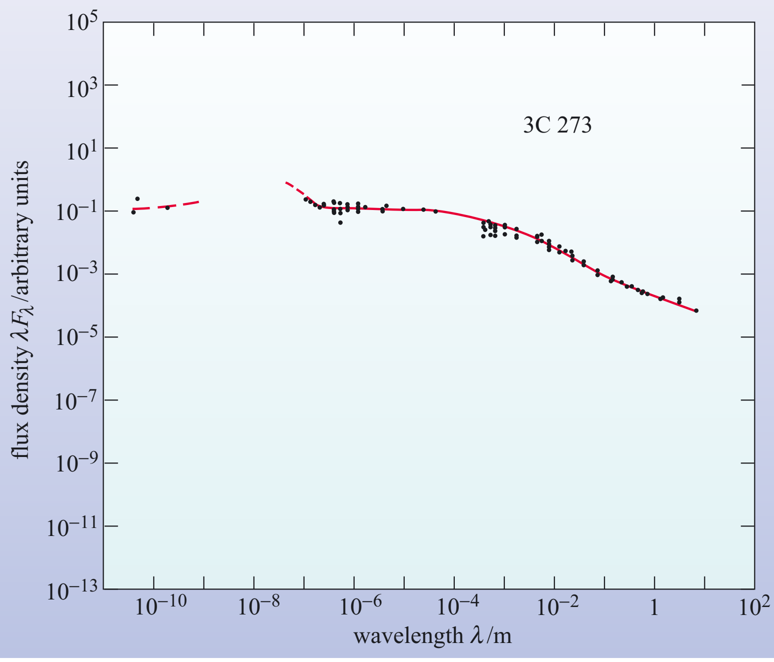

Figure 3.10 The spectral energy distribution of an active galaxy, the quasar 3C 273. The filled circles are measurements and the red curve shows the spectrum as determined from the data. (Data provided by NASA/IPAC Extragalactic Database)

- In broad terms, what is the major difference between the SED of the normal galaxy in Figure 3.9 and the SED of the active galaxy in Figure 3.10?
- Compared with the (unquantified) peak emission, the SED of the active galaxy is much flatter than that of the normal spiral galaxy. This indicates that there is relatively much more emission (by several orders of magnitude) at X-ray wavelengths and at radio wavelengths.

For the active galaxy (known from its catalogue number as 3C 273) the peak emission is in the X-ray and ultraviolet regions. Many other active galaxies are bright in this region and the feature is known as the 'big blue bump'. In some active galaxies, though not this one, the infrared emission is prominent. These galaxies emit a normal amount of starlight in the optical, so they must emit several times this amount of energy at infrared and other wavelengths – this is another feature that distinguishes active galaxies from normal galaxies. It means that we have to account for *several times* the total energy output of a normal galaxy, and possibly a great deal more. A normal galaxy contains 10^{10} to 10^{11} stars, so we need an even more powerful energy source for active galaxies.

The term **spectral excess** is used (rather loosely) to refer to the prominence of infrared or other wavelength regions in the broadband spectra of active galaxies. In particular, it is often used to indicate the presence of emission in a certain wavelength region that is over and above that which would be expected from the stellar content of a galaxy.

QUESTION 3.5

Now that you have some experience in interpreting the spectra of galaxies, look at the SED of the galaxy NGC 7714 in Figure 3.11. Describe as fully as you can what the diagram tells you about this galaxy. Can you guess what sort of galaxy it is?

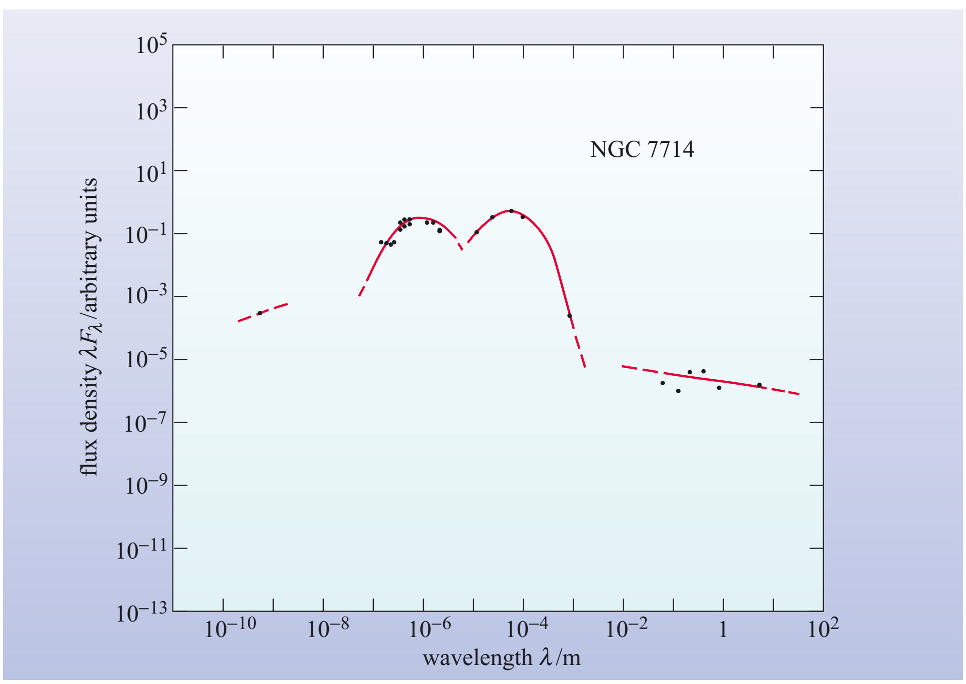

Figure 3.11 The spectral energy distribution of the galaxy NGC 7714 (for use with Question 3.5). (Data provided by NASA/IPAC Extragalactic Database)

3.3 Types of active galaxies

Active galaxies have occupied the attention of an increasing number of astronomers since the first example was identified in the 1940s. By one recent estimate, a fifth of all research astronomers are working on active galaxies, which indicates how important this field is. In this section you will learn about the observational characteristics of the four main classes of active galaxies: Seyfert galaxies, quasars, radio galaxies and blazars. This will set the scene for subsequent sections in which we will explore the physical processes that lie behind these different manifestations of active galaxies.

3.3.1 Seyfert galaxies

In 1943 the American astronomer Carl Seyfert (1911–1960, see Figure 3.14) drew attention to a handful of spiral galaxies that had unusually bright point-like nuclei. Figure 3.12 shows NGC 4051, one of the first **Seyfert galaxies** to be identified. Subsequently, it has been found that compared to normal galaxies, Seyfert galaxies show an excess of radiation in the far infrared and at other wavelengths. Even more remarkably, at some wavelengths, including the optical, this excess radiation is *variable.* Variability is discussed in detail in Section 3.4.1 – suffice it to say here that the variability implies that the emission from a Seyfert galaxy must come from a region that is *tiny* compared to the galaxy itself.

Spectra of the bright nuclei reveal that Seyferts can be classified into two types by the relative widths of their emission lines (Figure 3.13).

Type 1 Seyferts have two sets of emission lines (Figure 3.13a). The narrower set, which are made up largely of the forbidden lines discussed earlier, have widths of about 400 km s^{-1}. Despite this considerable width the region emitting these lines is known as the **narrow-line region**. The broader lines, consisting of permitted lines only, have widths up to 10 000 km s^{-1} and appear to originate from a denser region of gas known as the **broad-line region**. As noted above, forbidden lines are

Figure 3.12 NGC 4051 is a member of a class of galaxies known as Seyfert galaxies. In this optical image (at a wavelength of around 440 nm) a false colour scheme has been used to show features across a wide range of surface brightness. Blue and green regions have a low surface brightness, whereas yellow, red and white regions are relatively bright. The intense emission from the point-like nucleus of the galaxy is clearly evident. NGC 4051 is relatively close – lying at a distance of about 17 Mpc from the Milky Way. The field-of-view of this image is 4.0 arcmin × 4.5 arcmin. (Data provided by NASA/IPAC Extragalactic Database from the observations of Tully *et al*., 1996)

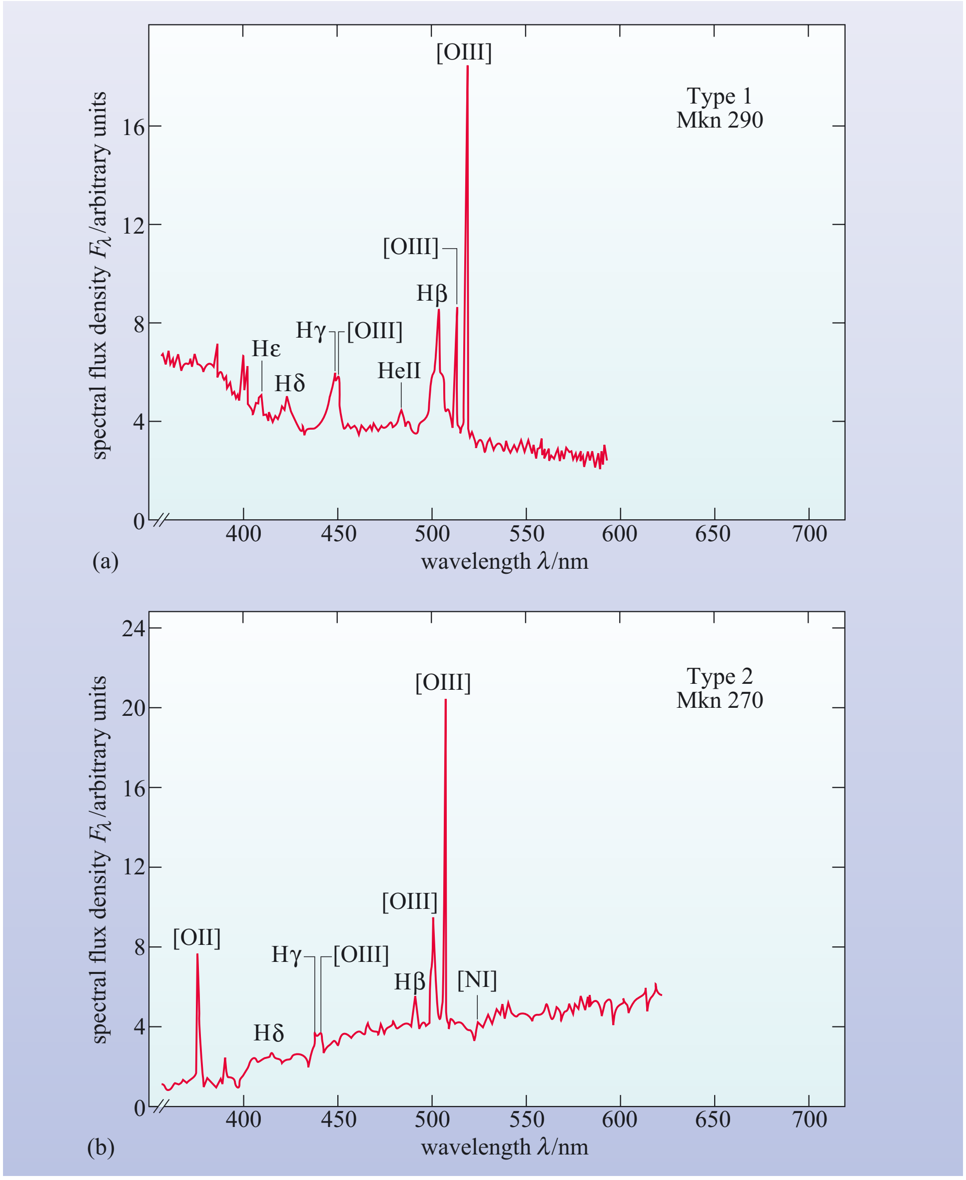

Figure 3.13 The optical spectra of two Seyfert galaxies.
(a) Markarian 290, a type 1 Seyfert.
(b) Markarian 270, a type 2 Seyfert.
Note that the broad hydrogen lines (especially Hβ) visible in (a) appear narrower in (b). (Netzer, 1990)

sensitive to the gas density in the emitting region. An analysis of which lines are present allows the densities of the gas in the broad- and narrow-line regions to be determined. These two regions are also characteristic of other types of active galaxy. Type 2 Seyferts only show prominent narrow lines (Figure 3.13b). The broad lines are either absent or very weak in the optical spectra of type 2 Seyferts.

In fact, these two types are not as clear cut as they first seemed, since weak broad lines have now been found in Seyferts previously classed as type 2. Types 1 and 2 are better understood as extreme ends of a range of intermediate Seyfert types classified according to the relative strengths of their broad and narrow lines. In a Seyfert 1.5, for example, there are broad and narrow lines, but the broad lines are not as strong as those seen in type 1 Seyferts.

CARL KEENAN SEYFERT (1911–1960)

Figure 3.14 Carl Seyfert with the 24 inch telescope (that is now named in his honour) at the Dyer Observatory at Vanderbilt University. (B. Poteete)

Carl Seyfert (Figure 3.14) was born and grew up in Cleveland, Ohio. He entered Harvard with the intention of studying medicine, but became diverted from this career path after attending an inspirational lecture course in astronomy given by Bart Bok. Seyfert switched his attention to astronomy and remained at Harvard to carry out his doctoral research under the direction of Harlow Shapley (Figure 1.27). Following a post at Yerkes Observatory he was employed at Mount Wilson Observatory from 1940 to 1942. It was during this time at Mount Wilson that he carried out his observations into the type of galaxies that now carry his name. During the Second World War he managed to juggle several tasks: teaching navigation to the armed forces, carrying out classified research, and still finding time to partake in some astronomical research. He is notable for producing some of the first colour photographs of nebulae and stellar spectra – some of which were used in the Encyclopedia Britannica. After the war Seyfert gained a faculty position at Vanderbilt University in Nashville, Tennessee. He was the driving force behind the development of their observatory and was also an enthusiastic popularizer of science. He also found time to present local weather forecasts on television! He was tragically killed in a motor accident in 1960 at the age of 49. He died before the significance of Seyfert galaxies became fully apparent – the field of active galaxy research only became a key area of astronomy after the discovery of quasars in 1963.

3.3.2 Quasars

One of the most unexpected turns in the history of astronomy was the discovery of **quasars**. When first recognized, in 1963, quasars appeared at radio and optical wavelengths as faint, point-like objects with unusual optical emission spectra. The name comes from their alternative designations of ‘quasi-stellar radio source’ (QSR) or ‘quasi-stellar object’ (QSO), meaning that they resemble stars in their point-like appearance. Their spectra, however, are quite unlike those of stars. The emission lines turn out to be those of hydrogen and other elements that occur in astronomical sources, but they are significantly red-shifted.

Figure 3.15 shows the optical spectrum of 3C 273, which was the first quasar to be discovered (you have already seen its broadband spectrum in Figure 3.10). The redshift is 0.158, which corresponds to a distance of about 660 Mpc according to Hubble’s law. Many other quasars are now known – a recent catalogue lists more than 7000 – and the vast majority have even greater redshifts, the record (in 2003) is more than 6. All quasars must therefore be highly luminous to be seen by us at all.

The optical spectra of quasars are similar to those of Seyfert 1 galaxies, with prominent broad lines but rather weaker narrow lines. A composite spectrum for 700 quasars is shown in Figure 3.16. To form this spectrum, the individual quasar spectra were all corrected to remove the effect of red-shift before being added together. Because many quasars have high redshifts, many of the features that are observed in the visible part of the spectrum correspond to emission

features in the ultraviolet. In particular, the spectrum shows the **Lyman α** (Lyα) line that arises from the electronic transition in atomic hydrogen from the state $n = 2$ to $n = 1$. This line, which occurs at a wavelength of 121.6 nm is clearly a very strong and broad line in quasar spectra.

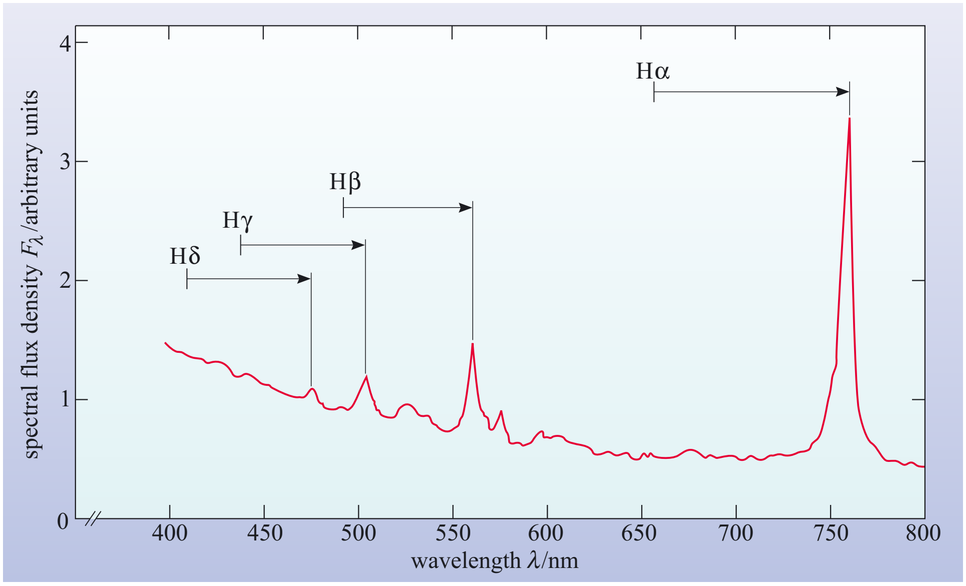

Figure 3.15 The optical spectrum of 3C 273, the first quasar to be discovered. The arrows show how the prominent hydrogen emission lines have been greatly red-shifted from their normal wavelengths. (Kaufmann, 1979)

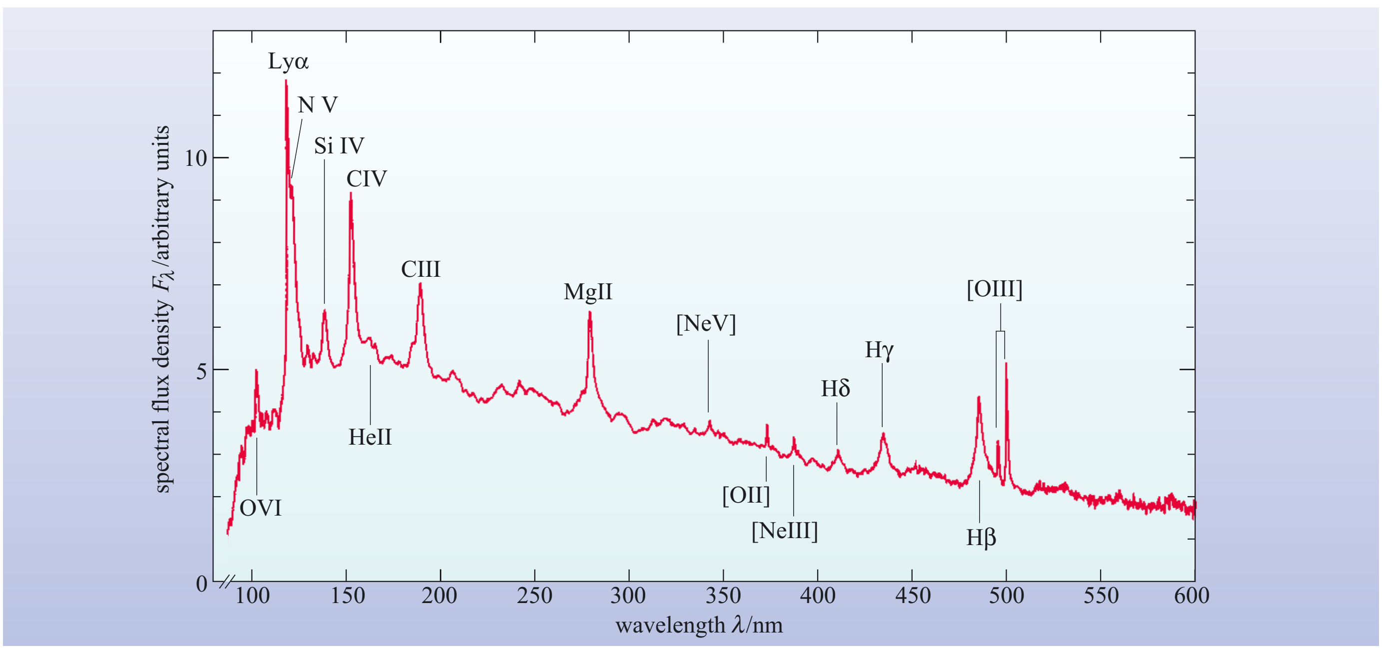

Figure 3.16 The mean optical spectrum of a sample of more than 700 quasars. The individual spectra were all corrected to remove the effect of red-shift before the spectra were averaged. Note the broad emission lines. (Peterson, 1997, from data described in Francis *et al*., 1991)

Quasars show spectral excesses in the infrared and at other wavelengths. About 10% of quasars are strong radio sources and are said to be *radio loud*. Some astronomers prefer to retain the older term QSO (quasi-stellar object) for *radio-quiet* quasars that are not strong sources of radio waves. The spectral energy distribution for a sample of radio-loud and a sample of radio-quiet quasars is shown in Figure 3.17. The big blue bump, hinted at in Figure 3.10, is particularly prominent here. Many quasars are also variable throughout the spectrum on timescales of months or even days.

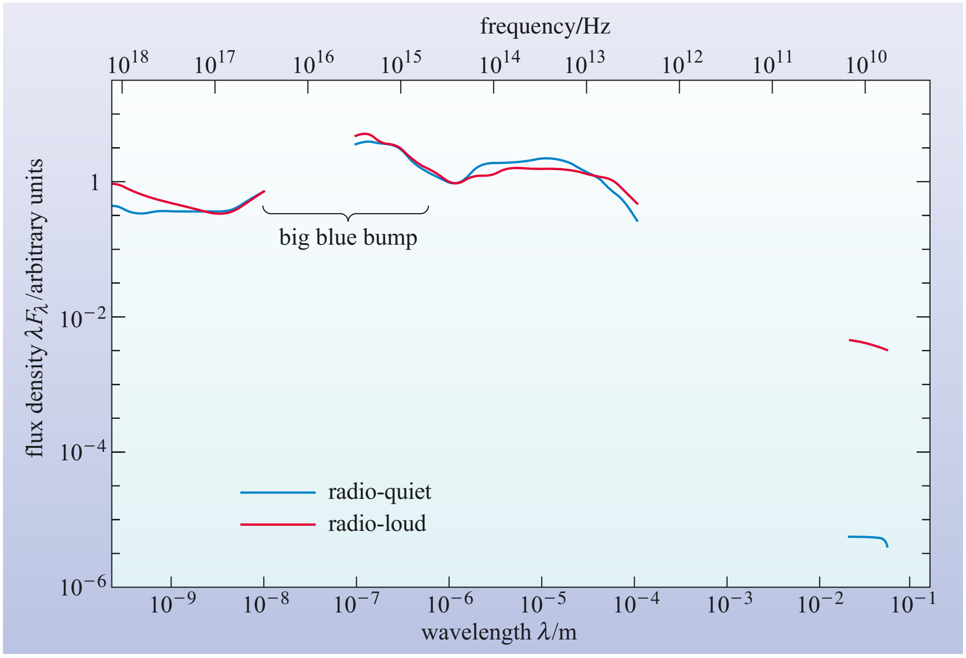

Figure 3.17 Mean SEDs for a sample of radio-quiet (blue line) and radio-loud (red line) quasars. The two curves are similar except at radio wavelengths. The 'big blue bump' is particularly prominent in this diagram. (Peterson, 1997, from data provided by Elvis *et al*., 1994)

Detailed radio mapping shows that many of the radio-loud quasars have prominent *jets* which appear to be gushing material into space. In 3C 273 the jet is even visible on optical images (Figure 3.18).

Because quasars are so distant, it has been difficult to study the **host galaxies** which contain them. Recent work seems to show that there is no simple relationship between a quasar and the morphology of its host galaxy – while many quasar host galaxies are interacting or merging systems, there are also many host galaxies that appear to be normal ellipticals or spirals (Figure 3.19). It has also been found that the radio-loud quasars tend to be found in elliptical and interacting galaxies whereas the radio-quiet quasars (the QSOs) seem to be present in both elliptical and spiral host galaxies. It should be stressed however that the relationship between quasar host and radio emission is not clear-cut, and that this is a topic of ongoing research.

Before their host galaxies were discovered in the 1980s quasars seemed much more puzzling than they do now. Indeed, for many years, there was a school of thought that supported the idea that quasars were not at such great distances as they are now thought to be, but were instead relatively close objects in which the red-shift arose from some unknown physical process. The study of quasar host galaxies has all but dispelled this view and the modern picture of a quasar is of a remote, very luminous AGN buried in a galaxy of normal luminosity. This is why astronomers now regard quasars as a type of active galaxy, though you will still see books referring to 'active galaxies and quasars'. Quasars are believed to be the most luminous examples of AGNs known.

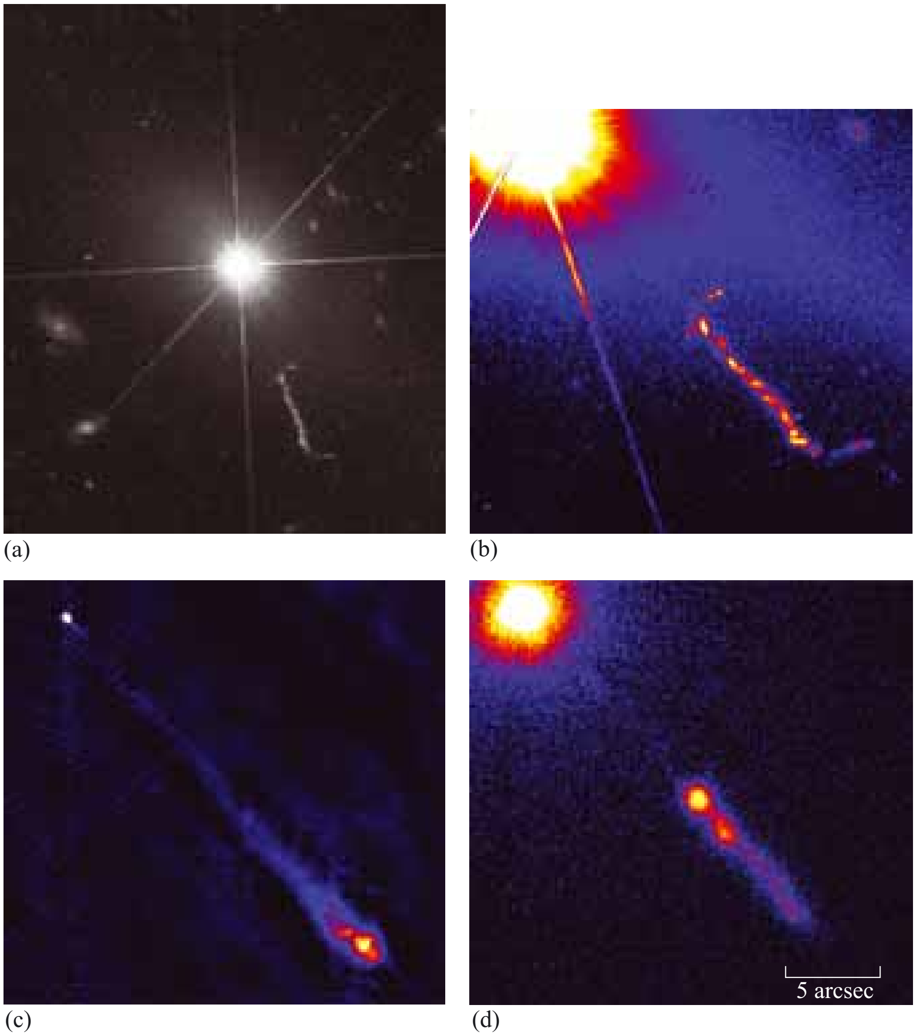

Figure 3.18 Images of the nearest quasar, 3C 273. (a) An optical (V band) image shows a faint jet of material emerging from the star-like nucleus. The panels show the jet in more detail at (b) optical, (c) radio and (d) X-ray wavelengths. (Note that the different colours in panels (b), (c) and (d) represent different levels of intensity.) ((a), (b) Hubble Space Telescope; (c) MERLIN/Jodrell Bank Observatory; (d) Chandra X-ray Observatory)

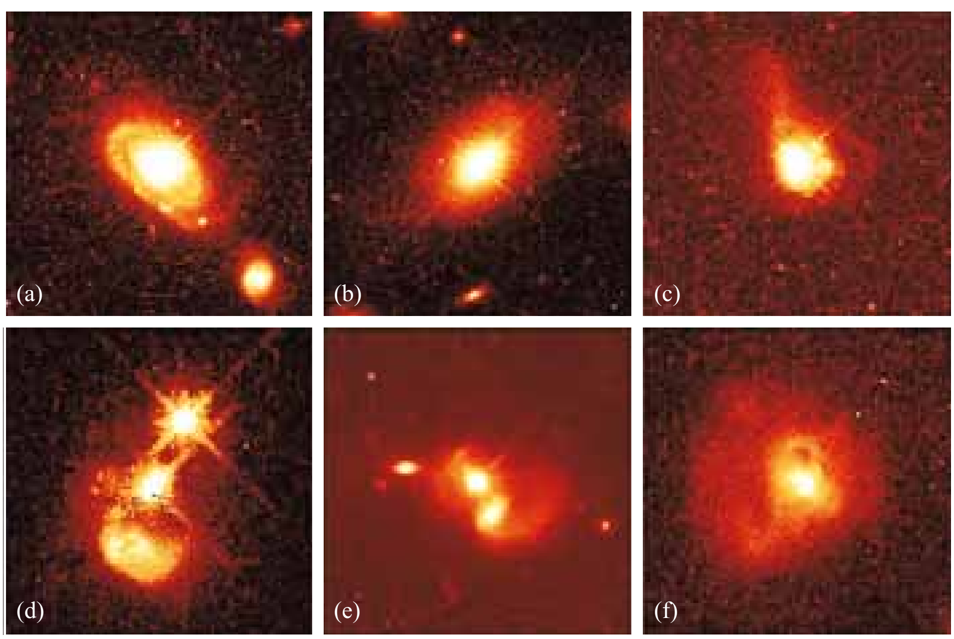

Figure 3.19 Examples of quasar host galaxies as observed at optical wavelengths with the Hubble Space Telescope. Quasars seem to occur in normal and interacting galaxies. The host galaxies shown here appear to be: (a) a normal spiral galaxy, (b) a normal elliptical galaxy, and (c) to (f) interacting or merging galaxies. (Note that the different colours represent different levels of intensity.) (J. Bahcall (Institute for Advanced Study, Princeton) and M. Disney (University of Wales, Cardiff))

3.3.3 Radio galaxies

Radio galaxies were discovered accidentally by wartime radar engineers in the 1940s, although it took another decade for them to be properly studied by the new science of radio astronomy. Radio galaxies dominate the sky at radio wavelengths. They show enormous regions of radio emission outside the visible extent of the host galaxy – usually these *radio lobes* occur in pairs.

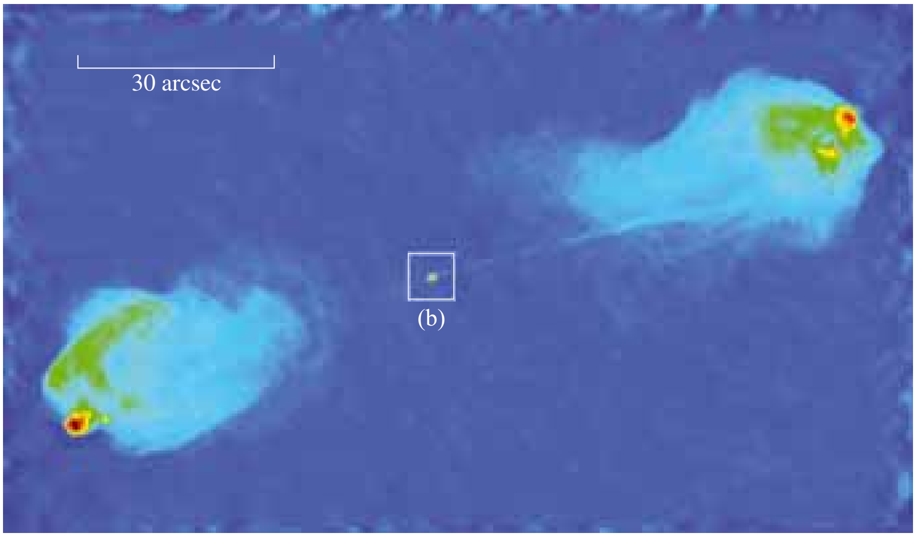

(a)

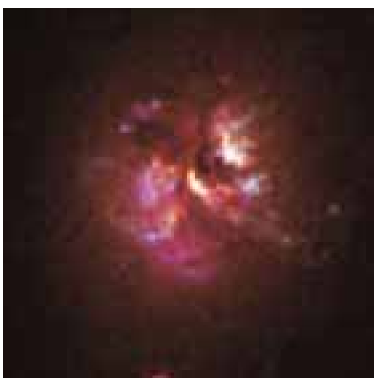

(b)

Figure 3.20 (a) The Cygnus A radio galaxy consists of two bright 'lobes' on either side of a compact nucleus. The lobe on the right is connected to the nucleus by a narrow jet. The white box shows the extent of (b), the host galaxy of Cygnus A. It is believed to be a giant elliptical galaxy with morphological peculiarities. The galaxy is at a distance of about 240 Mpc. This optical image combines observations made in the blue, visual (V) and near-infrared bands. ((a) Data provided by NASA/IPAC Extragalactic Database from the observations of Perley *et al.*, 1984; (b) R. Fosbury, ESO)

The first radio galaxy to be discovered, and still the brightest, is called Cygnus A (Figure 3.20). Radio maps show the two characteristic lobes on either side of a compact nucleus. A narrow jet is apparent to the right of the nucleus and appears to be feeding energy out to the lobe. There is a hint of a similar jet on the left. Jets are a common feature of radio galaxies, especially at radio wavelengths. They trace the path by which material is being ejected from the AGN into the lobes.

Cygnus A is an example of the more powerful class of radio galaxy with a single narrow jet. The second jet is faint, or even absent, in many powerful radio galaxies; we will consider the reasons for this shortly. Note the relatively inconspicuous nucleus and the bright edge to the lobes, as if the jet is driving material ahead of it into the intergalactic medium.

The jets of weaker radio galaxies spread out more and always come in pairs. These galaxies have bright nuclei, but the lobes are fainter and lack sharp edges. You can see an example in Figure 3.21. This is M84, a relatively nearby radio galaxy in the Virgo cluster of galaxies.

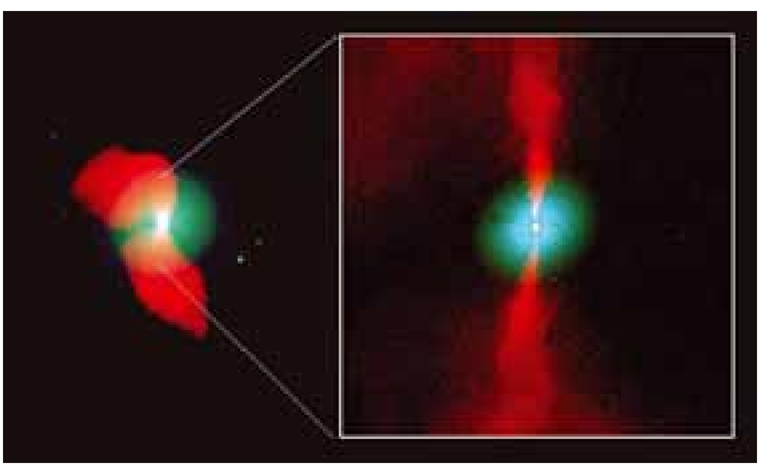

Figure 3.21 The radio galaxy M84. The radio emission is shown in red while the optical image of the galaxy is indicated in blue. The distance to M84 is about 18 Mpc. The inset shows an expanded view of the inner regions of the jets and the bright nucleus. (A. Bridle, NRAO)

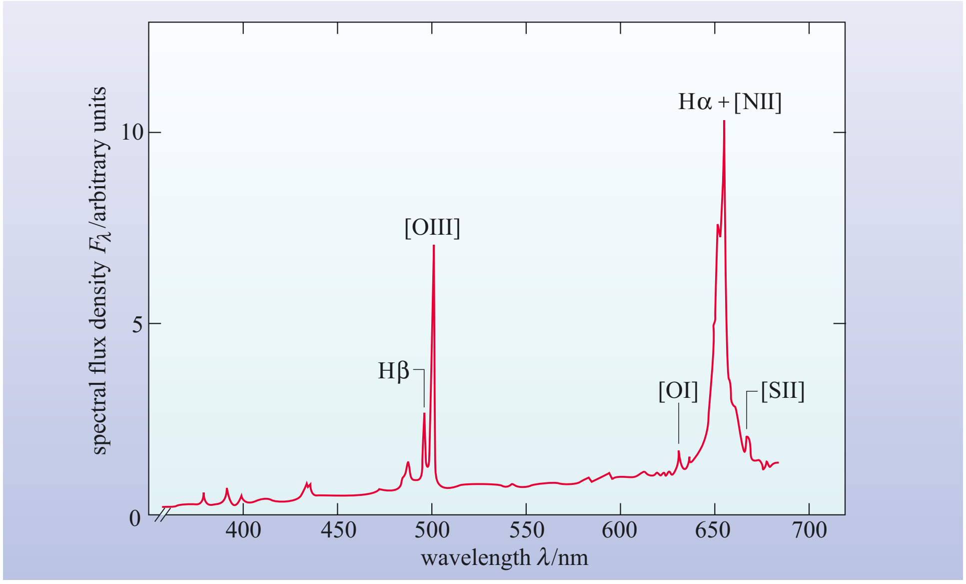

Figure 3.22 The optical spectrum of the nucleus of the radio galaxy 3C 445 (adjusted to zero redshift). (Osterbrock *et al*., 1976)

Each radio galaxy has a point-like radio nucleus coincident with the nucleus of the host galaxy. It is this feature that is reminiscent of other classes of active galaxies and which is believed to be the seat of the activity. The nucleus shows many of the properties of other AGNs, including emission lines, a broadband spectrum which is far wider than that of a normal galaxy, and variability.

The optical spectrum of the nucleus of a radio galaxy looks very much like that of any other AGN. Like Seyferts, radio galaxies can be classified into two types depending on whether broad lines are present (*broad-line radio galaxies*) or only narrow lines (*narrow-line radio galaxies*). Figure 3.22 shows an example of a spectrum of a broad-line radio galaxy.

Figure 3.23 shows maps of radio, optical and X-ray wavelengths of Centaurus A, which is the nearest radio galaxy to the Milky Way. The optical image (Figure 3.23b) shows that it is an elliptical galaxy with a dust lane bisecting it.

■ Given that Centaurus A is an elliptical galaxy, does anything strike you as incongruous about Figure 3.23b?

❑ Elliptical galaxies are supposed to have negligible amounts of dust, so the thick dust lane seems very strange indeed!

The galaxy is obviously not a normal elliptical and this is a clue to the nature of radio galaxies. In fact, it is now thought that Centaurus A was formed by the collision of a spiral galaxy with a massive elliptical, the dust lane being the remains of the spiral's disc. We will come back to this interesting topic later in the chapter.

M87 (also known as Virgo A) is such a well-known radio galaxy that it must be mentioned at this point. In the optical region it, too, appears as a giant elliptical galaxy at the centre of the nearby Virgo cluster of galaxies. It seems that most radio galaxies are ellipticals. The single bright jet in the galaxy (Figure 3.24) is reminiscent of the jet in the quasar 3C 273, shown in Figure 3.18.

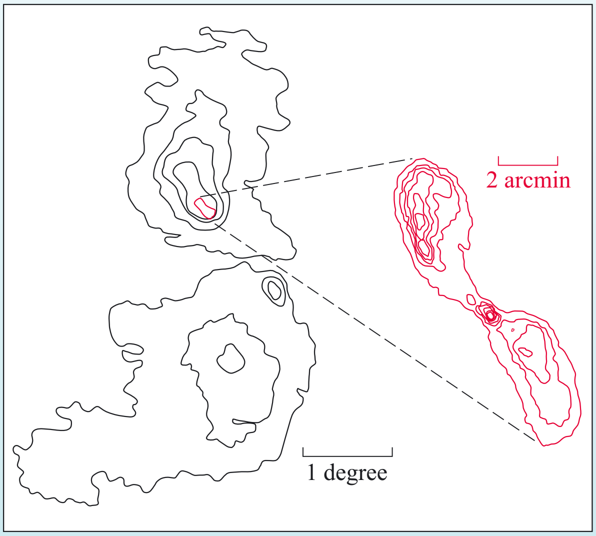

(a)

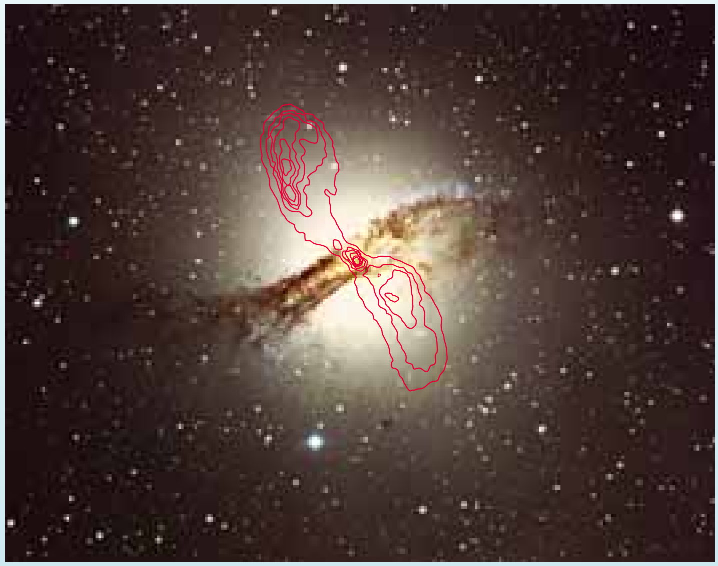

(b)

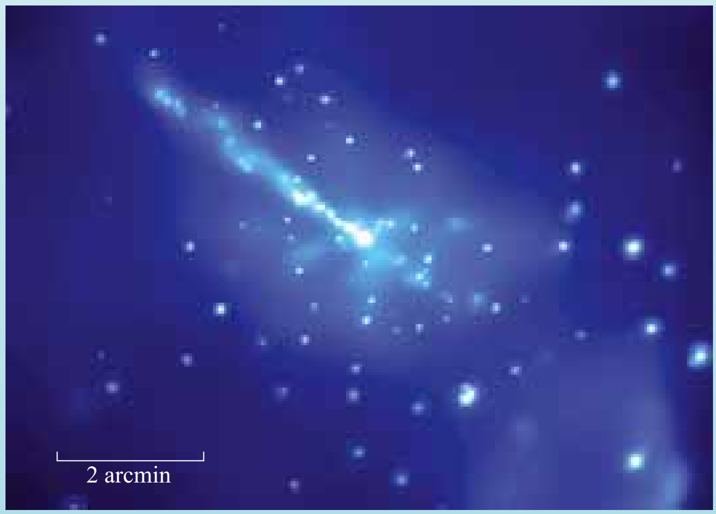

(c)

Figure 3.23 The Centaurus A radio galaxy.
(a) A radio map shows the lobes that extend over more than 9 degrees of the sky.
(b) An image at visible wavelengths shows that the host galaxy is an elliptical galaxy with a dust lane bisecting it (the inner radio lobes are shown superimposed on this image).
(c) An X-ray image from the Chandra X-ray Observatory clearly shows the jet and the point-like nucleus in the inner parts of the galaxy.
((a) Seeds, 1998; (b) D. Malin/AAO; radio contours in red are data provided by NASA/IPAC Extragalactic Database from the observations of Condon *et al.*, 1996; (c) R. Kraft, SAO/NASA)

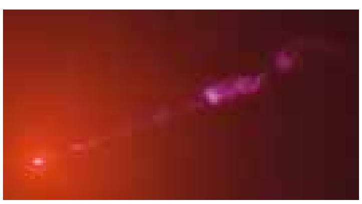

(a)

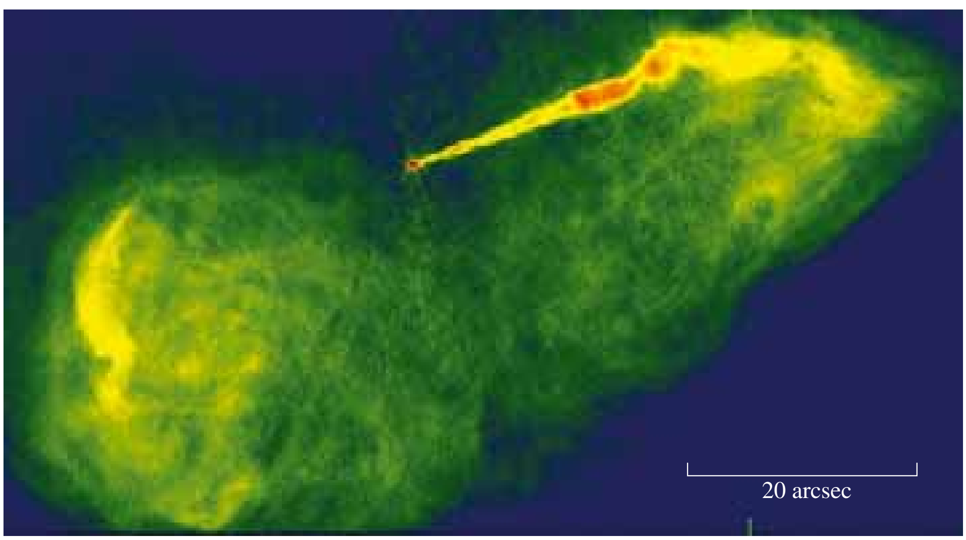

(b)

Figure 3.24 (a) Optical and (b) radio images of the giant elliptical galaxy M87 clearly show the presence of a 'one-sided' jet that extends from the active nucleus. Note that (a) and (b) are at the same scale. (NASA, NRAO and J. Biretta, STScI)

3.3.4 Blazars

Blazars appear star-like, as do quasars, but were only recognized as a distinct class of object in the 1970s. They are variable on timescales of days or less. All are strong and variable radio sources. There are two subclasses.

BL Lac objects are characterized by spectra in which emission lines are either absent or extremely weak. They lie at relatively low redshifts. At first, they were mistaken for variable stars until their spectra were studied. (Their name derives from BL Lacertae which is the variable-star designation originally given to the first object of this type to be studied.)

Just over 100 BL Lacs are known and evidence for host galaxies has been found for 70 or so. Figure 3.25 shows three examples of a survey of BL Lac host galaxies that was conducted with the Hubble Space Telescope. In most cases the host galaxy appears to be elliptical and the stellar absorption lines help to confirm the redshift of the object.

Optically violent variables (OVVs) are very similar to BL Lacs but have stronger, broad emission lines and tend to lie at higher redshifts.

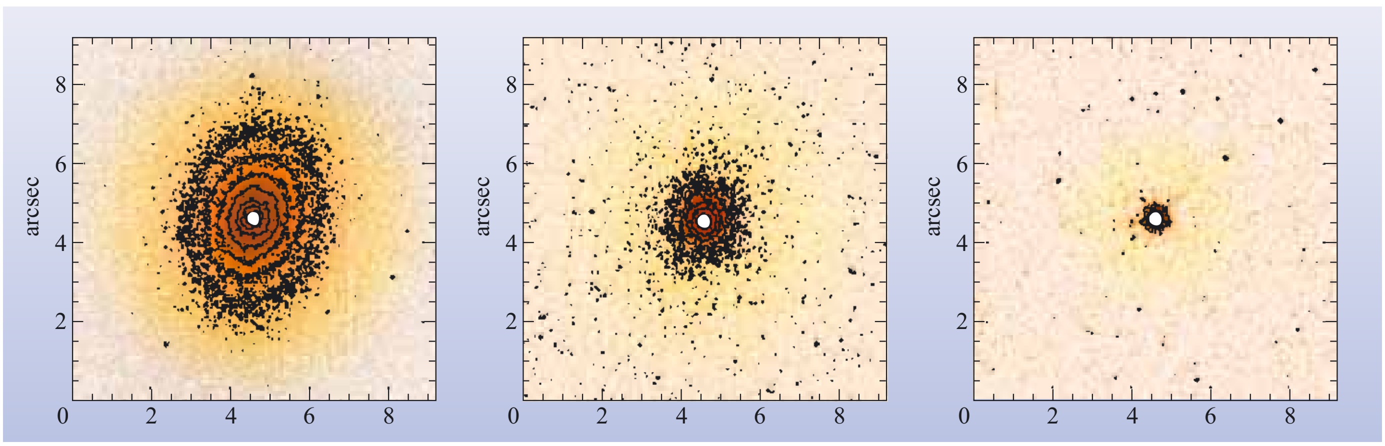

Figure 3.25 Examples of Hubble Space Telescope observations of BL Lac objects. This sequence shows the isophotes around three BL Lac objects: (left) 0548–322 – with a clearly imaged elliptical host galaxy, (middle) 1534+014 – which is resolved and can be shown to have isophotes that correspond to a normal elliptical galaxy, (right) 0820+255 – in which the host galaxy is unresolved. In all three cases the emission from the point-like AGN has been masked out. (Adapted from Scarpa *et al.*, 2000)

3.3.5 A 'non-active' class – the starburst galaxies

We end this section by drawing a distinction between the classes of active galaxy that are described above and the *starburst galaxies* mentioned earlier. As you have seen, starburst galaxies are essentially ordinary galaxies in which a massive burst of star formation has taken place. Their spectra show emission lines from their many HII regions and infrared emission from dust but, in the main, they do not show unusual activity in their nuclei. In the past they were regarded as active galaxies but modern practice is to place them in a class of their own.

Although it is clear that there are starburst galaxies that are not active galaxies, it does appear that some active galaxies are undergoing a burst of star formation. It is not clear at present whether there is a link between these two types of phenomenon where they are seen in the same galaxy but, as you will see later, it is possible that both types of phenomenon – rapid star formation and activity in the galactic nucleus – may be triggered by galactic collisions and mergers.

QUESTION 3.6

Take a few minutes to jot down as many differences that you can think of between normal galaxies and each of the four types of active galaxy. Are there any characteristics which all active galaxies have in common?

3.4 The central engine

From the previous section you will have discovered that one thing all active galaxies have in common is a compact nucleus, the AGN, which is the source of their activity. In this section you will study the two properties of AGNs that make them so intriguing – their small size and high luminosity – and learn about the energy source at the heart of the AGN, the central engine.

3.4.1 The size of AGNs

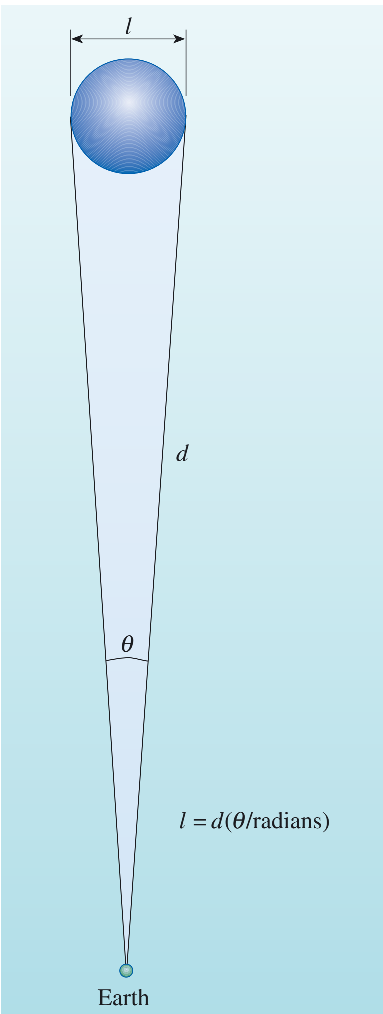

Figure 3.26 Schematic diagram to show how the linear size l of an AGN may be worked out from its angular size θ and distance d.

AGNs appear point-like on optical images. It is instructive to work out how small a region these imaging observations indicate. Optical observations from the Earth suffer from 'seeing', the blurring of the image by atmospheric turbulence. The result is that star-like images are generally smeared by about 0.5 arcsec or more. One can do much better with the Hubble Space Telescope where, thanks to the lack of atmosphere, resolved images can be as small as 0.05 arcsec. What does this mean in terms of the physical size of an AGN?

An arc second is 1/3600 of a degree and there are 57.3 degrees in a radian. So 0.05 arcsec corresponds to an angle of $0.05/(57.3 \times 3600)$ rad $= 2.4 \times 10^{-7}$ rad. For such a small angle, the linear diameter l of an object is related to its distance d by $l = d \times \theta$, where θ is its angular diameter in radians (Figure 3.26).

The nearest known AGN is NGC 4395, a Seyfert at a distance of 4.3 Mpc and it, too, is unresolvable with the Hubble Space Telescope. So its linear size l must be less than $(4.3 \times 10^6) \times (2.4 \times 10^{-7})$ pc $= 1.0$ pc. So, for a nearby AGN, we can place an upper limit of order 1 pc on its linear size. (For a more distant AGN, this upper limit is correspondingly larger.) A parsec is a tiny distance in galactic terms. Even the nearest star to the Sun is more than one parsec away, and our Galaxy is 30 kpc in diameter. So the point-like appearance of AGNs tells us that they are *much* smaller than any galaxy.

A second approach to estimating the size of an AGN comes from their variability. The continuous spectra of most AGNs vary appreciably in brightness over a one-year timescale, and several vary over timescales as short as a few hours (about 10^4 s), especially at X-ray wavelengths (see Figure 3.27). This variability places a much tighter constraint on the size, as you will see.

To take an analogy, suppose you have a spherical paper lampshade surrounding an electric light bulb. When the lamp is turned on, the light from the bulb will travel at a speed c and will reach all parts of the lampshade at the same time, causing all parts to brighten simultaneously. To our eyes the lampshade appears to light up instantaneously, but that is only because the lampshade is so small. In fact, light arrives at your eyes from the nearest point of the lampshade a fraction of a second

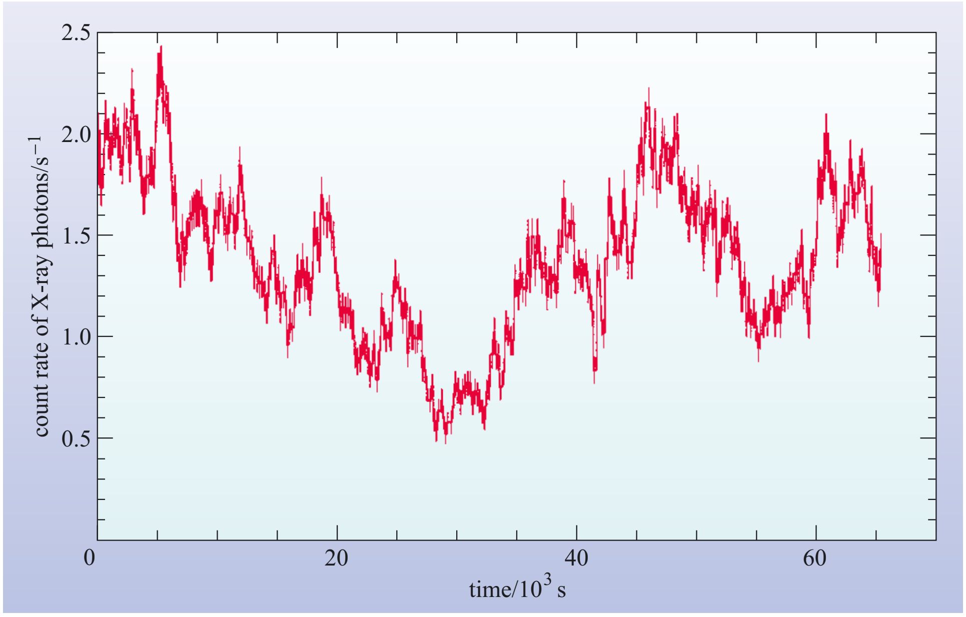

Figure 3.27 An example of X-ray variability, shown by the Seyfert galaxy MCG-6-30-15 during an observation made by the Chandra X-ray Observatory. The fastest fluctuations are spurious noise, but the variability over a few thousand seconds is a property of the AGN. (Lee *et al*., 2002)

before it arrives from the furthest visible point (Figure 3.28). The time delay for the brightening, Δt, is given by

$$\Delta t = R/c \tag{3.3}$$

where R is the radius of the lampshade.

Now imagine the shade to be much larger, perhaps the size of the Earth's orbit around the Sun, and the observer is far enough out in space that the shade appears as a point source of light.

- What is Δt for a lampshade with the same radius as the Earth's orbit?
- $\Delta t = (1.5 \times 10^{11}\ \text{m})/(3 \times 10^8\ \text{m s}^{-1}) = 500\ \text{s}$

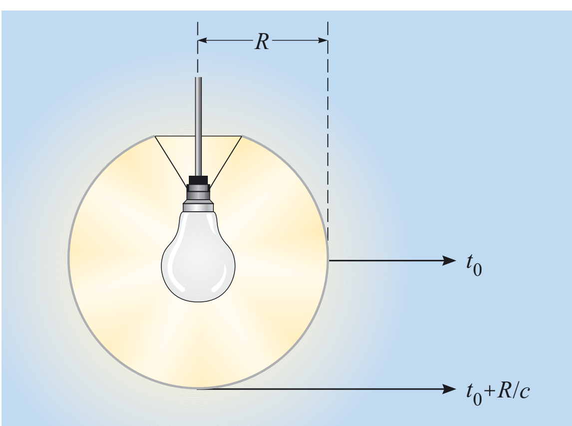

Figure 3.28 Light from the most distant visible point of a spherical lampshade will reach the observer a time R/c later than light from the near side. Fluctuations on timescales of less than R/c will not be observed.

So even if the lamp is switched on instantaneously, the observer will see the source take about eight minutes to brighten. Now suppose the bulb starts to flicker several times a second. What will an observer see? Even though the lampshade will flicker at the same rate as the bulb, it's clear that the flickering will have no effect on the *observed* brightness of the lampshade, since each flicker will take 500 seconds to spread across the lampshade and the flickers will be smeared out and mixed together. There is a limit to the rate at which a source (in this case the lampshade) can be seen to change in brightness and that limit is set by its size.

This argument may be inverted to state that if the observer sees a significant change in brightness of an unresolved source in a time Δt, then the radius of the source can be no larger than $R = c\Delta t$.

This kind of argument applies for any three-dimensional configuration where changes in brightness occur across a light-emitting surface. Of course, the argument is only approximate – real sources of radiation are unlikely to be perfectly represented by the idealized lampshade model that we have used here. The relationship between the maximum extent (R) of any source of radiation and its timescale for variability (Δt) is usually expressed as

$$R \sim c\Delta t \tag{3.3a}$$

(Where the symbol '$\sim$' is used to imply that the relationship is correct to within a factor of about ten.)

Returning now to the AGN, let us calculate the value of R for an AGN such as MCG-6-30-15. The timescale for variability that we shall use is the shortest time taken for the intensity of the source to double. By inspecting Figure 3.27 it can be seen that this timescale is about 10^4 s.

We have $R \sim c\Delta t$, so with $\Delta t = 1 \times 10^4$ s, we obtain $R \sim 3 \times 10^{12}$ m $= 1 \times 10^{-4}$ pc. This is a staggeringly small result – it is ten thousand times smaller than the upper limit we calculated from the size of AGN images – and corresponds to about 20 times the distance from the Sun to the Earth. The AGN would easily fit within our Solar System. The argument does not depend on the distance of the AGN. Hence the observed variability of AGNs places the strongest constraint on their size.

One note of caution: the variability of AGNs usually depends on the wavelength at which they are observed. Variations in X-rays, for example, tend to be faster than variations in infrared light. Does this imply that the size of an AGN depends on the wavelength? In a sense, yes, as we are seeing different radiation from different parts of the object. The X-rays seem to come from a much smaller region of the AGN than the infrared emission, so we must be careful when talking about 'the size' of an AGN.

QUESTION 3.7

An AGN at 50 Mpc appears smaller than 0.1 arcsec in an optical observation made by the Hubble Space Telescope, and shows variability on a timescale of one week. Calculate the upper limit placed on its size by (a) the angular diameter observation, and (b) the variability observation.

Other evidence also indicates the small size of AGNs. Radio astronomers operate radio telescopes with dishes placed on different continents. This technique of *very long baseline interferometry* (VLBI), is able to resolve angular sizes one hundred or so times smaller than optical telescopes can. Even so, AGNs remain unresolved.

3.4.2 The luminosity of AGNs

It is instructive to express the luminosity of an AGN in terms of the luminosity of a galaxy like our own. The figure may then be converted into solar luminosities, if we adopt the figure of $2 \times 10^{10} L_{\odot}$ for the luminosity of our Galaxy.

Consider a Seyfert galaxy first. At optical wavelengths the point-like AGN is about as bright as the remainder of the galaxy, which radiates mainly at optical wavelengths. But the AGN also emits brightly in the ultraviolet and the infrared, radiating at least three times its optical luminosity. So one concludes that for a typical Seyfert, the AGN has at least four times the luminosity of the rest of the galaxy.

We have seen that a characteristic of a quasar is that its luminous output is dominated by emission from its AGN. However quasar host galaxies are not less luminous than normal galaxies, so the AGNs of quasars must be *far* brighter than normal galaxies and must also be considerably more luminous than the AGNs of Seyfert galaxies.

In the case of a radio galaxy, the AGN may not emit as much energy in the optical as Seyfert and quasar AGNs, but an analysis of the mechanism by which the lobes shine shows that the power input into the lobes must exceed the luminosity of a normal galaxy by a large factor, and the AGN at the centre is the only plausible candidate for the source of all this energy.

A similar conclusion for AGN luminosity follows for blazars, which appear to be even more luminous than quasars. We examine why in Section 3.4.6 below.

QUESTION 3.8

Calculate the luminosity of an AGN that is at a distance of 200 Mpc, and appears as bright in the optical as a galaxy like our own at a distance of 100 Mpc. Assume that one-fifth of the energy from the AGN is at optical wavelengths.

One can conclude that AGNs in general have luminosities of more than $2 \times 10^{10} L_{\odot}$ produced within a tiny volume. Stop to ponder this statement for a minute. The power output of the Sun is so large that it is hard to comprehend; the number 2×10^{10} is even more difficult to imagine! Putting together over 2×10^{10} Suns' worth of luminosity inside an AGN is well beyond the powers of imagination of most of us. One Sun's worth of luminosity is about 4×10^{26} W, so a typical AGN has a luminosity of more than 8×10^{36} W. In fact, that's quite modest for an active galaxy, so for the purposes of this chapter we shall adopt a more representative value of 10^{38} W as the characteristic luminosity of an AGN.

You are now in a position to appreciate the basic problem in accounting for an AGN. It produces an *enormous* amount of power (luminosity) in what is astronomically speaking a *tiny* volume. This source of power is known as the engine. Current ideas about the workings of this engine are discussed in the next section.

3.4.3 A supermassive black hole

A **black hole** is a body so massive and so small that even electromagnetic radiation, such as visible light, cannot escape from it. It is its combination of small size and very strong gravitational field that makes it attractive as a key component of the engine that powers an AGN. You saw in Chapter 1 that there is good evidence of a black hole of mass $2.6 \times 10^6 M_\odot$ at the centre of the Milky Way. As you will see, it turns out that much more massive black holes are needed to explain AGNs, and these are referred to as *supermassive black holes*.

A black hole, supermassive or otherwise, is such a bizarre concept that it is worth recapping. The material of which it is made is contained in a radius so small that the gravity at its 'surface', the so-called **event horizon**, causes the escape speed to exceed the speed of light. According to classical physics, any object that falls into it can never get out again. Even electromagnetic radiation cannot escape, which is why the hole is called 'black'. What goes on inside the black hole is academic – no-one can see. What might be seen is activity just outside the event horizon where the gravitational field is strong, but not so strong as to prevent the escape of electromagnetic radiation. It is this surrounding region that is of most interest to astronomers.

The radius of the event horizon is called the **Schwarzschild radius** and is the distance at which the escape speed is just equal to the speed of light. It is given by

$$R_S = 2GM/c^2 \tag{3.4}$$

Let us now calculate the maximum mass M of a black hole that is small enough to fit inside an AGN. In Section 3.4.1 you found that an AGN that varies on a timescale of one day must have a radius less than 3×10^{12} m. We shall see later that all of the emission from the AGN must come from a region that is outside of the Schwarzschild radius and that the size of this emission region is a few times bigger than R_S. Consequently, for this approximate calculation we shall adopt a size for R_S that is a factor of ten smaller than the size we calculated above for the emission region, i.e. $R_S = 3 \times 10^{11}$ m. Then, from Equation 3.4,

$$\begin{aligned} M &= R_S \times c^2/2G \\ &= (3 \times 10^{11}\,\text{m}) \times (3.0 \times 10^8\,\text{m s}^{-1})^2/(2 \times 6.67 \times 10^{-11}\,\text{N m}^2\,\text{kg}^{-2}) \\ &= 2 \times 10^{38}\,\text{kg} \end{aligned}$$

which is equivalent to

$$(2.0 \times 10^{38}\,\text{kg})/(2.0 \times 10^{30}\,\text{kg})M_\odot = 1 \times 10^8 M_\odot$$

This result shows that is clearly possible to fit a black hole with an enormous mass within an AGN, although it does *not* prove that the central black hole has to be this massive. We will shortly see that there is a different argument that does show that mass of any black hole at the centre of an AGN must be about $10^8 M_\odot$. This is usually adopted as the 'standard' black hole mass in an AGN. It is some 10^7 times greater than the masses of the black holes inferred to exist in some binary stars that emit X-rays. Hence, the name **supermassive black hole** has been adopted.

3.4.4 An accretion disc

What will happen to matter that comes near a black hole? Consider a gas cloud moving to one side of the black hole, such as cloud A in Figure 3.29. The hole's gravity will accelerate the gas cloud towards it. The cloud will reach its maximum speed when it is at its closest approach to the black hole, but will slow down again as it moves away; it will then move away to a distance at least as great as the distance from which it started. Thus far nothing is new; the gas cloud will behave exactly as it would if it came near some other gravitationally attracting object, such as a Sun-like star.

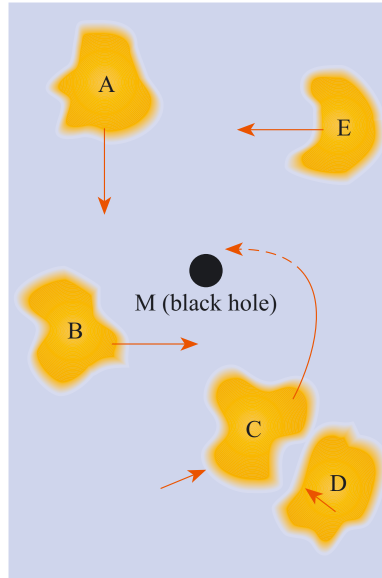

Figure 3.29 Schematic diagram of discrete gas clouds falling towards a black hole. Clouds C and D are shown colliding. This will allow the clouds to become trapped in an orbit around the black hole.

Now, let us extend the argument to a number of gas clouds being accelerated towards the black hole from different directions in space. This time, as the gas clouds get to their closest approach they will collide with each other, thus losing some of the kinetic energy they had gained as they fell towards the hole. Therefore some, but not all, of the clouds of gas will have slowed to a speed at which they cannot retreat, so they will go into an orbit around the hole. Further collisions amongst the gas clouds will tend to make their orbits circular, and the direction of rotation will be decided by the initial rotation direction of the majority of the gas clouds. The effect of the collisions will be to heat up the gas clouds; the kinetic energy they have lost will have been converted into thermal energy within each cloud, and so the cloud temperature will rise.

So far, we can envisage a group of warm gas clouds in a circular orbit about the black hole. But the clouds of gas are of a finite size and, because they move in a Keplerian orbit, the inner parts of the gas clouds will orbit faster than the outer parts. A form of friction (*viscosity*) will act between neighbouring clouds at different radii and they will lose energy in the form of heat. The consequence of this is that the inner parts of the gas clouds will fall inwards to even smaller orbits. This process will continue until a complete **accretion disc** is formed around the black hole (Figure 3.30). The accretion disc acts to remove angular momentum from most of the gas in the disc so that if you look at the path of a small part of one gas cloud, you can see that it will spiral inwards. Since angular momentum is a conserved quantity the accretion disc does not actually diminish the total angular momentum of the system – it simply redistributes it such that most gas in the disc will move inwards. This process occurs only for a *viscous* gas – planets in the Solar System do not show any tendency to spiral in to the Sun because interplanetary gas is very sparse. The viscosity causes the gas to heat up further, the thermal energy coming from the gravitational energy that was converted into kinetic energy as the gas fell towards the hole. The heating effect will be large for objects with a large gravitational field and so we might expect that accretion discs around black holes will reach high temperatures and become luminous sources of electromagnetic radiation.

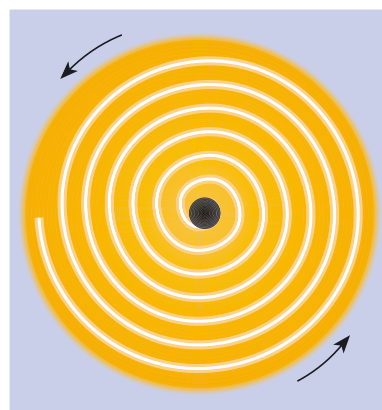

Figure 3.30 A rotating accretion disc; the line shows the spiral infall of one particle.

The gradual spiralling-in of gas through the accretion disc comes to an abrupt end at a distance of a few (up to about five) Schwarzschild radii from the centre of the black hole. At this point the infalling material begins to fall rapidly and quickly passes through the Schwarzschild radius and into the black hole. Note that the accretion disc is located *outside* the event horizon, where the heat can be radiated away as electromagnetic radiation. The accretion model is of such interest because an accretion disc around a massive black hole can radiate away a vast amount of energy, very much more than a star or a cluster of stars. It is this radiated energy that is believed to constitute the power of an AGN.

You may be wondering how large the accretion disc is; after all, the accretion disc as well as the black hole has to fit inside the AGN. The accretion disc gets hotter and therefore brighter towards its inner edge. The brightest, and hence innermost part is what matters. Since this is at only a few times the Schwarzschild radius, so there is no problem of size.

■ Estimate the extent of the brightest part of the accretion disc for a black hole of mass $10^8 M_\odot$. How does this compare with the radii of planetary orbits in the Solar System?

❑ From Section 3.4.3 we know that the Schwarzschild radius is about 3×10^{11} m, which is twice the radius of the Earth's orbit or 2 AU. The brightest part of the accretion disc could then extend to about five times this distance or about 10 AU, which is about the radius of Saturn's orbit.

3.4.5 Accretion power

Calculations based on the above accretion disc hypothesis show that if a mass m falls into the black hole, then the amount of energy it can radiate before it finally disappears is about $0.1mc^2$, or about 10% of its rest energy. Other than matter–antimatter annihilation, this is the most efficient process for converting mass into energy ever conceived. A comparable figure for the nuclear fusion of hydrogen in stars is only 0.7% of the rest energy of the four hydrogen nuclei that form the helium nucleus.

QUESTION 3.9

How much energy could be obtained from 1 kg of hydrogen (a) if it were to undergo nuclear fusion in the interior of a star, (b) if it were to spiral into a black hole? Would you expect to get more energy if it were to chemically burn in an oxygen atmosphere?

Now let us apply the idea of an accreting massive black hole to explain the luminosity of an AGN. We have to explain an object of small size and large luminosity. The Schwarzschild radius of a black hole is very small, and the part of the accretion disc that radiates most of the energy will be only a few times this size. The luminosity will depend on the rate at which matter falls in. Suppose that the matter is falling in at the rate Q (with units of kg s^{-1}), this is known as the **mass accretion rate**. We can now work out the value of Q to produce a luminosity L by writing

$$L = 0.1Qc^2 \quad \text{or} \quad Q = L/(0.1c^2) \qquad (3.5)$$

Using the values $L = 10^{38}$ W and $c = 3 \times 10^8$ m s^{-1}, we get $Q = 10^{22}$ kg s^{-1}. Converting this into solar masses per year using $1M_\odot \approx 2 \times 10^{30}$ kg and 1 year $\approx 3 \times 10^7$ s, we get $Q \approx 0.2M_\odot$ per year. Is there a large enough supply of matter for a fraction of a solar mass to be accreted every year? Most astronomers think that the answer is yes, and that even higher accretion rates are plausible – after all our own Galaxy has 10% of its baryonic mass in gaseous form, so there is at least $10^{10}M_\odot$ of gas available.

■ Does this estimate of the accretion rate require a supermassive black hole, or will any black hole such as one of $5M_\odot$ do?

❑ The mass of the black hole does not enter into the above calculation. So on this basis a $5M_\odot$ black hole would seem to be sufficient.

Moreover, the mass calculated in Section 3.4.3 is an upper limit. So, why is a *supermassive* black hole needed? To see why, we ask: is there any limit to the power L that can be radiated by an accretion disc around a black hole, or can one conceive of an ever-increasing value of L if there is enough matter to increase Q?

There *is* a limit to the amount of power that can be produced, and it is called the **Eddington limit**. As the black hole accretes faster and faster, the luminosity L will go up in proportion, that is to say the accretion disc will get brighter and hotter. Light and other forms of electromagnetic radiation exert a pressure, called **radiation pressure**, on any material they encounter. (This pressure is difficult to observe on Earth because it is difficult to find a bright enough light source.) Around an accreting black hole with a luminosity of 10^{38} W, the radiation will be so intense that it will exert a large outward pressure on the infalling material. If the force on the gas due to radiation pressure exactly counteracts the gravitational force, accretion will cease. This process acts to regulate the luminosity of an accreting black hole.

To work out the Eddington limit, it is necessary to balance radiation pressure against the effects of the black hole's gravity. Consider an atom of gas near the outer edge of the accretion disc. The force on it due to radiation pressure is proportional to L, whereas the gravitational force is proportional to the mass M of the black hole (assuming the mass of the accretion disc to be negligible). A balance is achieved when L_E = constant × M, where L_E is the Eddington limit. Full calculations give

$$L_E/\mathrm{W} = (1.3 \times 10^{31})M/M_\odot \qquad (3.6)$$

This is the upper limit of the luminosity of a black hole of mass M – the luminosity can be lower than L_E but not higher. The larger the mass M, the greater the value of L_E.

In fact, this is only a rough estimate. It assumes that the accreting material is ionized hydrogen (a good assumption) and that the hole is accreting uniformly from all directions (which is not a good assumption). The Eddington luminosity may be exceeded, for example, if accretion occurs primarily from one direction and the resulting radiation emerges in a different direction. Nonetheless, it is a useful approximation.

Putting $L = 10^{38}$ W into Equation 3.6, we find that $M = 7.7 \times 10^6 M_\odot$. So we see that we do need a *supermassive black hole* to account for the engine in an AGN, and $10^8 M_\odot$ is usually assumed.

In summary, then, the Eddington limit means that the observed luminosity of quasars requires an *accreting supermassive black hole* with a mass of order $10^8 M_\odot$; the accretion rate is at least a significant fraction of a solar mass per year; and the Schwarzschild radius is about 3×10^{11} m.

3.4.6 Jets

You have seen that two kinds of active galaxies – quasars and radio galaxies – are often seen to possess narrow features called jets projecting up to several hundred kiloparsecs from their nuclei. If these are indeed streams of energetic particles flowing from the central engine, how do they fit with the accretion disc model? How could the jets be produced?

The answers to these questions are not fully resolved, but there are some aspects of the model of the central engine which probably play an important part in jet formation. A key idea is that the jets are probably aligned with the axis of rotation of the disc – since this is the only natural straight-line direction that is defined by the system. This much is accepted by most astrophysicists, but the question of how material that is initially spiralling in comes to be ejected along the rotation axis of the disc at relativistic speeds (i.e. speeds that are very close to the speed of light) is an unsolved problem. One mechanism that has been suggested requires that at distances very close to the black hole the accretion disc becomes thickened and forms a pair of opposed funnels aligned with the rotation axis, as illustrated in Figure 3.31. Within these funnels the intense radiation pressure causes the acceleration and ejection of matter along the rotation axis of the disc. Unfortunately, this model fails in that it cannot produce beams of ejected particles that are energetic enough to explain the observed properties of real jets. Other variants of this scenario, and in particular those in which the magnetic field of the disc plays a major role in the ejection of jets are under investigation but do not yet offer a full explanation of the jet phenomenon.

If jets are ejected along the rotation axis of the disc, then why do quasars and the more powerful radio galaxies generally only appear to have a single jet? It seems improbable that the engine produces a jet on one side only, and it is thought that there are indeed two jets but only one is visible. In this model, two jets are emitted at highly relativistic speeds, and one of them is pointing in our direction and the other is pointing away. Due to an effect called *relativistic beaming*, the radiation from the jets is concentrated in the forward direction. The consequence of this is that if a jet is pointing even only very approximately towards us it will appear very much brighter than would a similar jet that is pointing in the opposite direction. (The special case of what happens when a jet is pointing directly at us will be considered in the next section.)

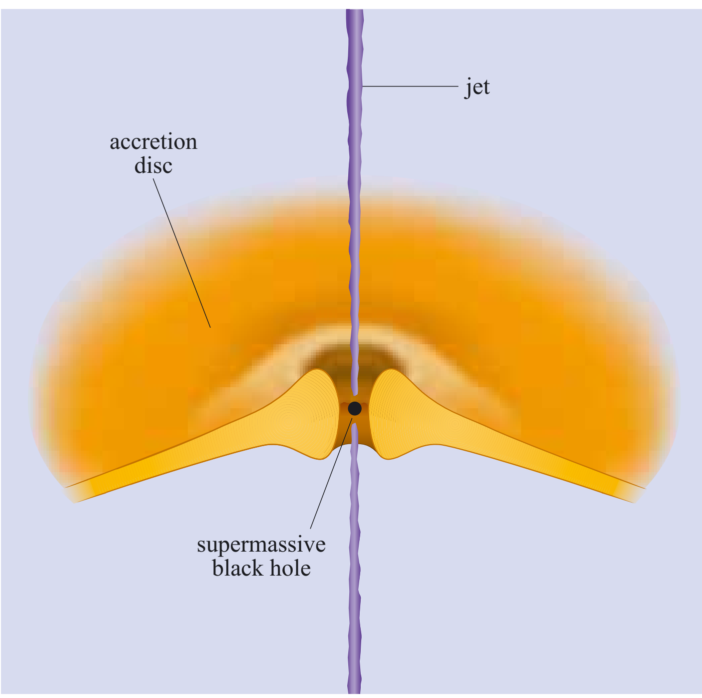

Figure 3.31 A scenario for the formation of jets in which the inner region of an accretion disc thickens to form two opposed funnels (for clarity, the accretion disc is cut-away to reveal the central black hole). The emission of radiation from the faces of the funnel leads to radiation pressure which acts to channel outflowing material into two relativistic particle beams called jets. Unfortunately this simple model cannot fully explain the observed properties of real jets.

QUESTION 3.10

Estimate the accretion rate on to a black hole needed to account for the luminosity of a Seyfert nucleus that has twice the luminosity of our Galaxy. Express your answer in solar masses per year. What, other than the mass accretion rate, limits the luminosity?

3.5 Models of active galaxies

So far we have seen how the properties of the central engine of the AGN can be accounted for by an accreting supermassive black hole. Though there are many questions still to be resolved, this model does seem to be the best available explanation of what is going on in the heart of an AGN. But of course all AGNs are not the same. We have identified four main classes and in this section we will attempt to construct models that reproduce the distinguishing features of these four classes.

Figure 3.32 shows the basic model that has been proposed for AGNs. It is a very simple model, and does not account for all AGN phenomena, but it does give you a flavour of the kinds of ideas that astrophysicists are working with. You can see that the central engine (the supermassive black hole and its accretion disc) is surrounded by a cloud of gas and dust in the shape of a torus (a doughnut shape). The gap in the middle of the torus is occupied by clouds forming the broad-line region and both in turn are enveloped by clouds forming the narrow-line region.

We begin by looking at the torus.

Figure 3.32 A generic model for an active galaxy. (a) The central engine is a supermassive black hole surrounded by an accretion disc with jets emerging perpendicular to the accretion disc. (b) The engine is surrounded by an obscuring torus of gas and dust. The broad-line region occupies the hole in the middle of the torus and the narrow-line region lies further out. (c) The entire AGN appears as a bright nucleus in an otherwise normal galaxy. Note that the jets extend to beyond the host galaxy and terminate in radio lobes.

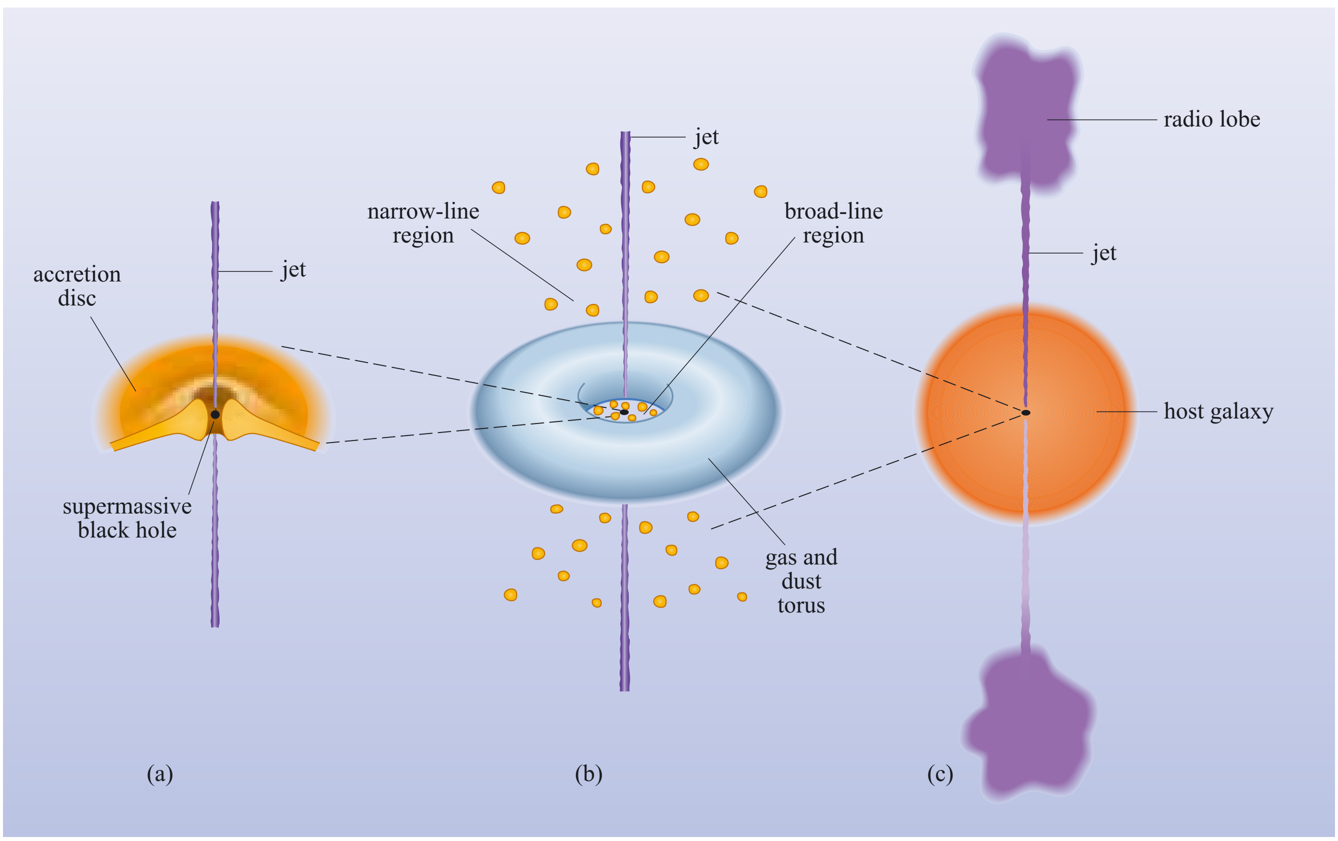

3.5.1 The obscuring torus

If an AGN consisted solely of the central engine, observers would see X-rays and ultraviolet radiation from the hot accretion disc (accounting for the 'the big blue bump' in Figure 3.17) and, apart from the jets, very little else. To account for the strong infrared emission from many AGNs, the model includes a torus of gas and dust that surrounds the central engine.

The dust particles – which are usually assumed to be grains of graphite – will be heated by the radiation from the engine until they are warm enough to radiate energy at the same rate at which they it receive it. As dust will vaporize (or sublimate) at temperatures above 2000 K, the cloud must be cooler than this.

QUESTION 3.11

Assuming that dust grains radiate as black bodies, estimate the range of wavelengths that will be emitted from the torus.

Note: A black-body source at a temperature T has a characteristic spectrum in which the maximum value of spectral flux density (F_λ) occurs at a wavelength given by Wien's displacement law

$$(\lambda_{\text{peak}}/\text{m}) = \frac{2.90 \times 10^{-3}}{(T/\text{K})}$$

So such a dust cloud will act to convert ultraviolet and X-ray emission from the engine into infrared radiation, with the shortest wavelengths coming from the hottest, inner parts of the cloud.

From a very simple dust cloud model, it is easy to understand why AGNs so often emit most of their radiation in the infrared. Almost certainly, dust heated by the engine is observed in most AGNs, although the dust may be more irregularly distributed than in our simple model, and the torus may have gaps in it. Some small amount of the infrared radiation will generally come from the engine itself, though, and in BL Lacs it is probable that most of the infrared radiation comes from the engine. The variability that was discussed in Section 3.4.1 applies to radiation from the engine at X-ray and optical wavelengths (and sometimes at radio wavelengths). The infrared emission from the torus is thought to vary much more slowly, as you would expect from the greater extent of the torus.

Note that this torus is *not* the same as the accretion disc surrounding the black hole, though it may well lie in the same plane and consist of material being drawn towards the engine.

It is possible, using a simple physical argument, to make a rough estimate of the inner radius of the torus by asking how far from the central engine the temperature will have fallen to 2000 K, the maximum temperature at which graphite grains can survive before being vaporized.

If the engine has a luminosity, L, then the flux density at a radius r from the engine will be $L/4\pi r^2$. A dust grain of radius a will intercept the radiation over an area πa^2 (Figure 3.33) and, if no energy is reflected, the power absorbed will be

$$\text{power absorbed} = \pi a^2 \times \frac{L}{4\pi r^2} = \frac{La^2}{4r^2}$$

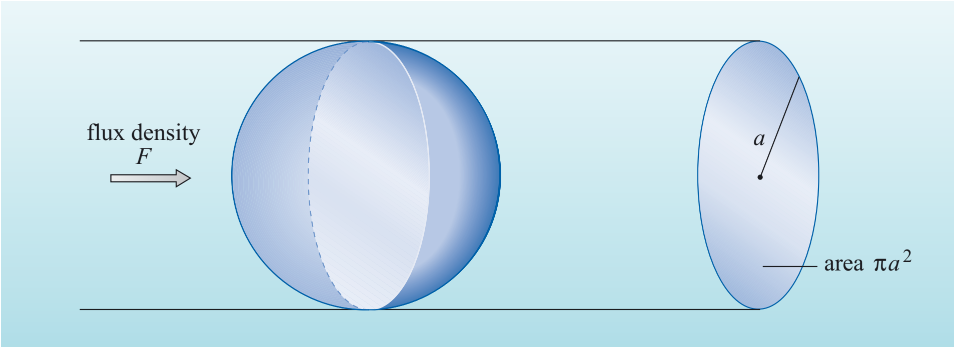

Figure 3.33 A spherical dust grain of radius a will intercept radiation over an area πa^2.

The temperature of the dust grain will rise until the power emitted by thermal radiation is equal to the power absorbed. If the grain behaves as a black body we can write

$$\text{power emitted} = 4\pi a^2 \sigma T^4$$

where σ is the Stefan–Boltzmann constant ($\sigma = 5.67 \times 10^{-8}\ \mathrm{W\,m^2\,K^{-4}}$).

Here we assume that the temperature of the grain is the same over its whole surface, which would be appropriate if, for instance, the grain were rotating. Next, we make the power absorbed equal to the power radiated

$$\frac{La^2}{4r^2} = 4\pi a^2 \sigma T^4$$

Finally, if we divide both sides by a^2, the radius a is cancelled out (as it should – the size of the dust grain should not come into it) and we can rearrange for r to get:

$$r = \left(\frac{L}{16\pi\sigma T^4}\right)^{1/2} \tag{3.7}$$

This distance is called the **sublimation radius** for the dust.

QUESTION 3.12

Calculate the dust sublimation radius, in metres and parsecs, for an AGN of luminosity 10^{38} W. (Assume that dust cannot exist above a temperature of 2000 K.)

For typical luminosities, the inner edge of the torus is three or four orders of magnitude (i.e. 1000 to 10 000 times) bigger than the emitting part of the accretion disc which is contained within the central engine in Figure 3.31. Even so, the torus cannot be resolved even in high-resolution images. However there is evidence in several galaxies of a much more extensive disc of gas and dust that encircles the AGN. It has been suggested, although not proven, that these discs provide a supply of material that can spiral down into the central regions of the active galaxy – passing into the torus, through the accretion disc, and eventually falling into the black hole itself. One example of such a disc is found in the radio galaxy NGC 4261 which is shown in Figure 3.34. On the left (Figure 3.34a) you can see a radio image of the jets, superimposed on an optical image of the host galaxy. The highly

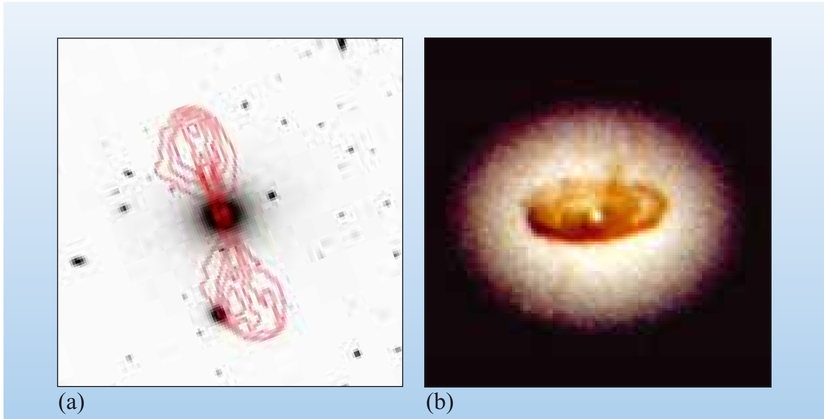

Figure 3.34 The radio galaxy NGC 4261 (also known as 3C 270) is about 31 Mpc away. (a) An optical image that shows the elliptical host galaxy, with contours of radio emission overlaid (in red). The full extent of the radio lobes is about 76 kpc. (b) An optical image from the Hubble Space Telescope of the central regions of NGC 4261, which reveals the presence of a disc of obscuring dust that is about 250 pc in diameter. ((a) Radio data provided by the NASA/IPAC Extragalactic Database from the observations of Condon and Broderick, 1998; optical data from the Digitized Sky Survey (STScI); (b) L. Ferrarese, Johns Hopkins University and NASA)

magnified image (Figure 3.34b), taken with the Hubble Space Telescope, shows a dark obscuring disc silhouetted against the stellar core of the elliptical host galaxy. This disc is about 250 pc across and very much bigger than the sub-parsec structures that make up the AGN itself. Note that its plane is perpendicular to the axis of the radio jets shown on the left of the figure. Thus the jets seem to be aligned along the rotation axis of the disc, and this lends support to the ideas of jet formation that were outlined in Section 3.4.6.

3.5.2 The broad- and narrow-line regions

In our model, the engine is surrounded by gas clouds (Figure 3.32). You have already seen how common these are in our own and other galaxies, so it is reasonable to expect them to be present in at least the spiral galaxies that contain AGNs. If these gas clouds are illuminated by ultraviolet or X-rays from the engine they will absorb the ultraviolet or X-ray energy, and will emit the characteristic lines of the gases making up the clouds. The most abundant gas in galactic clouds is hydrogen, and, sure enough, the Hα and other lines of hydrogen appear strongly in the observed spectra of AGNs.

What about other spectral lines that might be expected? Fortunately we get clues from objects in our own Galaxy, the HII regions, which consist of gas clouds illuminated by sources of ultraviolet radiation, albeit at a lower luminosity. These HII regions emit strong lines of nitrogen and oxygen, [NII] and [OIII], in the optical. Sure enough, the lines that appear in the optical spectra of AGNs turn out to be just what you would expect from a gas of normal cosmic composition surrounding an AGN.

As you have discovered, there appear to be two kinds of line-emitting regions known as the broad-line region (BLR) and narrow-line region (NLR). If we interpret the spectra in terms of the density (inferred from the presence or absence of forbidden lines) and motion of gas clouds (inferred from line widths), then the BLR corresponds to dense fast-moving clouds and the NLR to low-density, more slowly moving clouds.

It is not possible to see the motion in great detail, but these motions are probably associated with the strong gravitational field surrounding an AGN. The orbital speed of a cloud will increase as the distance from the central black hole decreases. Thus the faster moving BLR clouds are assumed to be closer to the centre than the slower moving NLR clouds.

Broad-line region

In the model, the clouds of the broad-line region surround the central engine within the opening in the middle of the dust torus. The radius of the BLR is of the order of 10^{14} m, placing it well inside the torus. At this distance from the black hole orbital speeds are several thousand kilometres per second, which is consistent with the typical speed of 5000 km s^{-1} that is measured from Doppler broadening. The clouds are fully exposed to the intense radiation from the engine (remember that any dust will have vaporized in this region) and will be heated to a high temperature. It is difficult to measure the temperature of BLR clouds, but it appears to be of the order of 10^4 K.

It has been estimated that the BLR of a typical AGN will have about 10^{10} clouds covering about 10% of the sky as seen from the central engine. The total mass of gas is less than $10M_{\odot}$, so it is utterly negligible compared with the black hole itself.

As you will have noted from Section 3.3, broad lines are not seen in every AGN. The general belief among astronomers is that every AGN has a broad-line region, but in some cases our view of the BLR clouds is obscured by the dust torus, so broad lines do not appear in the spectrum.

Narrow-line region

The model places the narrow-line region much further out from the central engine where orbital speeds are lower; 200–900 km s^{-1} is typical for the NLR.

An important consequence of the NLR being outside the dust torus is that it is always in view, so narrow lines will be seen even if the broad-line emitting gas is obscured.

QUESTION 3.13

The narrow-line region is the most extensive part of the AGN and envelops all the other components. Like the other parts, it is illuminated by the central engine. Bearing in mind the geometry of the dust torus, describe what the NLR might look like if a spaceship could get close enough to see it. From which direction would the observers have the best view?

So the model predicts that the NLR, if we could see it, would have a distinctive shape. You might think that such observations would be impossible, considering the tiny size of an AGN. But the NLR is the outer part of the AGN and has no real boundary. In fact, several NLRs have been imaged by the Hubble Space Telescope and one example, for the Seyfert galaxy NGC 5252, is shown in Figure 3.35. The double wedge shape reveals where the gas is illuminated by radiation shining from the centre of the torus. In this case the emission extends several kiloparsecs from the AGN and is known as an *extended narrow-line region*. The extended region is simply interstellar gas ionized by the radiation from the engine. This observation, and others like it, provides supporting evidence for the geometry of the dust torus and the NLR.

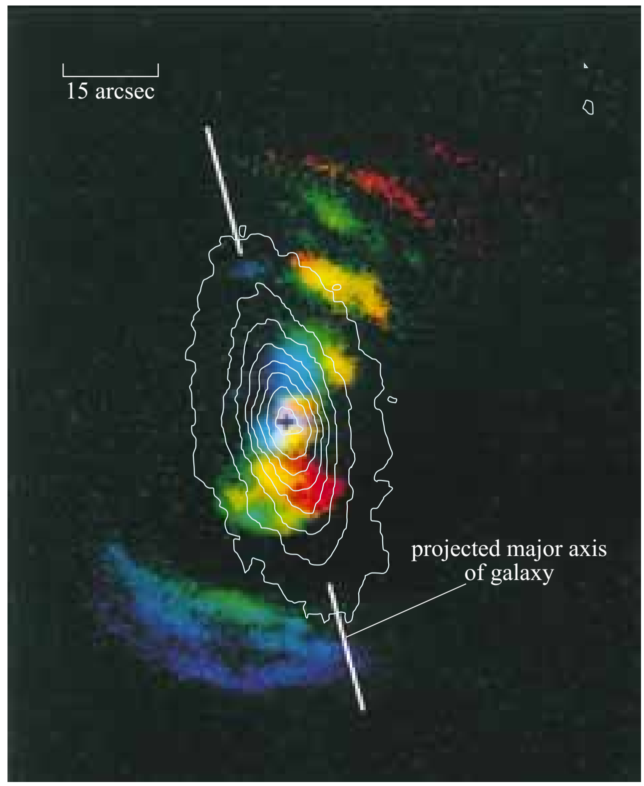

Figure 3.35 NGC 5252 is a type 2 Seyfert galaxy that is about 96 Mpc away. The white contours show the isophotes of the host galaxy (Hubble type S0). The coloured areas show emission from the extended narrow-line region: blue and red regions indicate emission from gas that is moving towards, or away from us, respectively (green and yellow regions have a low radial velocity). The emitting regions form two characteristic wedge shapes, or *ionization cones* that reveal where gas is illuminated by radiation escaping from the poles of the obscuring torus. (Morse *et al*., 1998 with isophotal data from the Digitized Sky Survey/STScI)

So even if we cannot observe the inner structure of an AGN, the regions around the nucleus are tantalizingly consistent with the model.

3.5.3 Unified models

You are now familiar with the main components for building models of AGNs: a central engine powered by an accreting supermassive black hole (with or without jets), clouds of dust, clouds of gas and accretion processes that can organize the gas and dust into a torus-shaped structure. Many attempts have been made to use these components to explain the different types of AGN. Two basic ideas – or perhaps hopes – underlie these models. First, all AGNs are essentially the same and differ chiefly in the luminosity of the central engine which in turn depends on the mass of the black hole and the mass accretion rate. Second, if the AGN contains a dust torus then the radiation observed will depend on the direction from which the AGN is viewed. Two possible schemes for such unified AGN models are shown in Figure 3.36. One is for radio-quiet AGNs and the other is for radio-loud AGNs.

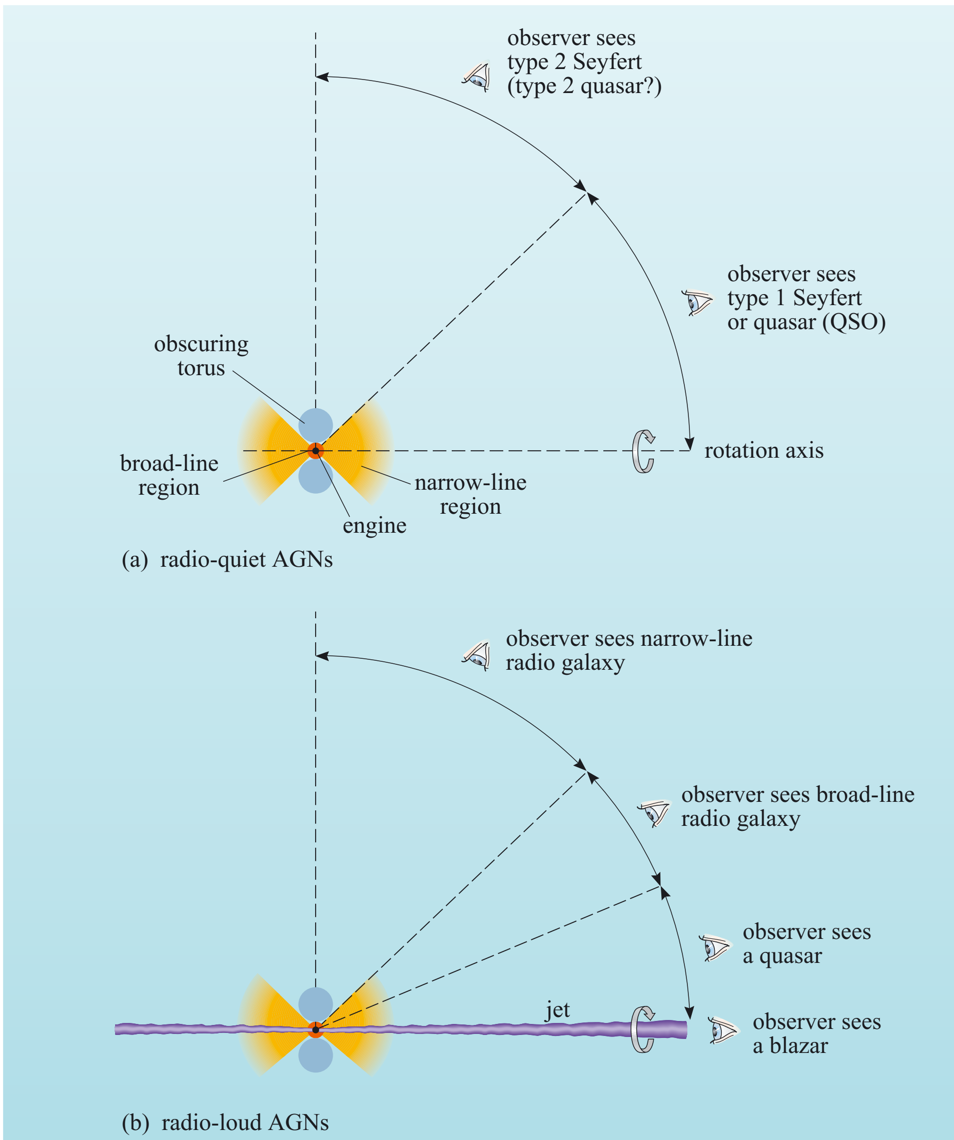

Figure 3.36 Two tentative unified models for AGNs. Note that, at present, it is not clear whether a class of quasar that is analogous to type 2 Seyferts exists. (a) Radio-quiet AGNs. (b) Radio-loud AGNs. (The angles are approximate.)

Radio-quiet AGNs

There has been a great deal of debate about whether there really are two different types of Seyfert or whether they can both be accounted for by the same model.

For example, suppose that you look at the model AGN in Figure 3.36a from a direction not too far from the rotation axis of the torus. You will see X-ray, UV (the 'big blue bump') and other radiation from the engine, broad lines from the broad-line region, narrow lines from the narrow-line region and infrared from the dust torus. You will observe the features associated with a type 1 Seyfert. If you look at the same model from a direction nearer to the plane of the torus, the X-rays and the broad optical emission lines will be hidden by the torus, and you will observe the features associated with a type 2 Seyfert. Observations strongly suggest that at least some type 2 Seyferts are essentially type 1 Seyferts seen from a different angle. This also accounts for the intermediate types, where the broad-line region is only partly in view.

- ■ The galaxy in Figure 3.35 is described as a type 2 Seyfert. Is this significant?
- ❑ Yes. In the unified model, type 2 Seyferts are seen from an angle close to the plane of the torus. This is the best viewing angle to see the shape of the NLR, as discussed in Question 3.13.

Does the same apply to other types of AGN? Radio-quiet quasars (QSOs) appear in many respects to be similar to type 1 Seyferts, showing both broad and narrow emission lines, but are much more luminous. There seems little doubt that Seyferts and radio-quiet quasars differ primarily in luminosity.

Much less is known about 'type 2'quasars without broad lines, analogous to the type 2 Seyferts. It may be that the dust torus around the more luminous quasars is diminished by the intense radiation, hence revealing the BLR from a large fraction of all possible orientations. On the other hand, some astronomers speculate that a recently discovered class of highly luminous galaxies that emit strongly in the far infrared may be the missing type 2 quasars concealed behind their dust clouds.

Radio-loud AGNs

The second model (Figure 3.36b) is similar to the first, but now the engine is producing a pair of jets that will eventually end in a pair of lobes, as seen in radio galaxies and some quasars.

Looking at the model from the side, one expects to see narrow lines in the spectrum (but not broad lines) and two jets surrounded by extended lobes. This is a narrow-line radio galaxy. At an angle closer to the jet axis the broad-line region comes into view and a broad-line radio galaxy is seen. So far this is analogous to the two types of Seyfert, but now another effect comes into play. As you saw in Section 3.4.6, relativistic beaming will cause an approaching jet to be brighter than a receding jet, so as the angle decreases one jet will fade at the expense of the other and a radio galaxy with a single jet will now be visible (though there may well be two lobes). As the angle continues to decrease the intense source of radiation surrounding the black hole comes into view and the object appears as a quasar, with never more than one visible jet. Finally, a blazar is seen when the torus is face-on to the observer who is looking straight down the jet. One distinguishing feature

of the blazars is that the spectrum is dominated by a smooth continuous spectrum which is what one would expect if the radiation is coming from the jet itself. Another feature of blazars is their rapid variability over a wide range of wavelengths, and this again is to consistent with the idea of the emission arising from a jet. BL Lacs would correspond to the less powerful radio galaxies and OVVs to the more powerful ones.

Unification of the radio-loud sources is more contentious and this model is by no means the last word on the subject. It has been difficult to reconcile all the observed properties of the AGNs with the model. For example, one test would be to examine whether the numbers of different kinds of AGN are consistent with what the model predicts.

■ Suppose that radio galaxies, radio-loud quasars and blazars were all the same kind of object but seen from different angles. From Figure 3.36b, which would you expect to be the most common? Which the least common?

❑ Radio galaxies would be seen over the widest range of angles, so these would be the most common. Blazars, on the other hand, would only be seen over a narrow range of angles and would be relatively rare.

This simple approach is complicated by two things. First, AGNs vary greatly in luminosity and distance, so the number observed is not necessarily a measure of how common they are. Powerful or nearby objects are more likely to show up in a survey than weak or distant objects. Second, AGNs are visible over such large distances that the light from the more remote ones started on its journey when the Universe was considerably younger than it is today. The most distant quasars may no longer exist in the form in which they are observed. We shall return to that idea shortly.

At the moment the jury is still out, as they say, but astronomers are confident that even if the different kinds of radio-loud AGNs are not identical siblings, they are at least close cousins.

Perhaps the most difficult question is why some AGNs are radio-loud while most are radio-quiet. You have seen that the radio-quiet AGNs appear to reside in spiral galaxies while the radio-loud AGNs are in ellipticals. It was once thought that the presence of gas in spiral galaxies acted to suppress the emergence of jets from the engine, but that idea is no longer favoured. Current thinking relates the presence of jets to the angular momentum of the black hole, with only the faster-spinning black holes able to produce jets. The novel element is that a high spin rate could be achieved not by accretion but by the merger of two massive black holes following the collision and merger of their host galaxies. As you saw in Chapter 2, there is other evidence that giant elliptical galaxies are formed from mergers, so this seems a plausible, if yet unproven, explanation as to why the radio-loud sources tend to be found in ellipticals.

3.6 Outstanding issues

The model described above is very attractive. Indeed, it is so attractive that it is easy to overlook the many problems that remain.

3.6.1 Do supermassive black holes really exist?

One outstanding feature of the black-hole model is that the black hole must be supermassive, for reasons argued in Section 3.4.3. Can one at least detect the presence of a massive central object?

- From what you have learned about galactic rotation curves, how might a massive central object be detected?
- By measuring rotation speeds near the nucleus of the galaxy. The faster the rotation speeds, the greater the enclosed mass.

So the answer is yes. In NGC 4151, a prominent type 1 Seyfert galaxy, the broad lines are observed to vary as well as the continuous spectrum. The line variations lag about 10 days behind associated variations in the continuous spectrum. The usual interpretation is that the variations commence in the engine, where the continuous spectrum originates, then take 10 days to 'light up' the broad-line region. So the broad-line region must be a distance r of about 10 light-days from the engine. Supposing that the broad lines are Doppler-broadened by rotation around the engine, then one has a picture of regions of gas moving at a speed v of about $7000\,\mathrm{km\,s^{-1}}$ around a central engine of mass M at a radius r. The value of M can now be calculated from v and r, in the same way that the mass of our Galaxy inside radius r was inferred in Chapter 1. Using Equation 1.5,

$$M = rv^2/G \tag{1.5}$$

with r = 10 light-days (3×10^{14} m), and $v = 7 \times 10^6\,\mathrm{m\,s^{-1}}$, and converting into solar masses, we obtain $M = 10^8 M_\odot$. This is consistent with the value of M for an accreting black hole calculated from consideration of the Eddington limit.

This approach has been very productive. One of the most studied active galaxies is the radio galaxy M87 which you have seen in Figure 3.24. Since the late 1970s astronomers have suspected it contains a supermassive black hole and the most recent observations with the Hubble Space Telescope reveal a rotating disc of gas only 16 pc from the centre. If Equation 1.5 applies, then the mass of the central object is around $3 \times 10^9 M_\odot$.

In the mid-1990s it became possible to probe even closer to the centre of an AGN. Measurements of rotating gas within 0.18 pc of the core of NGC 4258, a weak Seyfert galaxy, showed that an object of around $4 \times 10^7 M_\odot$ must be at the centre. Similar measurements have been made of other active galaxies.

Another intriguing observation comes from the Seyfert galaxy MCG-6-30-15, whose variability was illustrated in Figure 3.27. Its X-ray spectrum shows an extremely broad emission line, $100\,000\,\mathrm{km\,s^{-1}}$, which is believed to come from the accretion disc itself. The line is greatly distorted as if it originated in the intense gravitational field near a black hole, but it has not yet been possible to derive the mass of the black hole.

You have now heard some of the evidence that accreting massive black holes really do provide the engine power for AGNs. Do you think it is convincing?

If not, the alternatives are not very promising. The only other idea still in the running is a 'nuclear starburst' model, a cluster of young, massive stars with frequent supernova explosions, but this does not fit the observations so well. It remains interesting because of its similarity to the processes occurring in starburst galaxies. If a supermassive black hole is the leading contender, it is because no-one has yet thought of anything better.

QUESTION 3.14

How convincing is the scientific evidence for: (a) the existence of accreting massive black holes in AGNs; (b) the occurrence of nuclear fusion in the Sun and other stars; (c) the laws governing the orbits of the planets around the Sun?

3.6.2 Where are they now?

At the beginning of this chapter we asked whether active galaxies really are in a class of their own or whether most galaxies go through an active stage at some point in their lives. We can shed some light on this by looking for evidence that active galaxies evolve.

The first question is where AGNs came from. No-one knows how supermassive black holes formed, the question is intimately tied up with the origins of galaxies which, as you have seen in Chapter 2, is itself a vigorously debated topic. But it is likely that close interactions and collisions between galaxies were much more common than they are now, and such disturbances played an important part in providing material to feed a growing black hole and to stimulate AGN activity. Even today, active galaxies are more likely than normal galaxies to be within the gravitational influence of a companion galaxy – about 15% of Seyferts have companions compared with 3% of normal galaxies – and you have seen examples such as Centaurus A which seem to be the result of a recent merger.

Next we can ask how long AGNs live. As indicated earlier, we observe distant objects not as they are today, but as they were at the time their light was emitted. As electromagnetic radiation takes 3.2 million years to travel one megaparsec, even the relatively nearby quasar, 3C 273, is seen as it was some 2.5 billion years ago, and those with the highest observed redshifts are seen perhaps only a billion years after the beginning of the Universe. So by studying the most remote quasars and comparing them with closer ones, it should be possible to see if they have changed over the lifetime of the Universe.

Astronomers have worked out the numbers of quasars in a given volume of space for different redshifts. When the expansion of the Universe is taken into account, the number density of quasars seems to have reached a maximum around a redshift of 2–3 about 10 billion years ago and has been declining sharply ever since. Indeed, quasars were something like 10^3 times more common then than they are now. This suggests that the quasar phenomenon is short-lived, by cosmic standards. Where have they all gone?

- Bearing in mind what you already know about quasars, what would you expect a 'dead' quasar to look like?
- As a quasar is believed to be an AGN within an otherwise normal galaxy, a dead quasar would look like a normal galaxy *without* an AGN.

- How could you tell whether a normal galaxy once had a quasar inside it?
- Look in the nucleus! If the black hole model is correct, dead quasars will leave a supermassive black hole behind them.

So if quasars are indeed powered by supermassive black holes, it should be possible to find the 'relic' black holes in our local region of space, even where there are no obvious AGNs. If a galaxy was once a quasar the black hole will still be there; it is, after all, rather difficult to dispose of an object of $10^8 M_\odot$.

In the last section you learned about the rotation studies used to measure the masses of black holes in AGNs – M87 holds the record at about 3 billion $M_\odot$. The same methods have been used to examine the centres of normal galaxies and you already know one result from Chapter 1: a dark object with a mass of about $2 \times 10^6 M_\odot$ resides at the centre of the Milky Way. There is even more compelling evidence that M31 (the Andromeda Galaxy), which is the nearest big spiral to the Milky Way, contains an object of $3 \times 10^7 M_\odot$. Even its small elliptical companion, M32, hides an object of $2 \times 10^6 M_\odot$. Several more otherwise normal galaxies, most of them not far from the Milky Way, appear to possess supermassive objects, and the closer the observations get to the centre, the more confident astronomers are that these concentrations of mass are indeed black holes.

The modern view is that many, perhaps most, galaxies contain supermassive black holes, though we know that some do not (another nearby spiral, M33, has been shown to have no supermassive black hole, or at least nothing more massive than $3000 M_\odot$). The ubiquity of supermassive black holes means that it is possible that many of the galaxies that we observe as 'normal' at the present time might have gone through an active stage in the past. It should be stressed however that there is no definite proof that this scenario is correct.

The idea that extinct (or perhaps, dormant) quasars might be lurking quite close to us is intriguing and also, perhaps, alarming. One important question is why the quasars died. It cannot simply be because of a lack of fuel. As you saw earlier, less than one solar mass a year is needed to fuel a typical AGN. This is a relatively small amount and could easily be provided by the host galaxy. However, in order to fall into the central black hole, any surrounding gas clouds must also lose angular momentum. You saw earlier that very close to the black hole, material can only spiral inwards because of the viscosity of the gas in the accretion disc. The mechanism by which more distant orbiting clouds may spiral in towards the centre of an active galaxy is still something of a mystery, and this is one reason why the interpretation of the disc in NGC 4261 that you met in Section 3.5.1 is somewhat contentious. However, it seems likely that whatever process operates to cause material to spiral inwards, it will be the clouds that are closest to the AGN that will be most strongly affected. Thus it has been suggested that as time passes the AGN may 'sweep clean' the gas from its immediate environment. If, as is expected, this

gas is not replenished from clouds that are on orbits further away from the AGN then the mass accretion rate will drop, and the active galaxy will fade over time.

However this is not the end of the story, since if the central regions of the galaxy are disturbed – perhaps by a galactic collision or merger, then it is possible that the gas supply to the black hole could be temporarily restored and the AGN could then spring back into life. This may be what is currently happening in the case of the Centaurus A (Figure 3.23), which we have seen is a galaxy that appears to have undergone a recent merger. This scenario seems plausible, but is extraordinarily difficult to test in detail. However if this view of how AGN are fuelled is correct, then it is possible, although perhaps not very likely, that one day the black hole at the centre of the Milky Way could begin to accrete matter and start shining like a quasar.

3.7 Summary of Chapter 3

The spectra of galaxies

- The spectrum of a galaxy is the composite spectrum of the objects of which it is composed.
- The optical spectrum of a normal galaxy contains contributions from stars and HII regions. An elliptical galaxy has no HII regions and has an optical spectrum that looks somewhat like a stellar spectrum but with rather fainter absorption lines. A spiral galaxy has both stars and star-forming regions, and its optical spectrum is the composite of its stars and its HII regions (which show rather weak emission lines).
- The widths of spectral lines from a galaxy may be affected by Doppler broadening due either to thermal motion or to bulk motion of the emitting material.
- An active galaxy has an optical spectrum that is the composite of the spectrum of a normal galaxy and powerful additional radiation characterized by strong emission lines. The broadening comes from bulk motion of the emitting gas.
- A broadband spectrum comprises radiation from a galaxy over all wavelength ranges. To judge a broadband spectrum fairly, it is necessary to use a λF_λ plot on logarithmic axes which is called a spectral energy distribution (SED).
- The SEDs of normal galaxies peak at optical wavelengths while the SEDs of active galaxies show emission of substantial amounts of energy across a wide range of wavelengths that cannot be attributed to emission from stars alone.

Types of active galaxy

- All active galaxies have a compact, energetic nucleus – an AGN.
- Seyfert galaxies are spiral galaxies with bright, point-like nuclei which vary in brightness. They show excesses at far infrared and other wavelengths, and have strong, broad emission lines.
- Quasars resemble very distant Seyfert galaxies with very luminous nuclei. They are variable. About 10% are strong radio sources thought to be powered by jets of material moving at speeds close to the speed of light.

- Radio galaxies are distinguished by having giant radio lobes fed by one or two jets. They have a compact nucleus like Seyfert galaxies. The compact nucleus is variable, and its emission lines may be broad or narrow.
- Blazars exhibit a continuous spectrum across a wide range of wavelengths and emission lines, when present, are broad and weak. They are variable on very rapid timescales.

The central engine

- An object that fluctuates in brightness on a timescale Δt can have a radius no greater than $R \sim c\Delta t$.
- The point-like nature of AGNs and their rapid variability imply that the emitting region is smaller than the size of the Solar System.
- The central engine of a typical AGN is believed to contain a supermassive black hole of mass $\sim 10^8 M_\odot$ and Schwarzschild radius $\sim 3 \times 10^{11}$ m (2 AU).
- Infalling material is thought to form an accretion disc around the black hole, converting gravitational energy into thermal energy and radiation. A typical AGN luminosity of 10^{38} W can be accounted for by an accretion rate of $0.2 M_\odot$ per year.
- The maximum luminosity of an accreting black hole is given by the Eddington limit, at which the gravitational force on the infalling material is balanced by the radiation pressure of the emitted radiation.
- Jets are thought to be ejected perpendicular to the accretion disc.

Models of active galaxies

- The standard model of an AGN consists of an accreting supermassive black hole (the engine) surrounded by a broad-line region contained within a torus of infrared emitting dust and a narrow-line region.
- Unified models attempt to explain the range of AGNs on the assumption that they differ only in luminosity and the angle at which they are viewed.
- One type of model attempts to unify radio-quiet AGNs. Type 1 Seyferts and type 2 Seyferts differ only in the angle at which they are viewed. Radio-quiet quasars (QSOs) are similar to Seyferts but much more powerful. Evidence for this model is strong.
- Another set of models, in which the engine emits a pair of jets, attempts to unify radio-loud AGNs. The observer sees a radio galaxy, a quasar or a blazar as the viewing angle moves from side-on to the jets to end-on. These models remain controversial and there is not yet a consensus on whether such a unification is possible.
- The difference between radio-loud and radio-quiet AGNs may lie in the angular momentum of their black holes. The faster-spinning holes may have arisen from mergers of black holes resulting from the collision of their host galaxies.

Outstanding issues

- Evidence from rotation studies shows that some AGNs do indeed contain compact, supermassive objects within them, though there is no direct evidence that these are black holes.
- Quasars were most abundant at redshifts of 2–3 and have been declining in number for the last 10 billion years.

- It seems probable that AGNs fade with time as the supply of accreting material is used up. There is speculation that AGNs may be rejuvenated as a result of galactic collisions or mergers.
- Supermassive black holes found in the nuclei of the Milky Way and other galaxies may be the remnants of extinct AGNs.

Questions

QUESTION 3.15

Suppose that a galaxy has emission lines in its optical spectrum. A line of wavelength 654.3 nm is broadened by 2.0 nm. Estimate the velocity dispersion of the gas giving rise to the broadened spectral line. Is it likely to be a normal galaxy?

QUESTION 3.16

Calculate λF_λ flux densities in $\mathrm{W\,m^{-2}}$ in the radio, the far infrared and the X-ray regions, given the F_λ and λ values listed in Table 3.1. Which wavelength region dominates?

Table 3.1 For use with Question 3.16.

Region	λ	$F_\lambda/\mathrm{W\,m^{-2}\,\mu m^{-1}}$	$\lambda F_\lambda/\mathrm{W\,m^{-2}}$
radio	10 cm	10^{-28}	
far-IR	100 μm	10^{-23}	
X-ray	10^{-10} m	10^{-20}	

QUESTION 3.17

Suppose that an unusual galaxy has broadband spectral flux densities F_λ at wavelengths 500 nm, 5 μm and 50 μm, of 10^{-27}, 10^{-28}, and $10^{-28}\ \mathrm{W\,m^{-2}\,\mu m^{-1}}$, respectively. By calculating λF_λ, comment on whether it is likely to be a normal or an active galaxy.

QUESTION 3.18

A particular galaxy has a large luminosity at X-ray wavelengths. One astronomer believes it to be a galaxy that happens to contain a large number of separate X-ray stars. Another astronomer believes that the X-rays indicate an active galaxy. How, by measuring the *spectrum* of the galaxy, could this question be resolved?

CHAPTER 4
THE SPATIAL DISTRIBUTION OF GALAXIES

4.1 Introduction

Having looked at the properties of individual galaxies – both normal and active – in some detail, it is now appropriate to consider how these galaxies are distributed in space.

Surveys of the region outside our own Milky Way show that there are galaxies all around us. Deep field images such as those taken by the Hubble Space Telescope (Figure 2.40) have revealed that galaxies are present in great numbers out to very large distances. As suggested in Chapter 2, these galaxies are *not* distributed uniformly; there is structure present on all but the very largest distance scales.

At the smaller end of this range of scales, a proportion of galaxies are found in *groups* or *clusters*, which consist of local concentrations of tens to thousands of galaxies. Clusters of galaxies typically are no more than a few megaparsecs in diameter, but are themselves organized into larger structures called *superclusters* that can extend for tens of megaparsecs. On even larger scales, the matter in the Universe seems to resemble a three-dimensional network in which regions of high galaxy density are connected by *filaments* and *sheets*. These structures surround large *voids* in which very few galaxies are found. This appears to describe the current distribution of galaxies up to the largest observable scales.

In this chapter we will discuss how astronomers have come to their present understanding of the way in which galaxies, and more generally, matter is distributed throughout space. This has been one of the great scientific endeavours of the past fifty years or so, and is a process that continues with long-term projects that aim to produce accurate three-dimensional maps of vast regions of the Universe around us. We will look at some of these projects in detail and will also consider the efforts that are now being made to map the distribution of dark matter and tenuous intergalactic gas that pervades the Universe. Finally, we shall consider one of the techniques that astronomers use to describe the distribution of matter in the Universe – a process that is necessary if we are to come to an understanding of how cosmic structure was formed.

We start, however, by looking at the distribution of galaxies in our own neighbourhood.

4.2 The Local Group of galaxies

Our own Galaxy is a member of a small cluster – it belongs to a modest concentration of galaxies known as the **Local Group**. The Milky Way itself has about a dozen satellite galaxies, including two particularly prominent ones: the Large and Small Magellanic clouds. These irregular galaxies are visible to the naked eye as fuzzy patches in the southern sky (Figure 2.7b and c). (Note that images of many of the prominent members of the Local Group are given in Chapter 2.)

Slightly further away lies the largest of the Local Group galaxies – the Andromeda Galaxy or M31 (Figure 2.5). This spiral galaxy (type Sb) is somewhat more massive than the Milky Way and, at a distance of 0.8 Mpc, is the most distant object visible to the naked eye.

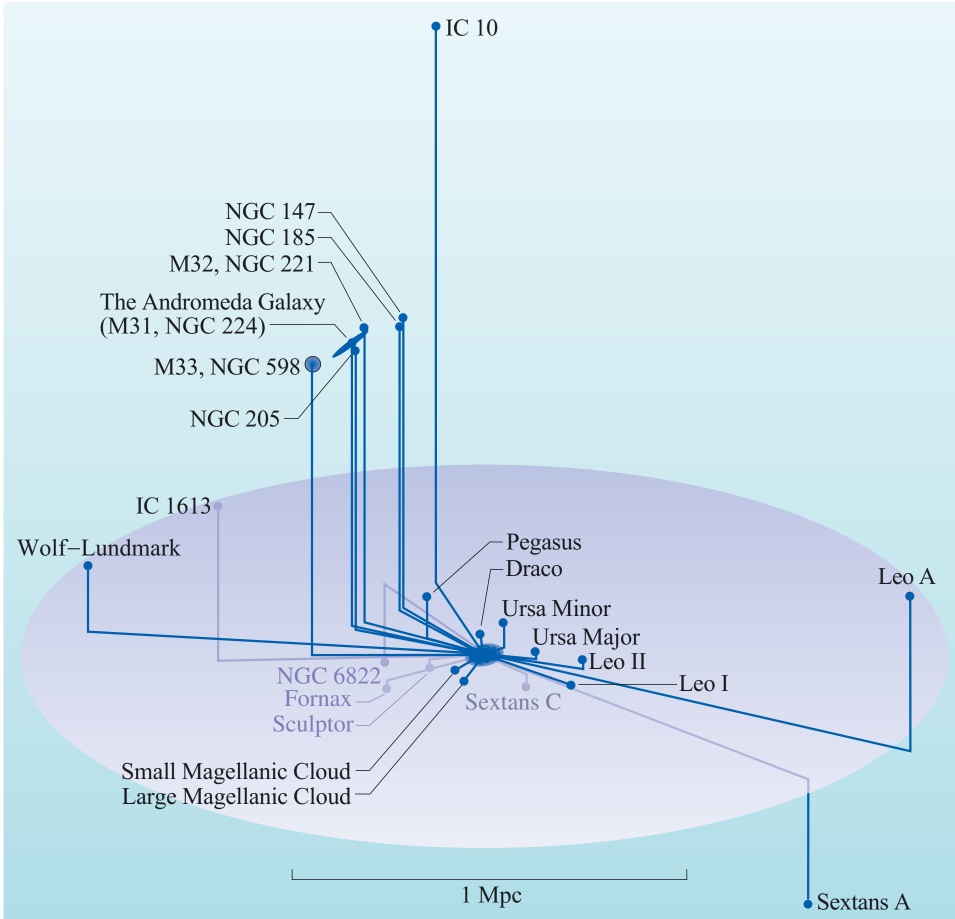

Figure 4.1 The main members of the Local Group of galaxies. Some are named after the constellations in whose directions they lie. In this diagram the Milky Way is located at the centre. (The disc separates the northern and southern halves of the celestial sphere.)

In total, the Local Group contains approximately 30 galaxies: Figure 4.1 shows how the main members of the Local Group are distributed in space.

The Local Group occupies a volume of space approximately 2 Mpc across. This is to be compared with the 0.03 Mpc diameter of the Milky Way. The Local Group is almost certainly not a transitory bunching of galaxies, but is **gravitationally bound**. Each member moves in an orbit determined by the gravitational influence of the whole Local Group. Furthermore, in a bound system, galaxies cannot normally escape unless ejected as the result of a collision between clusters or other perturbations.

Most of the members of the Local Group are much less massive than the Milky Way. After M31 and the Milky Way itself, the next most massive members of the Local Group are the two Magellanic Clouds and the more distant spiral galaxy M33 (Figure 4.2) – each having a mass approximately an order of magnitude less than that of the Milky Way. Of the remaining galaxies, most are dwarf elliptical galaxies with masses of typically just a few per cent of that of the Milky Way. M32 (visible in Figure 2.5 as a small galaxy just below the centre of the image) is a small companion of M31 and is classified as type E2 since it is slightly elongated. Leo I (Figure 2.8) is a dwarf elliptical at a distance of about 0.25 Mpc.

Dwarf ellipticals may be common but because they are very faint they are difficult to detect. Because of this we are uncertain of the exact number of galaxies in the Local Group; we have already noted that the current count is around 30, but it is

Figure 4.2 M33, a spiral galaxy in the Local Group. (D. Malin/IAC/RGO)

likely that further dwarf ellipticals will continue to be discovered as astronomical techniques improve. This difficulty in detecting faint objects has implications for deep surveys – as we look at more distant clusters, we see fewer of the less bright members. As clusters go, the Local Group contains only a small number of galaxies. Typically the term **group** is reserved for clusters with fewer than 50 members. The main characteristic of a **cluster** is that it is gravitationally bound and in this sense the terms 'group' and 'cluster' are interchangeable: the Local Group is simply a cluster with relatively few members. As will be seen in the next section, clusters can range from just a few members as in the Local Group, to much denser concentrations of thousands of galaxies.

4.3 Clusters of galaxies

Although the number of galaxies in a cluster can vary by a large factor, clusters do not vary so much in physical size: the typical cluster size of a few megaparsecs is not much different from the diameter of the Local Group. Thus *richer* clusters (those with more members) also tend to be more densely packed. Since we can observe galaxies out to distances of hundreds of megaparsecs, clusters are still very small structures on the overall scale of the observable Universe.

The most obvious way to study the distribution of galaxies is simply to photograph large areas of the sky and then to analyse the pattern of galaxies seen in the images. Historically, obtaining suitable images for such studies was a challenge: galaxies tend to be faint objects, so large aperture telescopes and long exposure times were required.

Technical difficulties aside, however, this approach is straightforward enough, and it has been applied since the 1930s. The first major survey was carried out by Harlow Shapley (Figure 1.27) who, together with Adelaide Ames in 1932, catalogued the positions of 1250 galaxies. The images taken by Shapley and Ames showed the first strong indication that galaxies are not distributed randomly in space: they found a number of compact regions containing significantly higher than average densities of galaxies. This survey thus provided early evidence for the clustering of galaxies.

Further surveys followed, adding more clusters to the total. Below we will discuss one of the most important – the Abell catalogue – in some detail. This survey is important because it was the first to introduce a classification scheme for clusters. More recent surveys have extended both the number of clusters discovered and the volume of space surveyed, but the Abell catalogue is still the starting point for astronomers embarking on a study of these objects.

Figure 4.3 shows images of two well-known nearby clusters – the Coma cluster, and the Virgo cluster.

These two examples illustrate some of the diversity and variety of clusters. The Coma cluster, which is at a distance of about 100 Mpc from our Galaxy, is a spherically symmetrical cluster consisting mainly of elliptical galaxies. By contrast, the Virgo cluster, which is about 20 Mpc distant, is much more irregular in shape, and contains a mixture of ellipticals and spirals. A feature that is common to both clusters however is the fact that each contains over a thousand galaxies.

Although clusters can contain many galaxies, it is important to appreciate that not all galaxies reside in clusters. In fact, the vast majority of galaxies exist outside of clusters. A galaxy that is not part of a cluster is called a **field galaxy**, and as we will see, care must be taken to identify and exclude these from cluster surveys.

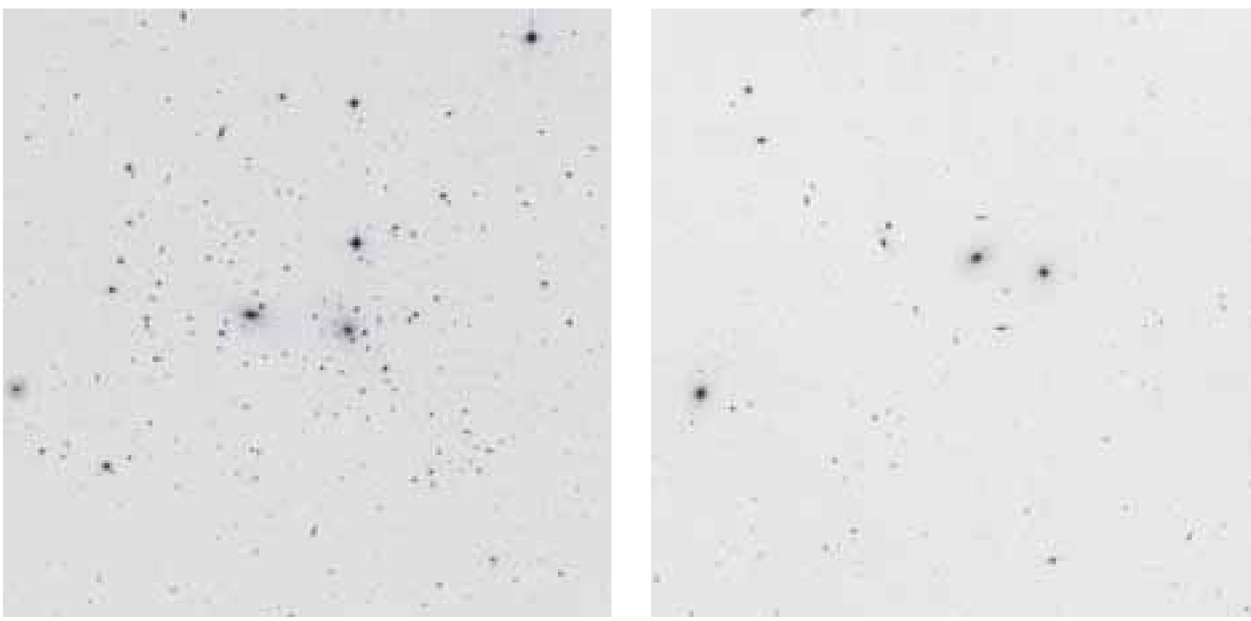

(a) Coma (b) Virgo

Figure 4.3 Optical images (visual band) of clusters of galaxies. (a) The Coma cluster of galaxies which lies at a distance of about 100 Mpc from our Galaxy. (b) The Virgo cluster of galaxies which is about 20 Mpc from the Milky Way. Both the Coma and the Virgo clusters of galaxies contain over a thousand galaxies. The fields of view of these images are relatively wide: $0.75° \times 0.75°$ in (a), and $2.5° \times 2.5°$ in (b). (Digitized Sky Survey/STScI)

4.3.1 The identification of clusters from imaging surveys

In 1958 George Abell (Figure 4.4) published a catalogue of 2712 clusters of galaxies which was the starting point for detailed study of these objects. In this section we will review the process by which Abell constructed this catalogue since it highlights some of the difficulties that have to be overcome by astronomers who endeavour to survey the Universe on large scales.

Abell's survey used plates taken using a special type of telescope called a Schmidt telescope (or Schmidt camera) that is well-suited to taking images that cover large areas on the sky. During the mid-1950s the 48-inch Schmidt telescope at the Mount Palomar Observatory (Figure 4.4) had been used to create a detailed photographic atlas of the sky. The images on these plates – each with a field of view just over 6 degrees square – together covered approximately 75% of the celestial sphere, including most of the northern sky and part of the southern. Abell used 879 of the 935 plates of the full survey as the basis for his search for clusters of galaxies. He examined the survey plates by eye to look for regions containing larger than average concentrations of galaxies. Later, he and his co-workers extended the catalogue to include more of the southern sky.

Abell's catalogue is significant because, for the first time, it contained a sufficiently large sample of clusters to allow a meaningful comparison of their different characteristics. The scale and extent of the survey also allowed the spatial distribution of clusters to be analysed for the first time.

Based on their visual differences, Abell was able to classify clusters according to various criteria. The most important of these is one which describes how many galaxies there are within a cluster. Abell called this property the **richness** of a

GEORGE OGDEN ABELL (1927–1983)

Figure 4.4 George Abell standing next to the Palomar 48 Inch Schmidt telescope. This design of telescope has a very wide field of view which facilitates the surveying of large areas of the sky. (California Institute of Technology)

George Abell (Figure 4.4) began his astronomical career as an observer on the Palomar Sky Survey (the survey on which his study of clusters of galaxies was based), and one of his early studies was to use the survey plates to examine low surface brightness planetary nebulae. Along with Peter Goldreich, Abell helped to establish the connection between these objects and the final stages of life of red giant stars.

For most of his career, he held a faculty position at the University of California, Los Angeles. He was an enthusiastic and popular teacher and subscribed to the view that in teaching science, it is more important to explain how we establish scientific knowledge than to simply present students with surprising or remarkable facts. He was committed to bringing science education to a broad audience: one example of this was his involvement in the production of a series of television programmes about relativity and cosmology in a collaboration between the Open University and the University of California.

cluster. Rich clusters are those that contain relatively high numbers of galaxies. However, as you saw in Chapter 2, it is difficult to detect faint galaxies, so a meaningful study of the number of galaxies in a cluster has to be based on the number of galaxies that exceed a certain threshold luminosity.

A vital piece of information that was needed in this process of detecting and classifying clusters was the distance of each. Abell had no direct means to measure the distances to all the galaxies in the survey, but he was able to use the apparent magnitudes of galaxies in a given cluster as the basis for estimating its distance. Specifically, he used the results of previous studies that indicated that the tenth brightest galaxy in each cluster should have about the same intrinsic luminosity. Thus the tenth brightest galaxy could be taken as a form of *standard candle*. This method did not allow Abell to calculate precise distances for each cluster – the values obtained were still very rough estimates. They were sufficient, however, to distinguish between clusters that were nearby and those that were more distant.

Abell's method of defining and selecting clusters was based on counting the galaxies within a circle of a certain radius on the photographic plate. Abell assumed that all clusters had roughly the same physical size: he estimated that clusters had a radius of about 2 Mpc. Subsequent studies have shown that this was a good assumption, and this 'standard' cluster radius is now known as the **Abell radius** R_A.

QUESTION 4.1

A cluster with an angular diameter of 1.9° is estimated to lie at a distance of 120 Mpc from the Earth.

(a) Calculate the diameter (in Mpc) of this cluster.

(b) What would the angular diameter of the same cluster be if it were at a distance of 420 Mpc?

Abell's work on defining clusters was very methodical – he was well aware that the presence of field galaxies and chance alignments between galaxies along a particular line of sight could give rise to spurious identifications of clusters. Since he wanted to minimize the number of false identifications in his catalogue he developed tests to identify clusters that are, to a high degree of statistical certainty, genuine associations of galaxies. The actual criterion used to define such a cluster was that the cluster must contain more than fifty members that exceeded a certain luminosity, and that these galaxies were located within a volume of space with radius R_A. Out of his original sample of 2712 suspected clusters, he identified 1682 cases which were statistically very likely to be genuine. Subsequent studies have shown that the vast majority of these objects are true clusters.

Abell also classified clusters of galaxies according to their symmetry, grading them on a scale running from *regular* to *irregular*. The regular clusters tend to be giant systems with spherical symmetry and a high degree of central concentration, and irregulars tending to be more open with low central concentrations and a significant amount of 'clumpiness' or sub-clustering.

Another type of study that can be based on imaging surveys relates to the morphogical types of galaxies that exist within clusters. It appears that the proportion of galaxies of different morphological type depends on the symmetry of the cluster. Regular

clusters such as the Coma cluster contain relatively few spiral galaxies, and are rich in lenticular and elliptical galaxies. This tendency is not exhibited by irregular clusters (such as the Virgo cluster), which seem to contain a higher proportion of spiral galaxies.

Abell's survey generated a number of interesting results: by adopting a methodical approach and introducing a classification scheme, Abell could do far more than merely catalogue the positions and richness of the clusters. He was also able to consider how the *distribution* of clusters – both over the surface of the sky and as a function of distance – might give information about the existence of larger scale structures.

One difficulty in mapping the distribution of clusters of galaxies is that it is not possible to observe the entire sky: external galaxies can only be seen in the part of the sky not obscured by our own Galaxy. This can be appreciated from maps that display the entire sky, such as Figure 4.5, which shows the positions of Abell clusters. Note that this map shows the celestial sphere in *equatorial* coordinates: the upper and lower halves of the map represent the northern and southern celestial hemispheres respectively. When a map of the celestial sphere is shown in such a way, the plane of the Galaxy snakes around the sky in an 'S'-shaped curve, as shown in the inset to Figure 4.5. It can be seen that only clusters that lie well away from the Galactic plane are visible.

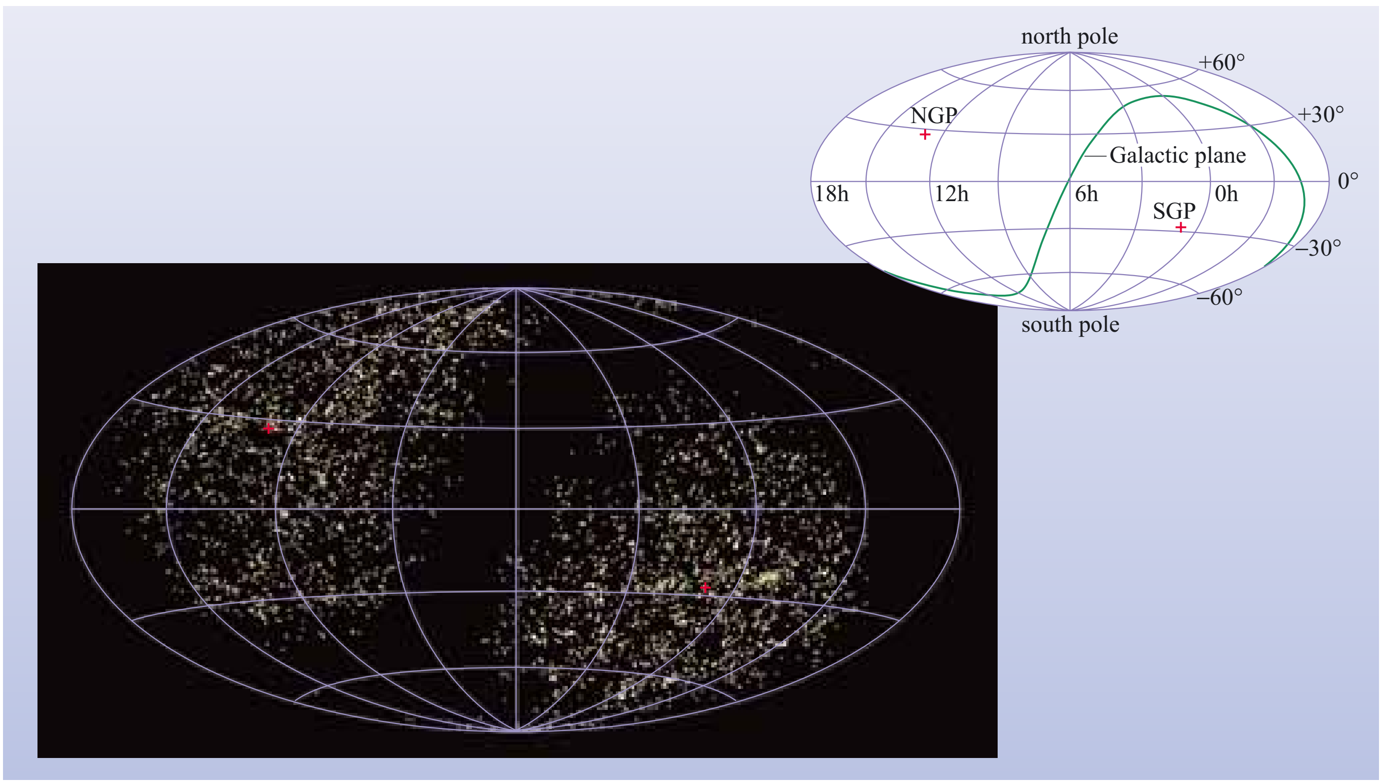

Figure 4.5 This map of the whole sky shows the distribution in equatorial coordinates of Abell clusters. Note that no clusters can be observed close to the Galactic plane because of obscuration due to the interstellar medium of the disc of our Galaxy. (The clusters are those identified in Abell's 1958 study of the northern hemisphere, and a similar study of the southern hemisphere that was published by Abell, Corwin and Olowin in 1989.) The red crosses show the North Galactic Pole (NGP) and the South Galactic Pole (SGP).

As mentioned above, another difficulty was that it was only possible for Abell to make rough estimates of distance. Modern redshift measurements together with improvements in the determination of the Hubble constant have allowed distances to clusters to be determined much more accurately. Within these constraints it was nevertheless possible to reach some overall conclusions on cluster distribution. Abell did not find much variation in the distribution of clusters with distance – there were just as many clusters at large distances as at smaller distances. Looking at the distribution *across* the sky, however, it was apparent that clusters are themselves *not* scattered randomly: although clusters were found in all parts of the observable sky their distribution, as can be seen from Figure 4.5, is far from uniform. Abell's data therefore suggested the existence of structure on larger scales than individual clusters.

QUESTION 4.2

The most distant Abell cluster has a redshift of 0.25. How far away is this cluster? (Assume that $H_0 = 72\,\mathrm{km\,s^{-1}\,Mpc^{-1}}$.)

More recent surveys have probed out to much greater distances than Abell's catalogue. As we look out to greater and greater distances from the Earth, galaxies become fainter, but they also become more numerous. For both these reasons it has become impractical to carry out such surveys by manual inspection of photographic plates, and modern surveys usually use computer-based methods in which digital images are analysed automatically.

Photographic and digital imaging surveys have catalogued many thousands of clusters and clearly shown that galaxies are not distributed randomly. But this type of survey has some limitations. In particular, imaging surveys are essentially *two-dimensional*: they show the positions of the galaxies as projected onto the celestial sphere but do not directly provide information on the *distance* from the Earth.

Space, however, is of course three-dimensional. In order to build up a clear picture of the large-scale structure of the Universe it is necessary to add *accurate* distance information to the two-dimensional position information. This allows a fully three-dimensional map to be built up showing the volume distribution of galaxies throughout space. More recent surveys are doing exactly this, and the techniques and results will be described in Section 4.4.

In order to work towards the ultimate aim of understanding how clusters form and evolve, it is necessary to learn something about the physical properties of clusters such as mass and composition, and it is to these two aspects of clusters of galaxies that we now turn.

4.3.2 The masses of clusters of galaxies

In common with most astronomical objects, it is the total mass of a cluster of galaxies that is the single most important physical property that astronomers are interested in determining. Once the mass of a cluster is known, it becomes possible to understand the gravitational influence that the cluster has on its environment. Furthermore, knowledge of the total mass of the cluster will allow estimates to be made of the relative proportions of luminous and dark matter.

Mass, however, is not a property that can be directly measured: instead it has to be inferred from measurements of observable quantities – such as the wavelengths of spectral lines. The following three sections describe different methods of determining the masses of clusters of galaxies. Although these techniques are based on different physical effects, it is found that all three give very similar answers for the cluster masses.

Estimation of cluster masses using velocity dispersion

In Chapter 2 you learned about the *virial theorem*, which is used to determine the masses of galaxies. The virial theorem states that the magnitude of the total gravitational potential energy of a bound system is equal to twice the total kinetic energy. In this way, the distribution of *velocities* (which is related to the kinetic energy) can be related to the overall *mass* of the system (which is related to the gravitational potential energy).

Clusters are collections of galaxies rather than stars, but the same principle applies – individual galaxies within a cluster will move under the influence of the gravitational field of the total mass in the cluster. The significance of this is that the velocities of galaxies within a cluster are observable quantities – they can be measured using Doppler shifts and this gives us a method for estimating the total cluster mass.

This is exactly the same principle as the method described in Chapter 2, Section 2.3.2 for determining the masses of elliptical galaxies using the velocity dispersion of individual stars within the galaxy. In the case of clusters, the only modification is that it is the velocity dispersion of galaxies within the cluster that is used rather than that of stars within a galaxy.

- ■ What assumptions need to be made for the virial theorem to hold?
- ❑ The system must be virialized – the cluster must be in a steady state – neither expanding nor contracting and the distribution of velocities of the galaxies must be unchanging. (See Box 2.1.)

When it first begins to form, a cluster may be far from being virialized. Over time, collisions and other interactions between the individual galaxies, gas and dark matter within the cluster will cause their energy to be redistributed. Eventually the motions will settle down into a steady state where further interactions do not change the distribution of kinetic and potential energies. This state is sometimes referred to by describing a cluster as being *relaxed* or in a state of *dynamic equilibrium*. Some clusters – especially those which show a high degree of symmetry are thought to be virialized. Clusters which appear irregular are far less likely to have reached this state, and so it may not be appropriate to apply this method of mass determination in such cases.

The redshifts of galaxies within clusters can be used to determine their velocities in the radial direction (i.e. along the line of sight). As for the case of stars within elliptical galaxies (Chapter 2) the kinetic energy can be characterized by the velocity dispersion. Then the mass of the cluster is given by:

$$M \approx \frac{R_\mathrm{A}\,(\Delta v)^2}{G} \tag{4.1}$$

where R_A is the Abell radius and Δv the dispersion in the line of sight velocities of the cluster members.

Clearly, it is important to ensure that only galaxies belonging to the cluster are included. Care must be taken to ensure that foreground or background galaxies along the line of sight are identified and excluded from the velocity dispersion measurements.

QUESTION 4.3

In the Virgo cluster the (elliptical) galaxies show a velocity dispersion Δv of 550 km s^{-1} (this value is given to a precision of 2 significant figures). Calculate the mass of this cluster. Express your answer in solar masses.

The Swiss-American astronomer Fritz Zwicky was the first to apply the virial theorem, using it in the 1930s to estimate the mass of the Coma cluster. Surprisingly, he found that the mass was much larger than the sum of the masses of the individual member galaxies. Historically, this was one of the first indications of the presence of dark matter in the Universe.

We saw in Chapters 1 and 2 that there is evidence for the existence of dark matter within our Galaxy and other galaxies. The results of studies of the masses of clusters of galaxies indicate that a cluster as a whole must include a large amount of dark matter surrounding the galaxies. The conclusion that has been reached is that the luminous matter in clusters accounts for only a small proportion of the mass, with the remaining 70% to 90% of the total cluster mass provided by dark matter.

FRITZ ZWICKY

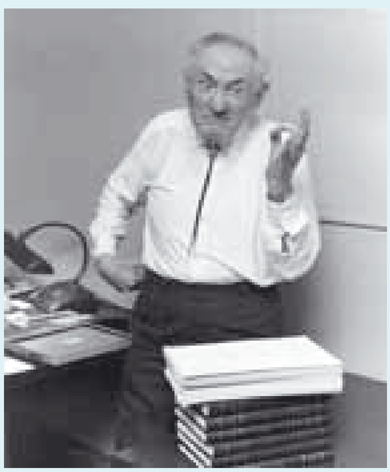

Figure 4.6 Fritz Zwicky (1898 – 1974). (California Institute of Technology)

Fritz Zwicky (Figure 4.6) was born in Varna, Bulgaria of Swiss parents. He studied in Switzerland and retained his Swiss nationality even when he moved to California Institute of Technology (Caltech), USA in 1925.

Zwicky originally trained as a crystallographer but became interested in the advances being made in astronomy at Caltech and nearby observatories. He remained professor of astronomy at Caltech until he retired in 1968. Zwicky was full of self-belief and came up with a lot of revolutionary ideas, largely intuitively.

His work on clusters of galaxies led to the idea of the existence of large amounts of dark matter in the Universe. Not only was Zwicky the first to infer the presence of dark matter but he also went on to suggest that the *gravitational lensing* of background galaxies would be the most direct way to probe the dark matter in the Universe. (As we will see in Section 4.5, such techniques are now being developed.)

Cluster mass from X-ray emission

Clusters of galaxies are not only visible in the optical part of the spectrum: they also produce strong X-ray emission. In 1971, results from the pioneering X-ray satellite Uhuru, confirmed what had been suspected from X-ray measurements made from sounding rockets – that clusters of galaxies are among the brightest X-ray sources in the sky. This X-ray emission arises from a vast quantity of very hot gas (typically at temperatures of between 10^7 to 10^8 K) that pervades the intergalactic space within the cluster.

In recent years, advances in X-ray astronomy have allowed clusters to be identified from X-ray surveys, often more efficiently than using optical imaging methods. Optical observations of clusters suffer from the problem of distinguishing true members of a cluster from other galaxies that are not associated with the cluster, but which happen to lie along the same line of sight. This is much less of a problem for X-ray observations because there are far fewer X-ray sources that could be incorrectly attributed to emission from a cluster. A cluster appears as an extended region of diffuse X-ray emission (Figure 4.7) that shows no variability with time. Other extragalactic sources of X-ray emission are normal and active galaxies and these are quite distinct from clusters of galaxies. As you saw in Section 3.2.2, normal galaxies typically have very low luminosities at X-ray wavelengths. Active galaxies, which can be luminous X-ray sources, are unresolved sources (i.e. point-like) that are often variable.

So how are the X-rays produced? Closer examination reveals that the X-rays from clusters form a broad continuous spectrum, with some emission lines (which we will discuss later). The broad continuous spectrum is characteristic of a mechanism known as **thermal bremsstrahlung**, which is normally associated with very hot ionized gas (Box 4.1, overleaf).

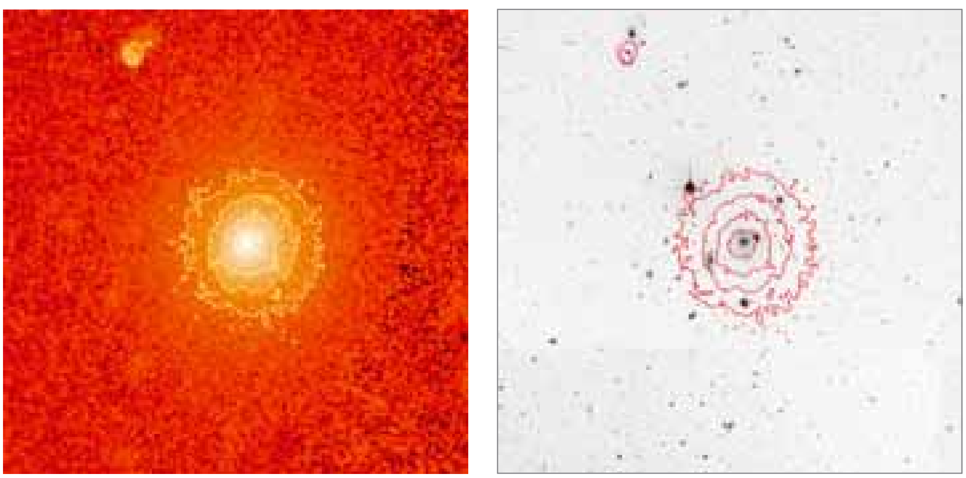

(a) (b)

Figure 4.7 A comparison of optical and X-ray images of Hydra A, a cluster of galaxies that is about 280 Mpc from Earth. (a) An X-ray image of Hydra A, as observed using the ROSAT X-ray Observatory. The image shows the emission from a large cloud of gas, several Mpc across that is at a temperature of about 3×10^7 K. (b) An optical image in the visual waveband of the Hydra cluster (shown as a photographic negative), with contours of X-ray emission overlaid. It can be seen that the hot X-ray emitting gas fills the space between the galaxies in the cluster. (Both (a) and (b) show the same field of view, and have an extent of 1° × 1°.) ((a) NASA; (b) Optical data from the Digitized Sky Survey/STScI)

BOX 4.1 THERMAL BREMSSTRAHLUNG

Thermal bremsstrahlung is an X-ray emission mechanism that typically takes place in a high-temperature, low-density plasma. As a free electron passes close to an ion in the gas it is deflected (Figure 4.8) without being captured. As a result of this acceleration the electron emits a photon while at the same time losing a corresponding amount of kinetic energy and slowing down a little.

X-rays generated in this way are known as *bremsstrahlung* (a German word that means *braking* or *deceleration* radiation). This type of X-ray emission is also called *free-free* emission because the electron moves freely both before and after the encounter with the ion.

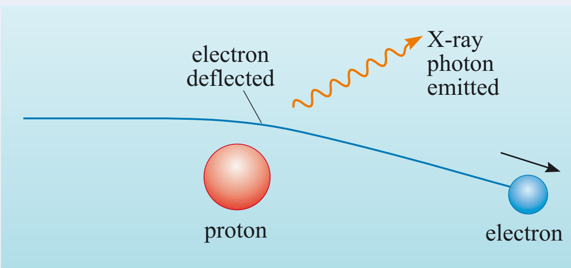

Figure 4.8 Mechanism for Bremsstrahlung emission

The energy $\varepsilon_{\rm ph}$ of a photon generated by this process depends on the average thermal energy of the electrons and is given approximately by:

$$\varepsilon_{\rm ph} \sim kT$$

where k is the Boltzmann constant (1.38×10^{-23} J K^{-1}) and T is the temperature of the gas. It is common in X-ray astronomy to express photon energies in terms of kilo-electronvolts (1 keV = 1.60×10^{-16} J). Photon energies in the range 1 to 10 keV are typical for X-ray clusters, corresponding to temperatures of about 10^7 to 10^8 K.

Because the X-rays are produced by the acceleration of *free* electrons, the spectrum of bremsstrahlung emission is a smooth continuum (Figure 4.9). This is characteristic of a fully ionized gas where the electrons are not bound to individual atoms. Bremsstrahlung spectra are thus distinct from the *line spectra* which are produced when electrons make transitions between the energy levels of atoms.

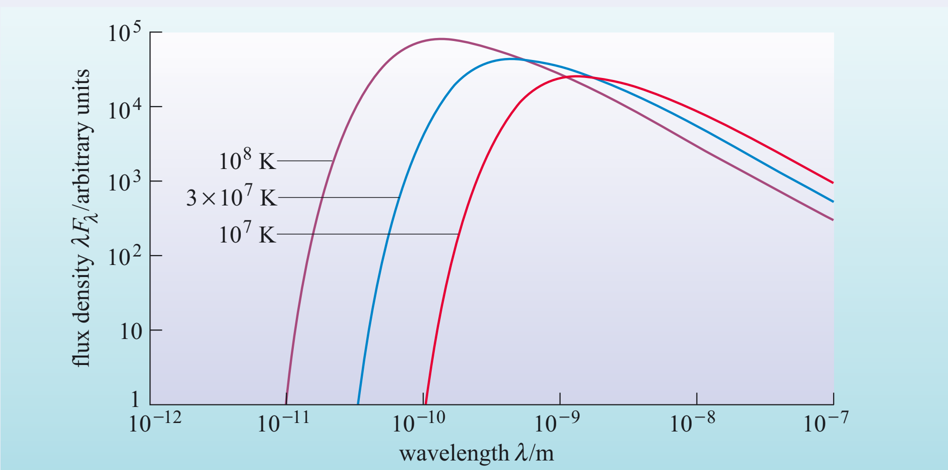

Figure 4.9 The spectral energy distribution due to hot gas (at three temperatures as indicated) emitting by the mechanism of thermal bremsstrahlung. Note the broad continuous spectrum that peaks at shorter wavelengths for higher gas temperatures.

The presence of bremsstrahlung X-ray emission is evidence for the presence of large quantities of hot ionized gas within the cluster. This gas is predominantly composed of hydrogen and helium, although it does contain a small fraction of heavier elements. As can be seen from Figure 4.7b this hot **intracluster medium** or **ICM**, is present between the galaxies, permeating the cluster out to a radius of a few megaparsecs. This makes clusters appear as extended, diffuse areas of X-ray emission.

With the benefit of X-ray images, our view of a typical cluster now becomes a large cloud of hot (10^7–10^8 K) ionized gas with the galaxies embedded in it.

■ The temperature of the intracluster medium at the centre of a cluster is typically around 10^7 to 10^8 K – similar to that found at the centre of the Sun. Why, then, do we not see strong X-ray emission from the hot plasma within the core of the Sun and other stars?

❑ X-rays generated in the core of a star do not escape directly: in the dense environment of the solar interior, photons are repeatedly scattered and reach thermal equilibrium with matter. Eventually, the energy that was originally in the form of X-ray photons escapes from the outer layers of Sun – the relatively cool photosphere – at ultraviolet, visible and infrared wavelengths.

Although the total mass of gas in a cluster is much larger than that of the Sun, it is spread out over a vast volume of space (2 Mpc compared to one solar radius). The overall density of the ICM is therefore many orders of magnitude lower than the density of material in a star, and this allows the X-rays to escape. In this respect the intracluster gas is similar to the tenuous gas in the Sun's corona – although it should be noted that intracluster gas is many orders of magnitude less dense than gas in the solar corona.

To appreciate how this X-ray emission can be used to estimate the mass of a cluster it is necessary to consider how the intracluster gas supports itself. An important idea here is the concept of *hydrostatic equilibrium* similar to that used to model the stability of a star. A spherical region of gas will tend to collapse under the influence of its own gravity. In the case of a cluster, the gravitational field is produced not only by the mass of the gas itself, but also by the mass of the galaxies in the cluster, together with the mass of any dark matter.

The ICM will be supported against this gravitational collapse by the pressure of the gas. In equilibrium, the pressure changes with distance from the centre of the cluster in a way that exactly balances the effect of gravity. The temperature and density of intracluster gas can be measured from X-ray observations. The pressure of the gas can be calculated once the temperature and density are known, and by using the relationship that balances gravity against the pressure gradient, the total mass of the cluster can be inferred.

The cluster masses that have been obtained from X-ray observations are typically much higher than the mass that can be accounted for by the galaxies and intracluster gas alone. For a given temperature, pressure gradients within the ICM are *higher* than expected. This suggests that the gravitational field within the cluster is *stronger* than that provided by the mass of the galaxies and intracluster gas alone. Total cluster masses of 10^{14} to $10^{15} M_\odot$ are typical.

Again, this is much greater than the mass that can be accounted for by the galaxies in the cluster – which only constitute about 10% of the total mass. Furthermore, X-ray observations also allow an estimate to be made of the mass of gas in the intracluster medium and this is typically found to account for between 10% and 30% of the total mass of a cluster. The remaining mass is believed to be made up mainly of dark matter.

Cluster mass from gravitational lensing

A completely different approach to measuring cluster masses is based on the effect that gravity has on light. Einstein's general theory of relativity makes a number of predictions. One of these predictions is that, in addition to affecting the paths of objects such as planets, gravity can also affect light: the path of light will be bent if it passes close enough to a sufficiently massive object. This prediction was confirmed in 1919 by an expedition to the island of Principe, off the coast of West Africa, led by Sir Arthur Eddington. By measuring the positions of stars during a total solar eclipse (Figure 4.10), the bending of starlight passing close to the surface of the Sun was measured and found to be in agreement with Einstein's theory.

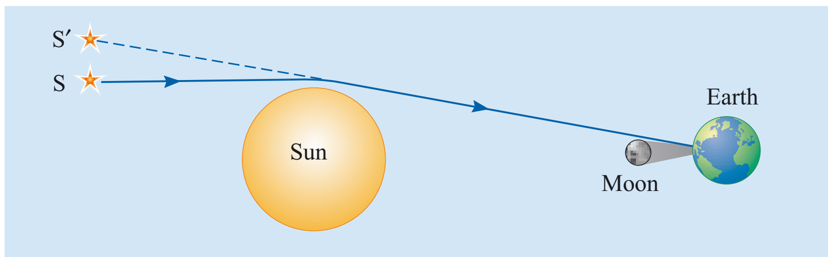

Figure 4.10 A schematic illustration of an eclipse observation of the gravitational bending of starlight. In order to be deflected by a significant amount, a ray of light from a distant star must pass very close to the surface of the Sun. Normally it would not be possible to see this effect, but during an eclipse the Moon obscures the extremely bright solar disc, allowing stars to be observed close to the limb of the Sun. Light from star S is deflected by a small amount, making its position appear to shift to S′.

This bending of light is a weak effect: Eddington's measurement was only possible when light passed very close to the surface of the Sun, and even then the angular deviation of just 1.74 arcsec was so small as to be barely measurable.

The deflection of rays of light becomes larger as the mass of the deflecting object increases. Since a cluster of galaxies typically has a high mass, we might expect that it could act as a **gravitational lens** and bend the paths of light rays from an object lying behind it, as shown in the simple arrangement in Figure 4.11. Rays of light from the galaxy at position S are deflected as they pass close to the cluster, and the observer at O, sees an image at position I. As well as this change in apparent position, the gravitational lens also causes the image of the background galaxy to be distorted, and typically produces multiple images.

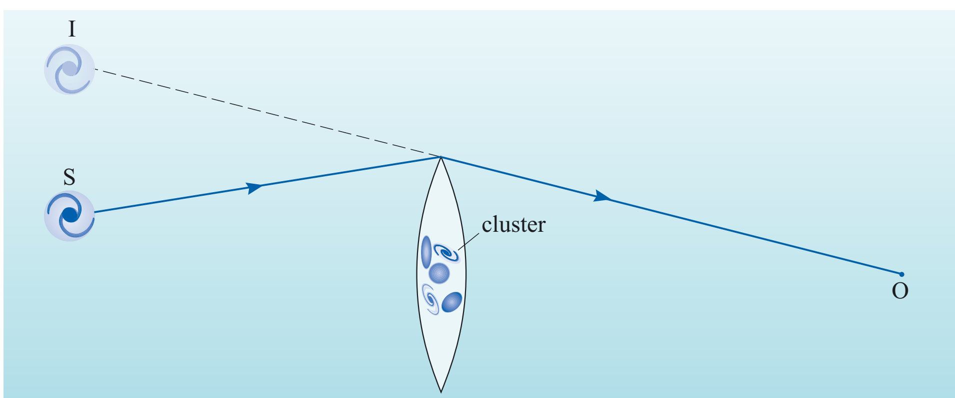

Figure 4.11 Schematic diagram of a gravitational lens. Light from the distant galaxy S is deflected as it passes a cluster of galaxies, causing a distorted image of the original galaxy to appear at I. Depending on the distribution of mass in the cluster, several images may be formed in different positions.

To date, over 50 cases of gravitational lensing have been observed. In addition to causing multiple or distorted images, gravitational lenses can also increase the apparent brightness of distant objects, in much the same way as a conventional lens focuses light. By concentrating light in this way, one effect of gravitational lensing is that it allows observation of distant objects which would normally have been too faint to be seen. One example of this is shown in Figure 4.12. Lensing in the cluster CL0024+1654 has produced five images of a more distant galaxy. The images of this galaxy are seen as blue elongated rings, one near the centre of the image and four others further out.

How can gravitational lensing be used to measure the masses of clusters of galaxies? Clearly the amount of distortion seen will depend in some way on the mass of the cluster that is acting as a lens. Calculating the exact distribution of mass in the lensing cluster can be quite difficult: just as with a glass lens, the exact shape of the lens will determine the nature of the image distortion and magnification. In cases like CL0024+1654 the pattern of distortions is very complicated – rather like looking at the distant galaxy through the bottom of a glass bottle.

In order to make reliable estimates of cluster mass, we need to look for simpler situations. Occasionally the multiple images resulting from gravitational lensing form symmetrical arcs surrounding the centre of the lensing cluster. A particularly spectacular example of this can be seen in the cluster Abell 2218 (Figure 4.13).

Figure 4.12 Lensing by CL0024+1654. Several distorted images of a distant blue galaxy can be seen encircling the yellower galaxies within the cluster. Analysis of these distorted images suggests that the background galaxy has an unusual shape. This may indicate that the distant galaxy is in the process of forming, or merging with another galaxy. (W. N. Colley and E. Turner (Princeton University), J. A. Tyson (AT & T Bell Labs, Lucent Technologies) and NASA)

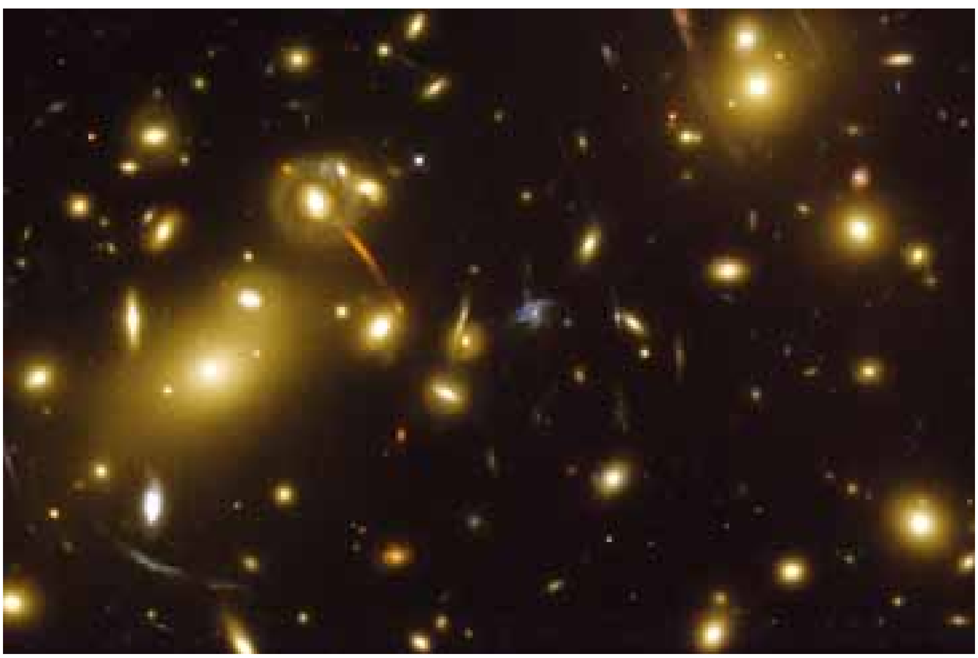

Figure 4.13 Gravitational lensing in Abell 2218. Note the arcs of concentric circles formed by the lens. (NASA, ESA, R. Ellis (Caltech) and J.-P. Kneib (Observatoire Midi-Pyrenees))

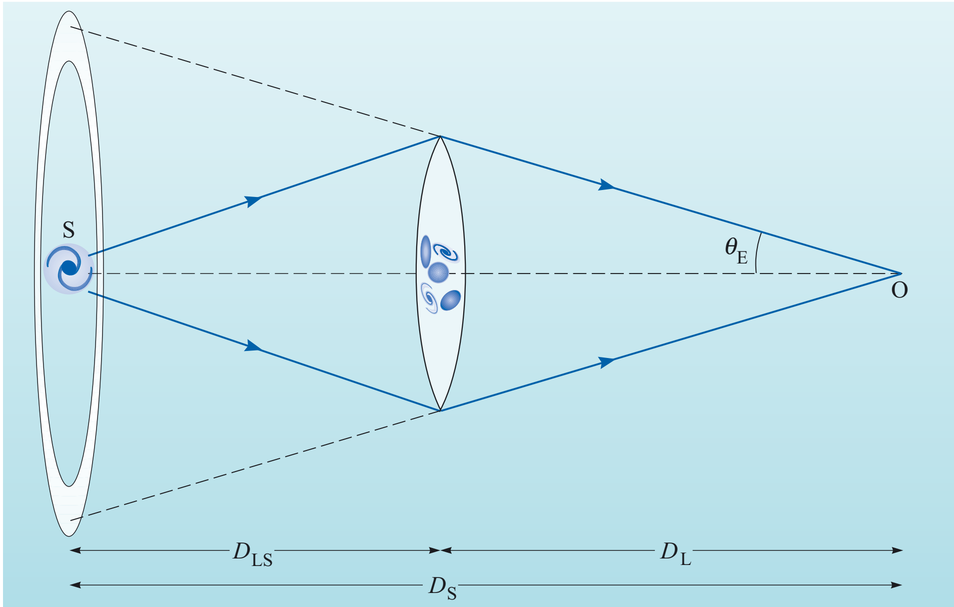

Figure 4.14 The geometry of a source imaged as a ring with angular radius θ_E.

Figure 4.14 shows a schematic view of this type of lensing situation. Here the distribution of mass in the lensing cluster is symmetrical and concentrated at the centre. The distant galaxy S is located exactly along the centreline. The paths of light rays passing either side of the cluster are distorted equally, resulting in symmetrical rings or arcs similar to those seen in Abell 2218.

If the alignment of source and lens is perfect, then the resulting image takes the form of a complete ring surrounding the lens. Such a ring is known as an **Einstein ring** and several examples like the one shown in Figure 4.15 have been discovered.

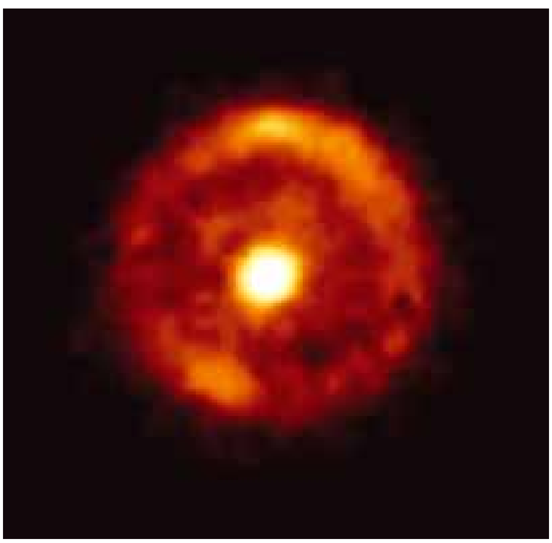

Figure 4.15 The Einstein ring B1938+666 as observed with the Hubble Space Telescope. In this case the foreground lens is a galaxy seen as the bright spot in the centre. (L. J. King (University of Manchester) and NASA)

■ For a given cluster-to-source distance, how would you expect the angular radius of the Einstein ring to depend on the mass of the lensing cluster?

□ The greater the mass of the cluster, the more the path of the light rays would be bent. So a more massive cluster would produce a ring of greater angular radius.

For the situation shown in Figure 4.14, the image of the distant object would appear as a complete ring with an angular radius θ_E that is given by:

$$\theta_E = \sqrt{\frac{4GM}{c^2}\frac{D_{LS}}{D_L D_S}} \qquad (4.2)$$

Where D_S is the distance between the observer and the distant source galaxy, D_L is the distance from the observer to the gravitational lens, and D_{LS} is the distance from the gravitational lens to the source.

Using Equation 4.2, the mass M of the lensing cluster can be estimated. (Note that similar calculations can be carried out for the less symmetrical situations where the lensing has not produced a complete ring.)

QUESTION 4.4

The largest lensed arcs in the image of Abell 2218 shown in Figure 4.13 have an angular radius θ_E of approximately 1.0 arcmin. This cluster is one of the most distant in the Abell catalogue: with a redshift of $z = 0.17$, it lies at a distance of approximately 700 Mpc from Earth. Using these values, and assuming that Equation 4.2 can be applied to this gravitational lens, estimate the mass of Abell 2218 in solar masses. Assume that the cluster is mid-way between the distant background galaxies and the Earth.

Gravitational lensing has an advantage over the other methods discussed in that it relies just on the distribution of mass within the cluster – we don't have to make assumptions about virialization or hydrostatic equilibrium. Of course, since lensing is a direct result of the gravitational field, it is sensitive to *all* the mass in the cluster, whether from galaxies, gas or dark matter.

Masses of clusters estimated from gravitational lensing lie within the range of 10^{14} to $10^{15} M_{\odot}$. This is consistent with the other two methods of mass determination and once again suggests the presence of significant quantities of dark matter within clusters.

4.3.3 The composition of clusters

As we have seen, cluster masses can be estimated by three independent methods: velocity dispersion, X-ray emission, and gravitational lensing. The results from these methods are all roughly consistent, typically agreeing within a factor of two or three. Typical masses range from less than $10^{14} M_{\odot}$ for the smallest clusters and groups to $10^{15} M_{\odot}$ for the richest clusters. Furthermore, the fact that three different techniques based on completely different physical principles are in such good agreement is compelling evidence for the existence of dark matter.

In addition to measuring mass, these three methods also enabled us to learn something about the different constituents of a cluster – galaxies, gas and dark matter. The results suggest that only a small percentage of the total mass of a cluster is contained in the galaxies themselves, with about 10%–25% in the intracluster medium, and the remaining 70%–90% as dark matter (see Table 4.1). The picture that has emerged is of a diffuse cloud of gas and dark matter which surrounds the galaxies and permeates the space between them.

Table 4.1 Relative contributions to the total mass of a cluster of galaxies due to its three major constituents.

Constituent	Contribution to total mass
galaxies	<10%
intracluster gas	10–25%
dark matter	70–90%

As described in Chapter 2, each individual galaxy has it own complement of gas (in the form of *interstellar* medium) and dark matter. We could therefore think of a cloud of gas and dark matter filling the whole cluster, with individual denser haloes around each galaxy. The density of material is highest around and within the member galaxies, but the large volume of the cluster compared to that of the galaxies means that the intracluster gas and dark matter – spread between individual galaxies – makes up most of the total mass of the cluster.

4.3.4 The formation and evolution of clusters

The study of the evolution of clusters is still in its infancy. As is the case in the study of the evolution and formation of galaxies (Chapter 2), the study of the evolution and formation of clusters takes the approach of trying to match simulations of the formation of structure to observations of the evolution of these objects.

The scenarios for the formation of structure that were described in Chapter 2, should also be scenarios that produce clusters as a natural outcome. As you saw in Chapter 2, the preferred scenario for the formation of structure is a hierarchical model in which small-scale structures (such as galaxies) form before larger ones (such as clusters).

The observational approach to studying the evolution of clusters is, at present, not well developed, but some advances are being made. For the remainder of this section we shall consider some of the results from studies of cluster evolution that may eventually help to confirm whether the scenarios of structure formation are correct.

The evolution of galaxies within clusters

We can start by looking at the evolution of galaxies within clusters. As noted earlier, clusters all have roughly the same size, with most of the galaxies being contained within the Abell radius of about 2 Mpc. The total number of galaxies within a cluster can vary greatly however, and it therefore follows that the density of clusters can also vary to a great extent. The richest clusters may contain hundreds of galaxies within the 2 Mpc radius, and towards the centres of such clusters the galaxies will be packed very densely.

■ What processes affecting the evolution of galaxies might depend on the density of packing of galaxies within a cluster?

❑ In the denser environments of rich clusters, there is more opportunity for collisions between galaxies.

During mergers the discs of spiral galaxies can be destroyed. Earlier it was mentioned that richer clusters tend to contain fewer spiral galaxies and a larger proportion of ellipticals. Such an observation seems consistent with the idea that rich clusters are an environment in which there have been many collisions and mergers of galaxies.

The role of mergers in cluster evolution

We have seen that within clusters, galaxies can collide and merge. What about the clusters themselves? Is there any evidence that clusters have built up from mergers of smaller clusters?

We can start by looking for evidence that mergers between clusters do actually occur, and to do this we have to make use of X-ray observations. Earlier, we saw how the strong X-ray emission from the hot intracluster gas can be used in estimating cluster masses. We can study the structure of the intracluster medium by looking at another aspect of the X-ray emission: in addition to the continuous thermal bremsstrahlung described in Box 4.1, the X-ray spectra of many clusters also contain *emission lines*, which signify the presence of elements heavier than hydrogen and helium.

As mentioned earlier, the intracluster medium consists mainly of hydrogen and helium. Why do line features in the spectra indicate that other, heavier, elements must also be present in the intracluster medium? The answer lies in *ionization energies*.

At temperatures of 10^7 to 10^8 K, hydrogen is fully ionized – that is, the electrons are completely separated from the hydrogen nuclei. Helium is also fully ionized at these temperatures. It is the free electrons in this plasma that give rise to the continuous bremsstrahlung emission. Being fully ionized, the hydrogen and helium will be not be able to produce line spectra, which come about as a result of transitions between energy levels within atoms.

It takes much more energy to remove all the electrons from the atoms of heavier elements such as iron: even at 10^8 K such atoms are not completely ionized. Any atoms of these elements will be present in the form of partially ionized atoms which have lost only some of their electrons. Transitions involving the tightly bound inner electrons in these ions give rise to line spectra in the X-ray part of the electromagnetic spectrum. Each element has its own characteristic spectral lines and this allows the presence of specific elements to be confirmed.

■ Elements heavier than hydrogen and helium – were not present in the primordial material from which the first stars and protogalaxies would have condensed. How could the intracluster medium have become enriched with these heavy elements?

❑ An early period of star formation within the galaxies of the cluster might have included many massive short-lived stars which ended their lives as supernovae. Material expelled from supernovae contains heavy elements, and shockwaves from the explosions could propel this material out of the galaxies thus enriching the intracluster medium with elements heavier than hydrogen and helium.

Further information on the physical properties of the intracluster medium can also be obtained from looking at the line emission X-ray spectra of specific elements. The line spectrum of *iron* in particular is very useful: measurements of the relative strengths of emission lines in the iron spectrum can give a much more precise measurement of temperature than can be obtained from the broad continuous bremsstrahlung spectrum of a cluster. This allows detailed maps of the temperature distribution within clusters to be produced.

A very interesting result from such maps is that many clusters do not have the smooth temperature distribution which would be expected if the clusters were in hydrostatic equilibrium.

Figure 4.16 shows observations (made with the Chandra X-ray observatory) of the cluster Abell 2142 that suggest that this cluster has undergone merger events. Firstly, the map of X-ray surface brightness (the contours in Figure 4.16a) shows that the cluster has sharp edge towards the upper right-hand side (this is where the contours are packed closely together). This edge is believed to be the shock front that resulted from the merger of two clusters. Secondly, the temperature map of the X-ray emitting gas (Figure 4.17b) shows substantial variation across the cluster. The regions of cooler gas in the centre of the cluster (the blue central region in Figure 4.17b) are interpreted as the dense cores of subclusters that have survived merger shockwaves. Thus, unusually, Abell 2142 has a cooler core surrounded by hot, shocked gas.

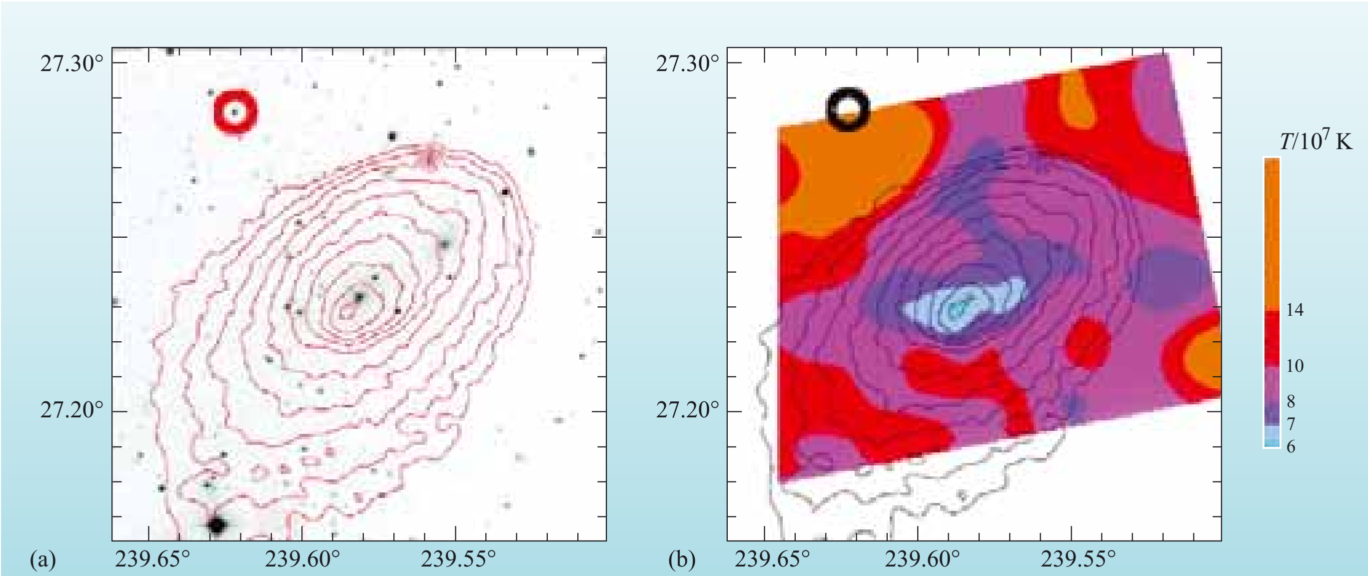

Figure 4.16 Observations of the cluster Abell 2142 which is possibly undergoing a merger event. (a) An optical image with the X-ray surface brightness contours overlaid. (b) A temperature map of the central region of the cluster with overlaid X-ray surface brightness contours. The central region is colder than the surrounding shocked region. (Markevitch *et al*., 2000)

These findings support the view that clusters appear to grow by the merger of smaller *subclusters* which are small concentrations of galaxies. Temperature maps indicate that this is an ongoing process in many clusters, where hot and cold regions are related to the shocks and other processes which occur as a result of the infall of subclusters. In some places, cold features within the intracluster medium have been identified with regions where subclusters appear to have collapsed inwards leaving behind volumes of cooler gas. In other places, collisions between subclusters have compressed and heated the ICM. The existence of these structures within the ICM suggests that many clusters are still in the process of evolving and have not yet reached an equilibrium state.

Although such observations show that mergers do occur, it is a much more difficult task to show that mergers have played an important role in the evolution of clusters. It might at first sight appear that all that is required is to look at the relative populations of clusters at different distances.

- Observing galaxies at great distances is equivalent to looking back in time. If the model of very rich clusters forming from the merger of smaller ones were correct, what would you expect to see when looking at clusters at greater and greater redshifts (and hence at earlier times)?

- You would expect to see that at high redshifts there was a greater proportion of sparse clusters (those with few members) and relatively fewer rich clusters. Over time clusters would merge, so the population of clusters with lower redshifts as seen from Earth would contain a progressively higher proportion of rich clusters.

The range and coverage of galaxy surveys continues to expand, but the population of very distant clusters has not yet been surveyed fully enough to provide a definite answer to this question: instead we must look for indirect evidence of cluster evolution.

You may recall one such piece of evidence – the *Butcher–Oemler effect* – from Section 2.5.3: out to redshifts of $z \approx 0.3$, clusters mostly look the same. More distant clusters seen at less than two-thirds of their present age have higher proportions of young blue galaxies. Many of these galaxies are deformed, probably as a result of interactions with their neighbours. This suggests a more violent past in which the galaxies within clusters were interacting with each other more vigorously than they are now, triggering bursts of star formation. This could certainly have been the case if smaller clusters were merging to form larger ones. Although rather indirect evidence, the Butcher–Oemler effect is at least consistent with the picture of clusters growing by mergers.

So, at present it seems plausible that clusters are formed by hierarchical growth, but the observational evidence to support such a claim is not strong. We will return to the formation of structure in the Universe in Chapter 6, where the role of dark matter in the formation of structure will also be examined. For now, we shall continue by looking at the problem of surveying structures larger than clusters.

4.4 The large-scale distribution of galaxies

Clusters of galaxies, with typical radii of 2 Mpc, are very much smaller than the overall scale of the Universe. As shown by Abell's survey (Figure 4.5), the distribution of clusters across the sky is not uniform – other surveys since the 1950s have confirmed this finding: clusters are not the largest scale objects in the Universe but are themselves organized into larger structures.

Much of this section will be concerned with the techniques that are currently being employed to map out the Universe on scales of hundreds of megaparsecs. However, before starting this discussion it is useful to take a quick tour of our 'local' part of the Universe beyond the Local Group.

Our Galaxy and the Local Group are part of a much larger structure: a **supercluster** – in this case, called rather unimaginatively, the **Local Supercluster** (Figure 4.17). This supercluster is centred on the Virgo cluster (Figure 4.3b), and is approximately 30 Mpc across. As suggested by Figure 4.17, this supercluster is a much more loosely organized structure than the individual clusters. Based on

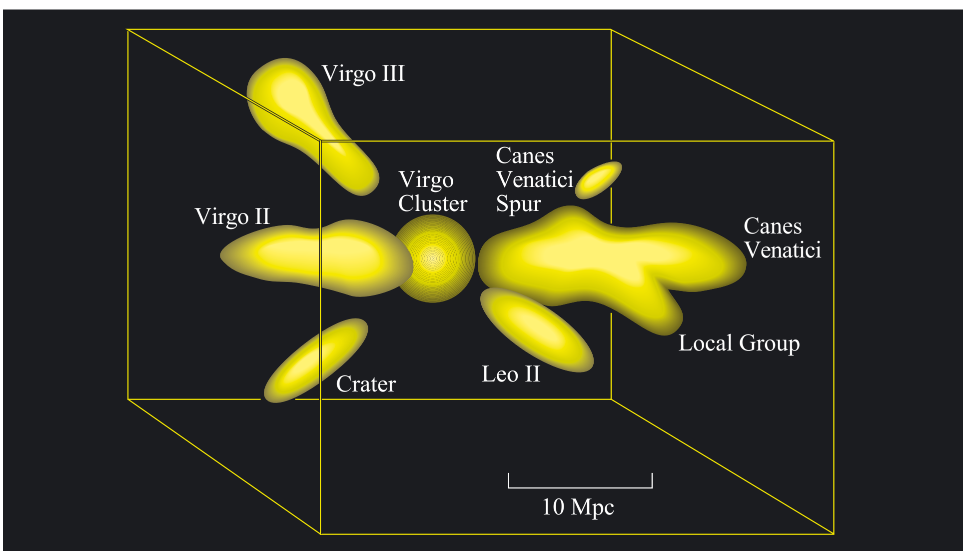

Figure 4.17 The Local Supercluster represented by a surface which separates high-density regions from lower density regions in the Universe, hence the 'empty' regions in this diagram correspond to locations were the density of galaxies is low but not zero. (R. Brent Tully)

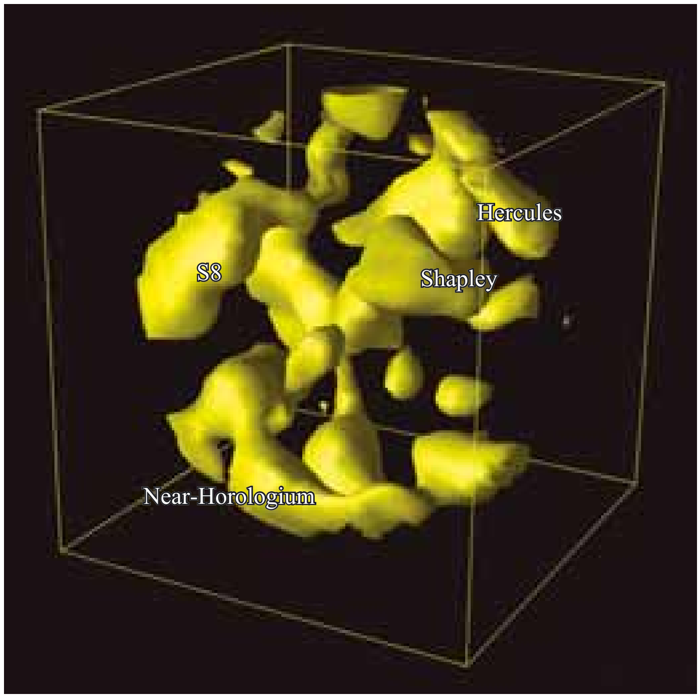

Figure 4.18 The results of a survey called PSC*z* (PSC – Point Source Catalog of the IRAS satellite, *z* – redshift) which mapped the density distribution in the Universe around us to a distance of about 250 Mpc. The locations of four superclusters are indicated: Shapley, Hercules, S8 and Horologium. Note that as in Figure 4.17, the distribution of matter is represented by a surface that separates high- from low-density regions. Also as in Figure 4.17, the 'empty' regions in this diagram correspond to locations were the density of galaxies is low but not zero. (Figure by L. Teodoro, based on data described in Saunders *et al.*, 2000)

velocity measurements of the galaxies making it up, the Local Supercluster appears not to be gravitationally bound in same way that clusters of galaxies are bound, and is certainly not a virialized system.

The Local Supercluster is not unique: other superclusters in our vicinity have also been mapped. Figure 4.18 shows the results of a three-dimensional survey which mapped the volume of space with a radius of about 250 Mpc from our location. This map clearly shows the location of some nearby superclusters – with typical extents of a few tens of megaparsecs.

Since there appears to be structure on the scale of superclusters, the obvious question is whether this organization continues hierarchically to larger and larger structures. It seems that this isn't the case. Moving upwards in distance scale, recent surveys are finding that superclusters are not themselves organized into ever larger clusters of superclusters, but instead are distributed in a vast network consisting of high-density regions connected by filaments and sheets wrapped around (relatively) empty **voids**. Any structure that is on the scale of superclusters or above is often referred to by the generic term of **large-scale structure**.

An impression of the large-scale distribution of matter in the Universe can be obtained from a remarkable map (Figure 4.19) of galaxy positions that was generated by automated scanning of plates from a Schmidt telescope survey. This map was developed by a group of astronomers using the Automatic Plate Measuring (APM) facility at the University of Cambridge from plates taken at the Anglo-Australian Observatory. Although it is a two-dimensional map, the filamentary structure of the distribution of galaxies is evident.

In the next section we shall discuss how this large-scale distribution is currently being surveyed so that we can better understand the structures in the Universe around us.

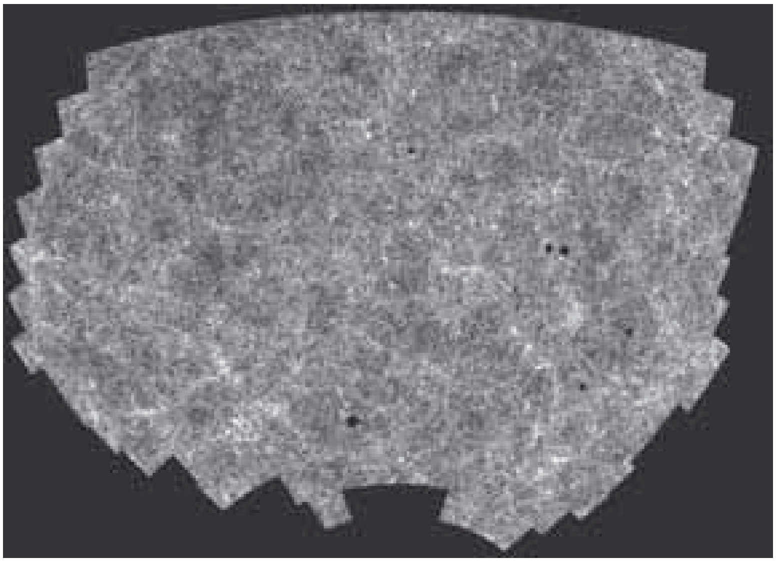

Figure 4.19 The APM map of galaxy positions. The map was generated by using automated routines to find galaxies on photographic plates. The survey contains about two million galaxies and covers an area of the southern sky that is about 4000 square degrees in extent. Note that the gaps in the map are areas that could not be scanned because of the presence of bright stars. Structure in the large-scale distribution of matter in the Universe is clearly evident in this map. (S. Maddox, W. Sutherland, G. Efstathiou and J. Loveday)

4.4.1 Redshifts of galaxies

The APM map (Figure 4.19) shows the distribution of galaxies or clusters of galaxies as a two-dimensional projection onto the celestial sphere. A comparison with constellations is appropriate here: as you may recall, the constellations do not generally represent physical groupings of stars: individual stars within a constellation may be at greatly differing distances from the Earth. Similarly, it is possible that the increased concentrations of galaxies seen in photographic surveys could be the result of coincidental alignments of galaxies at greatly different distances that just happened to be aligned along the same line of sight.

- How would you confirm that the galaxies that appear on a photographic plate to be within a cluster are indeed physically associated with each other, and not merely grouped as the result of chance alignment?
- You would need to show that the galaxies are all at a similar distance from the Earth.

This could be done by measuring the *redshift* of each individual galaxy within the cluster. If the galaxies are genuinely associated they should all have similar values of redshift. Foreground and background galaxies could be identified and eliminated by having either smaller or greater redshifts than those in the cluster. Historically, this was a difficult task due to the vast number of galaxies that had to be observed to build up a three-dimensional picture of the Universe around us. At the time that Abell carried out his initial work on clusters in the 1950s the spectra of galaxies had to be measured one at a time using a large telescope and recorded using photographic film.

Thanks to improvements in detector technology, modern telescope and detector systems can measure redshifts much more quickly. A dedicated programme of such observations can, in a matter of years, measure tens or hundreds of thousands of redshifts. Such surveys provide a basis for mapping the Universe in three dimensions. Some of the major programmes for mapping the Universe will be discussed in more detail in the following section, but first we need to take a closer look at how redshifts are related to distance.

The simple relationship $z = (H_0/c)d$ between redshift and distance introduced in Chapter 2 (Equation 2.12) is really only valid for small redshifts of up to $z \approx 0.2$: at larger redshifts this relationship no longer holds. As noted in Chapter 2, the redshift is a measure of the amount that the Universe has expanded since the light was emitted. At large distances the redshift increases more rapidly with distance than implied by Equation 2.12. For example an object with a redshift of 2.0 is not believed to be twice as far away as an object with redshift of 1.0.

There is little doubt that distance increases with redshift, but the exact relationship depends on a number of factors (or cosmological parameters) that characterize the behaviour of the expansion of the Universe. Different models of the cosmological expansion, and their consequences, will be discussed in more detail in Chapter 5. For now, it is sufficient to note that the precise relationship between redshift and distance depends on the model of the expansion used. The graph shown in Figure 4.20 represents one possible relationship between redshift and distance and will be used for the remainder of this chapter.

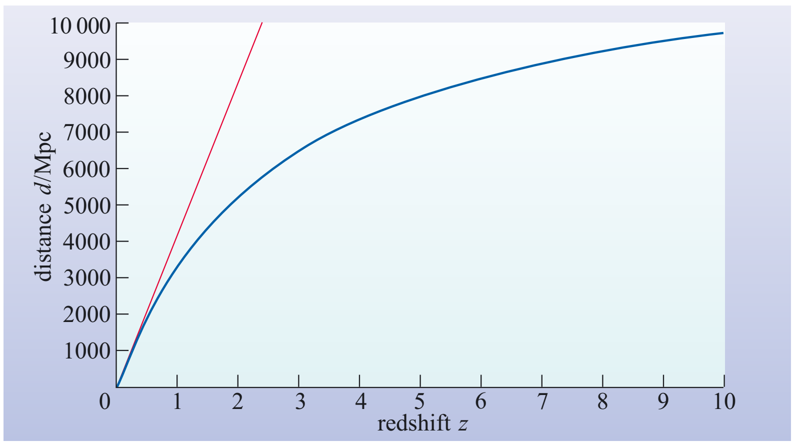

Figure 4.20 Redshift–distance relationship (blue curve) for one possible cosmological model. The simple relationship $z = (H_0/c)d$ (Equation 2.12), as indicated by the straight line (in red) holds only for low redshifts (below $z \approx 0.2$). For large redshifts, z is not proportional to distance.

4.4.2 Mapping the Universe in three dimensions

The surveys discussed in this section aim to provide accurate distance information by measuring redshifts of large numbers of objects – and some are also able to probe out to much greater distances by imaging fainter galaxies. In order to understand the scope of these surveys, we start by looking at some of the most distant galaxies imaged by the Hubble Space Telescope, such as those seen in the background of Figure 4.21.

Like the Hubble Deep Field images seen in Chapter 2, the background of this image of Abell 1689 illustrates the main difficulty with deep surveys: there are simply a huge number of very distant galaxies. The tiny portion of sky shown in Figure 4.21 contains thousands of galaxies yet the extent of the image is only 3 arcmin – one-tenth the diameter of the full moon.

■ The full moon is half a degree, or 30 arcmin, in diameter. How many images of 3 arc minutes square would be needed to survey a square area of sky 30 arcmin on a side (just large enough to cover the full moon)?

❑ You would need to assemble a mosaic of 10 × 10 images – a total of one hundred images to cover this small area of sky.

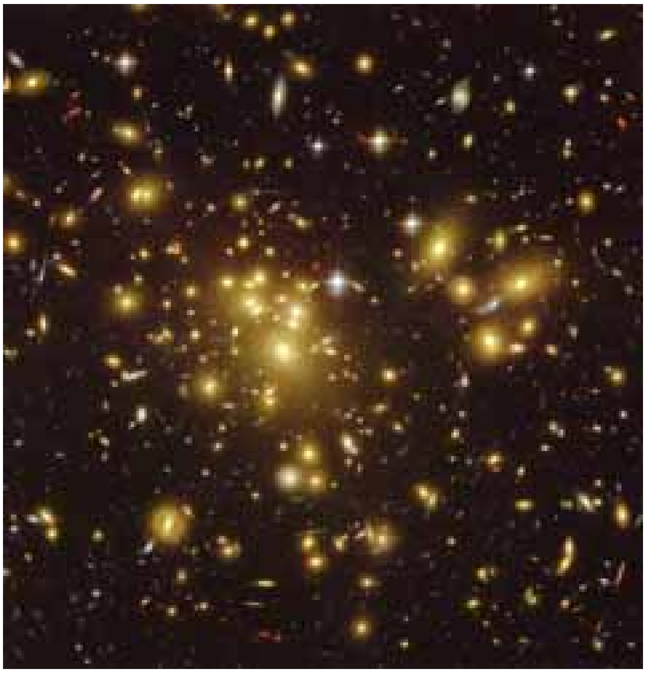

Figure 4.21 An image of the cluster Abell 1689 taken with the Advanced Camera for Surveys (ACS) on the Hubble Space Telescope. Although spectacular in its own right, the foreground cluster is overshadowed by the large number of distant galaxies that can be seen in the background. (NASA, N. Benitez (JHU), T. Broadhurst (Racah Institute of Physics/The Hebrew University), H. Ford (JHU), M. Clampin (STScI), G. Hartig (STScI), G. Illingworth (UCO/Lick Observatory), ACS Science Team and ESA)

A square image large enough to contain the full moon would be just half a degree on each side, giving an area of one-quarter of a square degree. In total there are approximately 40 000 square degrees in the whole sky. It is estimated that each square degree of sky may contain as many as 10^5 galaxies that could be detected in a long observation with the Hubble Space Telescope. Thus the total number of galaxies that we could potentially observe across the whole sky is in excess of a thousand million! Surveying the entire sky using the Hubble Space Telescope is clearly totally impractical – it would require making over ten million 3 arcmin square images.

The practical difficulties simply of imaging large numbers of galaxies are immense, but measuring their distances represents an even greater problem. Many of the galaxies imaged in the Hubble Deep Field are too faint for their redshifts to be determined. The practical constraint on the number of galaxies that can be studied in a reasonable length of time places a limit on the total volume of space that can be surveyed. Redshift surveys necessarily have had to compromise between sky coverage and distance probed: until recently it has been necessary to choose between imaging large areas of the sky to small redshifts, or small areas of sky to great distances.

Surveys carried out in the 1980s and 1990s followed one of these two paths. Some – such as the Harvard–Smithsonian Center for Astrophysics (CfA) survey (Figure 4.22a) and the IRAS (Infrared Astronomical Telescope) Point Source Catalogue *z*-survey (PSC*z* – Figure 4.18) – concentrated on measuring distances to galaxies within large volumes of the local Universe out to about 200 Mpc. Astronomers at Durham University and the University of California in Santa Cruz took a different approach, probing to much greater distances by concentrating on two much narrower regions of the sky. This **borehole survey** extended to about 2000 Mpc but covered only two narrow windows aimed towards the north and south galactic poles (Figure 4.22b).

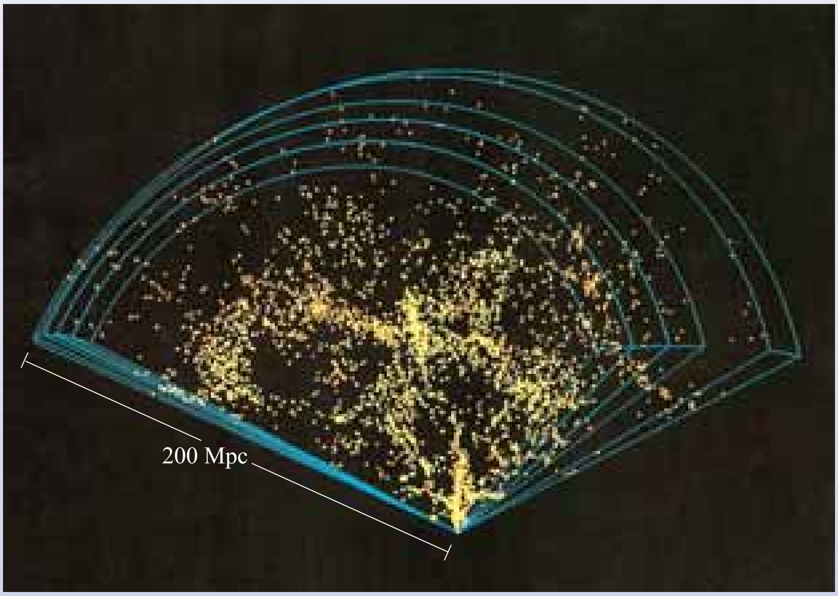

(a)

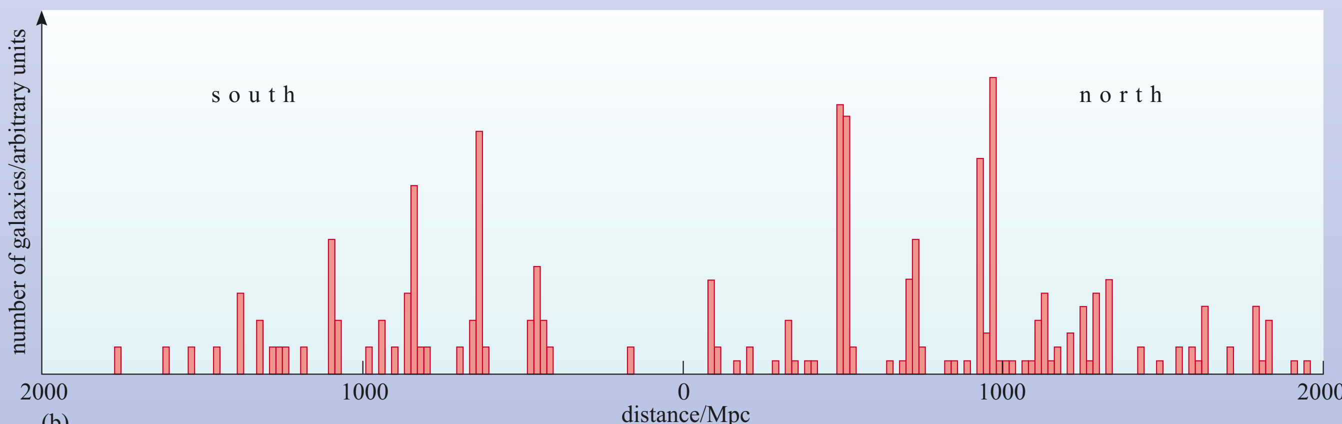

(b)

Figure 4.22 Examples of the structures revealed by the (a) CfA survey, and (b) the Durham–Santa Cruz borehole survey. Note the different distance scales. The CfA survey suggests a sponge-like distribution of galaxies with voids up to 60 Mpc across surrounded by walls and filaments. Although essentially a one-dimensional study, the Durham–Santa Cruz results also suggest the presence of walls separated by voids of low galaxy density. ((a) M. Geller and J. Huchra, SAO; (b) figure supplied by R. Ellis based on data described in Broadhurst *et al*., 1990)

Both the local surveys and the borehole survey confirmed the existence of features on scales larger than the Local Supercluster: these do not appear to be ever larger and larger clusters of clusters, but instead suggest a structure much more like a web or a network.

However, much larger volumes, going to greater depths, are needed in order to obtain a fair representation of the Universe and to see structures on the largest scales. Recent automated surveys using large-aperture telescopes are greatly extending the coverage of the sky. By contrast with the narrow views of the Hubble Deep Field, these telescopes observe with large fields of view (about 2 to 3 square degrees) allowing large areas of sky to be surveyed in a relatively short time.

The most ambitious of these projects is the Sloan Digital Sky Survey (SDSS), based at the Apache Point Observatory in the Sacramento Mountains of New Mexico (Figure 4.23). The goal of the Sloan Survey is to image one-half of the northern celestial hemisphere, as well as a smaller portion of the southern sky (see Figure 4.24). The northern sector covers roughly the same portion of the sky as Abell's 1958 cluster survey, but to a much greater depth and includes redshift

Figure 4.23 The 2.5-metre Sloan telescope has a remarkably wide-angle field of view, and is designed specifically to create a map of the sky. The telescope's detector includes an imaging camera and two spectrographs. The boxy metal structure that is prominent in this photograph is the outer wind baffle, which helps to minimize vibration of the telescope. (Sloan Digital Sky Survey)

measurements as well as simply imaging the galaxies. The aim is to determine the positions and brightness of over 100 million objects including stars, quasars and galaxies. By measuring the redshifts of a million of the nearest galaxies the survey will provide a three-dimensional picture of our neighbourhood of the Universe.

The survey has two elements: a deep sky imaging survey and a spectroscopic survey to determine redshifts. The imaging survey will record objects as faint as an apparent magnitude of 24. From these 100 million objects, the brighter ones (apparent magnitude 19 or brighter) will be selected for redshift measurements – this will include over a million galaxies and quasars. Hence only a small fraction of the objects imaged by SDSS will have their redshifts measured. It is expected that typical galaxies will be measured up to a redshift of about 0.25. The observational phase of the programme, which began in 2000, is due to be completed by 2005.

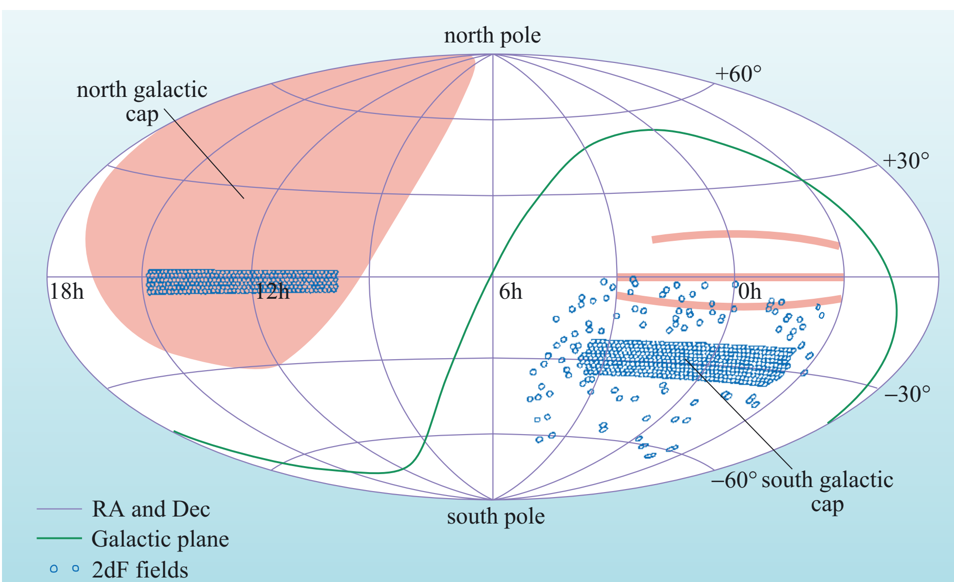

Figure 4.24 A map of the entire sky in equatorial coordinates showing the survey regions of the SDSS survey (pink shading), and the 2-degree Field (2dF) survey (blue shading). (Prepared with the assistance of M. Colless, Mount Stomlo Observatory)

The SDSS will cover most of the northern sky above 30° north of the galactic plane. Within this area it will generate a detailed three-dimensional map of our local neighbourhood out to ~800 Mpc, and a (two-dimensional) imaging survey out to much larger distances.

Another major redshift survey, albeit on a smaller scale than the SDSS, is the 2-degree Field (2dF) survey. This project, which had an observational programme that lasted three years (completed in 2002) was carried out using the 3.9 metre Anglo-Australian Telescope. Using a camera with a two-degree field of view, it surveyed two wedge shaped sectors of sky, one to the north and one the south of the galactic plane as shown in Figure 4.24. One aim of the survey was to use galaxy redshifts and positions to map the structure of the Universe out to distances of about 600 Mpc (this is the 2dF Galaxy Redshift Survey – 2dFGRS). The 2dF survey also mapped quasar positions and redshifts to much greater distances. Although the observational phase of the 2dFGRS is now complete, the analysis of the data will continue for many years.

The SDSS and the 2-degree Field survey use optical fibre systems to collect the spectra of hundreds of galaxies simultaneously. This means that the redshift measurements from many galaxies in a single field-of-view can be collected at the same time. Compared to older techniques in which only one spectrum could be measured at a time, modern fibre optic systems give a great advantage in the rate at which data can be collected.

In addition to surveying galaxies, both projects will also record the distances to hundreds of thousands of quasars and this will extend both our knowledge of the distribution of matter at high redshifts and provide information about the evolution of active galaxies (Section 3.6.2).

The improvements in imaging sensor technology over the past few decades are enabling these wide-scale surveys to be carried out in far more detail than was possible before, even using telescopes with relatively small apertures. When the same imaging technology is coupled to a large telescope, surveys can be extended to very high redshifts.

A group led by the University of California in Santa Cruz is doing exactly that in a project involving two of the most powerful telescope systems available. This Deep Extragalactic Evolutionary Probe project (DEEP) is using the twin Keck 10-metre telescopes on Mauna Kea, Hawaii, and the Hubble Space Telescope, to carry out a redshift survey that will include 50 000 galaxies to a limiting magnitude of 24.5 – equivalent to a redshift of 1.55 or a distance of about 4000 Mpc.

Like the earlier borehole survey, DEEP will cover only a very small area of sky, but will go out to much larger redshifts than the wide area surveys of the Sloan Digital Sky Survey and the 2-degree Field project. The patches of sky that will be examined include tiny portions of the area surveyed by SDSS and the area imaged in the original Hubble Deep Field. DEEP is designed to study the distribution and the evolution of galaxies out to high redshifts, thus exploring conditions earlier in the history of the Universe.

A summary of important redshift surveys that are either ongoing or have been completed is given in Table 4.2. Figure 4.25 shows the coverage in terms of area of sky and distance of these different surveys.

Table 4.2 A summary of five important galaxy redshift surveys. The CfA and the PSC*z* surveys were completed in 1989 and 1997 respectively.

Name	Number of galaxies in survey (approximate)	Mean redshift	Telescope diameter/m	Simultaneous spectral measurements[a]
CfA	1500	0.02	1.5	1
PSC*z*	15000	0.03	2.1	1
2dFGRS	250 000	0.10	3.9	400
SDSS	1000 000	0.10	2.5	640
DEEP	50 000	0.7–1.55	10	1

[a]The number of simultaneous spectral measurements describes how many galaxy redshifts can be measured in a single field-of-view at any one time.

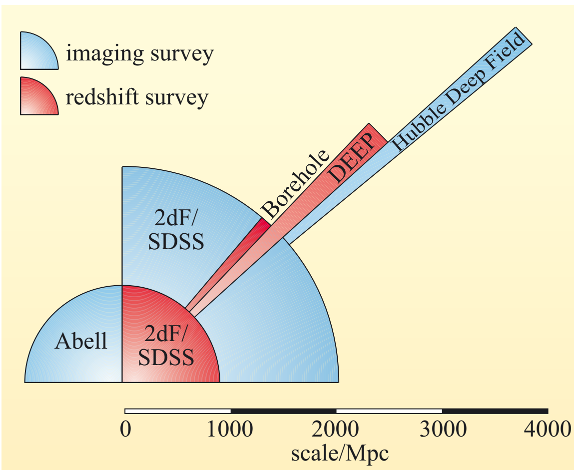

Figure 4.25 A schematic illustration of the relative scales of the different surveys. Imaging surveys can include fainter objects than redshift surveys, so the imaging elements of the SDSS and 2dF projects go out to much greater distances than their corresponding redshift elements. (Note that the extent of the sectors in this diagram are for illustration only – they do not correspond to the actual areas of sky covered by these surveys.)

4.4.3 Large-scale structure revealed

Although several of the surveys discussed in the previous section are still ongoing, early data releases are revealing ever larger glimpses of the structure of the Universe. One example is the result from the 2-degree Field survey shown in Figure 4.26.

The 2dF results clearly show that the web or sponge-like structure suggested by earlier studies extends out to great distances, forming a cosmic network. The densest points within this network are clusters of galaxies containing hundreds or thousands of galaxies. Loose collections of clusters form superclusters of perhaps 30 to 50 Mpc in size. On larger scales, there are low-density voids, of up to about 60 Mpc in diameter, separating the higher density collections of clusters. These voids are separated by filaments of galaxies strung out in long chains, and by two-dimensional sheets that enclose the voids rather like the pores in a sponge. Although difficult to discern from representations such as Figure 4.26, the density of galaxies in the filaments is very much less than that in the clusters, and only a factor of two or three greater than the density in the voids themselves. The largest structures appear to be on a scale of approximately 200 Mpc; above this, the Universe becomes uniform in the sense that one 200 Mpc region looks much like another.

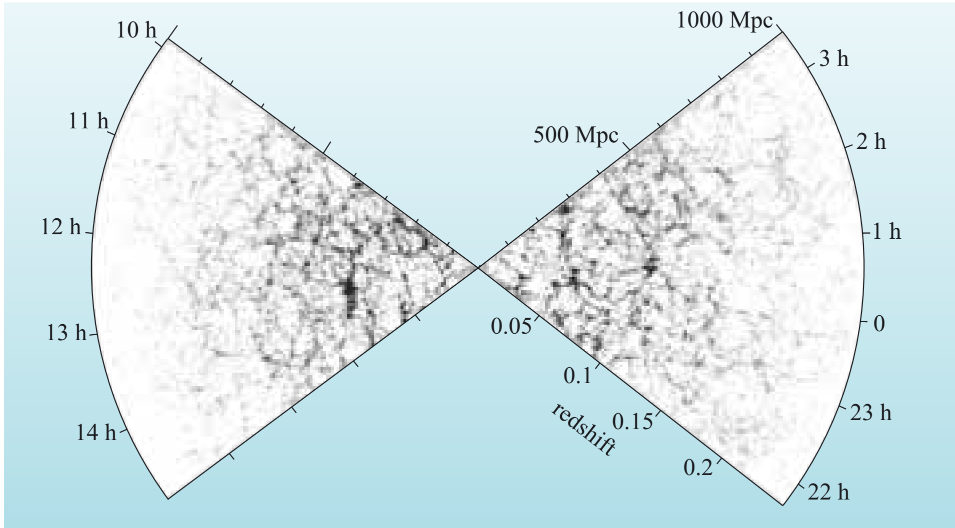

Figure 4.26 Early results from the 2-degree Field Galaxy Redshift Survey. This data release (May 2002) shows the positions of over 220 000 galaxies plotted in plan view on the two wedges covered by the survey. (M. Colless, Mount Stomlo Observatory)

QUESTION 4.5

Summarize the scales of different cosmic structures by completing Table 4.3. Note that only approximate values, or ranges of values, are required.

Table 4.3 The scales of different types of cosmic structures – for use with Question 4.5.

Feature	Distance or length/Mpc
Milky Way (diameter of the stellar disc)	
Distance to Large Magellanic Cloud	
Distance to the Andromeda Galaxy	
Extent of the Local Group	
Typical diameter of a cluster	
Distance to nearest rich cluster (Virgo)	
Extent of a typical supercluster	
Extent of voids	
Scale on which the Universe appears uniform	

4.5 The spatial distribution of intergalactic gas and dark matter

In the case of clusters of galaxies we saw that the galaxies themselves make only a small contribution to the total mass: clusters also contain significant amounts of intracluster gas, and the total mass is dominated by the contribution from dark matter. We also saw that in clusters the intergalactic gas and the dark matter are distributed in a somewhat different way from the galaxies. Specifically, the dark matter and the intergalactic gas seem to be more smoothly distributed in a cluster

than do the galaxies. So it is of great interest to astronomers to understand how intergalactic gas and dark matter are distributed on large scales – do they follow the large-scale structure that is mapped out by the luminous matter in galaxies, or is their distribution significantly different?

We will begin by considering how the gas that lies between galaxies and clusters can be studied, before moving on to discussing a technique that is now being developed to map the distribution of dark matter in the Universe.

4.5.1 Quasars and the Lyman α forest

We saw earlier that the intergalactic gas in clusters of galaxies is easily detectable because of its X-ray emission. However, in locations that are away from the gravitational influence of a rich cluster the intergalactic gas will not be a bright source of X-ray emission, or indeed, of any other form of electromagnetic radiation. A different type of approach is needed if we are to study such gas. Rather than looking for *emission* from this gas, astronomers examine how it *absorbs* electromagnetic radiation. Of course, to do this, there needs to be a convenient source of electromagnetic radiation that lies beyond the gas we wish to study. Fortunately, distant quasars provide us with such a source.

As you saw in Chapter 3, quasars are very bright, point-like objects with very high redshifts: quasars with redshifts up to about 6 have been discovered. Since they lie at such large distances from us, the electromagnetic radiation that is emitted by most quasars will cross vast tracts of the intergalactic medium as it travels towards the Earth. As this electromagnetic radiation passes through this medium we might expect that a certain amount of absorption may occur and give rise to spectral absorption lines at specific wavelengths (Figure 4.27).

The most common element in the Universe is hydrogen, and the distribution of intergalactic gas can be mapped by making use of the spectrum of this element. The spectrum of hydrogen consists of several series of spectral lines. Of these, the **Lyman series** has the highest energy (and hence shortest wavelengths). Within this series, the most prominent spectral line is the Lyman α line corresponding to the transition between $n = 2$ and $n = 1$ levels of the hydrogen atom. This line, which is often abbreviated to Lyα, lies in the ultraviolet part of the spectrum with a wavelength of 121 nm and is easily identified, even when red-shifted.

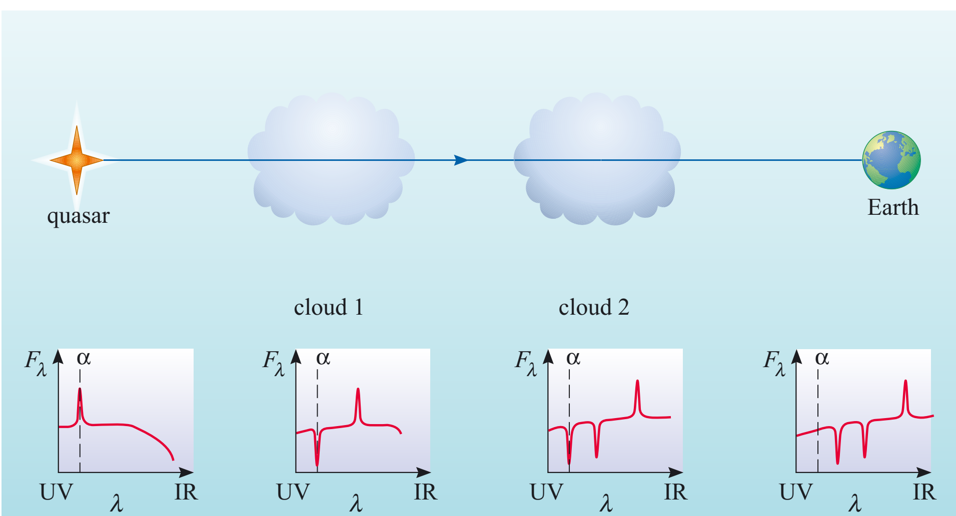

Figure 4.27 Intervening clouds in the line of sight from a quasar. Cloud 2 will have the smallest redshift when viewed from Earth.

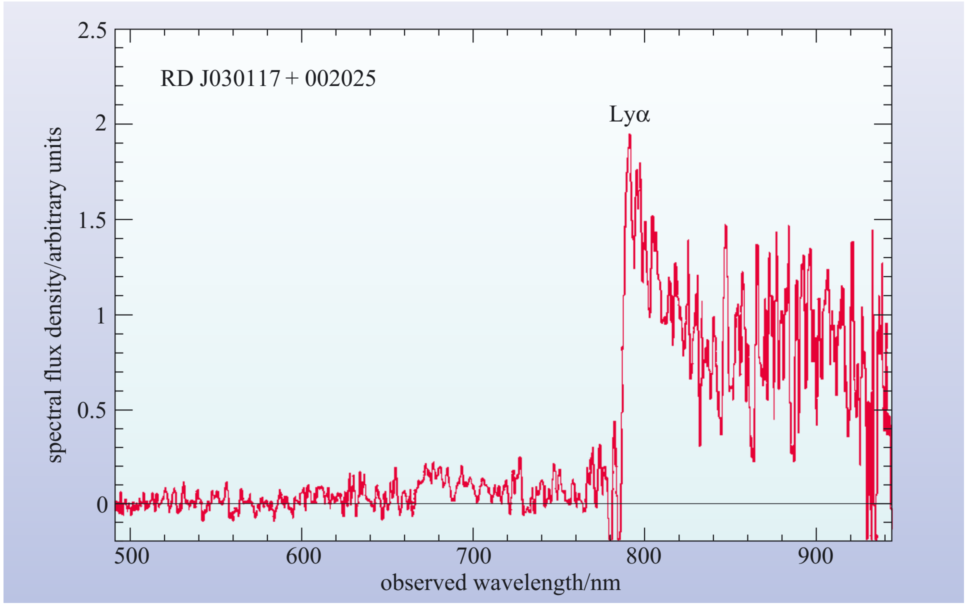

Figure 4.28 The spectrum of quasar RD J030117 + 002025 with redshift of $z = 5.5$. The redshift of this object is so large that the Lyman α emission line has been shifted from the ultraviolet (121 nm) to the infrared (786 nm). (Stern *et al*., 2000)

In the spectra of the most distant quasars the Lyman α spectral line gets shifted all the way from the ultraviolet, through the visible part of the spectrum and into the infrared (Figure 4.28). In the original spectrum from the quasar, this line is present as a bright *emission* line, which appears above the continuous spectrum produced by the AGN (see Figure 3.16).

As the electromagnetic radiation from the quasar passes through intergalactic space it encounters clouds of cool gas. Because the gas is cool, absorption will occur, and this will be prominent at the wavelength of the Lyman α line. To an observer within one of these clouds the spectrum from the quasar will appear red-shifted, so the original Lyman α emission line will have a longer wavelength than 121 nm. Ultraviolet light that arrives at the cloud with a wavelength of 121 nm would have been emitted by the quasar at wavelengths shorter than the Lyman α line. The cloud will absorb radiation at a wavelength of 121 nm and so an absorption line will be formed. This process of absorption will occur for every cloud that the light from the quasar passes through. However, these clouds are at differing distances from the quasar, so according to observers situated on these clouds, the observed emission from the quasar will be red-shifted by differing amounts. Consequently, as the electromagnetic radiation from the quasar passes through a series of clouds on its way to Earth, it produces a set of spectral lines at progressively shorter wavelengths. The distances to the clouds can be found from the redshifts of these absoption lines. An example of a spectrum from the quasar Q 0149+336 which displays such absorption features is shown in Figure 4.29.

Because of the many closely packed absorption lines, this structure in a spectrum is frequently referred to as the **Lyman α forest**.

- What does the presence of discrete absorption lines in the Lyman α forest suggest about the distribution of the material that the light has passed through? What would be seen if the absorbing material were distributed *uniformly* along the line of sight?

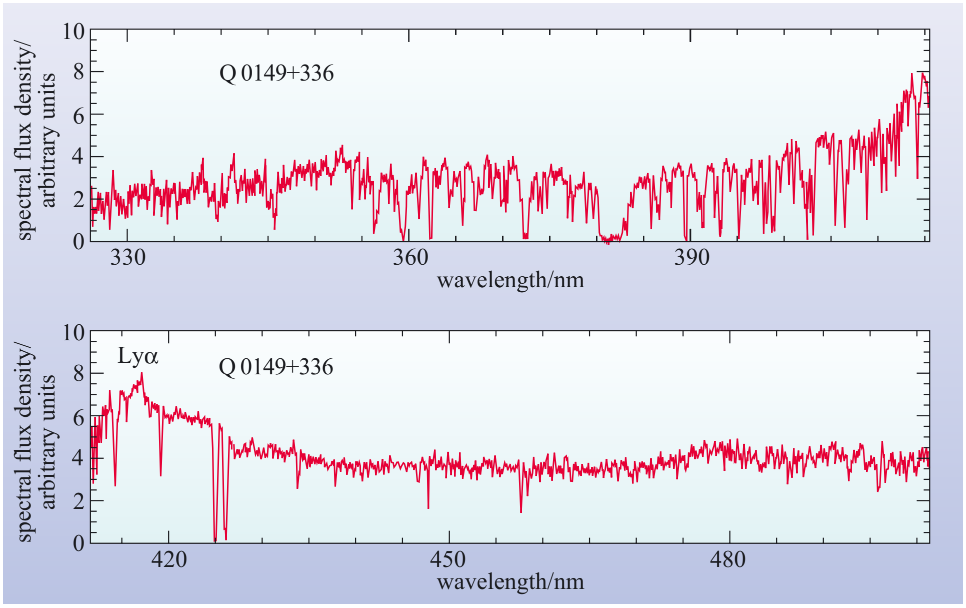

Figure 4.29 The spectrum of quasar Q 0149+336 ($z = 2.431$). The upper panel shows the spectrum from a wavelength of about 325 nm to 415 nm, the lower panel shows wavelengths from about 410 nm to 500 nm. The red-shifted Lyα line has an observed wavelength of 417 nm. At wavelengths shorter than the (red-shifted) Lyα line, there are a large number of absorption lines – due mainly to Lyα absorption by clouds of intergalactic gas at lower redshift than that of the quasar. At wavelengths longer than the red-shifted Lyα line there are relatively few absorption lines (the lines that are present are not due to Lyα absorption, but to absorption by elements heavier than hydrogen or helium in the intergalactic medium). (Wolfe *et al*., 1993)

❑ In order to produce a distinct absorption line at a given wavelength, the light must have passed through a concentration of material at the distance corresponding to that redshift. If the material were distributed uniformly, light would be absorbed gradually all along the line of sight with continuously varying redshift, giving constant absorption at all wavelengths rather than a 'forest' of individual lines.

So the fact that there are many Lyman α absorption lines in the spectrum from a distant quasar tells us that the intergalactic medium is not smoothly distributed – but instead is in the form of 'clumps' or clouds.

For example, an analysis of the absorption lines in the spectrum of the quasar Q 0149+336 (Figure 4.29) reveals seven clouds along the line of sight whose presence is confirmed by absorption lines due to elements heavier than hydrogen or helium ('metals'). Each of these clouds has a distinct redshift (ranging from about 0.5 to about 2.2 in this case). Note that there are many other lines, which are also due to absorption by intervening clouds, but that it is not possible to confirm the presence of any single cloud unless a *pattern* of spectral lines (Lyα and metal absorption lines) can be discerned in the spectrum.

QUESTION 4.6

In Figure 4.29, the spectrum shows a strong absorption line at a wavelength of 372 nm. Assuming this to be a red-shifted Lyman α line, calculate the redshift and hence estimate the distance of the cloud responsible for this absorption line.

So how does this distribution of intergalactic gas correspond to the distribution of matter as traced by galaxies? This is an ongoing area of research, but it does seem as though the Lyman α absorbing clouds are more uniformly distributed in space than the luminous matter. For instance, it has been mentioned that there are 'empty-

spaces' or voids in the galaxy distribution, but clouds of absorbing gas do seem to be present in these voids. There is no inconsistency here: most Lyman α absorbing clouds have very low densities – too low to be sites of star, and hence, galaxy formation, so it need not be the case that the distribution of intergalactic gas should exactly follow the distribution of galaxies.

Although the majority of Lyman α absorbing clouds are of low density, there are some clouds where the density enhancement is about a factor of 10^6 above the mean density of the intergalactic medium. The absorption lines from these clouds are very deep and broad, and are called **damped Lyman $\boldsymbol{\alpha}$ systems** (the terminology 'damped' refers to the physical effect that gives these lines their characteristic shape). The trough at roughly 380 nm in Figure 4.29 is an example of this effect. Damped Lyman α systems are of particular interest because, unlike the low-density Lyman α clouds, they *are* a plausible source of material for star formation. Indeed, it is suspected that the damped Lyman α systems may be clouds from which galaxies are about to, or have started to form. Unfortunately the evidence to make such a connection is, at present, rather circumstantial, but clearly these systems will be subject to a great deal of scrutiny in the coming years.

The fact that radiation from a distant quasar can reach us at all appears at first sight surprising. In Chapter 2, we saw that the big bang model suggests a Universe that is initially filled with a smooth distribution of hydrogen and helium which cools and forms neutral atoms. This is then followed by the growth of density perturbations by gravitational collapse. The matter that does not take part in this process might be expected to remain as un-ionized gas. The quantity of neutral gas that might naively be expected to remain in the intergalactic medium is such that it would cause very strong absorption of the light from distant quasars. This expected absorption by a neutral intergalactic medium is called the **Gunn–Peterson effect**. The fact that the absorption, as seen through the Lyman α forest, is much lower than expected suggests one of two possibilities: either that the expected hydrogen is not present, or (more likely) that any hydrogen is present but not as neutral hydrogen, rather it is in an *ionized* state, that prevents it from absorbing the radiation.

For light to reach us from distant quasars, intergalactic hydrogen must have been ionized by the time the light was emitted. The event that caused most of the neutral hydrogen in the Universe to become ionized is referred to as **reionization**. The time at which this occurred is called the **epoch of reionization**, and to be consistent with observations of high-redshift quasars this must have been when the Universe was less than 10% of its current age. So what could have caused this Universe-wide change? The most plausible explanation is that sources of ultraviolet radiation suddenly 'turned on' at this time.

■ Can you suggest two possible sources for this ultraviolet radiation?

❑ Star-forming regions and active galactic nuclei are both strong sources of ultraviolet radiation.

As we saw in Section 2.5.5, galaxies seen at high redshifts appear to be sites of energetic bursts of star formation. This was happening when the Universe was only about 10% of its present age, and could have provided the energy required to ionize the intergalactic hydrogen. Alternatively, you saw in Section 3.6.2 that in the past the density of quasars was much higher than it is now. So it is also possible that

active galaxies provided a source of ultraviolet radiation that ionized the bulk of the neutral hydrogen in the Universe. At present there is no consensus about which of these two processes was the more important as a cause of ionization of the neutral intergalactic medium.

If it were possible to look back to times earlier than the epoch of reionization, then we should expect quasar spectra to show strong absorption from neutral hydrogen. The search for the Gunn–Peterson effect at these early epochs is currently an active area of research. Recent observations of the most distant quasars are beginning to show signs that the expected absorption has indeed been detected at redshifts greater than $z \sim 6$. If confirmed, these results will allow estimates to be made of the time in the early Universe at which stars or active galaxies first started to form.

4.5.2 Cosmic shear

All the methods of determining masses discussed in Section 4.4 point to the existence of dark matter within galaxies and clusters. A fundamental question is whether the large-scale distribution of galaxies follows the distribution of dark matter as suggested by theoretical models. In many of these models, dark matter condenses first, creating a network within which galaxies form at locations where the dark matter is most densely concentrated.

Dark matter cannot be observed directly because it does not absorb or emit light. Within galaxies and clusters its presence can be detected by its gravitational effects on the velocities of individual stars or galaxies. Superclusters and larger structures however are not virialized so the large-scale distribution of dark matter cannot be studied in the same way.

■ Can you think of another way in which dark matter might reveal its presence on a large scale?

❑ Dark matter does not emit or absorb light, but it can be detected by its *gravitational* effects on light. The large-scale distribution of dark matter could be studied by looking for deflections of light from distant galaxies.

A strong form of gravitational lensing was seen in Section 4.3.2 where large local concentrations of mass such as clusters of galaxies acted as gravitational lenses causing severe distortions of background objects. Diffuse large-scale structures can also affect the paths of light rays causing a weaker form of the effect, where fluctuations in the density of matter cause the images of background galaxies to be very slightly stretched and distorted. This effect is known as **cosmic shear** and is similar to looking at the tiled bottom of a swimming pool through the ripples on the surface (Figure 4.30).

■ What effect would dark matter have on the passage of light if it were distributed uniformly throughout the Universe?

❑ None: if the distribution of dark matter were completely smooth, the light would not be deflected one way or the other. By analogy, the bottom of swimming pool would not appear distorted if the surface were smooth – it is the ripples that cause the distortion. Only if there is a non-uniform distribution of mass would deflections be seen.

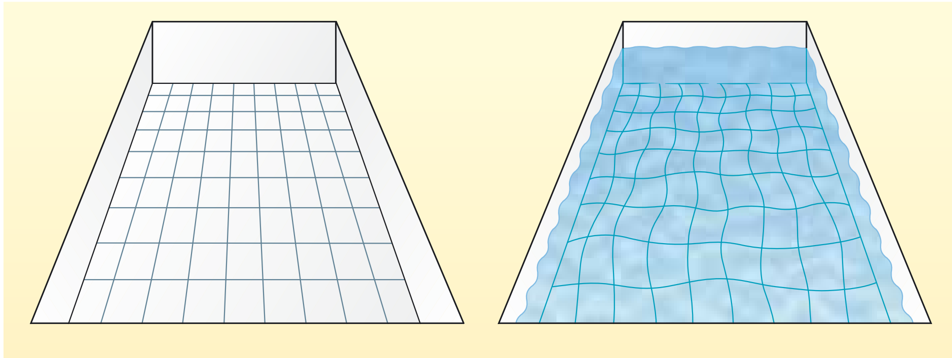

Figure 4.30 The bottom of a swimming pool can appear distorted when viewed through ripples on the surface. In a similar way, light from distant galaxies can be distorted as it passes through a non-uniform distribution of dark matter.

In the example of the swimming pool, the grid pattern of the tiles on the bottom of the pool makes even small distortions easy to see. The square tiles become distorted by the ripples on the surface: this type of distortion is known as a *shear*, hence the term *cosmic shear*. The sky, of course, does not have a convenient grid painted on it! Instead, use can be made of very distant galaxies such as those seen in long-exposure observations made using the Hubble Space Telescope (Figure 4.21): if you look to a great enough distance there are a vast number of background galaxies in every tiny patch of sky.

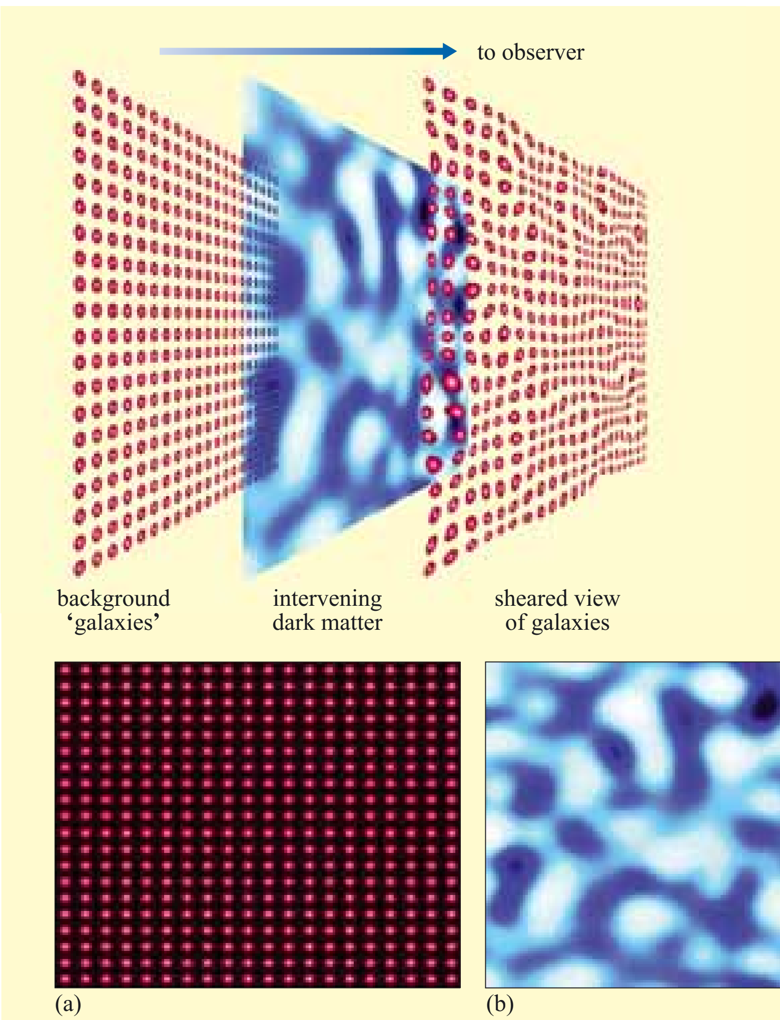

Figure 4.31 Cosmic shear: As light from a field of distant galaxies (a) passes through the web of dark matter (b) on its way to Earth, the image of each galaxy is slightly distorted by the non-uniform gravitational field (c). Although the distortion of each galaxy is small, the *average* distortion in a region of the image can be used to map the distribution of dark matter. (Adapted from figures produced by A. Refregier, University of Cambridge)

Figure 4.31 shows an imaginary situation in which a distant regular array of circular galaxies is viewed through a web of dark matter. Note how distortions indicate the presence of a high density of intervening dark matter. In other parts of the image, the 'galaxies' are relatively undistorted – showing that light rays have passed through a region with little variation in density. In reality, the distortions are much smaller – only one or two per cent, and the outlines of real galaxies are not necessarily circular to start with, so the distortion of an individual galaxy can be difficult to measure. But the images of galaxies that are near to one another will tend to be stretched in the same direction, and each small area of sky contains many galaxies. So even if the distortions are small they can still be measured by *averaging* over many neighbouring galaxies. This average distortion of galaxies can be used as a measure of the intervening dark matter.

Gravity is the one known way in which dark matter makes its presence felt. Because the distortions of background galaxies are caused by gravitational fields, cosmic shear provides one of the most direct means of mapping the distribution of dark matter.

This type of measurement is in its infancy, but the cosmic shear results published so far *do* suggest a network of dark matter that is consistent with the position of the visible matter in the Universe as mapped by redshift surveys. This is a vital piece of evidence with relevance to possible models of the formation and evolution of cosmic structure which will be taken up in more detail, in Chapter 6.

4.6 Describing cosmic structure

In this section we will introduce some of the ideas that are used to describe or characterize cosmic structure. We have already seen that the distribution of galaxies seems to suggest that at scales of about 200 Mpc or so, the Universe becomes uniform – one region that is about 200 Mpc across tends to look very much like another. However, theories of how structure is formed in the Universe need to be tested against real observations of the distribution of matter.

Computer simulations play an important role in the comparison between theory and observation. Different theoretical models make different predictions depending on the conditions built into the model. For example, changing the amount of dark matter in a computer simulation may make a large difference in the predicted distribution of galaxies. Theories can therefore be tested by varying the parameters within simulations (such as for instance, the density of dark matter) and comparing the results with data from the surveys.

It is unreasonable to expect that a computer simulation would reproduce the exact positions of all the individual galaxies in the Universe – rather, we expect theory to generate structures that are *similar* to those observed in the real Universe. For example, a good theoretical model should result in the formation of structure on scales that agree with observations – the *distribution* of galaxies should generate patterns similar in both shape and scale to those measured by redshift surveys.

The problem of describing the distribution of clusters can be tackled in various ways. As a very simplified example, look at Figure 4.32a, which shows a two-dimensional distribution of points. This could, for instance, correspond to a distribution of the positions of galaxies as seen on the sky. To describe this

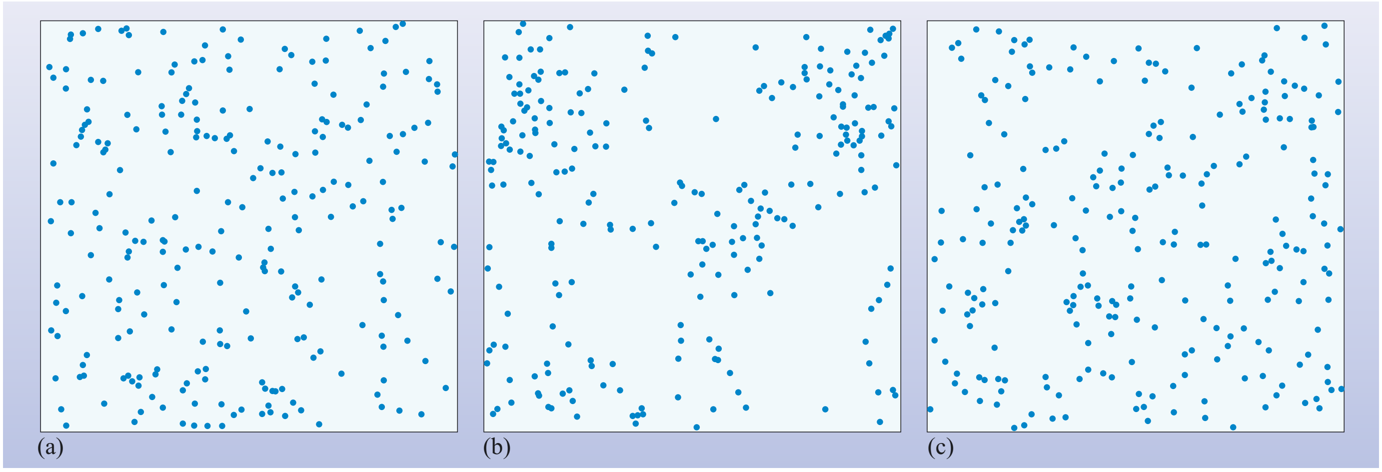

Figure 4.32 Three different two-dimensional distributions of points.

distribution the positions (for example, the x and y coordinates) could be given for each of the points. This would describe the distribution exactly, but it would not be useful to an astronomer who wants to make comparisons with a simulation. A description is needed which will easily allow comparison between different parts of the sky or between observations and simulated distributions, which will tell us how such a pattern may have formed.

The process of comparison of patterns is something that the human brain seems to be quite well adapted to do, as the following example should illustrate.

■ Look at Figure 4.32, and by eye, compare the pattern in (a) with those in (b) and (c). Which of (b) and (c) would you say most closely resembled (a)?

❑ Most people would choose (c) as being a pattern that resembles (a),

■ Why would you say that (c) more closely matches (a) than does (b)?

❑ Pattern (b) looks distinctly different. There seem to be clumps of galaxies and empty spaces that are not evident in (a) and (c).

The human brain does a remarkable job in being able to match patterns, but astronomers need a rigorous way of describing patterns which can be automated and applied to different sorts of data. To do this, astronomers use statistical methods that describe the average properties of a given distribution or pattern.

It would be a lengthy and highly mathematical diversion to explore all the various techniques that astronomers have adopted in order to compare maps of the Universe with the output from simulations. Indeed, the astronomical literature is littered with discussion about the advantages and disadvantages of using a particular statistical technique to characterize the large-scale distribution of matter in the Universe.

However, it is instructive to consider one type of method that is used, since it highlights the aim of all such techniques, which is to quantify how the relative variation in density in a map depends on length scale.

We will consider a simplified example of a technique that is called the **counts-in-cells** method. As the name suggests, the basis of the technique is to split a map (or three-dimensional survey region) up into cells and count the number of galaxies in each cell. As the following example shows, by carrying out this process using cells of differing sizes, it is possible to quantify how the density of galaxies varies on different length scales.

The maps that we will characterize in this example are two-dimensional, although the argument that we will follow can equally well be applied to three-dimensional surveys. To simplify the method, the maps are square and both have an area of 128 units by 128 units. These 'units' are our way of defining length in these maps.

Figure 4.33a (top left panel) shows the first map that we will be interested in – it shows a hypothetical distribution of galaxies all of the same mass, represented by points. In fact, this is a purely random distribution – the probability of finding a galaxy is the same at any location on the map, and we will call this distribution the 'random' map.

We are interested in investigating how fluctuations in density depend on length scale, so what we can do is to split the map up into cells and measure how the variation in density depends on the cell size. To start with we split the map up into 64 × 64 (= 4096) cells – so each cell has a size of 2 units × 2 units. In each of these cells we count the number of galaxies and hence calculate the density (remember that these are all 'galaxies' of identical mass). These densities are indicated in Figure 4.34a (top middle panel) by the shading of the cells (the brighter cells have a higher density). For all of the 4096 cells in this map we then work out a 'typical' variation $\Delta\rho$ – the amount by which the density of any one cell is likely to differ from the mean density ρ (taken over the entire map). The *relative variation* in density is then defined as $(\Delta\rho/\rho)$. In this first case, where the cell size is 2 units, the relative variation turns out to be 100%.

The next stage is to repeat this process with a smaller number of cells – in this case 32 × 32 (= 1024) (Figure 4.33a – top right panel). As you might expect, the relative variation is now smaller because the cells are larger – in fact, it is now only about 50%. This process can be repeated for cells in which the map is split up into increasingly larger cells: 16 × 16 (= 256), 8 × 8 (= 64) and 4 × 4 (= 16) cells (Figure 4.33a – second row of maps). When this is done the relative variation is found to have values of 24%, 11% and 4% respectively. As expected, the relative variation decreases as the size of the cell increases – the variation in the map is 'washed-out' as we look at the map at larger and larger scales.

The final stage is to plot a graph that shows how the relative variation changes when the map is split up into cells of different sizes. To do this a graph can be plotted of relative variation against the length of one side of the cell. For the example that we have just considered, such a graph is shown as the blue line in Figure 4.33c.

To illustrate how such a technique can provide a useful way to compare two maps, Figure 4.33b shows another hypothetical distribution of galaxies. As in the 'random' map, the map contains galaxies of identical mass, but in this case the distribution is strongly clustered. This will be referred to as the 'clustered' map. (Note that this distribution is much more clustered than the real distribution of galaxies.) Figures 4.33b show the results of applying the identical technique to that we have just described for the 'random' map to the 'clustered' map. The cores of the clusters have very high density, and this causes the relative variation to be very high (about 320%) when we analyse the map at a resolution of 64 × 64 cells.

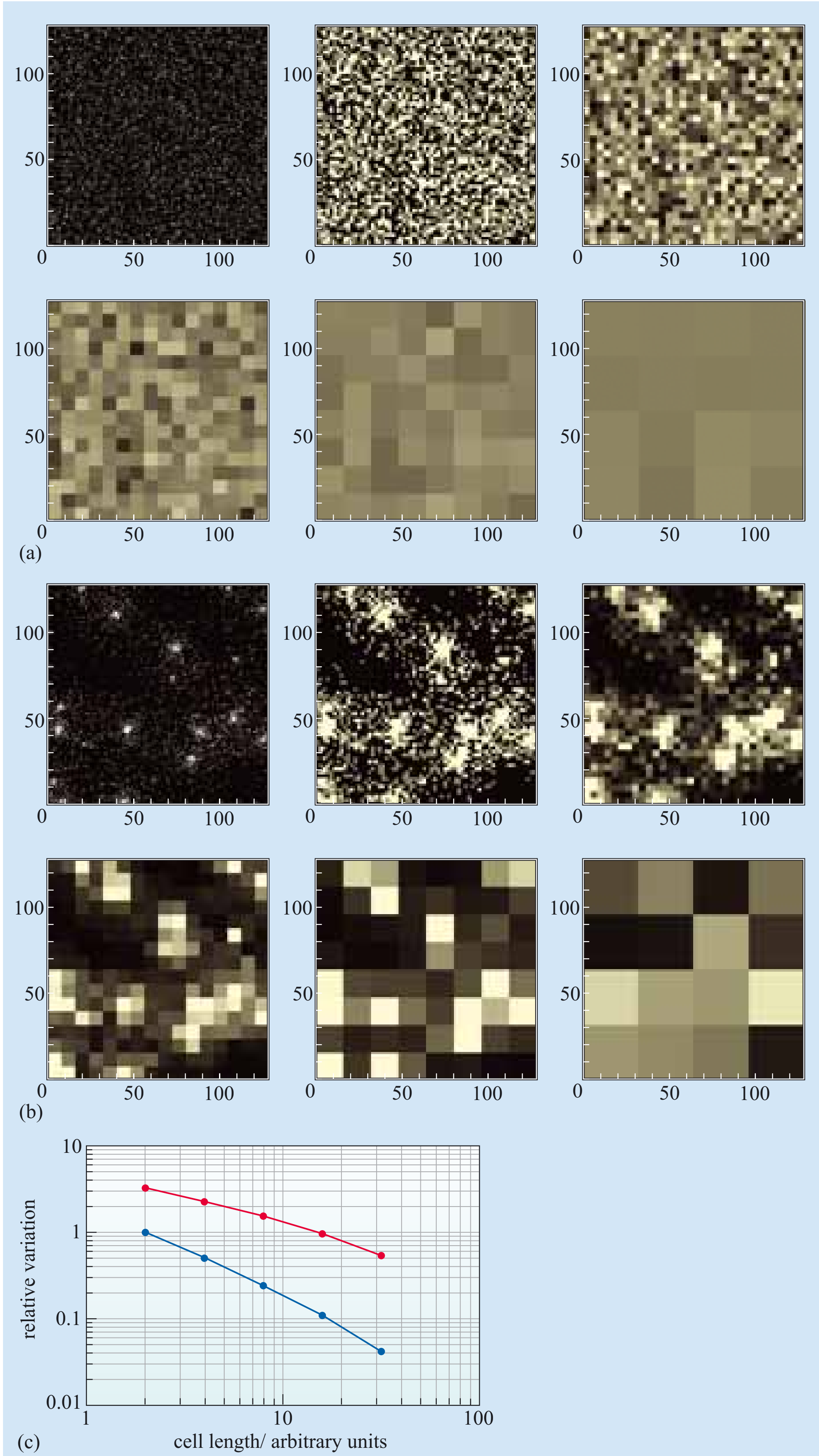

Figure 4.33 The counts-in-cells technique for measuring how the size of variations in density depend on the size of cell.
(a) Shows the original map (upper left), and five realizations of the same data binned into cells of increasingly larger sizes. The density within a cell is indicated by the intensity of its shading – brighter shading indicates higher density. The original map in this case is a purely random distribution of galaxies.
(b) Shows the same analysis as in sequence (a), but in this case for a highly clustered distribution.
(c) Shows a graph of how the relative variation depends on the size of the cell. The blue line shows the results from the 'random' map and the red line shows the results from the 'clustered' map. (M. Jones (Open University))

As cell size increases, the relative variation decreases, again because the variation is 'washed-out' in the larger cells. However, note that the clustering also causes large 'voids' and even when the map is analysed at a resolution of 4 × 4 cells, there is substantially more relative variation – typically 50% – than was found in the 'random' map.

The results of this analysis for the 'cluster' map are shown in Figure 4.33c (red line). Note that the results of the counts-in-cells analysis for the two maps are very different – not only does the cluster map show more relative variation at every length scale, but the shapes of the two curves in Figure 4.33c are also different. Of course, the technique that has been described here can be equally applied to a simulation as to real data – so by comparing the counts-in-cells analysis of real maps with simulations we may be able to discern which theoretical models for structure formation are consistent with observation.

In the analysis of real astronomical maps or surveys a similar approach can be adopted. Although the exact methods of carrying out the analysis are more sophisticated than the approach outlined here, the basic idea is the same. Figure 4.34 shows the results of a counts-in-cells analysis of a particular three-dimensional redshift survey of galaxies. (In fact, the galaxies were a subset of the PSC*z* survey that was mentioned above.) The observational data, which cover a range of scales from about 10 to 80 Mpc are shown by the red line in Figure 4.34. As might be expected, the relative variation decreases with length scale – such that for cells with sides of length 50 Mpc the relative variation is about 30%. The analysis that was carried out on the real data can also be applied to the results of simulations of the formation of large-scale structure. The results of the counts-in-cells analysis of one such theoretical model is shown as the blue line in Figure 4.34, and now we can start to see the power of this type of analysis. If a simulation produces a pattern of variation that is similar to that which is observed in the real Universe, then we might be able to discriminate between different scenarios under which structure formed in the Universe.

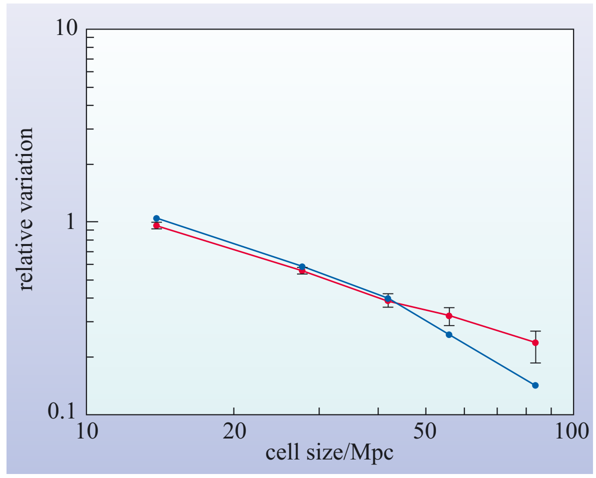

Figure 4.34 The results of a counts-in-cells analysis of three-dimensional survey data. The redshift survey was part of the program that constituted the PSC*z* survey (see Figure 4.18). The observational data are shown in red. The blue line shows the counts-in-cells results that would be expected from a particular model for the formation of structure. (Adapted from Oliver *et al*., 1996)

We won't dwell on the results of such comparisons here – since in order to put them into proper context, it is necessary to first develop the cosmological framework that we can use to describe the evolution of the Universe as a whole. However we will return to the topic of the formation of structure in Chapter 6. Furthermore, in Chapter 7 you will see how a similar type of analysis – which is based on characterizing the fluctuations in a map – is now enabling cosmologists to determine some of the fundamental physical parameters that describe the evolution of the Universe. In order to make further progress then, we need to consider how a scientific understanding of the Universe on the very largest scales has been developed; this is the subject of the next chapter.

4.7 Summary of Chapter 4

The large-scale distribution of galaxies

- Galaxies are gravitationally clustered into groups (containing up to about 50 galaxies) and clusters (which contain from about 50 to over a 1000 galaxies).
- Our Galaxy belongs to the Local Group of galaxies consisting of about 30 members but dominated by the Milky Way and Andromeda galaxy (M31).
- Medium-scale three-dimensional surveys confirm the existence of superclusters, loose collections of clusters which are about 30–50 Mpc in extent. Superclusters are not virialized systems.
- Our Local Group is at the outer edge of the Local Supercluster which is centred on, and dominated by the Virgo cluster.
- Redshifts can be combined with positions on the sky to obtain surveys of galaxies in three dimensions.
- The introduction of efficient electronic detectors and computer automation has resulted in a huge increase in the efficiency of redshift measurements. Current surveys are aimed at mapping large portions of the sky to great depth to look at the distribution of structure on scales of hundreds of megaparsecs.
- One method of describing of the large-scale cosmic structure is by using a counts-in-cells analysis. This quantifies how fluctuations in density vary with length scale. This allows comparisons to be made between the real distribution of galaxies and the results of numerical simulations of the formation of structure.

Clusters of galaxies

- Most clusters of galaxies have a radius of about 2 Mpc (the Abell radius). The mass of a typical cluster is of the order of 10^{14} to $10^{15} M_{\odot}$.
- Cluster masses can be estimated by three main methods: velocity dispersion, X-ray emission and gravitational lensing. The masses obtained by these methods typically agree within a factor of two or three.
- A cluster is said to be virialized if it is a gravitationally bound system and is in dynamical equilibrium. The mass of such a cluster can be obtained from the dispersion of the line of sight velocities (Δv) using $M \approx R_{\mathrm{A}}(\Delta v)^2/G$.
- Rich clusters are strong X-ray emitters due to the presence of hot intracluster gas. X-ray observations can be used to estimate the total mass of the cluster and the mass of X-ray emitting gas.
- A cluster can act as a gravitational lens of a distant galaxy, producing distorted multiple images. This is a means of detecting distant objects and can also be used to estimate the mass of the intervening cluster.
- Estimates of the masses of clusters from all three methods (virial theorem, X-ray emission and gravitational lensing) indicate that there is far more matter in clusters than the sum of the individual galaxy masses. This suggests the presence of dark matter in clusters. Typically galaxies will contribute less that about 10% of the mass of a cluster. The intracluster gas may constitute up to about 25% of the total mass. Dark matter makes up between 70% and 90% of the total mass of the cluster.

- X-ray spectra from clusters show that the hot intracluster medium contains an unexpectedly high metal content. This enrichment of the ICM is the result of supernova explosions in energetic young star-forming galaxies.
- Temperature maps of clusters indicate that many clusters are not in a state of hydrostatic equilibrium. This can give us information about the formation of clusters, and suggests that clusters may grow from the merging of smaller subclusters.

The intergalactic medium

- Some quasar spectra contain multiple absorption lines indicating the presence of gas (mainly neutral hydrogen) at different distances along the line of sight. This is called the Lyman α forest and can be used to detect the presence of neutral gas in the intergalactic medium.
- The absence of the Gunn–Peterson effect indicates that the density of any smooth neutral intergalactic medium must be very small out to large redshifts. Recent observations of very distant quasars ($z > 6$) are being used to look for the epoch of reionization using this effect.

The distribution of dark matter

- Dark matter forms the dominant contribution to the mass of clusters of galaxies (70–90%). Within clusters, the dark matter is distributed more smoothly than the matter that is present in the form of galaxies.
- The large-scale distribution of dark matter can be mapped by looking at small distortions in background galaxies – this effect is known as cosmic shear.

Questions

QUESTION 4.7

If the Universe is 13 billion years old, calculate the fraction of this age at which we see today (a) the Virgo cluster and (b) galaxies at the mean redshift of the galaxies in the SDSS.

QUESTION 4.8

Can you think why using Lyman α absorption spectra as a means to detect distant structure might give a biased view of the distribution of matter in the Universe? In particular, would you expect that Lyman α absorption would occur in regions where the density of galaxies is very high?

QUESTION 4.9

The masses of clusters of galaxies can be measured using methods based on three different physical processes. Name these methods and state what assumptions must be made about the physical state of the cluster in order for the individual methods to be applied.

CHAPTER 5
INTRODUCING COSMOLOGY – THE SCIENCE OF THE UNIVERSE

5.1 Introduction

Cosmology is the branch of science concerned with the study of the Universe as a whole. It involves questions such as: 'What is the composition of the Universe?'; 'What is its structure?'; 'How did it originate?'; 'How is it evolving?' and 'What is its ultimate fate?' These are obviously very challenging questions. They have been subjects of religious and philosophical speculation for thousands of years, but the development of scientific cosmology has brought them into the mainstream of astronomical debate over the past hundred years or so, and there is now real hope that their answers are coming into view.

Cosmology is a huge subject, and much of it concerns vast scales of time and distance. However, as you will see, cosmology has to concern itself with the physics of the very small (i.e. the physics of subatomic particles) as well as the physics of the very large. It is this combination of the very small and the very large – the microscopic and the macroscopic – that gives modern cosmology its distinctive flavour. It is also this combination that enables cosmology to cast new light on the nature of matter, and this gives it a vital role to play in answering one of the hardest questions in contemporary astronomy – 'Where did the galaxies come from?'

This chapter provides a broad introduction to scientific cosmology. Section 5.2 sets the scene by drawing together a number of facts about the Universe, most of which you have met in earlier chapters. Section 5.3 is concerned with 'modelling' the Universe: the process of formulating simplified descriptions of the Universe, usually expressed in mathematical form, that are consistent with modern physics, particularly with Einstein's theory of gravity – the general theory of relativity. The process of modelling the Universe involves a number of important cosmological parameters, such as the age of the Universe, the total density of matter in the Universe, and the Hubble constant, H_0. Section 5.4 concludes this introduction to cosmology by highlighting these cosmological parameters and considering the relationships between them that are predicted by the most popular models of the Universe. Later chapters build on this introduction by considering, in turn, the nature of the early Universe and the big bang (Chapter 6), the challenges and results of measuring the key cosmological parameters (Chapter 7), and the many important questions that are still unanswered at the current stage in the development of cosmology (Chapter 8).

5.2 The nature of the Universe

This section briefly introduces some of the main facts about the Universe, as revealed by astronomical observations. Many of these facts should already be familiar to you from earlier chapters, but some will be new. In neither case will much be said here about how the information was obtained. The main aim is simply to catalogue the basic facts that must be explained by any theoretical account of the origin and evolution of the Universe. Where necessary, greater detail is given later.

The term 'Copernican principle' recalls the work of Nicolaus Copernicus (1473–1543), who proposed a Sun-centred model of the Solar System at a time when the prevailing view favoured an Earth-centred model.

Before giving the observational 'facts' there is one important point that deserves special emphasis. All of our observations of the Universe are carried out from points on or near the Earth. In interpreting astronomical observations we have learned from experience *not* to assume that the Earth is in any particularly privileged position. We are not at the centre of the Solar System, nor are we at the centre of the Milky Way. It seems reasonable, therefore, to suppose that we are not at the centre of the Universe either. (This is absolutely opposed to the ancient pre-scientific view that placed us at, or close to, the centre of the Universe.) The assumption that we do not occupy a privileged position in the Universe is usually referred to as the **Copernican principle**, and is often invoked in interpreting observational data. If, for example, we find that distant galaxies are heading away from us in all directions (as we do), the Copernican principle tells us that the observations do not mean that we have the privilege of being at the fixed centre of an expanding Universe, but rather that the nature of cosmic expansion is such that the recession of distant galaxies is what would be observed from *any* typical point in the Universe.

5.2.1 The matter in the Universe

One of the most obvious facts about the Universe is that it contains matter. We humans are made of matter, as are the planets, stars, nebulae and galaxies that we observe. All of these visible objects are basically composed of oppositely charged *electrons* and *nuclei*. In some cases, such as ourselves and most of the Earth, the electrons and nuclei are combined together to form electrically neutral *atoms*, but the major part of the visible matter – most of that in stars for example – takes the form of a *plasma* in which the electrons and nuclei are separate and distinct, although the plasma as a whole remains electrically neutral.

Wherever large bodies of visible matter are found, whether they are composed of atoms or plasma, it is always the case that their mass is mainly accounted for by the *protons* and *neutrons* that make up nuclei, since these particles are far more massive than the electrons that accompany them.

■ The masses of the electron, proton and neutron are: $m_e = 9.109 \times 10^{-31}$ kg, $m_p = 1.673 \times 10^{-27}$ kg and $m_n = 1.675 \times 10^{-27}$ kg. Use these values to evaluate the following ratios: m_p/m_n, m_p/m_e and m_n/m_e. Roughly what fraction of the mass of a helium atom is attributable to the protons and neutrons contained in its nucleus?

❏ The required ratios are $m_p/m_n = 0.9988$, $m_p/m_e = 1837$ and $m_n/m_e = 1839$. Taking the view that the helium nucleus has the combined mass of two protons and two neutrons, while the helium atom has the combined mass of the nucleus and two electrons, we should expect the fraction of atomic mass attributable to protons and neutrons to be

$$(2m_p + 2m_n)/(2m_p + 2m_n + 2m_e) = 6696/6698 = 0.9997$$

(This is only an approximate value since we have ignored the effects of *binding energy*, which causes the mass of the nucleus to be slightly less than that of two protons and two neutrons.)

As you saw in Chapter 1, both the proton and the neutron (but not the electron) belong to a family of elementary particles called *baryons*, and the term *baryonic matter* is used to refer to all forms of matter in which the mass is mainly attributable to baryons. All the familiar atomic and molecular gases, liquids and solids, whatever their chemical composition, and all the plasmas found in stars, nebulae and galaxies, are therefore examples of baryonic matter.

Analyses of the chemical compositions of stars, nebulae and galaxies indicate that the most common form of baryonic matter is actually hydrogen plasma, and the second most common form is helium plasma. Although there are other significant forms of baryonic matter, we can, very crudely, say that the Universe has about 75% of its baryonic mass in the form of hydrogen nuclei and about 25% in the form of helium nuclei. We refine this crude recipe in later chapters, but it's worth remembering it as a first approximation to the true chemical composition of the Universe. Explaining the relative abundance of hydrogen and helium is a major challenge for any theory of the Universe, and is addressed in Chapter 6.

- Accepting that 75% of the baryonic mass of the Universe is due to hydrogen and 25% is due to helium, what are the relative numbers of hydrogen and helium nuclei in the Universe? In particular, how many hydrogen nuclei would you expect to find for each helium nucleus?

- Representing the masses of the hydrogen and helium nuclei by m_H and m_He, respectively, and using the symbols n_H and n_He to represent the number densities of hydrogen and helium nuclei, the question implies that

$$\frac{m_\mathrm{H}\, n_\mathrm{H}}{m_\mathrm{He}\, n_\mathrm{He}} = \frac{75}{25} = 3$$

Making the approximation that $m_\mathrm{He} = 4m_\mathrm{H}$ it follows that

$$\frac{n_\mathrm{H}}{4n_\mathrm{He}} = 3\text{, or equivalently, } \frac{n_\mathrm{H}}{n_\mathrm{He}} = 12$$

So, there should be 12 hydrogen nuclei for each helium nucleus.

It's clear that the Universe contains a great deal of baryonic matter, since it contains a lot of luminous stars, nebulae and galaxies. But earlier chapters have emphasized that many independent observations also indicate the presence of a great deal of non-luminous dark matter that has so far been detected only through its gravitational influence. Some scientists have suggested that dark matter may not actually exist at all, and that it may be our understanding of gravity that is at fault. However, the majority view at the time of writing is that dark matter does exist, and that it is far more common than baryonic matter. As stated in Chapter 1, it is expected that some of the dark matter is non-luminous *baryonic dark matter*, but there are good reasons to believe that most of it is non-baryonic, and that this *non-baryonic dark matter* is, at least in terms of density, the dominant form of matter in the Universe.

Recent cosmological observations indicate that the total density of non-baryonic dark matter is between five and six times greater than that of baryonic matter (see Figure 5.1). These measurements are discussed in Chapter 7, while the reasons for expecting only a limited amount of baryonic matter are covered in Chapter 6.

Figure 5.1 Galaxies represent large concentrations of matter. The visible parts of galaxies are certainly composed of baryonic matter, but most of the matter in galaxies is thought to be dark matter and the majority of that is expected to be non-baryonic. (Hubble Heritage Team (AURA/STScI/NASA))

QUESTION 5.1

For every 10 neutrons in the Universe, how many protons would you expect to find? Explain the assumptions you have made in arriving at your answer.

5.2.2 The radiation in the Universe

Another important fact about the Universe is that it is essentially full of *electromagnetic radiation*. All that we know of distant galaxies and clusters has been learnt by observing electromagnetic radiation (mainly radio waves, infrared radiation, visible light, X-rays and γ-rays) that has originated in those galaxies or clusters and then travelled through space until detected here on Earth. Of course, this direct observation only shows that there is a lot of radiation travelling towards the Earth, but the Copernican principle tells us that the Earth does not occupy any special place in the Universe, hence the belief that all parts of the Universe receive radiation from their cosmic surroundings, and the statement that the Universe is essentially full of radiation. This is supported by observations of the effects of the radiation on distant bodies.

One of the characteristic properties of electromagnetic radiation is its wavelength, λ, and an important feature of any observed radiation is its *spectral energy distribution* (defined in Chapter 3), which provides a description the amount of energy delivered per second and per unit area in any narrow range of wavelengths belonging to the radiation concerned. The radiation that reaches the Earth from space is dominated by the radiation from the Sun, and this is dominated by the visible light that our eyes have evolved to observe. However, this dominant role of visible light in our neighbourhood is a result of our close proximity to the Sun. Observations indicate that, in the Universe as a whole, the spectral energy distribution of radiation is actually dominated by microwave radiation, which occupies a range of wavelengths around 1 mm, between radio waves and infrared radiation.

Figure 5.2 The spectral energy distribution of background radiation. (Adapted from Sparke and Gallagher, 2000; based on work by T. Ressell and D. Scott)

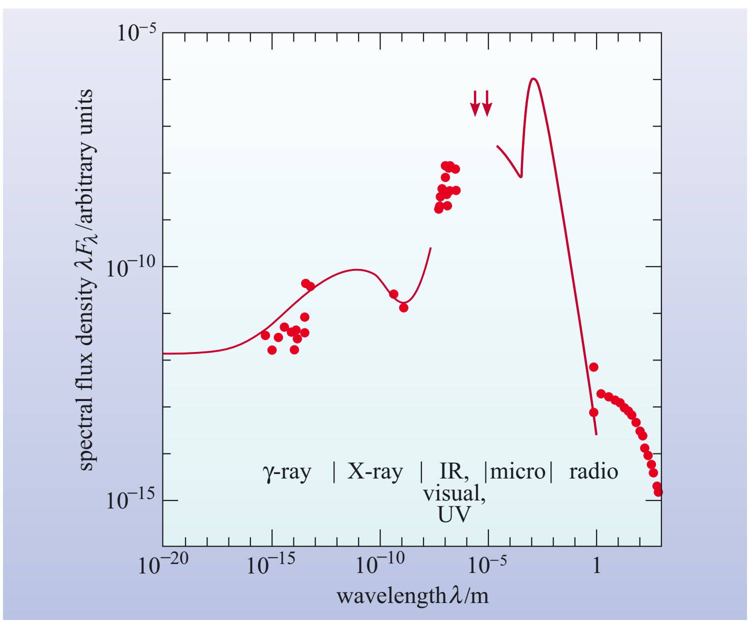

The predominance of microwave radiation is indicated in Figure 5.2, which shows the spectral energy distribution of so-called ‘background radiation’ at various wavelengths. This background radiation does not come from any identified source (such as the Sun or the Moon), and is in part thought to be truly ‘cosmic’ in the sense that similar distributions would be seen from anywhere in the Universe at the present time. The microwave contribution to the background radiation is usually referred to as the **cosmic microwave background (CMB)** and, at least in terms of the energy it carries, represents the dominant form of radiation in the Universe.

The discovery of the CMB, in 1965, was one of the most important events in the development of scientific cosmology and is described in Chapter 6. As you will see, it did a great deal to establish the ‘big bang theory’ as the best supported theory of cosmic evolution, and it continues to be of the utmost importance since detailed observations of the CMB now provide precise information about the nature, composition and evolution of the Universe.

5.2.3 The uniformity of the Universe

It is an obvious fact that what is normally above your head (probably some air, a ceiling, a roof, a lot more air and then outer space) is different from what is below your feet (probably a floor, some building foundations and the whole of the Earth). This provides clear evidence that, locally at least, the Universe is *not* uniform. However, rather than concentrate on your immediate surroundings, think instead about a sufficiently large region of the Universe that an astronomer or cosmologist might regard it as a 'typical' or 'representative' sample. In practice this means considering a region that is large enough to contain a few superclusters of galaxies, along with the voids that typically separate such superclusters. Such a region might well have a diameter of several hundred megaparsecs, and might represent, say, a millionth of the total volume of the observable part of the Universe. Provided the temptation to think about regions smaller than this is resisted, the view of modern cosmologists is that any part of the Universe is pretty much like any other at the present time. That is to say that, if we consider any two regions of the present Universe, each sufficiently large to be representative, then those regions will have the same average density, pressure, temperature, etc. In this sense, cosmologists say, provided we consider sufficiently large size scales, the Universe is uniform.

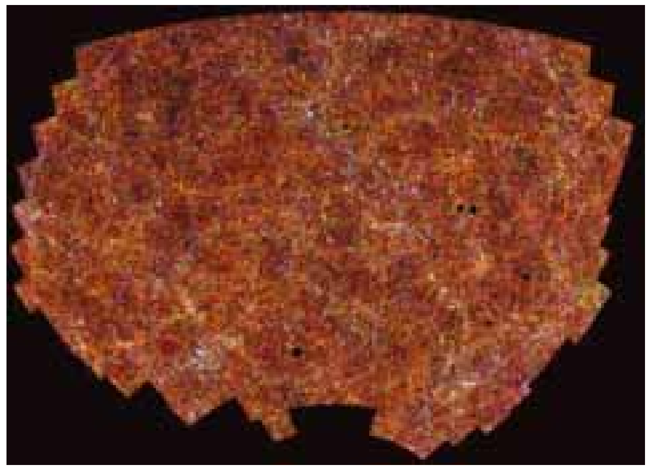

Figure 5.3 The observed distribution of galaxies across about 4300 square degrees of sky around the South Galactic Pole. (Steve Maddox, APM Galaxy Survey)

Belief in the large-scale uniformity of the Universe has always played an important part in scientific cosmology. In the early days of the subject this belief was based on assumption and the absence of any contradictory evidence, but in recent years it has come to rest more and more on positive observational support. One thing that observation certainly makes clear is that, on the large scale, the Universe is pretty much the same in all directions. This is fairly clear just from the large-scale distribution of galaxies, which can be seen to be reasonably even in all directions that are not obscured by parts of the Milky Way (see Figure 5.3). However, even better evidence is provided by the cosmic microwave background (see Figure 5.4), which is observed to come with equal intensity (to about a few parts in 10^5) from all regions of the sky, once allowance has been made for the 'local' effects of the Earth's motion.

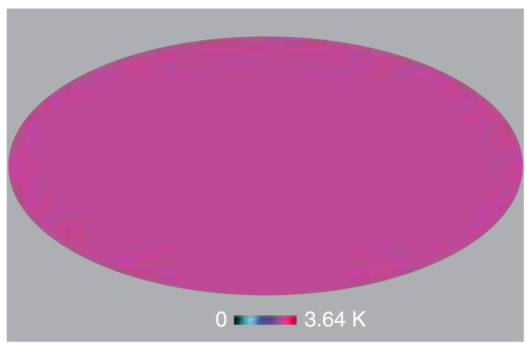

Figure 5.4 The observed intensity of the cosmic microwave background radiation across the whole sky. These data come from space-based measurements by the COBE satellite (Cosmic Background Explorer) and have been corrected to compensate for the motion of the detector. They are based on measurements made with an angular resolution of a few degrees and are sensitive to intensity variations of about one part in a thousand. (Douglas Scott)

By combining the evidence that the large-scale Universe appears the same in all *directions* when observed from our location, with the Copernican principle that we are not in any 'privileged' location, it follows that the large-scale Universe should appear to be the same in all directions from *every* location. This in turn implies that it should be the same everywhere, that is to say it should be uniform. This combination of observation and assumption is quite convincing in itself, but in recent years even more support has been provided by the increasingly ambitious surveys of galaxy redshifts that were described in Chapter 4. These really do provide evidence that galaxies are distributed uniformly on the large scale. There are signs of clustering and superclustering on scales of tens or hundreds of

megaparsecs, but there is no sign of any larger scale structure. It is *not* the case, for example, that the galaxies on one side of the Earth are significantly more clustered than those on the other side. The evidence for large-scale uniformity was discussed in detail in Chapter 4 and some results from the recent 2dF survey were shown in Figure 4.26. Other results from this survey are shown in Figure 5.5.

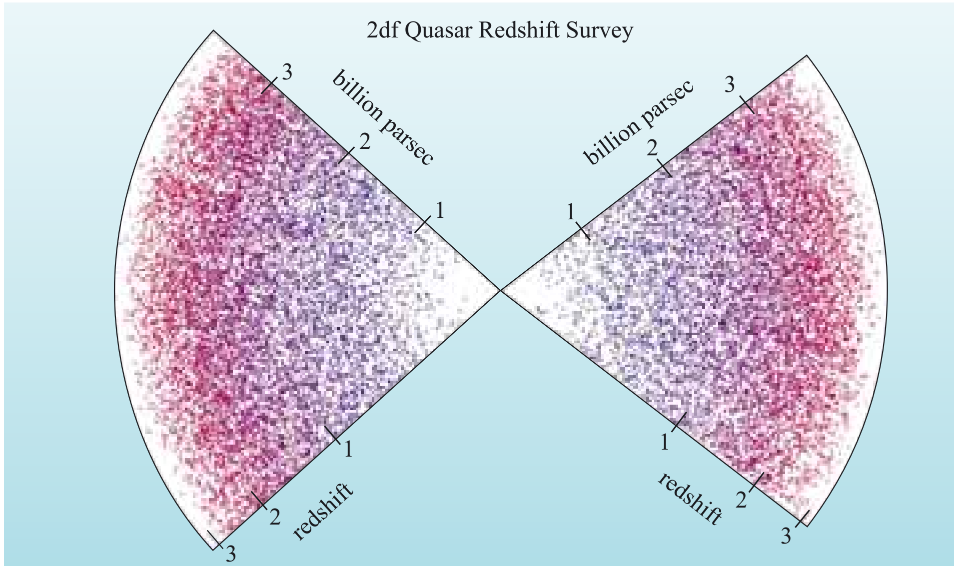

Figure 5.5 The distribution of quasars in two thin, wedge-shaped slices of the Universe. The quasars are observed out to such large distances that evolutionary effects allow changes in the number of quasars per unit volume to be observed as distance from the Earth increases. However, at any given distance the data give strong support to the claim that the large-scale distribution of quasars is the same in all directions. (Robert Smith, 2dF Quasar Redshift Survey)

QUESTION 5.2

In assuming that we can use the Copernican principle to interpret our observations of the CMB we are assuming that the CMB is a truly cosmic phenomenon, rather than a purely local one such as, say, sunlight. Describe a piece of observational evidence that makes it plausible to suppose that the CMB is a cosmic phenomenon, whereas sunlight is only a local astronomical one.

5.2.4 The expansion of the Universe

The nearest galaxies to the Milky Way are mainly dwarf galaxies that appear to be 'satellites' orbiting our own Galaxy. The closest large spiral galaxy – the Andromeda Galaxy, M31 – is actually heading towards us. But looking deeper into space it is found that all distant galaxies have a component of velocity which is directed away from the Earth, as revealed by the redshifts seen in their spectra. This finding, by Vesto Slipher (1875–1969), paved the way for the discovery of Hubble's law which was described in Chapter 2. As explained in Chapter 2, Hubble's law applies to galaxies with redshifts up to about 0.2, and implies a direct proportionality between redshift and distance that can be written as

$$z = \frac{H_0}{c} d \quad (\text{for } z \lesssim 0.2) \tag{5.1}$$

where H_0 is Hubble's constant and c is the speed of light in a vacuum. The redshift z can be related to the observed and emitted wavelengths, λ_{obs} and λ_{em}, of some identified spectral line by the equation (this is a repeat of Equation 2.11)

$$z = \frac{\lambda_{obs} - \lambda_{em}}{\lambda_{em}} \tag{5.2}$$

The two parts of Figure 5.6 provide a visual reminder of the meaning of redshift, as well as an indication of some of the observational data that support Hubble's law.

For reasons that will become clear later, it would be a mistake to interpret the redshift seen in the spectra of distant galaxies as a simple Doppler effect. Nonetheless, it is true that the observed redshifts do indicate that all distant galaxies are receding even though the Doppler formula can't generally be used to determine the speed of that recession. As mentioned earlier, such an observed recession is not thought to prove that the Earth is at the centre of an expanding cloud of galaxies, but rather that the whole Universe is in a state of expansion, with every galaxy, on average, moving away from every other *distant* galaxy. This overall expansion, described by Hubble's law, is sometimes called the **Hubble flow**. Galaxies provide imperfect tracers of the Hubble flow, since they interact gravitationally and may therefore be disturbed by the presence of nearby galaxies or other local effects. These local disturbances manifest themselves as movements relative to the Hubble flow, called *peculiar motions*, and are believed to be the main reason why a plot of redshift against distance, even for distant galaxies, is not the perfect straight line

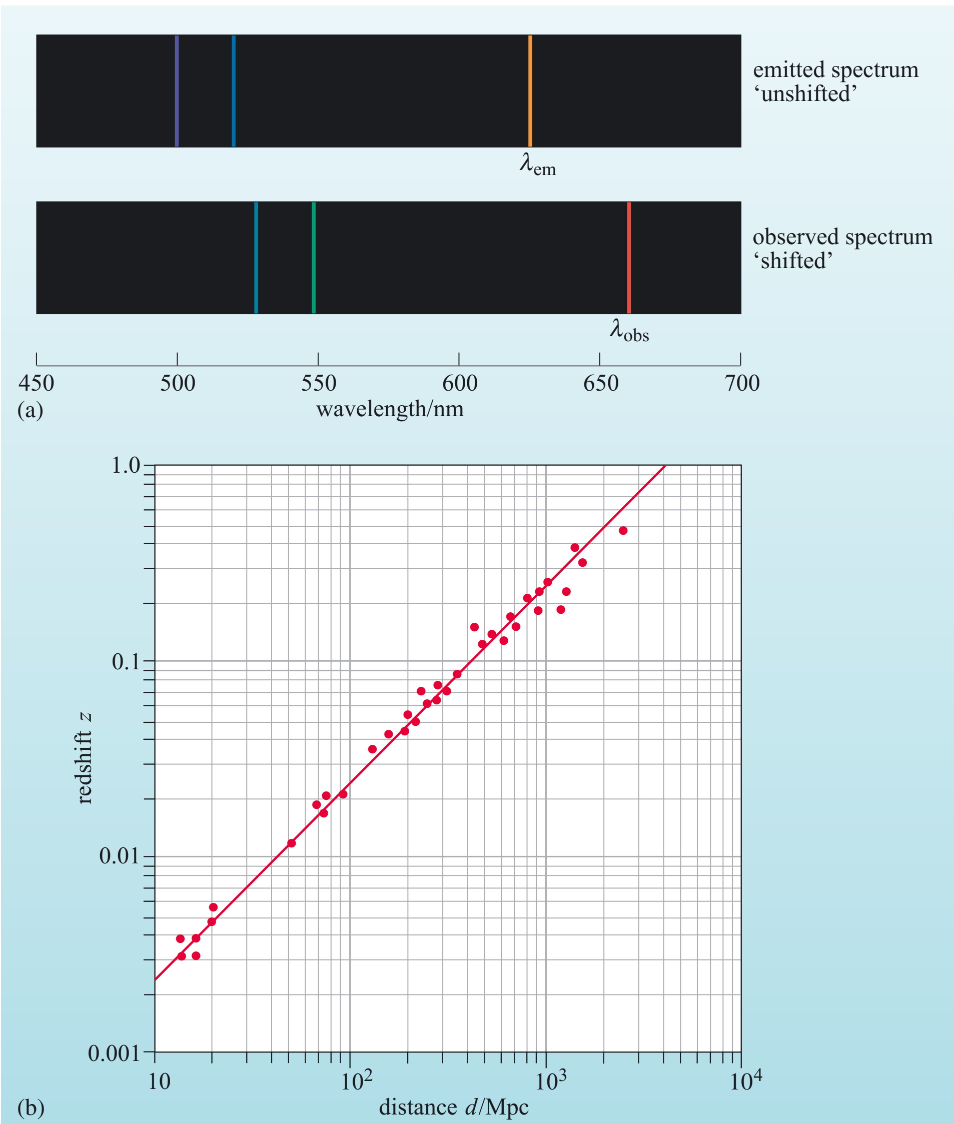

Figure 5.6 (a) The redshift z of a spectral line observed at wavelength λ_{obs} is a fractional measure of the line's displacement from the wavelength λ_{em} at which it was emitted by its source. (b) Observational evidence in support of Hubble's law.

that Hubble's law implies. The expansion of the Universe, like the uniformity of the Universe, is a large-scale phenomenon, and local departures such as the approach of M31 are only to be expected.

It's worth noting that if the uniformity of the Universe is to be preserved over time then the expansion of the Universe must also be uniform. At any time, the Universe should be expanding equally in all directions when viewed from any typical point. As you will see later, in an expansion described by Hubble's law, the current rate of expansion is measured by the Hubble constant, H_0. The uniformity of the Universe therefore implies that the Hubble constant should be a 'universal constant' with a value that is independent of where it is measured, though not necessarily of when it is measured. We have a lot more to say about this important constant later in our discussion.

■ Summarize the four main facts about the present state of the Universe that have been discussed in this section, giving detailed clarification where appropriate.

❑ The Universe contains matter. The matter is mainly non-baryonic dark matter, but about 1/5th or 1/6th is baryonic matter, mainly hydrogen (~75%) and helium (~25%).

The Universe contains radiation. The radiation is mainly cosmic microwave background radiation.

The Universe is uniform. All regions that are sufficiently large to be representative currently have the same average density, wherever they are located. This is consistent with the observed distributions of matter and radiation.

The Universe is expanding. For redshifts of ~0.2 or less, the expansion is thought to be well described by Hubble's law, implying that the current rate of expansion is described by the Hubble constant. Galaxies are thought to provide somewhat imperfect tracers of this expansion since they may have local motions relative to the large-scale Hubble flow.

5.3 Modelling the Universe

Physicists generally take the view that a scientific understanding of a phenomenon has been achieved when that phenomenon can be accurately described in terms of a few concise statements, or better still a well-formulated equation. A typical example is provided by the flow of electric current I through a sample of electrically conducting material in response to an applied voltage V. This is described by a relationship known as *Ohm's law*, which is expressed by the equation $V = IR$, where R is a parameter, called the *resistance*, that characterizes the electrical properties of the sample. Ohm's law provides a **mathematical model** of the process of current flow, implying that, for any given sample, V is proportional to I, but requiring the value of R to be determined before it can supply quantitative predictions.

Cosmologists adopt a similar view regarding the understanding of the Universe. One of the central concerns of modern cosmology is the formulation and investigation of mathematical models of the Universe. These are called **cosmological models**. They usually take the form of a few *equations* that imply general relations between observable quantities, but they also involve *parameters*, such as the Hubble constant, that must be determined by observation before the model can be used to provide detailed quantitative predictions.

ALBERT EINSTEIN (1879–1955)

Albert Einstein (Figure 5.7) was born in Ulm, Germany in 1879. From 1896 to 1901 he lived in Zurich, Switzerland, where he was a student at the Federal Institute of Technology (ETH). In 1905 he was working in the patent office in Bern when he completed some of the most important papers in the history of physics. These included a paper on the photoelectric effect, a paper on Brownian motion, and two papers on the special theory of relativity, the second of which introduced the equation $E = mc^2$. About ten years later, as Professor of Physics in Berlin, Einstein completed his general theory of relativity, a generalization of the 1905 theory that also turned out to be a theory of gravity. General relativity received its first systematic exposition in 1916, and was first applied to cosmology in 1917.

Observations made in 1919, during a total eclipse of the Sun, confirmed one of the key predictions of general relativity, that starlight passing close to the edge of the Sun should undergo a gravitational deflection of 1.74 arcsec (see Section 4.3.2). The success of this prediction was front-page news, and made Einstein an international celebrity. He was awarded the Nobel Prize for physics in 1921 (mainly for his work on the photoelectric effect), and received many other honours and awards. In 1932, shortly before the Nazis came to power, he left Germany for the United States where he took up a post at the Institute for Advanced Study in Princeton. With war approaching, in 1939, Einstein was persuaded to sign a letter to President Roosevelt, pointing out the military implications of atomic power. In his later years Einstein became a prominent commentator on world affairs, but had little direct impact on the development of science. He pursued a bold but fruitless search for a unified field theory that would unite gravitation and electromagnetism, and in 1952 he was offered the Presidency of Israel, which he declined. He died in Princeton in 1955.

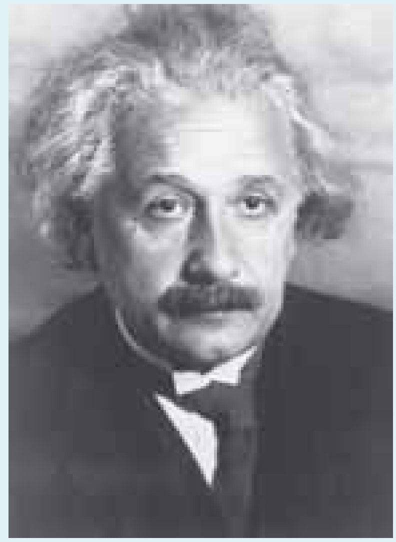

Figure 5.7 Albert Einstein. (Science Photo Library)

The aim of this section is to introduce you to some of the simplest but most important cosmological models that are currently in use, and to explore some of their implications. All of these models are based on **general relativity**, the theory of gravity published by Albert Einstein in 1916. For this reason, our discussion begins with a consideration of relativity and relativistic cosmology.

5.3.1 The relativistic Universe

The modern era of cosmology can be dated from the day in 1917 when Einstein's paper 'Cosmological Considerations of the General Theory of Relativity' was published in the Proceedings of the Prussian Academy of Science. An insight that is fundamental to this paper, and indeed to the whole of Einstein's theory of general relativity, is the crucial role that **space** and **time** must play in any attempt to model the Universe.

Before the advent of Einstein's theory of relativity, the view of most physicists was that space and time simply provided a sort of container for matter and radiation. Every particle of matter or radiation occupied some point in space at each instant of

time. Moreover, space and time were supposed to be *passive*. They provided a setting for the drama of physics, but they were not themselves players in that drama. The properties of space and time (basically geometric properties, as will be explained in the next section) were not thought to be in any way affected by the properties of the matter and radiation they contained.

Einstein changed this view radically and forever. Already, in 1905, his special theory of relativity (essentially a restricted form of the general theory that ignored gravity) had shown that the three dimensions of space and the single dimension of time should be melded together to form a unified four-dimensional entity usually referred to as **space–time**. But the general theory of 1916 went much further by showing that the geometric properties of this four-dimensional space–time were affected by the matter and radiation it contained, and that this could account for the cosmically important phenomenon of gravitation.

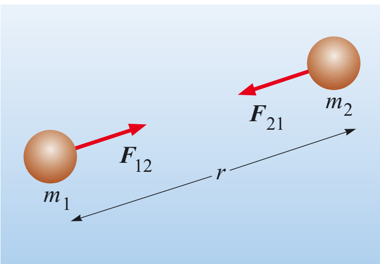

Figure 5.8 Newton's view of gravity: one body attracts another by means of a force that acts instantly across the intervening space.

According to the Newtonian theory of gravity, introduced in 1668, gravitational phenomena, such as the attraction between the Sun and the Earth, were due to a 'force' that acted instantly, between one body and another, across any intervening space (see Figure 5.8). Newton was able to describe the strength and direction of this force in terms of the masses of the bodies and the displacement (i.e. distance and direction) of one body from the other. However, he was not able to explain the origin of the gravitational force. He did not know the 'mechanism' that actually caused one body to influence another body at a remote location in space. He tried to explain his mysterious gravitational force in terms of something called 'vortex theory' that was popular with European scientists at the time, but his efforts only convinced him that this would not work, so he contented himself with *describing* the gravitational force and saying that as far as its origin was concerned 'I frame no hypothesis.' (In the Latin of his great work *Principia Mathematica*: 'hypotheses non fingo'.)

Two hundred and fifty years later Einstein was able to go much further in accounting for gravitational phenomena. According to Einstein there is no gravitational force. In Einstein's view, a body such as the Sun acts on the space–time in which it is located, giving rise to a geometrical distortion usually referred to as a **curvature** of space–time. Bodies moving in the vicinity of the Sun, such as the Earth, respond to this curvature by moving in a way that is different from the way they would have moved if the Sun had been absent and the space–time undistorted. In this way, a body such as the Sun is able to gravitationally influence the behaviour of a body such as the Earth, even though there is no 'gravitational force' acting between them. Gravitation, in Einstein's view, is a result of space–time curvature – a geometric phenomenon – and general relativity is Einstein's 'geometric' theory of gravity. This is illustrated schematically in Figure 5.9, where 'space' is represented by a two-dimensional sheet and gravity is indicated by the 'curvature' of that sheet.

Einstein was able to show that his theory of gravity agreed with all the correct predictions of Newton's theory. But general relativity went further, explaining anomalies for which Newton's theory had no account, and predicting entirely new phenomena that were outside the scope of Newtonian theory. Observations have consistently supported the novel predictions of general relativity, such as the gravitational deflection of starlight, which is why we now regard it as having superseded Newton's theory. Of course, we still use Newton's theory and speak of gravitational 'forces', but we do so because it is convenient, simple and sufficiently accurate for most purposes.

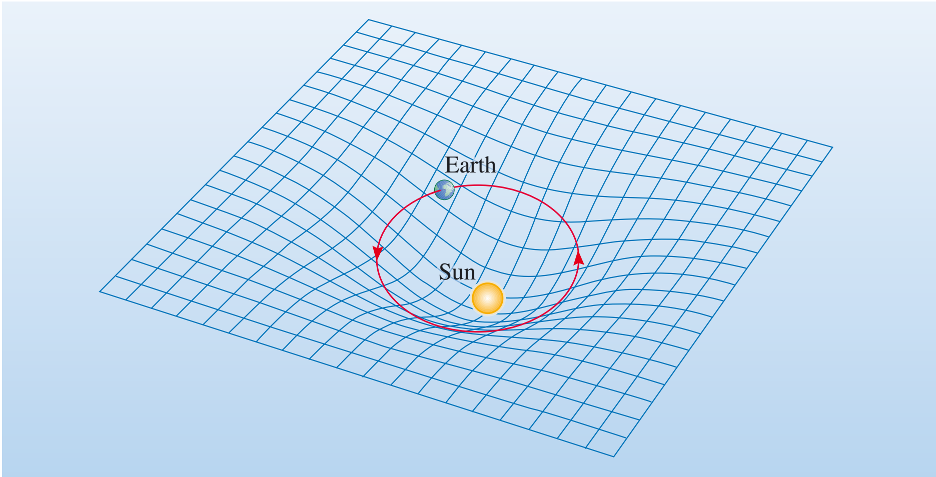

Figure 5.9 Einstein's view of gravity: a massive body (such as the Sun) significantly distorts the space–time in its vicinity. This space–time distortion (curvature) influences the motion of other bodies (such as the Earth) moving through that region of space–time, giving the impression that a 'force' is acting, although in reality there is only distorted space–time and motion in response to that space–time distortion.

What has all this to do with cosmology? Well, according to general relativity, what determines the curvature of space–time in any region of space–time is not simply the presence of massive bodies in that region, but rather the associated distribution of **energy** and **momentum** throughout the region. The notion that particles of matter and radiation have energy will already be familiar, so the idea that a distribution of matter and radiation can be associated with a distribution of energy should not seem strange. The theory of special relativity, however, adds new depth to this idea since the relation $E = mc^2$ implies that even a stationary particle can be associated with a certain amount of energy. The idea of momentum may be less familiar, but in essence it is simply another physical quantity that, like energy, can be associated with any particle of matter or radiation once the mass and velocity of that particle are known. (Particles of radiation, such as photons, have zero mass but, according to special relativity, a photon of energy E carries momentum of magnitude $p = E/c$.) As far as cosmology is concerned, you have already seen that matter and radiation are spread throughout the Universe, so you should expect there to be some corresponding large-scale distribution of energy and momentum associated with all that matter and radiation. It is this large-scale distribution of energy and momentum, together with the equations of general relativity, which allow us to obtain a mathematical description of space–time curvature on the large scale. This is the basis of relativistic cosmology.

QUESTION 5.3

On the basis of what you learned in Section 5.2 about the large-scale distribution of matter and radiation, what word would you expect to characterize the large-scale distribution of the associated energy and momentum?

Although the discussion in this section has been very qualitative and general up to this point, some important ideas have been introduced, so it's worth summarizing them here.

- The important ingredients of the Universe include space and time as well as matter and radiation.
- Einstein's special theory of relativity taught us to regard the three-dimensional space and one-dimensional time with which we are familiar as a four-dimensional space–time, in which all matter and radiation is contained.

- Einstein's general theory of relativity taught us that space–time has geometrical properties (e.g. curvature) that are determined by the distribution of energy and momentum associated with matter and radiation.
- By combining our beliefs about the large-scale distribution of energy and momentum with the general theory of relativity it should be possible to obtain a mathematical model of space–time on a large scale.

The next section concerns the meaning of the phrase the 'geometric properties' of space–time, and the way in which those properties can be summarized mathematically. The section after that considers the large-scale distribution of energy and momentum. Having dealt with those two topics, the central equations of general relativity – Einstein's field equations – are introduced. We can then discuss the mathematical models of space–time that are consistent with our observations of matter and radiation, and the associated distribution of energy and momentum.

5.3.2 The space and time of the Universe

Imagine you were asked to describe space: not just the outer space beyond the atmosphere, but space in general, including the space you are occupying right now, and the space in which you might wave your arms without leaving your seat. You might say that space is big, or that it had three dimensions (i.e. three independent directions in which things can move), but what else could you do to describe space?

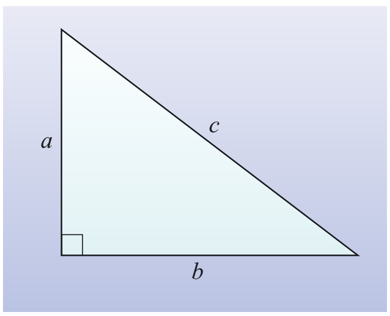

Figure 5.10 Pythagoras's theorem concerns the lengths, a, b and c, of the sides of a right-angled triangle (i.e. a closed, three-sided figure with one of its interior angles equal to 90°). In the notation of the figure, $c^2 = a^2 + b^2$.

The chances that you will be asked to describe space may be slim, but for a cosmologist the question is crucial and the conventional answer is well known. For cosmologists the description of space is essentially a matter of geometry. According to dictionaries, **geometry** is 'the study of the properties and relations of lines, surfaces and volumes in space'. It is by studying the properties and relations of objects *in* space that we learn about space itself. Now, geometry is a big subject, but 19th century mathematicians such as Carl Friedrich Gauss (1777–1855) and Bernhard Riemann (1826–1866) found powerful ways of summarizing the whole of geometry in just a line or two of mathematics. Gauss in particular, certainly one the greatest mathematicians who ever lived, initiated this development by recognizing the exceptional importance of **Pythagoras's theorem** about right-angled triangles.

According to Pythagoras's theorem, the square of the length of the longest side of a right-angled triangle is equal to the sum of the squares of the lengths of the other two sides. In symbols (see Figure 5.10), this can be expressed as

$$c^2 = a^2 + b^2 \tag{5.3}$$

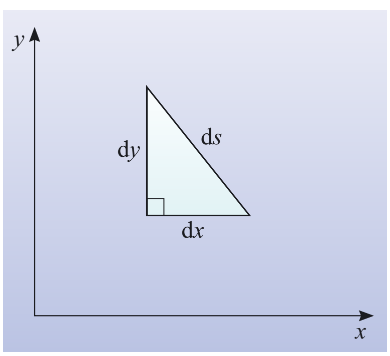

Figure 5.11 An infinitesimal version of Pythagoras's theorem.

Gauss realized that if this result held true for even the smallest conceivable right-angled triangles, then it could be used as the starting point for mathematical proofs of all the other known truths concerning the geometry of a two-dimensional plane. So, if we imagine an infinitesimally small version of Figure 5.10, and if we indicate its smallness by representing the lengths of its sides by $\mathrm{d}s$, $\mathrm{d}x$ and $\mathrm{d}y$ rather than c, a and b, then we can say that the whole of two-dimensional plane geometry is implicitly contained in the single expression

$$(\mathrm{d}s)^2 = (\mathrm{d}x)^2 + (\mathrm{d}y)^2 \tag{5.4}$$

where $\mathrm{d}s$ is the distance between two points whose x- and y-coordinates differ by the infinitesimal amounts $\mathrm{d}x$ and $\mathrm{d}y$ (see Figure 5.11). As far as a mathematician is concerned, Equation 5.4 is a complete answer to the question: 'Tell me all about the geometry of a two-dimensional plane.'

The form of Equation 5.4 immediately suggests an answer to the question 'Tell me all about the geometry of three-dimensional space.' If we describe any point in space by using the three-dimensional coordinate system with mutually perpendicular axes x, y and z (see Figure 5.12), then you can easily imagine that the distance $\mathrm{d}s$ between two points separated by infinitesimal coordinate differences $\mathrm{d}x$, $\mathrm{d}y$ and $\mathrm{d}z$ is given by a three-dimensional generalization of Pythagoras's theorem:

$$(\mathrm{d}s)^2 = (\mathrm{d}x)^2 + (\mathrm{d}y)^2 + (\mathrm{d}z)^2 \qquad (5.5)$$

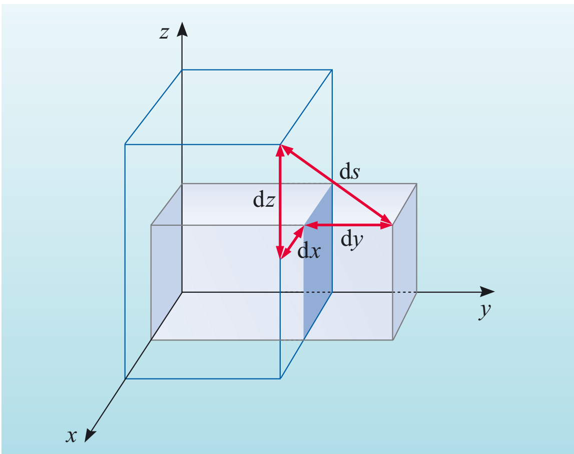

Figure 5.12 Two points in three-dimensional space with position coordinates that differ by the infinitesimal amounts $\mathrm{d}x$, $\mathrm{d}y$ and $\mathrm{d}z$. The points are separated by a distance $\mathrm{d}s$.

This equation provides a basis for three-dimensional geometry, just as Equation 5.4 provides a basis for two-dimensional geometry. However, it's important to note that since Equation 5.4 only applies to a plane, it describes geometry on a *flat* surface. It does not, for example, describe the geometry of shapes drawn on the *curved* two-dimensional surfaces shown in Figure 5.13. Concise mathematical statements that summarize the geometry of these curved two-dimensional surfaces can be written down, but those equations are inevitably somewhat more complicated than Equation 5.4. Similarly, for all its power, Equation 5.5 only describes the geometry of what is confusingly called a 'flat' three-dimensional space. Mathematicians are familiar with similar but more complicated expressions that describe the geometry of 'curved' three-dimensional spaces, but we shall not write them down here. There is little point in trying to picture what a 'curved' three-dimensional space would be like, but it is worth emphasizing that in a flat space familiar geometric results hold true, while in a curved space those same results may cease to be true. For example in a flat space the interior angles of a triangle add up to 180°, but in a curved space this may not be true. Similarly, 'straight' lines that are initially parallel do not necessarily remain parallel in curved space.

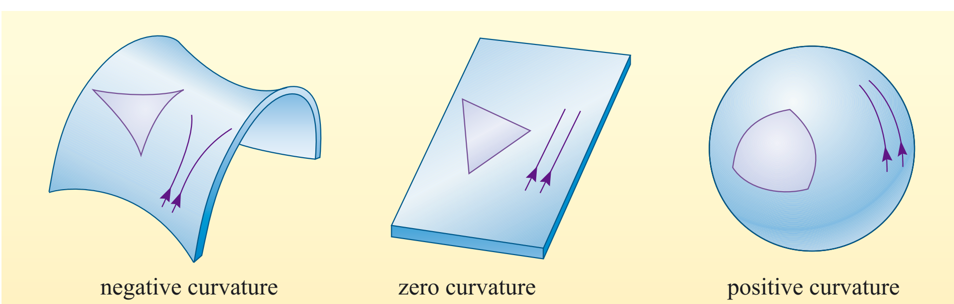

Figure 5.13 Some curved two-dimensional surfaces, viewed in three-dimensional space. The angles of triangles drawn on these surfaces do not add up to 180°, due to the curvature of the surfaces. Nor do lines that are initially parallel necessarily remain parallel.

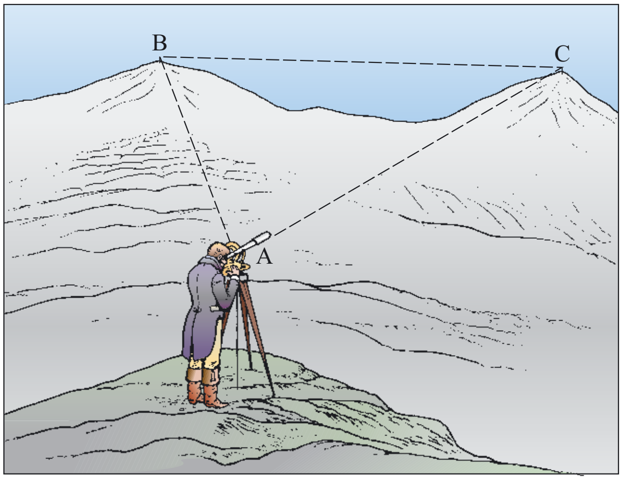

Figure 5.14 Gauss realized that mathematics provided many possible 'geometries' of space. The true geometry, flat or curved, could only be determined by experiment. He measured the interior angles of a triangle with vertices on three mountain tops, but found no deviation from 180° within the accuracy of his measurements. (Adapted from Kittel *et al*., 1965)

When Gauss realized that three-dimensional space might be curved he involved himself in a land survey that was being conducted, in order that he might investigate experimentally the properties of space (Figure 5.14). He hoped that accurate measurements of large triangles might reveal that their interior angles did not sum to 180°, implying that we are living in a curved space. (Note that Gauss was not concerned with triangles that followed the curvature of the Earth's surface; he was interested in the curvature of space itself – its *intrinsic* geometry – not the curvature of surfaces in space.) The results obtained in the survey did not provide any evidence that space is curved, but, as we now know in the light of Einstein's theory, that was simply because the curvature of space close to the Earth is too slight to be detected by the methods available to Gauss.

It has already been stressed that Einstein's theory of general relativity explains gravitational phenomena in terms of the curvature of space–time. So, you shouldn't be surprised that having discussed flat and curved three-dimensional spaces we now need to discuss the geometry of flat and curved four-dimensional space–times. Don't panic! As far as flat space–time is concerned all we need do is generalize Equation 5.5 so that instead of considering two narrowly separated *points* in space, we consider two neighbouring *events* in space–time. The two events can still differ in position by the infinitesimal amounts $\mathrm{d}x$, $\mathrm{d}y$ and $\mathrm{d}z$, but, being events, we can also choose them so that the times at which they occur differ by the infinitesimal amount $\mathrm{d}t$. Investigations based on Einstein's theory of special relativity, which does not include the effects of gravity and therefore concerns flat space–time, show that the appropriate generalization of Equation 5.5 is

Events play the same role in space–time that *points* play in space. Whereas a point in space can be specified by three position coordinates (x, y, z), an event in space–time requires three position coordinates and a time coordinate (x, y, z, t). A point is an idealized location; an event is an idealized occurrence.

$$(\mathrm{d}s)^2 = (\mathrm{d}x)^2 + (\mathrm{d}y)^2 + (\mathrm{d}z)^2 - c^2(\mathrm{d}t)^2 \qquad (5.6)$$

where c is the speed of light in a vacuum, a fundamental physical constant that would have been 'discovered' in the theory of relativity even if it had not already been known from studies of light.

It would be inappropriate to spend time justifying the precise form of Equation 5.6, but, as before, you should realize that Equation 5.6 describes the geometry of a 'flat' (i.e. zero curvature) space–time. The corresponding equation for a curved space–time will inevitably be more complicated.

5.3.3 The distribution of energy and momentum in the Universe

As explained in Section 5.2.3, the observation that the Universe appears to be the same in all directions, combined with the Copernican principle – that we are not observing from a privileged position – implies that the Universe should be the same everywhere, on the large scale. As was also stated, the implied uniformity in the large-scale distribution of matter and radiation is now being increasingly well confirmed by observations, particularly the deep redshift surveys that are being carried out. Even so, because the observational evidence is necessarily limited, it is still appropriate to treat uniformity on the largest scales as an assumption supported by increasingly good evidence rather than a proven fact.

Cosmologists usually call this assumption of large-scale uniformity the **cosmological principle**, and sometimes state it in the following way.

> On sufficiently large size-scales (i.e. averaged over regions that are several hundred megaparsecs across) the Universe is **homogeneous** (i.e. the same everywhere) and **isotropic** (i.e. the same in all directions).

The technical terms 'homogeneous' and 'isotropic' make precise the rather loose notion of 'uniformity' that we have been using up to this point. Both terms are needed because it is possible for a distribution to be homogeneous without being isotropic. For instance, a universe in which there was a homogeneous magnetic field that everywhere pointed in the same direction would not be isotropic, though it would be homogeneous.

■ What is the precise feature of the cosmological principle that rules out the uniformly magnetized universe that has just been described? Explain your answer.

❑ Although the magnetized universe would be homogeneous it would not be isotropic. No point in the universe would be distinguished from any other point, as homogeneity demands, but at any point it would be possible to identify a 'preferred' direction by using a compass to determine the direction of the magnetic field. The fact that all directions are not equivalent in that universe shows that it is not consistent with the requirement for isotropy in our Universe.

In the simplest cosmological models that are consistent with the cosmological principle it is usually imagined that the Universe is completely filled with a uniform gas or fluid. (You can think of superclusters of galaxies as being the equivalent of 'atoms' in this cosmic fluid.) One advantage of taking such a simplified view of the contents of the Universe is that describing the state of the gas at any time t only involves specifying the *density* and *pressure* at the relevant time. These two properties of the gas determine all the other properties, such as the temperature. Density and pressure are usually denoted by the symbols ρ (the Greek letter 'rho') and p, but in an expanding Universe the density and pressure should be expected to change with time and we can indicate this dependence on time by writing the density and pressure at any time t as $\rho(t)$ and $p(t)$. Cosmological discussions are often further simplified by assuming that the pressure is negligible. This seems to be a reasonable assumption throughout much of cosmic history, since there is no evidence of superclusters colliding and rebounding in the way that atoms in a gas are supposed to do. We shall assume that pressure is negligible throughout most of this chapter but not in Chapter 6, which deals with the hot, dense, early Universe.

Thanks to the simplifying assumptions outlined above, it is quite easy for a cosmologist to write down a mathematical description of the large-scale distribution of energy and momentum in the Universe. Like the uniformly distributed cosmic gas, the energy and momentum have a homogeneous and isotropic distribution that can easily be described mathematically. Armed with this mathematical description of the energy–momentum distribution, cosmologists are able to use the equations of general relativity to determine the large-scale geometry of space–time and hence formulate a cosmological model. The first models of this kind are discussed in the next section.

5.3.4 The first relativistic models of the Universe

According to general relativity, the distribution of energy and momentum determines the geometric properties of space–time, and, in particular, its curvature. The precise nature of this relationship is specified by a set of equations called the *field equations* of general relativity. In this book you are not expected to solve or even manipulate these equations, but you do need to know something about them, particularly how they led to the introduction of a quantity known as the *cosmological constant*. For this purpose, Einstein's field equations are discussed in Box 5.1.

BOX 5.1 EINSTEIN'S FIELD EQUATIONS OF GENERAL RELATIVITY

When spelled out in detail the **Einstein field equations** are vast and complicated, but in the compact and powerful notation used by general relativists they can be written with deceptive simplicity. Using this modern notation, the field equations that Einstein introduced in 1916 can be written as

$$\boldsymbol{G} = \frac{-8\pi G}{c^4}\boldsymbol{T} \tag{5.7}$$

Different authors may use different conventions for these equations. The bold symbols $\boldsymbol{G}$ and $\boldsymbol{T}$ represent complicated mathematical entities called *tensors* that it would be inappropriate to explain here, except to say that $\boldsymbol{G}$ describes the curvature of space–time while $\boldsymbol{T}$ describes the distribution of energy and momentum, and that both these quantities may vary with time and position. The other symbols just represent numerical constants and have their usual meanings, $G = 6.673 \times 10^{-11}\,\mathrm{N\,m^2\,kg^{-2}}$ is Newton's gravitational constant and $c = 2.998 \times 10^8\,\mathrm{m\,s^{-1}}$ is the speed of light in a vacuum.

Given the distribution of momentum and energy at all points in space and time (i.e. given $\boldsymbol{T}$), the field equations determine the geometrical quantity $\boldsymbol{G}$, from which it may be possible to derive a detailed description of space–time geometry along the lines of the infinitesimal generalizations of Pythagoras's theorem that were discussed in Section 5.3.2. In his 1916 paper, Einstein used these equations to investigate planetary motion in the Solar System and to predict the non-Newtonian deflection of light by the Sun.

Einstein published his first paper on relativistic cosmology in the following year, 1917. In that paper he tried to use general relativity to describe the space–time geometry of the whole Universe, not just the Solar System. While working towards that paper he realized that one of the assumptions he had made in his 1916 paper was unnecessary and inappropriate in the broader context of cosmology. This led him to introduce another term into the field equations, a term he had deliberately chosen to ignore in 1916. With this extra term included the field equations used in the cosmology paper of 1917 can be written

$$\boldsymbol{G} + \Lambda\boldsymbol{g} = \frac{-8\pi G}{c^4}\boldsymbol{T} \tag{5.8}$$

As you can see, the extra term takes the form $\Lambda\boldsymbol{g}$, where Λ is the upper case Greek letter 'lambda'. The $\boldsymbol{g}$ here is another of these tensor quantities that was actually already implicitly involved in $\boldsymbol{G}$, while Λ represents a new physical constant called the **cosmological constant**. Provided Λ is sufficiently small (which it is) the presence of the $\Lambda\boldsymbol{g}$ term does not invalidate any of the results that Einstein obtained in the 1916 paper but, in the context of cosmological calculations, a positive value of Λ implies the action of a long-range repulsion that might, under appropriate circumstances, balance or even overwhelm the attractive influence of gravity.

In 1917 there was no evidence to indicate that the Universe was either expanding or contracting. So, in developing the first relativistic cosmological model, Einstein sought a value for the cosmological constant Λ that would ensure everything was constant and unchanging with time. He was also guided by the cosmological principle, so he required that the average density of matter in the Universe, ρ, should be homogeneous (i.e. independent of position) as well as constant (i.e. independent of time). He ignored the possibility of pressure, effectively assuming $p = 0$. Using these assumptions together with the modified field equations (Equation 5.8), Einstein constructed the first relativistic cosmological model, which is now

known as the **Einstein model**. The need to balance the gravitational attraction of matter and the repulsive effect of the cosmological constant led Einstein to the relation

$$\Lambda = \frac{4\pi G\rho}{c^2} \tag{5.9}$$

Because it is not expanding, the Einstein model is not thought to represent the Universe we actually inhabit. In fact, after the expansion of the Universe had been discovered, Einstein himself described his first use of the cosmological constant as his 'greatest blunder'. Nonetheless, it is worth exploring the geometrical properties of the Einstein model since it can provide insight into some of the extraordinary possibilities of relativistic cosmology.

The universe described by the Einstein model is **static**, neither expanding nor contracting. In this model universe, space is **finite**, having a total volume that is proportional to $\Lambda^{-3/2}$. Despite being finite, space in the Einstein model is also **unbounded**, that is to say, you can travel as far as you like in any direction without ever hitting a wall or encountering anything like an 'edge' of space. However, if you were to travel far enough in a straight line, you would eventually find yourself back at your starting point.

How is this possible? How can a straight line close back upon itself? Very simply, because what we are discussing here is a straight line in a *curved* space. In the Einstein model, which is homogeneous and isotropic, the curvature of space must be the same everywhere and in all directions. In addition, this uniform curvature has a positive value at every point, which means that a 'straight' line will be uniformly bent back upon itself all along its length. The actual value of the positive curvature depends on the value of the cosmological constant Λ, with the consequence that a line that is as straight as it can be in any region (the kind of line defined by a light ray, say) will close on itself after a distance that is proportional to $\Lambda^{-1/2}$. Figure 5.15 attempts to provide some idea of the geometry of space–time in the Einstein model.

If we did inhabit the kind of universe described by the Einstein model, we might expect astronomical observations to reveal distant images of the Earth, Sun or Milky Way, due to light that had travelled along the closed paths that the model implies.

■ If we did live in the universe described by the Einstein model, how might we determine the value of the cosmological constant?

❑ By measuring the average density of matter on the large scale, ρ, and then using Equation 5.9 to determine Λ.

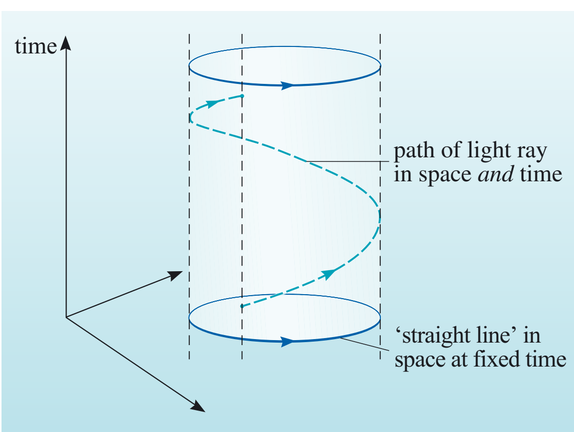

Figure 5.15 In this attempt to represent the four-dimensional space–time of the Einstein model, time is measured along the vertical axis. The whole of space at any time must therefore be represented in the horizontal plane, but because of the need to indicate that space is intrinsically curved, the circle that you see in the horizontal plane actually represents a 'straight' line. The helical path drawn above the circle might represent the path of a pulse of light that follows a 'straight' line through space while time passes. Because of the nature of this space–time diagram, the Einstein model is sometimes called 'Einstein's cylindrical world', but it's important to realize that the four-dimensional universe described by the Einstein model is no more akin to a real 'cylinder' than the 'flat' space of special relativity is akin to a pancake. (Adapted from Raine, 1981)

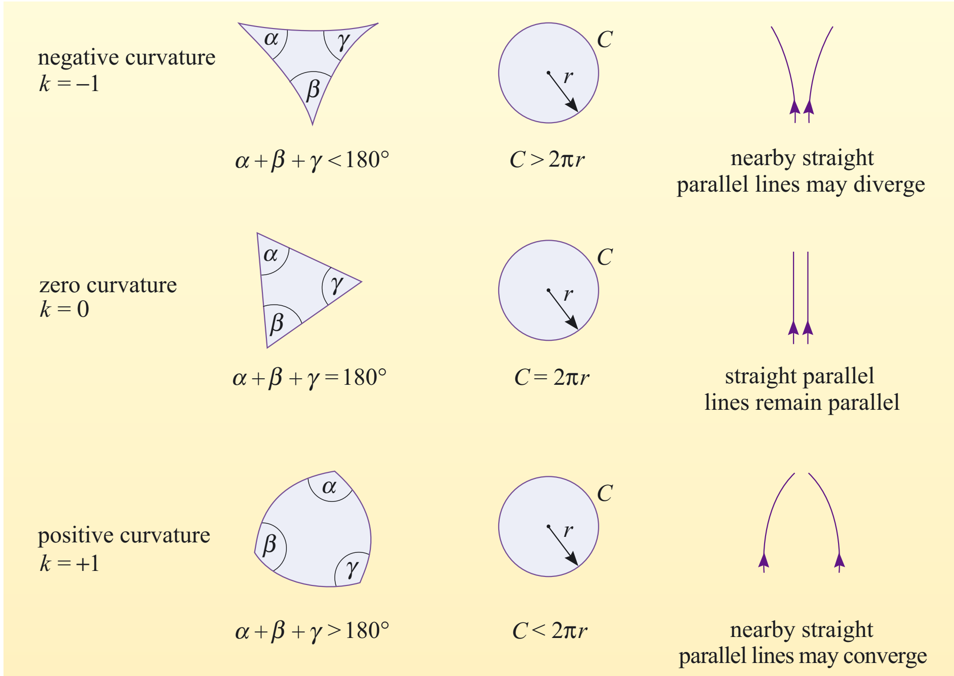

Figure 5.16 The effect of the curvature parameter, k, in determining the large-scale geometry of a cosmological model.

Figure 5.17 Willem de Sitter was a Dutch astronomer who devised the second relativistic cosmology in association with his colleague Paul Eherenfest (1880–1933). He realized that, in his model, observers would find that the light from distant galaxies was red-shifted, but he described the outward radial velocity this indicated as 'spurious'. (Science Photo Library)

As you have seen, an important feature of the Einstein model is that the curvature of space is everywhere positive. This is conventionally indicated by introducing a **curvature parameter**, k, that may take the value +1, 0 or −1, and by saying that in the Einstein model $k = +1$. You will shortly be meeting other cosmological models with $k = 0$ and $k = -1$, as well as more models with $k = +1$. The curvature parameter is one of the most important characteristics of these models, since it strongly influences the large-scale geometric properties of the model. The value of k immediately determines whether space is finite ($k = +1$) or infinite ($k = 0$ or −1). As Figure 5.16 indicates, it also determines whether the interior angles of cosmically large triangles will add up to be less than, equal to or greater than 180°, how the circumference of a circle is related to its radius, and whether parallel pathways will remain parallel. The significance of this should soon become apparent, because the next model we are going to discuss has zero curvature everywhere and is characterized by $k = 0$. In this model, space is infinite, and 'straight' lines do not close back upon themselves.

Within a year of Einstein's publication of the first relativistic cosmological model, a radically different model was proposed by the Dutch astronomer Willem de Sitter (1872–1934; Figure 5.17). As in the case of the Einstein model, the mathematical details of the **de Sitter model** can be found by solving the field equations (Equation 5.8). Like Einstein, de Sitter assumed that the Universe was homogeneous and isotropic, in accordance with the cosmological principle, but he did not require it to be static. Instead he took the view that the effect of matter was negligible, implying that both the average pressure and the average density could be taken to be zero. The geometric properties of space would therefore be determined by the cosmological constant alone. If positive, this would result in a never-ending expansion that would cause points in space to move apart perpetually. What little matter was actually present in the Universe would simply be carried along by the expansion of the space in which it was located (see Box 5.2). This is the key feature of de Sitter's model: it was the first model to describe an expanding Universe, although de Sitter himself seems not to have appreciated all the implications of this.

BOX 5.2 GALAXY RECESSION AND THE EXPANSION OF SPACE

At first sight, the observed recession of distant galaxies clearly suggests that those galaxies are moving through space. This, however, neglects the general relativistic view that space (or more properly space–time) has intrinsic properties that are influenced by the contents of the Universe. A useful way of thinking about space in general relativity is to imagine it as the three-dimensional analogue of a rubber sheet that may expand or contract as it is stretched or released.

If you picture galaxies as something like buttons placed on the rubber sheet, then it is clear that *one* way of causing them to separate is to move them across the sheet. This is the analogue of galaxies moving through space. But there is also a second way of increasing their separation. This other way of increasing their separation is to stretch the rubber itself. It is this latter view is that is most helpful when trying to interpret a phrase such as 'matter would be carried along by the expansion of space'.

The galaxies we actually observe can be thought of as moving for two reasons. On the one hand they are being carried along *by* space as a result of the uniform cosmic expansion described by the Hubble flow. On the other hand those same galaxies are also moving *through* space due to local effects, such as the gravitational attraction of nearby concentrations of matter. The local effects can be dominant on the small scale, thus explaining why *some* nearby galaxies are moving towards us, but on larger scales such effects are so overwhelmed by cosmic expansion that *all* distant galaxies are found to be moving away from us.

One way of describing the expansion of space mathematically is to start with a coordinate grid that can expand or contract along with space. Such coordinates are said to be **co-moving** and are widely used in cosmology. This sort of coordinate system is indicated schematically in Figure 5.18, although for the sake of clarity only a two-dimensional grid is shown, rather than the three-dimensional grid that would really be required to label all the points in space. Due to the use of co-moving coordinates, typical points in an expanding space have unchanging coordinates, even though those points are moving apart. Since the coordinates themselves do not describe the expansion of space, it is necessary to introduce another parameter that does. This is called the **scale factor** and is represented by $R(t)$, where the parenthesized t indicates that the scale factor can change with time, increasing or decreasing as the Universe expands or contracts. If $R(t)$ increases with time, so that its value at time t_2 is greater than its value at some earlier time t_1, then the physical distance between two points with fixed coordinates will also increase, as 'expansion' implies that it should (this is the case shown in Figure 5.18). If $R(t)$ decreases with time then the distance between typical points is reduced, and space may be said to be contracting.

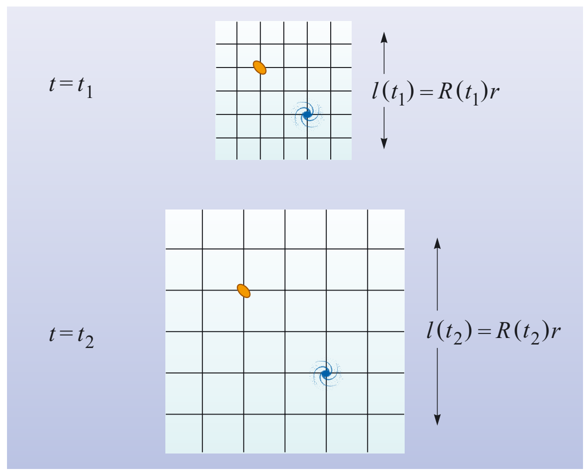

Figure 5.18 When co-moving coordinates are used to identify points, the expansion (or contraction) of space can be indicated by the behaviour of a scale factor, $R(t)$. If two points are separated by a co-moving coordinate distance r, the physical distance (in metres, say) between those two points, at time t, will be $l(t) = R(t)r$.

It's important to realize that the use of co-moving coordinates removes any direct relationship between the coordinate differences dx, dy and dz of two narrowly separated points and the actual physical distance, ds, between those points. In order to find the real physical distance between the two points (measured in metres, say), at time t, the scale factor $R(t)$ must be taken into account. In the simplest case of an expanding flat space with zero curvature, this can be indicated by writing

$$(\mathrm{d}s)^2 = [R(t)]^2[(\mathrm{d}x)^2 + (\mathrm{d}y)^2 + (\mathrm{d}z)^2] \tag{5.10}$$

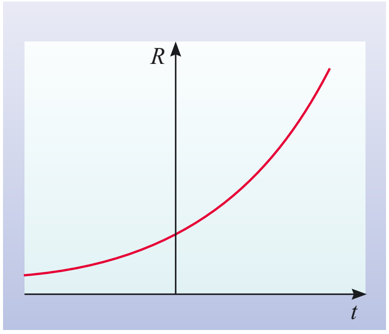

Figure 5.19 The behaviour of the scale factor in the de Sitter universe.

Equation 5.10 implies that if the 'coordinate distance' between the two points is dr, then the physical distance between them at time t is ds = $R(t)$ dr, where $\mathrm{d}r = \sqrt{(\mathrm{d}x)^2 + (\mathrm{d}y)^2 + (\mathrm{d}z)^2}$.

In the case of the de Sitter model, the field equations show that the scale factor grows exponentially with time, as indicated in Figure 5.19. The steepness of the curve increases at a rate that is determined by the value of the cosmological constant, since it is Λ that drives the expansion. In fact, it can be shown that in the de Sitter model

$$R \propto \mathrm{e}^{Ht} \quad \text{where } H = \sqrt{\frac{\Lambda c^2}{3}} \tag{5.11}$$

Willem de Sitter realized that if matter moved in accordance with the expansion of space in his cosmological model, then distant astronomical bodies would be driven apart by the cosmic expansion. He also realized that this would give rise to red-shifts in the spectra of those bodies. He didn't press this point with sufficient vigour to deserve the credit for 'discovering' the expansion of the Universe, but Hubble was aware of this consequence of the de Sitter model and referred to it in his 1929 paper showing that redshift increased with distance. If the density of matter in the Universe had been negligible, and de Sitter's model had been correct, then the Hubble constant would have determined the value of H in Equation 5.11, and this would have allowed the value of Λ to be determined from the motion of distant galaxies.

QUESTION 5.4

The scale factor was not discussed in the context of the Einstein model but, if it had been, what could have been said about its behaviour?

5.3.5 The Friedmann–Robertson–Walker models of the Universe

Alexander Friedmann (Figure 5.20) was a Russian mathematician who worked at the University of St Petersburg. In 1922 and 1924 he published two important papers which had the effect of showing that the cosmological models of Einstein and de Sitter were special cases of a much wider class of models, all of which were consistent with the field equations of general relativity and with the cosmological principle. Later, Howard P. Robertson (Figure 5.21) and Arthur G. Walker (Figure 5.22) independently found improved ways of describing these models mathematically and ensuring their generality. It was the work of these three, Friedmann, Robertson and Walker, which resulted in the general mathematical framework that is still used today when discussing relativistic cosmological models of a homogeneous and isotropic Universe.

The geometric properties of space–time in any of the **Friedmann–Robertson–Walker models** (usually abbreviated to **FRW models**) can be deduced from the following expression for the space–time separation ds of two events whose coordinates differ by the infinitesimal amounts dx, dy, dz and dt, and which are located at a coordinate distance r from the origin.

There are several different but equivalent ways writing Equation 5.12. The form given here is not the most conventional.

$$(\mathrm{d}s)^2 = \frac{[R(t)]^2}{\left(1 + \dfrac{kr^2}{4}\right)^2}[(\mathrm{d}x)^2 + (\mathrm{d}y)^2 + (\mathrm{d}z)^2] - c^2(\mathrm{d}t)^2 \tag{5.12}$$

ALEXANDER FRIEDMANN (1888–1925), HOWARD PERCY ROBERTSON (1903–1961) AND ARTHUR GEOFFREY WALKER (1909–2001)

Figure 5.20 Alexander Friedmann. (Science Photo Library)

Figure 5.21 Howard Percy Robertson.

Figure 5.22 Arthur Geoffrey Walker.

Alexander Friedmann (Figure 5.20) was born and educated in St Petersburg and returned there in 1920 to work at the Academy of Sciences. Mainly known for his work on theoretical meteorology, Friedmann became interested in general relativity and used his mathematical talents to undertake a highly original exploration of the cosmological consequences of the theory. His researches led him to the equation that determines the evolution of the scale factor $R(t)$ in a homogeneous, isotropic universe that is uniformly filled with matter. This is now known as the Friedmann equation.

Howard Percy Robertson (Figure 5.21) was an American mathematical physicist who specialized in the application of general relativity to practical situations. In 1929, using general arguments that did not depend on specific assumptions about the properties of matter, Robertson deduced the general expression for the separation of events in the space–time of any universe that is spatially homogeneous and isotropic at all times (see Equation 5.12).

Arthur Geoffrey Walker (Figure 5.22) spent most of his academic career at the University of Liverpool, initially as a lecturer and later as Professor of Mathematics. His expression for the separation of events in a homogeneous and isotropic universe was published in 1936, and was based on a somewhat different approach from the earlier work of Robertson.

Equation 5.12 is sometimes described as the **Robertson–Walker metric**. We shall not be using this expression as the basis of any detailed arguments, but you should notice three things about it. First, it is a generalization (to the case of curved space–time) of Equation 5.6, which provided a complete description of the geometric properties of a flat space–time. Second, it contains the curvature parameter k, which helps to characterize the curvature of a space–time and can take the values -1, 0 or $+1$. Third, it contains the scale factor $R(t)$ that describes the expansion or contraction of space as a function of time.

Equation 5.12 applies to all the FRW models, but in order to work out the details of any particular model it is necessary to specify the value of k and to determine the precise form of $R(t)$. In the case of a universe uniformly filled with pressure-free (i.e. $p = 0$) matter of density ρ, the form of $R(t)$ can be determined by solving a complicated equation known as the **Friedmann equation** (Box 5.3). This important equation relates the value of R, and the rate of change of R, to the curvature parameter k, the cosmic density ρ and the cosmological constant Λ. We do not go into the details of its solution, but different values of k and Λ can lead to quite different forms for $R(t)$, and these are indicated schematically in Figure 5.23. The implications of these solutions are discussed below.

BOX 5.3 THE FRIEDMANN EQUATION: EPISODE 1

It should be clear from what has already been said that the Friedmann equation is of the utmost importance in the process of cosmological modelling. The Friedmann equation determines the form of $R(t)$, and thereby fixes the evolutionary history of a model universe. In this sense, the fate of the Universe is determined by the Friedmann equation, and many cosmologists would say that it is certainly the most important equation in cosmology.

All of this might make you wonder why we have not actually written down the Friedmann equation at this point. The reason is simple. The Friedmann equation involves mathematical notation and concepts with which you may not be familiar at this stage, but which arise naturally in the next section. We are therefore delaying the explicit introduction of the Friedmann equation until then.

If you really can't wait to see it, take a look at Episode 2 in Section 5.4.3 (in Box 5.4).

Figure 5.23 contains a great deal of information and deserves careful study. The first thing to notice is that each of the small graphs of R against t corresponds to different values (or ranges of values) of the curvature parameter k and the cosmological constant Λ. For each set of values, the small graph shows the history of spatial expansion or contraction in a homogeneous and isotropic universe filled with pressure-free matter. For example, the left-hand column (the column headed $\Lambda < 0$) contains all the cases where the cosmological constant is less than zero. The uppermost of the three graphs corresponds to $k = +1$, the middle graph corresponds to $k = 0$, and the lowest graph corresponds to $k = -1$. In all three of these cases the graphs are similar: R is 0 at $t = 0$, increases up to some maximum value, and then decreases to zero again after a finite time. In other words, all these models describe universes with a finite lifetime that expand, reach a state of maximum expansion, and then contract again. It is important to remember that the quantity R plotted in these graphs represents the 'scale' of the universe, not its radius. Only in the case where $k = +1$, implying that space has a finite total volume, does the concept of a 'radius' of the universe have any meaning; in the other cases, where $k = 0$ and $k = -1$, space is infinite and the concept of a cosmic 'radius' has no meaning. However, even these spatially infinite universes can expand and contract. By recalling that R is a *scale factor*, and that it characterizes the changing separation of typical (co-moving) points in a uniform universe, you will avoid making, or being misled by, meaningless statements about the radius or diameter of the universe.

The second column in Figure 5.23 is especially interesting; it contains the models that have a vanishing cosmological constant ($\Lambda = 0$). Until recently, these were believed to be the most realistic models of the Universe we actually inhabit. The first of the models in this class has $k = +1$, implying that space is finite, and the corresponding graph of R against t once again indicates a cycle of expansion and contraction with a finite lifetime. In this and other models that begin with $R = 0$ at time $t = 0$, the early part of the expansion is now known as the **big bang**; the collapse that takes place at the other end of the cycle is known as the **big crunch**. Among the $\Lambda = 0$ models, all start with a big bang but only the $k = +1$ model ends with a crunch: it is known as the **closed model**. In the other two models of the

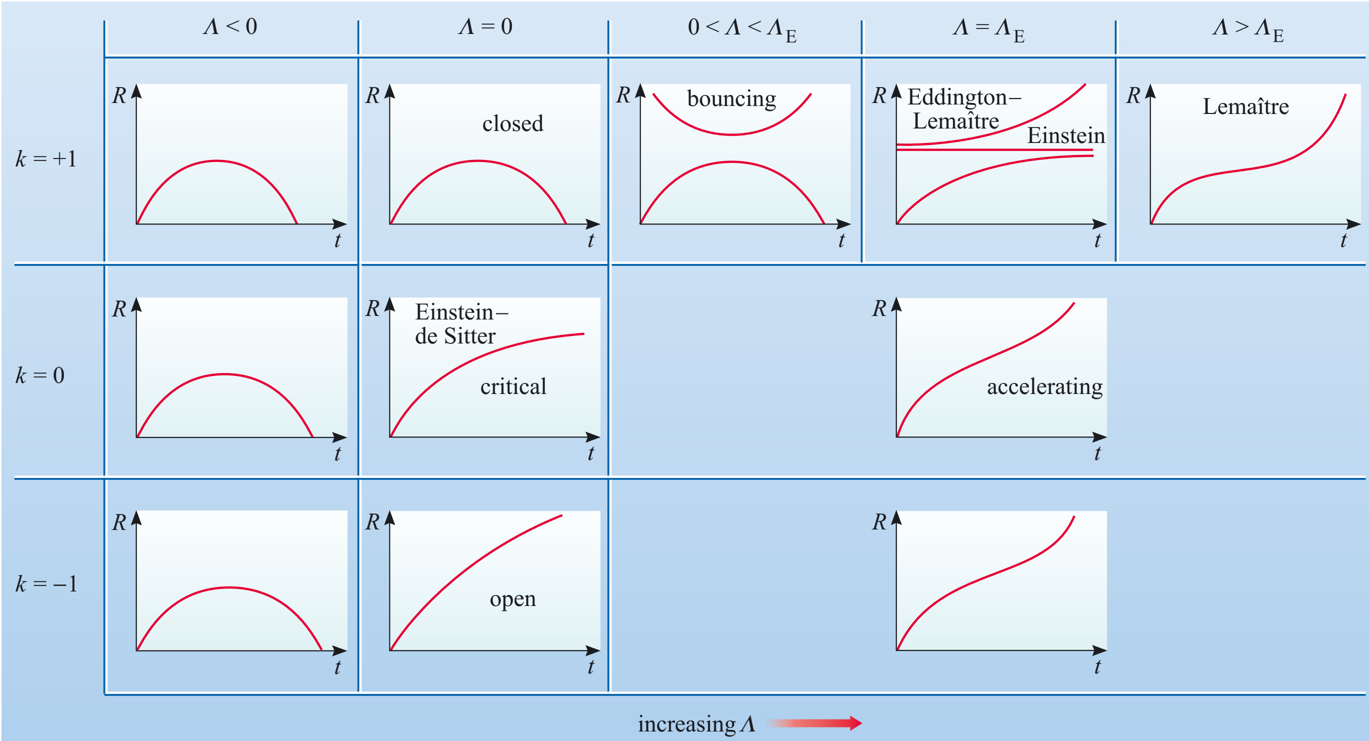

Figure 5.23 The Friedmann–Robertson–Walker models, classified according to the values of k and Λ. In each case the model is represented by a small graph of R against t, which encapsulates the history of spatial expansion and/or contraction implied by the model. Note that Λ_E represents the value of the cosmological constant in the Einstein model, $4\pi G\rho/c^2$. (Adapted from Landsberg and Evans, 1977)

$\Lambda = 0$ class, space is infinite and expands forever. The $k = -1$ model is called the **open model**. In this model, as t approaches infinity the relationship between R and t approaches the simple form $R \propto t$. The $k = 0$ model represents a special case between the open and closed models and is known as the **critical model**. In this case, the relationship between R and t takes the form $R \propto t^{2/3}$ for all values of t. Somewhat confusingly, the critical model is also known as the **Einstein–de Sitter model**, even though it has no direct relation to either the Einstein model or the de Sitter model.

In all of the remaining models of Figure 5.23 the cosmological constant is greater than zero ($\Lambda > 0$). It's best to regard all these models as occupying a single column, even though when $k = +1$ there are actually several quite distinct cases to discuss. But, before considering any of these models in detail, answer the following question.

■ (a) In Figure 5.23, locate the graph of R against t that characterizes the Einstein model, and write down the corresponding values of k and Λ.

(b) Can you see any graph in Figure 5.23 that corresponds to the de Sitter model?

❑ (a) The R against t graph for the Einstein model is the flat line shown in the middle of the top row of $\Lambda > 0$ models. According to Figure 5.23 it corresponds to $k = +1$ and $\Lambda = \Lambda_E$. (Note that Λ_E represents a particular value of the cosmological constant Λ. It follows from Equation 5.9 that, for a static universe of density ρ, that value is $\Lambda_E = 4\pi G\rho/c^2$.)

(b) There is no graph in Figure 5.23 that is obviously identical to the R against t graph of the de Sitter model shown in Figure 5.19. However, as you will see below, the de Sitter model is present in Figure 5.23 as a 'limiting case' of the $\Lambda > 0$, $k = 0$ model.

Let's examine the $\Lambda > 0$ models in turn, starting with the case where $k = +1$ and Λ is greater than zero, but less than Λ_E (i.e. $0 < \Lambda < \Lambda_E$). In this case the graph indicates two possible kinds of behaviour. One is the now familiar situation in which R starts from zero at time $t = 0$, increases up to some maximum value and then decreases to zero again in a finite time. The alternative behaviour, indicated by the higher of the two curves, is one in which there is no obvious time to choose as $t = 0$, since there is no equivalent of the big bang. Rather, this is an infinitely old model in which an infinitely long period of contraction leads to a 'bounce' (when the scale factor reaches its minimum value) followed by an infinitely long period of expansion. If the Universe we actually inhabit is represented by a Friedmann–Robertson–Walker model with $k = +1$ and Λ in the range $0 < \Lambda < \Lambda_E$, then its actual behaviour – whether it follows the upper curve or the lower one – will be determined by its behaviour in the distant past. If the Universe really started with a big bang, the upper curve would be ruled out.

The next case to consider is that in which the cosmological constant has the particular value Λ_E that allows the model to be static. We have already noted that the static behaviour of the Einstein model is one of the allowed modes of behaviour in this case, and that is indicated by the presence of the flat line in the R against t graph. But other kinds of behaviour are also possible, as indicated by the other two curves in this part of the figure. One possibility, shown by the lower curve, is that R starts from zero and increases, gradually approaching the value specified by the Einstein model. The other possibility, represented by the upper curve, describes a universe that starts out in something very close to the static state, but expanding just a little. Even the tiniest initial expansion of this kind will eventually lead to a perpetual expansion, making it possible that an expanding universe might have had an indefinitely long history before the expansion really took hold, a possibility that many cosmologists have found attractive. This last kind of behaviour characterizes the **Eddington–Lemaître model**. The model was introduced in 1925 by Georges Lemaître (1894–1966; Figure 5.24), a Belgian cleric who made several contributions to relativistic cosmology, but it was elaborated and strongly advocated in a 1930 paper by the Cambridge astrophysicist Sir Arthur Eddington (1882–1944; Figure 5.25), who felt that it might well describe the real Universe.

Despite his pioneering work on the Eddington–Lemaître model, Georges Lemaître is particularly associated with the $k = +1$ model in which Λ is greater than Λ_E, which is known as the **Lemaître model**. Lemaître advocated this model in the 1930s, when a number of scientists became interested in the origin of the chemical elements, or, more specifically, the origin of the nuclei of the various elements. The Lemaître model describes a universe that is homogeneous and isotropic, in which space has a finite total volume at any time, and where R starts from zero at time $t = 0$ but increases without limit. In this model the expansion passes through a 'pseudo-static' phase in which the R against t graph becomes almost flat, so that, for a while at least, it resembles a static universe even though it is never truly static. Lemaître argued that the late stages of this model could represent the expanding Universe we currently observe, that the intermediate 'coasting' phase provided the necessary time for the formation of stars and galaxies, and that the early, highly compressed state would have been so hot and dense that it could account for the 'cooking up' of some of the nuclei that certainly exist in the Universe. Although the details of Lemaître's argument are no longer accepted, his notion that the first nuclei were formed in a hot, dense phase of the early Universe is widely accepted, and Lemaître is therefore generally credited with recognizing the importance of the 'big bang' even though he did not use that specific term.

GEORGES LEMAÎTRE (1894–1966) AND ARTHUR EDDINGTON (1882–1944)

Georges Lemaître (Figure 5.24) was a Belgian cosmologist who was also a Catholic priest. He initially trained as a civil engineer, but after serving in World War I he entered a seminary, became a priest, and subsequently studied solar physics in Cambridge. While there he met Arthur Eddington, and then visited America where he became familiar with the work of Hubble and Shapley. After returning to Belgium, Lemaître became Professor of Astrophysics at the University of Louvain in 1927. In 1931 he formulated his notion of an ultra-dense ‘primeval atom’, the explosion of which might start the observed expansion of the Universe.

Figure 5.24 Georges Lemaître. (Science Photo Library)

Figure 5.25 Sir Arthur Stanley Eddington. (Royal Astronomical Society Library)

Sir Arthur Stanley Eddington (Figure 5.25) was a Cambridge-based astrophysicist who made several important contributions to the study of stellar structure, particularly through his recognition of the significance of radiation pressure in maintaining (or destroying) equilibrium. Eddington was an early supporter of Einstein’s general theory of relativity, and was the author of the first important book about the theory to appear in English. In 1919 he led the celebrated expedition that provided experimental support for the theory by observing the predicted deflection of starlight passing close to the edge of the Sun during a total eclipse.

In Figure 5.23, only one graph corresponds to $\Lambda > 0$ and $k = 0$. At the time of writing this is thought to be the model that most closely represents the real Universe. As you will see later, current astronomical evidence increasingly favours models in which $k = 0$. Observational evidence also favours $\Lambda > 0$. Hence this model represents the ‘best buy’ at the present time. As you can see from the R against t graph, this model represents a uniform universe that starts with a big bang and goes on expanding forever. The expansion undergoes a ‘slowdown’ at some stage, but does not exhibit the sort of ‘pseudo-static’ behaviour seen in the Lemaître model. After the slowdown, the rate of expansion increases continuously, and for this reason the model is sometimes referred to as the **accelerating model**.

The final graph in Figure 5.23 corresponds to $\Lambda > 0$ and $k = -1$. In a uniform universe of this type, space is infinite and has the kind of negatively curved geometry that causes cosmically large triangles to have interior angles that sum to less than 180°. This is another model that starts with a big bang. As in the accelerating model, the scale factor grows from zero, slows its growth temporarily and then accelerates again.

We have now discussed each of the FRW models, but we have still not found the de Sitter model among them. This is rather surprising, since Figure 5.23 should contain *all* the homogeneous and isotropic models that are filled by a pressure-free fluid. Where is the de Sitter model in this family? Well, the de Sitter model has $\Lambda > 0$ and $k = 0$, so we might expect to find it in the box that contains the accelerating model, and in fact that is where it is, but it is only present as a ‘limiting case’ of the behaviour that is illustrated in that part of the figure. The de Sitter model has a negligible amount of matter, so it corresponds to $\rho = 0$ as well as $p = 0$, whereas the graph that represents the $\Lambda > 0$ and $k = 0$ model in Figure 5.23 shows the

general case in which ρ may have a non-zero value. In this general case the density of matter decreases with time. As t increases the matter is eventually so thinly spread that such a universe increasingly resembles an essentially empty de Sitter model in which the cosmological constant is solely responsible for the expansion. As a result, the graph of R against t increasingly approaches the de Sitter form ($R \propto e^{Ht}$) as t approaches infinity. So, the de Sitter model is implicitly present in Figure 5.23, as a limiting case of what is shown. Though we shall not bother to discuss them, there are similar limiting cases elsewhere in Figure 5.23.

QUESTION 5.5

In the context of the Friedmann–Robertson–Walker models, which values or ranges of the parameters k and Λ correspond to universes with the following characteristics?

(a) The universe is neither homogeneous nor isotropic.

(b) There is no possibility of a big bang.

(c) A big bang is possible, but there is at least one other possibility (assume $\rho > 0$).

(d) The particular point in space where the big bang happened can still be determined long after the event.

(e) At any time, the large-scale geometrical properties of space are identical to those of a three-dimensional space with a flat geometry.

(f) Space has a finite volume, and 'straight' lines that are initially parallel may eventually meet.

(g) There is a big bang, but the volume of space is infinite from the earliest times.

5.4 The key parameters of the Universe

At the beginning of the last section it was stated that a cosmological model typically consists of:

- *equations* that imply general relations between observable quantities, together with
- *parameters* that must be determined by observation before the model can be used to provide detailed quantitative predictions.

You should fully appreciate the significance of this assertion now that you have examined the class of Friedmann–Robertson–Walker (FRW) models. You have just seen that in those models there is a general expression (Equation 5.12) that describes the geometry of space–time in terms of the separation of events. The form of this equation is enough to show a cosmologist that the universe being described is homogeneous and isotropic. However, a detailed appreciation of the properties of space–time in such a universe involves determining the parameters that arise in the model, specifically the curvature parameter k and a scale factor $R(t)$. Only when these are known does it become possible to evaluate quantities such as the curvature of space, which is determined at time t by the quantity $k/[R(t)]^2$. The importance of observable parameters is further emphasized by recalling that the behaviour of the scale factor is determined by the Friedmann equation, which involves the value of the curvature parameter k, the cosmological constant Λ and the average density of matter ρ, all of which are, in principle, observable parameters at any given time.

This section is concerned with the parameters that arise in the FRW models (basically k and $R(t)$), and their relationship to the observational parameters (such as the Hubble constant) that characterize our Universe. By determining and exploiting these relationships, it should be possible to use astronomical observations to determine which of the many cosmological models most closely resembles the Universe in which we live. This is one of the central challenges of the branch of cosmology known as *observational cosmology*.

Although this section concerns measurable parameters, its emphasis is on relationships rather than values. The values of the observable parameters, and the best ways of determining those values, are discussed much more fully in Chapter 7, which is entirely devoted to the subject of observational cosmology.

5.4.1 Hubble's law, the Hubble constant and the Hubble parameter

One observational result that finds a very natural explanation in the context of FRW cosmology is Hubble's law. You will recall that this law describes the general tendency for the redshift z of a galaxy to increase in proportion to its distance d from the observer, as described by the equation

$$z = \frac{H_0}{c}d \tag{5.1}$$

where the constant of proportionality, H_0/c, is made up of *Hubble's constant*, H_0, and the speed of light in a vacuum, c. You will also recall that for any particular galaxy the redshift z in Equation 5.1 can be related to the observed and emitted wavelengths, λ_{obs} and λ_{em}, of some identified spectral line by the equation

$$z = \frac{\lambda_{\text{obs}} - \lambda_{\text{em}}}{\lambda_{\text{em}}} \tag{5.2}$$

By measuring the redshifts of distant galaxies, and independently measuring the distances of those galaxies, it is possible to use Equation 5.1 to determine the value of the Hubble constant H_0, since the speed of light is well known. Hubble himself did this, although his result was wildly inaccurate due to poor and incorrectly interpreted data. More modern observations have allowed the value of H_0 to be determined with an uncertainty of about 10% and there are good prospects of reducing this uncertainty still further. A recent estimate of the Hubble constant suggests a value of

$$H_0 = (2.3 \pm 0.3) \times 10^{-18}\,\text{s}^{-1}$$

although, for historical reasons, this is more usually expressed in units of $\text{km s}^{-1}\,\text{Mpc}^{-1}$ (i.e. kilometres per second per megaparsec) giving

$$H_0 = (72 \pm 8)\,\text{km s}^{-1}\,\text{Mpc}^{-1}$$

H_0 is one of the most important observational parameters in cosmology, but how does it relate to the FRW models, where the obvious parameters are k and $R(t)$, and there is no H_0 to be seen? This is what we must now investigate.

Figure 5.26 indicates the basis of the relationship. The figure shows two snapshots of an expanding FRW universe, with a growing scale factor $R(t)$. Two galaxies, A and B, happen to be located at the grid points of a set of co-moving coordinates that expands with the universe. The first snapshot represents a time t_{em} at which some light is emitted from galaxy A, and the second snapshot represents a later

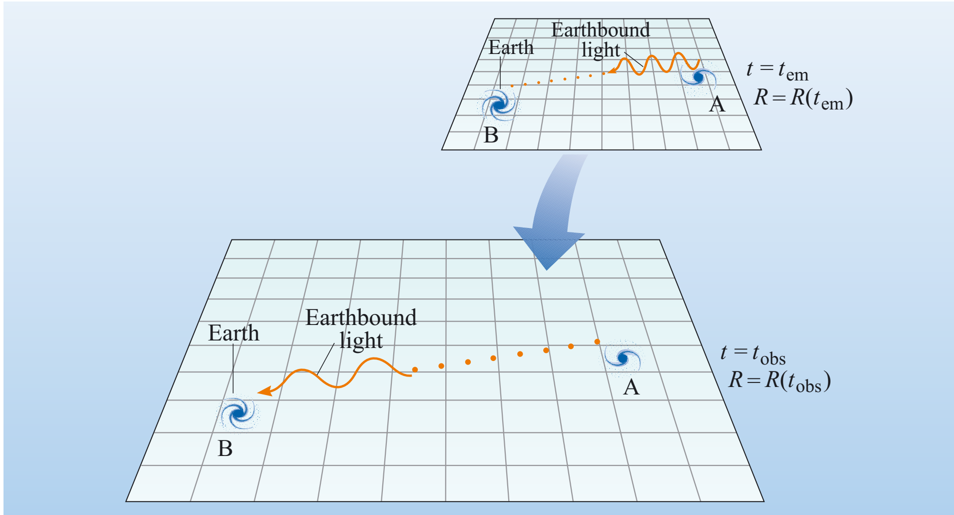

Figure 5.26 Cosmic expansion, measured by the increasing scale factor $R(t)$, as a cause of the cosmological red-shift of distant galaxies. The 'stretching' of space also stretches light waves travelling from one galaxy to another, causing the observed light to be red-shifted relative to the emitted light. (Adapted from Finkbeiner, 1998)

time t_{obs} at which that same light is observed in galaxy B. While the light is travelling from A to B, the (co-moving) coordinates of the galaxies do not change, but the physical distance between the galaxies does increase because it is proportional to $R(t)$, and $R(t_{obs})$ is greater than $R(t_{em})$. Whatever the distance from A to B at time t_{em}, it will have increased by a factor of $R(t_{obs})/R(t_{em})$ by the later time t_{obs}. Now, this expansion factor $R(t_{obs})/R(t_{em})$ represents the growth of space itself, so it will also influence the wavelength of the light that is moving freely between the two galaxies. As a result, light that is emitted from A at time t_{em} with wavelength λ_{em} will be observed at B at time t_{obs} with the longer wavelength $\lambda_{obs} = \lambda_{em} \times R(t_{obs})/R(t_{em})$. This increase in wavelength will, of course, be seen as a redshift by the observer in galaxy B.

- According to an observer in galaxy B at time t_{obs}, what is the redshift of galaxy A? Express your answer in terms of the expansion factor $R(t_{obs})/R(t_{em})$.

- Rearranging Equation 5.2

$$z = \frac{\lambda_{obs} - \lambda_{em}}{\lambda_{em}} = \frac{\lambda_{em}[(\lambda_{obs}/\lambda_{em}) - 1]}{\lambda_{em}}$$

Cancelling the overall factors of λ_{em}

$$z = \frac{\lambda_{obs}}{\lambda_{em}} - 1$$

Replacing $\lambda_{obs}/\lambda_{em}$ by the equivalent expansion factor $R(t_{obs})/R(t_{em})$, we find that

$$z = \frac{R(t_{obs})}{R(t_{em})} - 1 \qquad (5.13)$$

Note that according to the FRW model, the red-shift of a distant galaxy is primarily caused by the expansion of space, it is *not* a Doppler shift due to movement through space. These expansion-based redshifts are usually referred to as **cosmological redshifts** in order to distinguish them from Doppler shifts. Of course, real galaxies do not necessarily behave like the idealized galaxies of Figure 5.26. Real galaxies may have some 'peculiar' motion of their own relative to the

grid of co-moving coordinates, and this peculiar motion can give rise to Doppler shifts that cause the observed redshifts of galaxies to differ somewhat from the cosmological redshifts implied by a smoothly expanding FRW model.

We have now seen how redshifts can arise from expansion in a Friedmann–Robertson–Walker model, but the real point of Hubble's law is that the redshift z of distant galaxies *increases in proportion to their distance*. How do FRW models account for this? Very simply as it turns out. The greater the distance of a galaxy, the longer the light takes to reach us from that galaxy. The greater the time the light spends 'in flight' between the moments of emission and observation, the greater is the expansion factor $R(t_{\rm obs})/R(t_{\rm em})$, and the greater the redshift of the light, $z = [R(t_{\rm obs})/R(t_{\rm em})] - 1$.

The time-of-flight argument provides a qualitative explanation of Hubble's law in an expanding FRW model, but the explicit nature of the FRW models allows us to be even more precise about the exact nature of the relationship. In particular, it is possible to derive an equation that relates Hubble's constant to the scale factor. To see this, consider two galaxies separated by a relatively *small* distance d at time t when the scale parameter is $R(t)$. Because these galaxies are close together, the flight-time for light passing from one to the other, d/c, is also small and is represented by the quantity Δt. It follows from Equation 5.13 that the observed redshift of one of these galaxies, when observed from the other, is

$$z = \frac{R(t+\Delta t)}{R(t)} - 1 \qquad (5.14)$$

Due to the expansion of the Universe, $R(t + \Delta t)$ is greater than $R(t)$, and we can indicate this by writing $R(t + \Delta t) = R(t) + \Delta R(t)$, where the new quantity $\Delta R(t)$ represents the small increase in scale factor that occurs during the short time Δt. Note that $\Delta R(t)$ represents a single quantity, it is *not* the result of multiplying together quantities such as Δ and $R(t)$.

Replacing $R(t + \Delta t)$ in Equation 5.14 by the alternative expression $R(t) + \Delta R(t)$, shows that

$$z = \frac{R(t)+\Delta R(t)}{R(t)} - 1 \qquad (5.15)$$

and this can be rewritten as

$$z = 1 + \frac{\Delta R(t)}{R(t)} - 1 \qquad (5.16)$$

that is, $$z = \frac{\Delta R(t)}{R(t)} \qquad (5.17)$$

Now for the crucial step: $\Delta R(t)$ – the change in scale factor that occurs during the short time interval Δt – will be equal to the result of multiplying the interval Δt by the rate of change of R at the time t. (This is like saying that during a time Δt a car travelling with velocity v will change its position by an amount $\Delta t \times v$, since v is the rate of change of position.) It is conventional to represent the rate of change of the scale factor at time t by the symbol $\dot{R}(t)$ (read as 'R dot at time t'), so $\Delta R(t) = \Delta t \times \dot{R}(t)$, and to rewrite Equation 5.17 as:

$$z = \frac{\Delta t \times \dot{R}(t)}{R(t)} \qquad (5.18)$$

If you are familiar with differential calculus, you may find it helpful to know that $\dot{R}(t)$ is a common shorthand for the derivative $\mathrm{d}R(t)/\mathrm{d}t$.

Since $c/c = 1$, we can rewrite this as

$$z = \frac{c\Delta t}{c} \times \frac{\dot{R}(t)}{R(t)} \tag{5.19}$$

But, $c\Delta t = d$, the distance between the two galaxies. Using this, we can write

$$z = \frac{1}{c} \times \frac{\dot{R}(t)}{R(t)} \times d \tag{5.20}$$

Now, you should be able to see that this is similar to Hubble's law, according to which, at the present time t_0

$$z = \frac{H_0}{c} d \tag{5.1}$$

This similarity suggests that we should identify the time dependent quantity $\dot{R}(t)/R(t)$ in Equation 5.20 as a time dependent **Hubble parameter** that we can denote $H(t)$. Thus,

$$H(t) = \frac{\dot{R}(t)}{R(t)} \tag{5.21}$$

The value of this Hubble parameter varies with time, but the precise way that it varies depends on the precise way in which $R(t)$ varies with time, and will therefore differ from one FRW model to another. However, in any model that provides a good description of the real Universe, we expect to find that if we evaluate the 'theoretical' Hubble parameter at the present time t_0, then the value obtained should equal that of the observed Hubble constant, that is

$$H(t_0) = \frac{\dot{R}(t_0)}{R(t_0)} = H_0 \tag{5.22}$$

As you can see, we have now managed to relate an observational parameter, H_0, to the scale factor $R(t)$ – a parameter in the FRW model.

The function $\dot{R}(t)$ represents the rate of change of R at time t, so $\dot{R}(t)/R(t)$ represents the 'fractional' rate of change of the scale factor. Using this terminology we can say that in Friedmann–Robertson–Walker cosmology, the Hubble constant represents the fractional rate of change of the scale factor evaluated at the present time, t_0. More succinctly, we can say that the observed Hubble constant represents the current value of the model's Hubble parameter.

QUESTION 5.6

Figure 5.27 is a plot of redshift against distance for a number of galaxies. The plot includes a 'best fit' line drawn through the data. Assuming that our Universe can be well represented by an expanding Friedmann–Robertson–Walker model, state the significance of the gradient of the line, evaluate that gradient from the graph, and hence determine the value of the Hubble constant.

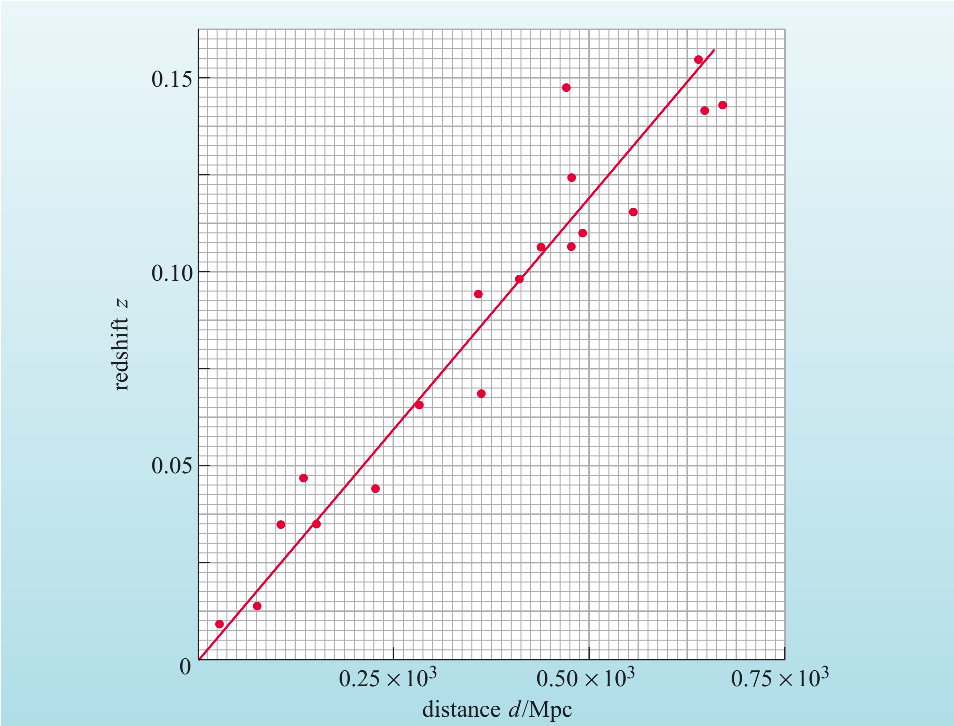

Figure 5.27 A plot of redshift against distance for a number of galaxies, together with a best-fit line through the data.

QUESTION 5.7

What is the rate of change of R in the Einstein model? What does your answer imply about the Hubble parameter in the Einstein model?

5.4.2 Systematic deviations from Hubble's law, and the deceleration parameter

At any time t, the Hubble parameter measures the rate expansion of the Universe and depends on the rate of change of R, which is indicated by the slope of the R against t graph. However, in most FRW models the expansion either speeds up or slows down as time progresses – that is to say the expansion is accelerating or decelerating – and this is indicated by the curvature of the R against t graph (see Figures 5.23 and 5.28).

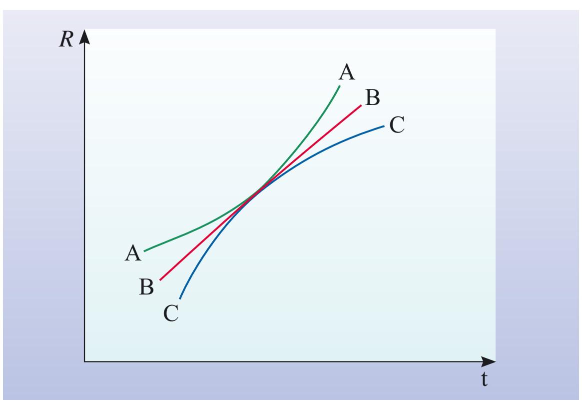

Figure 5.28 A plot of R against t, for large values of t, in three different FRW models denoted A, B and C. The upward curvature of A indicates acceleration, the downward curvature of C indicates deceleration and the relative lack of curvature in B indicates an almost steady expansion.

■ Referring back to Figure 5.23 (and the accompanying text), identify three named FRW models that might correspond to the curves A, B and C in Figure 5.28.

❑ A could represent the accelerating model ($k = 0$, $\Lambda > 0$)
B could represent the open model ($k = -1$, $\Lambda = 0$)
C could represent the critical model ($k = 0$, $\Lambda = 0$).

Just as the rate of change of R is indicated by $\dot{R}(t)$, so the rate of change of $\dot{R}(t)$ is indicated by $\ddot{R}(t)$ (read as 'R double dot at time t'). If the expansion of the Universe is speeding up at time t then $\ddot{R}(t)$ will be positive, if the expansion is slowing down, $\ddot{R}(t)$ will be negative, and if there is no acceleration or deceleration $\ddot{R}(t) = 0$.

In the context of the FRW models, it turns out that a useful way of characterizing an increasing or decreasing rate of expansion is in terms of a quantity called the **deceleration parameter**. This varies with time, and is conventionally denoted by the symbol $q(t)$. It is defined as follows

$$q(t) = \frac{-R(t)}{[\dot{R}(t)]^2}\ddot{R}(t) \tag{5.23}$$

Note the negative sign in this equation; this implies that if $\ddot{R}(t)$ is positive (i.e. if the expansion is accelerating) then the deceleration parameter will be negative. In the cases shown in Figure 5.28, at large values of t the deceleration parameter would be negative for curve A, zero for curve B, and positive for curve C.

■ What would you expect the corresponding results to be for small values of t in the three FRW models named in the last question?

❑ In all three models the R against t graph curves downwards at early times, similar to the behaviour of the Einstein–de Sitter model at very early times. This indicates that in its early phases the expansion is decelerating, and implies that $q(t)$ will be positive in all three cases.

Now, the detailed argument presented in the last section showed that the expanding FRW models predict a direct proportionality between z and d of just the kind described by Hubble's law. However, that argument was based on the behaviour of galaxies that were sufficiently close together for the time of flight of light passing from one to the other to be considered 'short'. When more distant galaxies are taken into account, the FRW models predict that the direct proportionality between z and d will break down, and systematic deviations from Hubble's law will be observed. Moreover, the models show that the systematic deviations from Hubble's law depend on the value of the deceleration parameter at the time of observation.

In fact, the FRW models predict that present-day observations of galaxy redshifts and distances should show, to a first approximation, that

$$d = \frac{cz}{H_0} \tag{5.24}$$

which is just a rearrangement of Hubble's law, and agrees with observations for redshifts of less than 0.2 or so. But the FRW models also predict that, to a better approximation

$$d = \frac{cz}{H_0}\left[1 + \frac{1}{2}(1 - q_0)z\right] \tag{5.25}$$

where q_0 is the current value of the deceleration parameter. Figure 5.29 illustrates this relationship by showing the kind of systematic deviations from Hubble's law that might be expected for various values of q_0 out to a redshift of about 1. It's worth noting that the distance d in these relationships represents the distance indicated by an object's luminosity at the time of observation, t_0.

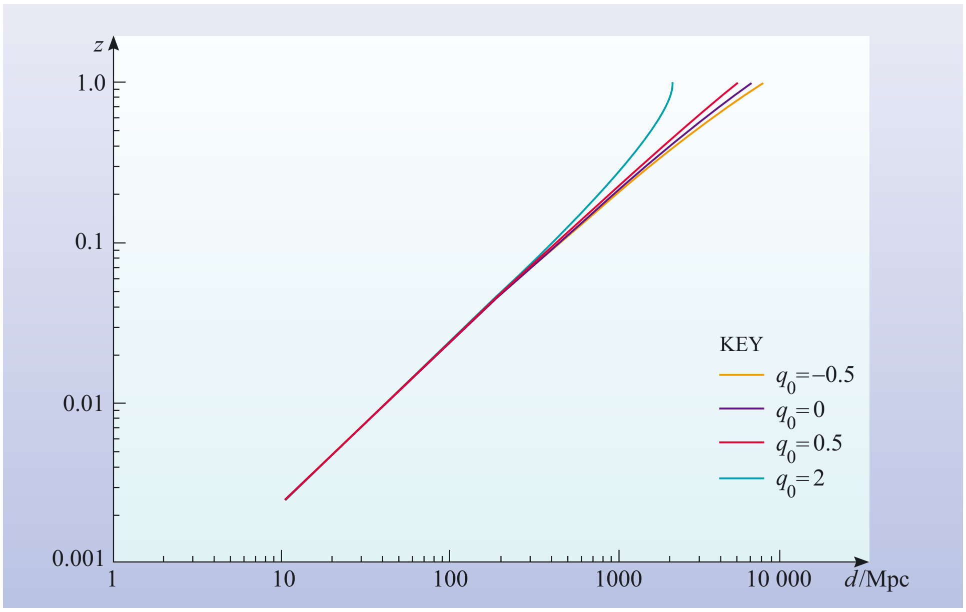

Figure 5.29 The current form of the graph of redshift against distance for galaxies, as predicted by expanding FRW models. The precise shape of the curve depends on the current value of the deceleration parameter, q_0, but all such models predict a straight part that is determined by the current value of the Hubble parameter, H_0. (In this case $H_0 = 72\,\mathrm{km\,s^{-1}\,Mpc^{-1}}$ has been assumed.)

In principle then, given sufficiently good observational data, the straight part of the redshift against distance graph can be used to determine the current value of the Hubble parameter, H_0, and the observed deviations from straightness can be used to determine the current value of the deceleration parameter, q_0. The determination of these two values, H_0 and q_0, was, for many years, the primary objective of observational cosmology. In fact, the American astronomer Alan Sandage (1926–), a former assistant of Hubble, once famously described observational cosmology as 'the search for two numbers', a characterization that was largely true until the 1970s.

Although there is now far more to observational cosmology than the determination of H_0 and q_0, the determination of those two numbers is still of very great importance. As mentioned earlier, recent observations have reduced the uncertainty in the value of H_0 to about 10% and even greater accuracy is to be expected soon. However, the determination of q_0 presents a much greater challenge. In order for the deviations from Hubble's law to be seen it is necessary to observe galaxies at large redshifts and to independently measure their distances. Finding high redshift galaxies is now relatively easy, but accurately determining their distances is very hard. A number of recent observations (see Chapter 7 for details) have indicated that q_0 is negative, implying that the expansion of the Universe is accelerating. If these results hold up, and if we do indeed live in a Universe broadly described by an accelerating FRW model, then it must also be the case that the cosmological constant is greater than zero.

QUESTION 5.8

Justify the assertion made in the last sentence above.

5.4.3 The critical density and the density parameters

An important parameter in any FRW model is the average density of cosmic matter. In an expanding or contracting Universe this quantity will change with time, so in the context of FRW models it is represented by the symbol $\rho(t)$. Observationally we might hope to determine the current value of the density, $\rho(t_0)$, by adding together the masses of all the galaxies and clusters in some sufficiently large region of the Universe, and dividing that sum by the volume of the region. Of course, this has been attempted many times, but the answers are fraught with uncertainties, partly due to the problems of measuring large distances and observing faint galaxies, but also due to the very great problem of determining the total mass of dark matter in any region. For this reason, more indirect approaches to the determination of ρ are usually necessary.

When discussing the cosmic density a useful reference value is the density of matter in the FRW model with $k = 0$ and $\Lambda = 0$. You will recall from our discussion of Figure 5.23 that this particular model is often referred to as the *critical model*, since it sits exactly on the borderline between the open and closed $\Lambda = 0$ models. It turns out that, in order to maintain this precarious position, the density of matter in the critical model must be precisely related to the value of the Hubble parameter at all times. In fact, if we denote the density of matter in the critical model at time t by $\rho_{\text{crit}}(t)$, the Friedmann equation (see Box 5.4) implies that

$$\rho_{\text{crit}}(t) = \frac{3H^2(t)}{8\pi G} \tag{5.26}$$

where G is Newton's gravitational constant. The quantity $\rho_{\text{crit}}(t)$ is known as the **critical density** at time t. Note that both $\rho_{\text{crit}}(t)$ and $H(t)$ vary with time, but, in the critical model, Equation 5.26 always relates their variations. So, it is always possible to work out the current value of the critical density from the current value of the Hubble parameter.

- ■ Until recently it was widely believed that our Universe was well represented by the critical model. If this belief had been correct what would have been a reasonable estimate of the current value for the density of the Universe?

- ❑ Under these conditions the current value of the density, $\rho(t_0)$, would be the current value of the critical density, i.e. $3H_0^2/8\pi G$. Using the value for H_0 given in Section 5.4.1, i.e. $72\,\text{km}\,\text{s}^{-1}\,\text{Mpc}^{-1} = 2.3 \times 10^{-18}\,\text{s}^{-1}$, we see that

$$\rho_{\text{crit}}(t_0) = \frac{3 \times (2.3 \times 10^{-18})^2}{8 \times \pi \times 6.67 \times 10^{-11}}\,\text{kg}\,\text{m}^{-3} \approx 1 \times 10^{-26}\,\text{kg}\,\text{m}^{-3}$$

Using the critical density as a reference value, we can express the actual density of cosmic matter at any time as a fraction of the critical density at that time. This fraction is called the **density parameter for matter**, and may be represented by the symbol $\Omega_{\text{m}}(t)$, so

Ω is the upper case Greek letter 'omega'.

BOX 5.4 THE FRIEDMANN EQUATION: EPISODE 2

This is a good place to finally write down the explicit form of the crucially important Friedmann equation that was first discussed in Section 5.3.5. The equation makes use of the symbol $\dot{R}(t)$ to represent the rate of change of the scale factor R, and may be written as

$$\dot{R}^2 = \frac{8\pi G R^2}{3}\left(\rho + \frac{\Lambda c^2}{8\pi G}\right) - kc^2 \qquad (5.27)$$

We have omitted the parenthesized t that should follow R and ρ for the sake of simplicity, but it is still the case that these are time-dependent quantities. Given the values of k and Λ, Equation 5.27 may be used to determine the behaviour of R, although in order to work out the precise details it is also necessary to know the value of ρ at some particular time. In fact, it can be shown that in a pressure-free universe $\rho(t)[R(t)]^3$ has a constant value, D say, so the density information is often provided by specifying the value of this constant, and replacing ρ in Equation 5.27 by D/R^3.

Note that in the case of the critical model, where $k = 0$ and $\Lambda = 0$, the Friedmann equation implies that

$$\dot{R}^2 = \frac{8\pi G R^2}{3}\rho \qquad (5.28)$$

Identifying ρ as $\rho_{\rm crit}$ in this case, and recalling that $[H(t)]^2 = \dot{R}^2/R^2$, the above equation can be rearranged to give Equation 5.26, $\rho_{\rm crit}(t) = 3H^2(t)/8\pi G$.

It is worth pointing out that on the basis of Newtonian physics (rather than general relativity), the Friedmann equation (Equation 5.27) can be derived by considering the total energy of an expanding spherical distribution of galaxies. In such a derivation kc^2 is related to the total energy of the sphere, $\dot{R}^2$ is related to the kinetic energy of the sphere, and the term involving G is related to the gravitational potential energy of the sphere. On this basis the Friedmann equation is sometimes referred to as the 'energy equation' of the Universe.

$$\Omega_{\rm m}(t) = \frac{\rho(t)}{\rho_{\rm crit}(t)} \quad \text{where } \rho_{\rm crit}(t) = \frac{3H^2(t)}{8\pi G} \qquad (5.29)$$

If, at some time t, the density of matter in the Universe was half the critical value, then $\Omega_{\rm m}(t) = 0.5$; if the actual density was one-quarter of the critical density then $\Omega_{\rm m}(t) = 0.25$, and so on. Note that this parameter includes *all* kinds of matter: dark matter as well as luminous matter, baryonic as well as non-baryonic.

Interestingly, it is possible to represent the value of the cosmological constant in a similar way. If you look at the Friedmann equation (Equation 5.27), you will see that the constant $\Lambda c^2/8\pi G$ enters the equation in a similar way to the matter density ρ. This suggests that we can interpret the term $\Lambda c^2/8\pi G$ as a sort of 'density' associated with the cosmological constant. Of course, $\Lambda c^2/8\pi G$ is a very odd sort of density because it is expected to remain constant while the Universe expands, whereas the matter density ρ is expected to decrease in proportion to $1/R^3$ in an expanding Universe. Nonetheless, if we use the symbol ρ_Λ to represent $\Lambda c^2/8\pi G$, then we can define the **density parameter for the cosmological constant** as

$$\Omega_\Lambda(t) = \frac{\rho_\Lambda}{\rho_{\rm crit}(t)} \quad \text{where } \rho_\Lambda = \Lambda c^2/8\pi G \qquad (5.30)$$

Note that although Λ and ρ_Λ are constants, the density parameter $\Omega_\Lambda(t)$ does depend on time, because it involves the critical density, and that is time-dependent.

Now, even though ρ_Λ doesn't make much sense as a matter density, if we multiply it by c^2 we obtain a quantity that can be measured in units of $\rm J\,m^{-3}$ (i.e. joule per

cubic metre). This quantity, $\rho_\Lambda c^2 = \Lambda c^4/8\pi G$, can be interpreted as an *energy density*, where the energy concerned can be thought of as a property of space itself – the energy density of a vacuum! As space expands there would be no reduction in the density of this particular kind of energy. Rather, an increase in the volume of space would simply produce a corresponding increase in 'vacuum energy'. There is no real need to interpret the cosmological constant in terms of a vacuum energy, but it is a fascinating thought that the effect of the cosmological constant might actually be caused by a vacuum energy. It has even been proposed that the vacuum energy might be the result of some sort of quantum physical effect in empty space. Attempts to formulate detailed theories along these lines have not been particularly successful, so rather than assuming that the cosmological constant is caused by some particular kind of vacuum energy, many scientists prefer to call the energy that *may* be associated with the cosmological constant **dark energy** and to admit that the nature of this enigmatic energy is still a complete mystery. Even so, it is now common practice to quote values for the dark energy density rather than for the cosmological constant itself. It is also common practice to refer to $\Omega_\Lambda(t)$ as the density parameter for dark energy.

A lot of observational effort is now going into the determination of the current values of $\Omega_\mathrm{m}(t)$ and $\Omega_\Lambda(t)$. Figure 5.30 gives some indication of the significance of these two parameters, which can be denoted $\Omega_{\mathrm{m},0}$ and $\Omega_{\Lambda,0}$. At all points on the red line, $\Omega_{\mathrm{m},0} + \Omega_{\Lambda,0} = 1$. If the observed values of $\Omega_{\mathrm{m},0}$ and $\Omega_{\Lambda,0}$ satisfy this condition, then the geometry of space will be flat, and it must be the case that $k = 0$ (Question 5.9 asks you to prove this). On the other hand, if $\Omega_{\mathrm{m},0} + \Omega_{\Lambda,0} > 1$ then $k = +1$, or if $\Omega_{\mathrm{m},0} + \Omega_{\Lambda,0} < 1$ then $k = -1$. Thus, the geometric properties of space depend crucially upon the sum of $\Omega_{\mathrm{m},0}$ and $\Omega_{\Lambda,0}$. As Figure 5.30 also indicates, another

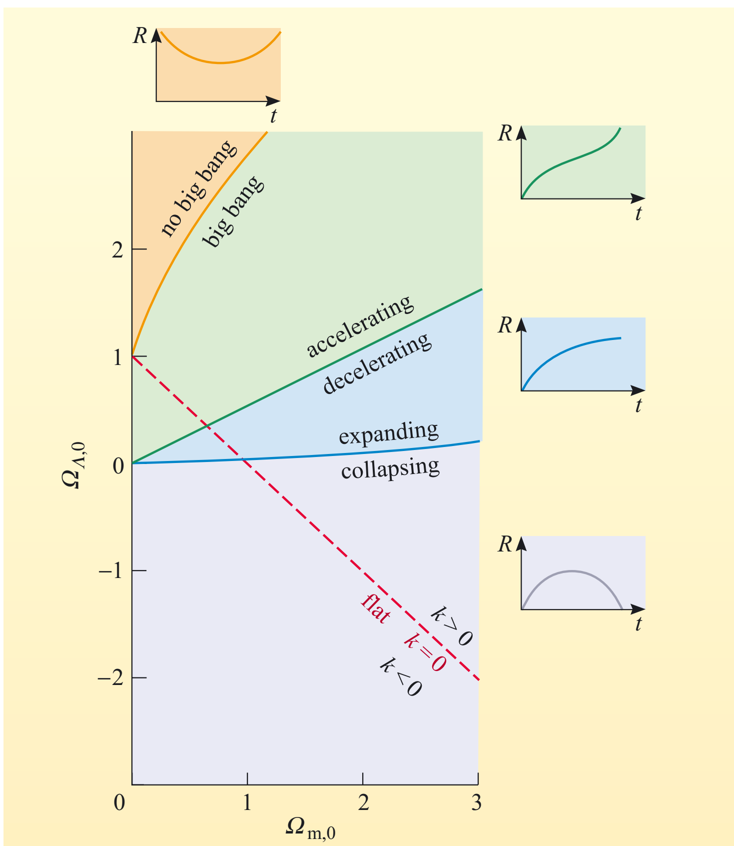

Figure 5.30 A plot of $\Omega_{\Lambda,0}$ against $\Omega_{\mathrm{m},0}$. The values of these two quantities determine important characteristics of a Friedmann–Robertson–Walker cosmological model, such as the sign of the curvature parameter k (red line), whether the Universe will expand forever and eventually collapse (blue line), whether that expansion will accelerate or decelerate (green line), and whether or not there was a big bang (yellow line).

condition involving $\Omega_{m,0}$ and $\Omega_{\Lambda,0}$ (represented by the blue line) determines whether the Universe will eventually collapse or continue expanding forever. And, if the fate of the Universe is perpetual expansion, yet another condition involving $\Omega_{m,0}$ and $\Omega_{\Lambda,0}$ (represented by the green line) will determine whether the expansion will accelerate or decelerate.

The current values of these density parameters are not easy to determine. However, recent measurements have indicated that $k = 0$, implying that $\Omega_{m,0} + \Omega_{\Lambda,0} = 1$, while other measurements suggest $\Omega_{\Lambda,0} > 0$. In fact, current estimates (see Chapter 7 for details) indicate that $\Omega_{m,0} \approx 0.3$ and $\Omega_{\Lambda,0} \approx 0.7$. If these figures are correct, then most of the energy in the Universe is dark energy, space has a flat geometry, and cosmic expansion will continue forever at an accelerating rate.

QUESTION 5.9

Show that the Friedmann equation can be rewritten as

$$H^2 = \frac{8\pi G}{3}\left(\rho + \frac{\Lambda c^2}{8\pi G}\right) - \frac{kc^2}{R^2}$$

and that this may itself be rewritten as

$$\Omega - 1 = \frac{kc^2}{R^2 H^2} \quad \text{(where } \Omega = \Omega_m + \Omega_\Lambda\text{)}$$

Hence justify the statement that if $\Omega_m + \Omega_\Lambda = 1$, then $k = 0$.

QUESTION 5.10

The Friedmann equation, together with the relation ρR^3 = constant, may be used to show (you are not expected to demonstrate this)

$$2\dot{R}\ddot{R} = -\frac{8\pi G}{3}(R\dot{R}\rho - 2R\dot{R}\rho_\Lambda)$$

Use this, and the definitions given above for $H(t)$, $q(t)$ and $\rho_{crit}(t)$ to show that at any time t

$$q(t) = \frac{\Omega_m(t)}{2} - \Omega_\Lambda(t)$$

Use this, together with the data given above, to estimate the value of q_0.

5.4.4 The Hubble time and the age of the Universe

The critical model not only provides a useful reference value for the cosmic density, it also provides useful insights into the age of the Universe. The usefulness of the critical model stems from the fact that its scale parameter varies with time in a very simple way

$$R(t) = At^{2/3} \quad \text{(where } A \text{ is a constant)}$$

(This relationship is found by solving the Friedmann equation with $k = 0$ and $\Lambda = 0$.)

Combining this with the definition of the Hubble parameter, $H(t)$, it can be shown that in the critical model

$$H(t) = \frac{2}{3t} \quad \text{(critical universe only)}$$

It follows from this that observers living in a universe that was well described by the critical model would find that, after their universe had been expanding for a time t_0, their observations of distant galaxies would indicate that the Hubble constant had the value $H_0 = 2/3t_0$. In other words, the observers in such a hypothetical universe would be able to deduce the age of their universe by measuring H_0 and using the relation

$$t_0 = \frac{2}{3H_0} \quad \text{(critical universe only)}$$

Since H_0 may be expressed in units of s^{-1}, the quantity $1/H_0$ may be expressed in time units, such as seconds or years. The quantity $1/H_0$ is known as the **Hubble time** and is often used as a reference value in discussions of cosmic age, just as ρ_{crit} is a useful reference value in discussions of cosmic density. The exact value of the Hubble time is somewhat uncertain, due to the uncertainties that still exist in measurements of H_0, but it is thought to be about 4.3×10^{17} s or, if you prefer, about 14 billion years (i.e. 1.4×10^{10} yr).

- If our Universe was well represented by the critical model, how old would it be?

- According to the critical model the age of the Universe, t_0, is two-thirds of the Hubble time. Since the Hubble time for our Universe is about 14 billion years, it follows that the age of our Universe, if it were well represented by the critical model, would be about 9 billion years. In fact, this is too short to be realistic.

The critical model is unusual in providing such a simple relationship between the age of the Universe and the observed value of the Hubble constant. Similar relationships exist in other FRW models, but they are generally less direct and therefore more complicated. Rather than trying to write down those relationships it is much easier to represent them graphically. First however, take a look at Figure 5.31, which should give you a general feel for what you can expect to see later.

Figure 5.31 shows the growth of the scale factor for four different FRW models; the models are numbered 1 to 4, and are, respectively,

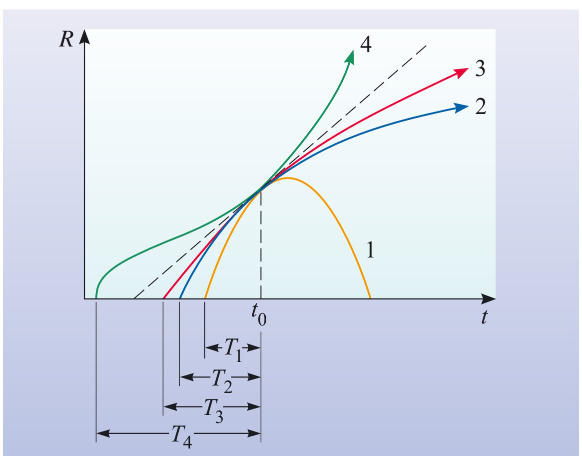

Figure 5.31 The evolution of the scale factor in closed, critical, open and accelerating FRW models that have the same Hubble constant at time t_0. The accelerating model, the only one of the four to have a non-zero cosmological constant, has the greatest age.

1 a closed model with $\Lambda = 0$ and $k = +1$

2 a critical model with $\Lambda = 0$ and $k = 0$

3 an open model with $\Lambda = 0$ and $k = -1$

4 an accelerating model with $\Lambda > 0$ and $k = 0$

The general behaviour of these four models was shown in Figure 5.23, but as redrawn in Figure 5.31 the curves have been shifted horizontally so that they all have the same values for R and $\dot{R}$ at the time t_0 that corresponds to the present. This amounts to saying that the curves have been drawn in such a way that they all indicate the same value for the Hubble constant. Given that the four curves in Figure 5.31 all correspond to the same Hubble constant, what do they tell us about the ages of these four kinds of universe? Well, the age of each model universe is represented by the time that elapses between the moment when R was first equal to zero and the time t_0. These times are different in the four models and are indicated by the values T_1, T_2, T_3 and T_4. As you can see, each is larger than its predecessor, with the closed universe having the smallest age and the accelerating universe the greatest.

You saw earlier that in our Universe the observed value of the Hubble constant is so large that a critical model would imply an unrealistically small age for the Universe. A number of cosmologists have taken this fact alone as *prima facie* evidence that the cosmological constant is non-zero.

Now look at Figure 5.32; this puts the implications of Figure 5.31 into a more general context by plotting curves that show the relationship between the age of the universe (i.e. the length of time it has been expanding) and the Hubble parameter in three different FRW models. The curves represent critical and open models with $\Lambda = 0$, and an accelerating model with the same density as the open model, but with a positive cosmological constant. It can clearly be seen that, for a given value of the Hubble parameter, the accelerating model is always the one that has been expanding longest.

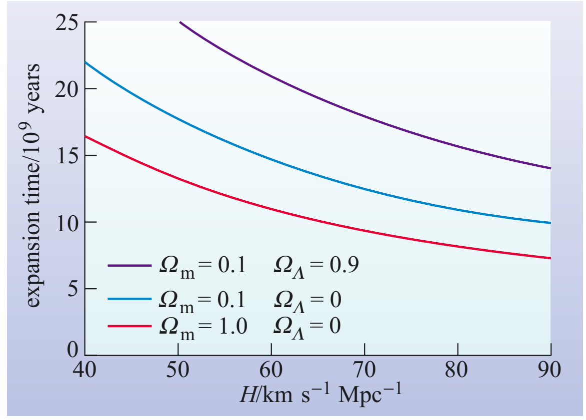

Figure 5.32 The age of the Universe plotted against the Hubble parameter for critical, open and accelerating universes of various densities. (Adapted from Roth, 1997, based on work by J. Primack)

Finally, Figure 5.33 provides an even broader context by showing the age of the universe for any value of the Hubble constant and for a wide range of possible values for $\Omega_{m,0}$ and $\Omega_{\Lambda,0}$. The possible values of the Hubble constant do not appear anywhere in the diagram, but the curved lines that sweep across the diagram indicate the ages of various models measured in multiples of the Hubble time, and this latter quantity implicitly depends on the value of Hubble constant. Note that the axes of Figure 5.33 are $\Omega_{m,0}$ and $\Omega_{m,0} + \Omega_{\Lambda,0}$, so the condition for flat space ($k = 0$) is now represented by the red vertical line through $\Omega_{m,0} + \Omega_{\Lambda,0} = 1$.

It was mentioned earlier that the currently favoured values of the density parameters for matter and dark energy are $\Omega_{m,0} \approx 0.3$ and $\Omega_{\Lambda,0} \approx 0.7$. These values mean that our Universe is represented by the large red dot in Figure 5.33. You can see from the figure that this location implies an age that is slightly less than the Hubble time, which was earlier estimated to be 14 billion years. This age estimate seems to be consistent with the ages of the oldest known objects in the Universe, the globular cluster stars mentioned in Chapter 1.

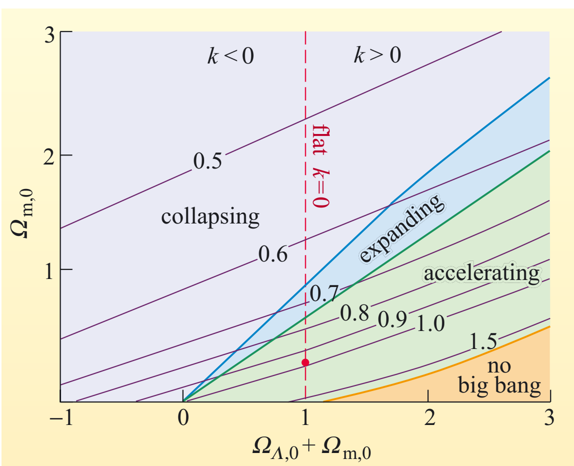

Figure 5.33 The age of the universe in units of the Hubble time is indicated by the various curves that cross this plot of $\Omega_{m,0}$ against $\Omega_{m,0} + \Omega_{\Lambda,0}$. (Adapted from Carroll *et al.*, 1992)

5.5 Summary of Chapter 5

The nature of the Universe

- The Universe contains matter. About 5/6ths of it is believed to be dark matter that may be non-baryonic, and the remaining 1/6th is baryonic matter. The baryonic matter is mainly hydrogen (~75% by mass) and helium (~25% by mass).
- The Universe contains (electromagnetic) radiation. Much of it is visible light, but the major part of the energy is contained in the cosmic microwave background (CMB) radiation.
- The Universe is uniform. That is to say, all regions that are sufficiently large to be representative have the same average density and pressure, wherever they are located. This claim is consistent with the observed distributions of matter and radiation.
- The Universe is expanding. As a result, the redshifts of distant galaxies are found, on average, to be proportional to the distances of those galaxies. This is described by Hubble's law, $z = (H_0/c)d$, where Hubble's constant, H_0, provides a measure of the rate of cosmic expansion at the present time.

Relativistic cosmology and models of the Universe

- According to Einstein's theory of general relativity the geometric properties of space–time are related to the distribution of energy and momentum within that space–time. The precise relationship is described by the field equations of general relativity, which provide the basis for Einstein's theory of gravity and for relativistic cosmology.
- The geometric properties of space–time include curvature. In a curved space, geometric results can take on unfamiliar forms. The interior angles of a triangle may have a sum that is different from 180°, straight lines may close upon themselves, and pairs of straight lines that are initially parallel may converge or diverge. The geometric properties of any particular space–time can be summarized by writing down an appropriate four-dimensional generalization of Pythagoras's theorem. In the case of a static (i.e. non-expanding), flat (i.e. zero curvature) space–time this takes the form

$$(\mathrm{d}s)^2 = (\mathrm{d}x)^2 + (\mathrm{d}y)^2 + (\mathrm{d}z)^2 - c^2(\mathrm{d}t)^2$$

- The distribution of energy and momentum throughout space–time is believed to be uniform on the large scale. This assertion is given precise form by the cosmological principle according to which, on sufficiently large size scales, the Universe is homogeneous and isotropic. Simple cosmological models that are consistent with this principle assume that a gas uniformly fills the Universe. Describing the state of this gas involves specifying its density and pressure, $\rho(t)$ and $p(t)$, both of which are expected to change with time due to the expansion or contraction of the Universe.
- In applying general relativity to cosmology, Einstein introduced a cosmological constant Λ. Thanks to this he was able to formulate a relativistic cosmological model that is neither expanding nor contracting, and in which space has a uniform positive curvature. Later, de Sitter presented a model in which the curvature of space was zero, but there was perpetual expansion.

- The work of Friedmann, Robertson and Walker resulted in the specification of the class of cosmological models that are consistent with general relativity and with the cosmological principle. These models involve a curvature parameter k, that characterizes the geometry of space, and a scale factor $R(t)$ that describes the expansion or contraction of space. The full range of FRW models includes cases that are closed, critical, open and accelerating. The Einstein model arises as a special case, and the de Sitter model as a limiting case.
- The behaviour of the scale factor in a pressure-free universe is determined by the Friedmann equation, and depends on the values of k, Λ and the density ρ at some particular time.

Key parameters of the Universe

- The FRW models provide a natural interpretation of the redshifts of distant galaxies as cosmological redshifts caused by the stretching of light waves while they move through an expanding space.
- The Hubble parameter, $H(t)$, provides a measure of the rate of expansion of space in any FRW model. It is defined by $H(t) = \dot{R}/R$, where $\dot{R}$ denotes the rate of change of R. Observations of distant galaxies are predicted to show that, to a first approximation, $d = cz/H_0$, where H_0 represents the value of the Hubble parameter at the time of observation.
- The deceleration parameter, $q(t)$, provides a measure of the rate of decrease of the rate of cosmic expansion in an FRW model. It is defined by $q(t) = -R\ddot{R}/\dot{R}^2$, where $\ddot{R}$ denotes the rate of change of $\dot{R}$. Observations of very distant galaxies are predicted to show systematic deviations from Hubble's law described by

  $$d = (cz/H_0)[1 + (1 - q_0)z/2]$$

  where q_0 represents the value of the deceleration parameter at the time of observation.
- The density parameters Ω_m and Ω_Λ provide a useful means of representing the cosmic matter density and the density associated with the cosmological constant at any time. The parameters are defined by $\Omega_\mathrm{m} = \rho/\rho_\mathrm{crit}$ and $\Omega_\Lambda = \rho_\Lambda/\rho_\mathrm{crit}$ respectively, where ρ is the cosmic matter density at the time of observation, $\rho_\Lambda = \Lambda c^2/8\pi G$ is a 'density' associated with the cosmological constant, and $\rho_\mathrm{crit} = 3H^2(t)/8\pi G$ is the density that the critical universe would have at the time of observation. The quantity $\rho_\Lambda c^2$ can be thought of as the density of dark energy: possibly a 'vacuum energy' associated with empty space. In a Universe with a flat space (i.e. $k = 0$), the Friedmann equation implies that $\Omega_\mathrm{m} + \Omega_\Lambda = 1$ at all times.
- The age of the Universe, t_0, may be conveniently expressed in terms of the Hubble time, $1/H_0$ in any FRW model. In the case of the critical model $t_0 = 2/3H_0$. In other models t_0 may be a different fraction of the Hubble time, depending on the values of Ω_m and Ω_Λ. Increasing the value of Ω_Λ increases the age of the universe for a given value of the Hubble constant.
- The various cosmological parameters are not all independent. The Friedmann equation implies that $\Omega_\mathrm{m} + \Omega_\Lambda - 1 = kc^2/(R^2H^2)$, and it may also be shown that $q = (\Omega_\mathrm{m}/2) - \Omega_\Lambda$.

Questions

QUESTION 5.11

A number of important events in the history of cosmology have been mentioned in this chapter. Compile a chronological listing of these events, starting with the publication of Einstein's theory of general relativity in 1916.

QUESTION 5.12

List the assumptions that underpin the Friedmann–Robertson–Walker models and the Friedmann equation.

QUESTION 5.13

Describe some of the possible consequences of positive curvature in a three-dimensional space, in the context of the FRW models.

QUESTION 5.14

The detailed argument given in Section 5.4.1 showed that the behaviour described by Hubble's law is an expected consequence of expansion in a FRW model. However, in Section 5.4.2 it was stated that this argument was only approximately true because it ignored the acceleration or deceleration of the expansion. Carefully reread the argument in Section 5.4.1 and identify the key step at which acceleration is ignored.

QUESTION 5.15

List the values that have been assigned to all the observational parameters mentioned in Section 5.4. Where a quantity is expressed in more than one unit system, confirm the equivalence of all the given values.

CHAPTER 6
BIG BANG COSMOLOGY – THE EVOLVING UNIVERSE

6.1 Introduction

In Chapter 5 we saw how general relativity can be used to construct models of the Universe. These models describe how the scale factor varies in a Universe that is filled with a smooth distribution of matter and radiation, but say very little about the properties and behaviour of these components. So, for instance, they do not account for the consequences of microscopic processes such as the interactions between the particles that make up the matter within the Universe.

However, such interactions play an important role in cosmology. One example that we shall see later in this chapter is that cosmological theories can offer an explanation for the observation that most of the stars in the Universe have a composition that is approximately 75% hydrogen and 25% helium (by mass). A fundamental aspect of the process that forms helium is that it involves reactions between nuclei and particles at an early stage in the history of the Universe. Thus physical processes on small scales *must* be taken into consideration in order to develop an understanding of the evolution of the Universe. This chapter starts by examining the conditions under which particles interacted in the early Universe (Section 6.2). The main focus, however, is to follow a chronological sequence from very early times in the history of the Universe (Section 6.3) through the formation of the first nuclei (Section 6.4) and the first neutral atoms (Section 6.5) to the stage at which gravitational clustering gives rise to the large-scale structure that we observe in the present-day Universe (Section 6.6).

At first sight, it might seem impossible to use the models in Chapter 5 to make any predictions about the small-scale behaviour of matter. Cosmological models describe how the scale factor varies with time, but at the present time any change in the scale factor certainly does not have any effect on, for instance, the atoms that make up your body. However one of the major assumptions made in Chapter 5 was that the matter in the Universe is smoothly distributed. This assumption of a uniform distribution of matter is a key to linking the large-scale dynamical behaviour of the Universe to small-scale effects.

To see why this is so, consider a volume of the Universe that, at some particular time, is bounded by an imaginary cube, as shown in Figure 6.1. Let us further suppose that we want to follow the evolution of the matter within this cube at all times using some particular Friedmann–Robertson–Walker model with scale factor $R(t)$. To do this, the edges of the cube must follow the expansion (or contraction) of the model universe.

■ Each edge of the cube has an associated length l. How must the length of each edge change with time if the cube is to follow the expansion or contraction of the model universe?

❑ The length of each edge of the cube must be proportional to the scale factor, i.e. $l \propto R(t)$.

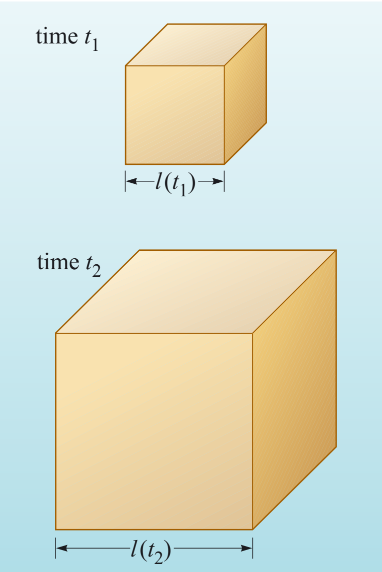

Figure 6.1 An imaginary cubic volume (with sides of length l) that evolves with the expansion of a model universe such that the mass within the volume is constant. Any volume that behaves in this way, whatever its shape, is called a co-moving volume.

Thus the volume ($= l^3$) of the cube at any time t is proportional to $R(t) \times R(t) \times R(t) = (R(t))^3$. This is illustrated by the change in volume shown in Figure 6.1. Although we have chosen to discuss a cubic volume here, a volume of *any* shape that follows the expansion (or contraction) of such a model universe will have a volume $V \propto (R(t))^3$. Such a volume is called a **co-moving volume**.

Because the volume V of a co-moving region, such as the cube, changes as the scale factor changes, but the mass M within it is constant, the density of matter within the co-moving volume, which we denote by ρ_m, also varies with scale factor. In fact,

$$\rho_m = \frac{M}{V} \propto \frac{1}{(R(t))^3} \tag{6.1}$$

Now, the density of matter is an important physical parameter in determining how interactions between particles progress on a microscopic scale. For example, the rate at which molecules in a sample of gas collide with one another increases as the density of the gas is increased. Thus, the large-scale behaviour *is* related to small-scale effects.

This still may not appear to be a great help in understanding the real Universe as opposed to a cosmological model, since we know that the matter in the Universe at the present time does not have a uniform density. Specifically, we saw in Chapter 4 that the distribution of matter is homogeneous only when we consider scales greater than about 200 Mpc: if we look at the Universe on smaller scales, we see large density variations. Thus the average density of the matter in the Universe would seem to be a quantity of limited practical use. However, we shall see later that there is good evidence that at times in the distant past the matter in the Universe was much more smoothly distributed than it is at present – even on relatively small scales. At such times, the average density *does* relate to the small-scale behaviour of matter.

The relationship between density and scale factor that is described by Equation 6.1 holds true for any of the cosmological models described in Chapter 5. The majority of these models are characterized by a scale factor $R = 0$ at time $t = 0$. As was noted in Section 5.3.5 the early expansion phase of any such model is referred to as the *big bang*. Current cosmological evidence strongly favours a model of the Universe that went through a big bang phase – and for the remainder of this chapter we shall only consider big bang models. An immediate consequence that can be noted from Equation 6.1, is that in a big bang model, early stages in the history of the Universe (when $R(t)$ was very small) are characterized by high densities. You may also have noticed that, strictly speaking, the mathematical relationship $\rho_m \propto 1/R^3$ implies an infinite density when $R = 0$. We shall return to consider the significance of such infinite quantities later.

Finally, we should make a brief note about terminology: much of the discussion of this chapter refers to specific times in the history of the Universe. A convention that we adopt throughout the chapter is that the age of the Universe is denoted by t (so, for instance, $t = 1$ s denotes the time at which the Universe was 1 second old). The time now, at which we observe the Universe, is referred to as t_0. So, t_0 represents the current value of the age of the Universe.

6.2 The thermal history of the Universe

A key physical parameter in particle interactions is temperature. It may seem to make no sense to talk of the 'temperature' of the Universe. The temperature of matter seems to range from a few degrees above absolute zero within giant molecular clouds, up to temperatures of over 10^7 K that are found in extreme astrophysical environments. However, we will see shortly that there *is* a cosmic temperature; it does not refer to temperature of the *matter* within the Universe, but to the *radiation* that pervades the Universe. This radiation, which is observable today as the cosmic microwave background (CMB), plays an extremely important role in modern cosmology. We shall discuss several aspects of the CMB in this, and in the following chapter, but in this section we shall consider how the existence of this background radiation in an expanding Universe allows us to determine how temperature has changed over cosmic history. The starting point for this discussion is to consider the cosmic microwave background in a little more detail.

6.2.1 The temperature of the background radiation

In Section 5.2.2 you saw that the most significant contribution to the radiation content of the Universe is the cosmic microwave background radiation. The spectral flux density of the CMB peaks at a wavelength of about 1 mm – this is illustrated in the spectrum of the background radiation that is shown in Figure 6.2. The form of this spectrum is highly significant: it is, to a very good approximation, a black-body spectrum – implying it can be associated with a particular temperature.

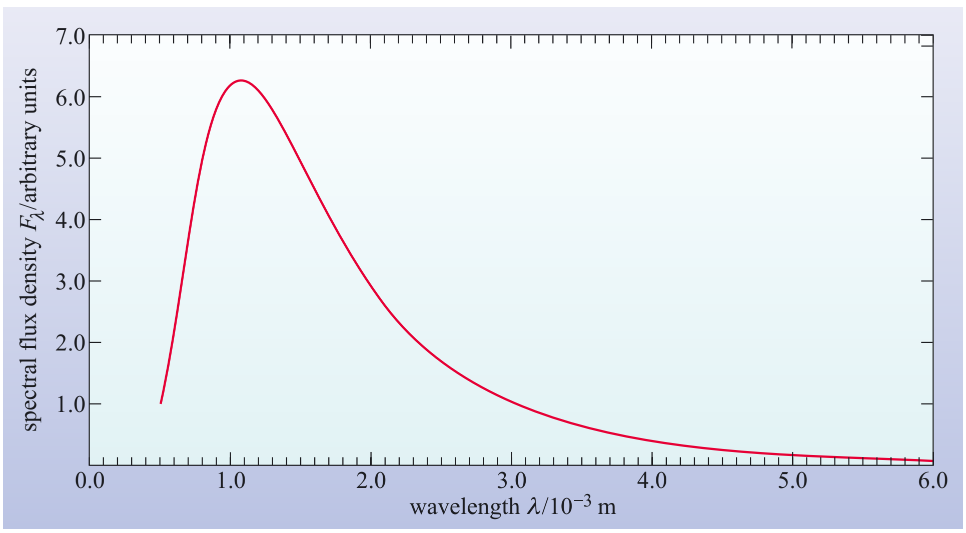

Figure 6.2 The spectrum of the cosmic microwave background. (Note that this spectrum shows the spectral flux density F_λ.)

The characteristic temperature T indicated by any given black-body spectrum is related to the wavelength λ_{peak} at which the spectral flux density (F_λ) is a maximum. According to Wien's displacement law,

$$(\lambda_{\text{peak}}/\text{m}) = \frac{2.90 \times 10^{-3}}{(T/\text{K})} \tag{6.2}$$

- Calculate the characteristic temperature of the cosmic microwave background radiation.

- Rearranging Equation 6.2

$$(T/\mathrm{K}) = \frac{2.90 \times 10^{-3}}{(\lambda_{\mathrm{peak}}/\mathrm{m})}$$

and using $\lambda_{\mathrm{peak}} \approx 1\ \mathrm{mm} = 1 \times 10^{-3}\ \mathrm{m}$

$$(T/\mathrm{K}) = \frac{2.90 \times 10^{-3}}{(1 \times 10^{-3})} = 2.90$$

So, to one significant figure, the temperature of the cosmic microwave background radiation is 3 K.

Detailed spectral measurements have been used to determine the temperature of the cosmic microwave background to a high degree of accuracy, with a value of $T = 2.725 \pm 0.002\ \mathrm{K}$ being widely accepted.

The fact that the CMB follows a black-body spectrum is, at first sight, puzzling. Black-body spectra are formed when photons are continually absorbed and re-emitted by matter. However, matter in the nearby Universe is transparent to cosmic microwave background photons. Thus there is no interaction between matter and photons, and so nearby matter could not give rise to the observed black-body spectrum. So, if the CMB did form by the interaction of radiation and matter – how could this have occurred? To answer this question we have to consider the effect of the expansion of the Universe on the photons of the cosmic microwave background.

6.2.2 The evolution of the temperature of background radiation

A clue to the origin of the microwave background lies in an effect that was introduced in Chapter 5 – the cosmological red-shift of photons. In Section 5.4.1 you saw that the effect of the expansion of the Universe on a single photon was to increase its wavelength. The relationship between the wavelength λ_0 of a photon that is observed now (when the scale factor has the value $R(t_0)$) and the wavelength λ that the photon had when the scale factor was $R(t)$ is

$$\frac{\lambda}{\lambda_0} = \frac{R(t)}{R(t_0)} \tag{6.3}$$

Thus, when the scale factor was smaller than it is at present, the wavelengths of photons that are now seen in the cosmic microwave background were all correspondingly smaller. In fact, the background radiation that is now observed as the cosmic *microwave* background, would, when the scale factor was much smaller, have had a peak in another part of the electromagnetic spectrum. For this reason we shall use the term **cosmic background radiation** to denote this radiation at any time in cosmic history. The cosmic microwave background is just the observable form of the cosmic background radiation at the present time.

■ If a microwave background photon currently has $\lambda = 1$ mm, what wavelength would it have had when the scale factor was 1000 times smaller than its present-day value? In which part of the electromagnetic spectrum does this wavelength lie?

❑ Using Equation 6.3, with values of $\lambda_0 = 1$ mm and $R(t)/R(t_0) = 1/1000$ gives

$$\lambda = 10^{-3}\,\text{m}/1000 = 10^{-6}\,\text{m}$$

So when the scale factor was 1000 times smaller than at present, photons that are currently at the peak of the cosmic microwave background had a wavelength of 10^{-6} m, which lies in the infrared part of the spectrum.

Thus, at high redshift, the wavelengths of photons in the cosmic background radiation would have been much shorter than at present, and consequently interactions between photons and matter would have been much more likely. However, before discussing this interaction, we need to consider the form of the red-shifted spectrum in a little more detail.

An important feature of the black-body spectrum is that if the photons that make up such a spectrum are all red-shifted by the same amount, then it will remain a black-body spectrum. Photons that are currently at the wavelength at which the spectrum has a peak, will always be at the peak, but the wavelength of that peak will change. The way in which this wavelength, λ_{peak}, changes with scale factor is given by Equation 6.3. $R(t_0)$ and λ_0 are the current values of $R(t)$ and λ respectively, and so can be considered as constants in Equation 6.3. Thus Equation 6.3 can be written as

$$\lambda_{\text{peak}} \propto R(t) \tag{6.4}$$

However, the temperature of a black-body spectrum is related to the wavelength of the peak of emission by Wien's displacement law (Equation 6.2) which can be rearranged and expressed as

$$T \propto \frac{1}{\lambda_{\text{peak}}} \tag{6.5}$$

Using the relationship between λ_{peak} and the scale factor (Equation 6.4) gives

$$T \propto \frac{1}{R(t)} \tag{6.6}$$

The temperature of the cosmic background radiation at any time is inversely proportional to the scale factor at that time.

This relationship is important because, in principle, it allows us to calculate the temperature of the background radiation at any given epoch for any cosmological model. Remember from Chapter 5 that different cosmological models provide different relationships for the scale factor R as a function of time (see, for example, Figure 5.23).

Even if we do not know the exact way in which the scale factor varies with time, Equation 6.6 shows that if the scale factor was once much smaller than it is at present, then the temperature of the background radiation at that time would have been much higher than it is at present.

- Use Equation 6.6 to express the ratio of the temperature at two times (t_1 and t_2) in terms of the scale factor at those two times.
- Equation 6.6 can be expressed as

$$T(t) = \frac{\text{constant}}{R(t)}$$

So for times t_1 and t_2 we can write

$$T(t_1) = \frac{\text{constant}}{R(t_1)} \quad \text{and} \quad T(t_2) = \frac{\text{constant}}{R(t_2)}$$

respectively. Dividing the first of these equations by the second gives

$$\frac{T(t_1)}{T(t_2)} = \frac{R(t_2)}{R(t_1)}$$

There is, however, a problem in applying Equation 6.6 which is highlighted by the following question.

- What is the predicted temperature of the Universe if the scale factor has a value of zero?
- Since $T \propto 1/R(t)$, if $R = 0$, the predicted temperature would be infinite!

A prediction of an infinite value of any physical quantity is treated with great suspicion by most physicists. Rather than taking this infinite value at face value, it is assumed that our understanding of physical processes is incomplete. The limits at which our knowledge of physical laws break down will be discussed briefly in Section 6.3 and taken up again in Chapter 8. However, for the present discussion, the important point is that at times when the scale factor was very small, the temperature would have been very high.

EXAMPLE 6.1

For the Lemaître cosmological model (in which $\Lambda > \Lambda_E$) and $k = +1$, use Figure 5.23 and Equation 6.6, to sketch a corresponding curve $T(t)$ that shows approximately how the temperature of the cosmic background radiation varies with time.

SOLUTION

The curve that shows how the scale factor R varies with time in the Lemaître cosmological model is shown in Figure 5.23 and is reproduced here as Figure 6.3a.

In order to draw a sketch of how the temperature T varies with time, we need to make use of the relationship between the temperature and the scale factor. This relationship is given by Equation 6.6, $T \propto 1/R(t)$.

The question asks for a *sketch* of how T varies with time. The implication of this is that the curve that shows $T(t)$ does not have to be exact, but that it should show the most important features of how the temperature varies with time. A way of doing this is to consider a few times (labelled A, B, C and D) on the corresponding curve of $R(t)$ as shown in Figure 6.3a. At each time, we shall use Equation 6.6 to deduce how T is behaving and use this information to help us draw a sketch of $T(t)$. The deductions that can be made about T at these times are shown in Table 6.1.

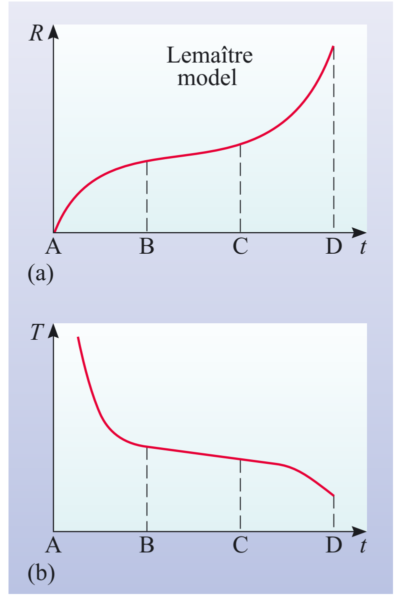

Figure 6.3 (a) Scale factor, and (b) temperature as functions of time for the Lemaître cosmological model. A, B, C and D are times that are referred to in Table 6.1.

Table 6.1 The behaviour of the scale factor R at various times indicated on Figure 6.3a and the inferred behaviour of the temperature T at those times.

Time	Behaviour of R at this time	Behaviour of T at this time
A	$R = 0$	$T = 1/R = \infty$
B	R has increased to some value and now does not vary much with time	T must decrease to some value and also only change slowly with time
C	R has a value that is slightly higher than that at B	T must have a value that is slightly lower than that at B
D	R is increasing to very high values	T must decrease to very low values

We can now use the deductions about the way in which T varies at these times to draw a sketch. Starting with time A, we clearly cannot plot an infinite temperature at A, so we simply show T as having a very high value as we approach $t = 0$. At time B, we simply choose a finite value of temperature, and note that the temperature at time C is slightly lower than at B. Finally, at time D, the temperature decreases to very low values. These points are shown on Figure 6.3b, and the final stage is to draw a smooth curve through these points to complete the sketch.

QUESTION 6.1

For all the Friedmann–Robertson–Walker models with $k = 0$, shown in Figure 5.23, use Equation 6.6 to draw a corresponding curve $T(t)$ that shows approximately how the temperature of the cosmic background radiation would vary with time.

The answer to Question 6.1 illustrates the point that in any big bang model (i.e. one that has $R = 0$ at $t = 0$) the temperature of the cosmic background radiation would have been very high in its early stages. Such a scenario is often referred to as the **hot big bang**.

The change in wavelength of the cosmic microwave background has a profound effect on the way in which photons interact with matter. At times when the temperature of the cosmic background radiation was very high, the typical photon energy would have been greater than the ionization energy of the hydrogen atom. Under these conditions, the baryonic matter in the Universe would have been in the form of a plasma.

The *opacity* of a medium is a measure of the extent to which the medium is opaque to radiation.

- What is the qualitative difference between the opacity of a plasma and that of an un-ionized gas?
- A plasma tends to have a much higher opacity than an un-ionized gas, i.e. un-ionized gases tend to be much more transparent than plasmas.

The reason for the dramatic difference in opacity between a plasma and an un-ionized gas is the presence of free electrons in the plasma. Photons interact with a plasma primarily by scattering from the free electrons in the plasma (Figure 6.4 – this process is called *Thomson scattering* after the discoverer of the electron J. J. Thomson). The degree of interaction between photons and electrons in a plasma can be very high, and this offers a clue as to the origin of the near perfect black-body spectrum of the background radiation. The conditions for forming a black-body spectrum are that there must be many collisions between the material that makes up a thermal source and the photons that are radiated by it. So an interpretation of the black-body spectrum of the cosmic microwave background is that it was formed at a time when the Universe consisted of a hot plasma, and so there were many collisions between the photons and the free electrons. As the Universe has expanded, the wavelengths of the photons have increased, and the black-body spectrum has shifted to longer wavelengths. Consequently, the temperature associated with this black-body spectrum has dropped with the expansion of the Universe.

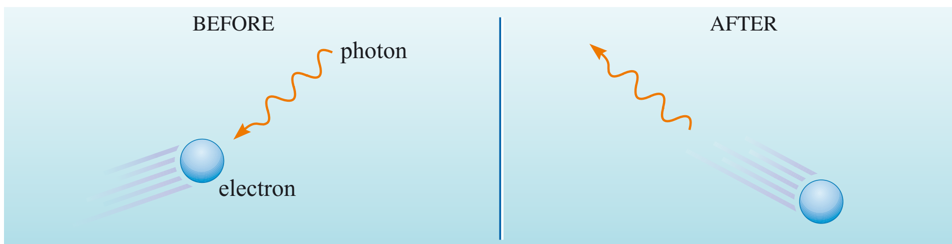

Figure 6.4 The interaction between photons and free electrons in a plasma.

6.2.3 The evolution of energy densities in the Universe

So far, we have only considered one physical property of the cosmic background radiation – its temperature. However, to establish whether this background radiation plays an important role in the evolution of the Universe, it is necessary to consider its *energy density* and how this quantity varies with scale factor.

Recall that in Chapter 5, the behaviour of cosmological models was shown to depend on the density of matter ρ_m, and on the cosmological constant Λ. In the models that we considered there, we simply assumed that electromagnetic radiation was a minor constituent of the Universe. However, we now want to question this assumption – so we must compare the importance of these three components: matter, cosmological constant, and electromagnetic radiation. The physical parameter that determines the importance of any one of these components within a cosmological model is the energy density, i.e. the energy per unit volume due to that component. If the energy density of any one component far exceeds that of the other two, then it is this component that will have the dominant effect on the dynamical behaviour of the Universe.

So, let us now consider the current energy densities due to radiation u_r, matter u_m and the cosmological constant u_Λ.

The energy density of the cosmic microwave background is the total energy of all the microwave background photons per cubic metre of space. Note that the energy density (like the mass density) is defined per cubic metre, i.e. for a physical volume of space that is *not* co-moving. In an expanding universe, the energy density can therefore be expected to decrease as the universe expands.

■ What are the SI units in which energy density should be expressed?

❏ Since the SI unit of energy is the joule, and the unit of volume is m^3, the SI unit of energy density is $\mathrm{J\,m^{-3}}$.

The current energy density of the cosmic background radiation can be found from measurements of the CMB and has a value of $u_{\mathrm{r},0} \approx 5 \times 10^{-14}\,\mathrm{J\,m^{-3}}$. ($u_{\mathrm{r},0}$ is a shorthand way of writing $u_\mathrm{r}(t_0)$ – the value of u_r at the present time.)

The energy density of matter $u_{\mathrm{m},0}$ can be found from density of matter in a straightforward way as the following question illustrates.

QUESTION 6.2

The current average *mass density* of all matter, both luminous and dark, is estimated to be about $\rho_{\mathrm{m},0} \approx 3 \times 10^{-27}\,\mathrm{kg\,m^{-3}}$. By using the equivalence between energy E and mass m given by $E = mc^2$, calculate the current average *energy density* due to matter.

The answer to Question 6.2 shows that at the present time, the energy density of matter is $u_{\mathrm{m},0} \approx 3 \times 10^{-10}\,\mathrm{J\,m^{-3}}$. Thus at the present time, the energy density due to matter exceeds the energy density in the cosmic microwave background by a factor of several thousand.

Finally, we consider the energy density due to the cosmological constant. In Chapter 5, it was noted that the cosmological constant Λ has an associated density

$$\rho_\Lambda = \Lambda c^2/8\pi G \tag{6.7}$$

■ Give an expression for the *energy* density (u_Λ) of the vacuum in terms of Λ.

❏ The energy density of the vacuum is obtained by multiplying Equation 6.7 by c^2,

$$u_\Lambda = \rho_\Lambda\, c^2$$

and so

$$u_\Lambda = \Lambda c^4/8\pi G \tag{6.8}$$

As was noted in Chapter 5, the energy that may be associated with the cosmological constant is often referred to as *dark energy*. Consequently the quantity u_Λ can be interpreted as the energy density of dark energy. The nature of this dark energy is a mystery, but recent observations imply that u_Λ has a value of about $9 \times 10^{-10}\,\mathrm{J\,m^{-3}}$. So, rather surprisingly, dark energy makes the dominant contribution to the total energy density of the Universe at the present time.

It might seem then that the cosmic background radiation is an insignificant component of the total energy density of the Universe. However, this was not always the case. To see why, it is necessary to compare the way in which the three energy densities u_r, u_m and u_Λ change with scale factor.

We start with the simplest case of the three, which is the energy density of the dark energy. By inspecting the terms on the right-hand side of Equation 6.8 we can see that this energy density depends only on values of physical constants (c, G and Λ). Thus, this energy density does not change with scale factor. As noted above, u_Λ currently has a value of about $9 \times 10^{-10}\,\mathrm{J\,m^{-3}}$, and this value has been constant throughout the history of the Universe (with perhaps one brief, but important, exception that we shall discuss later). However, the fact that u_Λ is constant and relatively large, does not mean that it has always been the most important factor in determining how the Universe evolves.

Next, let's consider the how the energy density due to matter changes with scale factor. This is found from the (normal) density of matter.

- For a cosmological model in which matter is uniformly distributed, write down an equation that describes how the density of matter changes with scale factor.

- We have already seen that the density of matter $\rho_m(t)$ varies according to Equation 6.1

$$\rho_m(t) \propto \frac{1}{R(t)^3} \tag{6.1}$$

The energy density of matter is related to the density of matter by $u_m = \rho_m c^2$, but c is a constant, so we can write

$$u_m(t) \propto \frac{1}{R(t)^3} \tag{6.9}$$

The behaviour of the energy density of *radiation* can be analysed by taking a similar approach to that taken when we examined the way in which the density of matter changes with scale factor. The first step is to consider the number of photons per cubic metre, i.e. the *number density* of photons $n(t)$. Assuming that cosmic background photons are neither created nor destroyed during the relevant part of the expansion we can expect that

$$n(t) \propto \frac{1}{R(t)^3} \tag{6.10}$$

So the number density of cosmic background photons behaves in a similar way to the density of matter. But what about the energy density? Here there is a difference. The energy of a photon of frequency f is given by

$$\varepsilon_{ph} = hf \tag{6.11}$$

where h is the Planck constant. The frequency f and wavelength λ of electromagnetic radiation are always related by $f = c/\lambda$, so we can also say

$$\varepsilon_{\mathrm{ph}} = \frac{hc}{\lambda} \tag{6.12}$$

But as the Universe expands (i.e. as $R(t)$ increases) the wavelength of a photon will also increase (Figure 6.5). The photon wavelength is proportional to the scale factor

$$\lambda \propto R(t) \tag{6.13}$$

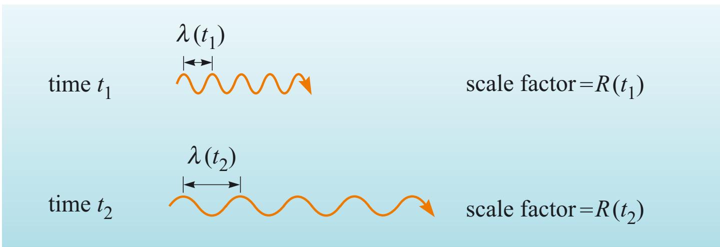

Figure 6.5 As the Universe expands (from scale factor $R(t_1)$ to $R(t_2)$), the wavelength of any photon will increase in proportion to the scale factor.

Hence for each photon in the cosmic background radiation

$$\varepsilon_{\mathrm{ph}} \propto \frac{1}{R(t)} \tag{6.14}$$

Now, the energy density of radiation $u_{\mathrm{r}}(t)$ is given at any time t by

$$u_{\mathrm{r}}(t) = n(t) \times \varepsilon_{\mathrm{ph}}(t) \tag{6.15}$$

It follows that

$$u_{\mathrm{r}}(t) \propto \frac{1}{R(t)^4} \tag{6.16}$$

Comparing this with Equation 6.9 shows that the energy density of radiation behaves differently from the energy density of matter. Specifically, the energy density of radiation is inversely proportional to the *fourth* power of the scale factor, whereas the energy density of matter is inversely proportional to the *third* power of the scale factor.

Figure 6.6 shows how all three energy densities (u_Λ, u_{m}, and u_{r}) vary as a function of scale factor. At the present, the energy densities of the dark energy ($9 \times 10^{-10}\,\mathrm{J\,m^{-3}}$) and of matter ($3 \times 10^{-10}\,\mathrm{J\,m^{-3}}$) are far in excess of the energy density of radiation ($5 \times 10^{-14}\,\mathrm{J\,m^{-3}}$). As we look back to earlier times however, when the value of the scale factor was smaller, we can see that both the energy densities of radiation and of matter were greater in the past than at present. When the value of $R(t)/R(t_0)$ was less than about 0.1, both the energy density of matter and of radiation exceeded the energy density of the dark energy.

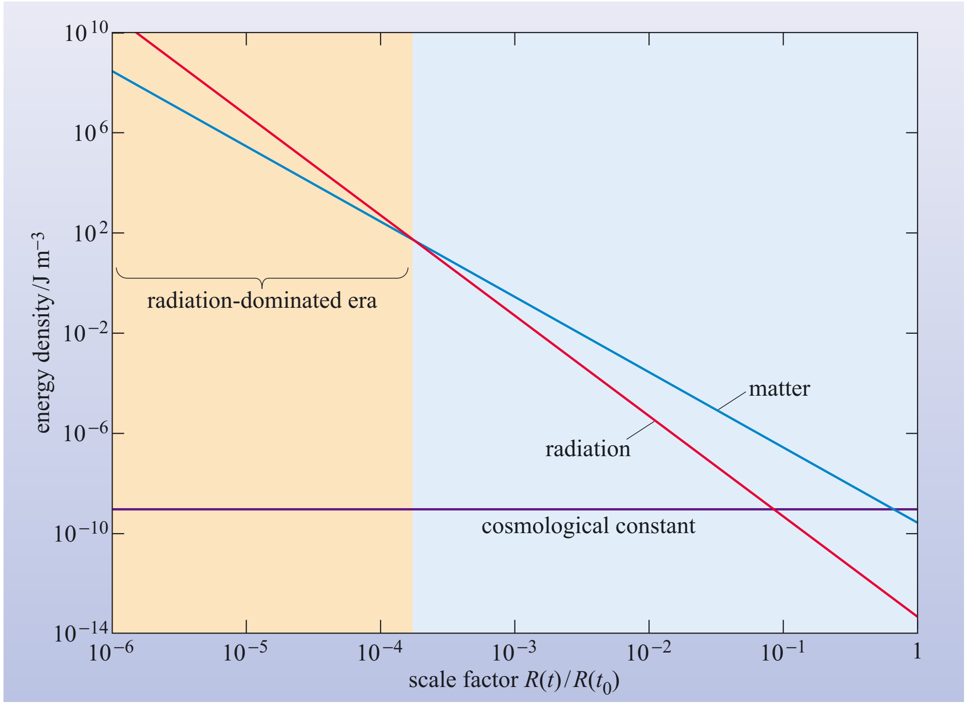

Figure 6.6 The energy densities of matter (blue line) and radiation (red line) as a function of scale factor. At a time when $R(t)/R(t_0) \approx 10^{-4}$ the energy densities of matter and radiation were equal. Prior to this time, the energy density of radiation exceeded that of matter – during this era the dynamical evolution of the Universe was determined by its radiation content. After this time, the energy density of matter was greater, so it was the matter in the Universe that controlled its dynamical evolution. The behaviour of the energy density due to the cosmological constant is also shown (purple line) – this does not vary with redshift and is exceeded by the energy densities in matter and radiation at early times.

Furthermore, as shown in Figure 6.6, the energy density of radiation has declined more rapidly than the energy density of matter. Indeed there was a time when the value of $R(t)/R(t_0)$ was such that these two energy densities were equal. This appears to have occurred when $R(t)/R(t_0) \approx 10^{-4}$. For most plausible cosmological models this corresponds to a time when the age of the Universe was a few times 10^4 years. As we look back to even earlier times, when $R(t)/R(t_0)$ was even smaller, we see that the energy density of radiation exceeded that of matter – this period of the history of the Universe is called the **radiation-dominated era**.

The key points of this discussion so far can be summarized as follows:

1 At the present time, the energy density due to radiation is much lower than the energy density of matter or the energy density of dark energy.

2 As the Universe expanded, the energy density of radiation decreased more rapidly than the energy density of matter. The energy density of dark energy has remained constant with time.

3 At times when the scale factor was less than about 10^{-4} of its current value, the energy density of radiation would have exceeded the energy density due to matter. At this time, the energy density of dark energy would have been negligible in comparison to the energy densities of radiation or matter.

As you will shortly see, the existence of an early radiation-dominated era has a profound effect on the dynamical evolution of the Universe.

At this point you may be wondering how is it that the energy density of matter and radiation change in different ways? The numbers of photons and particles within a co-moving volume remain constant, so this cannot be the origin of the difference. The answer lies in the fact that the energies of photons change with the expansion of the Universe, whereas the masses (and hence energies) of particles such as protons and electrons and of any cold-dark matter particles remain constant.

6.2.4 A radiation-dominated model of the Universe

We have just seen that in the early Universe, the dominant energy density is that due to the radiation within the Universe. The Friedmann equation that was described in Chapter 5 (Box 5.4) can be solved for such conditions and the way in which the scale factor varies with time for such a model is shown in Figure 6.7. One important feature of such a model is that the scale factor varies in the following way:

$$R(t) \propto t^{1/2} \tag{6.17}$$

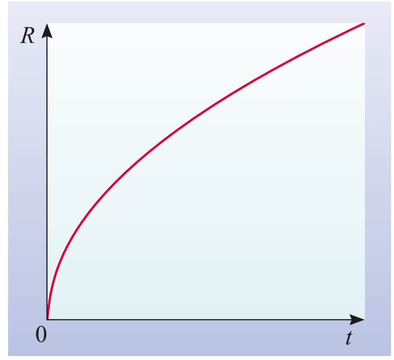

Figure 6.7 The evolution of the scale factor with time in a cosmological model in which the dominant contribution to the energy density arises from the radiation within the Universe (i.e. during the radiation-dominated era).

Because the energy density of radiation is dominant for times when $R(t)/R(t_0) < 10^{-4}$, all cosmological models which start at $t = 0$ with $R(0) = 0$, will go through a phase that is well described by this radiation-dominated model. Thus we are in the rather remarkable position that regardless of which type of cosmological model best describes the Universe at the present, we can be reasonably confident that we know how the scale factor varied with time in the first few tens of thousands of years of the big bang.

However, the temperature of the background radiation varies with scale factor according to $T(t) \propto 1/R(t)$ (Equation 6.6). It follows that during the radiation-dominated era the temperature of the background radiation varies with time according to

$$T(t) \propto t^{-1/2} \tag{6.18}$$

This describes how temperature changes with time in an expanding universe where the energy density of radiation is the dominant component. Of course, to use Equation 6.18 to predict the temperature, it is necessary to know the constant of proportionality between T and $t^{-1/2}$. In fact, this can be derived from the Friedmann equation and Equation 6.18 becomes

$$(T/\mathrm{K}) \approx 1.5 \times 10^{10} \times (t/\mathrm{s})^{-1/2} \tag{6.19}$$

(Note that T is measured in kelvin and t in seconds.) Equation 6.19 is an approximate relationship. As you will see later, other physical processes can change the temperature of the radiation in the real Universe during the radiation-dominated phase of its expansion.

■ What is the temperature when the age of the Universe is one second?

❑ By substituting a value of $t = 1$ s in Equation 6.19 the temperature is 1.5×10^{10} K.

Thus the temperature of the Universe in the first few seconds of the big bang was higher than the highest temperatures that are found in the cores of the most massive stars (where temperatures may reach about 10^9 K). This immediately suggests that nuclear reactions may have occurred in any matter that was present at this time. We will look into such processes in more detail in Section 6.4, but in the next section we will discuss even more extreme conditions: we will consider the processes that occurred when the Universe was less than 1 second old.

QUESTION 6.3

Rearrange Equation 6.19 to find an expression for the age of the Universe for a given temperature. What was the age of the Universe when the temperature was 10^6 K? Express your answer in terms of years.

6.3 The early Universe

We have seen that when considered together, the cosmic microwave background and the expansion of the Universe imply that there was an early phase of the history of the Universe which was characterized by high temperatures and high densities. In particular, the temperature at any time t can be estimated using Equation 6.19. A natural question to ask then is how far back towards $t = 0$ can we go in understanding processes in the Universe? This will be the first major question that we shall consider in this section, and we will find that there is a limit to our knowledge of the evolution of the Universe. The remainder of the section will be concerned with understanding the processes that occurred before the Universe was about 1 second old.

6.3.1 Cosmology and the limits of physical theory

We have seen that the Friedmann equation gives a model for a radiation-dominated Universe that is characterized by the scale factor having a value of zero at the instant of $t = 0$. As we said in Section 6.2.2, the naive interpretation of this is that the Universe came into existence with an infinitely high temperature; the truth of the matter is that we don't really understand the physical processes in the very early Universe. So, how early in the history of the Universe can we be confident that our physical theories really do apply? There are essentially two answers to this question, which reflect two levels of certainty in physical theory. The first approach is to say that theories are only well-tested for the ranges of physical conditions that can be explored by experiments. Thus, we may have a good deal of confidence in describing the Universe at times when the particle energies were similar to the highest values that can be imparted in large accelerator experiments. At present, this limit corresponds to being able to describe physical processes in the Universe that occurred after the temperature fell to below 10^{15} K, which corresponds to a time of $t \sim 10^{-9}$ s.

An alternative approach is to apply physical theories to conditions that never have been, and probably never will be, tested in the Earth-bound laboratory and to look for observable consequences in nature. Clearly, this is a somewhat more speculative approach than having to rely on 'tried-and-tested' physical theory. However, it is one way in which physical theories can be explored and developed, and is a very exciting field for cosmologists.

While it might be expected that physical theories could be extrapolated to describe processes at ever increasing temperatures, it turns out that there is a well recognized limit to our theoretical understanding of the processes of nature. This limit arises because of a surprising incompatibility between the physical theory that is used to describe the interactions of subatomic particles and the theory that describes gravity. The interactions of subatomic particles are described by a branch of quantum physics called the **standard model** of elementary particles. The gravitational interaction is described, as you saw in Chapter 5, by Einstein's general theory of relativity.

The general theory of relativity describes effects that were not explained by Newton's theory of gravity, and as far as the theory can be tested, there have been no observations or measurements to suggest that the theory is incorrect. The standard model of elementary particles is much more amenable to being tested by experiment than is general relativity, and its predictions have been well tested by laboratory measurements. Despite the fact that both theories appear to be sound, it has proven impossible to join them together to form a single consistent theory.

Thus physicists expect that neither general relativity nor the standard model offers a full description of the fundamental interactions of nature, and propose that there must be a unifying 'theory of everything' that is yet to be discovered. In particular, such a theory is needed to describe processes in the very extreme conditions that occurred when the Universe was less than about 10^{-43} s old. This limiting time is called the **Planck time** and represents the limit of how far back in time towards $t = 0$ can be investigated using current physical theory. (The Planck time is $t_{\mathrm{Planck}} = (Gh/2\pi c^5)^{1/2} = 5.38 \times 10^{-44}$ s.)

6.3.2 Conditions and processes in the early Universe

To set the scene for our account of the evolution of the Universe from a time of about 10^{-43} s, it is necessary to review some important physical concepts and processes. A key feature of the early Universe is that the radiation and matter were interacting so much that they were in a state of **thermal equilibrium**. This means the temperature of matter (as defined by the distribution of particle energies) and the temperature of radiation (as defined by the black-body spectrum) were equal.

At the high temperatures that existed in the early Universe, the composition of the Universe, in terms of the particles that were present, was determined by the typical energy that was available in particle interactions. This energy is termed the **interaction energy**, and is related to the temperature by

$$E \sim kT \tag{6.20}$$

where k is the Boltzmann constant ($k = 1.38 \times 10^{-23}\,\mathrm{J\,K^{-1}}$).

(The '~' sign is used to indicate a very approximate relationship. Note also that some books use $E \sim 3kT$, rather than Equation 6.20 given here.)

Note that it is common practice to express the interaction energy in terms of electronvolts (eV) where 1 eV = 1.60×10^{-19} J. The energies involved are usually expressed in MeV (1 MeV = 10^6 eV) or GeV (1 GeV = 10^9 eV).

■ Calculate the interaction energy when the temperature is 10^{14} K. Express your answer in joules and GeV.

❑ The interaction energy is found using Equation 6.20

$$E \sim kT = 1.38 \times 10^{-23}\,\mathrm{J\,K^{-1}} \times 10^{14}\,\mathrm{K} = 1.38 \times 10^{-9}\,\mathrm{J}$$

In terms of GeV

$$E = 1.38 \times 10^{-9}\,\mathrm{J}/(1.60 \times 10^{-19}\,\mathrm{J\,eV^{-1}}) = 8.63 \times 10^{9}\,\mathrm{eV} = 8.63\,\mathrm{GeV}$$

So the interaction energy is 9 GeV (to one significant figure).

The fundamental interactions and their evolution

A key idea in the cosmology of the very early Universe relates to the four *fundamental interactions* of nature: these are gravitational, electromagnetic, weak and strong interactions (see Box 6.1). In the context of the present-day Universe, these interactions seem quite distinct. They operate over quite different ranges – the weak and strong interactions act only over distances that are comparable to the size of an atomic nucleus. Furthermore, the 'strength' of these interactions can be defined in a way that allows sensible comparison. The weakest interaction is gravity, and then in ascending order of 'strength', there follows the weak interaction, the electromagnetic interaction, and appropriately enough, the strong interaction.

BOX 6.1 FOUR FUNDAMENTAL INTERACTIONS

At a fundamental level nature has just four types of interaction. This means that any physical process, for example, the scattering of a photon off an electron, or the generation of electricity in a nuclear power plant, can be analysed in terms of one or more of these four interactions.

The fundamental interactions are:

1. The *gravitational interaction*, which for instance, keeps the Earth in orbit around the Sun. This acts over large distances, so it is part of our everyday experience.
2. The *electromagnetic interaction*, which for instance, keeps electrons bound to atoms. Like the gravitational interaction, this interaction also acts over long distances.
3. The *strong interaction*. This interaction only acts over distances comparable to the diameter of a nucleus. An example of the effect of the strong interaction is the binding of the protons and neutrons together in the nucleus of an atom. The strong interaction overcomes the mutual repulsion that acts between the positively charged protons in a nucleus.
4. The *weak interaction*. This is also a short-range interaction, that acts only on scales comparable to that of the nucleus. An example of the effect of the weak interaction occurs in the transformation of a neutron to a proton in β^--decay.

The standard model of elementary particles explains the operation of the strong, weak and electromagnetic interactions in terms of so-called 'exchange particles' that carry energy and momentum between interacting particles and thereby account for the action of a 'force' in a fundamental way. The exchange particles for the various interactions are as follows:

- The *photon*: the exchange particle of the electromagnetic interaction.
- The *W^+, W^- and Z^0 bosons*: the exchange particles of the weak interaction.
  The masses of these particles are responsible for the short range of the weak interaction.
- The *gluons*: a family of eight similar particles that are responsible for the strong interaction. These particles are confined within the protons or neutrons that comprise a nucleus.

The gravitational interaction is described by the general theory of relativity. Within this theory gravity arises from the curvature of space–time rather than from a particle interaction.

It is suspected that all four interactions may be different manifestations of a single fundamental type of interaction. The reason for such a belief is partly philosophical and partly experimental. The 'philosophical' justification for the unification of interactions is that this type of approach – reducing the physical world to what appears to be the minimum number of particles and processes – has been outstandingly successful, and physicists see this as the next logical advance. If this sounds wildly idealistic, then the 'experimental' justification should offer some

reassurance. A key idea in demonstrating that two interactions are linked is that under certain physical conditions they should behave in the same way. So, for instance, the strength of two interactions may become the same.

Experiments using particle accelerators have revealed that the strength of interactions depends on the interaction energy. In particular, the strengths of the electromagnetic and weak interactions are observed to become closer to one another at high interaction energies. At interaction energies of about 1000 GeV, the strengths of these two interactions are predicted to be the same, and the electromagnetic and weak interactions should appear as different manifestations of a single underlying *electroweak* interaction.

It is believed that the unification of the other interactions occurs at very much higher interaction energies. The unification of the strong interaction with the electroweak interaction – which is termed 'grand unification' is predicted to occur at an interaction energy of about 10^{15} GeV. The theoretical framework that is used to describe this unified interaction is called a **grand unified theory** or **GUT**.

QUESTION 6.4

Calculate the temperature corresponding to the minimum interaction energy required for grand unification. Hence calculate the age of the Universe when the strong and electroweak interactions became distinct.

(It is appropriate to quote the results as order-of-magnitude estimates, i.e. to the nearest whole number power of ten.)

The energy at which the gravitational interaction might become unified with the other interactions, if such a thing happens at all, is expected to be higher still – about 10^{19} GeV. At such extreme interaction energies the gravitational interaction might become important for interactions between particles (at lower energies, the gravitational interaction has a negligible effect on particle interactions). In terms of the evolution of the Universe, an interaction energy of 10^{19} GeV corresponds to the Planck time ($\sim 10^{-43}$ s). As has already been mentioned, there is no accepted 'theory of everything' which allows the processes that occurred in this **Planck era** to be understood.

The interaction energies associated with GUT interactions and the Planck era are extreme – there is probably no environment in the present-day Universe in which particles interact with such energy. Thus, it is unlikely that direct experimental verification will ever be made of theories that describe interactions at such high energies.

The expected behaviour of the fundamental interactions over the first few moments of the history of the Universe can be summarized as follows. Prior to $t \sim 10^{-43}$ s all four fundamental interactions may have been unified. After this time, the gravitational interaction became distinct from the GUT interaction. Some time later, at $t \sim 10^{-36}$ s (see the answer to Question 6.4) the strong interaction and the electroweak interaction became distinct from one another. Finally, at $t \sim 10^{-12}$ s, when the typical interaction was about 1000 GeV, the weak and electromagnetic interactions took on the form in which they act in the present-day Universe. This evolution of the fundamental interactions is illustrated schematically in Figure 6.8.

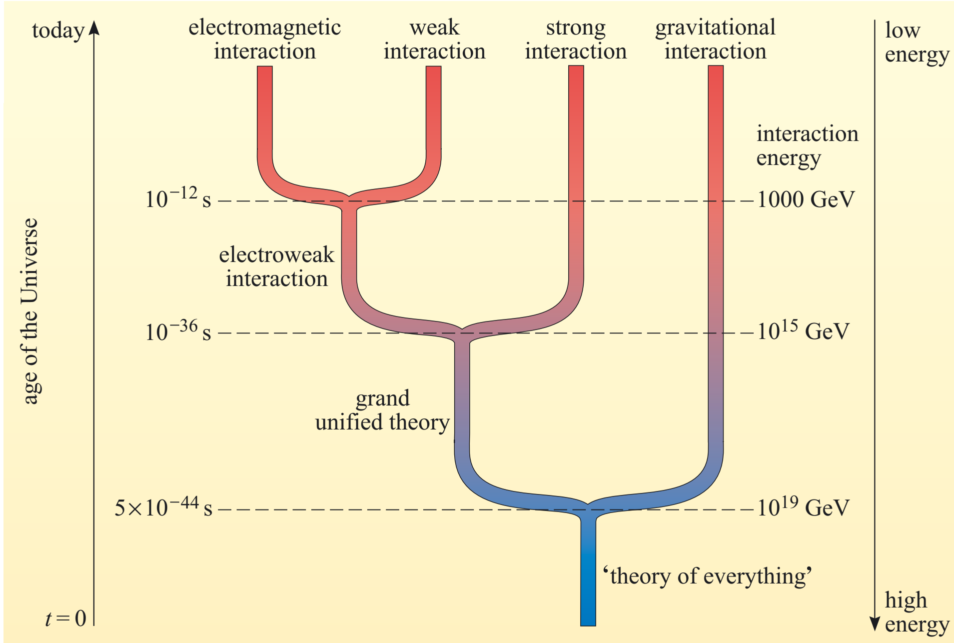

Figure 6.8 The evolution of the fundamental interactions with cosmic time.

Note that the earliest 'branch' shown in this diagram represents the end of the Planck era. The second branch corresponds to the time that grand unification ends – as we shall see later, it is speculated that this change is associated with a dramatic cosmological event, known as *inflation*. The third branch is associated with the separation of the electroweak interaction into the weak and electromagnetic interactions. This is the only one of the three branches that can currently be regarded as experimentally supported; the others are still very speculative.

Particle–antiparticle pair creation

An important process that occurs when interaction energies become very high is that particles and antiparticles can spontaneously form in pairs. This process is known as **pair-creation**, and it has an important effect on the composition of the Universe at early times. Interactions obey a set of conservation rules: the conserved quantities include energy, electric charge, and baryon and lepton numbers (See Box 6.2). The energy available in an interaction plays a vital role in determining which particles may form. Provided that all other conservation rules are obeyed, a particle that has a mass m can be formed if the available energy is equal to or exceeds its *mass energy*, which is given by $E = mc^2$.

For example, when the age of the Universe was 10^{-12} s (i.e. about the time at which electroweak unification ended) the temperature was 10^{16} K and the typical energy of a photon or particle was about 10^3 GeV. Thus any interactions that occurred could easily supply 10^3 GeV to create a new particle. This energy exceeds the mass energy of all of the quarks and the leptons (see Box 6.2). As a result, the material content of the Universe at this time includes all types of lepton and quark and their respective antiparticles.

BOX 6.2 QUARKS AND LEPTONS

The ultimate building blocks of matter are two families of fundamental particles called quarks and leptons. There appear to be six members of each family, as shown in Tables 6.2 and 6.3. Note that for each fundamental particle shown here there exists a corresponding antiparticle with the opposite charge, but the same mass.

Table 6.2 The six quarks.

	Name	Symbol	mass $\times c^2$/GeV
quarks with electric charge of $+2e/3$	up	u	5×10^{-3}
	charm	c	1.5
	top	t	1.8×10^{2}
quarks with electric charge of $-1e/3$	down	d	8×10^{-3}
	strange	s	0.16
	bottom	b	4.25

Table 6.3 The six leptons.

	Name	Symbol	mass $\times c^2$/GeV
leptons with electric charge $-e$	electron	e^-	5.11×10^{-4}
	muon	μ^-	0.106
	tauon	τ^-	1.78
leptons with zero electric charge	electron neutrino	ν_e	$< 1.5 \times 10^{-9}$
	muon neutrino	ν_μ	$< 1.7 \times 10^{-4}$
	tauon neutrino	ν_τ	$< 2.4 \times 10^{-2}$

Quarks are the fundamental particles that make up baryons, such as the proton and the neutron. A proton comprises two up quarks and a down quark, while a neutron comprises two down quarks and an up quark. Quarks are never found in isolation in laboratory experiments – they are always confined in clusters consisting of three quarks or three antiquarks, or in a pair comprising a quark and antiquark. The particles formed by such combinations of quarks are generally termed **hadrons**. A hadron that consists of three quarks is a **baryon**, and a hadron that comprises three antiquarks is an **antibaryon**. A quantity that is conserved in all known particle interactions is the **baryon number** – the baryon number of each quark is 1/3 while that of each antiquark is −1/3. So the baryon number of a baryon is +1, and that of an antibaryon is −1. The baryon number of all other particles is 0.

The family of **leptons** includes the electron (e^-) and two other charged particles: the muon (μ^-) and the tauon (τ^-). The other members of the lepton family are the three types of neutrino – there is one type of neutrino for each of the charged leptons (ν_e, ν_μ, ν_τ). As in the case of quarks, for each type of lepton there exists a corresponding antilepton. Unlike quarks, leptons are not confined and *can* be found in isolation in laboratory experiments.

In interactions that involve leptons, there is a conserved quantity called the **lepton number**. The lepton number of each of the leptons shown in Table 6.3 is +1 and that of each of the antileptons is −1. The lepton number of all other particles is 0.

QUESTION 6.5

Consider the following reaction in which a free neutron decays into a proton, an electron and an electron antineutrino ($\overline{\nu}_e$) (such a reaction is an example of β^--decay).

$$n \rightarrow p + e^- + \overline{\nu}_e$$

(a) What is the baryon number (i) before, and (ii) after this process? Hence show that baryon number is conserved.

(b) What is the lepton number (i) before, and (ii) after this process? Hence show that lepton number is conserved.

(c) What combination of quarks constitutes (i) a neutron, and (ii) a proton? Hence express β^--decay as a reaction involving quarks and leptons only.

The effect of the other conservation rules in determining which particles may be formed in an interaction is profound. Of particular importance are the conserved quantities known as total baryon number and total lepton number (described in Box 6.2). Consider a simple interaction in which two energetic photons interact to form particles

$$\gamma + \gamma \rightarrow \text{‘particles’}$$

- What is (a) the total lepton number of the two photons; (b) the total baryon number of the two photons?

- Photons have a lepton number of zero and a baryon number of zero. Thus (a) the total lepton number of the two photons is zero, and (b) the total baryon number of the two photons is zero.

Since lepton and baryon number are conserved, the two-photon reaction can only form products whose total lepton and baryon number is zero. This does not mean that the lepton and baryon number of each particle that is formed must be zero, but that the *sum* of the lepton and baryon numbers for all the particles that are formed must be zero. For instance, the reaction may result in the production of an electron (lepton number +1) and a positron (an antielectron, lepton number −1)

$$\gamma + \gamma \rightarrow e^+ + e^- \tag{6.21a}$$

Since electrons and positrons have a baryon number of zero, this reaction clearly conserves baryon number.

The pair-creation reaction described by Equation 6.21a is reversible – a positron and an electron can combine to produce two photons according to

$$e^+ + e^- \rightarrow \gamma + \gamma \tag{6.21b}$$

This process, in which a particle and its corresponding antiparticle interact and disappear is called **annihilation**. This process can occur for any particle–antiparticle pair, and the total energy of the photons can be found using the mass energy equivalence relation ($E = mc^2$).

QUESTION 6.6

Calculate the minimum interaction energy required for electron–positron pair production (Equation 6.21a). Express your answer in electronvolts. At what temperature is electron–positron pair production likely to occur?

Note that given sufficiently energetic photons, a two-photon reaction could generate any lepton–antilepton pair. Similarly, a two-photon reaction could generate a quark–antiquark pair

$$\gamma + \gamma \rightarrow \mathrm{q} + \overline{\mathrm{q}} \tag{6.22}$$

(Where the symbol $\overline{\mathrm{q}}$ represents an antiquark.) The photon–photon interaction is just one of many types of interaction that could occur, but without going into detail about these, we can see that the conservation rules will dictate that, provided a sufficiently high interaction energy is available, the Universe will be populated by a mixture of quarks and antiquarks and of leptons and antileptons.

We have concentrated here on quarks and leptons, but there are other particles too that were present in the early Universe. There are two categories of particles that deserve mention. The first are the exchange particles that act to transmit the fundamental interactions of nature (in the parlance of particle physics, these particles 'mediate' the interactions). The most familiar of these is the photon – a massless particle that mediates the electromagnetic interaction. In addition, there are other particles, as described in Box 6.1, that mediate the strong and weak interactions.

From an astronomical point of view, the other important category of particle comprises the massive, stable particle (or particles) that make up dark matter. As has been mentioned, the nature of dark matter is not known, but it is believed to be in the form of particles that are neither baryons or leptons. Presumably, such particles must have been present in the early Universe, but until we have a better idea of what they are, their origin remains a mystery. As far as this chapter is concerned, we shall assume that there are dark matter particles present in the early Universe, but we shall also assume they are essentially non-interacting, so we shall not need to mention them. We will however, consider the role of dark matter at later times – when structure begins to form as a result of gravitational collapse.

Having now reviewed some of the important processes in the early Universe, we can begin a chronological account of the evolution of the Universe. Throughout the following discussion we shall indicate the time t, and the temperature T and interaction energy E at these times (note that in most cases, these are order of magnitude estimates only).

So, let's start at (almost) the very beginning.

6.3.3 The Planck era

$$t < 5 \times 10^{-44}\,\mathrm{s},\ T > 10^{32}\,\mathrm{K},\ E > 10^{19}\,\mathrm{GeV}$$

We have already noted that there is no physical theory to describe processes of the Planck era ($t < 5 \times 10^{-44}$ s). When the age of the Universe was less than the Planck time, it is believed that the fundamental interactions would have had similar strengths, but without a consistent physical theory very little can be predicted about

what would happen at this time. We shall simply assume that the Universe was in an extremely hot and dense state. We shall return to consider these very early times again in Chapter 8 when we look at the way in which theoretical physicists are attempting to develop theories that describe this era.

6.3.4 Inflation and the end of grand unification

$t \sim 10^{-36}$ s, $T \sim 10^{28}$ K, $E \sim 10^{15}$ GeV

When the age of the Universe was about 10^{-36} s, the high-energy conditions under which the strong and electroweak interactions were unified came to an end. After this time, these two types of interaction would become distinct from one another.

Although the typical interaction energies at this time ($\sim 10^{15}$ GeV) are far in excess of laboratory experiments, physicists do have a theoretical framework within which some predictions about this era of cosmic history can be formulated. In fact, it was this approach that, in 1980, resulted in a significant advance in cosmological theory. A theoretical physicist named Alan Guth was tackling a problem which was that as the grand unified era came to an end, it seemed as though a vast number of particles called *magnetic monopoles* should be formed. Such a particle should not decay, and so, if the theory was correct, these magnetic monopoles should be easily detectable in the present-day Universe. The problem was that no such particle had ever been found.

The solution that Guth proposed was quite remarkable. It was based on an analysis of the behaviour of the vacuum. We saw in Chapter 5 that the dark energy may arise from the energy of the vacuum. Although we have no well-developed theory to explain the energy of the vacuum, Guth found that at the end of the grand unified era the vacuum could have had a different, and substantially higher energy density than it does in the present-day Universe. This peculiar state is referred to as the *false vacuum* to distinguish it from the *true vacuum*. This situation would not last for long – in a very short time the energy of the vacuum would drop to the value that it is observed at today – but during that time, something very dramatic would happen.

A high value of the energy density of the vacuum has the same physical effect as a high value of the cosmological constant. (Strictly speaking, the energy density of the false vacuum should not be referred to as being due to a 'cosmological constant' since it is hardly constant!) You saw in Chapter 5 that the cosmological model in which the cosmological constant plays a dominant role is the de Sitter model. The evolution of this model is described by Equation 5.11

$$R \propto e^{Ht} \qquad \text{where } H = \sqrt{\frac{\Lambda c^2}{3}} \tag{5.11}$$

In this model the scale factor undergoes exponential expansion. What Guth proposed was that in a very short interval of time – maybe only lasting from $t \sim 10^{-36}$ to 10^{-34} s – the Universe underwent a period of exponential expansion. During this time the scale factor increased by an enormous amount. The theory was not sufficiently well developed to say by exactly how much the scale factor would have increased, but such a process could have caused the scale factor to increase by a factor of as much as 10^{50} (Figure 6.9). This dramatic episode of expansion is termed **inflation**.

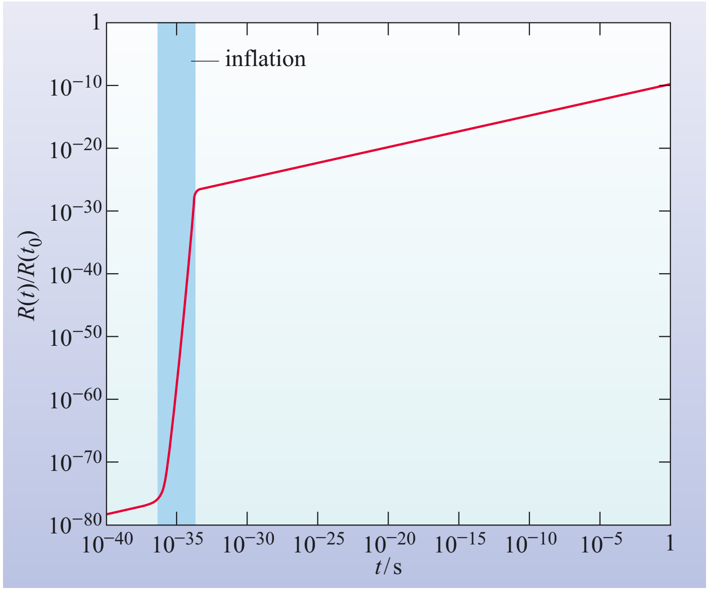

Figure 6.9 The evolution of the scale factor with time including the process of inflation. Note that the numerical values shown here are highly speculative.

So how would inflation solve the monopole problem? Well, the rapid expansion of space during inflation would result in any particles being swept apart from one another. Even if monopoles were abundant prior to inflation, the rapid expansion of space would spread them out so much that there would be a negligible chance of our detecting one in the present-day Universe.

The inflationary scenario has an important consequence for the material content of the Universe. As the period of inflation came to an end, the energy of the vacuum had to drop to the level we see today. So, as the vacuum made a transition to its ‘true vacuum’ state, energy was released and formed particle–antiparticle pairs. According to the inflationary model, the vast majority of particles in the Universe were created from the energy released as inflation came to an end. Thus, the matter now in the Universe may be a product of inflation.

It should be stressed that Guth’s original formulation of the inflationary model should not be considered to be a complete and consistent theory. Rather, it should be viewed as a starting point for exploring a new paradigm in cosmology. In fact, the exact mechanism behind inflation is essentially unknown. In view of this it might seem odd that such prominence is given to the inflationary model until it is appreciated that the *effects* of inflation – regardless of the underlying mechanism – provide solutions to a series of cosmological problems. We shall discuss these problems, and how inflation resolves them, in Chapter 8, but for now we shall simply assume that the process of inflation did occur.

After the process of inflation, the energy released by the false vacuum would have eventually formed all types of quarks and leptons (including their antiparticles). Furthermore, the numbers of quarks and antiquarks would have been almost, but not quite, equal, and a similar condition would have held true for leptons and antileptons. This slight inequality between matter and antimatter in the Universe is thought to have originated in physical processes that occurred at this time. (More will be said about this in Chapter 8.) As we shall shortly see, if this imbalance had not existed, then the present day cosmos would have contained no baryonic matter, and we would not be here to speculate on the origin of the Universe!

Thus, the time at which grand unification came to an end is suspected of playing a major role in the evolution of the Universe. However, from this time at around $t \sim 10^{-34}$ s to the time that the electromagnetic and weak interactions became distinct at $t \sim 10^{-12}$ s, no new physical processes occurred. This interval is often referred to as *the desert*.

6.3.5 The end of electroweak unification

$t \sim 10^{-12}$ s, $T \sim 10^{16}$ K, $E \sim 10^{3}$ GeV

The desert came to an end as electromagnetic and weak interactions became distinct. In contrast to the end of the grand unification, it is not thought that this caused any effects akin to inflation. The constituents of the Universe immediately after this time would have continued to be all types of quark and lepton and their antiparticles. There would also have been photons, and particles that mediate the strong interaction between quarks. However, the temperature was now too low for the creation of W^+, W^- and Z^0 bosons, so the particles that mediate the weak interaction would essentially disappear, thus separating the weak and electromagnetic interactions.

6.3.6 The quark–hadron transition

$t \sim 10^{-5}$ s, $T \sim 10^{12}$ K, $E \sim 1$ GeV

In the present-day Universe, quarks are never seen in isolation – they are always confined within particles called hadrons (see Box 6.2). In the high energy conditions of the early Universe however, quarks were not bound into hadrons; they existed as free individual particles. The existence of free quarks and antiquarks came to an end when the Universe cooled to such an extent that the typical interaction energy was about 200 MeV. At this stage the Universe underwent a phase transition (a process akin to the freezing of water to form ice) in which the quarks became bound into hadrons. This particular phase transition is called the **quark–hadron phase transition**. Although many different types of hadron were formed in this process, there are only two types of hadron that are stable enough to have any long-lasting effect on the composition of the Universe; the proton and the neutron.

The proton (and its antiparticle – the antiproton $\overline{\mathrm{p}}$) is, as far as is known, a stable particle. Both the proton and antiproton can participate in reactions with other particles but, left to themselves, no proton or antiproton has ever been observed to spontaneously decay. The fact that hydrogen exists in copious amounts in the present-day Universe is testament to the stability of the proton. In fact, there is some belief that the proton may decay on very long timescales – but experimental searches for proton decay have shown that its half-life must exceed 10^{33} years. The current age of the Universe is about 1.4×10^{10} years, so as far as this discussion is concerned we can assume the proton to be a stable particle.

Unlike the proton, the neutron (and its antiparticle – the antineutron $\overline{\mathrm{n}}$) is unstable: an isolated neutron will undergo the β^--decay reaction

$$\mathrm{n} \rightarrow \mathrm{p} + \mathrm{e}^- + \overline{\nu}_\mathrm{e} \qquad (6.23)$$

However, the half-life of the neutron is 615 s, and this is a very long time in comparison to the timescale on which the Universe is changing (remember that we are discussing processes that occur within about 10^{-4} s). So to a good approximation, the effect of this decay process can be ignored at this time – and we can say that the neutron is relatively stable.

The mass energies of the proton and the neutron are 938 and 940 MeV respectively. At the time that free quarks became bound into hadrons, the typical interaction energy was too low for proton–antiproton pairs to be produced. Thus, protons and antiprotons would have disappeared from the Universe as they annihilated one another according to the reaction

$$\mathrm{p} + \overline{\mathrm{p}} \rightarrow \gamma + \gamma \tag{6.24}$$

while there would have been no significant counter-conversion of photons into proton–antiproton pairs.

A reaction similar to that shown in Equation 6.24 would also have occurred for neutrons and antineutrons. Prior to this time, baryonic matter was in the form of particles and their antiparticles (either quarks or baryons), but at around this time the majority of such particles annihilated one another. Now we can appreciate the significance of the slight imbalance between matter and antimatter that had been present since the grand unified era. If there had been no imbalance, then at this time, all of the protons would have annihilated with an equal number of antiprotons, and a similar annihilation process would have resulted in the disappearance of all neutrons and antineutrons. The result would have been a Universe that contained no baryonic matter. Within such a Universe there would, of course, be no galaxies, stars, planets or life, so the fact that there was such an imbalance between matter and antimatter was vital to the Universe ending up as we observe it today.

The magnitude of this imbalance between the number of particles and antiparticles is small, but it can be measured from present-day observations. Neither the number of baryons nor the number of photons in a co-moving volume has changed significantly since this time. The present-day ratio of the number of CMB photons to the number of baryons thus provides an estimate of the imbalance between baryons and antibaryons at this time.

At present, there are approximately 10^9 photons in the cosmic microwave background for every stable baryon (proton or neutron) in the Universe.

Thus for every 10^9 baryon–antibaryon annihilation reactions that occurred there would have been one proton or neutron left over.

We have seen that quarks became confined into hadrons and that these hadrons decayed or annihilated one another leaving a residual number of relatively stable protons and neutrons. However, these protons and neutrons were not inert – they could undergo the following reactions that transformed one into the other.

$$\overline{\nu}_\mathrm{e} + \mathrm{p} \rightleftharpoons \mathrm{n} + \mathrm{e}^+ \tag{6.25a}$$

$$\nu_\mathrm{e} + \mathrm{n} \rightleftharpoons \mathrm{e}^- + \mathrm{p} \tag{6.25b}$$

When the age of the Universe was 10^{-2} s, there were large numbers of neutrinos, antineutrinos, electrons and positrons available for such reactions, and the rate of these reactions was high. Consequently the temperature of the neutrinos (as defined by the distribution of their energies) would have been the same as the temperature of the baryonic matter and the temperature of the radiation (as defined by the black-body spectrum).

In the following section (Section 6.4) we shall consider situations in which protons and neutrons participate in fusion reactions. The outcome of these reactions depends on the ratio of the number density of neutrons to the number density of protons (n_n/n_p), and so it is of interest to follow how this ratio varies with time. While the reactions described by Equation 6.25 were occurring, the ratio n_n/n_p depended on the difference in mass energy between these two types of baryon. The proton has a rest mass energy of 938.27 MeV whereas the neutron has a rest mass that is 1.29 MeV greater than this. When the interaction energy was much greater than this difference, i.e. much more than about 1 MeV, then the number densities of protons and neutrons would have been equal. However, once the interaction energy became similar to this energy difference, the number density of neutrons fell below that of protons. At $t = 10^{-2}$ s, when the interaction energy was 10 MeV, the value of $(n_n/n_p) \approx 0.9$, but by $t = 0.1$ s, the typical interaction energy had fallen to 3 MeV and the neutron to proton ratio was $(n_n/n_p) \approx 0.65$.

6.3.7 Neutrino decoupling and electron–positron annihilation

$$t \sim 1\,\text{s},\ T \sim 1.5 \times 10^{10}\,\text{K},\ E \sim 1\,\text{MeV}$$

By the time that the Universe reached an age of 0.7 s, conditions had changed to such an extent that some of the reactions described in Equation 6.25 no longer occurred. In particular, the probability of a neutrino (or antineutrino) interacting with another particle dropped as the density of the Universe decreased. Consequently the reactions shown in Equations 6.25a and 6.25b would only operate from right to left. This was the last occasion on which the bulk of the neutrinos in the Universe underwent any interaction apart from being influenced by gravitational fields. The effective end of the interaction between neutrinos and other particles is termed **neutrino decoupling**. As a result of this, huge numbers of neutrinos, usually referred to as *cosmic neutrinos* started to travel unimpeded through the Universe. They are thought to have been doing so ever since.

Just after neutrino decoupling, when the age of the Universe was about 1 second, the falling temperature of the Universe corresponded to a mean interaction energy of about 1 MeV, which is the energy required for the formation of an electron–positron pair (see Question 6.6). As the temperature fell further, electrons and positrons began to disappear because no new e^+e^- pairs were being created, whereas the annihilation reaction

$$e^+ + e^- \rightarrow \gamma + \gamma \tag{6.21b}$$

was continuing. The number of electrons and positrons decreased in a dramatic fashion. As was the case when baryons annihilated, there was a slight excess of matter over antimatter – a surplus of one electron for every 10^9 or so annihilation events. The number of negatively charged electrons that were left over is believed to be exactly the number to balance the charge of all the positively charged protons that were left over earlier, thus making the matter in the Universe electrically neutral overall.

An important effect of electron–positron annihilation is that energy was released and this would have been rapidly shared-out amongst the photons, baryons and remaining electrons. Because of this release of energy there was a short interval in which the temperature did not decrease as rapidly as Equation 6.19 would predict, and this is one reason why that equation was described as being approximate.

The process of electron–positron annihilation also leads to a prediction about cosmic neutrinos.

- Would the energy that is released by electron–positron annihilation be transferred to the neutrinos?
- No. We have just seen that neutrinos effectively stop interacting with the other constituents of the Universe just before electron–positron annihilation occurs.

So cosmic neutrinos do not gain any energy from the process of electron–positron annihilation. Consequently the temperature of cosmic neutrinos should be slightly lower than that of the background radiation. It is predicted that at the present time the cosmological background of neutrinos should have a temperature of about 1.95 K. Experimental confirmation of this would provide strong evidence that the big bang scenario that is described here is correct, but unfortunately, the detection of such low-energy neutrinos is unfeasible at present.

The disappearance of all of the positrons and most of the electrons further restricted the reactions shown in Equation 6.25 that converted protons into neutrons and vice versa. At the time that these reactions stopped completely, the ratio of the number density of neutrons to the number density of protons had a value of $(n_n/n_p) \approx 0.22$, i.e. for every 100 protons in the Universe there were 22 neutrons.

- There was however one reaction that causes neutrons to transform into protons which did not stop. Which reaction was this, and why didn't it stop?
- The reaction that continues is the β^--decay of the free neutron (Equation 6.23). It did not stop because, unlike the reactions in Equation 6.25 it does not require any other reactant apart from the neutron itself.

Thus, starting from a value of $(n_n/n_p) \approx 0.22$, the number of neutrons started to drop. Unless some new process intervened, the neutrons would have all decayed and we would have a Universe in which the only element that could form would be hydrogen. The way in which this fate was avoided is the next part of our story.

6.4 Nucleosynthesis and the abundance of light elements

$t <$ a few hundred seconds, $T >$ a few $\times\ 10^8$ K, $E >$ a few $\times\ 10^4$ eV

We have already seen that conditions in the early Universe led to a situation, such that at $t \sim 1$ s, the temperature was about 10^{10} K and the baryonic matter in the Universe was in the form of protons and neutrons. At this time the physical conditions became suitable for the onset of nuclear fusion reactions which lead to the formation of nuclides with a higher atomic mass than hydrogen. Such a process is believed to have occurred and is called **primordial nucleosynthesis** – a term that distinguishes it from the processes of stellar nucleosynthesis that create elements within stars.

There are some distinct differences between the nucleosynthetic processes that could have occurred in the early Universe and those which occur within stars.

One difference is that the conditions in the Universe were changing rapidly, as the following question illustrates.

QUESTION 6.7

Find the time t at which the temperature was (a) 10^9 K, and (b) 5×10^8 K.

As the answer to Question 6.7 shows, the temperature of the Universe dropped markedly in the first few hundred seconds after $t = 0$. In order for nuclear fusion reactions to have had a significant effect they must have progressed at a rapid rate, and this would have required temperatures in excess of 5×10^8 K. This is in marked contrast to the conditions in the cores of stars where fusion reactions progress at a relatively leisurely rate in lower temperature conditions.

As time progressed in the early Universe, one nuclear reaction that did not require high temperatures, the β^--decay of free neutrons, was proceeding. However, the presence of a large number of free neutrons highlights another difference between the early Universe and stellar cores – that of composition. As we shall now see, it is the declining number of free neutrons that plays an important role in determining how many nuclei can be formed before fusion reactions become ineffective at a temperature of about 5×10^8 K.

6.4.1 The formation and survival of deuterium

The first fusion reaction that could occur was that between a proton and a neutron to form a nucleus of deuterium (which is referred to as a **deuteron**). This is the neutron capture reaction:

$$\mathrm{p} + \mathrm{n} \rightleftharpoons {}^2_1\mathrm{H} + \gamma \tag{6.26}$$

Note that this is a reversible reaction: the deuteron can be broken apart by γ-rays in a process called **photodisintegration**. In order to cause the photodisintegration of a deuteron, an incident photon must have an energy that exceeds 2.23 MeV. Although at $t = 1$ s the average interaction energy is less than this, there were so many photons in comparison to the number of baryons, that there was a sufficient number of photons with energies greater than 2.23 MeV (i.e. well above the average value) to rapidly destroy any deuterium that formed. However, as the Universe continued to expand and cool, the average photon energy decreased. This decrease allowed deuterium to survive from about $t = 3$ minutes onwards.

To investigate this in more detail we need to know, for a given volume and at a given time (or temperature), what fraction of the photons have sufficiently high energy to cause the photodisintegration of deuterium. A quantity called the **photon energy distribution function** tells us this; it is defined as the fraction of the total number of protons that lie within a narrow energy range, divided by the width of that range. This definition may sound similar to the definition of the spectral flux density (F_λ) – and indeed there is a straightforward mathematical relationship between the two. As in the case of the spectral flux density, the photon energy distribution of a black-body source is a smooth function that has a peak value that depends on temperature.

Figure 6.10a shows the photon energy distribution expected over a range of temperatures in the early Universe. In all cases, of course, the photon energies follow a black-body distribution.

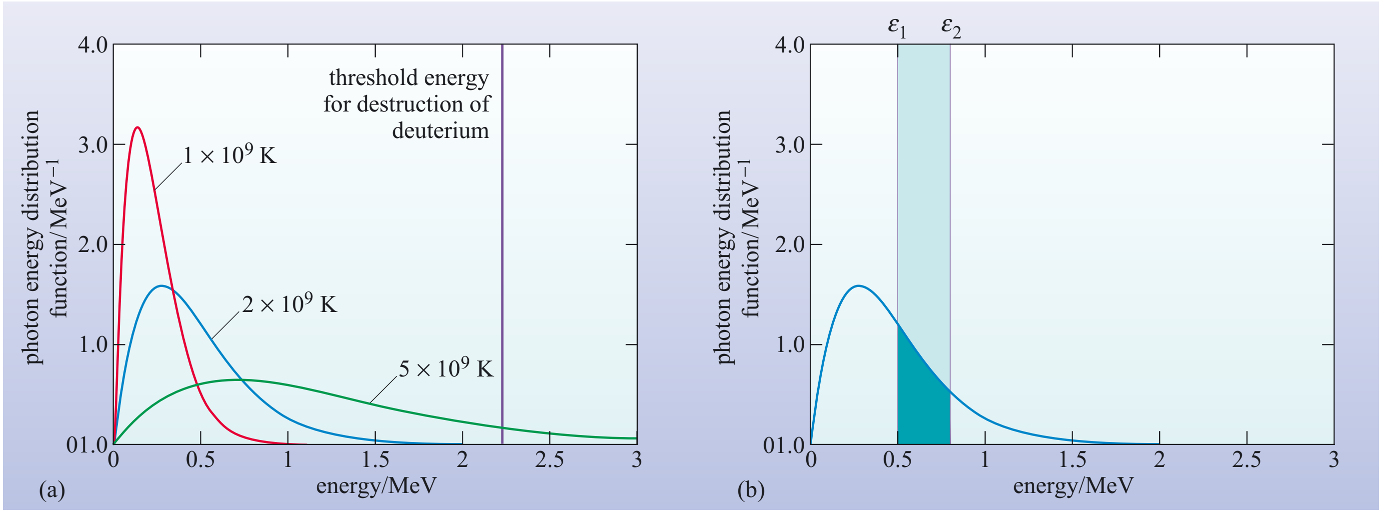

Figure 6.10 (a) Photon energy distributions at various temperatures. (b) The area under the curve of the photon energy distribution and between two energies, indicates the fraction of photons with energies in that range.

- By inspection of Figure 6.10a state qualitatively how the energy at peak of the photon energy distribution of a black-body source varies with temperature.
- The peak energy of the photon energy distribution of a black-body source decreases as the temperature decreases.

The key feature to note about the energy distribution function is that it indicates the fraction of photons that have energies in a certain range. The fraction of photons with an energy between ε_1 and ε_2 is given by the area under the curve between these two limits as shown by the shaded area in Figure 6.10b. Note that the units of the photon energy distribution function are 'per unit energy interval', i.e. $(\text{MeV})^{-1}$. Thus the area under the curve has units which are given by $(\text{MeV}) \times (\text{MeV})^{-1}$: it has no units, as would be expected for a quantity that represents the fraction of photons.

Returning now to the question of the destruction of deuterium, we know that the ratio of photons to baryons is about 10^9. Thus, if the photon energy distribution were such that more than about 1 in 10^9 photons had an energy greater than 2.23 MeV, then there would have been a sufficient number of energetic photons to destroy any deuterons that may have formed.

Conversely, we can say that deuterons only began to survive once the temperature was such that the fraction of photons with energies greater than 2.23 MeV became less than 10^{-9}. Figure 6.11 shows how this fraction varies with temperature.

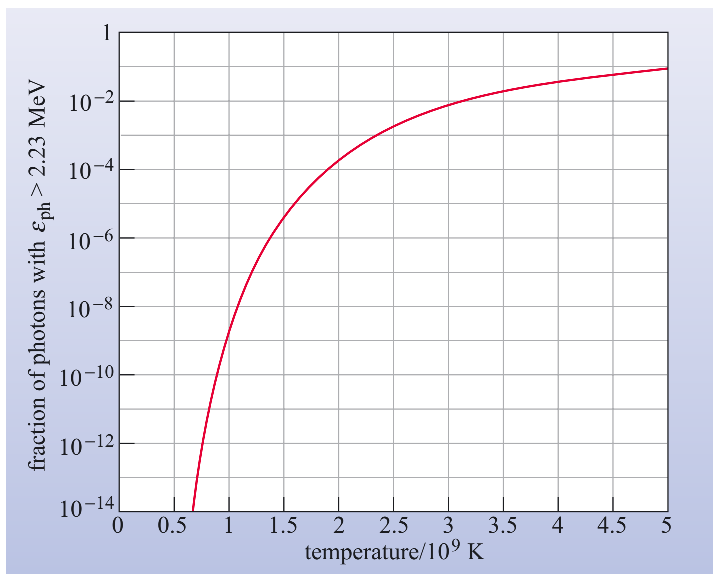

Figure 6.11 The variation with temperature of the fraction of photons with energies greater than 2.23 MeV in a black-body distribution of photon energies.

- From Figure 6.11 estimate the lowest temperature at which deuterium can survive, i.e. at which it does not undergo photodisintegration.
- From Figure 6.11 the temperature at which this fraction is 10^{-9} is 1.0×10^9 K.

Thus significant quantities of deuterium started to build up only after the temperature dropped below about 1.0×10^9 K. This temperature was reached when the age of the Universe was about 200 s (see answer to Question 6.7(a)).

It is interesting to compare the mean photon energy of a the black-body distribution with the energy required for the photodisintegration of deuterons. For a black-body distribution of photons, the mean photon energy $\varepsilon_{\text{mean}}$ is related to the absolute temperature T by the relation

$$\varepsilon_{\text{mean}} = 2.7kT \tag{6.27}$$

Where k is the Boltzmann constant. So at the time that deuterium starts to build up, (when $T = 1.0 \times 10^9$ K) the mean photon energy is $\varepsilon_{\text{mean}} = 0.233$ MeV. The ratio between the energy that can cause the photodisintegration of a deuteron and the mean photon energy is therefore 2.23 MeV/0.233 MeV = 9.6. Thus, the process of photodisintegration did not stop until the mean photon energy was about a factor of ten lower than the photodisintegration energy. This highlights the fact that because there are vastly more photons than baryons, the very small fraction of photons that have energies much higher than the mean photon energy can have a significant effect on physical processes.

The survival of deuterium has been considered in some detail, since similar considerations about the relative numbers of energetic photons play an important role at a much later time in the history of the Universe – the epoch at which electrons and ions combined to form neutral atoms.

6.4.2 Primordial nuclear reactions

As soon as there was a significant build up in the abundance of deuterium, other nuclear reactions could then proceed. In particular, there were several series of reactions that form the very stable nuclide helium-4 (i.e. ${}^4_2\text{He}$).

For instance, an isotope of hydrogen called tritium (${}^3_1\text{H}$) was formed by

The significance of the colour-coding is explained below.

$$\begin{aligned} &{}^2_1\text{H} + \text{n} \rightarrow {}^3_1\text{H} + \gamma \\ &{}^2_1\text{H} + {}^2_1\text{H} \rightarrow {}^3_1\text{H} + \text{p} \end{aligned} \tag{6.28a}$$

and the tritium thus formed could then undergo reactions to produce helium-4 as follows

$$\begin{aligned} &{}^3_1\text{H} + {}^2_1\text{H} \rightarrow {}^4_2\text{He} + \text{n} \\ &{}^3_1\text{H} + \text{p} \rightarrow {}^4_2\text{He} + \gamma \end{aligned} \tag{6.28b}$$

However deuterium also reacted to produce helium-3

$$\begin{aligned} &{}^2_1\text{H} + {}^2_1\text{H} \rightarrow {}^3_2\text{He} + \text{n} \\ &{}^2_1\text{H} + \text{p} \rightarrow {}^3_2\text{He} + \gamma \end{aligned} \tag{6.28c}$$

and this isotope of helium could undergo reactions to form helium-4 as follows

$$ {}^{3}_{2}\mathrm{He} + \mathrm{n} \rightarrow {}^{4}_{2}\mathrm{He} + \gamma \tag{6.28d}$$

$$ {}^{3}_{2}\mathrm{He} + {}^{2}_{1}\mathrm{H} \rightarrow {}^{4}_{2}\mathrm{He} + \mathrm{p} $$

These were the dominant reactions that led to the production of helium-4. (Although the direct fusion of two deuterons to form helium-4 was also a possible reaction, this did not occur to any great extent.)

If the plethora of reactions bothers you, you may be relieved to note that there are only four types of reaction at work here. The reaction equations have been colour coded to illustrate this. The reactions are of the following types:

- A neutron is captured and a photon is emitted (colour-coded green).
- A proton is captured and a photon is emitted (colour-coded red).
- A deuteron is captured and neutron is emitted (colour-coded blue).
- A deuteron is captured and proton is emitted (colour-coded purple).

The major product of primordial nucleosynthesis was helium-4. The fact that nucleosynthesis did not progress to produce large quantities of nuclides with higher mass numbers is due to two factors. Firstly, the rate at which two nuclei will fuse together depends very strongly on the temperature, and higher temperatures are required to fuse nuclei of higher atomic number. Because the deuteron is easily photodisintegrated, the process of nucleosynthesis could only start once the temperature was relatively low. As a consequence, the rate of fusion reactions that involved nuclides other than hydrogen and helium would have been very low.

A second factor is the lack of any stable nuclide with mass number 5 or 8. The lack of a stable nuclide with mass number 5 means that helium-4 could not react with the two most abundant species – protons and neutrons. This hurdle could, however, be overcome by reactions that involve tritium or helium-3,

$$ {}^{4}_{2}\mathrm{He} + {}^{3}_{1}\mathrm{H} \rightarrow {}^{7}_{3}\mathrm{Li} + \gamma \tag{6.29}$$

$$ {}^{4}_{2}\mathrm{He} + {}^{3}_{2}\mathrm{He} \rightarrow {}^{7}_{4}\mathrm{Be}\ \text{(unstable)} $$

$$ {}^{7}_{4}\mathrm{Be} + \mathrm{e}^{-} \rightarrow {}^{7}_{3}\mathrm{Li} + \nu_{\mathrm{e}} $$

One further reaction that is worth noting is that lithium-7 can react with a proton, but the result is the destruction of the newly formed lithium and the formation of two nuclei of helium-4

$$ {}^{7}_{3}\mathrm{Li} + \mathrm{p} \rightarrow {}^{4}_{2}\mathrm{He} + {}^{4}_{2}\mathrm{He} \tag{6.30}$$

The yield of lithium was small. The relative amount of lithium formed can be quantified by the mass fraction, i.e. the proportion of the baryonic mass that was in the form of this element. Since lithium is the only element heavier than hydrogen or helium that is formed at this time, the mass fraction of lithium corresponds to the metallicity Z. Primordial nucleosynthesis created lithium such that the metallicity was less than 10^{-9}, but as we will see, the abundance of lithium provides a useful way of probing the conditions during the first few minutes of the big bang.

It should be noted that the fusion reactions that are outlined above only operated for a brief period of time. By the time the Universe reached an age of about 1000 s (i.e. about 17 minutes) and had a temperature of about 5×10^8 K, all such reactions effectively ceased. However, this brief spell of history left a signature, in terms of the abundances of light elements, that can be read today.

6.4.3 The primordial abundance of helium

We can now investigate how much helium would have been produced in the first few minutes of the big bang. The approach that we take here is to estimate the mass fraction of helium (Y) that would have been produced given the processes outlined above.

The starting point for the calculation is the ratio of the number density of neutrons to the number density of protons.

- ■ What was the value of this ratio at the time that the reactions described by Equation 6.25 came to a halt. At what time did this happen?
- ❑ It was stated above that $n_n/n_p \approx 0.22$ at the time that these reactions stopped. This occurred a time $t \approx 0.7$ s.

The temperature at this time was much higher than the maximum temperature at which deuterium can survive.

- ■ Why is the temperature at which deuterons can survive relevant to the production of helium?
- ❑ The formation of deuterons is the first step in the sequence of nucleosynthesis reactions that leads to helium.

So there was a delay before helium synthesis could start. During this time the ratio n_n/n_p does not remain constant because the isolated neutron is not a stable particle. Free neutrons undergo β^--decay with a half-life of 615 s. The next step is to calculate how much time elapses from the instant at which $n_n/n_p \approx 0.22$ and the time at which deuterium can form.

- ■ At what time does the temperature drop to the point at which deuterium can survive? (*Hint*: See Question 6.7.)
- ❑ Deuterium survives once the temperature drops below 1×10^9 K. This temperature is reached at $t = 225$ s. (This was the answer to Question 6.7(a).)

Thus there was an interval of a few hundred seconds before helium production could start in earnest. The way in which the neutron number dropped with time is illustrated in Figure 6.12, which shows the fraction of the original sample of neutrons that would have remained at a given time.

QUESTION 6.8

Calculate the value of n_n/n_p at the time when deuterium started to be formed in significant amounts. (Figure 6.12 provides a way of estimating the number of neutrons that decay in a given time. Take care in calculating n_n/n_p that you account for particles that are created as well as those that disappear!)

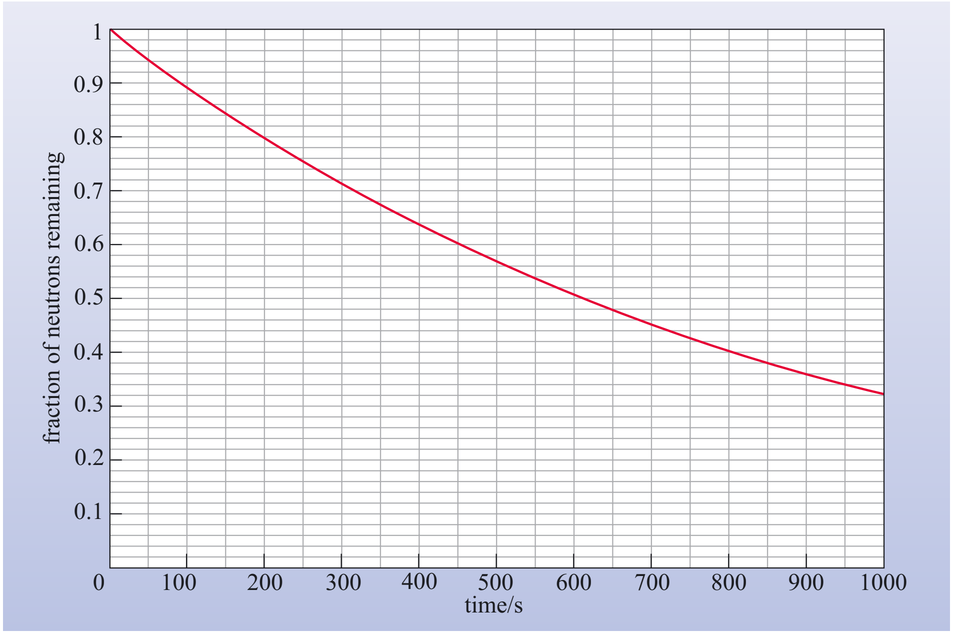

Figure 6.12 The fraction of the number of neutrons that would remain in a sample after a given interval of time. (For use with Question 6.8.)

The result of Question 6.8 shows that when deuterium began to be formed, the ratio of the neutron and proton number densities, n_n/n_p, had a value of about 0.16. The final stage of the calculation is to work out the mass fraction in helium that arises from this value. You have already seen that the major product of primordial nucleosynthesis was helium-4, and as far as calculating the helium abundance is concerned, it is a reasonable approximation to assume that *all* of the neutrons that were present ended up in nuclei of helium-4.

The quantity that we wish to calculate is the mass fraction contained in helium-4

$$Y = \frac{\text{mass of helium in a sample}}{\text{total mass of baryonic matter in the sample}} \tag{6.31}$$

For the purposes of this calculation the sample can be taken to be the baryonic matter in any co-moving volume. There are two contributions to the mass of this sample: that due to hydrogen and that due to helium (which, for simplicity, we assume here to be purely helium-4). If the number of hydrogen and helium nuclei present in our sample, after all nucleosynthesis reactions have stopped, are N_H and N_{He} respectively, then the mass fraction in helium can be written as

$$Y = \frac{N_{He}m_{He}}{N_H m_H + N_{He}m_{He}}$$

Where m_H and m_{He} are the masses of the hydrogen and helium nucleus respectively. This equation can be simplified by making the approximation that $m_{He} \approx 4m_H$.

$$Y = \frac{4N_{He}}{N_H + 4N_{He}} \tag{6.32}$$

Since there are two neutrons in each helium nucleus, the number of helium nuclei is simply half the number of neutrons. The number of hydrogen nuclei is the number of protons minus the number of protons that are locked up in helium nuclei,

$$N_{He} = N_n/2$$

$$N_H = N_p - 2N_{He} = N_p - N_n$$

These expressions for N_H and N_{He} can be substituted into Equation 6.32 to give

$$Y = \frac{2N_n}{N_n + N_p} = 2\left(\frac{1}{1+(N_p/N_n)}\right) \tag{6.33a}$$

The ratio of the number of protons to neutrons (N_p/N_n) in our co-moving sample is the same as the ratio of the *number density* of protons to that of neutrons (n_p/n_n). Hence

$$Y = 2\left(\frac{1}{1+(n_p/n_n)}\right) \tag{6.33b}$$

QUESTION 6.9

Using the value of n_n/n_p that you obtained in Question 6.8, calculate the value of the mass fraction in helium that you would expect from primordial nucleosynthesis.

The answer to Question 6.9 shows a remarkable result: the hot big bang model predicts that the mass fraction of helium-4 should have a value of about 28%. More refined calculations obtain a value that is lower than this – about 24%. This agrees very well with the observation that the mass fraction of helium-4 in low-metallicity interstellar gas seems to be about 24–25%. Until the development of the hot big bang model, the only other mechanism that was a plausible explanation for the production of helium was stellar nucleosynthesis. While it was known that this process does produce helium, it was a mystery how helium could have an almost identical abundance in every location that astronomers measured. The standard hot big bang model provides a more natural explanation for the abundance of helium-4. Such is the success of this outcome of the model, that it is generally interpreted as a key piece of evidence to support the big bang model.

6.4.4 Abundances of light elements as a cosmological probe

In the previous section we saw how the big bang model predicts the formation of helium-4 with an abundance close to that which is observed in the Universe. We have also seen that primordial nucleosynthesis forms other nuclides apart from helium-4.

■ Apart from helium-4, what other stable nuclides are formed by primordial nucleosynthesis?

❏ Deuterium, helium-3 and lithium-7 are the stable nuclides formed by primordial nucleosynthesis. (Note that tritium is unstable with a half-life of about 12 years.)

The abundances are sensitive to the density of matter that is in the form of protons and neutrons, i.e. the density of the baryonic matter in the early Universe. The density of baryonic matter at any time is usually expressed in terms of a baryonic density parameter $\Omega_b(t)$ which is defined as follows

$$\Omega_b(t) = \frac{\text{density of baryonic matter at } t}{\text{critical density at } t} \tag{6.34}$$

Where the critical density at any time $\rho_{crit}(t)$ is given by Equation 5.26

$$\rho_{crit} = \frac{3H^2(t)}{8\pi G} \tag{5.26}$$

The density of baryons in the early Universe can be related to the present-day density of baryonic material, which is expressed using the current value of the baryonic density parameter $\Omega_b(t_0)$. We shall refer to this value as $\Omega_{b,0}$.

The dependence of the abundances of the light elements on the value of $\Omega_{b,0}$ can be determined by detailed calculations: results of such calculations are shown in Figure 6.13. (The abundances also depend on the value of H_0: the calculation shown assumes a value of $H_0 = 72\,\text{km s}^{-1}\,\text{Mpc}^{-1}$.) The first notable aspect of Figure 6.13 is that the abundance of helium-4 does not vary dramatically with baryon density. Thus, the helium abundance is not very sensitive to the baryon density.

In contrast to helium-4, the abundances of deuterium and helium-3 *are* sensitive to the baryon density. The mass fraction in both of these nuclides decreases substantially as the baryon density increases. The behaviour of the abundance of lithium is somewhat more complex – the curve shows a dip to a minimum value that occurs at a value of $\Omega_{b,0} \approx 0.02$.

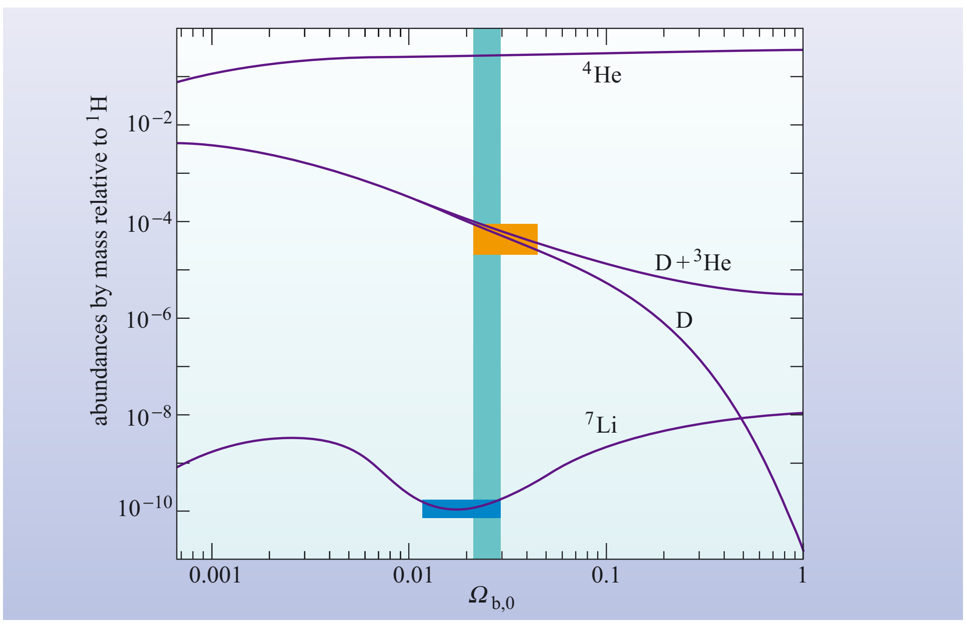

Figure 6.13 The abundances of the light elements as a function of the current value of the baryonic density parameter $\Omega_{b,0}$. Note that D stands for deuterium (^2_1H). The smooth curves show the prediction of nucleosynthesis calculations. The orange and blue boxes indicate the ranges of observed abundances. The vertical strip shows the values of $\Omega_{b,0}$ that are consistent with all observations. (Adapted from Walker *et al.*, 1991)

If the abundances of these light elements could be measured in material that has not undergone any change in composition since the time of primordial nucleosynthesis, then we could, in principle, measure the current baryonic density parameter of the Universe. A fundamental problem in this approach is highlighted by the following question.

QUESTION 6.10

Use Figure 6.13 to make an order of magnitude estimate of the maximum metallicity of material that has only undergone primordial nucleosynthesis, and has not been chemically enriched by stars. Is this value of metallicity consistent with the idea that the oldest observed stars were formed from primordial material?

The answer to Question 6.10 shows that even the oldest stars have undergone some chemical enrichment in a previous generation of stars; no stellar material appears to be left over from the big bang that has not undergone some subsequent nuclear processing by stars. Despite this complication, it is possible to make progress in this field by trying to work out how the abundances of deuterium, helium-4 and lithium may have been changed by nuclear processes that might have occurred since the end of primordial nucleosynthesis. When corrections of this sort are made, the result is a range of plausible values for the primordial abundances of deuterium, helium-4 and lithium. These ranges are shown as rectangular regions on Figure 6.13, and the overlap of these regions gives an allowed range of $\Omega_{b,0}$. The result is that $\Omega_{b,0}$ lies in the range 0.02 to 0.03. This immediately indicates that if the Universe has a flat geometry (implying $\Omega = 1$), then at most, 3% of the contribution to the density of the Universe can arise from baryonic matter. Given the difficulties in analysing primordial abundances, these figures should be treated with some caution, but it seems certain that baryonic matter can contribute no more than 5% to the total density of the Universe. As you will see in the next chapter, evidence is growing that $\Omega = 1$, which has the immediate implication that at least 95% of the density of the Universe is in a form that is different to the matter from which stars are made.

QUESTION 6.11

Suppose that the primordial abundances of light elements were measured in three 'hypothetical universes' as shown in Table 6.4. What would be the current value of the density parameter $\Omega_{b,0}$ of baryonic matter in each case? Could you determine the value of $\Omega_{b,0}$ from the lithium abundances alone?

Table 6.4 Some abundances in hypothetical universes – for use with Question 6.11.

Hypothetical universe	Lithium abundance by mass relative to hydrogen (^1_1H)	Deuterium abundance by mass relative to hydrogen (^1_1H)
A	1×10^{-9}	7×10^{-4}
B	1×10^{-9}	1×10^{-5}
C	$< 1 \times 10^{-9}$	1×10^{-4}

6.5 Recombination and the last scattering of photons

$t \approx 3$ to 4×10^5 years, $T \approx 4500$ to 3000 K, $E \sim$ a few eV

After the nucleosynthesis of light nuclei that occurred in the first few hundred seconds after $t = 0$, the Universe expanded and cooled for several hundred thousand years before it underwent another dramatic change. This next big event is called *recombination* and occurred when nuclei and electrons combined to form neutral atoms. In this section we will examine this epoch of the Universe and see how processes that took place at that time account for the cosmic microwave background that is detectable today.

6.5.1 The Universe in the post-nucleosynthesis era

As the temperature of the Universe dropped below 10^8 K, the nuclear reactions that resulted in the formation of light elements came to a halt. The composition of the Universe at this time was: protons; nuclei of deuterium, helium and lithium; electrons; neutrinos; photons; and dark matter particles (whatever they are!). The important interactions were those which shared energy out between the different constituents. In particular, photons and electrons interacted with one another to exchange energy. The electrons also collided with protons and nuclei and this also led to a sharing out of energy. These two types of interaction ensured that the radiation, electrons and nuclei remained in a state of thermal equilibrium.

■ Why were the neutrinos not in thermal equilibrium with the other particles at this stage in the evolution of the Universe?

❑ Because the rate of neutrino interactions was very small. Most neutrinos did not interact with any particle after the time of neutrino decoupling.

As the Universe expanded, the temperature of the background radiation dropped with time. Because the photons greatly outnumbered the electrons and nuclei, the temperature of the electrons and nuclei was kept in step with that of the cooling radiation.

It has already been noted that at early times the expansion of the Universe was dominated by the energy density of radiation. However as you saw in Figure 6.6, the energy density of matter became equal to that of radiation when the scale factor attained about 10^{-4} of its current value, and this would have occurred when the age of the Universe was a few times 10^4 years. Following that event, the rate of expansion would have been dominated by the energy density of matter, and the effect of radiation would have progressively declined. Despite this change in the expansion rate, the temperature would still have been that of the background radiation due to the incessant interactions between photons, electrons and nuclei. This state of affairs would have persisted until the interactions between cosmic background photons and free electrons became negligible.

6.5.2 The era of recombination

An important type of interaction between electrons and nuclei is that which results in the formation of a neutral atom. As an electron becomes bound into an atom, energy is released in the form of a photon. This process is called **recombination**.

As the Universe expanded and cooled, conditions became favourable for recombination to occur. (In this context, the term 'recombination' may seem somewhat of a misnomer as electrons and nuclei had never been 'combined' as neutral atoms before this time!)

The process of recombination is the opposite of ionization. The reaction can be written as

$$\mathrm{p} + \mathrm{e}^- \underset{\text{ionization}}{\overset{\text{recombination}}{\rightleftarrows}} ({}^1_1\mathrm{H})_{\text{neutral}} + \gamma \qquad (6.35)$$

In the case of neutral hydrogen, the energy required to ionize the atom from its lowest energy (ground) state is 13.6 eV. Thus, if conditions were such that for every atom, there were many photons with an energy of at least 13.6 eV, then the neutral atom would not have survived for long, but would have soon been re-ionized. Alternatively, the atom may have undergone a collision with an electron or proton that could also have supplied the 13.6 eV of energy required to ionize the atom. Either way, at high temperatures, the reaction described in Equation 6.35 favours the production of protons and electrons, and the number density of neutral atoms is exceedingly low.

As the temperature of the Universe fell, the equilibrium of Equation 6.35 shifted to favour the production of neutral atoms and photons. The temperature at which this change occurred was subject to very similar constraints as those you met earlier in connection with the photodisintegration of deuterium. The number of photons exceeds the number of hydrogen atoms by a factor of about 10^9. Thus if only one in 10^9 photons had an energy of 13.6 eV, then this will be sufficient to ionize any neutral hydrogen.

QUESTION 6.12

By analogy with the case of deuterium photodisintegration, estimate the temperature at which recombination of hydrogen occurs.

Recombination started to occur when the temperature was about 4500 K. This temperature was reached when the Universe was about 3×10^5 years old. As neutral atoms formed, the density of free electrons (i.e. electrons that are not bound up in atoms) decreased. This had an important effect on the interrelationship between photons in the background radiation and matter in the Universe. Scattering interactions between free electrons and photons became infrequent. By the time the temperature had dropped to 3000 K, the number density of free electrons was so low that the Universe essentially became transparent and photons could travel unhindered from this time on. As we shall shortly see, the radiation that we observe now as the cosmic microwave background was last scattered at the time of recombination.

The lack of scattering interactions had important thermal and dynamical effects. As we saw above, prior to recombination, the energy of photons was 'shared' with the thermal energy of matter in the Universe, and this ensured that matter had the same temperature as the background radiation. After recombination the temperature of the matter and the background radiation evolved independently of one another. The temperature of the background radiation changed with scale factor according to Equation 6.6 – indeed it was from this relationship we were able to infer that the cosmic microwave background that is observed at present implies a hot early Universe.

The important dynamical role of the coupling between photons and electrons relates to the stability of over-dense regions against gravitational collapse. Prior to recombination, the radiation pressure played an important role in opposing the gravitational collapse of over-dense regions. After recombination, the rate of interactions between photons and electrons dropped dramatically, and this suddenly allowed over-dense regions that had been expanding with the Hubble flow to start to begin to contract under gravity. We will explore this aspect of the post-recombination Universe in more detail in Section 6.6, but first we will consider the evolution of the background radiation to form the cosmic microwave background.

6.5.3 The formation of the cosmic microwave background

The major change that occurred to the photons as they travelled after their last scattering was that they were red-shifted by the expansion of the Universe. As has already been mentioned, cosmological expansion causes the wavelengths of photons to increase, and if those photons are distributed according to a black-body spectrum, then this form of the spectrum is retained even though its characteristic temperature is reduced. We have now reached a detailed explanation for the formation of the cosmic microwave background: it is the cooled 'gas' of red-shifted photons that were in thermal equilibrium with matter at the time of last scattering.

QUESTION 6.13

Calculate the redshift at which the last scattering occurred. Assume that at the time of last scattering the temperature of the background radiation was 3.0×10^3 K. (*Hint*: Start by using Equation 6.6 to determine the change in scale factor.)

As the answer to Question 6.13 shows, the last scattering of photons in the cosmic background radiation occurred at a redshift of about 1100.

One way of thinking about how such photons should appear to us now is illustrated schematically in Figure 6.14: the diagram shows our vantage point – 'here and now' – at the centre, and the radial direction from this point represents a direction on the sky. The radial distance from our viewpoint on this diagram represents time, such that the present is at the centre whilst the outermost circle of the diagram is at $t = 0$, i.e. at the first instant of cosmic expansion. Whatever direction we look in we see the radiation from the time that the Universe became transparent. This transition, from being opaque to being transparent occurred when the Universe was about 3×10^5 years old. At times before this, the Universe was opaque due to the scattering of photons by electrons.

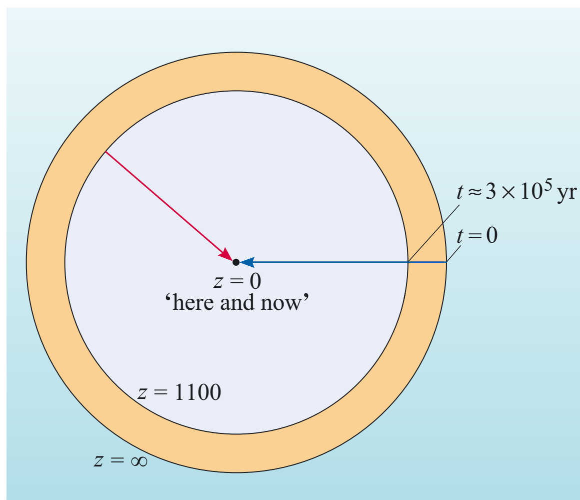

Figure 6.14 A schematic figure showing the origin of photons in the cosmic microwave background as observed from the Earth. In this diagram the radial direction from the Earth represents a direction on the sky and the radial distance from the Earth represents time.

Thus the cosmic background radiation appears to come from a spherical surface called the **last-scattering surface**, that is centred on us. Of course, this does *not* mean that we are at the centre of the Universe! An analogy may help here: if you go for a walk on a foggy day when the visibility is 30 m, then you will be able to see up to 30 m away in any direction.

Your view of the 'foggy world' is that you are at its centre, and that it has a radius of 30 m. Of course, this is just *your* view of the world; any other observer in the fog will have a similar view even though they might be somewhere else, see Figure 6.15. Thus the boundary defined by how far any single observer can see has no global significance. Likewise the last-scattering surface simply represents as far as we can see from our location in the Universe. The situation is somewhat different from viewing the world through a uniform fog – since in viewing the CMB we are essentially looking back in time to an era when the Universe was, in a sense, 'foggy'. However, the principle is the same: observers at another location in the Universe would also see a last-scattering surface, but it will not correspond physically to the last-scattering surface that we observe.

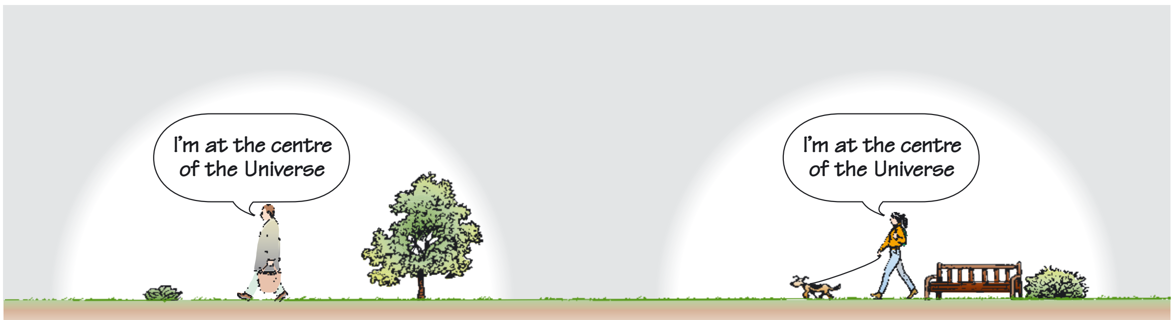

Figure 6.15 Observers walking on a foggy day can see a fixed distance in any direction. Despite the naive claims of the observers, the boundary defined by this distance has no global significance!

6.5.4 Observing the cosmic microwave background

Now that we have developed an explanation for the cosmic microwave background in terms of red-shifted radiation that was last scattered by free electrons at a redshift of $z \approx 1100$, it is appropriate to consider its observed properties in more detail and how such observations are made.

The properties of the cosmic microwave background radiation that have already been described can be summarized as follows:

- The CMB has a black-body spectrum, with a characteristic temperature of 2.725 ± 0.002 K.
- The CMB is highly uniform in every direction that we observe (Section 5.2.3).

We shall shortly see that the CMB is not perfectly uniform, and that this is an important source of information about the Universe. However we shall begin by considering how measurements of the spectrum of the CMB are made.

The cosmic microwave background was discovered in 1965 by Arno Penzias and Robert Wilson (Box 6.3). Penzias and Wilson could not measure the spectrum of this signal since their receiver was tuned to work at a single wavelength (of 7.35 cm), so initially there were no data to support the idea that the background had the spectrum of a black body. However, the surface brightness of the radiation was characteristic of emission from a black body at a temperature of 3 K.

BOX 6.3 THE DISCOVERY OF THE COSMIC MICROWAVE BACKGROUND

In 1964, two researchers at Bell Laboratories in Holmdel, New Jersey, Arno Penzias and Robert Wilson (Figure 6.16), were charged with the task of calibrating a radio antenna to be used for telecommunication and galactic radio astronomy. The antenna, which is shown in the background of Figure 6.16, was in the form of a horn: radio waves entered through the aperture and were directed onto a detector at the narrow end of the horn. A feature of this type of design of radio antenna is that the signal that is received at the detector should be relatively free from any contamination that arises from sources that are outside the field of view (this is a problem that most other designs of antenna, such as a dish, do suffer from). Soon after starting, Penzias and Wilson measured the signal from an airborne radio emitter, and found that there was an unexplained source of noise within the system. For the next year or so, they tried to track down the source of this noise; eliminating the possibility that it may be due to faulty electronics, rivets in the antenna – or even pigeon droppings in the horn. One characteristic of this noise was that it seemed to be the same wherever on the sky the antenna was pointed. Another was that the intensity of the signal was as would be expected if the whole sky were a black-body source at a temperature of 3 K.

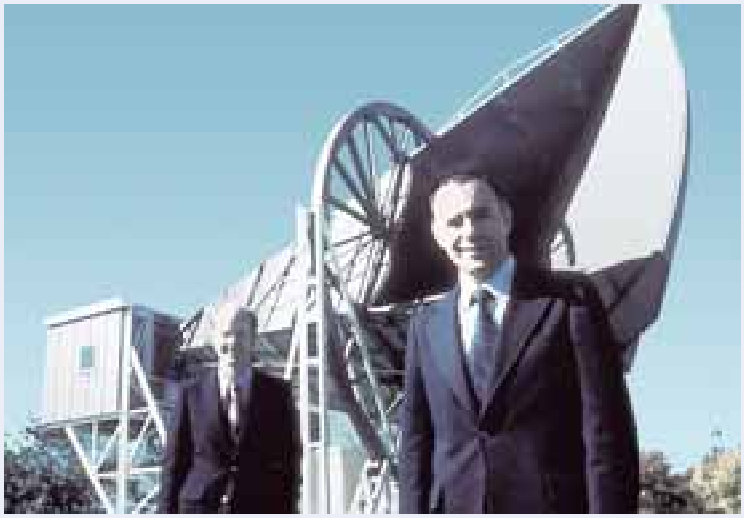

Figure 6.16 Arno Penzias (right) and Robert Wilson (left) in front of the horn antenna with which they discovered the cosmic microwave background. Penzias and Wilson were awarded the 1978 Nobel Prize in Physics for their discovery of the cosmic microwave background. (Bell Laboratories, AT&T)

In seeking an explanation for this signal, Penzias and Wilson were put in touch with Robert Dicke, a professor at Princeton University (which is only a few miles away from Holmdel). Dicke had realized several years earlier that the early stages of the big bang would have been characterized by very high temperatures, and that the radiation from this phase of the history of the Universe should be detectable today with a black-body spectrum and a temperature of a few kelvin. He had also realized that with the then current state of radio technology it should have been possible to detect such a signal. His research group were in the process of building a dedicated detector when Penzias and Wilson contacted him. Although Dicke and his team were beaten to the discovery of the signal, they were in a prime position to offer an interpretation of the result. The discovery was published as two papers in 1965; one by Penzias and Wilson which described only the observational result, and another by Dicke and his co-workers that offered an interpretation of the result as the signal being a relict of the hot big bang.

A further twist in the tale arose after the results were first published. Dicke received a terse letter from George Gamow, a Russian-born American physicist. In 1948, Gamow, with his collaborators, Ralph Alpher and Robert Herman had predicted that the temperature during the early stages of the big bang were sufficiently high that nuclear reactions would have taken place (Section 6.4). Furthermore, he suggested that a remnant of this high temperature phase should exist as background radiation with a temperature of about 5 K. Having made a prediction about the background radiation seventeen years earlier, Gamow was justifiably annoyed that his work had been overlooked. However, in the years since the discovery of the cosmic background radiation, Gamow's contribution to the implications of the hot big bang model have become widely recognized.

As we have already seen, the peak of emission from a black-body spectrum at a temperature of 3 K occurs at wavelengths of about 1 mm. The Earth's atmosphere partially absorbs radiation in this part of the electromagnetic spectrum, which makes it difficult to measure the spectrum of the cosmic microwave background using a ground-based antenna. The obvious solution to this is to place a detector above the Earth's atmosphere. During the 1970s and 1980s measurements were made using balloon-borne instruments that went some way to confirming that the cosmic microwave background has a black-body spectrum. But a major advance came from a satellite-based experiment called the Cosmic Background Explorer or COBE. This mission was launched in 1989, and was designed to measure various characteristics of the cosmic microwave background. One striking result from COBE was the measurement of the spectrum of the microwave background radiation as shown earlier in Figure 6.2. This spectrum follows the theoretical black-body curve to a very high degree – in fact, it is the best example of a black-body spectrum that has ever been observed in nature.

The second major aspect of the cosmic microwave background that has been subject to intense observational scrutiny is its uniformity. The largest variations in the microwave background as we look from one position to another correspond to a variation in temperature of less than one part in 10^3. It is difficult to make absolute measurements of the intensity of the CMB, and so experiments that measure variations in intensity do so by comparing signals from two different regions of the sky. Typical observing strategies involve making a large number of these comparison measurements across the area of sky that is of interest (which may be the entire celestial sphere). In this way, instrumental uncertainties are reduced, and levels of *relative* variation in the CMB can be measured to better than one part in 10^5. We will return to this topic in Chapter 7, but now we will take a first look at the implications of the measured uniformity of the cosmic microwave background.

6.5.5 Interpreting the cosmic microwave background

Much of this chapter has been based on interpreting one aspect of the cosmic microwave background – its spectrum. Thus we have studied the significance of the black-body form of the cosmic background radiation, and explored the consequences of the presence of such radiation in an expanding Universe. However there is a lot more to be learnt from the cosmic microwave background than can be deduced from its spectrum alone. In particular, the uniformity of the cosmic microwave background, and departures from this uniformity, also need to be explained in terms of cosmological processes. It is to this aspect of the cosmic microwave background that we now turn.

The uniformity of the cosmic microwave background

The view of the formation of the cosmic microwave background as illustrated by Figure 6.14 seems reasonable but gives rise to a puzzle. The temperature of the cosmic microwave background is, to a very high degree, uniform in whichever direction we look. The uniformity in the microwave background implies that at the time of recombination, the temperature at any point on the last-scattering surface was also highly uniform. The puzzling aspect of this is that the last-scattering surface is too large to have settled down to a uniform temperature in the 3 to 4×10^5 years that the Universe had been expanding.

A limit to the size of a region that can come to thermal equilibrium can be found by a similar argument to that used in Chapter 3 to constrain the size of AGN. The underlying principle is that a physical signal cannot propagate at a speed that is greater than the speed of light. In this case the 'physical signal' is the heat flow caused by a difference in temperature between two locations. If we consider one location in the Universe at the instant when the expansion of the Universe began, then at subsequent times, the most distant point that could possibly be in thermal equilibrium with our starting point would be at the distance that light could travel in the age of the Universe. This distance, which is the limiting size of a region that can be expected to be in thermal equilibrium at a given time is called the **horizon distance**. This is illustrated schematically in Figure 6.17: the point X represents an initial point and X′ is the same point at recombination (i.e. X and X′ have the same co-moving coordinates). The maximum distance that could be covered by any signal at a given time prior to recombination is shown by the line from X to A, and the distance from X′ to A is the horizon distance at the time of recombination. If the horizon distance is calculated for the last-scattering surface, it turns out that it corresponds to an angle θ on the sky of about 2°. Regions of the last-scattering surface that are separated by more than this angle could not have affected each other.
The fact that the microwave background has almost the same temperature over scales that are much greater than the horizon scale of 2° is a problem that the standard big bang model fails to address. We will return to consider a solution to this *horizon problem* in Chapter 8.

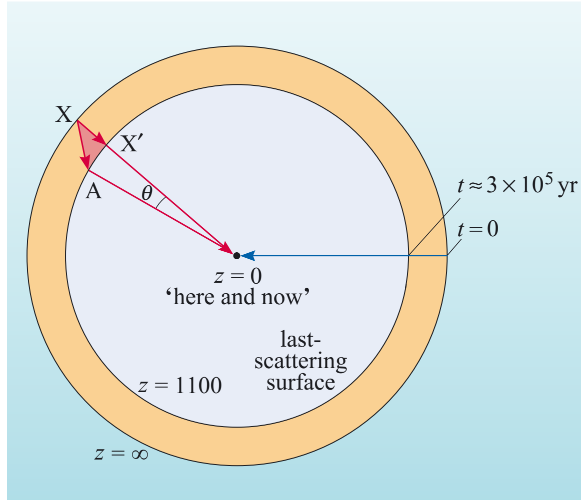

Figure 6.17 The horizon distance at the time of recombination as it appears on the last-scattering surface. Point X represents a location in the Universe just after $t = 0$. X′ is the location with the same co-moving coordinates as X at the time of recombination. The distance from X′ to A is the maximum distance that a signal could travel prior to recombination. The angular separation of points A and X′ is about 2°. (Note that this diagram is not to scale.)

Although the cosmic microwave background is remarkably smooth there are departures from perfect uniformity. These variations – or **anisotropies** – are at a very small level. As discussed in the following two subsections, there are two distinctly different mechanisms that give rise to anisotropies in the microwave background.

The dipole anisotropy

Mapping of the cosmic microwave background reveals that in one direction in the sky the temperature is 3.36 mK higher than the mean temperature, whereas in the opposite direction it is 3.36 mK lower than the mean. Between these two directions there is a smooth variation between the maximum and minimum temperatures. This is illustrated by the all-sky map shown in Figure 6.18 – the blue and pink areas are above and below the average temperature respectively. Because the variation is symmetric about two opposite directions, or poles, on the celestial sphere, it is referred to as the **dipole anisotropy**.

Figure 6.18 A map from COBE showing the dipole anisotropy. The elliptical map area covers the entire sky. The blue and pink coloured regions represent temperatures that are higher and lower, respectively, than the mean. (Goddard Space Flight Center)

The interpretation of the dipole anisotropy is that it arises from our motion relative to the co-moving reference frame. Figure 6.19 indicates the effect of observer motion on the measured wavelength of cosmic microwave background photons.

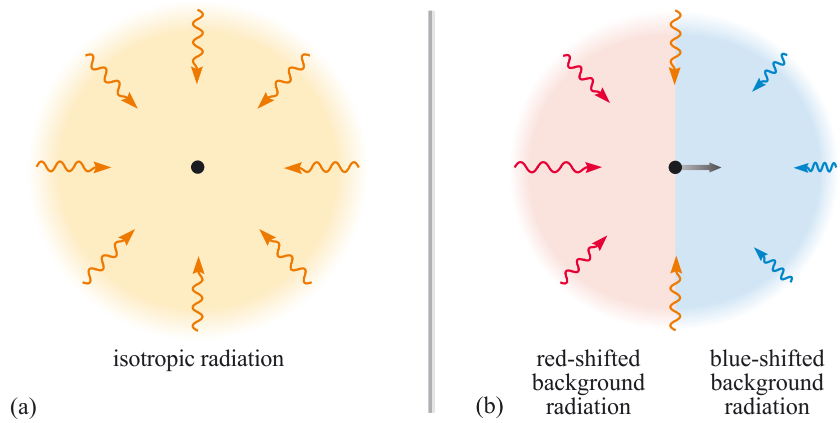

Figure 6.19 The view of the cosmic microwave background according to (a) an observer who is stationary with respect to the frame of reference of co-moving coordinates, and (b) an observer who is moving with respect to this frame of reference. According to the observer in case (a) the background is isotropic, whereas the observer in case (b) measures a blue-shift in the direction of motion and red-shift in the opposite direction.

Figure 6.19 concerns two observers at the same location in space, but who are moving with respect to one another. Observer (a) sees the cosmic microwave background as being perfectly uniform in all directions, whereas observer (b) sees the same last-scattering surface, but the radiation is Doppler shifted. The perfectly uniform case arises for an observer who is stationary in co-moving coordinates, i.e. one who is perfectly following the Hubble flow of the expanding Universe. Any motion relative to this frame of reference, such as that of observer (b), would cause the observer to see the cosmic microwave background blue-shifted in the direction of motion and red-shifted in the opposite direction. When radiation with a black-body spectrum is subject to a Doppler shift, the spectrum retains its black-body form, but the peak wavelength is shifted and the characteristic temperature changes accordingly. Red- and blue-shifts result in lower and higher temperatures respectively. Thus the direction on the sky in which the temperature increases the most corresponds to the direction in which we are moving with respect to the Hubble flow.

■ Why is it unlikely that the Earth would be stationary with respect to the frame of reference of co-moving coordinates? List possible contributions to the Earth's velocity with respect to this frame?

❏ The Earth is unlikely to be stationary in co-moving coordinates because (i) the Earth is in motion around the Sun, (ii) the Sun is in motion around the centre of our Galaxy, and (iii) the Galaxy has a peculiar motion with respect to the Local Group, and (iv) the Local Group is likely to have a random motion with respect to the Hubble flow.

Analysis of the dipole anisotropy shows that the Sun has a speed of about 365 $\mathrm{km\,s^{-1}}$ with respect to the local co-moving frame of reference. When the Sun's motion around the Galaxy, and the Galaxy's motion with respect to the Local Group are accounted for, it is found that the Local Group has a speed of about 630 $\mathrm{km\,s^{-1}}$ with respect to the local co-moving frame of reference.

Intrinsic anisotropies in the cosmic microwave background

Even when the effect of the dipole anisotropy is removed the cosmic microwave background is still not perfectly smooth – it exhibits smaller scale variations in temperature from one point to another. Figure 6.20 shows a map of these fluctuations over a region of sky that is about 10° across. The magnitude of such variations is small: at most they correspond to a fractional change in temperature of only a few parts in 10^5. The significance of these intrinsic anisotropies is that, although they mainly represent temperature variations in the Universe at the time of recombination, they are intimately linked to the small variations in *density* that are believed to have arisen at very early times in the history of the Universe. In particular, it is hypothesized that these density fluctuations may have their origin in the process of inflation that occurred at $t \sim 10^{-36}$ s. We shall consider the origin of these so-called *primordial fluctuations* in Chapters 7 and 8, but we note here that the analysis of intrinsic anisotropies in the cosmic microwave background can potentially provide information about processes in the very early history of the Universe.

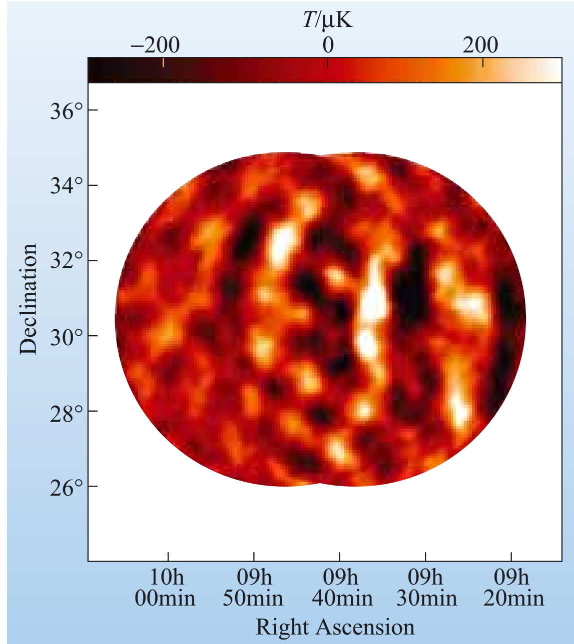

Figure 6.20 A map of the fluctuations in the cosmic microwave background as measured by an experiment called the Very Small Array. (University of Cambridge, Jodrell Bank Observatory, and the Instituto de Astrofísica de Canarias)

Temperature variations in the cosmic microwave background are also useful because the photons that were last scattered at the time of recombination have been moving freely, apart from the effects of gravity, ever since. So the anisotropy pattern can also provide information about the geometry of space–time. For this reason, the analysis of anisotropies in the cosmic microwave background is a key area of observational cosmology, and will be discussed more fully in Chapter 7. However, here we continue our discussion of the evolution of the Universe in the post-recombination era by considering how the small variations in density that were present at recombination helped to form structure in the Universe.

6.6 Gravitational clustering and the development of structure

The small amplitude of temperature anisotropies in the cosmic microwave background indicates that the distribution of baryonic matter in the Universe was very smooth at the time of recombination. This is in marked contrast to the present-day Universe in which the baryonic matter is concentrated into stars, galaxies, clusters and large-scale structure. An outline of how the Universe evolved from an almost, but not quite, uniform state into such structures was given in Chapter 2, and here we consider the formation of structure in the light of our account of the big bang model. Our starting point is to consider a simple, but rather unrealistic scenario in which all the matter in the Universe is assumed to be baryonic. We shall then see how the study of the growth of structure can provide some clues as to the nature of the non-baryonic matter that is actually believed to have been present.

6.6.1 Gravitational collapse in a baryonic matter Universe

You have already seen (Chapter 2) that structure is believed to form as a result of the gravitational collapse of a region that is initially denser than average. The early stages of this process are very gradual. Remember that the Universe is expanding, and initially, over-dense regions will simply expand at a slower rate than average. Furthermore, the density variations in the early Universe are at a low level. Since the density of the Universe is changing with time, it is useful to express the magnitude of density variation using the **relative density fluctuation**, which is defined as follows

For clarity, we have used ρ rather than ρ_m to denote the density of matter in this equation. We shall continue to use this simplified notation in the next chapter.

$$\frac{\Delta\rho}{\rho} = \frac{\text{density within a fluctuation} - \text{mean density of the Universe}}{\text{mean density of the Universe}}$$

The level of the primordial fluctuations suggests that in the early Universe $\Delta\rho/\rho \sim 10^{-5}$.

Whether a particular density enhancement will grow by gravitational collapse depends on the balance between two effects. One effect is the self gravity of the matter within the over-dense region which, of course, tends to cause collapse. The opposing effect is due to pressure which acts to stabilize over-dense regions against collapse. Which of these two effects is dominant under specified conditions depends on the mass of the region. The British scientist Sir James Jeans, who first analysed gravitational collapse in relation to the formation of stars, discovered that a key parameter is a quantity that is now known as the **Jeans mass**. The Jeans mass represents the boundary between two different types of behaviour. If the mass of an over-dense region exceeds the Jeans mass then it will collapse. However, a region that contains less than the Jeans mass would be supported by its internal pressure and hence be stable.

The horizon distance plays an important role in the discussion of stability against collapse. An over-dense region that is larger than the horizon distance cannot be supported by its internal pressure. This is because any changes in pressure are propagated at a speed that is lower than the speed of light. Nevertheless, the relative density fluctuation within this over-dense region *does* grow with time, albeit slowly, since the over-dense region is expanding at a lower rate than the Universe around it. However, the horizon distance increases with time, so eventually, the over-dense region will lie within the horizon distance and can respond to internal pressure changes. After this time, an over-dense region can be stable against collapse provided that the mass within this region is less than the Jeans mass.

The Jeans mass depends on the density and pressure of the region under consideration. In an expanding Universe, the density and pressure change as the scale factor changes. This causes the Jeans mass also to vary with time – this behaviour is shown in Figure 6.21. Note that the Jeans mass increases steadily with scale factor during the radiation-dominated phase, but it then flattens out and then drops at the time of recombination. To help in interpreting this diagram, it is useful also to indicate the criterion that the diameter of an over-dense region must be less than the horizon distance before it can become stable against collapse. To do this, Figure 6.21 also shows a quantity called the **horizon mass** which is the mass contained within a sphere with radius equal to the horizon distance. As expected, the horizon mass increases with time because the horizon distance increases with time (because light has had the time to travel further). The region above the horizon mass line represents over-dense regions that have a diameter greater than the horizon, and as mentioned above, these grow in a rather sedate fashion.

Figure 6.21 implies that, prior to the time when matter and radiation energy densities became equal, any over-dense region with a mass of up to about $10^{16}M_\odot$ will at some time be overtaken by the horizon – that is, the mass within the region will be overtaken by the horizon mass. However the horizon mass and the Jeans mass are very close to one another, so almost immediately, the mass of such an over-dense region will also be overtaken by the Jeans mass. Thus, the over-dense region will become stable against collapse, and the amplification of fluctuations as a result of gravitational contraction comes to a halt – at least temporarily.

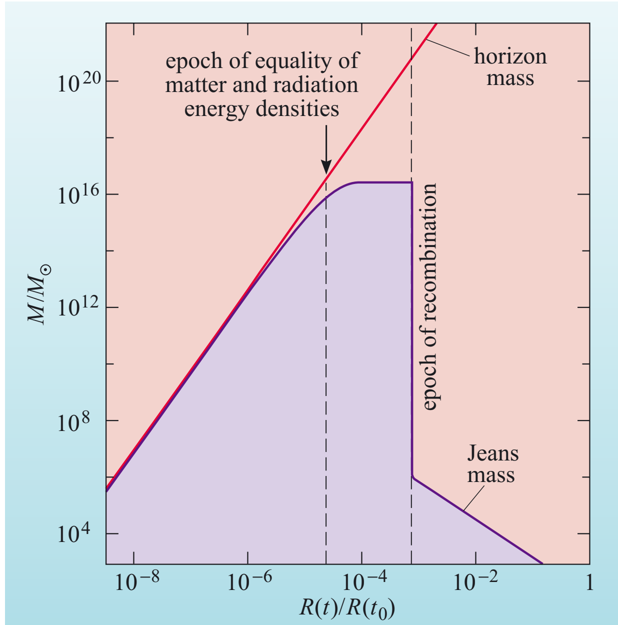

Figure 6.21 The variation of the Jeans mass (purple line) and the horizon mass (red line) as a function of the scale factor ($R(t)/R(t_0)$). Gravitational collapse only occurs for regions of the diagram that are shaded in pink. Regions that are shaded in lilac are stable against collapse. (Adapted from Longair, 1998)

An important change occurs at the time of recombination: the Jeans mass drops dramatically. Prior to recombination the major contribution to the pressure arose from the interaction of photons with free electrons. After recombination electrons become bound into neutral atoms which do not interact with the background photons. The radiation pressure becomes negligible and the only source of support against collapse comes from the thermal pressure of the gas. This thermal pressure is much smaller than the radiation pressure prior to recombination, so much smaller masses suddenly become unstable to gravitational collapse. The Jeans mass drops from a value of about $10^{16}M_\odot$ just before recombination to about $10^5M_\odot$ just after. Thus, any fluctuations in the mass range from $10^5M_\odot$ to $10^{16}M_\odot$ that had previously been stabilised, suddenly find themselves, in a manner of speaking, without any visible means of support. Collapse then proceeds in earnest, and it is the smaller fluctuations, with masses close to $10^5M_\odot$, that will most rapidly collapse to form virialized systems.

So far, this account of the formation of structure looks promising. Gravitational collapse is essentially arrested until the time of recombination, but soon after this the Jeans mass drops to a value of $10^5M_\odot$, a mass that is typical for the oldest known stellar systems – the globular clusters. There is however a fundamental problem with this scenario that relates to the level of relative density fluctuation that would be required at recombination in order for this model to produce the structure that we observe in the present-day Universe. Detailed calculations show that this purely baryonic model would require fluctuations in density at recombination that would be detectable now as temperature fluctuations in the cosmic microwave background at the level of about 1 part in 10^3.

■ Why is this a problem for this model?

❑ The observed amplitude of fluctuation in temperature in the cosmic microwave background is about 1 part in 10^5 – about a hundred times too small to give rise to the structures observed in the present-day Universe.

An alternative way of viewing the problem is that there has been insufficient time since recombination for fluctuations to grow from their observed value at that time (1 part in 10^5) to give the structure that we observe today.

We have seen throughout this book that dark matter plays an important dynamical role in many astrophysical systems, so it seems sensible to consider whether dark matter may help in resolving the problem of structure formation.

■ If the dark matter was baryonic in nature, could that help in resolving the problem of formation of structure?

❏ No. We have just seen that any baryonic matter – whether it ends up being luminous or dark – could not give rise to the structure that we see in the present-day Universe.

In the next section we will see how the formation of structure might be modified by the presence of non-baryonic dark matter.

6.6.2 Gravitational collapse with dark matter

In Chapter 2 we saw that numerical simulations of the formation of structure usually incorporate a dark matter component.

It was also noted that hot dark matter scenarios typically cannot reproduce structures across the range of scales that are observed in the present-day Universe. Cold dark matter models seem somewhat more successful, and here we will consider how cold dark matter could play a vital role in forming structure in the Universe.

In the context of cold dark matter, the term 'cold' refers to the fact that the particles have been moving at speeds much slower than the speed of light since very early times in the history of the Universe. This in itself does not help in the formation of structure – since this is essentially the same as the behaviour of the normal baryonic matter in the Universe. As you saw in the previous section, the formation of structure requires a higher degree of density fluctuation at the time of recombination than is observed. This could happen if the cold dark matter particles do not interact to any significant extent with photons or with the baryonic matter. This would mean that the cold dark matter particles would not be supported by the radiation pressure, and so gravitational collapse of density fluctuations of this cold dark matter could start before the time of recombination.

This lack of interaction with photons or electrons is an important characteristic of cold dark matter particles. The term **weakly interacting massive particle** or (**WIMP**) is often used to denote the hypothetical cold dark matter particles. The term 'weakly' refers to the fact that such particles only interact by the weak interaction and do not take part in electromagnetic or strong interactions (they do however respond to gravitational fields). The issue of what WIMPs might actually be is considered in Chapter 8.

In cold dark matter scenarios, primordial fluctuations can start to grow at much earlier times than the epoch of recombination. There is ample time for the density fluctuations in this matter to reach a value of one part in 10^3 at the time of recombination. This level of fluctuation is not evident on the last-scattering surface because there is no significant interaction between WIMPs and photons. Furthermore the behaviour of the baryonic matter is dominated by radiation pressure up until recombination, and thus its distribution appears smooth to one part in 10^5, just as if the Universe contained only baryonic matter.

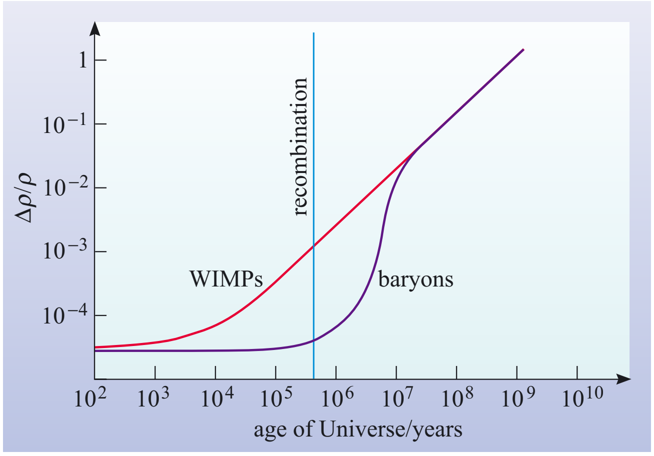

Figure 6.22 The evolution of density perturbations for matter in the form of WIMPs and baryons. The magnitude of a perturbation is characterized by the typical fractional change in density ($\Delta\rho/\rho$). (Adapted from Kolb and Turner, 1990)

After recombination however, the dominant effect on baryonic matter is the gravitational attraction of regions in which over-densities of cold dark matter have accumulated. In a sense the baryonic matter 'falls into' the density enhancements of cold dark matter. This behaviour is summarized in Figure 6.22 which shows the evolution of density enhancements, characterized by the typical relative density fluctuation ($\Delta\rho/\rho$) of matter in the form of WIMPs and in baryons.

Models of the formation of structure under the influence of cold dark matter have undergone scrutiny by conducting computer-based simulations and comparing the resulting structure to that which is measured in the real Universe. The comparison that is made between the outcome of a simulation and real observations usually involves some statistical measure of the structure such as a counts-in-cells analysis as described in Section 4.6. An added, and major, complication is that it is not clear how closely the visible mass in the Universe traces the distribution of dark matter.

Such studies are able to constrain some cosmological parameters relating to the distribution of cold dark matter. For instance, it is possible to rule out the cosmological model which has a mass density parameter $\Omega_m = 1$, no cosmological constant ($\Lambda = 0$), and in which the matter in predominantly in the form of cold dark matter – this is often referred to as the 'standard cold dark matter' (SCDM) model (a simulation of this case is shown in Figure 6.23a). However, other variants of cold dark matter models do produce structure that is similar to that which occurs in

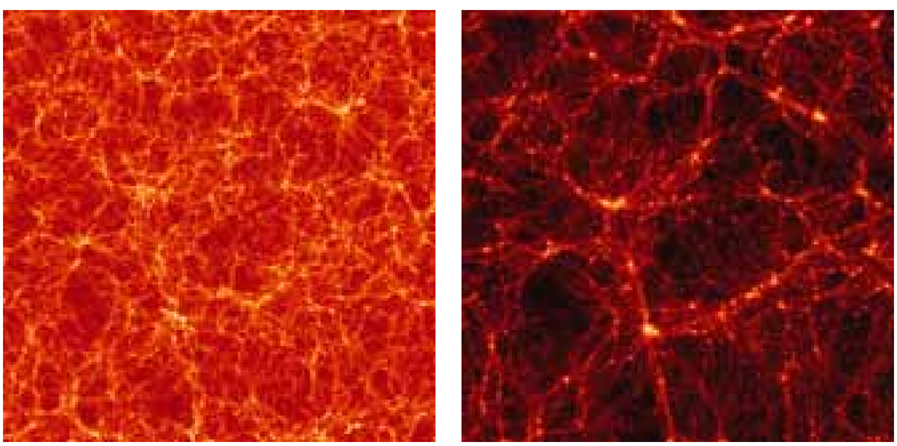

(a) (b)

Figure 6.23 The results of numerical simulations of the formation of structure in two different dark matter scenarios. Both of the models shown have cold dark matter as the dominant contribution to mass. The simulations show the distribution of matter at the present time. (a) A model with no cosmological constant and $\Omega_m = 1$. (b) A model with a non-zero cosmological constant and with $\Omega_m + \Omega_\Lambda = 1$. The model in (a) is incompatible with the observed structure in the real Universe, whereas model (b) gives rise to structure that is similar to that which is observed. (Jenkins *et al.*, 1998/The Virgo Consortium)

the real Universe. For instance one cosmological model with cold dark matter, a non-zero cosmological constant and a flat geometry (the so-called ΛCDM model) appears to be a good representation of reality (Figure 6.23b).

So study of the formation of structure can provide useful information about the nature of dark matter, but it cannot simultaneously determine the values of the cosmological parameters. However, there are other observational techniques that do allow the cosmological parameters to be constrained, and it is to this topic that we turn in the next chapter.

6.7 Summary of Chapter 6

The evolution of the cosmic background radiation

- The cosmic background radiation has a black-body spectrum and its current temperature is about 2.73 K.
- The temperature T of the cosmic background radiation varies with scale factor $R(t)$ according to

$$T \propto \frac{1}{R(t)} \tag{6.6}$$

- At times when the scale factor of the Universe was much smaller than at present, the temperature of the cosmic background radiation would have been much higher.
- At early times the dominant contribution to the energy density of the Universe was that due to radiation. At such times, the temperature is related to time by

$$(T/\mathrm{K}) \approx 1.5 \times 10^{10} \times (t/\mathrm{s})^{-1/2} \tag{6.19}$$

The very early Universe

- Current physical theory breaks down in describing events that took place at, or before, the Planck time ($t \sim 10^{-43}$ s).
- It is speculated that major physical effects could have arisen when grand unification ended ($t \sim 10^{-36}$ s). At this time, the strong and electroweak interactions became distinct. One such effect may be the process of inflation, which resulted in the scale factor increasing very rapidly for a short period of time.
- At early times, the content of the Universe would have been all types of quark and lepton and their antiparticles. There were also particles present that mediate the fundamental interactions (such as the photon), as well as dark-matter particles. There was a slight excess of matter over antimatter.
- At $t \sim 10^{-5}$ s free quarks became bound into hadrons. Most of these hadrons either decayed or annihilated with their antiparticles, leaving only protons and neutrons. For every 10^9 or so annihilation events that occurred, there would have been one proton or neutron left over.
- At $t \approx 0.7$ s neutrinos had their last significant interaction with other particles (apart from the effects of gravity). Shortly after this, electron–positron pairs annihilated, leaving only a residual number of electrons whose summed electric charges exactly balance the charge on the protons.

Primordial nucleosynthesis

- In the first few hundred seconds of the history of the Universe, the physical conditions were such that nuclear fusion reactions could occur. Such reactions led to the formation of deuterium, helium and lithium.
- The first step in the production of helium is the formation of deuterium. This nuclide is unstable to photodisintegration at temperatures above 10^9 K. The formation of helium did not start until $t \approx 225$ s. During this time, some neutrons decayed to protons, and this had an effect on the mass fraction of helium that was produced by primordial nucleosynthesis.
- The mass fraction of helium that is predicted by primordial nucleosynthesis is about 24%. This is in good agreement with measurements of the helium abundance in interstellar gas and stars, and provides very strong evidence to support the hot big bang model.

The scattering of photons and the cosmic microwave background

- The cosmic microwave background that is observed at the present time, is radiation that was last scattered at a redshift of about 1100 ($t \sim 3$ to 4×10^5 years). The radiation appears to originate from the last-scattering surface which is at this redshift.
- The scattering of background radiation photons stopped when the number density of free electrons became very low, and this occurred because of the recombination of electrons and nuclei to form neutral atoms.
- The observed high degree of uniformity of the cosmic microwave background leads to the horizon problem – which is that regions of the last-scattering surface that are more than about 2° apart could not have come into thermal equilibrium by the time that last scattering occurred.
- Our motion relative to co-moving coordinates can be determined by analysis of the observed dipole anisotropy of the cosmic microwave background.
- The cosmic microwave background shows intrinsic anisotropies in temperature at a level of a few parts in 10^5. These anisotropies result from density variations in the early Universe.

The formation of structure

- The formation of structure in the Universe would have proceeded by gravitational collapse from density fluctuations in the early Universe.
- Prior to recombination, the high degree of scattering between photons and electrons prevented density fluctuations in baryonic matter from growing substantially.
- If all matter was baryonic in form, then the level of fluctuation that is observed on the last scattering surface is too small to explain the structure that we observe at the present time.
- The observed level of structure in the present-day Universe can be explained if density fluctuations in non-baryonic matter had begun to grow prior to recombination, and baryons were subsequently drawn into those collapsing clouds of dark matter.

Questions

QUESTION 6.14

Draw a 'time-line' for the history of the Universe that indicates the major events that occurred at different times from the Planck time to the present day. Include on this time-line an indication of the temperature at the times of these events.

QUESTION 6.15

Briefly summarize what is meant by a 'theory of everything'. Why is such a theory required to understand the processes that occurred in the very early Universe?

QUESTION 6.16

During the process of inflation, the scale factor would have increased by an enormous factor. What consequences would this have for the temperature at this time?

QUESTION 6.17

State what the qualitative effect would be on the mass fraction of helium-4 produced by primordial nucleosynthesis if the photodisintegration of deuterium required photons of much higher energy than 2.23 MeV.

QUESTION 6.18

Suppose we received a message from (hypothetical) astronomers in a galaxy that has a current redshift of $z = 2.5$. What would they say they found as the temperature of the cosmic microwave background at the time of their transmission?

CHAPTER 7
OBSERVATIONAL COSMOLOGY – MEASURING THE UNIVERSE

7.1 Introduction

Observational cosmology is the branch of science concerned with measuring the parameters that characterize the Universe. Some of the most important of those parameters were introduced in Chapter 5, including the Hubble constant H_0, the current value of the deceleration parameter q_0, the age of the Universe t_0, and the current values of the density parameters for matter and for the cosmological constant (dark energy), $\Omega_{m,0}$ and $\Omega_{\Lambda,0}$, respectively. (The cosmological constant, Λ, can be given as an alternative to $\Omega_{\Lambda,0}$.) The study of the early Universe in Chapter 6, with its emphasis on nuclear and subnuclear processes, introduced several more parameters, including the current value of the density parameter for baryonic matter $\Omega_{b,0}$ (one of the contributions to $\Omega_{m,0}$). Other parameters may arise from any detailed proposal regarding the nature of dark matter. Yet more parameters can be associated with the cosmic microwave background radiation (CMB). Since the CMB has a black-body spectrum, one of the most important of these parameters is the present temperature of the CMB. This is currently one of the best determined of all the cosmological parameters: according to a widely quoted result, its value is $T_{cmb} = (2.725 \pm 0.002)\,K$.

This chapter is mainly concerned with the determination of just a few of these parameter values, particularly H_0, q_0, $\Omega_{m,0}$, $\Omega_{\Lambda,0}$ and $\Omega_{b,0}$. The first four of these determine which of the various Friedmann–Robertson–Walker models (FRW models; introduced in Chapter 5) provides the best description of the Universe we actually inhabit. The fifth, the current value of the density parameter for baryonic matter, represents a particularly familiar contribution to the total matter density. The current 'best values' for these five parameters are discussed, along with the methods used to arrive at those values and the degree of uncertainty in each result. As you will see, there is growing confidence among observational cosmologists that they are finally closing in on the true values of these parameters. If this confidence is well placed, it should soon be possible to eliminate much of the uncertainty that has traditionally been associated with determining the most appropriate model for our Universe.

One topic that arises at several different points in our discussion is the CMB. You have already seen that its absolute temperature is known to better than one part in 10^3, which is an extraordinary level of precision for any cosmological parameter. The precision of this result is an indication of what is now happening throughout observational cosmology. In the view of many cosmologists, we are just entering an age of *precision cosmology*, in which the values of the key cosmological parameters will be determined accurately and precisely. As is explained later, it is our ability to measure and understand the CMB that is leading the way into this new era. However, other methods are still important, since the confidence in precise CMB measurements is based on their agreement with several more traditional kinds of measurement. For this reason, the more traditional methods are discussed in Sections 7.2, 7.3 and 7.4, while Section 7.5 is entirely devoted to the CMB and precision cosmology.

Any account of observational cosmology is likely to become quickly outdated. Even as this chapter was being written, new observational data became available from a space probe called WMAP. These data are discussed in Section 7.5, and give just one indication of the need to be always alert for new findings and new developments in a

subject as vibrant and active as observational cosmology. This chapter can provide nothing more than a snapshot of this fast-moving field.

7.2 Measuring the Hubble constant, H_0

The Hubble constant is in many ways the most fundamental of the cosmological parameters. Of them all, it is the one most easily related to the 'theoretical' parameters that characterize the FRW models, and the value of H_0 plays an important part in almost all determinations of the other constants. In this section we discuss two methods of determining H_0. A third method, based on the CMB, is discussed in Section 7.5. First, though, here are some questions to help you recall what you learned about the Hubble constant and the related Hubble parameter in Chapter 5.

■ Briefly describe the curvature parameter k, and the scale factor $R(t)$ that appear in the FRW models, and state which aspects of space–time they describe.

❏ The *curvature parameter* k may be −1, 0 or +1. It indicates the sign of the curvature of space, and helps to determine geometric properties such as the sum of the interior angles of a triangle, the relationship between the radius and the circumference of a circle, and whether neighbouring straight lines that are initially parallel will converge or diverge. The positive value, $k = +1$, indicates that space has a finite total volume; the values $k = 0$ and $k = -1$ indicate that space is infinite.

The *scale factor* $R(t)$ varies with time, t. It describes the uniform expansion or contraction of space. If the positions of galaxies are expressed in terms of co-moving coordinates (i.e. ones that expand with the Universe) then the coordinate separation of two galaxies might have the fixed value r, but the physical distance between those galaxies (measured in metres, say) will be proportional to $R(t)$, and will increase as $R(t)$ grows and the Universe expands.

■ What is the precise relationship between the Hubble constant H_0 and the scale factor $R(t)$? You may find it useful to start by defining the Hubble parameter.

❏ The *Hubble parameter*, $H(t)$, is a fractional measure of the rate of change of the scale factor (see Section 5.4.1). In terms of symbols, this relationship may be written as

$$H(t) = \frac{\dot{R}(t)}{R(t)} \tag{7.1}$$

where $\dot{R}(t)$ represents the rate of change of R at time t. The *Hubble constant*, H_0 is simply the value of the time-dependent Hubble parameter $H(t)$ at the present time t_0; that is to say,

$$H_0 = H(t_0) \tag{7.2}$$

■ Write down Hubble's law and suggest a way in which this can be used to determine the Hubble constant from observations.

❏ According to Hubble's law, the redshift (z) of galaxies increases in proportion to their distance (d) from us, provided the redshift is not too great (less than

about 0.2, say). If the constant of proportionality is identified as H_0/c, then Hubble's law may be written

$$z = \frac{H_0}{c} d \tag{7.3}$$

This suggests that if the redshifts of a sample of galaxies are measured, and if the distances of the same galaxies are determined independently of the redshifts, then those observational data can be used to determine H_0/c, and hence H_0, since c is well known. One way of doing this would be to plot a graph of z against d, determine the best straight line through the data points and then measure the gradient of that line, since this gradient should be H_0/c.

7.2.1 Determinations of H_0 using the Hubble diagram

The first determination of the Hubble constant was by Hubble himself, and was published in 1929. The determination appeared in the paper in which Hubble announced the law that is now named after him, and was based on measurements of the distances of 24 relatively nearby galaxies. The redshifts of these galaxies were already known thanks to the work of Vesto M. Slipher (1875–1969), who had systematically measured the redshifts of almost all the spiral galaxies that were known at the time. Hubble determined the distances of the 24 galaxies by using Cepheid variables and other distance indicators in the manner described in Chapter 2. For those galaxies where Cepheid variables could be seen, the distances were deduced as follows.

- The *period* of each Cepheid was measured by recording the rise and fall of its apparent magnitude and determining the time between successive maxima. Technically this amounts to measuring the *light curve* of the Cepheid – a plot of apparent magnitude against time over a complete period.
- A previously calibrated *period–luminosity relation* for Cepheids was then used to determine the luminosity or (equivalently) the *absolute magnitude* of each Cepheid.
- The absolute magnitude M determined in this way was then combined with a measurement of the apparent magnitude m to determine the *distance* of each of the Cepheids, and this was assumed to be the distance of the galaxy that contained the Cepheid.

Independently of these distance measurements, the formula $v = cz$ was used to assign a 'naive' recession speed v to each of the 24 galaxies on the basis of its measured redshift z. We refer to v as the 'naive' recession speed since the use of $v = cz$ was based on the assumption that the redshift z is the result of a simple Doppler shift, which is not true. The value of v differs from the real recession speed of the galaxy, and the discrepancy increases with the redshift. Nonetheless, the measurements made it possible for Hubble to represent each of the 24 galaxies by a single point on a plot of naive recession speed against distance, as shown in Figure 7.1.

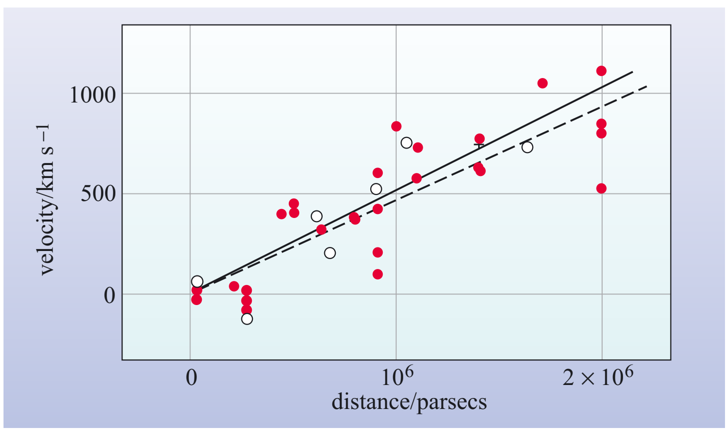

Figure 7.1 The original 'Hubble diagram', based on a figure that appeared in 1929. The 24 galaxies are represented by the red dots; the solid line represents the best straight line through the data. The open circles and the dotted line refer to nine groups of galaxies that Hubble also considered. (Courtesy of the National Academy of Sciences)

The data points were somewhat scattered, but Hubble detected a linear trend, and on this basis claimed that the recession speed of galaxies increased in proportion to their distance from us. From the gradient of the straight line in Figure 7.1, Hubble deduced that the rate of increase of recession speed with distance was $500\,\mathrm{km\,s^{-1}\,Mpc^{-1}}$. Using the notation and terminology of modern astronomers, the relation that Hubble proposed can be rewritten as $\upsilon = H_0 d$, where $\upsilon = cz$, and H_0 is Hubble's constant. From this we obtain the modern form of Hubble's law, $z = (H_0/c)d$, and we can see that $500\,\mathrm{km\,s^{-1}\,Mpc^{-1}}$ represents the first determination of the Hubble constant H_0. This value is far outside the range of values that are currently thought to be credible, but the measurement is historically important as the start of a long campaign to measure H_0.

There have now been hundreds of attempts to determine the Hubble constant. Like all observational results, these determinations are subject to various kinds of uncertainty. There are, for instance, the **random uncertainties** that beset any measurement, and which generally cause different determinations of a measured quantity to vary about some mean value. In addition there may be **systematic uncertainties**, which will always influence the measured value in the same way, no matter how many times the measurement is repeated. It is now known that there were substantial systematic uncertainties in the early determinations of the Hubble constant. Some of these were the result of studying only nearby galaxies where the motion was dominated by 'local' effects, such as the attraction of the local supercluster (see Chapter 4), rather than the large-scale Hubble flow. Others arose from the mistaken belief that two different kinds of variable star were actually the same kind of Cepheid. However, even after these sources of error were removed, different determinations of the Hubble constant still tended to disagree by substantial amounts. This is indicated in Figure 7.2, where the results of various determinations of H_0 are plotted against the year in which they were made. Note that uncertainty ranges, represented by vertical bars through the data points, have been used to show the range of values that are consistent with the measured results, rather than pretending that each measurement results in a unique value. Estimating the appropriate size for the uncertainty range in an astronomical

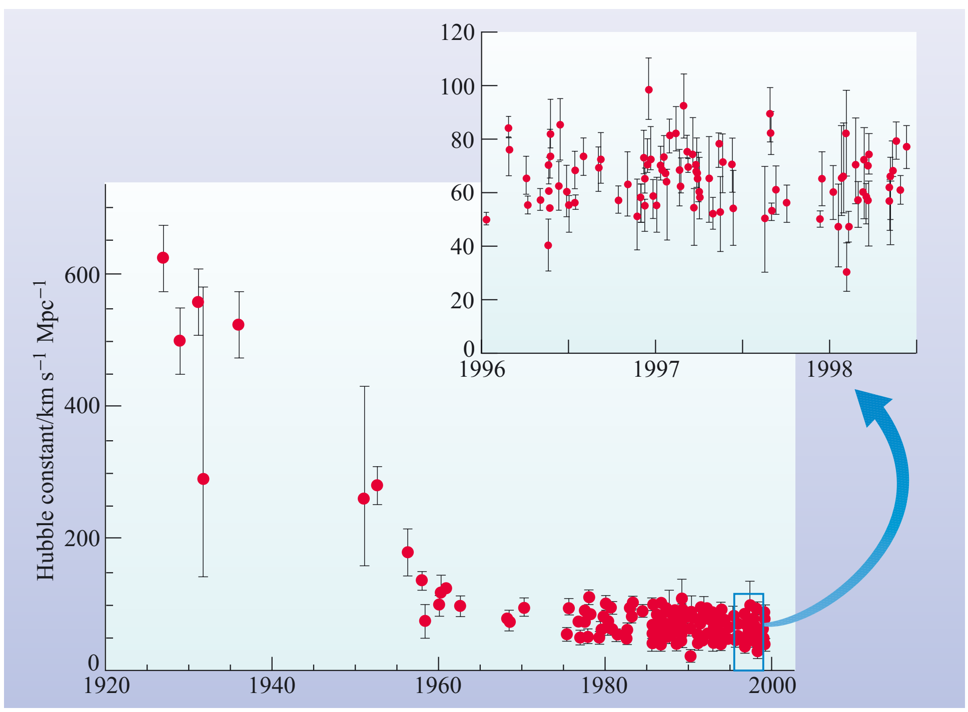

Figure 7.2 The evolution of the measured value of the Hubble constant H_0. Over 300 measurements performed since 1975 have yielded values between 50 and $100\,\mathrm{km\,s^{-1}\,Mpc^{-1}}$. (Adapted from *Sky and Telescope*, based on work by J. Huchra and the HST Key Project on the Distance Scale)

measurement is often highly complicated and very time consuming, but it is vital if other scientists are to properly appreciate the significance of the results.

As the figure shows, by the 1980s a large number of determinations indicated that the Hubble constant was probably somewhere in the range between 50 and 100 $\mathrm{km\,s^{-1}\,Mpc^{-1}}$, and for a while there were strong proponents of either end of that range. Perhaps the most notable were Gerard de Vaucouleurs who favoured a high value of the Hubble constant, and Allan Sandage who favoured a low value. The disagreement between these eminent astronomers was not caused by the inherent difficulty of making the observations, but rather by the different procedures they adopted when interpreting their observations and correcting them for various observational effects.

In an effort to reduce the uncertainty, one of the designated '*key projects*' of the Hubble Space Telescope (HST) in the 1990s was a programme to determine the Hubble constant to an accuracy of about 10%. The efforts of a team of astronomers, led by Canadian-born US astronomer Wendy Freedman, resulted in the value $H_0 = 72 \pm 8\,\mathrm{km\,s^{-1}\,Mpc^{-1}}$, which has now been supported by more recent CMB-based measurements.

The basis of the HST Key Project to measure H_0 was to use the Cepheid period–luminosity relationship to calibrate other methods of distance measurement. The period–luminosity relation that was used was based on studies of Cepheids in our neighbouring galaxy, the Large Magellanic Cloud (LMC), which is sufficiently close for large numbers of Cepheids to be observed. The calibration of the Cepheid period–luminosity method required the distance to the LMC to be known, and it was assumed, on the basis of measurements made by other researchers, that the LMC is at a distance of 50 kpc from the Sun.

The first stage of observations was to search for Cepheids in selected galaxies which lie between about 3 and 25 Mpc from the Milky Way. At these distances the 'local' motion of galaxies still has a significant effect on their measured redshifts, so the selected galaxies could not themselves be used to determine the Hubble constant. However, once the Cepheids had been found and measured, the distances of the selected galaxies could be precisely determined. Once this had been done, a variety of measurements made in those selected galaxies could be used to calibrate other methods of distance measurement that could be applied to more remote galaxies, which were more likely to represent the Hubble flow. The galaxies that were searched for Cepheids were carefully chosen so as to allow the calibration of not one, but five other methods of distance measurement, all of which were discussed in Chapter 2.

■ On the basis of Chapter 2, name five methods of galactic distance determination (excluding the use of Hubble's law) that are appropriate for measuring distances to about 100 Mpc. Briefly explain the nature of the 'calibration problem' that these methods must confront.

❑ The five methods appropriate for measuring distances to about 100 Mpc are: the Type Ia supernova method; the Type II supernova method; the methods based on the Tully–Fisher and fundamental plane relations; and the method based on surface brightness fluctuations.

The calibration problem consists of making measurements in relatively nearby galaxies at known distances (between about 3 and 25 Mpc in the case of the HST Key Project) that enable the 'relative' distances indicated by standard candles in more remote galaxies to be converted into 'absolute' distances that may be expressed in units such as megaparsecs.

Table 7.1 A summary of the different methods used to measure H_0 from the HST Key Project.

Distance measurement method	Number of Cepheid calibration measurements	Number of measurements used to obtain H_0	Range of redshift in the measurements used to obtain H_0	Value of H_0 obtained/km s^{-1} Mpc^{-1}
Type Ia supernovae	6	36	0.013–0.10	71
Type II supernovae	4	4	0.006–0.047	72
Tully–Fisher relation	21	21	0.003–0.030	71
fundamental plane	3	11	0.003–0.037	82
surface brightness fluctuations	6	6	0.013–0.019	70

The five methods used to determine H_0, along with their results, are shown in Table 7.1. The numbers of measurements used to calibrate the five methods are shown in the second column. The fact that some techniques were calibrated using a small number of galaxies highlights the difficulty of the calibration problem: prior to the HST measurements, some of the methods that are listed had never before been calibrated against the Cepheid period–luminosity method.

Having calibrated the five methods, the next stage was to use those methods to determine the distances of galaxies that are sufficiently far away that their measured redshifts are dominated by the expansion of the Universe rather than by any 'local' effects. The typical uncertainty in redshift caused by local effects is roughly 10^{-3}, so in order to bring this uncertainty to below 10% of the measured redshift, that measured redshift must be at least $z \approx 10^{-2}$. The actual ranges in redshift that were sampled using the five different methods of distance determination are shown in Table 7.1, along with the number of measurements that were used to obtain a value of H_0.

The correlation between redshift and distance for a number of galaxies and clusters, based on the HST Key Project results, is shown in Figure 7.3. One of the remarkable outcomes, evident from the fifth column of Table 7.1, is that the five different methods, which are based on quite different physical principles, agree well with one another. The values obtained for H_0 vary from 70 to 82 km s^{-1} Mpc^{-1}. This level of agreement provides some reassurance that there are no gross systematic differences

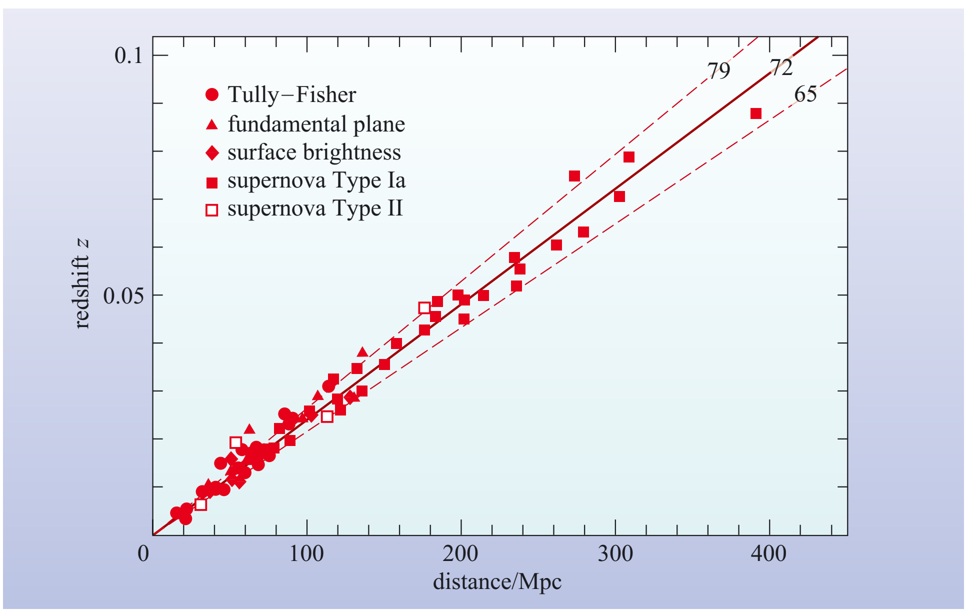

Figure 7.3 A modern version of the Hubble diagram from the HST Key Project, with recession speed replaced by redshift. Note that in this case the gradient of the graph will be equal to the quantity H_0/c. Various straight lines through the data are shown, together with the corresponding values of H_0 measured in km s^{-1} Mpc^{-1}. (Adapted from Freedman *et al*., 2001)

between the five methods that were adopted, and leads, after further analysis, to the result quoted earlier: $H_0 = 72 \pm 8\,\mathrm{km\,s^{-1}\,Mpc^{-1}}$.

Plots such as those in Figures 7.1 and 7.3 are examples of what are generally called **Hubble diagrams**. They still play an important part in the determination of the Hubble constant, although in modern versions, such as Figure 7.3, it is often the redshift z that is plotted along the vertical axis (rather than the 'naive' recession speed) and the range of redshifts is generally much greater than in the original Hubble diagram of Figure 7.1. This last point is important since it is only by extending the Hubble diagram to sufficiently distant galaxies, as the HST Key Project did, that there is any hope of escaping the effects of local motion and determining the true rate of expansion of the Universe.

7.2.2 Other methods of determining H_0

Because it has been so difficult to obtain convergence amongst measurements of H_0 based on the use of the Hubble diagram, there has always been an interest in other methods that might be used to determine the Hubble constant. A method based on detailed observations of the cosmic microwave background radiation is discussed in Section 7.5. Yet another method involves the phenomenon of *gravitational lensing* that was introduced in Chapter 4.

You will recall from Chapters 4 and 5 that, according to general relativity, matter and radiation cause space–time to curve, and the path of a light ray responds to that space–time curvature. This means that concentrations of matter, such as galaxies or clusters of galaxies, can act as 'gravitational lenses', which can magnify and distort an observer's view of objects that lie beyond the lens. A possible outcome of gravitational lensing is the formation of multiple images of the kind shown in Figure 7.4. In this case, the gravitational lens consists of a large, elliptical galaxy and a surrounding cluster of galaxies, while the two-part image provides two views, A and B, of a single quasar, QSO 0957+561 (quasars and their variable luminosities were discussed in Chapter 3). The redshift of this quasar is 1.41, while that of the elliptical galaxy is 0.36. The way the lens forms this image is shown in Figure 7.5.

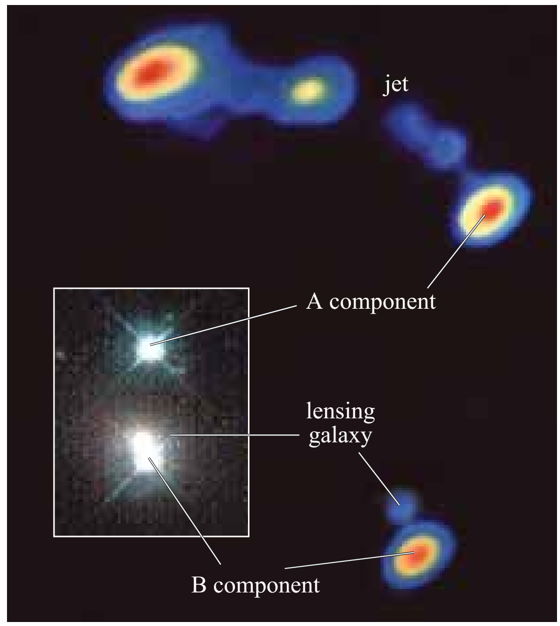

Figure 7.4 The two-component image of the gravitationally lensed quasar QSO 0957+561. The large, elliptical galaxy that is partly responsible for the lensing can be seen just above the B component of the quasar image. The main image was recorded by a radio telescope, the inset is an optical image. The jet is part of the quasar. (NRAO/AUI)

As Figure 7.5 indicates, the two images of the quasar reach the observer by different pathways that have different lengths. This means that any change that occurs in the quasar, such as a sudden brightening, will be observed in one image some time after it is observed in the other. In other words, as the two images fluctuate

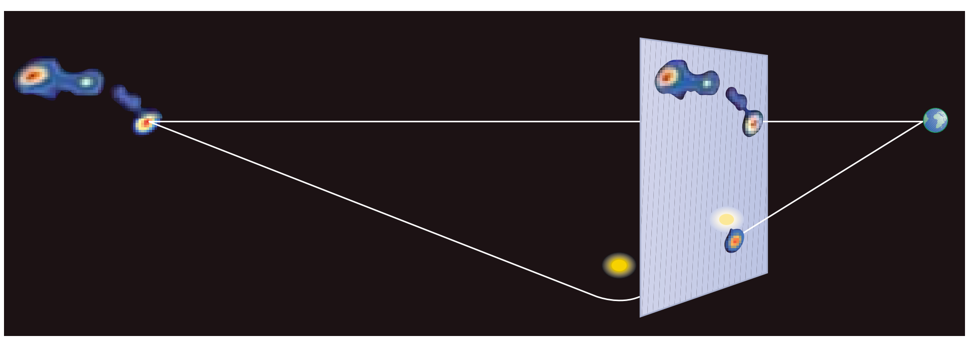

Figure 7.5 A schematic diagram, with an exaggerated angular scale, showing how the double image of QSO 0957+561 is formed. The distance to the lensing galaxy is a little over 1000 Mpc, about one-third of the distance to the quasar. Note that the two routes from the quasar to the observer are not of equal length. (Adapted from Henbest and Marten, 1983)

in response to changes in the quasar itself, there will be some time lag between the observed patterns of fluctuation of the two images due to the different path lengths from the quasar. Unfortunately, the difference in path length is not the only cause of a time lag between fluctuations in the two images. The distribution of material within the gravitational lens determines the detailed geometry of space in the neighbourhood of the lens, and this influences the time of passage for light as it passes through the gravitational lens. Light passing through the denser part of the lens is generally delayed relative to light passing through the less dense parts. Since the light responsible for the two images passes through different parts of the lens, just such a density-dependent time-of-passage contribution to the observed time lag between fluctuations in the two images can be expected. The total time lag, including both the path-length and the time-of-passage effect, has been measured for QSO 0957+561 and for a few other gravitational lenses (see Figure 7.6). In the case of QSO 0957+561 the time lag is about 415 days.

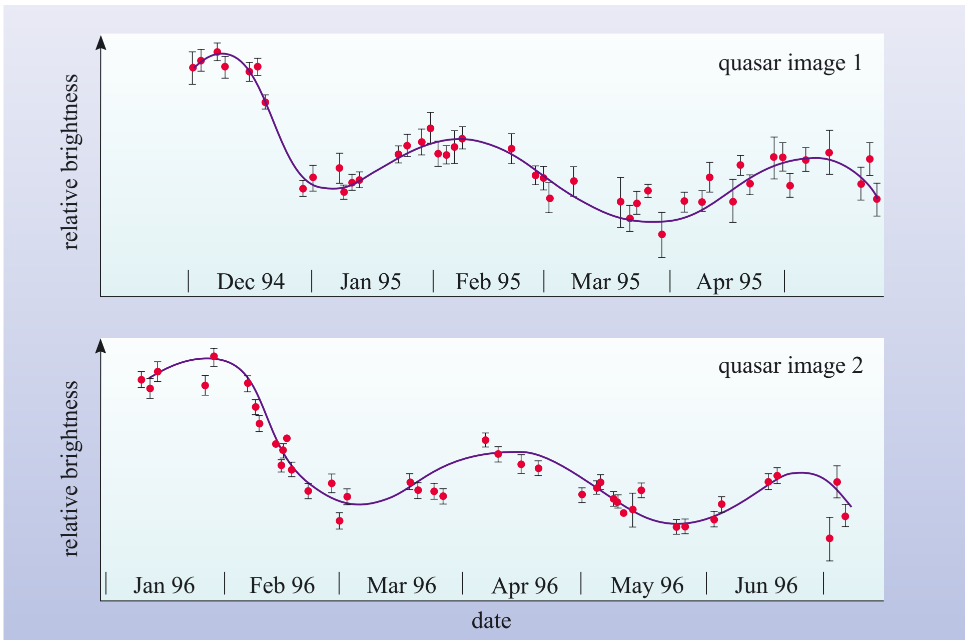

Figure 7.6 The observed patterns of brightness fluctuation in the two images of a double quasar differ by a fixed time lag. (Adapted from Schild and Thomson, 1997)

In the 1960s, well before the discovery of the first gravitational lens, it was known from theoretical calculations that the path length contribution to the time delay would depend on the Hubble constant. So, in principle, this part of the observed total time lag can be used to determine the Hubble constant without the need for calibration. However, in order to carry out such a determination it is first necessary to calculate the time-of-passage delay and to subtract that from the observed total time lag. Performing such a calculation involves formulating a theoretical ‘model’ of the lens and making a number of assumptions about the way that gravitating material is distributed within the lens. The need to model the lens in this way introduces a large degree of uncertainty into what might otherwise be a rather precise way of evaluating the Hubble constant. In the particular case of QSO 0957+561, the lens is dominated by a large, elliptical galaxy that is fairly simple to model. Even so, there are still several remaining uncertainties. At the time of writing, the best current estimate of H_0 from this particular source is about $(61 \pm 6)\,\mathrm{km\,s^{-1}\,Mpc^{-1}}$, but this is about 30% different from the ‘best’ value provided by the same source just a few years ago – the difference being almost entirely due to changes in the modelling.

Because of this sensitivity to modelling assumptions it's probably best to regard the gravitational lensing technique as providing a useful cross-check on the broad value of the Hubble constant, but to still need considerable improvement (at least in the certainty of theoretical modelling) before it can match other methods.

QUESTION 7.1

Listed below are some possible sources of error and uncertainty in a determination of the Hubble constant based on gravitational lensing. Classify each as either random or systematic, justifying your decision in each case.

(a) Uncertainty about the distribution of dark matter in the lensing galaxy.

(b) Failure to detect a small companion galaxy located directly behind the lensing galaxy.

(c) Difficulty, due to incomplete data, in determining the total time lag between fluctuations in the two images of the lensed galaxy.

7.3 Measuring the current value of the deceleration parameter, q_0

In the context of the Friedmann–Robertson–Walker models, the Hubble constant, H_0, measures the rate of expansion of the Universe. However, the Hubble constant only represents the *current* rate of expansion: the *current* value of the more general Hubble parameter $H(t)$ that describes the rate of expansion at *any* time t. The rate of expansion might have been higher or lower in the past, and may, in principle at least, be greater or smaller in the future. The observable quantity that tells us whether the cosmic expansion rate is currently increasing or decreasing is the current value of the deceleration parameter q_0, the current value of the time-dependent deceleration parameter $q(t)$ that was introduced in Chapter 5. A positive value of q_0 would indicate that the expansion is slowing down, a negative value that it is speeding up.

The current value of the deceleration parameter is expected to influence the relationship between the distance and the redshift of distant galaxies. As you saw in Chapter 5, to a first approximation this relationship is described by Hubble's law:

$$d = \frac{cz}{H_0}$$

but a more accurate relationship, according to the Friedmann–Robertson–Walker models, is given by

$$d = \frac{cz}{H_0}\left[1 + \frac{1}{2}(1 - q_0)z\right] \tag{7.4}$$

As was shown in Figure 5.29, these two different expressions agree well at low redshift, but they differ significantly when z is greater than about 0.2.

Equation 7.4 provides a way of determining the current value of the deceleration parameter from observation. It implies that a plot of d against z for distant galaxies will show systematic deviations from the straight line implied by Hubble's law if q_0 has any value other than $q_0 = 1$. In principle, then, we can expect to determine q_0 by

making accurate independent measurements of d and z and then determining which values of H_0 and q_0 in Equation 7.4 provide the best fit to the observed data. In practice, of course, this procedure is nothing like as simple as it sounds. You saw in the last section the enormous difficulty that astronomers have had in using this kind of approach to pin down the value of H_0, without the added complication of determining q_0 as well. With this in mind, you will not be surprised that many of the early attempts to measure q_0 were not particularly successful. Nonetheless, they deserve a brief discussion because of the light they shed on the observational challenges of measuring cosmic deceleration.

7.3.1 Early attempts to determine q_0

The direct proportionality between redshift and distance indicated by Hubble's law is in excellent agreement with the data obtained from galaxies out to redshifts of 0.1 or so. Hence any attempt to detect departures from Hubble's law must involve galaxies with redshifts greater than 0.1. Such measurements were not really possible until the late 1940s, when the 200-inch telescope on Mount Palomar (see Figure 7.7) was commissioned. Even then, observing individual bright stars in such distant galaxies was not possible, so distance determinations had to make use of clusters of stars, or even whole galaxies.

Early attempts to measure deceleration using the Palomar telescope concentrated on whole galaxies. Hubble had pointed out in 1936 that, if galaxies had some natural upper limit to their brightness, then the brightest galaxies in clusters that contained hundreds or thousands of galaxies might be expected to be close to that limit. Thus the brightest galaxy in a cluster might represent a 'standard candle' (i.e. a source of fixed luminosity or absolute magnitude), and once that absolute magnitude had been determined it should be possible to work out the distance of any such galaxy from an observation of its apparent magnitude. (This was the basis of the technique used by George Abell to determine the distances of the rich clusters discussed in Chapter 4.) Accepting this idea, an extensive survey involving clusters with redshifts up to $z = 0.18$, published in 1956, found evidence of curvature in the Hubble diagram and led to the value $q_0 = 3.7 \pm 0.8$. However, another study soon gave $q_0 = 1.0 \pm 0.5$, and a reconsideration of earlier work led to a claim that $q_0 = 0.2 \pm 0.5$. Clearly, this approach was not yielding consistent results, although there did seem general agreement that q_0 was probably positive, as might be expected in a Universe where gravity gradually slowed the cosmic expansion. By the late 1970s extensive studies of galaxies, theoretical as well as observational, were showing that attempts to use the brightest galaxies in clusters as standard candles were being seriously undermined by evolutionary effects, since the galaxies themselves showed signs of changing over time. The larger the redshift of the galaxy, the greater the time its light had spent travelling to the Earth, and the 'younger' the galaxy in cosmic terms; these youthful, bright galaxies did not, it was becoming clear, have the same luminosity as their more evolved 'older' counterparts at lower redshifts. Since these evolutionary effects were overwhelming the effects due to cosmic deceleration, the brightest-galaxy approach became discredited and some other technique had to be used to determine q_0.

Figure 7.7 The 200-inch telescope at the Mount Palomar observatory. The large, white structure that supports the open lattice-work of the telescope itself is aligned with the Earth's rotation axis to facilitate the tracking of stars. (Caltech Archives)

The alternative that came to the fore was based on the use of *supernovae*. As you know from earlier discussions, supernovae are highly luminous events that mark the explosive death of certain kinds of star. They can be classified into various types according to their spectra, with Type I supernovae being the most luminous. Astronomers are now keenly aware of the existence of various subclasses of Type I supernovae, such as the Type Ia supernovae that were discussed in Chapter 2. However, the early attempts to use supernovae to determine q_0 treated all Type I supernovae on the same basis.

Type I supernovae can easily be observed in galaxies with redshifts that are greater than 0.1, and may even be detected at redshifts as great as $z = 1$. This ensures that the galaxies containing the more distant supernovae are so far away that they are unlikely to be significantly influenced by local disruptions of the Hubble flow. Hence any value of q_0 based on observations of distant supernovae might be expected to be free of the systematic uncertainties that might affect more 'local' measurements.

Making the assumption that all Type I supernovae attain the same maximum luminosity, attempts were made to use them to determine q_0. The basic approach was similar to that based on brightest galaxies in clusters: measurements of the supernova's apparent magnitude were combined with the assumed 'standard' value of the absolute magnitude to determine the distance, while a separate measurement yielded the supernova's redshift. The way that the redshift varied with distance, for an appropriate sample of Type I supernovae, was expected to reveal the value of q_0. Unfortunately this particular approach was recognized as unreliable when it was realized that the broad class of Type I supernovae actually included several quite distinct types of supernova that differed in intrinsic brightness. However, this failure paved the way for the more recent attempts to measure the current value of the deceleration parameter using the carefully studied subclass of supernovae known as Type Ia supernovae. The results of this study have had such a significant impact on observational cosmology that they deserve to be discussed in a separate section.

QUESTION 7.2

Use Hubble's law to calculate the distance of a supernova in a galaxy with redshift $z = 1.0$. Explain why the distance you have estimated may not be a good estimate of the true distance to the galaxy. How does the distance you calculated compare with the size of the local supercluster, as discussed in Chapter 4?

7.3.2 Determinations of q_0 using Type Ia supernovae

Type Ia supernovae are believed to occur when a white dwarf star in a close binary system accretes so much matter from its binary companion that it exceeds a critical mass (about 1.4 times the mass of the Sun) and collapses under its own weight. In a rapid succession of events the collapse is transformed into an explosion that causes a rapid brightening of the supernova, followed by a more gradual decline that can typically be observed for a month or more.

Because the mass required to initiate the supernova is thought to be the same in all cases, and because the physical processes involved are believed to be always very similar, it is expected that all Type Ia supernovae attain approximately the same maximum brightness. This means that Type Ia supernovae might be used as 'standard candles' just like Cepheid variables with a known period.

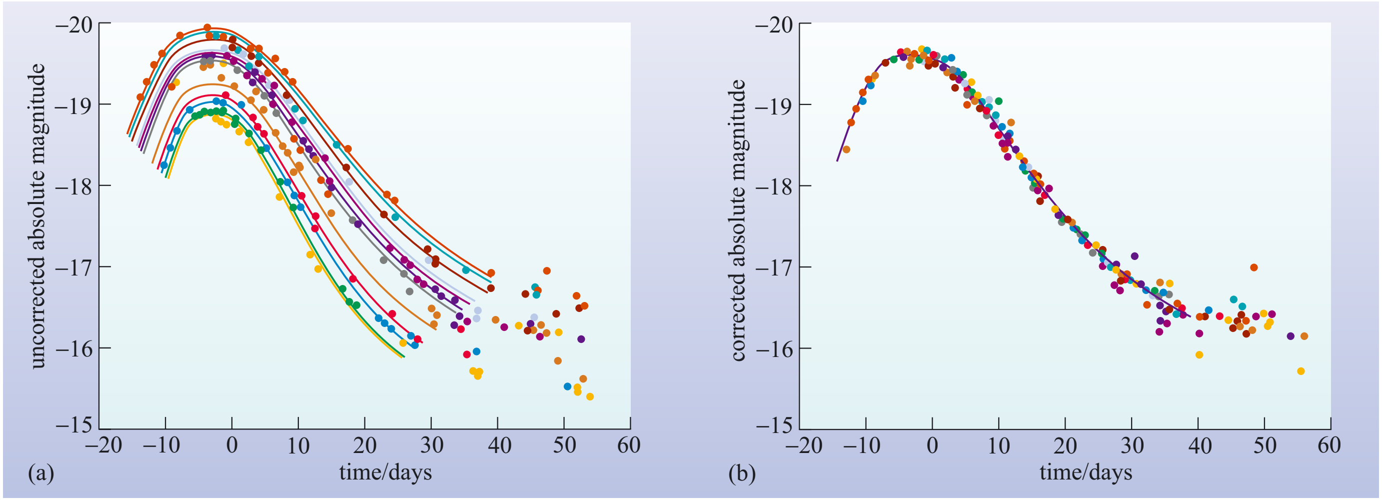

Figure 7.8 The light curves in (a) show the absolute magnitude of relatively nearby Type Ia supernovae as a function of time. Note that the greater the maximum luminosity the slower the decline in brightness from that maximum. (Crudely, the higher the curve, the wider it is.) Part (b) shows the effect of 'correcting' all the light curves according to a standard prescription derived from the observations. The 'corrected' light curves show much less intrinsic spread in maximum luminosity. (Adam Reiss)

In practice, simply expecting all Type Ia supernovae to have approximately the same luminosity is not a sufficiently good basis for a major observational research programme. Such a programme must also be supported by an extensive and painstaking investigation of Type Ia supernovae that enables any intrinsic differences between Type Ia supernovae to be studied, understood and, as far as possible, eliminated as a source of uncertainty. This constitutes the process of *calibration* that was described in general terms in Chapter 2. In this case it can be achieved by studying Type Ia supernovae that occur in galaxies whose distances can be determined independently of the supernovae. This work was effectively carried out in the early 1990s by a number of investigators, each pursuing their own goals. As a result, it was found that even within the tightly defined subclass of Type Ia supernovae there were still differences of around 35% in the maximum luminosity attained by different Type Ia supernovae. However, it was also found that the value of the maximum brightness correlates with the rate at which the brightness of the supernova declines from its maximum (see Figure 7.8). Thanks to this correlation it became possible to 'correct' the observed brightness of any particular Type Ia supernova in such a way that it behaved as though its maximum luminosity was actually within 15 to 20% of the maximum luminosity of any other Type Ia supernova. Unfortunately this correction lacks a sound theoretical basis, but it does appear to be what is needed to substantially reduce the intrinsic differences in luminosity between different Type Ia supernovae. Calculations indicated that 'corrected' observations of thirty or so Type Ia supernovae with redshifts roughly in the range 0.5 to 1 should provide a good indication of cosmic deceleration.

■ In general terms, what sort of observations would be necessary in order to 'correct' the brightness of any particular Type Ia supernova with the aim of minimizing the effect of intrinsic differences in luminosity?

❑ The apparent magnitude of the supernova would have to be measured repeatedly over a sufficiently long period (about a month) to determine the rate of decline of its light curve, and hence the supernova's peak luminosity relative to other Type Ia supernovae.

By the mid-1990s Type Ia supernovae were sufficiently well understood that they could reasonably be used to determine the current value of the deceleration parameter, and two independent teams of researchers set out to do this. The two

groups – the High-z Supernova Search Team and the Supernova Cosmology Project – faced similar challenges. Each group had to detect a reasonable number of Type Ia supernovae, measure the redshift of each, and carry out sufficient follow-up observations over a period of several weeks to determine the rate of decline in brightness of each supernova. They would then be able to ‘correct’ their observations in order to minimize the effect of the intrinsic differences in maximum brightness that exist between different Type Ia supernovae.

This programme presents many observational challenges and requires the involvement of several astronomers using a range of telescopes and detectors. The High-z Supernova Search Team, for example, included about two dozen astronomers from fifteen different institutions spread over four continents. Their search for distant Type Ia supernovae involved recording large-area images of the sky with sufficient sensitivity to detect the faint images of supernovae out to redshifts of about $z = 1$. This was initially done using large-area CCD detectors on the 4-metre telescope at the Cerro Tololo Inter-American Observatory (CTIO) in Chile, where the team was able to image about three square degrees of sky per night, down to a limiting magnitude of about 23. In order to identify candidate supernovae they imaged the same area of sky 21 days later and then compared the two images, looking for point-like objects that had changed in brightness over that time. (The period of 21 days was chosen to reflect the ‘rise time’ of a typical Type Ia supernova – the time it takes for the light curve to build up to a maximum, before starting its much slower decline.) The comparison was mainly an automatic process in which a computer program aligned the two images, compensated for various observational effects, and eliminated known stellar sources in our own Galaxy before presenting the astronomers with the data from which to make a final selection of candidate Type Ia supernovae. This resulted in about five to 20 candidates for each night of observation, most of which were later confirmed as Type Ia supernovae.

Once the candidates had been identified the detailed follow-up work could begin. This involved studying each candidate individually, both *spectroscopically* (to determine its redshift and to confirm that it really was a Type Ia supernova), and *photometrically* (to determine the light curve and hence the ‘corrected’ maximum brightness of the source). In the case of the High-z Supernova Search Team, the spectra were obtained using one of the 10-metre Keck telescopes in Hawaii (Figure 7.9). A very large telescope was needed because many of the candidates were very faint, so recording the light in their spectra required a large-aperture telescope that could capture as much light as possible in a relatively short time. The photometric (brightness) studies were carried out using a range of telescopes in both the northern and southern hemispheres. For some of the sources, even the Hubble Space Telescope was used. Accurate photometry generally involves comparing the object being studied with stars whose brightness has already been determined with great care, and often requires the observations to be made through a set of standard filters designed to pass light in specific ranges of wavelength. The use of filters allows the effects of obscuration (by dust in the host galaxy) to be determined and eliminated.

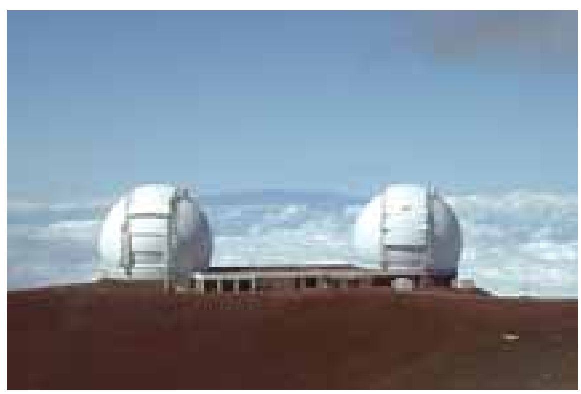

Figure 7.9 The twin domes of the two 10-metre Keck telescopes in Hawaii. (WY’east Consulting, 2002)

It’s important to note that the procedure adopted by the High-z Team was not designed to accurately determine the absolute magnitude of the high redshift supernovae. Rather, the aim was to

determine their brightness relative to one another (and relative to lower redshift Type Ia supernovae). This approach has the advantage of being simpler than methods requiring accurate measurements of absolute magnitudes, while still allowing deviations from Hubble's law to be detected.

The results from both the High-z Team and from the Supernova Cosmology Project began to appear in 1998. In both cases the crucial data took the form of a graph of 'corrected' apparent magnitude against redshift (see Figure 7.10), and indicated that distant Type Ia supernovae have smaller redshifts than would be expected on the basis of observations of nearer Type Ia supernova and Hubble's law. Amazingly, the results actually imply that the cosmic expansion is accelerating. So, in contrast to all the early determinations of q_0 discussed in the last section, it now appears that the current value of the deceleration parameter is negative, probably in the range $-0.6 < q_0 < 0$.

More recent results from various sources have tended to confirm these initial findings, but, given the history of measurements in this field, there is still considerable concern about the reliability of the results. The quality of the work that has been done is not doubted, but the possibility exists that systematic uncertainties may have influenced the results.

- On the basis of what you learned in the last section, suggest one possible source of systematic error that might influence the Type Ia supernova measurements.

- Evolution. Just like the brightest galaxies in clusters, the more distant Type Ia supernovae might differ in some significant way from their nearer counterparts at smaller redshift. This factor has been considered, but it is hard to know what its precise effect might be.

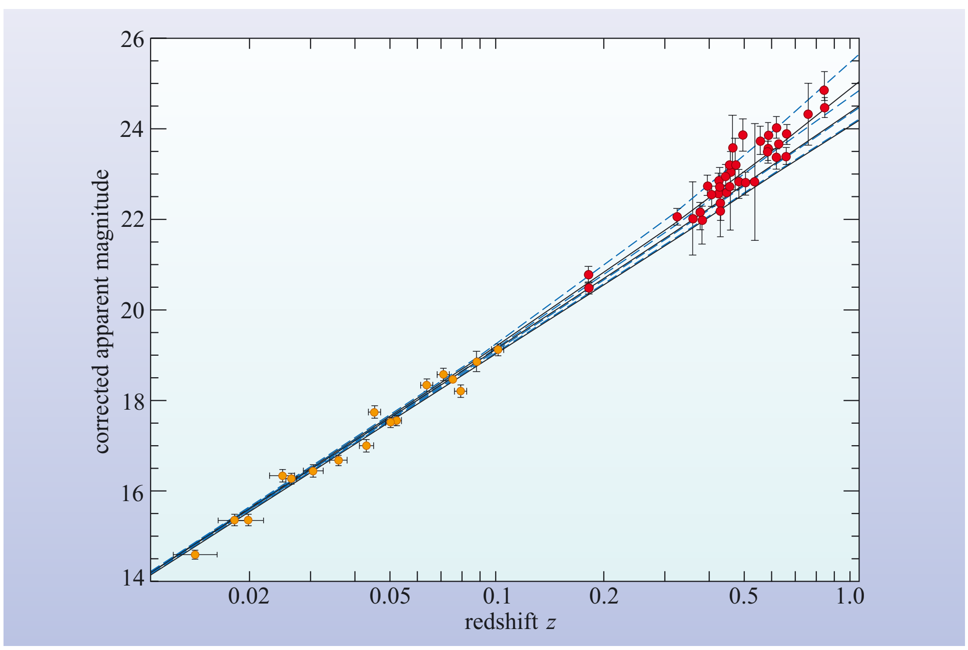

Figure 7.10 A plot of apparent magnitude against redshift for Type Ia supernovae that have been 'corrected' for various factors, including the intrinsic differences in brightness indicated by the differing rates of decline of their light curves. The 40 red dots represent observations by the Supernova Cosmology Project. The yellow data points represent the nearer supernovae that were used to calibrate the Type Ia light curve. The various lines shown on the graph correspond to different values of q_0. (Adapted from Schwarzschild, 1998, based on the work of S. Perlmutter *et al.*)

Further confirmation of cosmic acceleration has come from the observation of individual, very distant, supernovae such as one found in the Hubble Deep Field at a redshift of 1.7. These too indicate that the rate of cosmic expansion is currently greater than it has been in the past.

Despite the remaining concerns, the Type Ia supernova results have led to a major reassessment of the viability of the various FRW models. An accelerating cosmic expansion implies a non-zero cosmological constant, and in such a situation the cosmological implications of the Type Ia supernova measurements are not well described by simply quoting a value for q_0. The results are better described in terms of their implications for various contributions to the cosmic density, so it is to measurements of those quantities that we now turn.

QUESTION 7.3

Studies of Type Ia supernovae have been used in the attempt to measure the Hubble constant, but the high redshift measurements detailed in this section are not appropriate for this purpose. Why not? (*Hint*: look at the quantities that have been plotted in Figure 7.10.)

7.4 Measuring the current values of the density parameters $\Omega_{\Lambda,0}$, $\Omega_{\mathrm{m},0}$ and $\Omega_{\mathrm{b},0}$

Chapters 5 and 6 introduced a number of density parameters that play an important role in characterizing the contents of the Universe. Each of these parameters was defined as the ratio of some kind of density to the critical density $\rho_{\mathrm{crit}}(t)$, where $\rho_{\mathrm{crit}}(t) = 3H^2(t)/8\pi G$ represents the density in a 'critical Universe' with Hubble parameter $H(t)$ where both the cosmological constant and the curvature parameter are zero (i.e. $\Lambda = 0$ and $k = 0$). The three density parameters that will be mainly of concern in this section are:

the density parameter for matter

$$\Omega_{\mathrm{m}}(t) = \frac{\rho(t)}{\rho_{\mathrm{crit}}(t)} \tag{7.5}$$

the density parameter for baryonic matter

$$\Omega_{\mathrm{b}}(t) = \frac{\rho_{\mathrm{b}}(t)}{\rho_{\mathrm{crit}}(t)} \tag{7.6}$$

the density parameter for the cosmological constant

$$\Omega_{\Lambda}(t) = \frac{\rho_{\Lambda}}{\rho_{\mathrm{crit}}(t)} \tag{7.7}$$

where $\rho(t)$ represents the average cosmic density of all kinds of matter (baryonic and non-baryonic), $\rho_{\mathrm{b}}(t)$ represents the density of baryonic matter, and ρ_{Λ} has no simple physical interpretation but is probably best regarded as a convenient way of representing the cosmological constant, since $\rho_{\Lambda} = \Lambda c^2/8\pi G$. (You will recall that Ω_{Λ} is also referred to as the density parameter for dark energy.) Note that all three of these density parameters, $\Omega_{\Lambda}(t)$, $\Omega_{\mathrm{b}}(t)$ and $\Omega_{\mathrm{m}}(t)$ depend on time, since $\rho_{\mathrm{crit}}(t)$, $\rho_{\mathrm{b}}(t)$

and $\rho(t)$ all vary with time (though ρ_Λ does not). As in earlier sections, our concern is with determinations of the *current* values of these time-dependent parameters, which we denote $\Omega_{\Lambda,0}$, $\Omega_{b,0}$ and $\Omega_{m,0}$.

7.4.1 Constraints on $\Omega_{\Lambda,0}$ and $\Omega_{m,0}$ from Type Ia supernovae

In the context of the FRW models, the deceleration parameter is related to a combination of density parameters (see Section 5.4.3). If the very small contribution due to radiation is ignored, the Friedmann equation implies

$$q(t) = \frac{\Omega_m(t)}{2} - \Omega_\Lambda(t) \tag{7.8}$$

As this suggests, the results of both the Supernova Cosmology Project and the High-z Supernova Team can be expressed in terms of constraints on the current values of $\Omega_\Lambda(t)$ and $\Omega_m(t)$. In fact, this is the best way of presenting those results, and both research groups chose to present their findings in this way. The results obtained by the two groups are very similar: those of the Supernova Cosmology Project are shown in Figure 7.11. On a plot of $\Omega_{\Lambda,0}$ against $\Omega_{m,0}$ the results appear as a set of ellipses, marked with figures that represent various **confidence levels**. This is a way of indicating the uncertainties that attend any experimental or observational result. The mauve ellipse showing the 99% confidence level, for instance, indicates that, given the measured results, there is a 99% chance that the true values of $\Omega_{\Lambda,0}$ and $\Omega_{m,0}$ are located within the contour. The narrower contours represent increasingly tight constraints on the values of $\Omega_{\Lambda,0}$ and $\Omega_{m,0}$ and are presented with decreasing levels of confidence. All these confidence levels implicitly assume that all sources of uncertainty have been properly taken into account. In the case of the supernova results there is, of course, great concern about the possibility of unrecognized systematic uncertainties, possibly due to evolution, but also possibly due to some other cause. The blue dashed curves indicate the observers' estimates of the 'worst case' implications of various systematic uncertainties, but concerns still remain.

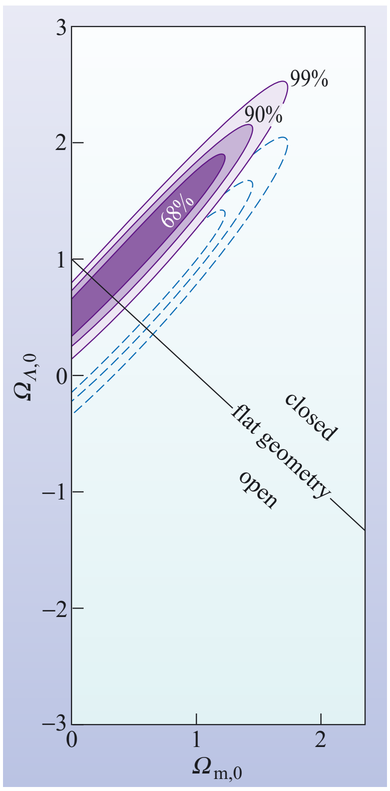

Figure 7.11 Results of the Supernova Cosmology Project, plotted as constraints (indicated by confidence level) on the current values of Ω_Λ and Ω_m. The results effectively rule out the kind of Universe in which $\Omega_{\Lambda,0} = 0$ and $\Omega_{m,0} = 1$ that was favoured by many cosmologists prior to the publication of the supernova data. (Adapted from Schwarzschild, 1998, based on the work of S. Perlmutter *et al*.)

As you can see, the results of supernova cosmology are consistent with a whole range of values for $\Omega_{\Lambda,0}$ and $\Omega_{m,0}$. A significant feature of these results however, is that they strongly exclude a FRW model in which $\Omega_{\Lambda,0} = 0$ and $\Omega_{m,0} = 1$, which was exactly the kind of model Universe favoured by many cosmologists until the supernova data were published.

Although the supernovae results alone do not determine $\Omega_{\Lambda,0}$ and $\Omega_{m,0}$ very precisely, the results have been used in conjunction with the outcomes of other studies to deduce tight constraints on these two values. Some of these additional studies are described later, but they broadly support the idea that the Universe has a flat spatial geometry, implying that $k = 0$ and, consequently, $\Omega_{\Lambda,0} + \Omega_{m,0} = 1$. In the context of Figure 7.11 this implies that the point representing the true values of $\Omega_{\Lambda,0}$ and $\Omega_{m,0}$ lies on the diagonal line marked 'flat geometry'. Accepting this and working to a reasonable level of confidence, the results of the Supernova Cosmology Project indicate that

$$\Omega_{m,0} = 0.28 \pm 0.09 \tag{7.9}$$

while the High-z Supernova Team find

$$\Omega_{m,0} = 0.32 \pm 0.10 \tag{7.10}$$

The agreement between these results (within the quoted uncertainties) is impressive, and while there must always be concerns about systematic uncertainties, there is now widespread agreement that $\Omega_{m,0}$ is within the range indicated by these results. Further evidence of this is presented in Section 7.5.

QUESTION 7.4

From Figure 7.11, estimate the range of possible values for $\Omega_{\Lambda,0}$ at the 99% confidence level. Making the additional assumption that the Universe has a flat spatial geometry, what is the likely range of values for $\Omega_{\Lambda,0}$?

7.4.2 Determination of $\Omega_{m,0}$ from mass-to-light ratios

There are many methods of determining the current value of Ω_m apart from supernova measurements. Some of these methods are of dubious reliability, and recent results for $\Omega_{m,0}$ have ranged from about 0.2 to 1.5, often with substantial uncertainties. A selection of these results is shown in Figure 7.12, where the uncertainty associated with each determination is represented by a horizontal bar. The method used in each of these determinations has been named in the figure, but the details of most of those methods are not explained here. One method, however, is regarded as being particularly important, and that will be discussed in this section. This is the method of mass-to-light ratios.

The **mass-to-light ratio** of an astronomical system, such as a star or galaxy or even a cluster of galaxies, is the value obtained by dividing the mass M of the system by its luminosity L. The luminosity in this definition is normally restricted to some specified range of wavelengths, usually the optical range. So, in the case of the Sun where the mass is $M_\odot$ and the (optical) luminosity is $L_\odot$, the mass-to-light ratio is given by $M_\odot/L_\odot$.

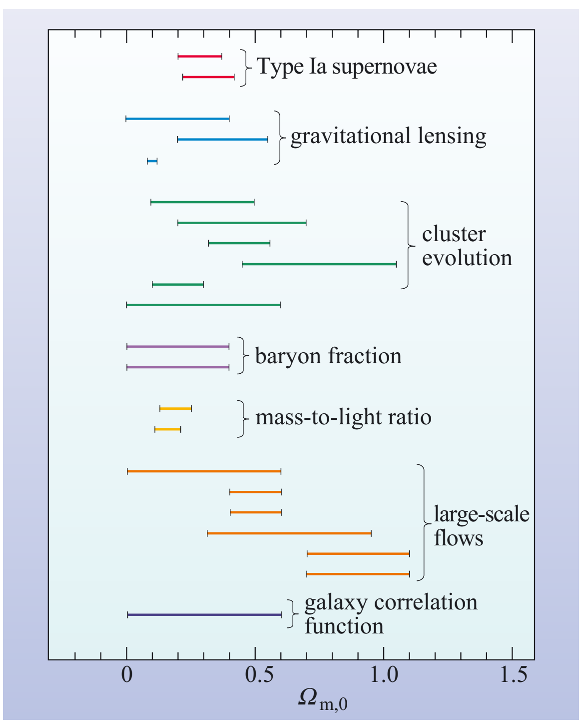

Figure 7.12 A selection of recent results for the current value of Ω_m. In some cases, such as those from supernovae, the actual observational results have been additionally restricted by assuming that the Universe has a flat spatial geometry on the large scale. Observational support for this assumption is provided in Section 7.5. This figure summarizes a great deal of modern research literature and is based on an original figure by Sabine Schindler.

The mass-to-light ratio of the Sun is not of much direct interest in cosmology, but if observers could determine the mass-to-light ratio of a representative portion of the Universe then they could multiply that quantity by the observable luminosity density of the Universe, $j_{\rm Univ}$, to obtain the average matter density ρ and hence the density parameter for matter $\Omega_{\rm m}$. In terms of symbols

$$\Omega_{\rm m} = \rho/\rho_{\rm crit} = [(M/L)_{\rm Univ} \times j_{\rm Univ}]/\rho_{\rm crit} \tag{7.11}$$

where $(M/L)_{\rm Univ}$ represents the mass-to-light ratio of the Universe.

■ What would be appropriate SI units of $(M/L)_{\rm Univ}$ and $j_{\rm Univ}$?

❑ $(M/L)_{\rm Univ}$ could be expressed in terms of $\rm kg\,W^{-1}$ (i.e. kilogram per watt) and $j_{\rm Univ}$ could be measured in $\rm W\,m^{-3}$ (i.e. watt per cubic metre). In practice, astronomers are quite likely to use $M_\odot/L_\odot$ as a unit of mass-to-light ratio, and to express the luminosity density in terms of solar luminosities per cubic parsec ($L_\odot\,\rm pc^{-3}$), but these are not SI units.

Any attempt to use mass-to-light ratios to determine $\Omega_{\rm m,0}$ must, of course, take account of many details. For instance, the same range of wavelengths must be used in determining $(M/L)_{\rm Univ}$ and $j_{\rm Univ}$, and the range over which all quantities are measured, although large enough to be cosmologically representative, must also be small enough to ensure that it is the *current* values of $(M/L)_{\rm Univ}$ and $j_{\rm Univ}$ that are being determined. (Presumably, the values of both $(M/L)_{\rm Univ}$ and $j_{\rm Univ}$ have changed over time.) Nonetheless, the basic challenges of this method are clear: determine $(M/L)_{\rm Univ}$ and measure $j_{\rm Univ}$.

Over the years, these challenges have been confronted by a number of astronomers, starting with Fritz Zwicky (see Section 4.3.2) in the 1950s. The two attempts to use this method that are shown in Figure 7.12 date from 1997 and 2000 and are, respectively, the work of Raymond G. Carlberg *et al*. and Neta Bahcall *et al*. Bahcall and her collaborators restricted luminosities to blue wavelengths, and it was assumed that $(M/L)_{\rm Univ}$ would be well represented by the mass-to-light ratio of clusters of galaxies. The masses of the clusters were measured using the optical and X-ray techniques that were described in Chapter 4.

■ List and briefly describe the optical and X-ray techniques for determining cluster masses that were described in Chapter 4.

❑ *The virial mass method*, which is based on Doppler measurements of the velocity dispersion within the cluster and the assumption that the cluster is in dynamical equilibrium (i.e. relaxed or virialized).

The X-ray emission method, which is based on X-ray spectra and X-ray surface brightness measurements (to determine the temperature and density distribution of the intracluster gas) and the assumption that the gas is in hydrostatic equilibrium.

The gravitational lensing method, which is based on observations of distorted images of more distant galaxies and models of the mass distribution within the lensing cluster.

It has been clear for a long time that mass-to-light ratios of astronomical systems tend to increase as the size of the system becomes larger, at least up to scales of hundreds of kiloparsecs. When dealing with galaxies and clusters of galaxies this

growth is usually interpreted as signifying the presence of large amounts of dark matter, since dark matter tends to increase the mass of a system without producing any corresponding increase in luminosity. In fact, the growth of mass-to-light ratios with the size scale on which they are measured is often quoted as evidence of the existence of dark matter. However, there is also evidence that, as the size of the systems considered increases to a megaparsec and beyond, so the growth in the mass-to-light ratio ceases and M/L attains a constant value. It is this constant limiting value that is taken to represent the average 'cosmic' value of the mass-to-light ratio.

Figure 7.13 provides a highly schematic representation of the way that observed mass-to-light ratios increase with the scale on which they are measured. As you can see, for the visible parts of galaxies (corresponding to measurement scales of about 10 kpc) the mass-to-light ratio is about five times $M_\odot/L_\odot$, while on the larger scale of entire galaxies (a scale of 100 kpc or so, that would include the galaxy's dark halo) the mass-to-light ratio is about 20 times $M_\odot/L_\odot$, and on the even larger scale of groups and clusters (scales around 1 Mpc) the mass-to-light ratio is more like 240 times $M_\odot/L_\odot$. The belief that the mass-to-light ratio becomes roughly constant on the largest of these scales is supported by various measurements, including the finding that the mass-to-light ratio of the supercluster MS302 is essentially equal to the mass-to-light ratios of the clusters of which it is composed. (In this latter case, all the masses were determined using the gravitational lensing method.)

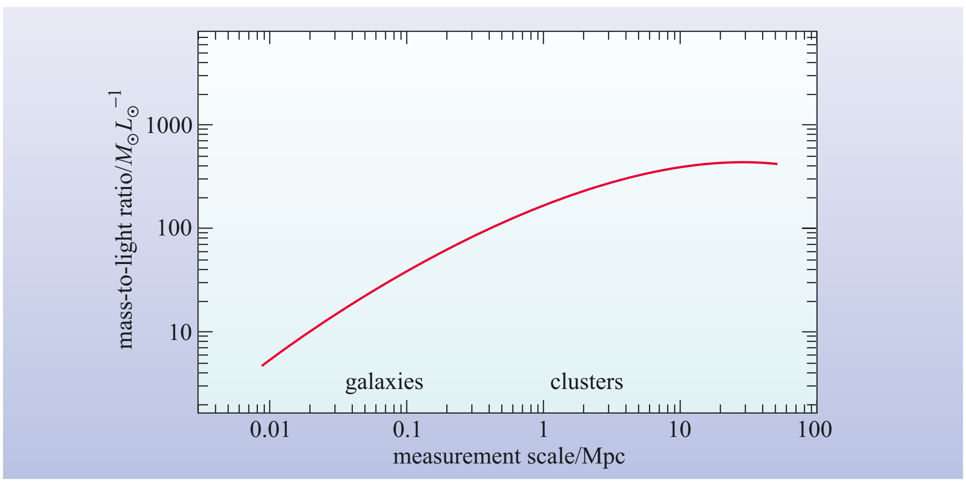

Figure 7.13 A schematic representation of the mass-to-light ratio as a function of measurement scale.

According to Bahcall *et al.*, mass and light do share the same overall distribution on the large scale (i.e. the mass-to-light ratio does become constant) but there is still a great need for caution when making measurements because relatively dense regions such as rich clusters of galaxies exhibit higher mass-to-light ratios than do lower density regions. This so-called 'bias' effect is attributed to the relatively more highly evolved state of the high-density regions, where the emission of blue light from stars has declined more than in the relatively less evolved, lower density regions. Taking this bias into account, their conclusion is that

$$\Omega_{\mathrm{m},0} = 0.16 \pm 0.05 \qquad (7.12)$$

This is somewhat lower than the widely favoured value obtained from supernova cosmology ($\Omega_{\mathrm{m},0} \approx 0.3$), but not vastly different given the difficulty of the measurements and the range of results indicated in Figure 7.12. Some cosmologists regard the estimated uncertainty in Equation 7.12 as rather optimistic. Perhaps the

real significance of these results is the support they give to the idea of dark matter becoming increasingly important on larger size scales, and the insight they provide into the poorly understood relationship between the distribution of light and mass.

7.4.3 Determinations of $\Omega_{b,0}$

The methods of density determination that have been discussed in the last two sections have both been sensitive to dark matter, and have indicated its presence in substantial amounts. On the basis of mass-to-light ratios, it is widely assumed that much of this dark matter is contained in dark-matter halos of galaxies. However, these measurements give little indication of the nature of the dark matter. One obvious possibility is that it might be some form of ordinary baryonic matter. One way to investigate this possibility is to determine the density parameter for baryonic matter $\Omega_b(t)$; if the current value of this quantity, $\Omega_{b,0}$, is significantly less than the current value of the density parameter for all kinds of matter, $\Omega_{m,0}$, then much of the dark matter must be non-baryonic.

This section presents two arguments for the belief that the current average density of baryonic matter is much less than the current total density of matter. The first of these arguments is based on the requirement that the relative abundances of light elements predicted by the theoretical account of *primordial nucleosynthesis* (as discussed in Chapter 6) should agree with the observational evidence regarding those abundances. The second argument is based on direct observational assessments of the density of baryonic matter in various parts of the Universe; that is to say a *baryon inventory*. In addition to these two arguments, a third argument based on observations of the cosmic background radiation is presented in Section 7.5.

Primordial nucleosynthesis

According to Chapter 6, the abundances of light elements (essentially hydrogen, helium and lithium) predicted by primordial nucleosynthesis are related to the current value of the density parameter for baryonic matter. This link exists because the total number of baryons in the Universe is a *conserved* quantity that is not expected to change with time. So the current mean density of baryonic matter is related to the density of baryonic matter at the time of cosmic nucleosynthesis, and this primordial density played an important role in determining the extent to which light nuclei were synthesized between about three and 30 minutes after the start of cosmic expansion.

One of the great successes of big bang cosmology is its ability to simultaneously predict primordial abundances of deuterium, helium and lithium that are consistent with the abundances currently observed in stars and gas clouds (once allowances have been made for more recent astronomical processes such as stellar nucleosynthesis). In order to achieve this consistency, however, it is necessary that the current value of the density parameter for baryonic matter should be in the range

$$0.02 \leq \Omega_{b,0} \leq 0.05 \tag{7.13}$$

This is much lower than the estimates of $\Omega_{m,0}$ based on supernova cosmology which, as you saw earlier, are around 0.3. So it seems that baryons account, very roughly, for only somewhere between about a fifteenth and a sixth of the total density of matter in the Universe.

A baryon inventory

Where are the baryons (protons, neutrons, etc.) in the Universe? Well, some are in you and me. We each contain about 2 to 4 × 10^{28} protons and neutrons. But there

are many more in the Earth, far more in the Sun, and enormously more in the Milky Way and other galaxies. Perhaps surprisingly, stars and their remnants are thought to account for less than 30% of the baryonic matter in the Universe. The majority of the baryons are believed to reside in the various forms of ionized gas that exist within and between the galaxies.

Table 7.2 is adapted from a baryon inventory that was published in 1998. The table shows the estimated contribution to $\Omega_{b,0}$ from various sources. The authors of the inventory based their estimates on a wide range of observational data. When dealing with the well-determined contribution from hot, ionized gas in rich clusters they made use of the kind of X-ray observations described in Chapter 4. X-ray observations at somewhat lower energies provided estimates of the cooler ionized gas in sparser groups of galaxies, while Lyman α absorption measurements (also described in Chapter 4) allow the quantity of ionized gas in cool clouds to be inferred. Unfortunately these last two estimates, although important to the final sum, are less reliable than many of the other values that appear in the table.

Table 7.2 The main repositories of baryons in the Universe, and their respective contributions to the current value of the density constant for baryonic matter.

Repositories of baryons	Contribution to $\Omega_{b,0}$
stars in elliptical galaxies and the spheroids of spirals	0.0026
stars in discs (for spiral galaxies)	0.0009
stars in irregular galaxies	0.0001
neutral atomic gas	0.0003
molecular gas	0.0003
ionized gas in clusters of galaxies	0.0026
ionized gas in groups of galaxies	0.0056
ionized gas in cool clouds	0.0020

A baryon inventory of this kind is open to the criticism that many of the entries, including some of the most important, are hard to estimate. It is also the case that some repositories of baryons may have been overlooked. In Table 7.2, for example, it is certainly the case that warm, ionized gas in the voids between superclusters has been ignored, and so has the contribution of baryons in dwarf galaxies and in galaxies of low surface brightness. The contribution from these and other neglected sources are thought to be small, but there is inevitably some uncertainty about this.

The general conclusion, after taking account of all known repositories of baryons and making reasonable estimates wherever data are lacking, is that $\Omega_{b,0}$ is in the range

$$0.007 \leq \Omega_{b,0} \leq 0.041 \tag{7.14}$$

with a 'best guess' value of

$$\Omega_{b,0} \approx 0.021 \tag{7.15}$$

Because of the uncertainties this 'best guess' should not be taken too seriously. However, the upper part of the range given in Equation 7.14 is consistent with the requirements of primordial nucleosynthesis, and gives further evidence that the dark matter cannot be entirely, or even mainly, baryonic matter.

QUESTION 7.5

Justify the rough claim made earlier that 'baryons only account for somewhere between about a fifteenth and a sixth of the total density of matter in the Universe'.

7.5 Anisotropies in the cosmic microwave background and precision cosmology

The cosmic microwave background (CMB) radiation was introduced in Chapter 5 and then explored more fully in Chapter 6. Among the many features of the CMB that were described in those earlier discussions were the following.

1. The CMB radiation is intrinsically uniform to better than one part in 10 000. This means that, after correcting for effects due to the motion of the detector, the CMB comes with very nearly equal intensity from all directions.
2. The CMB is 'thermal radiation' with a characteristic temperature of 2.725 K. This means that the intrinsic spectrum of the radiation is well described by a black-body curve with a peak in intensity at a wavelength of about 1 mm.
3. The CMB radiation is believed to have originated at the time of recombination, when the mean temperature of cosmic matter became low enough to allow electrons and protons to form hydrogen atoms that were not immediately ionized again. This means that the photons that make up the CMB were last scattered about 3 to 4×10^5 years after the start of cosmic expansion, when the temperature was about 3000 K.
4. The radiation has been expanding and cooling since it was last scattered, during which time its temperature has decreased by a factor of about 1100. This means that the 'last-scattering surface' from which the radiation was released is now at a redshift of about 1100. (The most distant observed galaxies are at a redshift of about 6.)
5. Despite its high degree of intrinsic uniformity, anisotropies in the intensity of the radiation have been observed, at a level of a few parts in 100 000, over a range of angular scales. These tiny variations in intensity represent fluctuations in the temperature of the CMB and are believed to hold the key to the precise measurement of the cosmological parameters.

This section is concerned with the anisotropies in the CMB, and discusses the origin of the anisotropies, how they can be measured and described, and how they can be used to determine the key cosmological parameters. It also contains very recent results that improve and make more precise some of the values quoted in earlier chapters and in the points listed above.

QUESTION 7.6

In the numbered list above, no mention is made of the 'dipole anisotropy' that was introduced in Chapter 6. Briefly describe the dipole anisotropy, explain its origin and identify the words and phrases in points 1, 2 and 5 that imply the dipole anisotropy has been taken into account, despite the lack of any explicit reference to it.

7.5.1 Detecting the anisotropies in the CMB

The discovery of the CMB by Penzias and Wilson in 1965 was a turning point in observational cosmology. Following the discovery, many observers reoriented their research in order to concentrate on the CMB and the other implications of big bang cosmology. Penzias and Wilson had made their serendipitous discovery using a ground-based radio detector working at a wavelength of about 70 mm, but much of the subsequent work tried to cover wavelengths closer to the expected peak in the CMB spectrum, at about 1 mm. At such relatively short wavelengths, radiation coming from space is absorbed by the Earth's atmosphere, so many of the observations were made using detectors carried by balloons or high-flying aircraft. The existence of the dipole anisotropy was first established in this way, in 1977, using a detector fitted to an American U-2 aircraft. (U-2s had been employed as spy planes during the Cold War, but were extensively used for scientific work from the mid-1970s.) Other high-altitude work gave a strong indication that the CMB spectrum was thermal (i.e. described by a black-body curve), but left open the possibility that there might be small departures from a pure black-body spectrum. However, none of the balloon or aircraft observations revealed any anisotropies in the CMB, apart from the large-scale dipole anisotropy. Small-scale anisotropies were predicted by big bang cosmology, but highly sensitive detectors with at least moderate resolution were needed to identify them. The observation of those small-scale anisotropies, and the confirmation of the purely thermal nature of the CMB spectrum, had to await the launch of the first space satellite to be dedicated to the study of the cosmic background radiation.

COBE, the Cosmic Background Explorer (Figure 7.14) was launched on 18 November 1989. COBE was about the size and mass of a large car, and carried three main experimental packages:

- DMR, a set of three differential microwave radiometers designed to search for anisotropies in the cosmic background radiation;
- FIRAS, the Far-Infrared Absolute Spectrophotometer, designed to measure the CMB spectrum; and
- DIRBE, the Diffuse Infrared Background Experiment, designed to search for cosmic infrared background radiation, and to assess local sources of diffuse infrared radiation, including the Milky Way.

Within a short time of starting its astronomical observations, the FIRAS detector gave powerful support to the big bang prediction of a very pure black-body spectrum. It is now known that, over the wavelength range from 0.1 mm to 5 mm, the CMB spectrum follows a 2.725 K black-body spectrum very precisely. Observations of small-scale anisotropies by the DMR took longer to emerge and longer still to be refined.

As mentioned in Chapter 6, absolute measurements of the intensity of the CMB are difficult to make, so the DMR was designed to look for differences in the intensity of the CMB from pairs of regions separated by 60° on the sky.

Figure 7.14 COBE, the Cosmic Background Explorer. COBE's three main scientific instruments, FIRAS, DMR and DIRBE, made their observations from behind a collapsible thermal shield that was deployed after the satellite was placed in orbit. COBE followed a relatively low Earth orbit that took it over the Earth's poles. The plane of the orbit processed at the rate of about one degree per day; this allowed the shielded instruments to scan all parts of the sky over a period of six months. (NASA)

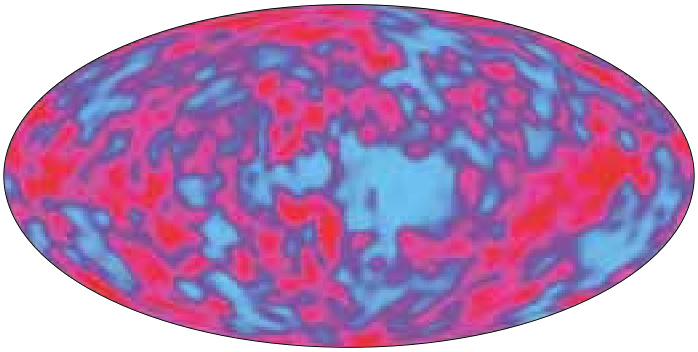

Figure 7.15 An all-sky CMB anisotropy map based on data from the DMR experiment on COBE. The angular resolution of this map is about 7°. Contrast this map with the highly isotropic distribution measured at lower sensitivities, shown in Figure 5.4. (Edward L. Wright)

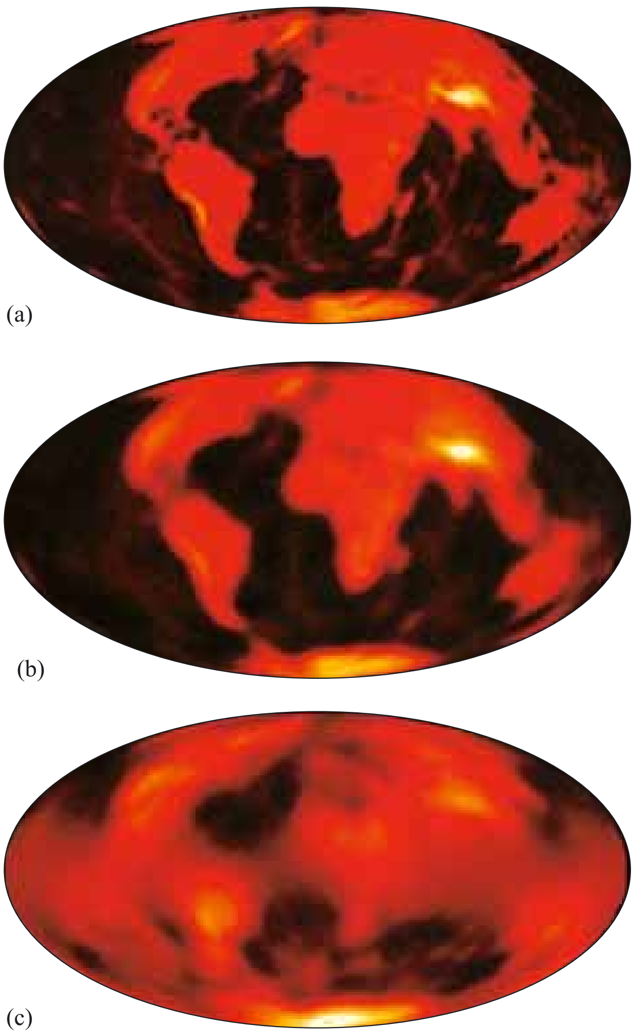

Figure 7.16 (a) A map of the Earth. (b) The same map viewed with the angular resolution that is inherent in the COBE anisotropy map. (c) The addition of noise makes the underlying pattern even harder to discern. (Courtesy of Ted Bunn)

The same technique had been used to detect the dipole anisotropy in the 1970s, and the DMR on COBE was a direct descendant of the detector that had been carried to high altitude by a U-2 spy plane. The COBE DMR actually consisted of three pairs of detectors working at wavelengths of 3.3, 5.7 and 9.6 mm. By comparing observations at these three wavelengths, the effects of microwave emission from the Milky Way could be identified and eliminated, leaving just the cosmic signal, albeit contaminated by unavoidable detector 'noise'. Thanks to COBE's rotation (it turned on its axis once every 75 seconds), the satellite's 103-minute orbital period, and the gradual precession of the orbital plane, the DMR was eventually able to examine all parts of the sky and to produce the all-sky CMB anisotropy map shown in Figure 7.15.

The publication of the first anisotropy map in April 1992 was another very significant development in observational cosmology. Nonetheless, it is important to recognize the limitations of the COBE findings. In the first place, the data on which the map was based were very noisy. This means that much of the visible structure in the map may be illusory. A statistical analysis of the data justified the claim that anisotropies had been observed, but it did not guarantee that the coloured boundaries that appear in the map were accurately located. Moreover, the nature of the DMR's collecting horns meant that each of the paired regions being compared was about 7° across, so this was the minimum angular scale on which anisotropies might reliably be detected. To give some idea of the significance of this, Figure 7.16 shows a map of the Earth viewed with the same kind of resolution. As you can see, even the major continents are indistinct, while finer details, such as the existence of the British Isles, are completely lost. The features become even more obscure when 'noise' is deliberately added to the data to make the comparison with the DMR results more apposite. Clearly, despite COBE's success, much work remained to be done.

In the early 1990s, further measurements and analyses by the COBE Science Team confirmed and refined the original results for angular scales of about 7°. Since then other groups of researchers, mainly using ground-based or balloon-borne equipment, have struggled to measure CMB anisotropies on smaller angular scales. One particularly notable effort was that of the BOOMERanG collaboration, an international team that used equipment suspended from a high-altitude balloon (Figure 7.17). BOOMERanG (which stands for 'balloon observations

Figure 7.17 The high-altitude balloon and instrument package used by the BOOMERanG team to measure CMB anisotropies from Antarctica. (BOOMERanG Collaboration)

of millimetric extragalactic radiation and geophysics') mapped CMB anisotropies over only a limited region of sky, but did so with high sensitivity and an angular resolution of better than 1°. The greatly improved resolution was achieved by cooling the detectors to 0.28 K and placing them at the focus of a small (1.3 m aperture) telescope. The BOOMERanG team published their results in Spring 2000. They were based on 10.5 days of continuous observation from an altitude of 35 km above Antarctica. The Antarctic air is exceptionally clear, clean and dry, so the effects of absorption are minimized there. Some of the results from BOOMERanG are shown in Figure 7.18.

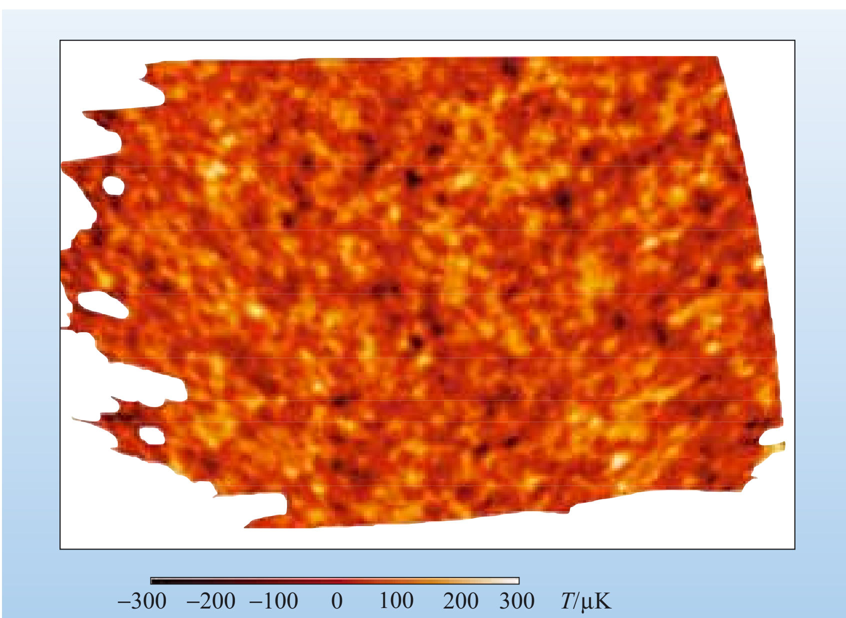

Figure 7.18 Some results from BOOMERanG, which examined only a limited part of the sky but did so at an angular resolution of about 1°. The CMB anisotropies are portrayed as variations in the effective temperature of the radiation. Note that the range of variation is only ±300 μK, while the mean temperature is about 3 K. (BOOMERanG Collaboration)

Figure 7.19 shows a comparison between the CMB anisotropies actually observed by BOOMERanG and those predicted by big bang cosmology in the context of some Friedmann–Robertson–Walker models with different values of the curvature parameter k. As you can see, even a simple comparison 'by eye' favours the model with $k = 0$. This conclusion is supported by more detailed analyses of the data that will be outlined later.

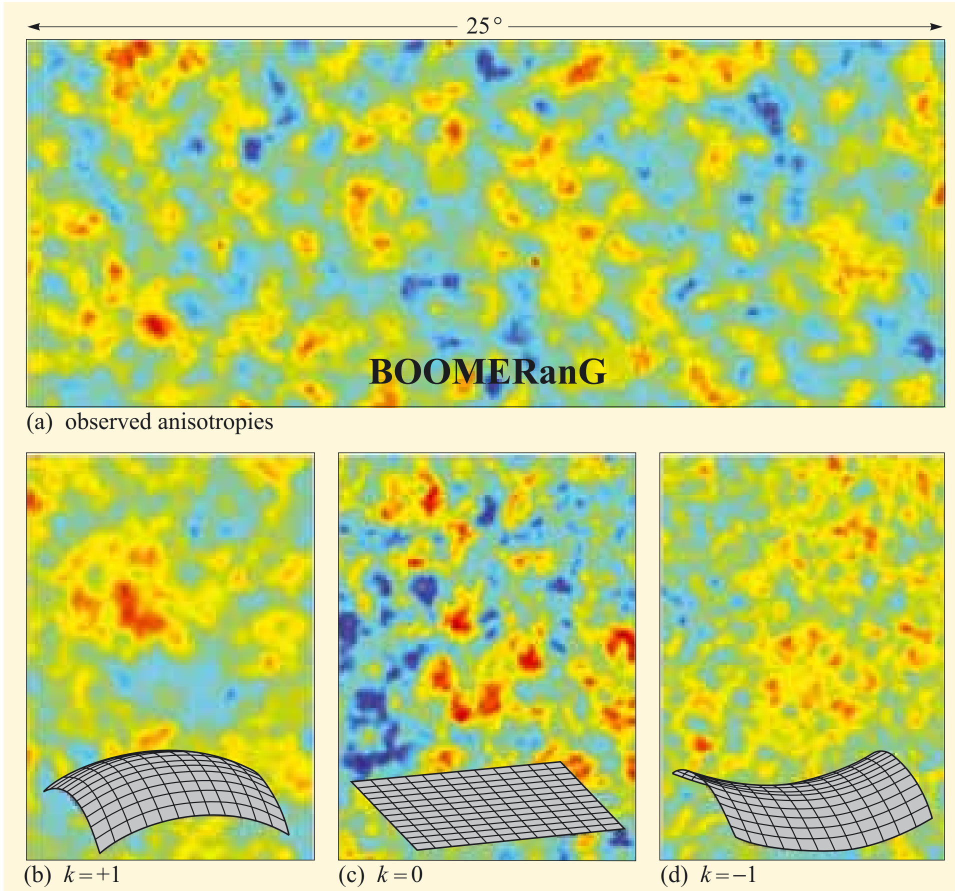

Figure 7.19 Evidence that the Universe has a flat ($k = 0$) spatial geometry. (a) When the anisotropies observed by BOOMERanG are compared with computer predictions (b, c and d) based on various cosmological models, it is the $k = 0$ predictions that provide the best agreement with the observations. The small grids printed at the bottom of the computer simulations provide a reminder of the geometric properties that correspond to the different values of k. (BOOMERanG Collaboration)

Many other degree-scale anisotropy observations have followed those of BOOMERanG, some from balloon experiments, others from ground-based detectors. However, the most recent results at the time of writing are the keenly awaited findings of an American space mission, the Wilkinson Microwave Anisotropy Probe (WMAP), which was launched in June 2001 (Figure 7.20). This is the successor to COBE and, like COBE, it has produced an all-sky anisotropy map, although this time with an angular resolution of about 0.1°. The WMAP anisotropy map is shown in Figure 7.21; it is based on the first year's observations and may be refined somewhat by further observation and analysis. However, as you can see, it is already far more detailed than the COBE map that was produced roughly ten years earlier.

Analysis of the small-scale anisotropies that can be seen in Figure 7.21 has already resulted in the publication of revised values for a whole range of cosmological parameters, with many of them being quoted to unprecedented levels of precision. How these values have been derived is explained later; first we must examine how the observed anisotropies can be described mathematically, so that the analysis can begin.

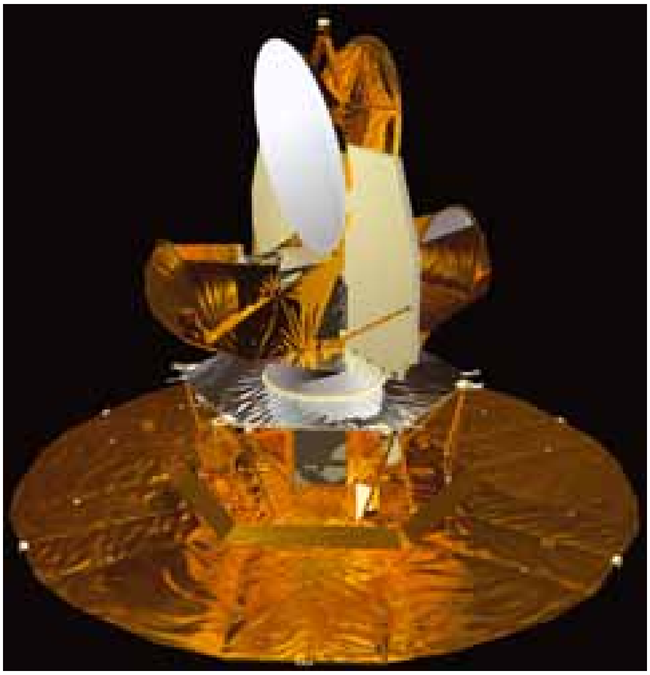

Figure 7.20 Computer image of the WMAP spacecraft. (NASA)

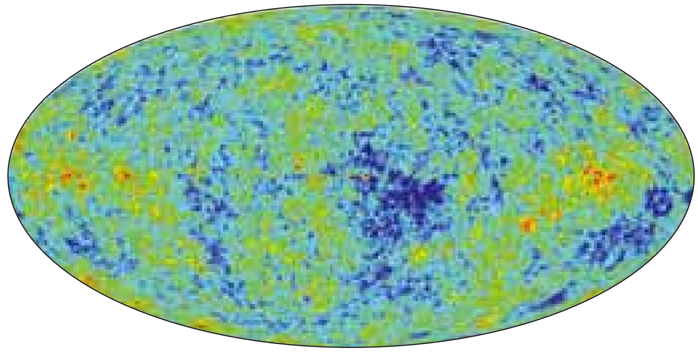

Figure 7.21 An all-sky CMB anisotropy map, based on data obtained by the WMAP space probe. The angular resolution of this map is about 0.1°. Compare this map with the lower resolution COBE data shown in Figure 7.15.
(Bennett *et al.*, 2003)

QUESTION 7.7

When comparing the predictions with the observations in Figure 7.19, would you expect the big bang prediction to show precisely the same pattern of anisotropies as that observed by BOOMERanG, or simply something 'similar' to the observations? Justify your answer.

7.5.2 Describing the anisotropies in the CMB

Any observation of anisotropies in the CMB (such as shown in Figure 7.21), made from the Earth or anywhere in the Solar System, represents nothing more than a single 'sample' of a cosmic phenomenon. The CMB, viewed from anywhere else in the Universe at the present time, is expected to be similar in its general aspects but different in detail. From a cosmologist's point of view, what is interesting about any single view is not the detailed information it provides about the directions in which the CMB is slightly warmer or slightly cooler, but the *statistical* insight it provides into CMB anisotropies in general. This is analogous to saying that cosmologists value observations of the large-scale distribution of galaxies (described in Chapter 4) not for what they reveal about the locations of particular clusters of galaxies, but rather for the statistical information they provide about the scale of clusters in general. The locations are a *local* concern, the scales are a *cosmic* one.

The quantity that contains all the *statistically* important data in an anisotropy map such as Figure 7.21 is called the **angular power spectrum**. It is constructed from the same data that are used to plot the map, but it effectively discards the detail that depends on our particular location, and makes apparent the cosmically important features of the data. It provides a way of showing graphically the strength of

fluctuations on different scales and bears comparison with methods used to describe large-scale structure in Chapter 4. The angular power spectrum derived from the first year of WMAP observations is shown in Figure 7.22. The aim of this section is to introduce the main features of such a spectrum, and to explore the relationship between an anisotropy map and the corresponding angular power spectrum.

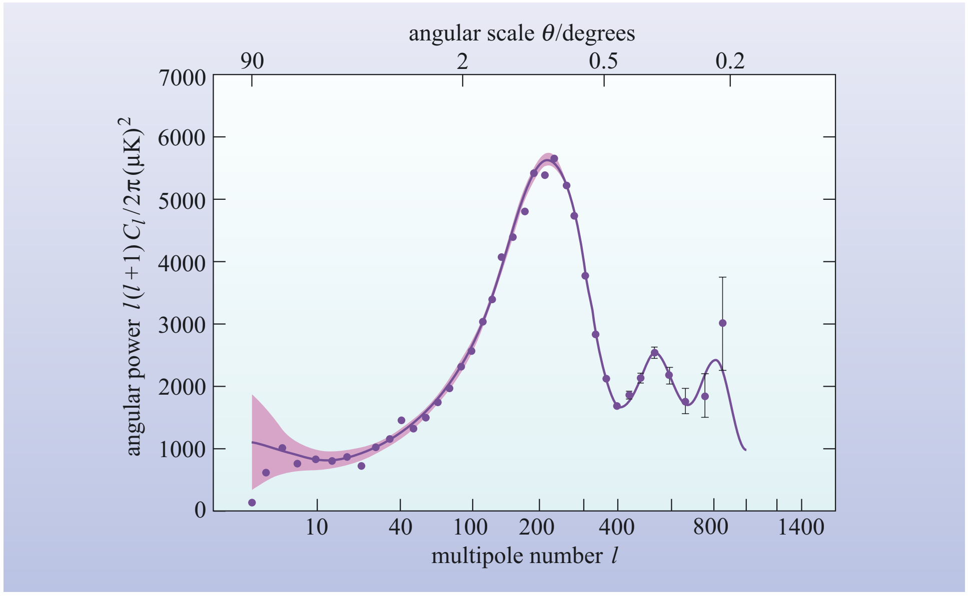

Figure 7.22 The angular power spectrum of the CMB as determined by WMAP. (Bennett *et al*., 2003)

The data points and uncertainty ranges plotted in Figure 7.22 show what WMAP has revealed about the angular power spectrum of the CMB as a whole. The smooth curve represents the 'best fit' to these data from a range of theoretical predictions based on various FRW models (more will be said about these predictions in the next section), and the shaded band enclosing the best-fit line represents an effect known as **cosmic variance**. The cosmic variance is a consequence of the fact that we are compelled to estimate the angular power spectrum of the CMB from observations made at one cosmic location (i.e. on the basis of a single 'sample' of the CMB, made from within the Solar System). As a result, even though theories may predict a precise form for the CMB's angular power spectrum (represented by the best-fit line), measurements of that spectrum from a single location should only be expected to show consistency with the broadened band that surrounds the line.

The angular power spectrum is usually presented as a graph in which a variable called *angular power* is plotted along the vertical axis, while an independent variable called *multipole number* is plotted along the horizontal axis. Both of these variables are explained below.

In the context of CMB anisotropy studies, the **multipole number** (usually denoted by the italic letter l), provides a natural, if somewhat unfamiliar, way of describing angular separations. The difference between two directions can always be described in terms of the angle θ between them. The angle θ may be associated with a multipole number l using the relation

$$l = 180°/\theta \tag{7.16}$$

implying that the multipole number l is the number of times the angle θ can be fitted into a 180° arc. Because of this relationship between multipole number and angle, the horizontal axis of an angular power spectrum is sometimes shown as an angular

scale, but with the angle *decreasing* in unequal steps from left to right. (A scale of this kind is shown at the top of Figure 7.22.) In what follows we mainly make use of the multipole number, but we sometimes refer to the corresponding angle derived from Equation 7.16.

- ■ COBE was only able to detect anisotropies of angular size 7° or above. What is the corresponding range of l values?
- ❑ From Equation 7.16, $\theta = 7°$ corresponds to an l value of about 26. Larger angles correspond to smaller values of l, so we can say that the COBE results were confined to the range $l = 0$ to $l = 26$ or thereabouts. Looking at Figure 7.22 you can see that this is a very small range compared with the WMAP results; it doesn't even cover the first peak.

For any given value of l in Figure 7.22, the corresponding value of the **angular power**, usually denoted $l(l + 1)C_l/(2\pi)$, indicates how much variation is present in the anisotropy measurements on that angular scale. The precise definition of angular power is complicated and too technical to merit discussion here. However, the important quantity C_l can be determined directly from the data used to plot the anisotropy map, and reveals the extent to which the temperature measured at one point will, on average, be *correlated* with the temperature at some other point an angular distance θ away. To get some feeling for the significance of this, consider the two artificial anisotropy maps shown in Figure 7.23. The map in Figure 7.23a shows no small-scale variation in the temperature; the anisotropy is on a scale of 90°, and the corresponding angular power spectrum would show a peak at $l = 2$. In contrast, the map in Figure 7.23b consists of anisotropies that share a common angular scale of about 11°; in this case the corresponding angular power spectrum would peak at $l = 16$. In neither case would the angular power spectrum reveal anything about the precise location of the coloured boundaries in the maps, but it would indicate the angle that, on average, separates a region of one colour from the next region of that colour.

The WMAP results represent a major contribution to the effort to determine the angular power spectrum of the CMB anisotropies. Over the range of l values shown, the WMAP measurements provide almost as much information about the angular power spectrum as it is possible to obtain from a single location in the cosmos. Figure 7.24 shows a compilation of recent measurements (excluding those from WMAP), along with the best-fit line to the WMAP data shown in Figure 7.22. As you can see, despite some large uncertainties in the older measurements, there is an impressive level of agreement about the shape of the

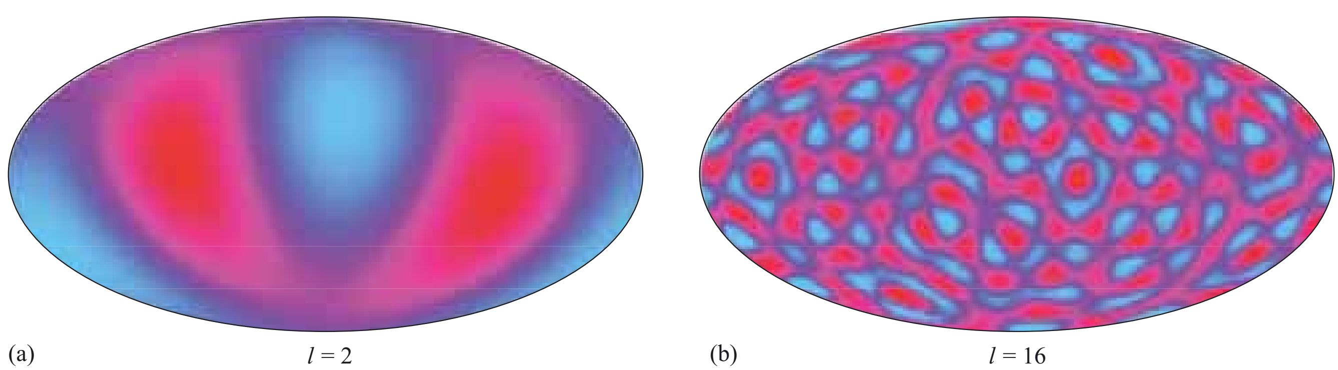

Figure 7.23 Two artificial all-sky maps showing different patterns of anisotropy. (a) A large-scale anisotropy for which all the angular power is concentrated at $l = 2$. (b) Smaller anisotropies that share a common angular scale of about 11°, and for which the angular power is concentrated at $l = 16$. (Edward L. Wright)

angular power spectrum. As Figure 7.24 indicates, the observed CMB anisotropies have some angular power at all angular scales, but there is a pronounced peak around $l = 220$, which corresponds to an angle of slightly less than 1°, and there are lesser peaks at larger values of l. These peaks show the angular scales at which temperature variations in the CMB are strongest. The next section concerns our theoretical understanding of those peaks in the angular power spectrum, and our ability to predict them on the basis of big bang cosmology.

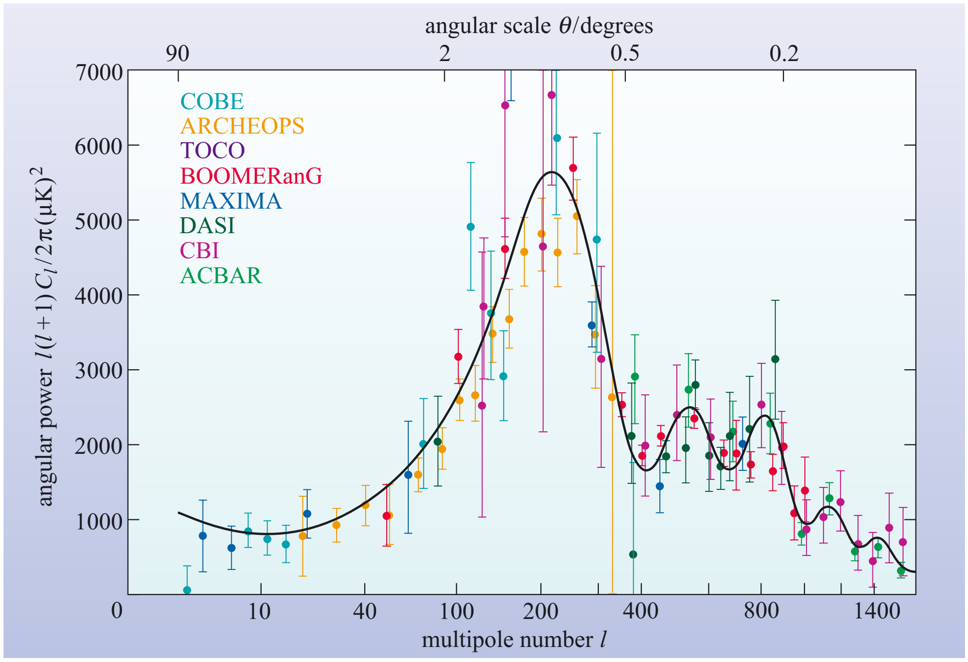

Figure 7.24 A compilation of recent measurements of the angular power spectrum of CMB anisotropies (excluding those from WMAP), together with the best-fit line obtained from the WMAP data. There is good agreement, despite some large uncertainties in some of the measurements. (Hinshaw *et al*., 2003)

QUESTION 7.8

At what values of l are the second and third peaks in the angular power spectrum in Figure 7.24? What are the corresponding angular scales? What is the maximum angular power of these two peaks according to Figure 7.24?

7.5.3 Predicting the anisotropies in the CMB

Cosmologists treat the Universe as highly uniform on the large scale, but they know that this is not a valid approximation on the small scale. The existence of people, planets, stars, galaxies and clusters of galaxies all demonstrate that there are non-uniformities in the Universe, and the anisotropies in the CMB provide our earliest view of those non-uniformities. An all-sky CMB anisotropy map, such as Figure 7.21, is essentially a snapshot of the spherical surface, centred on the Earth, at which the CMB radiation now reaching us was last scattered. That surface was discussed in Chapter 6, where it was referred to as the *last-scattering surface*. According to Chapter 6, the last scattering occurred at the time of recombination, when matter and radiation became decoupled. The time of this decoupling is usually supposed to be about 3 to 4 × 10^5 years after the start of cosmic expansion, but the recent WMAP data support a more precise value: $t_{dec} = 3.8 \times 10^5$ years, which we adopt from here on. So Figure 7.21 shows that when the Universe was about 380 000 years old some parts of it were slightly warmer or slightly cooler than others.

The existence of these **temperature fluctuations** at the time of decoupling indicates the presence of a corresponding set of **density fluctuations** in the distribution of cosmic matter (i.e. regions where the density of matter was slightly higher or slightly lower than the average density). Chapter 6 explained the link that is thought to exist between density fluctuations in the early Universe and the large-scale clustering of galaxies that we see in the present-day Universe. In this section, our main concern is the relationship between the density fluctuations and the anisotropies in the CMB. In particular we shall see how the effects of density fluctuations can be related to the features seen in the CMB's angular power spectrum. Note that the emphasis here is on *statistical* features. You will shortly see how the density fluctuations can be characterized statistically, and how that statistical characterization allows us to predict the *statistical* features of the CMB anisotropies. No attempt is made to predict the particular pattern of anisotropies shown in the all-sky map of Figure 7.21: it is the statistically significant angular power spectrum of Figure 7.22 that is of interest.

It is widely assumed that the density fluctuations present in the early Universe first arose as a natural consequence of quantum processes in the very early Universe, and were then amplified by the process of *inflation* that was discussed in Chapter 6. One of the exciting things about modern observational cosmology is that it is now beginning to test this assumption, and some speculative proposals concerning inflation have already been ruled out by measurements of the CMB. However, whatever the role of inflation may have been, there is general agreement that the early Universe contained density fluctuations on essentially all size scales and with a range of strengths. Any detailed assumptions we make about the relative strengths of fluctuations of different sizes can be presented in the form of an assumed 'spectrum' of fluctuations, and this can be characterized mathematically by introducing some more cosmological parameters. The simplest credible spectrum of density fluctuations involves two new cosmological parameters: a *power spectrum normalization*, denoted A, and a *scalar spectral index*, denoted n_s. We shall not be much concerned with these two parameters, but we should add them to the list of cosmological parameters that observational cosmologists are trying to determine, and keep in mind the possibility that more parameters might be needed to fully describe the fluctuation spectrum.

To work out how a spectrum of density fluctuations, characterized by A and n_s, influences the anisotropy of the CMB, we need to consider the interaction of matter and radiation in the early Universe, at least up to the time of decoupling ($t_{dec} = 3.8 \times 10^5$ years). This is best done by considering the various constituents of the Universe separately, and then considering the way they interact with each other.

Before decoupling, most of the matter in the Universe would have been non-baryonic dark matter, just as it is now, since the relative densities of baryonic and non-baryonic matter are not expected to change with time. The density fluctuations would have been largely composed of dark matter, and can be roughly thought of as dark matter 'halos', of various densities and sizes. These halos would have been expanding, like the rest of the Universe, but those that had a slightly greater than average density would have been growing a little less rapidly than average, and would have been increasing in 'strength' as a result.

The radiation in the Universe, prior to decoupling, would have been plentiful and energetic. As in the present-day Universe, the radiation would not have had much direct interaction with the dark matter. However, the radiation would have incessantly interacted with the electrically charged particles of baryonic matter (such as nuclei of hydrogen and helium). As a result, the baryons and the radiation would jointly form a

sort of fluid, with a common temperature and pressure. This **photon–baryon fluid** would be subject to the gravitational influence of the dark-matter halos and would be drawn towards those halos. However, as indicated in Chapter 6, the gravitational tendency to compress the photon–baryon fluid would have been resisted by the internal pressure of the fluid.

When the Universe had been expanding for a time t, effects due to the pressure in the photon–baryon fluid would not have been able to make themselves felt over distances greater than ct. (The speed of light represents an upper limit to the speed at which signals of any kind can travel.) Consequently, the photon–baryon fluid inside a dark-matter halo that is larger than ct at time t expands along with the halo, essentially undisturbed by the effects of pressure. However, as time passes, t increases and the scale of pressure effects grows. As ct comes to exceed the size of any particular dark-matter halo, the photon–baryon fluid collapsing into that halo will be subject to an increasing pressure that will halt the collapse, and then allow the photon–baryon fluid to 'spring back'. The photon–baryon fluid contained in some dark-matter halos can undergo several of these oscillations, allowing the density fluctuations to act as the generators of **acoustic waves** (i.e. sound waves) in the photon–baryon fluid. An important point to remember is that at time t the greatest wavelength that any of these waves may have will be roughly ct. We make use of this later.

When the Universe gets to be about 380 000 years old, recombination occurs. This allows the photons to decouple from the baryons. It is the decoupled photons streaming away from the surface of last scattering at $t_{\mathrm{dec}} \approx 380\,000$ years that eventually produce the CMB we now observe. The anisotropies that we see in the CMB are mainly caused by the unevenness of the last-scattering surface, and this is due to the density fluctuations and the acoustic waves that are present there. Now that we have identified the cause of the anisotropies we can account for the main features of their angular power spectrum.

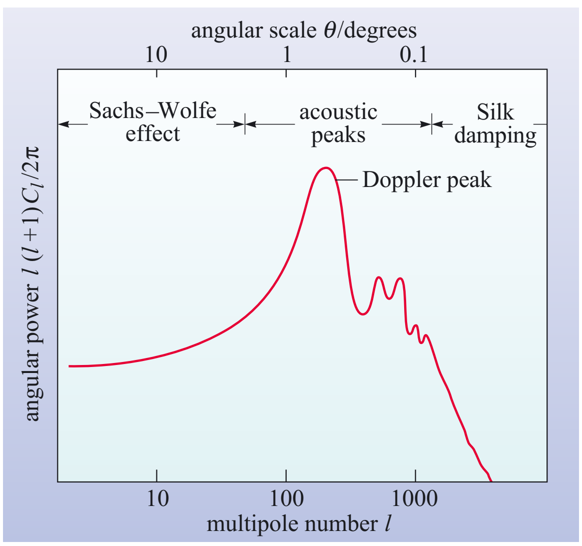

Figure 7.25 The causes of the main features in the angular power spectrum. The various effects named on the graph are discussed in the text. Note that in this case the multipole number has been plotted logarithmically, to allow the inclusion of large values of l.

On angular scales of a few degrees or more (i.e. multipole numbers of about 50 or less), the main source of anisotropy is called the **Sachs–Wolfe effect**. This is largely due to the general relativistic phenomenon of *gravitational red-shift*, which causes photons coming from the denser parts of the last-scattering surface to be observed with slightly longer wavelengths than identical photons leaving other parts of the last scattering surface. This causes the denser parts to appear slightly cooler and leads to the flat plateau seen on the left of the angular power spectrum in Figure 7.25.

On intermediate angular scales (i.e. multipole numbers between 50 and 1000, say), the angular power spectrum shows the effect of the acoustic waves at the time of decoupling. At that time there are some long wavelength waves that are just reaching their state of maximum compression for the first time. These compressions heat the photon–baryon fluid, causing the photons that escape from them to create temperature anisotropies. The moving charged particles associated with the waves will also cause the wavelengths of scattered photons to change (this is a Doppler effect), and this too will create temperature anisotropies. The size scale of the anisotropies would be comparable to the wavelength of the waves, and of the order of ct_{dec}.

- Evaluate ct_{dec} in light-years.
- Since $t_{\text{dec}} \approx 380\,000$ years, it follows that $ct_{\text{dec}} \approx 380\,000$ light-years.

In a Universe with a flat geometry (i.e. $k = 0$), a feature of this size on the last-scattering surface would span an angle of about two degrees. A more precise calculation, based on the same effects, predicts that there should be strong temperature anisotropies on a scale of about one degree, rather than two, and thus accounts for the prominent peak in the angular power spectrum around $l = 220$. The other, lesser peaks in the angular power spectrum can be attributed to waves that have fully expanded once, recollapsed once, fully expanded twice and so on. The big peak in the angular power spectrum is often referred to as the Doppler peak, but it and the lesser peaks are all caused by essentially the same phenomenon and are sometimes collectively referred to as **acoustic peaks**.

At small angular scales (multipole numbers of 1000 or more), signs of the acoustic waves are expected to fade away. This is due to an effect called **Silk damping** and occurs where the acoustic waves would have such short wavelengths that they are effectively smeared out by the free movement of photons between encounters with charged particles. A similar effect connected with the finite sizes of molecules prevents sound waves of extremely short wavelength from travelling through air.

Now that the main influences on the angular power spectrum have been identified, we can ask how the angular power spectrum can be predicted on the basis of a given cosmological model (i.e. given values of H_0, $\Omega_{\text{m},0}$, $\Omega_{\Lambda,0}$ and $\Omega_{\text{b},0}$ etc.) and some particular assumptions about the spectrum of density fluctuations (i.e. particular values of A and n_{s}). Making such a prediction is not easy. Fortunately for those who would like to do so, there are now publicly available computer programs such as ‘CMBFAST’, which can be used to calculate the shape of the angular power spectrum in a specified FRW model of the Universe. The ability to make such complicated predictions with relative ease is the key to using the observed CMB anisotropies to determine the main cosmological parameters, as is explained in the next section.

7.5.4 Determining cosmological parameters from the anisotropies in the CMB

Figure 7.26 shows a set of predictions for the shape of the CMB angular power spectrum based on fixed values for all the main cosmological parameters apart from $\Omega_{\text{b},0}$. The different curves in the figure show the effect of increasing the assumed current value of the baryon density parameter while keeping all the other parameters fixed. As you can see, the shape of the power spectrum changes significantly as $\Omega_{\text{b},0}$ is increased. Altering the other parameters would have different but analogous effects.

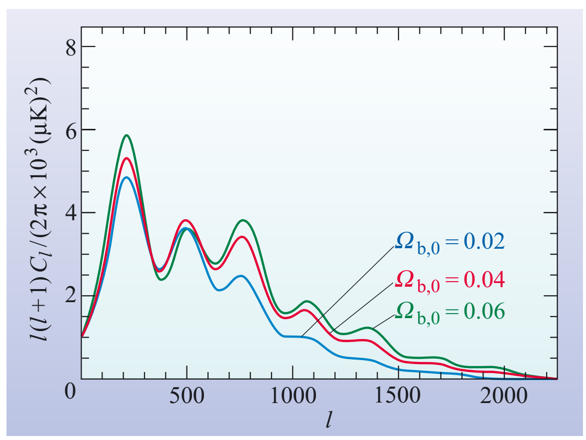

Figure 7.26 The angular power spectrum of CMB anisotropies, as predicted by big bang cosmology, for a range of values of the density parameter for baryonic matter, $\Omega_{\text{b},0}$. The differently coloured traces correspond to values of $\Omega_{\text{b},0}$ ranging from 0.02 to 0.06.

The general lesson to be drawn from Figure 7.26 is that the predicted shape of the angular power spectrum depends on the values of H_0, $\Omega_{\text{m},0}$, $\Omega_{\Lambda,0}$, $\Omega_{\text{b},0}$, A, n_{s} etc. that are used in its calculation. This is an important point because it provides a method of deducing the values of all the cosmological parameters simultaneously. By comparing a large number of predicted power spectra with the available observational data regarding the power spectrum it is possible to identify a ‘best-fit’ spectrum, and hence

to come to some conclusions about the most probable values for the various cosmological parameters. More detailed analysis even allows uncertainties to be estimated.

This process of determining cosmological parameters from CMB anisotropy observations has already been carried out by a number of observational cosmology research groups. The latest values at the time of writing, those obtained by the WMAP team, are shown in Figure 7.27. Some of the parameters listed will be unfamiliar since they refer to aspects of cosmology that have not been discussed in this book. However from the list it is possible to draw the following values for the key cosmological parameters.

$$H_0 = (71 \pm 4)\,\mathrm{km\,s^{-1}\,Mpc^{-1}}$$

$$\Omega_{\mathrm{m},0} = 0.27 \pm 0.04$$

$$\Omega_{\Lambda,0} = 0.73 \pm 0.04$$

$$\Omega_{\mathrm{b},0} = 0.044 \pm 0.004$$

Also included in the list are the values of some 'secondary' parameters that depend on the key parameters. Among them is a value for the age of the Universe which provides a valuable cross-check on the reasonableness of the 'primary' results. In the case of the WMAP findings, the favoured value for the age of the Universe is

$$t_0 = 13.7 \times 10^9 \text{ years}$$

Pleasingly, this does seem to be a realistic estimate for t_0, since it makes the Universe older than the oldest stars we know of, the Population II stars in globular clusters. In view of this and other consistency checks the WMAP results have been well-received by cosmologists and are widely thought to represent the best numerical characterization of the Universe currently available.

7.5.5 Precision cosmology

The term **precision cosmology** was coined in 1996 by the American cosmologist Michael Turner. It expresses rather well the direction in which cosmology is thought to be heading. Gone are the days when cosmologists were free to speculate about the origin and evolution of the Universe with hardly any observational data to guide or fetter them. Cosmologists, like most other scientists, are now fenced in by large amounts of data, some of them very precise. Hubble's original estimate of the constant that bears his name was wrong by a factor of about 10. The estimate based on WMAP's anisotropy observations is thought to be within about 5% of the true value. Many of the other cosmological parameters are now thought to be known with a similar level of precision.

Studies of the CMB have certainly led the way into the era of precision cosmology and are expected to provide much of the data that will help to sustain it. A European space probe called *Planck*, planned for launch in 2007 or later, is expected to measure the CMB anisotropies on even finer scales than WMAP, and to determine the angular power spectrum almost as well as cosmic variance will permit. This will allow the cosmological parameters to be determined with even greater precision, perhaps with uncertainties of only 1% in some cases. However, the feeling among observational cosmologists that they are finally closing on the correct values of the cosmological parameters is not based on CMB measurements alone.

What has really boosted the confidence of observational cosmologists is finding that several independent lines of investigation are leading them towards the same

Description	Symbol	Value	+ uncertainty	− uncertainty
Total density	Ω_{tot}	1.02	0.02	0.02
Equation of state of quintessence	w	<-0.78	95% CL	–
Dark energy density	Ω_Λ	0.73	0.04	0.04
Baryon density	$\Omega_{\text{b}}h^2$	0.0224	0.0009	0.0009
Baryon density	Ω_{b}	0.044	0.004	0.004
Baryon density (cm^{-3})	n_{b}	2.5×10^{-7}	0.1×10^{-7}	0.1×10^{-7}
Matter density	$\Omega_{\text{m}}h^2$	0.135	0.008	0.009
Matter density	Ω_{m}	0.27	0.04	0.04
Light neutrino density	$\Omega_\nu h^2$	<0.0076	95% CL	–
CMB temperature (K)[a]	T_{cmb}	2.725	0.002	0.002
CMB photon density (cm^{-3})[b]	n_γ	410.4	0.9	0.9
Baryon-to-photon ratio	η	6.1×10^{-10}	0.3×10^{-10}	0.2×10^{-10}
Baryon-to-matter ratio	$\Omega_{\text{b}}\Omega_{\text{m}}^{-1}$	0.17	0.01	0.01
Fluctuation amplitude in $8h^{-1}$ Mpc spheres	σ_8	0.84	0.04	0.04
Low-z cluster abundance scaling	$\sigma_8\Omega_{\text{m}}^{0.5}$	0.44	0.04	0.05
Power spectrum normalization (at $k_0 = 0.05\ \text{Mpc}^{-1}$)[c]	A	0.833	0.086	0.083
Scalar spectral index (at $k_0 = 0.05\ \text{Mpc}^{-1}$)[c]	n_{s}	0.93	0.03	0.03
Running index scope (at $k_0 = 0.05\ \text{Mpc}^{-1}$)[c]	$dn_{\text{s}}/d\ln k$	-0.031	0.016	0.018
Tensor-to-scalar ratio (at $k_0 = 0.002\ \text{Mpc}^{-1}$)	r	<0.90	95% CL	–
Redshift of decoupling	z_{dec}	1089	1	1
Thickness of decoupling (FWHM)	Δz_{dec}	195	2	2
Hubble constant	h	0.71	0.04	0.03
Age of Universe (Gyr)	t_0	13.7	0.2	0.2
Age at decoupling (kyr)	t_{dec}	379	8	7
Age at reionization (Myr, 95% CL)	t_{r}	180	220	80
Decoupling time interval (kyr)	Δt_{dec}	118	3	2
Redshift of matter-energy equality	z_{eq}	3233	194	210
Reionization optical depth	τ	0.17	0.04	0.04
Redshift of reionization (95% CL)	z_{r}	20	10	9
Sound horizon at decoupling (°)	θ_A	0.598	0.002	0.002
Angular diameter distance to decoupling (Gpc)	d_A	14.0	0.2	0.3
Acoustic scale[d]	ℓ_A	301	1	1
Sound horizon at decoupling (Mpc)[d]	r_{s}	147	2	2

[a] from COBE (Mather *et al.* 1999)

[b] derived from COBE (Mather *et al.* 1999)

[c] $l_{eff} \approx 700$

[d] $\ell_A \equiv \pi\theta_A^{-1}$ $\quad \theta_A \equiv r_{\text{s}} d_a^{-1}$

Figure 7.27 The values of the various cosmological parameters obtained by comparing the WMAP observations with a range of cosmological models; CL indicates confidence limit. These values are taken from a paper by C. L. Bennett *et al*. and draw on the results obtained by many different observational cosmologists. (Note that some of these parameters have not been described in this book.)

conclusion. You saw evidence of this earlier, in the many different ways of trying to determine the key cosmological parameters. Some are inherently less accurate than others, but over the past few years they have been leading towards the same general conclusion. We live in a homogeneous and isotropic Universe with a flat ($k = 0$) spatial geometry and a scale factor $R(t)$ that is growing at an accelerating rate. The Universe is dominated by dark energy, but also contains a substantial amount of non-baryonic dark matter, a much smaller quantity of baryonic matter and an almost negligible amount of radiation.

Evidence concerning the composition of the Universe provides a good example of many different lines of investigation coming together. You saw in Section 7.4.1 that observations of Type Ia supernovae provide information about q_0 which is related to the combination $(\Omega_{\mathrm{m},0}/2) - \Omega_{\Lambda,0}$. The study of CMB anisotropies provides independent information and has tightly constrained $\Omega_{\mathrm{m},0} + \Omega_{\Lambda,0}$ since the time of BOOMERanG, and even more precise information has come from WMAP. Yet another line of argument involves the study of the large-scale distribution of galaxies that was briefly discussed in Chapter 4. The three-dimensional distribution of galaxies can also be described by a power spectrum, although it is very different from the angular power spectrum of the CMB. Nonetheless, the galaxy power spectrum contains features that limit the plausible range of values for $\Omega_{\mathrm{m},0}$. Although it is the study of CMB anisotropies that provides the most precise values for these density parameters, it is the agreement and combined effect of all the results that persuade many cosmologists that they are on the right track.

Cosmology is a speculative field of enquiry, but the constraints and tests provided by observational cosmology ensure that the core of that enquiry will be disciplined and effective. The new era of precision cosmology will be challenging, but it is safe to predict that it will also be exciting.

7.6 Summary of Chapter 7

Measuring the Hubble constant, H_0

- H_0 measures the current rate of expansion of the Universe.
- H_0 is traditionally determined by means of the Hubble diagram, a plot of redshift against distance for distant galaxies. When making such a plot the redshift and the distance must be determined independently. The Hubble constant is obtained from the gradient of the plotted line.
- The HST Key Project team used Cepheid variables to calibrate five other methods of distance measurement. Using these together with independent measurements of galaxy redshifts they concluded that $H_0 = 72 \pm 8\,\mathrm{km\,s^{-1}\,Mpc^{-1}}$.
- Other methods of determining H_0 include those based on gravitational lensing (via time delays between fluctuations in different images of the same lensed galaxy) and those based on observations of anisotropies in the cosmic microwave background radiation (CMB).

Measuring the current value of the deceleration parameter, q_0

- q_0 measures the current rate of change of cosmic expansion.
- q_0 may be determined from the Hubble diagram by observing the curvature of the plotted line at $z > 0.2$, but early attempts to do this were highly inconsistent.

- Results obtained using Type Ia supernovae as distance indicators suggest that q_0 is negative, implying that the expansion of the Universe is speeding up. It has become traditional to express the value of q_0 in terms of $\Omega_{\text{m},0}$ and $\Omega_{\Lambda,0}$, using the relation

$$q_0 = \frac{\Omega_{\text{m},0}}{2} - \Omega_{\Lambda,0}$$

Measuring the current values of the density constants, $\Omega_{\Lambda,0}$, $\Omega_{\text{m},0}$ and $\Omega_{\text{b},0}$

- The current values of the density parameters $\Omega_{\Lambda,0}$, $\Omega_{\text{m},0}$ and $\Omega_{\text{b},0}$ measure the densities associated with the cosmological constant (dark energy), matter of all kinds and baryonic matter, relative to the critical density $\rho_{\text{crit}} = 3H_0^2/8\pi G$.
- Results based on observations of anisotropies in the CMB strongly favour $\Omega_{\Lambda,0} + \Omega_{\text{m},0} = 1$.
- When these are combined with the results of observations of Type Ia supernovae, favoured values of $\Omega_{\Lambda,0}$ and $\Omega_{\text{m},0}$ are typically $\Omega_{\text{m},0} = 0.30 \pm 0.10$ and $\Omega_{\Lambda,0} = 0.70 \pm 0.10$.
- The current value of the density constant for baryonic matter can be determined in a number of ways. This quantity is constrained by primordial nucleosynthesis calculations which, if they are to agree with observations, require $0.02 \leq \Omega_{\text{b},0} \leq 0.05$.
- Direct assessments of $\Omega_{\text{b},0}$, based on baryon inventories, are beset by many uncertainties, but generally favour lower values: $0.007 \leq \Omega_{\text{b},0} \leq 0.041$.

Anisotropies in the CMB and precision cosmology

- Although highly isotropic, the CMB exhibits anisotropies in intensity at the level of a few parts in 100 000 over a range of angular scales. These can be mapped, and are usually shown as variations in the temperature of the CMB.
- The angular power spectrum of an anisotropy map shows the level of variation that is present on any specified angular scale (or, equivalently, the angular power at multipole number l).
- Values of cosmological parameters may be extracted from anisotropy measurements by comparing the observed angular power spectrum with that predicted by big bang cosmology. Recent results from the WMAP space probe indicate $\Omega_{\Lambda,0} = 0.73 \pm 0.04$, $\Omega_{\text{m},0} = 0.27 \pm 0.04$, and $\Omega_{\text{b},0} = 0.044 \pm 0.004$, implying a Universe dominated by dark energy, and in which most of the matter is non-baryonic dark matter.
- WMAP measurements also indicate that $H_0 = (71 \pm 4)\,\text{km s}^{-1}\,\text{Mpc}^{-1}$, and that the age of the Universe is $t_0 = 13.7 \times 10^9$ years.
- The results may indicate that we are now entering an era of precision cosmology in which cosmological speculations will be tightly constrained by measurements, and quantities that were previously very uncertain will become accurately known.

Questions

QUESTION 7.9

Using a variety of measurements (not just CMB), outline the observational basis of the claim that

(a) the Universe is dominated by dark energy

(b) most of the matter is dark

(c) most of the dark matter is non-baryonic.

QUESTION 7.10

On the basis of the very incomplete account given in this chapter, outline the role that space technology has played in observational cosmology and the role that it is expected to play in the future development of the subject.

QUESTION 7.11

Quote some examples to show the importance of terrestrial (as opposed to space-based) observations in cosmology.

CHAPTER 8
QUESTIONING COSMOLOGY – OUTSTANDING PROBLEMS ABOUT THE UNIVERSE

8.1 Introduction

> 'Don't let me catch anyone talking about the Universe in my department.'
>
> Lord Rutherford

Rutherford – the discoverer of the atomic nucleus – was a practical man. Perhaps one of the greatest experimental physicists of all time, he was profoundly sceptical of notions that were not grounded in hard experimental evidence. We can guess that he might not have been happy with some of the ideas of modern cosmology! But, however challenging the concepts of cosmology – and ideas about space being curved or expanding, and the vacuum possessing energy are certainly challenging – there can be no doubt that Rutherford would have been deeply impressed and intrigued by the vast amount of observational evidence that cosmologists have now acquired. His main interest, however, might well have been in those areas of cosmology where there are still clear gaps in our knowledge; the areas where work remains to be done and where new insights can be expected to arise.

The last few chapters have been largely concerned with the development and testing of models of the Universe. By a model we mean some simplified representation of the real world that helps us to understand reality by focusing on some specific aspects of it. The model should be simple, but not so simple that the phenomena of interest are inadequately represented. The Earth's orbit around the Sun, for example, can be modelled by a circle. This is an adequate model for explaining the occurrence of certain annual events, but a better model, such as an ellipse, is required to explain finer details such as the precise timing of those events. Neither model fully represents reality, but both are useful within their own ranges of validity, and the greater precision of the elliptical model is bought at the price of greater mathematical complexity.

■ In what important way did the FRW cosmological models of Chapter 5 simplify reality?

❑ They treated the contents of the Universe as a simple uniform fluid, the properties of which could be specified at any time by a density $\rho(t)$ and a pressure $p(t)$. Small-scale departures from uniformity, such as stars and galaxies, or even whole clusters of galaxies, were ignored.

■ In what important way did the big bang model of Chapter 6 improve on this, and how was the modelling further extended in Chapter 7?

❑ In Chapter 6 the matter in the Universe was treated more realistically by taking account of the variety of interacting particles that it contains, and by acknowledging the presence of density fluctuations. In Chapter 7 a spectrum of density fluctuations was considered (characterized by the parameters A and n_s) and related to the observed anisotropies in the cosmic microwave background radiation.

Despite its conceptual difficulty, the big bang is now widely accepted as the best available model of how the Universe evolved into its present state. However, it is quite clear that the model, as it has been presented in this book, and insofar as it is accepted by the majority of cosmologists, is still inadequate in several important respects. There are a number of major questions about our Universe that the standard big bang model does not address. This does not mean the model is wrong, but it does indicate deficiencies in certain areas and the model may need to be extended in those areas. This chapter concerns some of these outstanding problems, and considers the ways in which the standard big bang model might be extended to provide a more adequate account of reality.

The questions we shall consider are these:

Problem 1: What is the dark matter? (Section 8.2)

Problem 2: What is the dark energy? (Section 8.3)

Problem 3: Why is the Universe so uniform? (Section 8.4.1)

Problem 4: Why does the Universe have a flat ($k = 0$) geometry? (Section 8.4.2)

Problem 5: Where did the structure come from? (Section 8.5)

Problem 6: Why is there more matter than antimatter? (Section 8.6)

Problem 7: What happened at $t = 0$? (Section 8.7)

Problem 8: Why is the Universe the way it is? (Section 8.8)

8.2 The nature of dark matter

As you have seen many times in this book, the visible matter in the Universe – the stuff of stars and nebulae – accounts for only a small fraction of the whole. By recent estimates about 85% of the matter in the Universe is dark matter, and its nature is still a mystery. This is hardly satisfactory! So far you have been asked to accept the existence of dark matter without really enquiring what it is, but the time has now come to address that question – Problem 1 in our list – head on.

To prepare for that, we will review some of what you have already learned about dark matter.

- What do you understand by baryonic and non-baryonic dark matter?
- Baryonic dark matter is non-luminous matter in which most of the mass is attributable to baryons, most probably neutrons and protons. Non-baryonic dark matter is non-luminous matter made from something else.

In Chapter 6 you saw that the physics of the early Universe, especially the nucleosynthesis of the elements, puts constraints on the density of baryonic matter. No more than about 15% of the matter in the Universe can be baryonic. If we can trust the physics, then some of the dark matter may be baryonic but most of it has to be non-baryonic. Figure 8.1 summarizes our current understanding of the composition of the Universe.

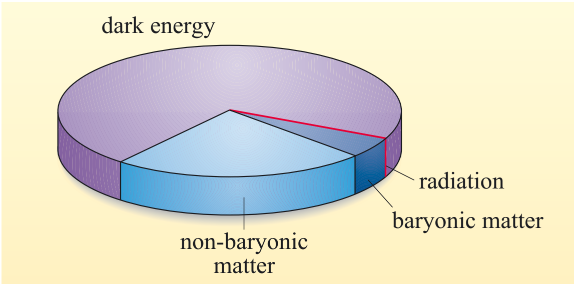

Figure 8.1 The contributions to the total (energy) density of the Universe from various sources. According to recent estimates, about 73% of the density of the Universe is currently due to dark energy, and about 27% is due to matter of all types. Only 4.4% of the total density is due to baryonic matter (i.e. roughly 15% of the matter). The contribution from radiation is only about 0.005%.

What can the dark matter be? Two broad classes of candidates have been proposed and they have been given the colourful names of MACHOs and WIMPs.

8.2.1 MACHOs

An obvious possibility, first mentioned in Chapter 1, is that at least some of the dark matter is simply normal matter – baryonic matter – that we cannot see and cannot detect other than by its gravitational influence. Stars are visible because they glow; if they did not we would regard them as dark matter.

QUESTION 8.1

Make a list of all the *known* types of astronomical object that could make up the dark matter in the halo of our own Galaxy.

In answering Question 8.1 you may have noticed that these dark objects fall into one of two categories – they are either *stellar remnants* or they are bodies that have masses lower than that of main sequence stars. All such objects are called **MACHOs**, a name that stands for 'massive astrophysical compact halo object'. (Astrophysicists are known for their occasional lapses into whimsy.) MACHOs, if they exist, are simply 'familiar' objects that happen to emit little or no radiation of their own and have therefore evaded detection except by their gravitational effect.

Some MACHOs (dead stars, etc.) might reasonably be expected to exist, so an important question to answer is whether the dark matter in our Galaxy – and by extension that in other galaxies and clusters of galaxies – can be *entirely* accounted for by MACHOs or whether something else is needed. One approach is a theoretical one. From what we know about stellar evolution and the age of the Galaxy we can estimate how many of these different kinds of objects might have been formed and work out their total contribution to the cosmic density. Helpful though it is, that approach is not as compelling as an observational one. Is there any way we can actually detect and count MACHOs?

Yes, there is. In Chapter 4 you saw how gravitational lensing could be used to study the distribution of dark matter in a cluster of galaxies. A similar technique can be used to search for MACHOs in the Milky Way. Dark objects in the Galaxy will occasionally pass in front of background stars, bending their light and causing them to brighten. Even a planet-size object can act as a gravitational lens. This smaller scale phenomenon is known as **gravitational microlensing**. All we need to do is look at a sufficiently distant star and wait for it to brighten as a MACHO passes in front of it.

- What problems do you see with this idea?
- Since both MACHOs and stars will have very small angular sizes, lensing events are likely to be rare. You would have to monitor a very large number of stars to stand a chance of seeing a single event. Also, you would have to be sure that the star was not variable, or that the brightening was not caused by some other effect.

Fortunately, any brightening caused by microlensing is expected to be characterized by a particular kind of light curve. The shape of this curve can be used to distinguish microlensing events from other types of variability. There are other checks too as the following question illustrates.

- How would you expect a microlensing event to affect the colour of a star?
- Not at all. Light at all wavelengths should be affected in the same way, so microlensing will not affect the colour of the star.

Despite its difficulties, this technique has been successfully employed to search for MACHOs against the dense stellar background of the Galactic bulge and the two Magellanic Clouds, that are located just outside the Milky Way. Many dozens of microlensing events have been seen since the first detection in 1992. An example is shown in Figure 8.2.

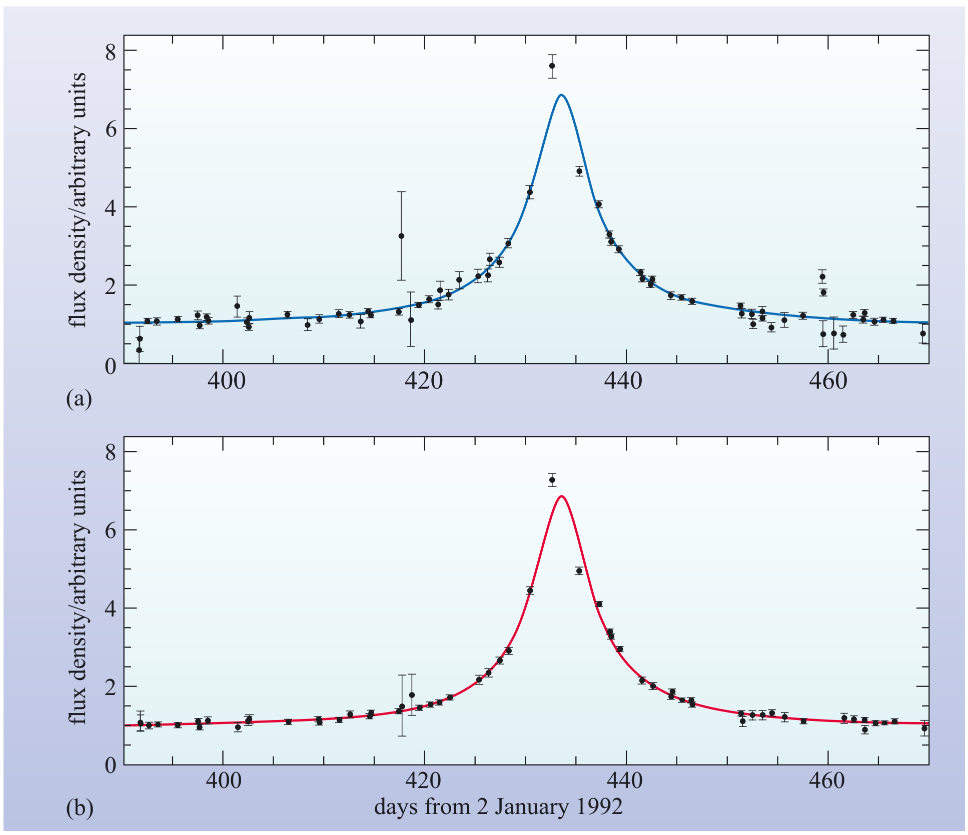

Figure 8.2 Gravitational microlensing. A star in the Large Magellanic Cloud brightens by a factor of 7 as an unseen dark object passes in front of it. The shape of the light curve is characteristic of microlensing and can be predicted from gravitational theory. As expected, the light curves are identical within experimental uncertainty in (a) blue and (b) red light. (Alcock *et al*., 1993)

The observations to date suggest that no more than about 20% of the mass of the Milky Way's dark-matter halo could be accounted for by MACHOs. So, although some of the dark matter in the halo may be MACHOs, most of it is not. In fact, this is not so surprising. As you have seen, there are very good theoretical reasons for believing that most of the dark matter cannot be made of MACHOs or any other kind of baryonic matter – we have to look elsewhere.

8.2.2 WIMPs

Weakly Interacting Massive Particles or WIMPs were introduced in Chapter 6 when we discussed the growth of structure under the influence of gravity in the early Universe. In that context, the justification for introducing the idea of a particle that responds only to gravity and the weak interaction was that density fluctuations composed of such particles would be able to grow prior to recombination. It should be stressed that at present no one knows what the WIMPs are, but several candidates have been proposed.

The original WIMP candidate, and the only one known to exist, is the neutrino. Neutrinos were plentiful in the early Universe, but ceased significant interactions with other forms of matter when the Universe was about 1 s old, just prior to the large-scale annihilation of electrons and positrons (see Section 6.3.7). As a result, the Universe should still be filled by a 'gas' of cosmic neutrinos, which should now have cooled to a temperature of roughly 2 K and a number density of about 10^8 per cubic metre. Individually, these neutrinos carry so little energy that they are currently undetectable, but collectively they might make a significant contribution to the density of dark matter.

Until recently it was thought that neutrinos had zero rest mass and always travelled at the speed of light. Such massless neutrinos would still contribute to the total density parameter Ω since this includes all kinds of energy, but the total contribution from massless neutrinos would be small. However, physicists have long recognized that there is no fundamental reason why neutrinos should not have mass, and neutrinos with mass, even a very small mass, might make a substantial contribution to the cosmic density. Recent measurements involving neutrinos from the Sun have indicated that the mass of a neutrino is roughly five million times smaller than the mass of the electron. Although this is an important result, such a tiny mass is not enough to let neutrinos account for a significant proportion of the dark matter. Neutrinos must make up some of the non-baryonic dark matter, but only, it seems, a tiny fraction amounting to about 0.3% of the total cosmic density.

Another serious objection to the neutrino is that because of its speed it could only be a candidate for *hot* dark matter. As was noted in Chapter 2, the hot dark matter scenario has fallen out of favour since it results in the formation of structure that is inconsistent with observations. For this reason, most cosmologists now reserve the term 'WIMP' for the proposed particles of *cold* dark matter.

Unlike the neutrino, all the candidates for cold WIMPs are hypothetical – no known particles fit the bill. There are several possibilities, but we shall consider only one, or rather only one class of candidates. This one class of candidate WIMPs is associated with a proposed new symmetry of nature known as **supersymmetry**. The notion of symmetry plays an important part in the standard model of elementary particles, since it implies various relationships between the fundamental particles and between the laws that govern them. Supersymmetry – first proposed

in the 1970s but still unconfirmed – would, if it existed, greatly extend the known symmetries of nature and imply the existence of many kinds of particles that have not yet been observed in nature.

Members of one class of supersymmetric particles, called **neutralinos**, have attracted particular attention from cosmologists. It is expected that there should be a stable neutralino with a relatively high mass – about 20 to 1000 times the mass of the proton. Like neutrinos, neutralinos are predicted to interact with other particles only through the weak interaction and through gravity. If the theory of supersymmetry is correct then some of the neutralinos created in the early moments of the big bang will still be present in the Universe today and these might be the WIMPs mainly responsible for cold dark matter. How could we find out whether neutralinos really exist?

There are two ways of going about this. One is to try to create a neutralino by simulating the high-energy conditions that were present in the big bang. This is not as dangerous as it sounds, since extreme conditions are routinely achieved in particle accelerators by making particles collide with each other at high energies. New particles are formed in the collision, and the hope is that, at the right energy, some of them will be neutralinos. Present-day accelerators are not powerful enough to achieve the required energies, but the new Large Hadron Collider being built at the European Laboratory for Particle Physics (CERN) near Geneva, may be able to do it (Figure 8.3). Early experiments with less powerful colliders have failed to create a neutralino but they have shown that, if it exists, the neutralino mass must be at least 30 times the mass of the proton.

Figure 8.3 The Large Hadron Collider at CERN near Geneva will occupy a circular tunnel 27 km in circumference, which currently houses the Large Electron–Positron Collider. When operational it may be possible to create neutralinos, the candidate particles of cold dark matter. (CERN)

Another approach is to try to detect cosmic WIMPs directly. You saw in Chapter 6 how particles of high mass could be created from radiation in the very earliest moments of the big bang when temperatures were extremely high. It is possible to estimate how many neutralinos might have been formed and so gauge how likely we are to detect them.

Although dark matter in the Milky Way is believed to form a widely dispersed dark-matter halo, the visible parts of the Galaxy lie within this halo. Thus the dark matter particles are expected to permeate the entire Galaxy, and we may expect to find neutralinos in our neighbourhood. They interact only weakly with ordinary matter, so they will pass freely through the Earth. The predicted number density of these particles is such that over ten million of them will pass through your head as you read this sentence.

This opens up the attractive possibility of detecting neutralinos in a laboratory experiment. Many such experiments are under way. They all work on the principle that if presented with a suitable target, a small proportion of the neutralinos passing through the Earth might interact with that target to produce a tiny flash of light or a minute rise in temperature.

Several materials are being used as targets but sodium iodide, in the form of large crystals up to 100 kg in mass, is a common one. The sodium and iodine atoms will recoil when hit head-on by a neutralino, and the recoil energy will be released as a flash of light that can be detected. Estimates suggest that a 10 kg crystal could be used to detect one neutralino a day. The biggest problem is to distinguish between genuine neutralinos and various kinds of background radiation. One series of experiments, by the UK Dark Matter Collaboration, is being conducted 1100 metres below ground in a potash mine where the detectors are shielded from cosmic rays (Figure 8.4). Other events can cause flashes of light, too, and the physicists work on the principle that when all other possible events have been eliminated then whatever remains must be a neutralino. At the time of writing, none of the various experiments around the world have unambiguously detected a neutralino. However, detector sensitivity is improving all the time, and if a future experiment does give a positive detection of a dark matter particle it will mark a major advance in cosmology.

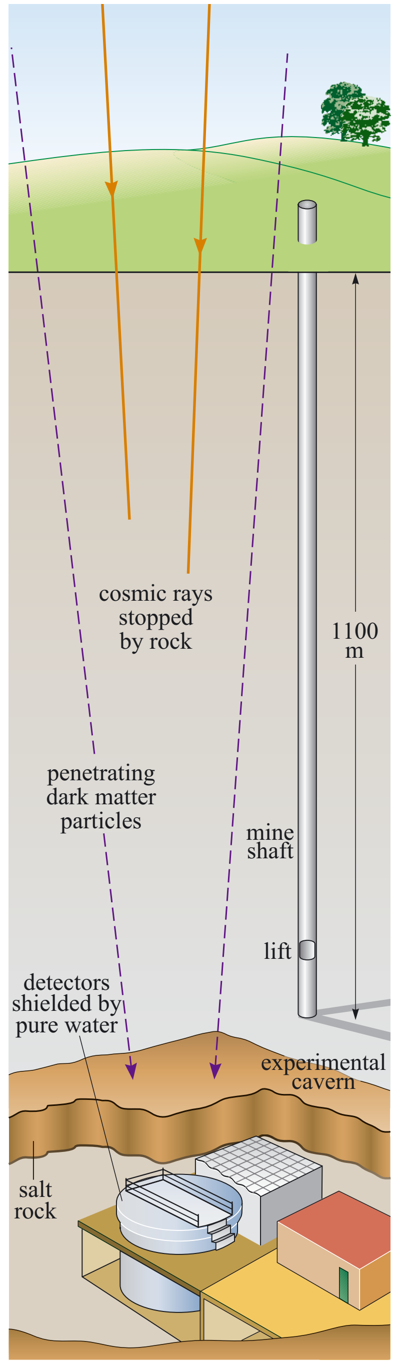

Figure 8.4 The UK Dark Matter Collaboration's WIMP detector is buried 1100 metres below ground at the Boulby Mine in the North York Moors National Park (in northern England). The deep location of the detector provides some shielding from cosmic rays, which are a source of 'noise' for dark matter experiments.

QUESTION 8.2

Table 8.1 presents a number of candidates for dark matter. Classify each candidate by placing ticks in the appropriate columns.

Table 8.1 For use with Question 8.2.

Dark matter candidate	Baryonic	Non-baryonic	MACHO	WIMP	Cold	Hot
brown dwarfs						
neutrinos						
neutron stars						
black holes						
neutralinos						

8.3 The nature of dark energy

While the prospect of a Universe filled with exotic new matter has itself challenged our understanding of the physical world, an even more startling cosmological discovery has come to light in the last few years. Until the late 1990s cosmologists took it for granted that the expansion of the Universe was slowing down under the mutual gravitational attraction of the matter within it. The main question was whether the expansion would eventually stop and go into reverse, or else carry on forever. Things are no longer so simple. As we saw in Chapter 7, studies of remote Type Ia supernovae imply that cosmic expansion is not slowing down but speeding up, and recent measurements of CMB anisotropies have given support to this finding. The accelerating expansion can be accounted for by attributing about 73% of the energy density of the Universe to a so-called dark energy, the effect of which is to oppose the deceleration of cosmic expansion. The presence of dark energy allows the Universe to maintain the critical density, even though the density of matter is low and decreases with time.

■ What is the connection between dark energy and dark matter?

❑ None that we know of! Although the names are similar, they refer to completely different phenomena. In particular, dark energy is *not* the energy equivalent of dark matter.

The dark energy acts to oppose the gravitational attraction of the matter in the Universe. But what does that mean physically? In general relativity, gravity is a consequence of space–time curvature, and that is determined by the distribution of energy and momentum, not just by the presence of massive bodies. Even the pressure in a fluid influences its gravitational effect since, as the fluid expands or contracts, the pressure will affect the internal energy of the fluid, and this energy will influence the curvature of space. (This is one way in which general relativity differs from Newtonian gravity.) A normal fluid uniformly filling the Universe, as envisaged in the Friedmann–Robertson–Walker models, would exert a positive pressure at every point, and this, like the density of the fluid, would have the gravitational effect of decelerating the cosmic expansion. The accelerating effect of dark energy indicates that it, in contrast to a normal fluid, is a source of *negative* pressure. The *density* of dark energy actually tends to retard cosmic expansion, but the negative pressure more than compensates for this, so the overall effect of dark energy is to accelerate the expansion. The negative pressure, or rather the associated gravitational effect, can be thought of as driving the cosmic acceleration. (Incidentally, if you think that *positive* pressure is normally responsible for pushing things apart, you are probably thinking of the effect of *differences* in pressure between one region and another. FRW cosmology is concerned with uniform universes, where there are no pressure differences, but where uniform pressure, like uniform density, does have a gravitational effect.)

Negative pressure may be unfamiliar but it is not unphysical. A phenomenon known as the **Casimir effect** (see Figure 8.5) shows that the presence of two narrowly separated, parallel metal plates modifies the electrical properties of the vacuum between them, producing a negative pressure in that region. In this case there *is* a pressure difference, and it creates an effective attraction between the plates that can be demonstrated and measured experimentally. This is not a gravitational effect, but it is a demonstration of negative pressure. Don't worry if you find the idea of

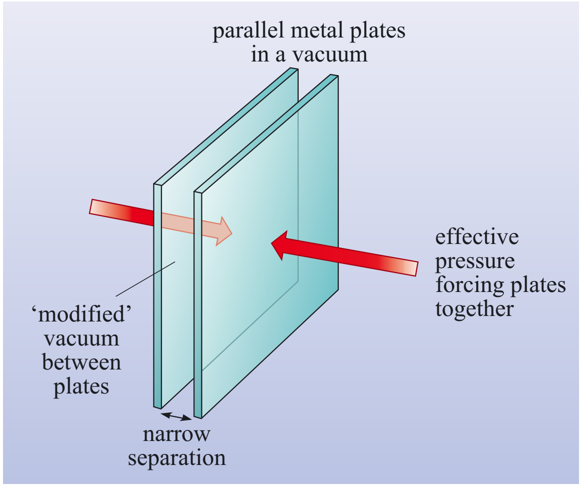

Figure 8.5 The Casimir effect. Two narrowly separated, uncharged conducting plates, located in a vacuum will be attracted towards one another. The attraction arises from the influence that the plates have on the region between them and the negative pressure that this produces in that region.

negative pressure hard to grasp. Accept for now that a uniform distribution of dark energy with negative pressure will have a repulsive gravitational effect, and such a distribution of dark energy will tend to accelerate the Hubble expansion.

What could this mysterious (and, let's face it, rather weird) dark energy possibly be? This is our Problem 2, and cosmologists have come up with three plausible answers.

The first possibility is that the dark energy simply represents the effect of a cosmological constant Λ, and has no deeper explanation. Unlike matter and radiation, the energy associated with the cosmological constant would not be diluted by the expansion of the Universe. It would stay the same, exerting a constant negative pressure throughout the expansion of the Universe. The value of the constant, Λ, would then be a new constant of nature, much like the gravitational constant, G. We would not be able to explain why it had the value it had, any more than we can explain why G has the value it has. It's just one of those things. Many cosmologists are unhappy about simply attributing the dark energy to the cosmological constant. Because its value is arbitrary and can be chosen to fit any acceleration, it seems too much of a 'just so' explanation.

The second possibility comes not from general relativity but from quantum physics. One of the central features of quantum theory is **Heisenberg's uncertainty principle**, which can be expressed in several ways, including the simple formula

$$\Delta E \Delta t > h/2\pi \tag{8.1}$$

where h is the Planck constant. Its usual interpretation is that we cannot know both the precise energy of a particle and the precise time we measure that energy. If we wish to know the energy of a particle to an uncertainty ΔE, then the time we take to measure it must be at least Δt. We cannot know both the energy and the time to greater precision.

The implications of this are profound and not a little disturbing when we apply it to empty space. Let's do a thought experiment. Suppose we take a small box, as small as we wish, and clear it of all particles. We also shield it from the outside world to make sure no fields are present within it. It's as empty as we can get it.

■ What would be the energy density inside this box?

❑ Common sense tells is that if the box is empty the energy density inside must be zero. But the uncertainty principle tells us otherwise!

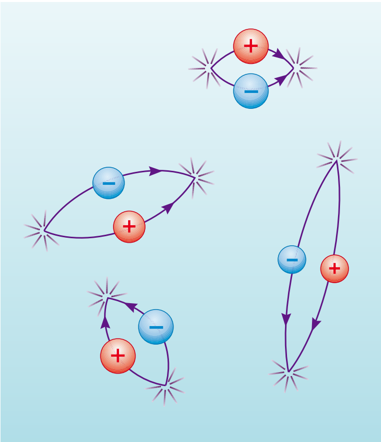

Figure 8.6 Virtual particles. According to quantum physics pairs of particles and antiparticles are continually being created and destroyed in empty space. The more massive the particle, the shorter its life.

If space were devoid of particles we would be able to say 'the energy in this part of space at this time is zero'. But we would then know the energy exactly and that would violate the uncertainty principle! The uncertainty principle forces us to recognize that even in 'empty' space, particles of energy ΔE could exist for a time Δt. It also implies that more massive particles (with greater mass energy) will be shorter lived than less massive particles. These **virtual particles**, which always appear as pairs of particles and antiparticles, are created and destroyed before they can be observed. (The process is similar to the process of pair production that was discussed in Chapter 6.) Space, far from being empty, is teeming with particles continually popping in and out of existence (Figure 8.6). The collective energy of these particles is known as **vacuum energy**.

There is no doubt that vacuum energy exists. It provides the explanation of the Casimir effect. The presence of the parallel conducting plates limits the kinds of virtual particles that can form in the region between the plates, and it is this that causes that region of 'empty space' to have different properties from the surrounding 'empty space'. The fact that vacuum energy is a property of the vacuum itself ensures that it will not be 'diluted' by the expansion of the Universe, and that it will have the required negative pressure.

In fact, the vacuum energy would have the same effect as a cosmological constant. Nonetheless, a distinction should be drawn between the cosmological constant as an irreducible term in the field equations of general relativity, and the quantum physical vacuum energy as a particular contribution to the cosmic distribution of energy and momentum. They may have similar effects, and either may account for the dark energy, but strictly speaking, they have a different origin.

This similarity has led to a lot of confusion, with some authors using the terms dark energy, vacuum energy and cosmological constant interchangeably. But it also means that the behaviour of possible universes, as described by the equations of Chapter 5 and 6, is just the same whether Λ represents Einstein's cosmological constant or a quantum vacuum energy with the same properties.

There is one important difference, though. Since vacuum energy is a consequence of quantum physics, it should be possible to calculate its density from first principles, to see how it compares with the measured density of the dark energy. This is something that cannot be done for the cosmological constant.

Can we calculate the density of the vacuum energy? Yes we can, though with some difficulty, and it comes out to about a factor of 10^{120} – 120 orders of magnitude – higher than the measured density of dark energy! This seems bizarre. Can there really be so much energy in empty space? Wouldn't we notice it? The repulsive gravitational effect of so much vacuum energy would be so great that the Universe would expand explosively (much like inflation in fact, where the vacuum energy is also implicated, as you saw in Chapter 6). If the vacuum energy is as high as it seems it's a real puzzle why it does not make itself felt.

Despite the huge discrepancy between the observed and calculated energy densities (Nobel laureate Steven Weinberg has called it 'the worst failure of an order-of-magnitude estimate in the history of science'), theoretical physicists seek solace in the knowledge that our understanding of particle physics is not complete. Until it is, they cannot allow for all the possible particles that may appear in the vacuum. In some theories particle energies may cancel each other out, so physicists hope that when a more complete theory is available the vacuum energy may yet turn out to account for the dark energy, but there is no proof of that at present.

The third candidate for dark energy is called **quintessence**. The name alludes to the fifth element of the ancient Greeks (after earth, air, fire and water), which was supposed to constitute the heavenly bodies. In its modern cosmological usage, quintessence can be thought of as an exotic form of matter. However, to account successfully for the observed properties of dark energy, quintessence would have to be such an odd form of matter that it actually makes more sense to think of it as a distribution of energy that fills the Universe. This makes it sound like vacuum energy, but unlike vacuum energy, quintessence is assumed to vary in time and space. Vacuum energy is a very specific form of energy whereas quintessence encompasses many possibilities. Quintessence would have to exert negative pressure to cause the observed acceleration in cosmic expansion, but its properties might be such that in the early Universe it behaved in a way similar to the energy of ordinary radiation and, though dominant at present, its influence might decline in the future allowing the cosmic acceleration to cease and even permitting the eventual deceleration of the Universe. Changes in the rate of cosmic acceleration should make it possible to distinguish the effects of quintessence from those of vacuum energy or the cosmological constant. Such measurements are not conclusive at present, but they may become so in future with improved observations of supernovae and CMB anisotropies.

Figure 8.7 summarizes the three main candidates for dark energy. So you thought space was empty? US physicist Hans Christian von Baeyer put it rather well. 'Space,' he said, 'is empty of matter but filled with surprises.'

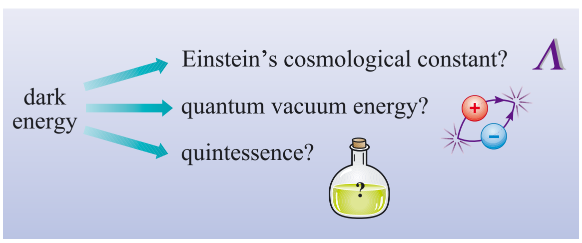

Figure 8.7 The three main candidates for dark energy.

8.4 The horizon and flatness problems

Two observed properties of the Universe that should be accounted for by cosmological models relate to its uniformity and the flatness of its three-dimensional spatial geometry. Neither of these properties is a natural outcome of the hot big bang model. Consequently the issues of explaining the uniformity and spatial flatness of the Universe have been labelled as 'problems' called, respectively, the horizon and flatness problems.

We start by considering the problem of explaining the uniformity of the Universe (Problem 3 in our list).

8.4.1 The horizon problem

You first came across the horizon problem in Chapter 6, when we considered the uniformity of the cosmic background radiation. This problem arises from the observation that the temperature of the cosmic background radiation is uniform to a few parts in 10^5 across the sky, yet points on the sky more than about two degrees apart are separated by a distance that is greater than the *horizon distance* at the time of last scattering (Figure 8.8). Remember that the horizon distance at a given time represents the maximum distance that a physical signal could propagate through space in the time elapsed since the very first instant of the big bang.

Although we have concentrated on the horizon distance at the time of last scattering, it is possible to consider the horizon distance and uniformity of the Universe at later times, and to arrive at a similar conclusion about the existence of the horizon problem. The advantage of discussing horizon distances in terms of the last-scattering surface is that it is readily observable through observations of the CMB. Thus, according to the standard account of the big bang, there is no reason to expect the CMB to be uniform on scales greater than about 2°.

One solution to the horizon problem is that, despite the arguments we have advanced to suggest that regions of the last-scattering surface could not have been in communication with each other, nevertheless, they *have* colluded together. Somehow or other, in the very early stages of the Universe's development, they *were* in contact with each other and reached a state of thermal equilibrium. What is required then is that these regions were somehow separated. A key idea here is that such a separation would create large-scale uniformity by the expansion *of space* rather than the propagation of a physical signal *through space*. The expansion would have to be by an enormous factor so that two regions that were once in contact, would later appear to be separated by many horizon distances.

- ■ What process in the early Universe could have had this effect?
- ❑ The process of inflation – a brief period of very rapid expansion could have caused regions that were once in contact to become separated by more than the horizon distance. (Inflation was discussed in Chapter 6.)

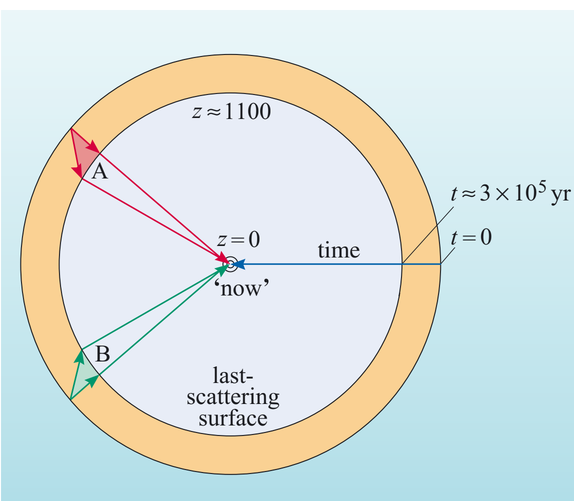

Figure 8.8 Regions A and B individually have an extent equal to the horizon distance at the time of last scattering. Both A and B subtend an angle of about 2° on the last-scattering surface (note that these angles are exaggerated in this diagram). However, A and B are separated by an angle greater than 2° and so lie outside each other's horizon at the time of last scattering, and hence no physical communication could have occurred between these two regions. The fact that the CMB appears to have the same temperature at A and B, despite this apparent lack of communication, is an example of the horizon problem.

To recap, the key idea of inflation is that close to the time that the grand unified era came to an end, the Universe underwent a brief but rapid phase of exponential expansion. The net result was that by the time that inflation was over the scale factor had increased by a huge amount. As noted in Chapter 6, the growth in the scale factor during inflation is very uncertain – but it is thought that an increase by a factor of as much as 10^{50} or more could have occurred during this process. Thus a region of the Universe, having first had a chance to become homogeneous and to reach thermal equilibrium before inflation, might have expanded to a size that is much greater than the horizon distance.

So inflation can solve the horizon problem by enlarging and sweeping apart regions of the Universe that had already become homogenized and leaving them separated by vast distances. When the cosmic background radiation became decoupled from matter (when the age of the Universe was about 380 000 years), it was necessarily isotropic because it was emitted by matter that was already homogeneous.

It is important to appreciate that inflation should be considered as an addition to the standard hot big bang model. Whereas the predictions of the standard hot big bang model from times of about 10^{-9} s onwards are widely accepted and stand up to observational scrutiny, the inflationary hypothesis is far more speculative. Indeed, as we noted in Chapter 6, the mechanism that drives the process of inflation is essentially unknown. The appealing aspect of inflation is that it offers a single solution to several cosmological problems; not only the horizon problem that we have just considered, but also the problems of structure formation and spatial flatness. It is to the latter problem that we now turn.

8.4.2 The flatness problem

The next outstanding problem on our list, Problem 4, relates to the observation that the average density of the Universe is almost equal to the critical density, i.e. $\Omega = 1$. In the context of the Friedmann–Robertson–Walker models this causes the curvature parameter, k, to be zero (see Question 5.9) and implies that three-dimensional space will have a flat geometry. Why should this be a problem?

In order for the total density parameter, $\Omega(t)$, to be close to 1 today, it had to be even closer to 1 in the past. This is because the extent to which $\Omega(t)$ differs from 1 is predicted to grow with time. If $\Omega(t)$ were *exactly* equal to 1 today, at time t_0, then at any earlier time, it would also have been exactly equal to 1. If, however, the current value of the density parameter turned out to be somewhat less than 1, $\Omega(t_0) = 0.90$ say, what would its value have been at some earlier time when the age of the Universe was only a fraction of t_0? The answer depends on the details of the FRW model used to represent the Universe, but in one case, for example, the difference grows at a rate proportional to $t^{2/3}$. In this particular case, a current difference of 0.1 implies that when the Universe was a thirtieth of its present age the difference between $\Omega(t)$ and 1 would have been smaller by a factor $30^{2/3} \approx 10$. Thus if $\Omega(t_0) = 0.90$, then $\Omega(t_0/30) \approx 0.99$. The fact that the Universe is now about 10^{17} seconds old, and has a density parameter that is still close to 1 means that at very early times, $t < 10^{-6}$ s say, $\Omega(t)$ must have been *extremely* close to 1. Explaining why $\Omega(t)$ should be so close to 1 at very early times is the crux of the flatness problem.

Now, of course, it is possible that the total density of the Universe just happens to have the critical value, in which case $k = 0$ and $\Omega(t)$ will always be equal to one.

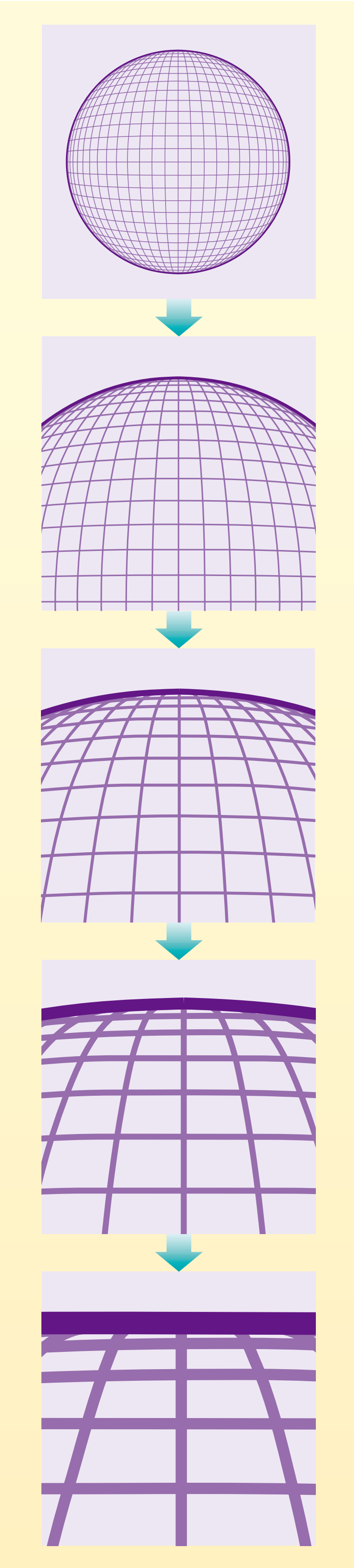

However, this would be another of those 'just so' explanations that, though possible, are never much trusted by cosmologists. Their preference is always for 'mechanisms' or 'processes' that force the cosmological parameters to take on their observed values. One of the motivations for proposing that there might have been an era of inflation in the very early Universe is that this can solve the flatness problem just as neatly as it solves the horizon problem.

The most direct result of inflation is an enormous increase in the cosmic scale factor $R(t)$, perhaps by a factor of 10^{50} or more. As suggested by Figure 8.9, this will have the effect of reducing the curvature of space, which depends on the quantity k/R^2. A sufficient amount of inflation will result in such a small value of k/R^2 that the effective value of k is zero, and space is geometrically 'flat', irrespective of the true value of k prior to inflation.

Now a geometrical argument of this kind might seem quite convincing at first sight, but you might still wonder how such an argument can have any bearing on the density of the Universe. Figure 8.9 might suggest that, in effect, $k = 0$, but how can it account for the fact that $\Omega(t)$ is correspondingly close to 1? To understand this you have to recognize that the link between the effective curvature and the density comes directly from the Friedmann equation and remains true no matter what the source of the cosmic energy density may be. Thus, near the end of inflation, when space is effectively flat, the Universe might have become quite cold and most of its energy might take the form of some exotic kind of vacuum energy, but the density of that vacuum energy will be just what is required to produce an effectively flat geometry. The usual assumption is that as the Universe ceases to inflate, some of this vacuum energy is converted into more conventional forms of matter and radiation, and that the Universe is reheated to a temperature similar to that it would have had in the absence of inflation. This has the interesting effect of causing all the matter and radiation in the observable Universe to be a direct consequence of inflation (any pre-existing matter or radiation will have been so diluted by inflation as to be unobservable), but it will not alter the fact that when all forms of matter and radiation are taken into account, as well as any dark energy, the total density of the Universe will be very close to the critical density and $\Omega(t)$ will be correspondingly close to 1.

Though inflation leads in a natural way to a Universe that is close to having to a critical density, it does not convert the Universe into one that has *exactly* the critical density. If the density before the onset of inflation was greater (or less) than critical, it will still be greater (or less) afterwards, though only barely so.

- ■ Supposing that prior to inflation the density were *less* than critical, what would be the analogue of Figure 8.9 for a Universe undergoing inflation?
- ❑ It would be a saddle-shaped rubber sheet which, after inflation, had been almost completely flattened over the tiny part constituting the 'observable' Universe.

Figure 8.9 A spherical balloon analogue for illustrating how the inflation of the Universe at an early epoch would have resulted in a flat spatial geometry for the observable Universe regardless of the curvature prior to inflation.

As you have seen in Chapter 7, the best current measurement of the cosmic density parameter is 1.02 ± 0.02, showing that the Universe is indeed very close to the critical density and very close to having a flat geometry. You have also seen that the contribution from the dark energy is about 73% of the critical density with matter at 27%. Hence the observation that two apparently unconnected components of the Universe, matter and dark energy, add up to the critical density is simply explained by inflation. Otherwise this coincidence seems very hard to understand.

At a stroke, the inflation idea solves both the horizon *and* flatness problems that afflict the standard model of the big bang. We have solved Problems 3 and 4! Indeed, it might even be that inflation holds the key to understanding the slight inhomogeneities that do occur – those responsible for triggering the formation of galaxies and those that manifest themselves as the ripples in the microwave background radiation. We shall learn more about this in the next section.

8.5 The origin of structure

In Chapter 2 you were introduced to the idea that galaxies formed from primordial fluctuations in the density of matter in the early Universe. Later, in Chapter 4, you saw how astronomers study the large-scale distribution of galaxies to test theories of how galaxies formed and infer something about the nature of the early fluctuations. Then, in Chapters 6 and 7 you learned how these fluctuations left their imprint on the cosmic background radiation.

Now it is time to address our Problem 5: where did those primordial fluctuations come from? In a sense this is the inverse of the uniformity problem. Earlier we asked why is the Universe so uniform, and now we ask why it is not perfectly uniform. From where did all this diverse structure come?

Inflation enlarges a tiny region of space by a huge factor. Solving the horizon problem may require space to expand by many orders of magnitude. This implies that current cosmological scales, tens to hundreds of megaparsecs, corresponded to subatomic scales during inflation. This intense magnification means that large-scale structures in the present-day Universe may have been rooted in subatomic irregularities in the pre-inflationary Universe. But where could such irregularities have come from in the first place?

As you have seen in the discussion of vacuum energy, empty space is seething with virtual particles that flit in and out of existence as a consequence of the Heisenberg uncertainty principle. Similar **quantum fluctuations** occurring during inflation would have been enlarged by the very rapid expansion of the Universe and could have been the cause of macroscopic variations in density. These, after much subsequent evolution might have been the source of the large-scale structure we see around us today.

Although there is no agreement about exactly what caused inflation, there are a number of proposed models that make quite detailed predictions about the quantum fluctuations that might have occurred. Generally speaking these fluctuations would have been caught up in inflation and would have grown in size until they exceeded the horizon scale of the then-observable Universe (Figure 8.10). Once this happened, information could no longer travel from one side of a fluctuation to the other, so the fluctuation would have been unable to smooth itself out and would have become 'frozen in', expanding along with space as the scale factor $R(t)$ continued to grow.

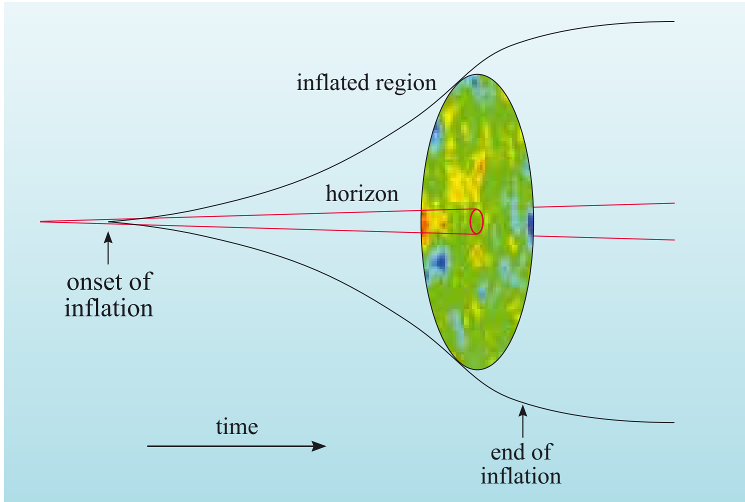

Figure 8.10 A schematic illustration of the expansion of a small region of the Universe due to inflation. Quantum fluctuations within this region are expanded beyond the horizon distance, at which point they become 'frozen in' and form the primordial density fluctuations from which subsequent structure in the Universe develops.

As earlier fluctuations were stretched beyond the horizon scale, newer quantum fluctuations were generated, creating more small-scale density variations that were stretched in their turn. The precise outcome varies from one model of inflation to another, but the general result is a range of density fluctuations with roughly the same 'strength' on a wide range of size scales, i.e. variations in density that are much the same on large scales and on small scales.

Following inflation, the Universe continued to expand, but the rate of expansion was so much reduced that the growing cosmic horizon would have encompassed more and more of the matter in the Universe as time passed. As the horizon expanded at the speed of light, material that had been swept over the horizon during inflation re-entered the horizon bringing the frozen-in density variations with it. The last density fluctuations to be inflated beyond the horizon would have been the first to re-enter, but these would have been followed by other density variations on larger and larger scales. Once back inside the horizon, the variations in density ceased to be 'frozen-in' and were able to become stronger or weaker depending on the prevailing conditions at the time they re-entered the horizon. It has been known for some time that the pattern of density variations predicted by inflation (with the same amplitude on all scales) is just what is required to give rise to the observed range of superclusters, clusters, etc. Hence inflation provides a possible explanation for the origin of all of the structure we see in the Universe – it might all have come from quantum fluctuations. Intriguingly, according to the inflationary hypothesis, the largest macroscopic structures might have had their origin in the microscopic quantum world.

8.6 The matter of antimatter

Inflation can explain many things, but it cannot account for the fact – Problem 6 – that the Universe contains far more matter than antimatter. Why should this be so?

In the account of inflation given in Chapter 6, it was noted that the end of inflation would have been accompanied by the release of a vast amount of energy in the form of particle–antiparticle pairs. At a later stage the antiparticles annihilated with the particles, so by now we might expect the Universe to be devoid of matter but full of radiation. In numerical terms this is very nearly the case: there are about a

billion photons (mainly in the cosmic microwave background) for each proton or electron in the Universe. Even so, the fact that there are any matter particles at all, implies that rather more matter than antimatter must have been formed.

Another way of stating this problem is in terms of the baryon number of the Universe. If, for every baryon in the Universe, there was a corresponding antibaryon, the baryon number of the Universe would be zero. However, we know that in the real Universe there is a surplus of baryons over antibaryons – so the baryon number of the Universe is a positive number. The conservation of baryon number in nuclear reactions is an important principle of physics, and we might naively expect that because the baryon number of the Universe currently has a positive value, this must always have been the case. However, physicists are reluctant to accept that the Universe must have started out with a positive baryon number. It seems more natural for the baryon number of the Universe to have originally been zero – in much the same way that the net electric charge of the Universe is zero. So if the Universe started out with a baryon number of zero – how did it reach its present non-zero value? One possible answer is that there may have been an era in the history of the Universe when baryon number was *not* conserved, i.e. reactions may have occurred which violate the principle of conservation of baryon number. Such reactions could have caused the baryon number of the Universe to change from an initial value of zero to the positive value we observe in the present-day Universe.

In Chapter 6 you saw that the unification of the strong and electroweak forces (grand unification) is believed to occur at energies of around 10^{15} GeV. The speculative grand unified theories that describe reactions at these enormous energies predict that baryon number need not always be conserved. Particle interactions at such energies could therefore give rise to the slight excess of matter that we see in the present-day Universe. Note that such interactions must have occurred *after* the process of inflation. According to the inflationary model, the vast majority of particles in the Universe were created from the energy released at the end of inflation. The imbalance between matter and antimatter could only have developed after these particles were created, and so inflation must have occurred at, or before, the end of the grand unified era.

Reactions in which baryon number is not conserved occur at such high energies that they are far beyond anything we can reproduce in laboratories today. However, it might still be possible to find experimental evidence in support of grand unification theories. The fundamental processes that allowed an excess of baryons to form in the very early Universe might also, very rarely, allow protons to decay in the present-day Universe. So far, no proton has ever been observed to decay, despite many attempts to detect such a process. However, if the proton had a mean life of the order of 10^{33} years, this failure could be understood and there would still exist the possibility of observing proton decay in the future.

Before we leave this subject, we need to address an assumption we have made, namely that there are no significant amounts of antimatter in today's Universe. How do we know this? If matter and antimatter could somehow have become segregated in the early Universe, then there may be regions of space in which antimatter dominates. Antiprotons, antineutrons and antielectrons (i.e. positrons) could have come together to form antiatoms which in turn could have formed antimolecules and eventually antistars, antiplanets and antipeople. Are there intelligent creatures out there made of antimatter?

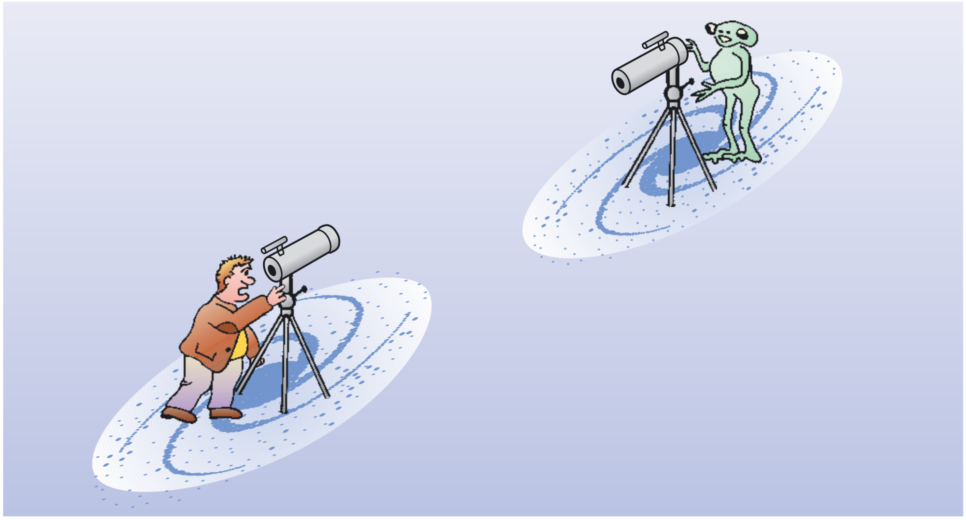

Figure 8.11 How could we tell whether a distant galaxy was made of antimatter?

QUESTION 8.3

Suppose you suspected that a newly discovered galaxy was made of antimatter (Figure 8.11).

(a) Could you tell from its emitted radiation whether the galaxy was made of matter or antimatter?

(b) Given that matter and antimatter will annihilate each other to form γ-rays, are there any other observations you could make?

8.7 Towards $t = 0$

According to the classical Friedmann–Robertson–Walker models, the Universe started expanding from a condition in which the scale factor was zero, implying a state of infinite density, often referred to as the **initial singularity**. How can we talk about the physics of something in that state? What actually happened at $t = 0$? This is our Problem 7, and it is a difficult one. If we naively extrapolate the big bang model back towards $t = 0$, many of its physical properties (the energy density of matter and radiation, the pressure and temperature, and the curvature of space–time) approach infinity, i.e. they diverge. When a model predicts infinite values we can take it as a warning that we have probably pushed the model beyond its limits of validity.

This should not come as a great surprise. You saw in Chapter 6 that quantum physics sets a natural limit – represented by the Planck time, about 10^{-43} seconds – on the earliest moment at which we can have any confidence in the big bang model. As we approach the Planck time quantum effects become as important as general relativistic effects and behaviour cannot be understood within the framework of existing physical theory. Neither general relativity nor conventional quantum physics are much help to us here. So before we can think about $t = 0$ we need a new theory that will take us back beyond the Planck time. First, however, we consider the possible cause of inflation.

8.7.1 The origin of inflation

We would like to know how inflation began. There is no agreement about the fundamental physics underlying the inflationary hypothesis, unlike, say the big bang model, which is based on general relativity. Inflation implies a wealth of physics beyond what we already understand. One of the major aims of current research involves trying to link inflation to known particle physics.

Without a fundamental theory backing it, the question of how an inflationary period may arise in the Universe is open to speculation. Inflating even a small initial patch to form the observable Universe we see today puts restrictions on what came before. For instance, any initial patch must have been sufficiently uniform on average to allow inflation. How did this arise? Were these conditions predetermined – or did they arise by chance? As one possible solution to this, the cosmologist Andrei Linde has suggested a model called **chaotic inflation**, where the initial condition of the Universe is random. In this model the Universe is much larger than we can see, and is partitioned into *domains* with differing laws of physics (see Figure 8.12). We live in a region where the right conditions for inflation have arisen by chance. This region has inflated and has provided the right conditions for life, but other domains may not be capable of this.

A problem with this suggestion is that we cannot probe these other domains unless they impinge on our domain. This model is therefore not testable. One day, inflation may be found to be part of testable theory that explains how the right conditions could arise. At present however, it is not clear if this will ever be the case.

Inflationary theory has dominated thinking about the very early Universe since the 1980s. Its ability to explain a range of diverse features of the Universe with a small number of assumptions makes it an attractive model. The main 'predictions' of inflation – a spatially flat Universe that is highly but not perfectly uniform, and a specific spectrum of density variations – appear to have been validated by observation. This success has led cosmologists to take seriously the key elements of the inflationary scenario, but it has also left them with a strong awareness of the need for further tests and an interest in searching for alternative theories that might be equally successful. The next two subsections briefly discuss two of these alternatives.

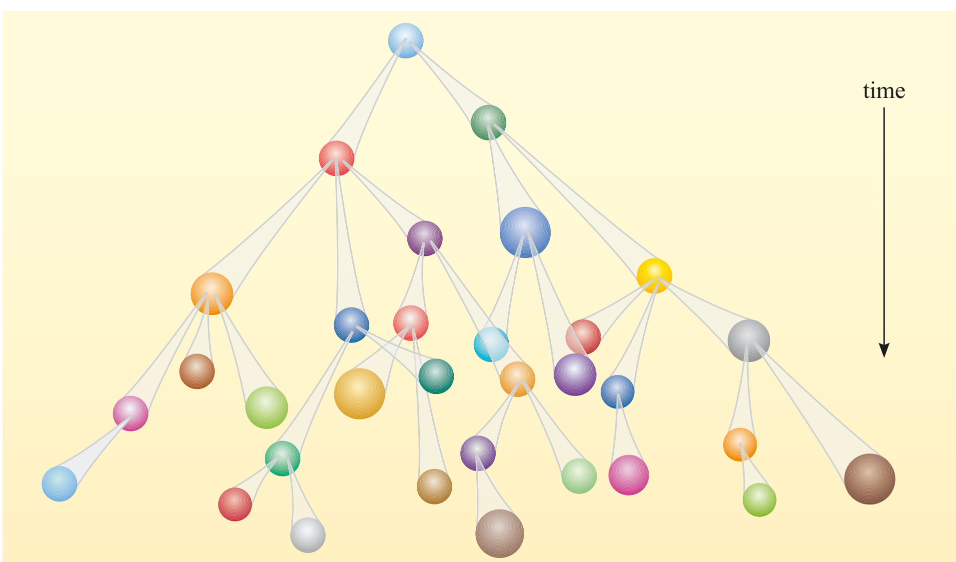

Figure 8.12 Chaotic inflation suggests that the Universe may consist of numerous inflationary domains each with different laws of physics (different colours in this diagram). Our observable Universe is just a tiny part of one of these domains.

8.7.2 Quantum cosmology

Quantum cosmology is used to describe one particular attempt to describe what went on before the Planck time. It employs a particular (and highly speculative) approach to the unification of quantum physics and general relativity that was pioneered by John Wheeler and Bryce DeWitt in the 1960s. Unfortunately, their theory is difficult to interpret as it does not refer directly to evolution in time, but rather to other properties of the Universe, such as its size. Remarkably, the Wheeler–DeWitt theory can be used to calculate the probability that the Universe came into being from nothing, though doing so involves making a number of assumptions. James Hartle and Stephen Hawking attempted this in 1983, basing their thinking on the assumption that the Universe should have no boundary in time or space. Others, using different assumptions have found a different answer and it is not clear which, if any, is correct. However it is interesting that one can make progress by assuming that the laws of physics are somehow ‘beyond’ the Universe itself and can describe its creation. This is in distinct contrast to the philosophy of chaotic inflation, where it is assumed that the laws of physics are very much ‘within’ the Universe, and may vary from place to place.

8.7.3 M-theory

Over the past few years a new line of research has opened up in cosmology. **M-theory** (which subsumes the earlier ideas of *superstring theory*) tries to unify not only general relativity and quantum theory, but also all the known forces in the Universe. It is widely regarded as the best candidate so far for a ‘theory of everything.’ In M-theory the fundamental objects are not particles, as usually assumed, but strings or even sheets. These strings and sheets can vibrate, and the different vibrations describe the different particles and their masses. One of the attractive features of these models is that they predict a massless particle that looks like the graviton, the quantum particle of the gravitational field. Hence M-theory ‘predicts’ gravity and all of the results of general relativity.

One of the stranger features of M-theory is that it predicts more than four dimensions. In fact it requires 11 dimensions to work at all. Usually it is assumed that the extra dimensions are ‘rolled up’ and hidden away to leave the familiar three dimensions of space and one of time – the extra dimensions would only become apparent at very high energies. However it seems that some of the extra dimensions need not be rolled up. One line of development regards our Universe as residing on a sheet (known as a ‘brane’ since it is derived from the term membrane) that itself resides in a five-dimensional space called the bulk. This picture has allowed cosmologists to develop new models of the early Universe, including one that does not require inflation to have occurred at all. According to this **ekpyrotic model** (the name means ‘out of fire’), a key event in cosmic history was a collision between the brane on which our Universe resides and some other ‘parallel’ brane (Figure 8.13). This collision would have been the cause of the fluctuations that led to large-scale structures being formed. In an extension of this model, the sheets collide over and again, allowing an infinite number of past big bangs in a ‘cyclic’ universe. Just before the collision, the forces on the sheets cause an accelerated expansion, which would look like the currently observed acceleration, and which flattens and smoothes out the Universe thus dispensing with the flatness and horizon problems.

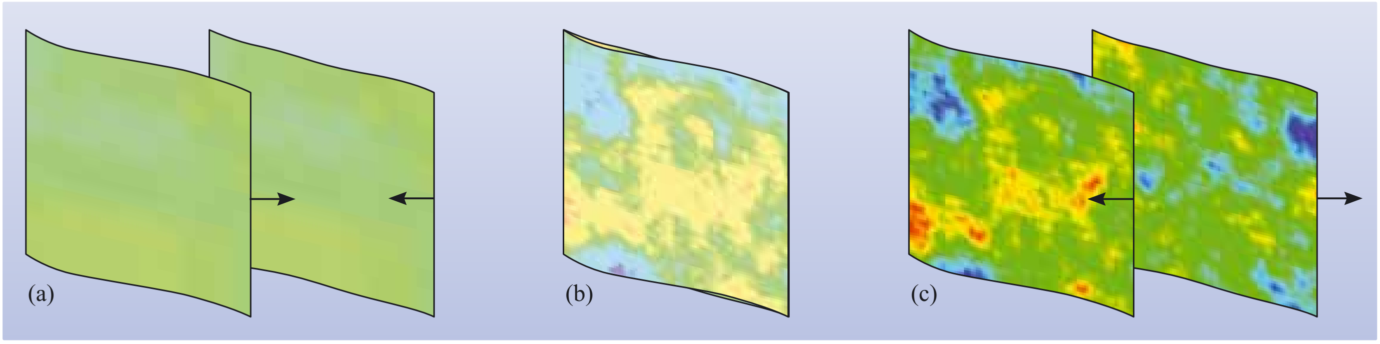

Figure 8.13 The ekpyrotic model, which invokes colliding sheets or 'branes' (representing our Universe and a parallel universe). (a) Two branes come together, resulting in (b) a collision that creates (c) the primordial fluctuations that are required to give rise to the observed large-scale structure and to the observed anisotropies in the cosmic microwave background.

In this theory the dark energy is a manifestation of the energy that controls the separation of the colliding branes, so it plays a vital role in the evolution of the cosmos rather than being a sort of 'uninvited guest'.

No one seems to know what the 'M' of M-theory stands for, though one of the theory's leading protagonists, Edward Witten, suggests 'magic, mystery or membrane, according to taste'.

8.8 The anthropic Universe

There seem to be a multitude of possible universes, but only one Universe. Why is our Universe the way it is? (This was the last question posed at the beginning – Problem 8.) Why do the fundamental constants of nature have the values they do? Could they have been different? In particular, if the Universe had started out with different conditions would we, or someone like us, still be here to puzzle about it?

The notion that the Universe must be able to give rise to life (and cosmologists!), has been given the status of a principle, the **anthropic principle**. It comes in two basic forms, the weak and the strong, and there are various versions of each.

The *weak anthropic principle* holds that the initial conditions of the big bang were such as to allow the eventual emergence of carbon-based life. Universes with different initial conditions – perhaps different values of the speed of light, the Planck constant, the gravitational constant, and so on – may have been possible, but if those conditions were not favourable to life then we would not be here. We would not, therefore, expect to find anything in the Universe incompatible with our own existence. So far the anthropic principle is not saying anything remarkable.

But the *strong anthropic principle* goes further, and holds that the Universe *necessarily* had the initial conditions that eventually allowed carbon-based life to emerge. Proponents of the strong principle argue that of all possible universes our Universe is so extraordinarily improbable that it cannot be an accident. Some go further and hold that the Universe was in some sense destined to develop not only life but self-awareness. They point to numerous coincidences that seem to imply that the Universe is finely tuned to favour the emergence of life.

The classic example, which actually pre-dates the anthropic principle, is the nucleosynthesis of carbon. Carbon is produced in post main sequence stars by the triple-alpha reaction. Two helium nuclei fuse to form an unstable nucleus of beryllium. Before the beryllium can fall apart again it is hit by a third helium nucleus to form a stable carbon nucleus. The trouble is, such a triple collision is so improbable that it's hard to explain the amount of carbon seen in stars today. The puzzle was solved in 1953 by the cosmologist Fred Hoyle, who predicted that carbon must possess a 'resonant' state such that at a certain collision energy a carbon nucleus is formed much more readily than expected. Without Hoyle's resonant state – which was later confirmed by experiment – there would be no carbon and no cosmologists. The energy of the resonant state is so finely tuned that if it were a little higher, the carbon would be rapidly converted into oxygen and there would again be no cosmologists. Hoyle himself was deeply affected by his discovery.

There are many other supposed coincidences of this nature though, unlike Hoyle's prediction, they have all been recognized in hindsight. Stable orbits are only possible in a universe with three spatial dimensions. Any more than three and there would be no planets for life to make its home on and no atoms either. The initial expansion of the big bang must have been just right – any faster and galaxies and stars would not have been able to form, any slower and the Universe would have collapsed again before life could emerge. Gravity must also be the right strength. If G is too big, only massive stars will form and burn out before life can take hold. If G is too small, stars will not get hot enough to start nuclear reactions.

Many people are unimpressed by such arguments, pointing out that no one should be surprised that the Universe permits us to exist. For them the anthropic principle begins and ends with its weak form and is not saying anything very profound. Douglas Adams, the author of the *Hitchhiker's Guide to the Galaxy*, liked to tell the story of a puddle of water lying in the road. Suppose the puddle suddenly becomes conscious and starts to contemplate its situation. It starts to sense its surroundings, probing the surface of the road beneath it, and notes that the depression in which it lies is the same shape as its own body. It comes to the conclusion not only that the Universe is perfectly adjusted to the emergence of puddles but that its own existence was somehow predestined. Can it be a coincidence?

You win the National Lottery against odds of 14 million to one. What an extraordinarily improbable coincidence! Yet someone had to win, and your win has to be seen in the context of millions of ticket holders who did not win. On this view, our Universe may one of countless possible past and future universes – perhaps arising from chaotic inflation – the difference being that ours holds the winning ticket.

Others argue that aside from the meaninglessness of hypothetical and unobservable 'other universes', such critics are missing the point. Russell Stannard, a physicist at the Open University, cites a counter-example of a prisoner sentenced to be executed by firing squad. At the crucial moment all ten marksmen miss their target and the prisoner is reprieved. Asked to explain his amazing deliverance the prisoner is unimpressed. 'Of course they missed, or else I wouldn't be here.' Such an explanation is not wholly satisfactory, since it fails to address *why* all ten skilled marksmen so improbably missed their target. Likewise, some people seek an explanation for why the Universe is set up the way it is beyond the explanation that it just has to be that way or else we would not be here to ask the question.

QUESTION 8.4

What do you think about the anthropic principle? Do you find it trivial, like Douglas Adams, or profound, like Russell Stannard? Can you find flaws in either of their stories? Can you reconcile the two views? How much is your opinion coloured by your own philosophical or religious beliefs? These are questions you will not find answered at the back of the book!

8.9 Epilogue

This chapter started with a quotation so it will finish with one too. Albert Einstein, whose insights into the nature of space and time made modern cosmology possible, once remarked that 'the most incomprehensible thing about the Universe is that it is comprehensible.' Perhaps after reading about multidimensional sheets banging together in 11-dimensional space, you may be inclined to think that Einstein, on this occasion, got it wrong!

But stay with us. Einstein was saying two things. First, he was expressing a faith that underpins all science, not just cosmology, namely that we will be able to understand the Universe and find it makes sense. The world is not chaotic and that makes science possible. But he was also saying something else, namely that we really have no right to expect the Universe to be that way. Why *should* we find the Universe comprehensible?

This could be a cue for another excursion into the anthropic principle, but we shall not do that. The models we have been discussing in the last few chapters may stretch your imagination to the limit (and beyond!) but they are the cosmologist's way of making the Universe comprehensible. So far our models have been able to keep up with new surprises sprung on us by the Universe. One day our luck and our imagination may run out and we may then have to admit that the Universe makes no sense after all. Until that happens, cosmology will continue to be one of the most exciting and mind-stretching of all the sciences.

QUESTION 8.5

Make brief notes *in your own words* to answer each of the questions posed at the beginning of this chapter. How satisfied are you with the answers? Check them against the summary at the end of this chapter.

8.10 Summary of Chapter 8

The models devised by cosmologists are simplified representations of the Universe. Like all models, they are only partial analogies to reality and break down outside their limits of validity. The big bang model is successful as far as it goes, but there are several problems it cannot answer.

- *Problem 1: What is the dark matter?* Dark matter makes up about 23% of the Universe. A little of it is baryonic, in the form of MACHOs, which are simply familiar objects that are too faint to see. Some of them can be revealed by

gravitational microlensing. About 85% of the dark matter has to be non-baryonic but apart from a very small proportion of neutrinos its nature is largely unknown. The best candidate is the neutralino, a form of WIMP, which may soon be discovered in laboratory experiments.

- *Problem 2: What is the dark energy?* Dark energy is a source of negative pressure that fills the Universe and drives the accelerating expansion. It should not be confused with dark matter. Its nature is still a mystery, but the leading contenders are Einstein's cosmological constant (a source of 'repulsive' gravity arising from general relativity), quantum vacuum energy (a consequence of Heisenberg's uncertainty principle) or 'quintessence' (an exotic form of matter).
- *Problem 3: Why is the Universe so uniform?* This is the horizon problem, which asks why widely separated regions have the same temperature and density, even though each has been beyond the horizon of the other throughout the history of the Universe. Inflation provides a possible answer. A small region of the Universe that had become homogeneous might have expanded so rapidly and by such an enormous factor that the whole of the currently observable part of the Universe (and perhaps more) is contained within the inflated homogeneous region.
- *Problem 4: Why does the Universe have a flat ($k = 0$) geometry?* Again, inflation may make it so. During the inflationary period large amounts of matter and energy were released into the Universe from the vacuum energy, leaving its density very close to the critical density, which corresponds to a flat geometry. Equivalently, whatever curvature the early Universe may have had would have been smoothed out by inflation leaving the spatial geometry of the observable Universe indistinguishable from that of a 'flat' space.
- *Problem 5: Where did the structure come from?* Clusters of galaxies were formed from density fluctuations in the early Universe which have left their imprint on the cosmic background radiation. Those fluctuations in turn may have arisen from tiny quantum fluctuations which were stretched by inflation from the microscopic scale up to and beyond the size of the then-observable Universe. At that point they would have become 'frozen in' as large-scale primordial fluctuations from which galaxies could condense.
- *Problem 6: Why is there more matter than antimatter?* Although one might expect equal numbers of particles and antiparticles to have been created in the early Universe, grand unified theories of physics allow a slight imbalance of matter over antimatter of 1 part in 10^9. The matter now in the Universe is that left over when the bulk of the matter and antimatter annihilated.
- *Problem 7: What happened at $t = 0$?* It's still anyone's guess. General relativity breaks down at the Planck time of 10^{-43} s, and to progress to earlier times requires a theory of quantum gravity that unifies general relativity with quantum physics. Inflation, too, remains without a firm grounding until this very early era is better understood. Limited progress has been made with quantum cosmology but the new all-encompassing M-theory offers several intriguing lines of enquiry.
- *Problem 8: Why is the Universe the way it is?* According to the anthropic principle, because we are here to ask the question!

ANSWERS AND COMMENTS

QUESTION 1.1

Since $v = d/t$, the time it takes the Sun to travel a distance d around its orbit at speed v is given by $t = d/v$.

The distance d the Sun travels in one orbit is the circumference of a circle of radius $R = 8.5\,\text{kpc}$, so $d = 2\pi R = 2 \times 3.14 \times 8.5\,\text{kpc} = 53.4\,\text{kpc}$. As the speed is given in km s^{-1} rather than kpc s^{-1}, it is convenient to convert this distance to units of km. Since $1\,\text{pc} = 3.09 \times 10^{13}\,\text{km}$, $d = 53.4 \times 10^{3}\,\text{pc} \times 3.09 \times 10^{13}\,\text{km pc}^{-1} = 1.65 \times 10^{18}\,\text{km}$.

We can then calculate the time taken to complete one orbit of the Galactic centre as

$$t = d/v = 1.65 \times 10^{18}\,\text{km}/220\,\text{km s}^{-1} = 7.50 \times 10^{15}\,\text{s}$$

The number of seconds in one year is $60 \times 60 \times 24 \times 365.25 \approx 3.16 \times 10^{7}$. Therefore

$$t = 7.50 \times 10^{15}\,\text{s}/3.16 \times 10^{7}\,\text{s yr}^{-1} = 2.37 \times 10^{8}\,\text{yr}$$

Note that since R is given to only two significant figures, we should round the final results to the same accuracy: $t = 7.5 \times 10^{15}\,\text{s}$ (in SI units) and $t = 2.4 \times 10^{8}\,\text{yr}$ (in years).

QUESTION 1.2

(a) Baade found that the stars in the spheroid of M31 were all red giants, whereas those in the disc of that galaxy were blue stars. Moreover, the red stars in the spheroid of M31 resembled those of Galactic globular clusters, and his observations of the blue stars in the disc of M31 resembled those seen in the plane of the Milky Way. His observations showed that different types of stars occupied different parts of a galaxy.

(b) When a star finishes burning hydrogen in its core, it evolves from the main sequence to become a red giant. In a young population, there are plenty of massive main sequence stars (which are blue), but with time they evolve onto the red giant branch. Hence a population of old stars is dominated by the light of red giants. You can therefore infer that the stars in the spiral arms of M31 and the plane of the Milky Way must be young, whereas the stars in the nuclear bulge of M31 and in Galactic globular clusters must be old.

QUESTION 1.3

The locations to which stars travel within the Galaxy are determined by their motions. For example, stars with higher speeds are more likely to be able to travel to great distances away from the Galactic centre. Hence location is also an indicator of motion.

QUESTION 1.4

As massive stars evolve, they convert hydrogen into helium, helium into carbon and oxygen, and carbon and oxygen into still heavier elements. Some of these freshly synthesized elements are ejected into the interstellar medium when stars reach the end of their lives, so the metallicity of the interstellar medium increases with time. Surviving Pop. II stars are very old and hence formed from material with a low metallicity, whereas Pop. I stars are much younger and hence formed more recently from more metal-rich gas.

QUESTION 1.5

While this view is understandable, it is flawed for the following reason. During their main sequence lifetimes, stars convert H into He, but do not produce additional heavier elements. Not until helium burning begins during the giant phase do they produce carbon and oxygen, and even then it occurs only in the core of the star, and is not observed at the surface until late in the evolution of the star.

QUESTION 1.6

(a) The circumference of a circle of radius R is $d = 2\pi R$, so the distance the Earth travels in each orbit is $d = 2 \times \pi \times 150 \times 10^6 \times 10^3\,\text{m} = 9.425 \times 10^{11}\,\text{m}$. (This should be rounded to three significant figures in the final answer.)

(b) The speed of the Earth, v_E, can be calculated from the known distance, d, around the orbit, and the time taken, $T = 365.25 \times 24 \times 60 \times 60\,\text{s} \approx 3.156 \times 10^7\,\text{s}$

i.e. $v_E = 9.425 \times 10^{11}\,\text{m}/3.156 \times 10^7\,\text{s} = 2.986 \times 10^4\,\text{m}\,\text{s}^{-1}$ (about $30\,\text{km}\,\text{s}^{-1}$)

(c) The formula of the rotation curve gives

$$M_\odot = v_E{}^2 r/G = (2.986 \times 10^4\,\text{m}\,\text{s}^{-1})^2 \times 150 \times 10^9\,\text{m}/(6.673 \times 10^{-11}\,\text{N}\,\text{m}^2\,\text{kg}^{-2})$$
$$= 2.004 \times 10^{30}\,\text{m}\,\text{s}^{-2}\,\text{N}^{-1}\,\text{kg}^2$$

Since $1\,\text{N} = 1\,\text{kg}\,\text{m}\,\text{s}^{-2}$, we can write

$$M_\odot = 2.004 \times 10^{30}\,\text{m}\,\text{s}^{-2}\,(\text{kg}\,\text{m}\,\text{s}^{-2})^{-1}\,\text{kg}^2 = 2.004 \times 10^{30}\,\text{kg}$$

(d) The distance from the Earth to the Sun was given to three significant figures, whereas all other values are known to higher precision, so the final answer is also known to three significant figures, $2.00 \times 10^{30}\,\text{kg}$.

QUESTION 1.7

(a) To use the equation $M(r) = v^2 r/G$, we need to know the speed the Sun moves, v, the radius of its orbit, r, and G the universal gravitational constant.

$$M_{\text{MW}}(8.5\,\text{kpc}) = v^2 r/G$$
$$= (220 \times 10^3\,\text{m}\,\text{s}^{-1})^2 \times 8.5 \times 10^3\,\text{pc} \times 3.09 \times 10^{16}\,\text{m}\,\text{pc}^{-1}/(6.673 \times 10^{-11}\,\text{N}\,\text{m}^2\,\text{kg}^{-2})$$
$$= 1.905 \times 10^{41}\,\text{m}^2\,\text{s}^{-2}\,\text{m}\,\text{N}^{-1}\,\text{m}^{-2}\,\text{kg}^2$$
$$= 1.905 \times 10^{41}\,\text{m}^3\,\text{s}^{-2}\,(\text{kg}\,\text{m}\,\text{s}^{-2})^{-1}\,\text{m}^{-2}\,\text{kg}^2$$
$$= 1.905 \times 10^{41}\,\text{kg}$$

This should be quoted to at most two significant figures, $1.9 \times 10^{41}\,\text{kg}$.

Since $M_\odot = 1.99 \times 10^{30}\,\text{kg}$, we can write

$$M_{\text{MW}}(8.5\,\text{kpc}) = 1.905 \times 10^{41}\,\text{kg}/1.99 \times 10^{30}\,\text{kg}\,M_\odot{}^{-1}$$
$$= 9.6 \times 10^{10} M_\odot$$

(b) As the distance of the Sun from the Galactic centre is given to two significant figures, we could quote the result to this many figures. However, you might wonder whether the result really has that much accuracy because we know the Galaxy does not perfectly meet one of the assumptions of the method – that the mass in the Galaxy is distributed in a way that is spherically symmetric. You might justifiably wonder whether only the first digit is really significant. It would be appropriate to quote the result as $M_{\text{MW}}(8.5\,\text{kpc}) = 1 \times 10^{11} M_\odot$.

QUESTION 1.8

The rotation curve is a plot of speed against distance from the centre, so the more useful form of the rotation-curve equation is $v(r) = (GM(r)/r)^{1/2}$. To sketch the rotation curve, we need to know how v varies with r.

(a) $M(r) = kr$ so $v(r) = (GM(r)/r)^{1/2}$ becomes $v(r) = (Gkr/r)^{1/2} = (Gk)^{1/2}$ = constant. That is, the speed has the same value, irrespective of the distance from the centre, and hence the rotation curve is a horizontal straight line (it is flat) (see Figure 1.38a).

(b) $M(r) = \rho \times \frac{4}{3}\pi r^3$ so $v(r) = (GM(r)/r)^{1/2}$ becomes $v(r) = (G\rho\frac{4}{3}\pi r^3/r)^{1/2} = (G\rho\frac{4}{3}\pi \times r^2)^{1/2}$ = const $\times\, r$. That is, the speed rises in proportion to the distance from the centre, and hence the rotation curve is a straight line passing through the origin (see Figure 1.38b).

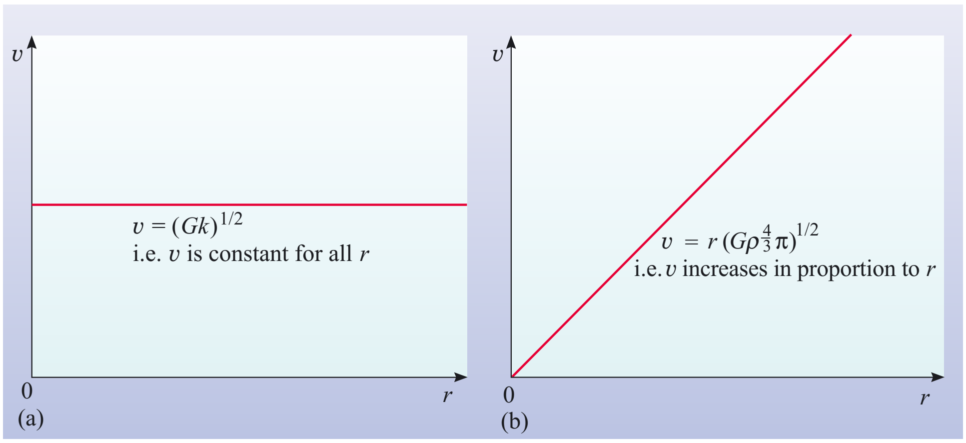

Figure 1.38 Rotation curves for (a) a mass distribution increasing linearly with radius, and (b) a uniform density sphere.

QUESTION 1.9

(a) The time, t, to complete one orbit is given by the distance travelled, d, divided by the speed, v. For a circular orbit, $d = 2\pi r$, where r is the radius of the orbit.

Hence

$$t = d/v = 2\pi r/v = 2\pi \times 4 \times 10^3\ \text{pc} \times 3.09 \times 10^{16}\ \text{m pc}^{-1}/(220 \times 10^3\ \text{m s}^{-1})$$
$$= 3.53 \times 10^{15}\ \text{s}$$

Since the conversion factor from years to seconds is $365.25 \times 24 \times 60 \times 60\ \text{s yr}^{-1} \approx 3.16 \times 10^7\ \text{s yr}^{-1}$, we can write $t = 3.53 \times 10^{15}\ \text{s}/31.6 \times 10^6\ \text{s yr}^{-1} = 1.12 \times 10^8\ \text{yr}$. Therefore, over 4.5×10^9 yr, at 4 kpc the arm would make $4.5 \times 10^9\ \text{yr}/1.12 \times 10^8\ \text{yr}$ = 40 rotations.

(b) Similarly, at 10 kpc an arm would complete one revolution in

$$t = 2\pi \times 1.0 \times 10^4\ \text{pc} \times 3.09 \times 10^{16}\ \text{m pc}^{-1}/(220 \times 10^3\ \text{m s}^{-1}) = 8.83 \times 10^{15}\ \text{s}$$

or $\quad 8.83 \times 10^{15}\ \text{s}/3.16 \times 10^7\ \text{s yr}^{-1} = 2.79 \times 10^8\ \text{yr}$

Over 4.5×10^9 yr, at 10 kpc the arm would make $4.5 \times 10^9\ \text{yr}/2.79 \times 10^8\ \text{yr} = 16$ rotations.

(c) Over this length of time, the parts at 4 kpc would have made 40 − 16 = 24 more rotations than the 10 kpc part, which means the spiral arm would be wound around the Galaxy 24 times. However, images of other galaxies, (e.g. Figure 1.4b), and even the limited maps of our own Galaxy (e.g. Figure 1.23a), suggest that this does not happen. Spiral arms can usually be traced for *at most* a few circuits of a galaxy.

QUESTION 1.10

If the co-rotation distance is at 15 kpc, then the spiral-arm speed and star speed must be the same at this distance. From Figure 1.13c, the speed here is about 235 km s^{-1}. Since the arms rotate rigidly, the speed must increase linearly with distance from the Galactic centre, so the graph of the rotation curve must resemble Figure 1.39.

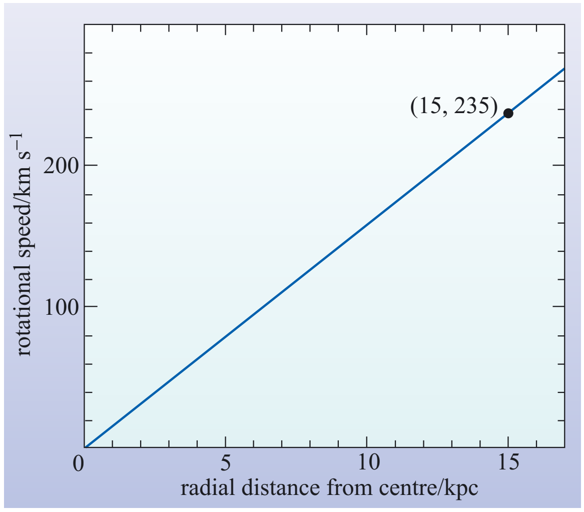

Figure 1.39 Rotation curve for a rigidly rotating spiral pattern that rotates at 235 km s^{-1} at 15 kpc from the Galactic centre. Note that although this rotation 'curve' passes through the centre of the Galaxy, the spiral arms do not extend to radial distances smaller than about 2 kpc from the centre.

The speed of the spiral pattern at 8.5 kpc is therefore (8.5/15) × 235 km s^{-1} = 133 km s^{-1}. Since the Sun is travelling at 220 km s^{-1}, it will approach the wave at 220 km s^{-1} – 133 km s^{-1} = 87 km s^{-1}.

QUESTION 1.11

(a) At the centre of a globular cluster, the number density of stars is 10^4 pc^{-3}, so each star can occupy a volume $1/(10^4\ \text{pc}^{-3})$ which equals 10^{-4} pc^3. To ensure we leave no gaps between adjacent volumes, we must consider cubic spaces rather than spherical ones. Since a cube with sides of length s has a volume s^3, we can write $s^3 = 10^{-4}$ pc^3, so $s = 10^{-4/3}$ pc = 0.046 pc. So the average separation between stars at the centre of a globular cluster is 0.05 pc (to 1 significant figure).

(b) 0.046 pc/1.3 pc ≈ 0.035, so the stellar separation at the centre of a globular clusters is typically 0.035 (i.e. about 1/28) times the distance to alpha Centauri. Clearly stars are packed together much more tightly in globular clusters than they are in the region of the Galaxy near the Sun.

QUESTION 1.12

The given equation can be rearranged to give the logarithm of the distance in terms of the other quantities:

$$\log_{10}(d/\text{pc}) = (m_V - M_V + 5)/5$$

This can be evaluated using the magnitudes provided ($m_V \approx +20.5$, $M_V \approx +0.5$)

$$\log_{10}(d/\text{pc}) = (20.5 - 0.5 + 5)/5 = 5$$

This implies (from the definition of the $\log_{10}$ function) that $d = 10^5$ pc. That is, RR Lyrae stars having $m_V \sim 20.5$ could be seen to a distance of 100 kpc, well out into the most distant parts of the stellar halo.

QUESTION 1.13

Initially, losses to stellar remnants will continue, so the total amount of ISM will decrease below the current 10% of the stellar mass, and for a time, the metallicity will continue to increase due to mass loss from stars. However, as there will be fewer new stars forming in the Galaxy in future because it will have less gas, there will be fewer high-mass stars to enrich the ISM. The ISM will then be replenished only slowly, by the evolution of long lived, low-mass stars. Ultimately the intergalactic medium will be the main means of replenishment, assuming (boldly) that this source is unlimited. Then, the metallicity of the ISM will begin to reflect that of the infalling intergalactic gas.

QUESTION 1.14

High-velocity stars are not part of the disc population (Population I), they really belong to the halo population (Population II). As members of this older population they formed from material which had not yet been enriched in heavy elements by nucleosynthesis and mass loss from stars and supernovae. Therefore they are expected to have, on average, lower metallicity than the Sun.

QUESTION 1.15

According to Figure 1.13c, a star 8.5 kpc from the Galactic centre will have a rotation speed of $220\,\mathrm{km\,s^{-1}}$. The circumference of a circular orbit of radius 8.5 kpc is $d = 2\pi r = 2\pi \times 8.5 \times 10^3\,\mathrm{pc} \times 3.09 \times 10^{16}\,\mathrm{m\,pc^{-1}} = 1.65 \times 10^{21}\,\mathrm{m}$.

Thus the time required for a star, such as the Sun, to execute such an orbit is

$$t = \frac{d}{v} = \frac{1.65 \times 10^{21}\ \mathrm{m}}{2.2 \times 10^5\ \mathrm{m\,s^{-1}}} = 7.50 \times 10^{15}\ \mathrm{s}$$

There are 3.16×10^7 s in one year. So the time required for one complete orbit by the Sun is

$$\frac{7.50 \times 10^{15}\ \mathrm{s}}{3.16 \times 10^7\ \mathrm{s\,yr^{-1}}} = 2.37 \times 10^8\ \mathrm{yr}$$

Since the Sun has existed for 4.5×10^9 yr, it follows that the number of orbits is

$$\frac{4.5 \times 10^9\ \mathrm{yr}}{2.37 \times 10^8\ \mathrm{yr}} = 19$$

Thus there will have been 19 orbits. (Of course, the two-figure 'precision' in this calculation is largely spurious, given the uncertainties that arise in such a calculation.)

QUESTION 1.16

The disc has a radius of about 15 kpc. Thus the area of the disc is $\pi(15\,\mathrm{kpc})^2$ and, since it is $\approx$1 kpc thick, its volume is $\pi(15)^2\,\mathrm{kpc}^3$. By similar reasoning, the optically observable volume of the disc is $\pi(5)^2\,\mathrm{kpc}^2 \times 1\,\mathrm{kpc} = \pi(5)^2\,\mathrm{kpc}^3$. Thus the fraction of the disc's volume that can be observed is

$$\frac{\pi(5)^2}{\pi(15)^2} = \frac{25\pi}{225\pi} = \frac{1}{9}$$

This limitation is mainly the result of dust in the plane of the Galaxy.

QUESTION 1.17

The Sun is about 4.5×10^9 years old. This is older than all but a very few of the longest-lived open clusters. Thus, even if the Sun was originally part of an open cluster, it would have long since escaped from the cluster. Possible causes of the escape are gravitational disruption (possibly through an encounter with a giant molecular cloud complex), the ‘evaporation’ of the cluster due to stars occasionally exceeding the escape speed, or simply the dispersive effect of differential rotation over a long period of time.

QUESTION 1.18

In the density wave theory, the spiral pattern moves around rigidly with an unchanging shape, and does not wind up. Matter in the Milky Way revolves differentially, with a longer orbital period for matter at a greater distance from the Galactic centre. Such matter passes into the spiral arms and then out again. Thus the matter highlighting the spiral arms at any time is not permanently present within the arms and thus the arms have no tendency to wind up.

QUESTION 1.19

Tracers of spiral arms include:

- open clusters
- OB associations
- bright HII regions
- dense molecular clouds
- clouds of neutral hydrogen
- T Tauri stars, O and B stars, supergiants and classical Cepheid stars.

QUESTION 1.20

Orange. The brightest stars in a globular cluster will be those at the highest point on the H–R diagram of a cluster of *old* stars. In the globular cluster H–R diagrams the stars in this position are cool red giants, i.e. orange in colour.

QUESTION 1.21

The evidence that the galaxy continues to evolve can be summarized by the following points:

- Star formation is still occurring;
- Enriched gas is returned to the ISM via stellar winds, planetary nebulae and supernovae;
- Infall of intergalactic gas is inferred from gas recycling and high-velocity clouds;
- Some gas from the ISM becomes locked away in the cores of stellar remnants;
- Young stars have higher metallicities than older stars;
- The Sagittarius dwarf galaxy is currently merging with the Milky Way;
- Open star clusters are disrupted by differential rotation of the Galaxy long before most of their stars die;
- Many high-velocity clouds have large velocities towards the Milky Way.

QUESTION 2.1

High-mass main sequence stars, open clusters, HII regions and an abundance of Population I stars (relative to Population II stars), are all indicators of continuing star formation. Since new stars are unlikely to be formed in the absence of cool gas (the raw material needed to make them) it is to be expected that each of these types of object will increase or become more significant in going from ellipticals (which have little cool gas) to spirals, which are actively forming stars in their discs.

QUESTION 2.2

The completed Table 2.1 is shown below.

Property	Ellipticals	Spirals	Irregulars
approximate proportion of all galaxies	$\gtrsim$60%	$\lesssim$30%	$\lesssim$15%
mass of molecular and atomic gas as % of mass of stars	small, 1% say	5–15%	15–25%
stellar populations	Population II	Populations I and II	Populations I and II
approximate mass range	$\sim 10^5 M_\odot$ to $\sim 10^{13} M_\odot$	$\sim 10^9 M_\odot$ to a few times $10^{12} M_\odot$	$\sim 10^7 M_\odot$ to $10^{10} M_\odot$
approximate luminosity range	a few times $10^5 L_\odot$ to $\sim 10^{11} L_\odot$	$\sim 10^9 L_\odot$ to a few times $10^{11} L_\odot$	$\sim 10^7 L_\odot$ to $10^{10} L_\odot$
approximate diameter range [a]	(0.01–5) d_{MW}	(0.02–1.5) d_{MW}	(0.05–0.25) d_{MW}
angular momentum per unit mass	low	high	low

[a] d_{MW}, diameter of Milky Way.

It is important to realize that many of the properties in the table are difficult to determine and that approximate figures are often poorly determined.

QUESTION 2.3

(a) The diameter of the ring $2a$ can be found using Equation 2.2

$$2a = \frac{c\Delta t}{\sqrt{\left(1 - \left(\frac{b}{a}\right)^2\right)}} \tag{2.2}$$

The time delay is 340 days, so

$$c\Delta t = (3.00 \times 10^8\ \text{m s}^{-1}) \times (340 \times 24 \times 60 \times 60\ \text{s}) = 8.81 \times 10^{15}\ \text{m}$$

The ratio (b/a) can be measured from Figure 2.21 as the ratio between the short and long axes of the ellipse (which is $(2b/2a) = (b/a)$)

(b/a) = (short axis of ellipse)/(long axis of ellipse) = (49 mm)/(69 mm) = 0.710

Substituting these values into Equation 2.2

$$2a = \frac{8.81 \times 10^{15}\ \text{m}}{\sqrt{(1-(0.710)^2)}} = \frac{8.81 \times 10^{15}\ \text{m}}{0.704} = 1.25 \times 10^{16}\ \text{m}$$

So the diameter of the ring around SN 1987A is 1.3×10^{16} m.

(b) To find the distance to a feature of length l that subtends an angle θ as viewed from the Earth, we use the relation $l = d \times (\theta/\text{radians})$ given in Section 2.4.1. Thus

$$d = \frac{l}{(\theta/\text{radians})}$$

From part (a), the diameter of the ring is 1.25×10^{16} m. The angular diameter of the ring is given as 1.66 arcsec, and this needs to be expressed in radians

$$(\theta/\text{radians}) = (\theta/\text{arcsec}) \times (1/57.3) \times (1/3600) = 8.05 \times 10^{-6}$$

It follows that the distance to SN 1987A is

$$d = \frac{1.25 \times 10^{16}\ \text{m}}{8.05 \times 10^{-6}} = 1.55 \times 10^{21}\ \text{m} = \frac{1.55 \times 10^{21}\ \text{m}}{3.09 \times 10^{16}\ \text{m pc}^{-1}} = 5.02 \times 10^{4}\ \text{pc}$$

So the distance to SN 1987A using this method is found to be 50 kpc. (This is consistent with the value of 52 ± 3 kpc that is given in the text.)

QUESTION 2.4

(a) Absorption will reduce the flux received from an object in comparison with the flux that would be measured in the absence of absorption. Thus a distance estimate that is based on applying Equation 2.3 to the flux received when there is absorption will be greater than the value obtained if there were no absorption. So if the effects of absorption are simply ignored, distances will be overestimated.

(b) If the flux is measured over a narrow range of wavelengths, the standard candle method can still be used provided that the luminosity used is that which is emitted over an identical range of wavelengths. Thus, in the visual band (V-band), we could write Equation 2.3 in the form

$$d = [L_V/(4\pi F_V)]^{1/2}$$

Where L_V and F_V are the luminosity and flux in the V-band respectively. (This assumes that radiation does not undergo any significant shift in wavelength between the source and the observer.)

QUESTION 2.5

For a Cepheid with a period of 10 days, Figure 2.25 shows that the average absolute visual magnitude M_V is –4.2.

QUESTION 2.6

The following items of information are needed.

(i) The observed flux density from each supernova at peak brightness. (In practice this would be limited to particular wavebands.)

(ii) A value for the distance, d, to each host galaxy. (In principle this might be based on observations of Cepheid variable periods, but in practice the distances used in these particular cases were based on other bright star observations.)

(iii) An estimate of the amount of radiation absorbed or scattered between the supernova and the flux detector. (Again, in practice this would be limited to a particular waveband.)

The observed flux density should be increased by the amount that was lost due to scattering and absorption, and the resulting total, F, used in conjunction with the distance, d, to find the luminosity, L, where:

$$L = 4\pi d^2 F$$

(If F had been limited to some particular band of wavelengths then L would be limited in the same way. In practice, the calibration of the Type Ia supernova method uses other information besides the three nearby examples mentioned in the question. For example, a number of Type Ia supernovae have been observed in the Virgo cluster of galaxies. Despite the uncertainties about the distance of the Virgo cluster, these observations have also been used in the calibration.)

QUESTION 2.7

The luminosity of a black-body source is given by Equation 2.4

$$L = 4\pi R^2 \sigma T^4 \qquad \text{(i)}$$

and the flux F is related to luminosity and distance d by Equation 2.3

$$d = \sqrt{\frac{L}{4\pi F}}$$

Squaring both sides gives

$$d^2 = \frac{L}{4\pi F}$$

and rearranging gives

$$F = \frac{L}{4\pi d^2} \qquad \text{(ii)}$$

So the flux from a black-body source can be found by combining Equations (i) and (ii)

$$F = \frac{4\pi R^2 \sigma T^4}{4\pi d^2} = \frac{R^2 \sigma T^4}{d^2}$$

At two different times, which are denoted by the subscript 0 and 1, respectively, this equation gives

$$F_0 = \frac{R_0^2 \sigma T_0^4}{d^2}$$

$$F_1 = \frac{R_1^2 \sigma T_1^4}{d^2}$$

Thus F_1/F_0 can be found by dividing the right-hand side of second equation by the right-hand side of the first equation. Note that the terms in d and σ cancel out.

$$\frac{F_1}{F_0} = \frac{R_1^2 T_1^4}{R_0^2 T_0^4}$$

As required, this is Equation 2.5.

QUESTION 2.8

Let quantities relating to the two galaxies be denoted by subscripts A and B. The relationship between the velocity dispersions of galaxies A and B can be expressed as

$$(\Delta v)_A = 1.2(\Delta v)_B$$

(a) The luminosities are related to the velocity dispersion according to the Faber–Jackson relation (Equation 2.10)

$$L_A \propto (\Delta v)_A^4$$

$$L_B \propto (\Delta v)_B^4$$

Hence $(L_A/L_B) = ((\Delta v)_A/(\Delta v)_B)^4 = (1.2)^4 = 2.07$

Thus the luminosity of galaxy A is 2.1 times greater than that of galaxy B.

(b) The velocity dispersion, mass M and length scale R are related according to the relation quoted in Section 2.3.2

$$(\Delta v) \propto (M/R)^{1/2}$$

Which can be rearranged to give

$$M \propto (\Delta v)^2 R$$

Thus $M_A \propto (\Delta v)_A^2 R_A$

and $M_B \propto (\Delta v)_B^2 R_B$

These relations imply that

$$(M_A/M_B) = ((\Delta v)_A/(\Delta v)_B)^2 (R_A/R_B)$$

But the radii are identical and hence the length scale R is the same for both galaxies, i.e. $R_A = R_B$,

so $(M_A/M_B) = ((\Delta v)_A/(\Delta v)_B)^2 = (1.2)^2 = 1.44$

So the mass of galaxy A is a factor of 1.4 times greater than that of galaxy B.

QUESTION 2.9

The first stage is to rearrange Equation 2.12

$$d = \frac{cz}{H_0}$$

Using the measured redshift of $z = 0.048$, the assumed value of $H_0 = 72\,\text{km}\,\text{s}^{-1}\,\text{Mpc}^{-1}$, and ensuring that c is expressed in units of $\text{km}\,\text{s}^{-1}$, the distance is

$$d = \frac{(3.00 \times 10^5\ \text{km}\,\text{s}^{-1}) \times 0.048}{72\,\text{km}\,\text{s}^{-1}\ \text{Mpc}^{-1}} = 200\,\text{Mpc}$$

So, using Hubble's law, the distance of this galaxy is 200 Mpc.

QUESTION 2.10

To express the Hubble constant in SI units, speed should be expressed in $m\,s^{-1}$ and distance in terms of m.

$$H_0 = 72\,\text{km}\,\text{s}^{-1}\,\text{Mpc}^{-1}$$

$$H_0 = 7.2 \times 10^4\,\text{m}\,\text{s}^{-1}/(10^6 \times 3.09 \times 10^{16}\,\text{m})$$

$$H_0 = 2.33 \times 10^{-18}\,\text{s}^{-1}$$

So a value of H_0 of $72\,\text{km}\,\text{s}^{-1}\,\text{Mpc}^{-1}$ is equivalent to $2.3 \times 10^{-18}\,\text{s}^{-1}$.

QUESTION 2.11

(a) The redshift due to a random motion is a Doppler shift. The equation that relates Doppler shift and radial velocity is Equation 1.7

$$\upsilon = c(\lambda_{\text{obs}} - \lambda_{\text{em}})/\lambda_{\text{em}}$$

But $\quad z = (\lambda_{\text{obs}} - \lambda_{\text{em}})/\lambda_{\text{em}}$

So, $\quad \upsilon = cz$

Rearranging

$$z = \upsilon/c$$

So if $\upsilon = 300\,\text{km}\,\text{s}^{-1}$,

$$z = (300 \times 10^3\,\text{m}\,\text{s}^{-1})/(3.00 \times 10^8\,\text{m}\,\text{s}^{-1})$$

i.e. $\quad z = 1.0 \times 10^{-3}$

The typical random velocities of galaxies will give rise to redshifts typically of the order of 0.001. Since the motions are random they are equally likely to be towards us as away from us, and so the redshifts may be negative or positive.

(b) The distance at which the redshifts due to Hubble's law will be a factor of ten greater than the redshifts caused by random motion is found using Hubble's law. From part (a) we know that random motions cause a redshift of 0.001, thus we need to find the distance at which Hubble's law predicts $z = 10 \times 0.001 = 0.01$. Using

$$d = \frac{cz}{H_0}$$

$$d = \frac{(3.00 \times 10^5\ \text{km}\,\text{s}^{-1}) \times 0.01}{72\,\text{km}\,\text{s}^{-1}\,\text{Mpc}^{-1}} = 42\,\text{Mpc}$$

So the redshifts predicted by Hubble's law will be a factor of ten greater than the redshifts due to random motion for distances greater than about 40 Mpc.

QUESTION 2.12

As the stars all grow older together, the massive blue stars would exhaust their core hydrogen first and leave the main sequence. They would then become progressively redder and soon disappear by way of a supernova. (Though this conclusion might be modified in the case of high-mass stars due to the effects of strong stellar winds.) As this process continues, stars of lower and lower mass would gradually leave the main sequence, evolve through the giant stage and eventually end their

lives as white dwarfs. The overall effect would be to reduce the luminosity of the galaxy (because of the growing predominance of lower main sequence stars) and to make it redder. (However, within this general development there are many subtleties that must be considered, mainly arising from the complicated evolution of luminosity and colour of each individual star or type of star.)

QUESTION 2.13

The flattening factor for an elliptical galaxy is $f = (a - b)/a$. For the ellipse shown in Figure 2.3, a is 24 mm and b is 13 mm, so

$$f = \frac{23\,\text{mm} - 13\,\text{mm}}{23\,\text{mm}} = 0.43$$

In assigning a Hubble type to an elliptical galaxy, the number that follows the E is the nearest integer to $10 \times f$. So in this case the appropriate Hubble type would be E4.

QUESTION 2.14

(a) NGC 7479 has wide-flung arms, and there is a bar across its centre; it is an SBc galaxy.

(b) M101 also has wide-flung arms and a relatively small bulge; it is a spiral galaxy of type Sc.

(c) NGC 4449 has no symmetry; it is an irregular galaxy (Irr).

QUESTION 2.15

The ellipsoid is the only three-dimensional shape that presents an elliptical outline to all observers, irrespective of the direction from which it is observed. Oblate and prolate spheroids (and triaxial ellipsoids) are special cases of the general ellipsoid.

QUESTION 2.16

Shortcomings of the standard candle methods include the following.

(i) The difficulty of selecting classes of objects or bodies that have a definite luminosity (i.e. standard candles).

(ii) The difficulty of determining the luminosity of those standard candles (i.e. the calibration problem).

(iii) The likelihood that the standard candles, whatever they may be, will simply be too faint to be seen at all in the more distant galaxies.

(iv) The problems associated with the absorption and/or scattering of radiation along the pathway between the source and the detector. These effects generally reduce the flux density received from the source and make it seem further away than it really is.

(v) The possibility, particularly in the case of spirals, that it may be necessary to take into account the orientation of the galaxy relative to the observer (for example, when using the Tully–Fisher method).

(It is also possible that standard candles observed at great distances (and hence at earlier times, because of the finite speed of light) may not be the same as those relatively nearby objects used for calibration due to evolutionary effects.)

QUESTION 2.17

See Figure 2.44.

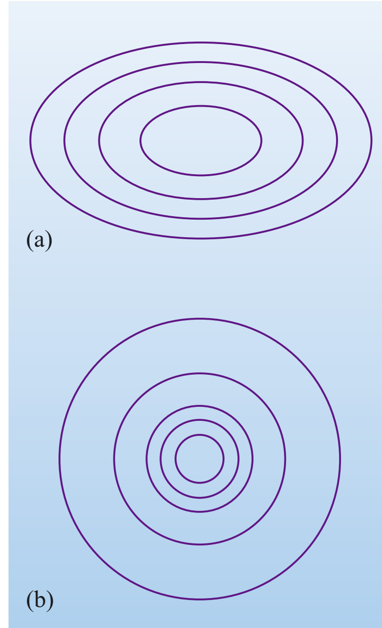

Figure 2.44 The answer to Question 2.17: (a) an E4 galaxy; (b) a face-on S0 galaxy.

QUESTION 2.18

The rotation curve method depends on the stars in a galaxy moving in near circular orbits (Box 1.3). Stars in elliptical galaxies are moving randomly, unlike the fairly orderly rotation of matter in spirals, so there is little net rotation. Consequently the rotation curve analysis cannot be applied to matter in elliptical galaxies.

QUESTION 2.19

(a) M31 is a spiral galaxy, like the Milky Way. Therefore it is to be expected that the central bulge will mainly consist of Population II stars whereas the disc will be dominated by Population I stars. Since these populations are significantly different, it makes sense to model them separately.

(b) In an E2 galaxy, where there is little or no active star formation, the stars will be mainly long-lived types of the sort common in Population II. Thus, lower main sequence stars (i) and red giants (ii) should be well represented, whereas upper main sequence stars (iii) and Cepheid variables (iv) will be rare.

QUESTION 2.20

The correct sequence is (c), (a), (b). In Figure 2.43c, all the stars have formed and the main sequence is well populated, although massive blue stars are much less common than low-mass red stars. A few million years later (Figure 2.43a) the very massive blue stars have burnt themselves out and some of the slightly less massive stars have already left the main sequences and started to become cooler, although no less luminous. Overall, by this stage there has been some reduction in luminosity and a definite change towards a yellower integrated spectrum. After billions of years (Figure 2.43b) even intermediate-mass stars have started to leave the main sequence before entering their giant phase. Overall, owing to the exhaustion of the more massive stars, there has been a further lowering of luminosity and a movement towards a redder spectrum. (Note that the chronological sequence of these H–R diagrams is similar to that shown for the three clusters of stars shown in Figure 1.29.)

QUESTION 3.1

For the Sun's photosphere we have $T = 6000\,\text{K}$ and $m = m_{\text{H}} = 1.67 \times 10^{-27}\,\text{kg}$.

So the velocity dispersion is given by

$$\Delta v \approx \left(\frac{2kT}{m}\right)^{1/2} = \left(\frac{2 \times 1.38 \times 10^{-23}\,\text{J}\,\text{K}^{-1} \times 6000\,\text{K}}{1.67 \times 10^{-27}\,\text{kg}}\right)^{1/2} = 9960\,\text{m}\,\text{s}^{-1}$$

So hydrogen atoms in the Sun's atmosphere are moving at around $10\,\text{km}\,\text{s}^{-1}$.

Rearranging Equation 3.1 we have

$$\Delta\lambda = \frac{\lambda \Delta v}{c} = \frac{656.3\,\text{nm} \times 9960\,\text{m}\,\text{s}^{-1}}{3.0 \times 10^{8}\,\text{m}\,\text{s}^{-1}} = 0.022\,\text{nm}$$

so the Doppler broadening of the solar Hα line is 0.02 nm (to 1 significant figure). (This is a tiny broadening, about 1 part in 30 000, and rather difficult to observe.)

QUESTION 3.2

The rotation curve shows that the Galaxy is rotating at between roughly 200 and 250 km s^{-1}. Edge-on, this is the approach speed at one extremity and the recession speed at the other. So the line-width that would be observed if the Galaxy were viewed edge-on is 400–500 km s^{-1}.

QUESTION 3.3

The Hβ line has a wavelength of about 485 nm and a width of roughly 6 nm. So the velocity dispersion is

$$\Delta v = \frac{c\Delta\lambda}{\lambda} = \frac{3.0 \times 10^5 \text{ km s}^{-1} \times 6 \text{ nm}}{485 \text{ nm}} \approx 3700 \text{ km s}^{-1}$$

Rearranging Equation 3.2 and putting $m = m_{\text{H}}$ we have

$$T = \frac{m_{\text{H}}(\Delta v)^2}{2k} = \frac{1.67 \times 10^{-27} \text{ kg} \times (3.7 \times 10^6 \text{ m s}^{-1})^2}{2 \times 1.38 \times 10^{-23} \text{ J K}^{-1}} = 8 \times 10^8 \text{ K}$$

In view of the difficulty of measuring the width of the line, it would be appropriate to give the temperature as approximately 10^9 K. (As is explained in the text following this question, the Hβ emitting region does *not* have such a high temperature.)

QUESTION 3.4

In the optical region (λ = 0.5 μm) galaxy A has $\lambda F_\lambda = 0.5 \times 10^{-29}$ W m^{-2}. For galaxy B, $\lambda F_\lambda = 0.5 \times 10^{-30}$ W m^{-2}. So galaxy A is 10 times brighter in the optical.

In the far-infrared (λ = 100 μm), the upper limit to λF_λ is 10^{-30} W m^{-2} whereas galaxy B has $\lambda F_\lambda = 10^{-28}$ W m^{-2}. The far-infrared flux density of galaxy B is not only greater than that of galaxy A at this wavelength, but also exceeds the flux density at optical wavelengths of both galaxies. On the basis of these (very sparse!) data, it is concluded that galaxy B is the more luminous galaxy.

QUESTION 3.5

The spectrum shows two distinct peaks, one at the red end of the optical (similar to a normal galaxy) and one far into the infrared, near 100 μm. The far-infrared peak is at a similar wavelength to the small peak in a normal spiral galaxy, but it is higher than the optical peak, suggesting that this galaxy emits most of its energy in the far-infrared. There is no significant emission in the UV or X-ray region.

This is not a normal galaxy and you might have guessed that it is an active galaxy. In fact, it is a starburst galaxy. The infrared radiation is coming from dust heated by the continuing star formation and is another distinguishing characteristic of a starburst galaxy, in addition to the strong narrow optical emission lines that you encountered earlier.

QUESTION 3.6

There are several things you may have thought of. Table 3.1 summarizes many of the characteristics and includes some pieces of new information as well. What all active galaxies have in common is a powerful, compact nucleus which appears to be the source of their energy.

Table 3.1 Features of active galaxies compared to those of normal galaxies.

Characteristic		Active galaxies			
	Normal	Seyfert	Quasar	Radio galaxy	Blazar
Narrow emission lines	weak	yes	yes	yes	no
Broad emission lines	no	some cases	yes	some cases	some cases
X-rays	weak	some cases	some cases	some cases	yes
UV excess	no	some cases	yes	some cases	yes
Far-infrared excess	no	yes	yes	yes	no
Strong radio emission	no	no	some cases	yes	some cases
Jets and lobes	no	no	some cases	yes	no
Variability	no	yes	yes	yes	yes

QUESTION 3.7

(a) An angular size limit of 0.1 arcsec corresponds to an angle in radians of

$$(\theta\,/\mathrm{rad}) = 0.1 \times (1/3600) \times (1/57.3) = 4.8 \times 10^{-7}$$

Multiplying this by the distance shows that the upper limit on the size is $= (50 \times 10^{6}\,\mathrm{pc}) \times (4.8 \times 10^{-7}\,\mathrm{rad}) = 24\,\mathrm{pc}$.

(b) A week is 7 days which is $7 \times 24 \times 60 \times 60\,\mathrm{s}$. The upper limit from the variability is

$$R \sim \Delta t c = (3.0 \times 10^{8}\,\mathrm{m\,s^{-1}}) \times (7 \times 24 \times 60 \times 60\,\mathrm{s}) = 1.8 \times 10^{14}\,\mathrm{m} = 0.006\,\mathrm{pc}$$

(Thus variability constraints provide a much lower value for the upper limit to the size of the AGN than does the optical imaging observation.)

QUESTION 3.8

The relationship between flux density F, luminosity L and distance d is given by Equation 2.3 which can be rearranged to give

$$F = \frac{L}{4\pi d^{2}}$$

Using this relationship it can be seen that if the AGN is at twice the distance but appears as bright as the normal galaxy in the optical, then it must be emitting four times the optical light of the normal galaxy like our own. If only one-fifth of the AGN's energy is emitted in the optical, then its luminosity is $4 \times 5 = 20$ times that of the normal galaxy like our own, assuming that (as usual) the normal galaxy emits mostly at optical wavelengths. The AGN luminosity is thus about $20 \times 2 \times 10^{10} L_{\odot} = 4 \times 10^{11} L_{\odot}$.

QUESTION 3.9

A mass m has a rest energy of mc^2.

(a) If 1 kg of hydrogen were to undergo nuclear fusion to produce helium, the energy liberated would be 0.007 (i.e. 0.7%) of its rest energy:

$$E = 0.007mc^2 = 0.007 \times 1\,\mathrm{kg} \times (3 \times 10^8\,\mathrm{m\,s^{-1}})^2\,\mathrm{J} = 6 \times 10^{14}\,\mathrm{J}$$

(b) If 1 kg of hydrogen were to fall into a black hole, the energy liberated would be approximately $0.1mc^2 = 0.1 \times 1 \times (3 \times 10^8\,\mathrm{m\,s^{-1}})^2\,\mathrm{J} = 9 \times 10^{15}\,\mathrm{J}$.

You would expect much *less* energy from the chemical reaction.

QUESTION 3.10

For the Seyfert nucleus, $L = 4 \times 10^{10} L_\odot = 1.6 \times 10^{37}\,\mathrm{W}$. By Equation 3.5, $Q = L/(0.1c^2)$. Substituting for L,

$$Q = \frac{1.6 \times 10^{37}}{(0.1 \times 9 \times 10^{16})}\,\mathrm{kg\,s^{-1}} \approx 2 \times 10^{21}\,\mathrm{kg\,s^{-1}}$$

This can be converted into solar masses per year, by using 1 year $\approx 3 \times 10^7$ s, and $M_\odot \approx 2 \times 10^{30}$ kg, giving

$$Q \approx \frac{(2 \times 10^{21} \times 3 \times 10^7)}{2 \times 10^{30}} M_\odot\,\mathrm{yr^{-1}} = 0.03 M_\odot\,\mathrm{yr^{-1}}$$

The Eddington limit places an upper limit on the luminosity for a black hole of given mass.

QUESTION 3.11

Wien's displacement law relates the temperature of a black body to the wavelength at which the spectral flux density has its maximum value. In this case, the dust grains on the inner edge of the torus will be at 2000 K, so their peak emission will be at

$$(\lambda_{\mathrm{max}}/\mathrm{m}) = \frac{2.9 \times 10^{-3}}{(T/\mathrm{K})} = \frac{2.9 \times 10^{-3}}{2000} \approx 1.5 \times 10^{-6}$$

So, λ_{max} is about 1.5 μm.

Grains further from the engine will be cooler, and their emission will peak at longer wavelengths, so the torus can be expected to radiate in the infrared at wavelengths of 1.5 μm or longer. (Note that although the spectrum emitted by dust grains is *not* a black-body spectrum, it is similar enough for the above argument to remain valid.)

QUESTION 3.12

From Equation 3.7 we have

$$r = \left(\frac{L}{16\pi\sigma T^4}\right)^{1/2} = \left(\frac{1 \times 10^{38}\,\mathrm{W}}{16\pi \times (5.67 \times 10^{-8}\,\mathrm{W\,m^{-2}\,K^{-4}}) \times (2000\,\mathrm{K})^4}\right)^{1/2}$$

$$\approx 1.48 \times 10^{15}\,\mathrm{m}$$

$$= \frac{1.48 \times 10^{15}\,\mathrm{m}}{3.09 \times 10^{16}\,\mathrm{Mpc^{-1}}} = 4.8 \times 10^{-2}\,\mathrm{pc}$$

Thus, according to this calculation, the radius of the inner edge of the dust torus is 1.5×10^{15} m or 0.05 pc. (A more rigorous calculation, which takes account of the efficiency of graphite grains in absorbing and emitting radiation, gives a radius of 0.2 pc.)

QUESTION 3.13

The NLR is illuminated by radiation from the central engine. As the engine is partly hidden by the dust torus, radiation can only reach the NLR through the openings along the axis of the torus. Any gas near the plane of the torus lies in its shadow and will not be illuminated. The visible NLR would take the form of a double cone of light corresponding to the conical beams of radiation emerging from either side of the torus.

The best view would be from near the plane of the torus, where a wedge-shaped glow would be visible on either side of the dark torus.

QUESTION 3.14

(a) An accreting massive black hole is a hypothesis that has been thought up to account for AGNs. There is really no *conclusive* evidence to support the hypothesis. However, no-one has a *better* idea of how to produce enough power for an AGN in the small volume.

(b) The occurrence of nuclear fusion in the Sun was originally a hypothesis proposed to explain the Sun's energy source. The whole theory of the structure and evolution of stars of different mass and different composition has been based on the nuclear fusion idea. The agreement of this theory with observations is strong confirmation that the nuclear fusion idea is correct.

(c) The laws governing the motion of the planets round the Sun account for all planetary motions ever observed and allow future motions to be predicted. This is the strongest evidence for their correctness. It could even be said that people have conducted experiments by launching spacecraft that are found to move according to these same laws.

QUESTION 3.15

For the gas motion use Equation 3.1, $\Delta\lambda/\lambda = \Delta v/c$, where Δv is the velocity dispersion. Then $\Delta\lambda/\lambda = 2.0\,\text{nm}/654.3\,\text{nm} \approx 0.0030$. Thus the overall spread of internal speeds is $\Delta v \approx 0.0030 \times c \approx 900\,\text{km s}^{-1}$, which is too large for a normal galaxy.

QUESTION 3.16

In the radio wave region, $\lambda = 10^5\,\mu\text{m}$ so

$$\lambda F_\lambda = 10^5\,\mu\text{m} \times 10^{-28}\,\text{W m}^{-2}\,\mu\text{m}^{-1} = 10^{-23}\,\text{W m}^{-2}$$

In the far infrared region $\lambda = 100\,\mu\text{m}$ so that

$$\lambda F_\lambda = 100\,\mu\text{m} \times 10^{-23}\,\text{W m}^{-2}\,\mu\text{m}^{-1} = 10^{-21}\,\text{W m}^{-2}$$

In the X-ray region, $\lambda = 10^{-4}\,\mu\text{m}$ so

$$\lambda F_\lambda = 10^{-4}\,\mu\text{m} \times 10^{-20}\,\text{W m}^{-2}\,\mu\text{m}^{-1} = 10^{-24}\,\text{W m}^{-2}$$

The largest of these λF_λ values is $10^{-21}\,\text{W m}^{-2}$, so we conclude that the far-infrared emission dominates.

QUESTION 3.17

The wavelengths λ are 0.5 μm, 5 μm and 50 μm, therefore the λF_λ values are 5×10^{-28} W m^{-2}, 5×10^{-28} W m^{-2} and 5×10^{-27} W m^{-2}, respectively. The largest of these values is 5×10^{-27} W m^{-2}, so the dominant flux is at 50 μm, which is in the far infrared. The object is likely to be either a starburst galaxy or an active galaxy.

QUESTION 3.18

If the galaxy were active, one would expect to see strong emission lines in the optical and spectral excesses at non-optical wavelengths.

QUESTION 4.1

(a) First, we must convert the angular diameter θ into radians:

$$\theta = 1.9° \times 1/57.3 = 0.0332 \text{ rad}$$

The cluster diameter ($2R$) is given by $d \times \theta$ where d is the distance to the cluster:

$$2R = d \times \theta = 120 \text{ Mpc} \times 0.0332 \text{ radians} = 3.98 \text{ Mpc}$$

So the diameter of the cluster is 4.0 Mpc (to 2 significant figures).

(This is a typical cluster with a radius equal to the Abell radius.)

(b) The cluster is now viewed from distance $d = 420$ Mpc, and we know that the diameter ($2R$) of the cluster is 3.98 Mpc

$$\theta = 2R/d$$

$$\theta = 3.98 \text{ Mpc}/420 \text{ Mpc} = 9.48 \times 10^{-3} \text{ rad} = 9.48 \times 10^{-3} \times 57.3° = 0.543°$$

So as seen from a distance of 420 Mpc, the angular diameter of the cluster would be 0.54°.

QUESTION 4.2

Using Equation 2.12:

$$z = \frac{H_0}{c} d$$

gives $$d = \frac{cz}{H_0} = \frac{3 \times 10^5 \text{ km s}^{-1} \times 0.25}{72 \text{ km s}^{-1} \text{ Mpc}^{-1}} = 1042 \text{ Mpc}$$

So the distance to is 1.0×10^3 Mpc (to 2 significant figures).

(Note that later in this chapter (Section 4.4.1) you will see that the simple linear relationship between redshift and distance (Equation 2.12) only holds for redshifts less than 0.2. Consequently the result of the answer to this question should be regarded as an *upper limit* to the distance. The deviations from Equation 2.12 for a redshift of 0.25 will be small, so it is reasonable to say that the distance to the furthest cluster in the Abell survey is *approximately* 1000 Mpc.)

QUESTION 4.3

We start by converting the Abell radius of 2 Mpc into metres

$$R_A = 2 \times 10^6 \times (3.09 \times 10^{16})\ \text{m}$$

$$R_A = 6.18 \times 10^{22}\ \text{m}$$

Using Equation 4.1,

$$M = \frac{R_A (\Delta v)^2}{G}$$

$$= \frac{6.18 \times 10^{22}\ \text{m}}{6.67 \times 10^{-11}\ \text{m}^3\ \text{kg}^{-1}\ \text{s}^{-2}} (5.5 \times 10^5\ \text{m s}^{-1})^2 = 2.80 \times 10^{44}\ \text{kg}$$

$$= \frac{2.80 \times 10^{44}\ \text{kg}}{1.99 \times 10^{30}\ \text{kg}} M_\odot = 1.41 \times 10^{14} M_\odot$$

So, using the virial mass method, the mass of the Virgo cluster is found to be $1 \times 10^{14} M_\odot$ (to 1 significant figure).

QUESTION 4.4

Equation 4.2 is an expression for the angular radius of the Einstein ring

$$\theta_E = \sqrt{\frac{4GM}{c^2} \frac{D_{LS}}{D_L D_S}} \tag{4.2}$$

This needs to be rearranged to give an expression for the mass M of the cluster. So both sides of Equation 4.2 are squared

$$\theta_E^2 = \frac{4GM}{c^2} \frac{D_{LS}}{D_L D_S}$$

and this is then rearranged to give

$$M = \frac{\theta_E^2 c^2 D_L D_S}{4GD_{LS}} \tag{i}$$

The question states that we can assume that the cluster is mid-way between Earth and the background galaxies, and so $D_{LS} = D_L$. Substituting this value for D_{LS} into Equation (i) gives

$$M = \frac{\theta_E^2 c^2 D_L D_S}{4GD_L} = \frac{\theta_E^2 c^2 D_S}{4G} \tag{ii}$$

D_S is the distance to the background *source* galaxy, which is twice as far away as Abell 2218 itself, so $D_S = 1400$ Mpc.

We must also convert the angle θ_E into radians

$$\theta_E = (1.0/60) \times (1/57.3)\ \text{rad} = 2.91 \times 10^{-4}\ \text{rad}$$

Substituting these values into Equation (ii) gives

$$M = \frac{(2.91\times10^{-4})^2 \times (3\times10^8\ \mathrm{m\,s^{-1}})^2 \times 1400 \times 3.09\times10^{22}\ \mathrm{m}}{4\times6.67\times10^{-11}\ \mathrm{N\,m^2\,kg^{-2}}}$$

$$= 1.24\times10^{45}\ \mathrm{kg}$$

$$M = \frac{1.24\times10^{45}\ \mathrm{kg}}{1.99\times10^{30}\ \mathrm{kg}} M_\odot = 6.23\times10^{14} M_\odot$$

So the mass of the cluster is $6.2 \times 10^{14} M_\odot$ (to 2 significant figures).

(As mentioned in the text, cluster masses typically lie between 10^{14} and $10^{15} M_\odot$, so this estimate is towards the upper end of the range of cluster masses. This is consistent with the fact that Abell 2218 is one of the richest clusters in the Abell catalogue.)

QUESTION 4.5

The completed table of distances and lengths is given as Table 4.4.

Table 4.4 The scales of different types of cosmic structures. (Completed version of Table 4.3.)

Feature	Distance or length/Mpc
Milky Way (diameter)	0.03
Distance to Large Magellanic Cloud	0.05
Distance to the Andromeda Galaxy	0.8
Extent of the Local Group	~2
Typical diameter of a cluster	~4
Distance to nearest rich cluster (Virgo)	20
Extent of a typical supercluster	30–50
Extent of voids	~60
Scale on which the Universe appears uniform	~200

QUESTION 4.6

Redshift is given by Equation 2.11

$$z = \frac{\lambda_{\mathrm{obs}} - \lambda_{\mathrm{em}}}{\lambda_{\mathrm{em}}}$$

The original wavelength λ_{em} of the Lyman α line is 121 nm. (Note that although the original wavelength is called λ_{em}, this is of course the wavelength of an *absorption* line due to atomic hydrogen in the intergalactic medium.)

A red-shifted wavelength of λ_{obs} = 372 nm gives

$$z = \frac{372 - 121}{121} = 2.07$$

From Figure 4.20 a redshift of 2.07 corresponds to a distance of approximately 5.4×10^3 Mpc.

QUESTION 4.7

(a) The Virgo cluster is at a distance of about 20 Mpc. One parsec equals 3.26 light-years, so light will take 3.26 × 15 million years, or about 65 million years to travel 20 Mpc. Therefore we are seeing the Virgo cluster as it was about 65 million years ago. Expressed as a fraction of the age of the Universe this is $(65 \times 10^6$ years$)/(1.3 \times 10^{10}$ years$) = 5.0 \times 10^{-3}$, or about 0.5% of the age of the Universe.

(b) The mean redshift of galaxies in the SDSS is $z = 0.1$ (Table 4.2). Taking $H_0 = 72\,\text{km s}^{-1}\,\text{Mpc}^{-1}$ then the corresponding distance is given by:

$$d = \frac{cz}{H_0} = \frac{3 \times 10^5\ \text{km s}^{-1} \times 0.1}{72\,\text{km s}^{-1}\ \text{Mpc}^{-1}} = 416\,\text{Mpc}$$

The time taken for light to travel this distance = $3.26 \times 416 \times 10^6$ years = 1.35 billion years. Thus the mean redshift of the SDSS mapping survey corresponds to light travel times of about 10% of the age of the Universe.

QUESTION 4.8

Since the absorption is due to atomic hydrogen, the structures detected would be biased towards those which contain neutral gas. However we know that the densest regions in the Universe – the cores of rich clusters – are regions where density of neutral gas is very low. This follows from the fact that spiral galaxies are rare in the cores of rich clusters and from the fact that any intracluster gas is at too high a temperature for any hydrogen to remain un-ionized. So studies of the distribution of matter based on Lyman α absoption may be biased towards revealing regions of low density.

QUESTION 4.9

The three methods for determining the total mass of a cluster of galaxies are: (i) using the velocity dispersion of galaxies within the cluster, (ii) from X-ray observations of the intracluster gas, and (iii) from the effect that the cluster has as a gravitational lens.

For the velocity dispersion method it is assumed that the cluster is relaxed or virialized. The determination of mass from X-ray measurements assumes that the intracluster gas is in a state of hydrostatic equilibrium such that the outward pressure of gas balances gravity. The method of using gravitational lensing to determine the cluster mass does not rely on making any assumptions about the physical state of the cluster.

QUESTION 5.1

In a Universe where the baryonic matter is 75% hydrogen and 25% helium (by mass), it has already been shown that there will be 12 hydrogen nuclei for each helium nucleus. Assuming that all the helium is helium-4, it follows that for the two neutrons in each helium-4 nucleus there will be 14 protons (two from the helium-4 nucleus and 12 from the 12 hydrogen nuclei).

Thus, for every 10 neutrons there will be 70 protons. In arriving at this conclusion we have assumed that all hydrogen nuclei consist of a single proton, that all helium nuclei are helium-4, that neutrons and protons have identical mass, and that the universal mix of 75% hydrogen and 25% helium (by mass) is accurate.

QUESTION 5.2

The uniformity of the CMB argues (but does not prove) that the CMB is cosmic. In the case of sunlight, for example, it is clear that there is a nearby source since part of each day is dark when the Earth is between us and the Sun. Most other sources of radiation give similar indications of their local origin by being non-uniform.

QUESTION 5.3

In Section 5.2.3 it was argued that the matter and radiation in the Universe are uniformly distributed at any time. On this basis it is to be expected that the energy and momentum associated with that matter and radiation are also uniformly distributed.

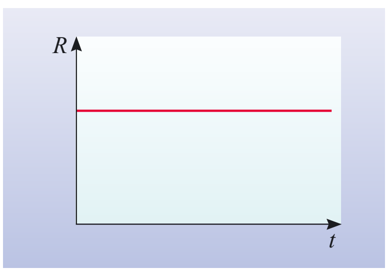

Figure 5.34 *R* against *t* graph for the scale factor of the Einstein model.

QUESTION 5.4

In the Einstein model the scale factor *R* is constant. This means that the graph of *R* against *t* will be a horizontal line, as shown in Figure 5.34.

QUESTION 5.5

(a) There are no such ranges, all the FRW models are consistent with the cosmological principle which demands homogeneity and isotropy. (Questions have been raised about the possibility that some models, such as the Eddington–Lemaître model, might evolve into an inhomogeneous state, but these are beyond the scope of this chapter.)

(b) All ranges of k and Λ allow a big bang, but $k = +1$ models with $0 < \Lambda < \Lambda_E$ allow the possibility of universes that began without a big bang. The case $k = +1$, $\Lambda = \Lambda_E$ allows the possibility that the universe might be static (hence no big bang) or that there might not have been a big bang in a non-static universe. Among the limiting cases (like the de Sitter model) that arise as the density approaches zero, there are cases in which the big bang happened an infinitely long time ago.

(c) This is possible for $k = +1$ and $0 < \Lambda \leq \Lambda_E$. (The symbol $\leq$ means 'less than or equal to'.)

(d) There are no ranges that allow the big bang to be associated with a unique point in space. Such an association would violate the cosmological principle. Take good note of this point since it is a widespread misconception to suppose that the big bang was the 'explosion' of a dense primeval 'atom' located at some particular point in space. Rather than thinking of the big bang as an event in space you should think of it as giving rise to space (or rather space–time).

(e) This is true in any model with $k = 0$.

(f) This is true in any model with $k = +1$.

(g) This is true in all models with $k = 0$ or -1. Of course, due to the finite speed of light we can have no direct observational knowledge of those parts of the Universe that are so distant that light emitted from them has not yet reached us.

QUESTION 5.6

The line is described by Hubble's law, $z = (H_0/c)d$, so the gradient of the line represents H_0/c, i.e. the Hubble constant divided by the speed of light in a vacuum. The gradient of the graph is found by dividing the vertical 'rise' Δz of the line by the corresponding horizontal 'run' Δd. In the case of Figure 5.27, this implies

$$\frac{H_0}{c} = \frac{\Delta z}{\Delta d} = \frac{0.15}{0.64 \times 10^3\ \text{Mpc}} = 2.34 \times 10^{-4}\ \text{Mpc}^{-1}$$

It follows that

$$H_0 = 3.00 \times 10^5\ \text{km s}^{-1} \times 2.34 \times 10^{-4}\ \text{Mpc}^{-1}$$

i.e. $$H_0 = 70\ \text{km s}^{-1}\ \text{Mpc}^{-1}$$

Note that this question is based on artificial data, not real measurements.

QUESTION 5.7

In the Einstein model R does not change with time, so $\dot{R} = 0$ at all times. This implies that for the Einstein model, the Hubble parameter will also be zero at all times. So, $H(t) = 0$. (Einstein produced this model before Hubble's law was discovered, so he did not appreciate the need for an expanding Universe.)

QUESTION 5.8

Figure 5.23 indicates that all the accelerating FRW models correspond to $\Lambda > 0$. So, if q_0 is indeed negative, as recent observations indicate, then we should expect that $\Lambda > 0$ if the real Universe is well described by an FRW model.

QUESTION 5.9

According to the Friedmann equation

$$(\dot{R})^2 = \frac{8\pi G R^2}{3}\left(\rho + \frac{\Lambda c^2}{8\pi G}\right) - kc^2$$

Now $H(t) = \dot{R}(t)/R(t)$, so to get H^2 on the left-hand side of the Friedmann equation, divide both sides by R^2:

$$\left(\frac{\dot{R}}{R}\right)^2 = \frac{8\pi G}{3}\left(\rho + \frac{\Lambda c^2}{8\pi G}\right) - \frac{kc^2}{R^2}$$

i.e. $$H^2 = \frac{8\pi G}{3}\left(\rho + \frac{\Lambda c^2}{8\pi G}\right) - \frac{kc^2}{R^2}$$

as required.

Multiplying both sides of this equation by $3/8\pi G$ gives

$$\frac{3H^2}{8\pi G} = \rho + \frac{\Lambda c^2}{8\pi G} - \frac{3kc^2}{8\pi G R^2}$$

i.e. $$\rho_{\text{crit}} = \rho + \rho_\Lambda - \frac{3H^2}{8\pi G}\frac{kc^2}{H^2R^2}$$

Dividing both sides by ρ_{crit} gives

$$1 = \frac{\rho}{\rho_{\text{crit}}} + \frac{\rho_\Lambda}{\rho_{\text{crit}}} - \frac{kc^2}{H^2R^2}$$

i.e. $$1 = \Omega_{\text{m}} + \Omega_\Lambda - \frac{kc^2}{H^2R^2}$$

Letting $\Omega = \Omega_{\text{m}} + \Omega_\Lambda$ gives

$$\Omega - 1 = \frac{kc^2}{H^2R^2}$$

If $\Omega_{\text{m}} + \Omega_\Lambda = 1$ then $\Omega = 1$, so $\Omega - 1 = 0$

Therefore $\dfrac{kc^2}{H^2R^2} = 0$, so $k = 0$.

QUESTION 5.10

Multiplying both sides of the given equation by $\dfrac{-R}{2\dot{R}^3}$ gives

$$\frac{-R\ddot{R}}{\dot{R}^2} = \frac{8\pi G}{3}\frac{R^2}{\dot{R}^2}\left(\frac{\rho}{2} - \rho_\Lambda\right)$$

But $\dfrac{R^2}{\dot{R}^2} = \dfrac{1}{H^2}$ and $\dfrac{-R\ddot{R}}{\dot{R}^2} = q$

So, $$q = \frac{8\pi G}{3H^2}\left(\frac{\rho}{2} - \rho_\Lambda\right)$$

Now, $$\frac{8\pi G}{3H^2} = \frac{1}{\rho_{\text{crit}}}$$

So, $$q = \frac{1}{2}\frac{\rho}{\rho_{\text{crit}}} - \frac{\rho_\Lambda}{\rho_{\text{crit}}}$$

i.e. $$q = \frac{\Omega_{\text{m}}}{2} - \Omega_\Lambda$$

Substituting the currently favoured values $\Omega_{\mathrm{m},0} = 0.3$ and $\Omega_{\Lambda,0} = 0.7$ gives

$$q_0 = 0.15 - 0.7$$

i.e. $$q_0 = -0.55$$

QUESTION 5.11

1916	Einstein's theory of general relativity published. This included the field equations in their original form.
1917	Einstein modified the field equations to include the cosmological constant and published the first (static) cosmological model. The de Sitter model was also published within a year.
1919	Eddington led the eclipse expedition that confirmed the general relativistic prediction that starlight passing close to the edge of the edge of the Sun would be bent.
1922 and 1924	Friedmann published papers on the behaviour of the scale factor in homogeneous and isotropic relativistic cosmologies.
1925	Lemaître introduced the model (later championed by Eddington) that allowed cosmic expansion to follow an indefinitely long period of effectively static behaviour.
1929	Robertson improved and generalized Friedmann's work.
1931	Lemaître formulated his theory of the primeval atom, a crude precursor of the modern big bang theory.
1936	Walker published his independent work on the improvement and generalization of Friedmann's investigations.
1965	Cosmic microwave background radiation discovered.

QUESTION 5.12

The assumptions underpinning the FRW models are that:

- space and time behave in accordance with general relativity; and
- energy and momentum are distributed homogeneously and isotropically on the large scale. (This is the cosmological principle.)

An additional assumption underpinning the Friedmann equation is that:

- the Universe is uniformly filled with a gas of density ρ (that may depend on time).

There are of course other unstated assumptions behind these, such as the belief that space and time are three-dimensional and one-dimensional respectively.

QUESTION 5.13

Since the question concerns FRW models, which are homogeneous and isotropic, it follows that the curvature must be uniform (i.e. the same everywhere and in all directions) at any given time. In a three-dimensional space of (uniform) positive curvature, space will have a finite total volume, straight lines will close back upon themselves, pairs of nearby parallel lines will converge and may meet, any plane triangle will have interior angles that sum to more than 180°, and the circumference of any circle will be less than 2π times its radius.

QUESTION 5.14

In making the step from Equation 5.17 to Equation 5.18 it is stated that

$$\Delta R(t) = \Delta t \times \dot{R}(t)$$

This would be exactly true if the rate of change of R was constant, and it *is* approximately true because we have limited the discussion to cases where Δt is small. However it is not *exactly* true if $\dot{R}$ is changing, i.e. if there is acceleration or deceleration.

QUESTION 5.15

$$H_0 = (72 \pm 8)\,\mathrm{km\,s^{-1}\,Mpc^{-1}}$$

and $$H_0 = (2.3 \pm 0.3) \times 10^{-18}\,\mathrm{s^{-1}}$$

$$\Omega_{\mathrm{m},0} \approx 0.3$$

$$\Omega_{\Lambda,0} \approx 0.7$$

$q_0 \approx -0.55$ (see answer to Question 5.10)

The age of the Universe t_0 is quoted as slightly less than 14×10^9 years.

To show that the two values of H_0 are equivalent, note that

$$1\,\mathrm{Mpc} = 3.09 \times 10^{22}\,\mathrm{m} = 3.09 \times 10^{19}\,\mathrm{km}$$

Dividing both sides by 1 Mpc shows that

$$1 = 3.09 \times 10^{19}\,\mathrm{km\,Mpc^{-1}}$$

The units make the right-hand side of this equation a complicated way of writing 1. Dividing the first quoted value of H_0 by this conversion factor gives

$$H_0 = \frac{(72 \pm 8)\,\mathrm{km\,s^{-1}\,Mpc^{-1}}}{3.09 \times 10^{19}\,\mathrm{km\,Mpc^{-1}}} = (2.3 \pm 0.3) \times 10^{-18}\,\mathrm{s^{-1}}$$

QUESTION 6.1

The approach to drawing sketches of how the temperature T varies with time t for all Friedmann–Robertson–Walker models with $k = 0$ shown in Figure 5.23, is similar to that adopted in Example 6.1. We shall look at each model in turn.

$k = 0, \Lambda < 0$ model

The curve showing $R(t)$ is shown in Figure 6.24a. The behaviour of the scale factor R at times A, B and C, and the inferred behaviour of the temperature T at these times is summarized in Table 6.5. The sketch of $T(t)$ is shown in Figure 6.24b.

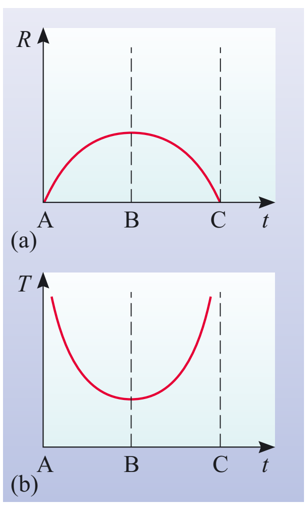

Figure 6.24 (a) Scale factor, and (b) temperature as functions of time for a Friedmann–Robertson–Walker model with $k = 0, \Lambda < 0$. A, B and C are times that are referred to in Table 6.5.

Table 6.5 The behaviour of the scale factor R at various times indicated on Figure 6.24a and the inferred behaviour of the temperature T at those times.

Time	Behaviour of R at this time	Behaviour of T at this time
A	$R = 0$	$T = 1/R = \infty$
B	R has increased to a maximum value and now does not vary much with time	T must decrease to some minimum value and also only change slowly with time
C	$R = 0$	$T = 1/R = \infty$

k = 0, Λ = 0 model (the Einstein–de Sitter model)

The curve showing $R(t)$ is shown in Figure 6.25a. The behaviour of the scale factor R at times A, B and C, and the inferred behaviour of the temperature T at these times is summarized in Table 6.6. The sketch of $T(t)$ is shown in Figure 6.25b.

Table 6.6 The behaviour of the scale factor R at various times indicated on Figure 6.25a and the inferred behaviour of the temperature T at those times.

Time	Behaviour of R at this time	Behaviour of T at this time
A	$R = 0$	$T = 1/R = \infty$
B	R is increasing rapidly	T must decrease rapidly
C	R is increasing slowly	T must decrease slowly

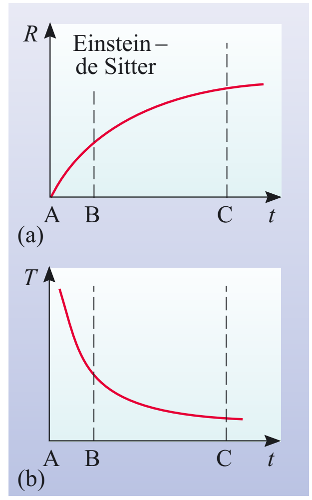

Figure 6.25 (a) Scale factor, and (b) temperature as functions of time for a Friedmann–Robertson–Walker model with $k = 0$, $\Lambda = 0$ (the Einstein–de Sitter model).

k = 0, $\Lambda = \Lambda_E$ model

The curve showing $R(t)$ is shown in Figure 6.26a. The behaviour the scale factor R at times A, B, C and D and the inferred behaviour of the temperature T at these times is summarized in Table 6.7. The sketch of $T(t)$ is shown in Figure 6.26b.

Table 6.7 The behaviour of the scale factor R at various times indicated on Figure 6.26a and the inferred behaviour of the temperature T at those times.

Time	Behaviour of R at this time	Behaviour of T at this time
A	$R = 0$	$T = 1/R = \infty$
B	R is increasing rapidly	T must decrease rapidly
C	R is increasing slowly	T must decrease slowly
D	R is increasing to very high values	T must decrease to very small values

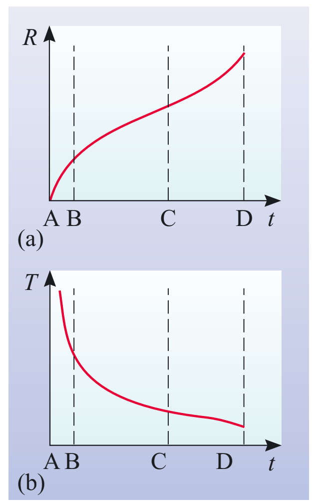

Figure 6.26 (a) Scale factor, and (b) temperature as functions of time for a Friedmann–Robertson–Walker model with $k = 0$, $\Lambda = \Lambda_E$.

QUESTION 6.2

The question states that the current average mass density of luminous and dark matter, $\rho_m \approx 3 \times 10^{-27}\,\mathrm{kg\,m^{-3}}$.

The definition of mass density is that if a volume V contains a mass m, then $\rho_m = m/V$.

The energy density u is defined in an analogous way; if a volume of space V contains an energy E, then $u = E/V$.

To find the energy density due to matter u_m we need to calculate the energy equivalent of the mass m that is contained within the volume V. To do this we use the mass-energy equivalence relation $E = mc^2$,

$$u = E/V = mc^2/V = (m/V)c^2$$

but $(m/V) = \rho_m$, so

$$u = \rho_m c^2$$

Using the value of ρ_m given in the question,

$$u = 3 \times 10^{-27}\,\mathrm{kg\,m^{-3}} \times (3.00 \times 10^8\,\mathrm{m\,s^{-1}})^2$$

i.e. $$u = 2.7 \times 10^{-10}\,\mathrm{J\,m^{-3}}$$

Thus the average energy density due to matter is currently $3 \times 10^{-10}\,\mathrm{J\,m^{-3}}$ (to 1 significant figure).

QUESTION 6.3

The temperature T at time t is given by Equation 6.19

$$(T/\mathrm{K}) \approx 1.5 \times 10^{10}(t/\mathrm{s})^{-1/2}$$

This can be rearranged to give

$$(t/\mathrm{s})^{1/2} \approx 1.5 \times 10^{10}/(T/\mathrm{K})$$

Squaring both sides gives

$$(t/\mathrm{s}) \approx (1.5 \times 10^{10}/(T/\mathrm{K}))^2 \qquad \text{(i)}$$

When $T = 10^6\,\mathrm{K}$,

$$(t/\mathrm{s}) \approx (1.5 \times 10^{10}/(10^6\,\mathrm{K/K}))^2 = (1.5 \times 10^4)^2 = 2.25 \times 10^8$$

$$t = 2.25 \times 10^8\,\mathrm{s} = 2.25 \times 10^8\,\mathrm{s}/(365 \times 24 \times 60 \times 60\,\mathrm{s\,yr^{-1}}) = 7.13\,\mathrm{yr}$$

So when the temperature was $10^6\,\mathrm{K}$, the age of the Universe was 7 years (to 1 significant figure).

QUESTION 6.4

It is stated in the text that grand unification occurs at an interaction energy of about $10^{15}\,\mathrm{GeV}$. Thus the strong and electroweak interaction became distinct when interaction energies dropped below this value. The corresponding temperature can be found using Equation 6.20, which can be rearranged to give

$$T \sim E/k$$

An interaction energy of $10^{15}\,\mathrm{GeV}$ therefore corresponds to a temperature of

$$T \sim (10^{15} \times 10^9\,\mathrm{eV} \times 1.60 \times 10^{-19}\,\mathrm{J\,(eV)^{-1}}/(1.38 \times 10^{-23}\,\mathrm{J\,K^{-1}})$$

$$T \sim 1.16 \times 10^{28}\,\mathrm{K}$$

So, grand unification occurs when the temperature exceeds $10^{28}\,\mathrm{K}$.

In order to calculate the time at which the temperature was $10^{28}\,\mathrm{K}$, we can use Equation (i) from the answer to Question 6.3,

$$(t/\mathrm{s}) \sim (1.5 \times 10^{10}/(10^{28}\,\mathrm{K/K}))^2 = 2.25 \times 10^{-36}$$

So, expressing this to the nearest power of ten, the time at which grand unification occurred was $t \sim 10^{-36}\,\mathrm{s}$.

QUESTION 6.5

(a) (i) Before the decay, the only particle is a single neutron. This has a baryon number of +1. (ii) The baryon numbers of the products of the decay are +1 (proton), 0 (electron) and 0 (electron antineutrino). The baryon number before and after the decay is thus +1 and so baryon number is conserved.

(b) (i) The single neutron has a lepton number of 0. (ii) The lepton numbers of the products are 0 (proton), +1 (electron) and −1 (electron antineutrino). The lepton number before and after the decay is thus 0 and so lepton number is conserved.

(c) (i) A neutron comprises one up and two down quarks (u d d). (ii) A proton comprises two up and one down quark (u u d). The β^--decay reaction thus involves a down quark being transformed into an up quark. Hence β^--decay can be expressed in terms of quarks and leptons as

$$\mathrm{d} \to \mathrm{u} + \mathrm{e}^- + \overline{\nu}_\mathrm{e}$$

QUESTION 6.6

Electron–positron pair production requires an amount of energy given by

$$E = 2m_\mathrm{e}c^2$$

(note that the mass of the positron is equal to the mass of the electron m_e). The value of $m_\mathrm{e}c^2$ is given in Table 6.3 as being 0.511 MeV, thus

$$E = 2 \times 0.511\,\mathrm{MeV} = 1.02\,\mathrm{MeV} = 1.02 \times 10^6\,\mathrm{eV}$$

So the interaction energy required for electron–positron pair production is 1.02×10^6 eV.

The temperature can be found interaction using Equation 6.20

$$E \sim kT$$

Which can be rearranged as

$$T \sim E/k = (1.02 \times 10^6\,\mathrm{eV} \times 1.60 \times 10^{-19}\,\mathrm{J})/(1.38 \times 10^{-23}\,\mathrm{J\,K^{-1}}) = 1.18 \times 10^{10}\,\mathrm{K}$$

So the temperature for electron–positron pair production is about 1×10^{10} K. (This is called the *threshold temperature* for electron–positron pairs.)

QUESTION 6.7

The temperature T at time t is given by Equation (i) of the answer to Question 6.3.

(a) When $T = 10^9$ K, then

$$(t/\mathrm{s}) \approx (1.5 \times 10^{10}/(10^9\,\mathrm{K/K}))^2 = 15^2 = 225$$

So the temperature was 10^9 K when $t = 2 \times 10^2$ s (to 1 significant figure).

(b) When $T = 5 \times 10^8$ K, then

$$(t/\mathrm{s}) \approx (1.5 \times 10^{10}/(5 \times 10^8\,\mathrm{K/K}))^2 = 30^2 = 900$$

So the temperature was 5×10^8 K when $t = 9 \times 10^2$ s (to 1 significant figure).

QUESTION 6.8

At around $t \approx 1$ s the ratio $n_\mathrm{n}/n_\mathrm{p}$ had a value of 0.22. After this time, the dominant reaction affecting free neutrons was β^--decay. If we consider a region of the Universe that contained 100 neutrons at $t \approx 1$ s, then the number of protons in this region would have been $N_\mathrm{p} = 100/0.22 = 455$. After this time, the neutrons decayed according to the curve shown in Figure 6.12. The time at which deuterium was first formed was $t = 225$ s. From Figure 6.12 it can be seen that a fraction of 0.78 of the sample of neutrons would remain at this time. Thus the sample would have contained

78 neutrons ($N_n = 78$). However, due to β^--decay, the number of protons would have *increased* by $(100 - 78) = 22$, so the total number of protons (N_p) in the sample would have been $455 + 22 = 477$. So

$$N_n/N_p = 78/477 = 0.164$$

The ratio N_n/N_p is the same as the ratio of number densities of neutrons and protons n_n/n_p. So at the time that deuterium started to form, $n_n/n_p = 0.16$ (to 2 significant figures).

QUESTION 6.9

The mass fraction in helium (Y) is given by Equation 6.33b. The value of n_n/n_p that was obtained in Question 6.8 is 0.16, so

$$Y = 2\left(\frac{1}{1+(n_p/n_n)}\right) = 2\left(\frac{1}{1+(1/0.16)}\right) = 0.276$$

So the mass fraction in helium is 0.28 (to 2 significant figures).

QUESTION 6.10

The metallicity Z of a sample of material is defined as the mass of the sample that is in metals divided by the total mass of the sample. Since lithium is the only metal (i.e. element with mass number greater than 4) produced in the big bang, the metallicity will be

$$Z = (\text{mass of lithium})/(\text{mass of sample})$$

The mass of the sample can be found from the definition of the hydrogen mass fraction

$$X = (\text{mass of hydrogen})/(\text{mass of sample})$$

$$(\text{mass of sample}) = (\text{mass of hydrogen})/X$$

So the metallicity can be expressed as

$$Z = X \times (\text{mass of lithium})/(\text{mass of hydrogen})$$

This is a useful expression because Figure 6.13 gives the abundance of lithium as the ratio of the mass of lithium to the mass of hydrogen within a sample.

Using the approximation that $X \sim 0.75$,

$$Z = 0.75 \times (\text{mass of lithium})/(\text{mass of hydrogen})$$

For the purposes of this order of magnitude calculation it is reasonable to equate the metallicity to the relative abundance of lithium shown in Figure 6.13. Since the maximum value of the lithium abundance is about 10^{-8}, the maximum metallicity of material formed in the big bang would be of order of magnitude $Z \sim 10^{-8}$.

The oldest observed stars have measured values of $Z \sim 10^{-6}$ (Chapter 1). Thus the metallicity of material formed in the big bang is expected to be at least a factor of 10^2 smaller than the metallicities observed even in the least chemically enriched stars. So the oldest stars cannot be formed from material that has not been subject to some enrichment after the era of primordial nucleosynthesis.

QUESTION 6.11

In all three cases, A, B and C, the value of $\Omega_{b,0}$ can be found by identifying the locations on the curves in Figure 6.13 that correspond to the given abundances. The values of $\Omega_{b,0}$ are shown in Table 6.8.

In cases A and B the lithium abundances correspond to three different values of $\Omega_{b,0}$. In case C, the lithium abundance corresponds to a range of values of $\Omega_{b,0}$. Thus, in all cases, the lithium abundances on their own do *not* allow $\Omega_{b,0}$ to be determined uniquely.

Table 6.8 The values of $\Omega_{b,0}$ determined from the abundances in Question 6.11.

Case	$\Omega_{b,0}$
A	0.006
B	0.07
C	0.02

QUESTION 6.12

The energy required for the ionization of hydrogen is 13.6 eV. Because the number of photons exceeds the number of protons by a factor of 10^9, by analogy with the case of the photodisintegration of deuterium, recombination will only occur once the mean photon energy is a factor of 9.6 lower than the ionization energy (see Section 6.4.1).

So the mean photon energy

$$\begin{aligned}\varepsilon_{\text{mean}} &= (13.6\,\text{eV})/9.6 = 1.42\,\text{eV} = 1.42\,\text{eV} \times 1.60 \times 10^{-19}\,\text{J}\,\text{eV}^{-1} \\ &= 2.27 \times 10^{-19}\,\text{J}\end{aligned}$$

However, $\varepsilon_{\text{mean}}$ is related to the absolute temperature T by Equation 6.27

$$\varepsilon_{\text{mean}} = 2.7kT$$

Thus $$T = \frac{\varepsilon_{\text{mean}}}{2.7k} = \frac{2.27 \times 10^{-19}\,\text{J}}{2.7 \times 1.38 \times 10^{-23}\,\text{J}\,\text{K}^{-1}} = 6092\,\text{K}$$

So recombination occurred at a temperature of 6.1×10^3 K.

(This is, in fact, something of an overestimate. The ionization of hydrogen may occur, not only by an atom in the ground state absorbing a photon with energy greater than 13.6 eV, but also by an atom absorbing a photon such that it is in an excited state, and then absorbing another photon. The effect of this is to lower the temperature at which recombination starts to occur – to about 4500 K.)

QUESTION 6.13

The relationship between temperature and scale factor is given by Equation 6.6,

$$T \propto \frac{1}{R(t)}$$

Thus the relationship between the temperature of the background radiation at the present time T_0 and that at the time of last scattering T_{last} is

$$\frac{T_{\text{last}}}{T_0} = \frac{R(t_0)}{R(t_{\text{last}})}$$

where t_{last} is the time at which the last scattering of photons occurred.

The relationship between redshift and scale factor is given by Equation 5.13. In this case, the time at which the photon is observed is t_0 and the time at which the photon was emitted is t_{last}, so Equation 5.13 can be written as

$$z = \frac{R(t_0)}{R(t_{\text{last}})} - 1$$

So $$z = \frac{T_{\text{last}}}{T_0} - 1 \qquad \text{(ii)}$$

The question states that $T_{\text{last}} = 3.0 \times 10^3$ K, and $T_0 = 2.7$ K, so

$$z = \frac{3.0 \times 10^3 \text{ K}}{2.7 \text{ K}} - 1 = 1110$$

So the redshift at which the last scattering of cosmic background photons occurred is 1.1×10^3 (to 2 significant figures).

QUESTION 6.14

A 'time-line' for the history of the Universe is shown in Figure 6.27.

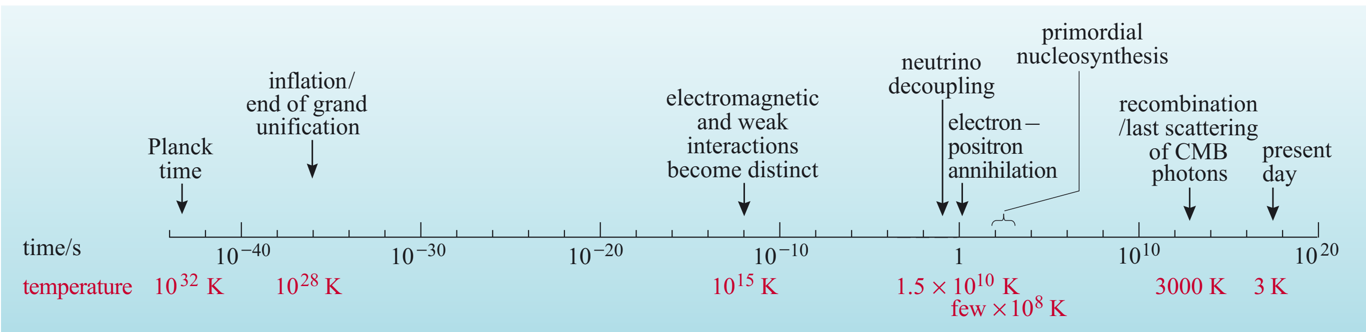

Figure 6.27 The major events in the evolution of the Universe from the Planck time ($t \sim 10^{-43}$ s) to the present day.

QUESTION 6.15

A 'theory of everything' is a theory that accounts for all four of the fundamental interactions of nature in a unified manner. In particular, such a theory would provide a consistent way to describe processes that are currently described by two separate and mutually incompatible theories: the standard model of elementary particles and general relativity (which describes gravitational interactions). Such a theory is needed to describe processes in the very early Universe; before the Planck time (10^{-43} s) the strength of all four fundamental interactions would have been similar, and gravity would have played a role in particle interactions.

QUESTION 6.16

The relationship between scale factor and temperature is given by Equation 6.6, which shows that temperature is inversely proportional to scale factor. Thus a dramatic *increase* in scale factor would cause a dramatic *fall* in temperature. An increase in the scale factor by, for example, a factor of 10^{50}, would cause the temperature to fall by the same factor. Even if the temperature prior to inflation was about 10^{28} K, it would plummet to 10^{28} K/10^{50} = 10^{-32} K at the end of inflation. So the temperature at the end of inflation would be expected to be extremely low.

(This might seem at odds with the whole idea of a hot big bang model. How could the Universe that is a tiny fraction of a degree above absolute zero at the end of inflation have proceeded to cause, for example, primordial nucleosynthesis? It turns out that the energy that is released at the end of inflation re-heats the Universe, and it does so as if the cooling due to inflation had never occurred!)

QUESTION 6.17

If the photodisintegration of deuterium required photons of a much higher energy than 2.23 MeV, then, in comparison to the real Universe, a significant amount of deuterium would have been formed at earlier times when the temperature was higher. Thus deuterium would have formed at an earlier time, when the ratio of neutron to proton number densities (n_n/n_p) would have been higher. Most of the neutrons that are present at the time that deuterium production starts, end up in helium nuclei. A higher value of (n_n/n_p) at the start of deuterium production would therefore result in a higher value of the helium mass fraction.

QUESTION 6.18

Following the same reasoning as is used to arrive at Equation (ii) in the answer to Question 6.13, the redshift z is related to the temperature T_{em} of the background radiation at that redshift by

$$z = \frac{T_{em}}{T_0} - 1$$

This can be rearranged to give

$$T_{em} = T_0(z + 1)$$

Inserting the given values leads to

$$T_{em} = (2.73\,\text{K}) \times (2.5 + 1) = 9.56\,\text{K}$$

So, their measurement of the temperature of the cosmic microwave background would be 9.6 K (to 2 significant figures).

(Although we don't have any communication with astronomers anywhere else in the Universe, a similar principle applies to a real observational technique: it is possible to measure the temperature of the cosmic background radiation as experienced by Lyα clouds at redshifts of $z \sim 2$. Such measurements, which are based on detailed analysis of spectral lines, show that the temperature of the cosmic background does increase with redshift in this way.)

QUESTION 7.1

(a) Systematic. This uncertainty would influence the modelling of the lensing galaxy and hence the calculation of the time-of-passage lag, but it would influence repeated measurements in the same way, and would therefore be a systematic effect rather than a random one.

(b) Systematic. Repeated measurements will be affected in the same way each time they are performed.

(c) Random. Performing similar observations several times will lead to different results due to this source of uncertainty.

QUESTION 7.2

Using Hubble's law $d = cz/H_0$, with $z = 1$ and $H_0 = 72\,\mathrm{km\,s^{-1}\,Mpc^{-1}}$ (the HST value), gives

$$d = (3.0 \times 10^5\,\mathrm{km\,s^{-1}})/(72\,\mathrm{km\,s^{-1}\,Mpc^{-1}})$$

i.e. $$d = 4.2 \times 10^3\,\mathrm{Mpc}$$

The simple form of Hubble's law used above should not be trusted as a reliable indicator of distances at such large redshift, since it ignores the effect of any acceleration or deceleration in the rate of cosmic expansion. For instance, from the more accurate Equation 7.4, it can be seen that if $q_0 = 0$, then d would increase to 150% of the quoted value. In either case, this would be very much larger than the diameter of the local supercluster, which was described in Chapter 4 as being 20 to 50 Mpc across.

QUESTION 7.3

In the supernova cosmology measurements the emphasis was on determining the magnitude of distant Type Ia supernovae relative to nearer ones. For this purpose it is only necessary to measure the apparent magnitudes of the supernovae rather than the absolute magnitudes. To measure the Hubble constant we would also need to know the absolute magnitudes, in order to determine the distances.

QUESTION 7.4

From Figure 7.11, the lowest point on the 99% confidence contour corresponds to $\Omega_{\Lambda,0} = 0.1$, while the highest point on that contour corresponds to $\Omega_{\Lambda,0} = 2.5$. In contrast, the points at which the 99% contour crosses the 'flat geometry' line correspond to $\Omega_{\Lambda,0} = 0.6$ and $\Omega_{\Lambda,0} = 0.9$.

QUESTION 7.5

The claim that 'baryons only account for somewhere between about a fifteenth and a sixth of the total density of matter in the Universe' was based on Equation 7.13, according to which

$$0.02 \leq \Omega_{\mathrm{b},0} \leq 0.05$$

The widely favoured value for $\Omega_{\mathrm{m},0}$, based on supernova cosmology and measurements of the cosmic microwave background radiation is

$$\Omega_{\mathrm{m},0} \approx 0.3$$

This suggests that

$$0.067 \leq \frac{\Omega_{\mathrm{b},0}}{\Omega_{\mathrm{m},0}} \leq 0.167$$

i.e. between a fifteenth and a sixth.

QUESTION 7.6

The dipole anisotropy is a large-scale non-uniformity in the CMB, as observed from Earth. It causes the direction of maximum intensity (or effective temperature) to be diametrically opposite the direction of minimum intensity (or temperature), with the intensity increasing progressively from the minimum to the maximum. The dipole anisotropy is caused by the motion of the Earth relative to the frame of reference in which the CMB shows large-scale isotropy. (In other words the dipole anisotropy is a result of the Doppler effect.)

The existence of the dipole anisotropy is implicitly acknowledged in Point 1 by saying that the radiation (CMB) is 'intrinsically' uniform to better than one part in 10 000. It is more explicitly recognized in the next sentence by the inclusion of the phrase 'after correcting for effects due to the motion of the detector'.

In Point 2, the word 'intrinsic' is again used to indicate 'after correcting for effects due to the motion of the detector'.

Point 5 also includes the word 'intrinsic' with the same implication.

QUESTION 7.7

The predictions are based on the general principles of big bang cosmology and specific assumptions about the values of the cosmological parameters. Since the predictions don't relate to specific features such as the exact region of sky being observed, or the detailed history of that region, the predictions cannot be expected to show anything more than 'general' agreement even when the appropriate values for the cosmological parameters have been chosen.

QUESTION 7.8

From Figure 7.24, the second and third peaks are located at $l \approx 500$ and $l \approx 800$, respectively.

From Equation 7.16, these values correspond to angular scales $\theta = 0.36°$ and $\theta = 0.23°$, respectively.

The maximum angular power associated with these peaks is roughly $2500\,(\mu\text{K})^2$ in each case.

QUESTION 7.9

(a) The CMB anisotropy measurements indicate that $\Omega_{\Lambda,0} + \Omega_{\text{m},0} = 1.02 \pm 0.02$.

However, Type Ia supernovae, mass-to-light ratios and CMB measurements all indicate that $\Omega_{\text{m},0}$ is much less than 1, probably about 0.3. This implies that $\Omega_{\Lambda,0} \approx 0.7$. Thus the energy associated with the cosmological constant (dark energy) dominates the density of the Universe. The nature of this energy is not well understood at the time of writing.

(b) Among other results discussed in earlier chapters, the growth of mass-to-light ratios with the scale of observations indicates that most of the matter in the Universe is dark matter.

(c) Although observations indicate that $\Omega_{\text{m},0} \approx 0.3$, estimates of $\Omega_{\text{b},0}$ based on primordial nucleosynthesis constraints, baryon inventories and CMB measurements, indicate that $\Omega_{\text{b},0} \approx 0.04$. Hence most of the (dark) matter must be non-baryonic.

QUESTION 7.10

Even from the incomplete account given in this chapter it is clear that space technology has profoundly influenced observational cosmology. This is clear from:

- the role of the HST in facilitating the determination of the Hubble constant from Cepheid variable observations;
- the use of the HST to study some of the faintest (and therefore most distant) Type Ia supernova candidates used in the determination of the current value of the deceleration parameter;
- the role of space-based X-ray observations in the determination of cluster masses that are an essential ingredient in measurements of the mass-to-light ratio on large scales;
- the additional role of X-ray and other space-based observations in compiling a baryon inventory;
- the importance of COBE in confirming the black-body nature of the CMB spectrum, determining the mean temperature of the radiation and revealing the existence of anisotropies in that temperature; and
- the role of WMAP and the expected role of the Planck mission in measuring the CMB angular power spectrum with great precision so that the key cosmological parameters can be precisely determined.

QUESTION 7.11

Terrestrial observations, including those performed from planes and balloons, are still of enormous importance in cosmology, despite the many advances that can be attributed to space technology. Examples of important ground-based or air-based experiments include:

- observations of gravitational lensing using optical and radio telescopes (although important results have also come from the HST);
- studies of supernovae carried out by large telescopes at sites such as Mount Palomar and, more recently, Cerro Tololo and Hawaii (Keck);
- observations of various kinds used in establishing mass-to-light ratios, baryon inventories and the relative abundances of light elements that are needed to check primordial nucleosynthesis predictions;
- a range of CMB observations including the initial breakthrough by Penzias and Wilson, the discovery of the dipole anisotropy and the anisotropy measurements carried out by BOOMERanG and various other projects; and
- the large-scale galaxy surveys that are helping to refine our knowledge of the galaxy power spectrum.

QUESTION 8.1

Some examples of known objects that could make up the dark matter are:

Brown dwarfs – stellar bodies whose masses are too low for hydrogen burning to have commenced in their cores.

Stellar remnants – cooled white dwarfs, neutron stars, black holes

Minor bodies – planets, asteroids, comets

Note that all of these candidates contain baryonic matter. Strictly speaking, black holes should not be counted as being a form of baryonic matter, but we shall treat them as such on the basis that they were probably formed from baryonic matter.

QUESTION 8.2

The answer is given in Table 8.2.

Table 8.2 The completed Table 8.1 (Question 8.2).

Dark matter candidate	Baryonic	Non-baryonic	MACHO	WIMP	Cold[a]	Hot[a]
brown dwarfs	✓		✓			
neutrinos		✓		✓		✓
neutron stars	✓		✓			
black holes	✓		✓			
neutralinos		✓		✓	✓	

[a] Note that the terms hot and cold only apply to WIMPs, since they refer to the speed of particles at the time of decoupling and not to temperature in the conventional sense.

QUESTION 8.3

(a) An antihydrogen atom (made from an antiproton and a positron) would have the same energy levels as normal hydrogen and would absorb and emit photons in the same way. The photons themselves would be identical to photons produced in our own Galaxy. The same applies to all other atoms. So the spectrum of an antigalaxy would look much the same as an ordinary galaxy.

(b) If the galaxy really is an antigalaxy, then somewhere between the galaxy and our own Milky Way there must be a boundary between matter and antimatter. We would expect annihilations to be taking place at the boundary, perhaps in the intergalactic medium, and the boundary could revealed by a search for γ-rays. In fact, the absence of such γ-radiation is strong evidence that there are no significant amounts of antimatter in our part of the Universe.

QUESTION 8.4

You didn't really expect to find an answer to this one, did you?

QUESTION 8.5

The end-of-chapter summary provides an overview of the current status of the cosmological problems that were outlined at the beginning of the chapter.

APPENDIX

Useful quantities

Quantity	Symbol	Value[a]
Physical constants		
speed of light in a vacuum	c	$3.00 \times 10^{8}\,\mathrm{m\,s^{-1}}$
Planck constant	h	$6.63 \times 10^{-34}\,\mathrm{J\,s}$
Boltzmann constant	k	$1.38 \times 10^{-23}\,\mathrm{J\,K^{-1}}$
gravitational constant	G	$6.67 \times 10^{-11}\,\mathrm{N\,m^{2}\,kg^{-2}}$
Stefan–Boltzmann constant	σ	$5.67 \times 10^{-8}\,\mathrm{W\,m^{-2}\,K^{-4}}$
charge of electron	$-e$	$-1.60 \times 10^{-19}\,\mathrm{C}$
mass of hydrogen atom	m_{H}	$1.67 \times 10^{-27}\,\mathrm{kg}$
mass of electron	m_{e}	$9.11 \times 10^{-31}\,\mathrm{kg}$
Astronomical data		
mass of the Earth	M_{E}	$5.98 \times 10^{24}\,\mathrm{kg}$
radius (equatorial) of the Earth	R_{E}	$6.38 \times 10^{6}\,\mathrm{m}$
mass of the Sun	$M_{\odot}$	$1.99 \times 10^{30}\,\mathrm{kg}$
radius of the Sun	$R_{\odot}$	$6.96 \times 10^{8}\,\mathrm{m}$
luminosity of the Sun	$L_{\odot}$	$3.84 \times 10^{26}\,\mathrm{W}$
Hubble constant[b]	H_0	$72 \pm 8\,\mathrm{km\,s^{-1}\,Mpc^{-1}}$

[a]Values are given to 3 significant figures. Many of these are known more accurately.

[b]Freedman, W. L. *et al*. *Astrophysical Journal*, **533**, 47–72, (2001).

Units

Quantity	SI Unit	Other units	In SI	Alternative SI units
length	metre, m	Astronomical unit, AU	$1.50 \times 10^{11}\,\mathrm{m}$	
		parsec, pc	$3.09 \times 10^{16}\,\mathrm{m}$	
time	second, s	year, yr	$3.16 \times 10^{7}\,\mathrm{s}$	
frequency	hertz, Hz			$\mathrm{s^{-1}}$
force	newton, N			$\mathrm{kg\,m\,s^{-2}}$
pressure	pascal, Pa			$\mathrm{kg\,m^{-1}\,s^{-2}}$, $\mathrm{N\,m^{-2}}$
temperature	kelvin, K	°C	(kelvin − 273)	
energy	joule, J	electronvolt, eV	$1.60 \times 10^{-19}\,\mathrm{J}$	$\mathrm{kg\,m^{2}\,s^{-2}}$
power	watt, W			$\mathrm{kg\,m^{2}\,s^{-3}}$, $\mathrm{J\,s^{-1}}$
angle	radian, rad	degree, °	1/57.3 rad	
		1° = 60 arcmin = 3600 arcsec		
		arcsec, ″	1/206265 rad	

GLOSSARY

21 centimetre radiation Electromagnetic radiation with a wavelength of 21 cm, in the radio part of the spectrum, which is emitted or absorbed by a hydrogen atom when it undergoes a spin–flip transition. The spin–flip transition of a hydrogen atom may be described in term of classical (i.e. non-quantum) physics by saying that the proton and electron which comprise the atom change from having their spins aligned parallel with one another to being antiparallel (180° out of alignment), or vice versa.

Abell radius The typical radius of a cluster of galaxies. It is now known to be about 2 Mpc.

absolute visual magnitude An intrinsic property of a star, equal to the apparent visual magnitude the star would have if observed from a standard distance of 10 parsecs, in the absence of interstellar absorption. The absolute visual magnitude provides a measure of the star's luminosity.

accelerating model A cosmological model, belonging to the class of Friedmann–Robertson–Walker models, in which the rate of change of the scale factor is itself changing at a positive rate (i.e. $\ddot{R} > 0$). Although any FRW model with a sufficiently large cosmological constant Λ may exhibit accelerated expansion at late times in its development, the term 'accelerating model' is often used to refer specifically to the model with positive cosmological constant ($\Lambda > 0$) and zero curvature parameter ($k = 0$).

accretion disc A disc of gas and dust which forms around a massive object such as the accreting star in an interacting binary system, or around the massive black hole in the engine of an AGN. Material spirals inwards within the disc and falls onto the central object from the inner edge of the disc.

acoustic peaks A set of peaks, the largest of which is called the Doppler peak, seen in the angular power spectrum of the cosmic background radiation for multipole numbers in the range from about $l = 50$ to $l = 1000$ (i.e. on angular scales between about 0.1 degrees and a few degrees). The phenomenon is partly due to the localized heating of the last-scattering surface caused by the acoustic waves in the photon–baryon fluid that is present there, and partly due to the effect that the moving charged particles, associated with those waves, have on the wavelengths of scattered photons.

acoustic waves Waves in a fluid arising from the tendency of localized concentrations of pressure or density to return to some preferred equilibrium value by increasing the pressure or density in neighbouring regions. Acoustic waves are also known as sound waves.

active galactic nucleus (AGN) The bright, point-like object at the centre of an active galaxy. AGNs typically have high luminosities and often exhibit rapid variability.

active galaxy A galaxy that typically exhibits an unusually high and varying luminosity, and which may additionally show signs of energetic processes connected with its central regions. The term embraces: Seyfert galaxies, quasars, radio galaxies and blazars.

age–metallicity relation The tendency for older stars to have lower metallicities.

AGN *See* active galactic nucleus.

angular power The quantity, usually denoted as $l(l+1)C_l/2\pi$ and measured in units of $(\mu K)^2$, that is plotted on the vertical axis of an angular power spectrum, and which measures the amount of variation present in the corresponding (anisotropy) map on the angular scale $\theta = 180°/l$.

angular power spectrum A mathematical entity, often presented as a plot of angular power against multipole number, that is used to describe the statistically important data contained in a two-dimensional map of temperature anisotropies in the cosmic microwave background.

anisotropies (in the cosmic microwave background) Variations in the intensity of the cosmic microwave background radiation over the celestial sphere.

annihilation The interaction between a particle and its corresponding antiparticle in which both the particle and antiparticle are destroyed and energy is released. This is the opposite process to pair-creation.

anthropic principle An assertion that the existence of intelligent life in the Universe is of cosmological significance. In its weak form, the anthropic principle states that conditions in the Universe are those which allowed the emergence of intelligent life. In its strong form, the principle states that the Universe necessarily had conditions that led to the emergence of intelligent life.

antibaryon An elementary particle that comprises three antiquarks. An example of an antibaryon is the antiproton.

apparent surface brightness The quantity that describes the apparent brightness at any point on an extended object, such as a galaxy. The apparent surface brightness at any chosen point is the amount of radiant flux that would reach 1 m^2 at Earth from a small, uniformly bright, square region, of angular area 1 $(arcsec)^2$, surrounding the chosen point. An acceptable SI unit of apparent surface brightness is the $W\,m^{-2}\,arcsec^{-2}$.

apparent visual magnitude A quantity that describes the apparent brightness of a body. For a star, it is a measure of the flux density received in the V band, i.e. a band that approximates the response of human vision versus wavelength.

atomic hydrogen Hydrogen in the electrically neutral state in which it contains a single proton bound to a single electron. This form may be distinguished from other common forms of hydrogen such as molecular hydrogen and ionized hydrogen.

band-shifting The effect whereby electromagnetic radiation from a highly red-shifted object will be observed in a different wavelength band to that in which it was emitted.

bar instability The process by which a system of stars orbiting their common centre of gravity in a flattened (disc-like) configuration, tends to develop an elongated (bar-shaped) rather than circular distribution.

barred galaxy Any spiral, lenticular or irregular galaxy with a central bar-like feature.

barred spiral galaxy Any spiral galaxy whose central stars form an elongated (bar shaped) distribution, with the long axis lying in the plane of the disc.

baryon An elementary particle that comprises three quarks. Protons and neutrons are examples of particles that are baryons.

baryon number A quantity that is conserved in all particle interactions (with the exception of some speculative interactions predicted by grand unified theories). The baryon number of any baryon is +1 and that of any antibaryon is −1 respectively (or equivalently, the baryon number of any quark is +1/3, whereas that of any antiquark is −1/3). The baryon number of any other particle is zero.

baryonic dark matter Dark matter consisting of baryons that do not produce any detectable radiation. It is generally believed that most dark matter is non-baryonic.

big bang The early part of the expansion of the Universe, as described by those Friedmann–Robertson–Walker models that start with the scale factor R equal to zero at time $t = 0$ and with the rate of change of the scale factor being positive ($\dot{R} > 0$).

big crunch The late part of the contraction of the Universe, as described by those Friedmann–Robertson–Walker models that end with the scale factor R equal to zero and with the rate of change of the scale factor being negative ($\dot{R} < 0$).

BL Lac object (BL Lacertae object) A subclass of blazar. In contrast to optically violent variables, the spectra of BL Lac objects show no emission lines.

black hole A region of space from which, according to general relativity, signals (including particles of matter and electromagnetic radiation) are unable to escape due to the action of gravity. Such regions are bounded by an event horizon, and may be created by the catastrophic collapse of massive stars.

black-body spectrum The spectrum of an ideal thermal source of radiation (i.e. a black body). This is a continuous spectrum with a characteristic ‘humped’ shape, the peak wavelength depending on the temperature of the source, in accord with Wien’s displacement law. A characteristic of sources that produce spectra that are close to the black-body form is that there is a degree of interaction between electromagnetic radiation and the material that makes up the source. (This leads to the formal definition of a black-body source as one that has the property of absorbing perfectly any electromagnetic radiation that is incident on it and emits a black-body spectrum.)

blazar A kind of active galaxy, characterized by a point-like appearance, a relatively featureless optical spectrum, and rapid variability across the electromagnetic spectrum. Blazars may be subclassified as BL Lac objects or optically violent variables.

borehole survey A survey of galaxies in which a wide range of redshifts is measured over a narrow range of directions (angles). Such surveys extend out to very great distances and are generally described as ‘deep’ surveys.

bottom-up scenario *See* hierarchical scenario.

broadband spectrum A spectrum covering a wide range of wavelengths or frequencies, which indicates the energy distribution of a source. It does not generally show narrow features such as absorption lines.

broad-line region (BLR) The body of gas responsible for emitting the broad emission lines in an AGN. The typical width of broad emission lines corresponds to radial velocity variations of about $5000\,\mathrm{km\,s^{-1}}$.

bulge The region around the centre of a spiral galaxy, where the galaxy is thicker and brighter and the concentration of matter is greater than elsewhere. Its outer parts are dominated by the light of old stars, but towards the centre it contains material associated with the inner parts of the disc including sites of star formation.

Butcher–Oemler effect The observation that young galaxies (i.e. those observed at very large distances) tend to have more blue stars than older galaxies (i.e. those nearby). This provides evidence for the evolution of stellar populations.

calibration problem The difficulty of establishing the relationship between various methods for measuring relative distances and of deducing absolute distances from relative distances, arising largely from difficulties in determining the luminosity of standard candles.

Casimir effect The effect whereby two parallel, uncharged, metal plates will experience a mutual attraction, of electromagnetic origin, when narrowly separated in a vacuum. The effect arises because the plates modify the physical properties of the intervening vacuum. In particular, the pressure of the vacuum between the metal plates is lower than the pressure of the surrounding vacuum, giving rise to the forces that act on the plates.

cD galaxy Any supergiant elliptical galaxy with a large diffuse envelope.

Cepheid variable method The use of a (classical) Cepheid as a standard candle for the purposes of distance determination. The method is based on the fact that for classical Cepheids the absolute magnitude is proportional to the period of brightness variation.

chaotic inflation A hypothesis which assumes that the entire Universe is partitioned into domains, and that the laws of physics may differ from one domain to another. In the chaotic inflation scenario, the physical laws that lead to inflation occur by chance in some of these domains. Such a scenario avoids the need to explain why conditions in a single Universe were ‘just right’ to produce inflation.

chimneys Regions of hot, low-density gas in the disc of the galaxy where supernova explosions have heated the local interstellar medium and caused it to break out from the disc. Such structures are believed to provide channels whereby gas from the disc can flow into the tenuous halo.

classical Cepheids A type of giant/supergiant star which pulsates regularly with a period in the range from about a day to about 100 days. The changes in radius, temperature, and hence luminosity, arise from instabilities in the envelopes of such evolved giant or supergiant stars. Classical Cepheids, which are Population I stars, can be distinguished from another category of stars with similar but nevertheless distinct properties, the Population II Cepheids.

closed model A cosmological model, belonging to the class of Friedmann–Robertson–Walker models, that starts with a big bang and ends with a big crunch. The closed model is characterized by zero cosmological constant ($\Lambda = 0$) and a positive curvature parameter ($k = +1$). In such a model the cosmic density is always greater than the critical density.

cluster (of galaxies) A concentration of galaxies in a region of space, of order 4 Mpc across.

cold dark matter (CDM) Dark matter that is comprised of particles whose speeds are low in comparison to the speed of light.

collisional excitation The process in which an ion, atom or molecule is raised to a higher energy state as a result of its collision with another particle.

colour index The quantity that describes the colour of a star, obtained by subtracting its apparent magnitude in one wavelength band (e.g. its apparent visual magnitude) from its apparent visual magnitude in a different band (e.g. in blue light). In this example, the colour index would be denoted $B - V$. The colour index of a star depends primarily on its temperature.

co-moving A term used to indicate a state of expansion or contraction matched to that of the Universe as a whole. The term is typically applied to ‘co-moving coordinates’ which allow points moving with the Hubble flow to be described by fixed coordinate values despite their increasing physical separation.

co-moving volume Any volume of space whose boundary is fixed in co-moving coordinates.

confidence level A numerical quantity, usually expressed as a percentage, describing the likelihood that the true value of a measured quantity lies within some specified range of values.

Copernican principle The principle that the Earth does not occupy a privileged position in the Universe.

co-rotation radius The distance, measured from the centre of a spiral galaxy, at which the orbital speed of the stars about the galaxy and the pattern speed of the spiral arms is the same.

cosmic background radiation The electromagnetic radiation that pervades the Universe. At the present time, the peak of the spectral energy distribution of the cosmic background radiation occurs at microwave wavelengths and is observed as the cosmic microwave background.

cosmic microwave background (CMB) The contribution to the observed astronomical 'background radiation' that has no identifiable stellar or galactic source and which occupies the wavelength range from about 0.1 mm to 0.1 m. The cosmic microwave background is of great importance in modern cosmology and is often represented by the abbreviation CMB. In terms of total energy content, the CMB represents the dominant form of radiation in the Universe. It is characterized by a black-body spectrum corresponding to a temperature of (2.725 ± 0.002) K, and has a highly isotropic distribution with intrinsic temperature anisotropies of no more than a few parts in 10^5.

cosmic recycling The cycling of gas through various forms in the Galaxy, from the interstellar medium into stars and then back into the interstellar medium (towards the end of the star's life). In this process the metallicity of the gas is increased by the production of heavier elements in stars.

cosmic shear The effect whereby distant galaxies appear to be distorted and displaced due to the gravitational deflection of the light from those galaxies as it encounters non-uniformities in the large-scale distribution of matter. An analysis of the consequences of cosmic shear provides a way of mapping the distribution of matter in the Universe.

cosmic variance A source of uncertainty in the determination of the angular power spectrum of the cosmic microwave background, arising from the fact that the temperature anisotropies on which the determination is based are being measured from just one location in the Universe (i.e. the spectrum of a cosmic phenomenon is being estimated on the basis of a single sample of data).

cosmological constant A constant, usually denoted Λ, that appears in the Einstein field equations of general relativity, and through them plays a role in many relativistic cosmological models. A positive cosmological constant causes an effective repulsion between distantly separated points in space, and may result in an eventual acceleration in the rate of cosmic expansion. *See also* dark energy.

cosmological model A mathematical model of the Universe as a whole, usually involving equations and parameters. Typically, a cosmological model describes the large-scale geometry of space and time, the contents of space and time, and the evolution of the parameters that describe the geometry and contents of space and time. *See also* Friedmann–Roberston–Walker models.

cosmological principle The principle (essentially an assumption based on increasingly good observational evidence) that on sufficiently large size scales, the Universe is homogeneous and isotropic. In this context, the phrase 'sufficiently large size scales' is usually taken to mean a few hundred megaparsecs or more.

cosmological redshift The contribution to the redshift (i.e. the fractional increase in wavelength $z = (\lambda_{obs} - \lambda_{em})/\lambda_{em}$) of radiation emitted from a distant source which arises from the large-scale expansion of the Universe. Note that the observed redshift of a distant galaxy is usually the sum of a cosmological redshift and another contribution arising from the peculiar motion of the galaxy relative to the large-scale expansion.

cosmology The branch of science concerned with the Universe as a whole, including its origin, structure, composition, evolution and eventual fate.

counts-in-cells (method) A method of characterizing the non uniformities in a distribution (such as the distribution of galaxies on the sky) based on the relative variation in density of the distribution when it is divided into cells of a given size, and the way that relative variation in density changes as the cell size is altered.

critical density The value of the cosmic density, $\rho_{crit}(t) = 3[H(t)]^2/(8\pi G)$, that would cause a Friedmann–Robertson–Walker model with Hubble parameter $H(t)$ at time t and zero cosmological constant ($\Lambda = 0$) to be a critical model. The critical density provides a useful reference value in discussions of the cosmic density and is used in defining the density parameter for matter and the density parameter for the cosmological constant. (In a FRW model where $H(t_0) = 72\,\mathrm{km\,s^{-1}\,Mpc^{-1}}$ at some time t_0, the critical density at that time is $\rho_{crit}(t_0) \approx 1 \times 10^{-26}\,\mathrm{kg\,m^{-3}}$.)

critical model A cosmological model, belonging to the class of Friedmann–Robertson–Walker models, that starts with a big bang and expands continuously but in such a way that the rate of change of the scale factor approaches zero as the time t approaches infinity. The critical model is characterized by zero cosmological constant ($\Lambda = 0$) and zero curvature parameter ($k = 0$). In such a model the cosmic density is always equal to the critical density. The critical model is also referred to as the Einstein–de Sitter model.

curvature A geometric property of space, or of space–time, that may be used to describe departures from 'flat' geometry.

curvature parameter A parameter (i.e. a quantity that may vary from case to case, but which takes a constant value in any given case) that appears in the Robertson–Walker metric, and which helps to characterize the curvature of space or space–time, and which may take the value +1, 0, or −1.

damped Lyman α system A relatively dense cloud of un-ionized gas that is detectable from the very strong Lyman α absorption that it causes in the spectrum of a background quasar. It is speculated that such clouds may be galaxies that are in the process of forming.

dark energy The energy, whatever its nature, that may be associated with an effective cosmological constant Λ via the relation $\rho_\Lambda = \Lambda c^2/(8\pi G)$, where $\rho_\Lambda c^2$ represents the (uniform) energy density of the dark energy.

dark matter Matter that can be detected through its gravitational attraction, but which appears neither to emit nor absorb electromagnetic radiation, and hence gives few clues as to its nature. Some fraction of the dark matter is made up of baryons (baryonic dark matter), but most is believed to be composed of something else (non-baryonic dark matter).

dark-matter halo An approximately spherical volume surrounding the luminous parts of a galaxy where a large quantity of dark matter resides. The luminous parts of galaxies probably occupy the highest density part of the dark-matter halo and are held in place by the gravity of the dark matter.

de Sitter model A cosmological model describing a universe in which there is a negligible amount of matter and the cosmological constant Λ is positive. In the de Sitter model, space is infinite and in a state of perpetual expansion, as described by the scale factor $R \propto e^{Ht}$, where $H = (\Lambda c^2/3)^{1/2}$. The de Sitter model is a limiting case of the Friedmann–Robertson–Walker model with $k = 0$ and $\Lambda > 0$.

deceleration parameter The time-dependent quantity $q(t) = R\ddot{R}/[\dot{R}]^2$ that arises in any Friedmann–Robertson–Walker model in which the scale factor at time t is $R(t)$, its rate of change at the time t is $\dot{R}(t)$ and the rate of change of $\dot{R}(t)$ at that time is $\ddot{R}(t)$. To the extent that such a model describes the real Universe, the current value of the deceleration parameter $q(t_0)$ should equal the quantity q_0 that quantifies departures from Hubble's law in the formula $H_0 d = cz[1 + (1 - q_0)z/2]$.

deep survey An astronomical survey that is performed with sufficient sensitivity to detect very faint sources. Typically, deep surveys require long observation times and are consequently restricted to small areas of the sky.

dense cloud One of the coldest and densest kinds of cloud to be found in the interstellar medium, usually rich in molecules. Dense clouds give birth to stars, mainly in the form of open clusters.

density fluctuations Variations in the average density, on a given size scale, within a density distribution, such as that of matter in the early Universe.

density parameter for matter The time-dependent quantity $\Omega_{\rm m}(t) = \rho(t)/\rho_{\rm crit}(t)$ that arises in any Friedmann–Robertson–Walker model where the density of matter at time t is $\rho(t)$ and the critical density at that time is $\rho_{\rm crit}(t) = 3[H(t)]^2/(8\pi G)$.

density parameter for the cosmological constant The time-dependent quantity $\Omega_\Lambda(t) = \rho_\Lambda/\rho_{\rm crit}(t)$, that arises in any Friedmann–Robertson–Walker model where $\rho_\Lambda = \Lambda c^2/(8\pi G)$ is the 'density' associated with the cosmological constant Λ and $\rho_{\rm crit}(t) = 3\,[H(t)]^2/(8\pi G)$ is the critical density at time t. Note that $\rho_\Lambda c^2$ is sometimes referred to as the density of dark energy and that $\Omega_\Lambda(t)$ may accordingly be referred to as the density parameter for dark energy.

density wave theory An explanation of the formation and maintenance of the density enhancements thought to be responsible for spiral arms. The density wave sweeps around the galaxy, compressing the material it traverses and triggering star formation.

deuteron A nucleus of deuterium. It comprises one proton and one neutron.

differential rotation A pattern of rotation in which the rotation period of one part of the rotating system may differ from that of another. In the case of the Milky Way, for example, the rotation period of different parts of the disc varies with their distance from the centre. *See* rotation curve.

dipole anisotropy The large-scale variation in the intensity of the cosmic microwave background due to the Earth's motion with respect to the Hubble flow.

disc A major structural component of spiral galaxies, containing most of the visible matter of the galaxy in a highly flattened distribution.

distance ladder A synthesis of techniques for measuring astronomical distances. The distance ladder is based on using one method of distance determination to calibrate another method that is appropriate to measurements of larger distances – which can then be used to calibrate a method that is used over yet larger distances and so on.

Doppler broadening The effect whereby the width of a spectral line is increased as a result of movements within the region where the line originates. *See* Doppler effect; Doppler shift.

Doppler effect The effect whereby the observed frequency of waves received from a source depends on the motion of the source relative to the observer. There is a corresponding change in the observed wavelength.

Doppler shift The difference, arising from the relative motion of an observer and a source of radiation, between the observed wavelength (or frequency) of the radiation and the wavelength (or frequency) of that radiation at its point of emission.

dust Small solid particles, around 10^{-7} or 10^{-6} m across, found mixed with interstellar gas. Dust grains are predominantly composed of graphite and silicates, but may be surrounded by an icy mantle. Dust is very effective at absorbing and scattering ultraviolet and visible light.

dwarf elliptical Any small, intrinsically faint, elliptical galaxy, typically of type E0 and with a mass of about $10^6 M_\odot$.

Eddington limit The limiting luminosity of an accreting body such as an accreting massive black hole which is set by the outward radiation pressure on infalling material. This limit is proportional to the mass of the accreting body.

Eddington–Lemaître model A cosmological model belonging to the class of Friedmann–Robertson–Walker models, in which the rate of change of the scale factor is positive at any positive time t (i.e. $\dot{R} > 0$ for all $t > 0$) implying perpetual expansion, but in which $\dot{R}$ approaches zero as t approaches zero indicating a long period of quasi-static behaviour (similar to the behaviour of the Einstein model) before the expansion really takes hold. The Eddington–Lemaître model is characterized by a positive cosmological constant ($\Lambda = 4\pi G\rho/c^2$) and a positive curvature parameter ($k = +1$).

Einstein–de Sitter model An alternative name for the critical model.

Einstein field equations The key equations of general relativity that relate the geometric properties of space–time (such as curvature) to the distribution of energy and momentum. In applying general relativity to problems in cosmology, Einstein argued for the inclusion of a term involving the cosmological constant, Λ, that was absent from his original formulation of the field equations. The significance of this modification has remained controversial since its introduction.

Einstein model A cosmological model describing a static universe in which space is finite but unbounded and 'straight' lines close back upon themselves. The Einstein model was the first relativistic cosmological model and is now regarded as a special case in the family of Friedmann–Robertson–Walker models characterized by a uniform distribution of matter with density ρ, a positive cosmological constant $\Lambda_E = 4\pi G\rho/c^2$ and a curvature parameter $k = +1$.

Einstein ring The circular image produced when a point source of light lies directly behind a symmetrical gravitational lens.

ekpyrotic model A speculative model for the early Universe which does not invoke the process of inflation. In the ekpyrotic model, our Universe corresponds to a sheet or 'brane' that moves through a higher dimensional space (the 'bulk'). The collision of the brane on which our Universe resides, with the brane of another 'Universe' may give rise to the effects that are commonly attributed to inflation.

ellipsoid A three-dimensional shape whose cross-section is always elliptical. It has three principal axes.

elliptical (galaxy) Any member of the Hubble class of galaxies characterized by an overall elliptical shape and central concentration of brightness. Membership of this class is indicated by the letter E, followed by a number that denotes the flattening factor of the galaxy.

energy A property of systems (such as arrangements of particles of matter or distributions of radiation) that measures their ability to do work. According to general relativity, the distribution of energy throughout a region of space–time is one of the factors that plays a role in determining the curvature of that region of space–time. The SI unit of energy is the joule (J).

engine The power source within an AGN. It is generally believed, but not proven, that the engine is an accreting massive black hole.

epoch of reionization The stage in the evolution of the Universe at which the neutral gas that had been present since the time of recombination first became ionized, possibly due to the intensity of ultraviolet radiation from newly formed stars or AGN. It is believed that reionization occurred when the age of the Universe was less than 10% of its current value.

evaporation The process by which there is a gradual loss of stars from an open cluster due to their acquiring sufficient kinetic energy to escape. The energy to escape is provided by gravitational forces exerted by other stars.

event horizon The bounding surface of a black hole, at which the escape speed is equal to the speed of light in a vacuum. According to general relativity, the event horizon encloses a region of space from which signals (including particles of matter and electromagnetic radiation) cannot escape.

exponential function A mathematical function of the form $y = y_0 e^{ax}$, where $e \approx 2.718$, a is a parameter which may be positive or negative, and y_0 is the value of y when $x = 0$. Many natural processes can be described quantitatively by the exponential function.

Faber–Jackson relation A relationship between the luminosity and the velocity dispersion of elliptical galaxies.

field galaxy Any galaxy that is not a member of a cluster of galaxies.

finite A property of certain cosmological models (or more specifically of certain space–times) implying that the total volume of space is of limited extent.

flux density (F) A quantity describing the rate at which energy transferred by radiation is received from a source, per unit area facing the source. The SI unit of flux density is the watt per square metre ($\mathrm{W\,m^{-2}}$).

forbidden line A spectral line that can only be produced in a very low density gas. Forbidden lines cannot normally be produced in the laboratory.

frequency The rate at which wavelengths of a wave pass a fixed point (i.e. the number per second passing the fixed point). The SI unit of frequency is the hertz (Hz), where $1\,\mathrm{Hz} = 1\,\mathrm{s^{-1}}$.

Friedmann equation An equation, arising in the context of the Friedmann–Robertson–Walker models, that relates the value of the scale factor $R(t)$ and its rate of change $\dot{R}(t)$ to the curvature parameter k, the cosmic density ρ and the cosmological constant Λ. Given the value of the parameters k, ρ and Λ, the process of 'solving' the Friedmann equation leads to an expression for R as a function of the time t that may be presented as a graph of R against t. Such an expression (or graph) substantially determines the evolution of the cosmological model.

Friedmann–Robertson–Walker models A class of cosmological models based on general relativity and the assumption that the Universe is homogeneous and isotropic (i.e. the cosmological principle). The geometric properties of space–time in these models are described by the Robertson–Walker metric which includes a curvature parameter k, and a scale factor $R(t)$ that satisfies the Friedmann equation.

FRW models A common abbreviation of Friedmann–Robertson–Walker models.

Galactic coordinates A coordinate system on the sky, whose two elements are Galactic longitude l, and Galactic latitude b, resembling longitude and latitude on the Earth. The orientation of the coordinate system is defined to make it useful for describing the locations of objects in the Galaxy from the viewpoint of the Sun. The Galactic equator is chosen to coincide more-or-less with the Galactic plane, the direction $(l, b) = (0°, 0°)$ is roughly in the direction of the Galactic centre, $(l, b) = (90°, 0°)$ is roughly in the direction of motion of the Sun around the Galactic centre, and $b = 90°$ is the direction in the sky perpendicular to the disc, that lies above the northern hemisphere of the Earth.

Galactic disc A major structural component of the Galaxy, containing most of the visible matter, which lies in a highly flattened distribution. The Sun is located in the disc.

Galactic equator The directions in the sky, close to the Galactic plane, whose Galactic latitude is $b = 0°$. *See* Galactic coordinates.

Galactic fountain A flow of hot gas away from the disc of the Galaxy due to heating by supernova explosions. The gas is believed to cool and then be attracted back to the disc by gravity.

Galactic latitude The Galactic coordinate, denoted *b*, that measures the angular position of an object relative to the plane marked out by the Galactic equator, which is similar to its angular position relative to the Galactic plane.

Galactic longitude The Galactic coordinate, denoted *l*, that measures the angular distance of an object around the Galactic equator, from a reference point $l = 0°$ roughly in the direction of the Galactic centre.

Galactic plane The plane defined by the distribution of stars in the flattened disc of the Galaxy, with equal amounts of material on either side. The Sun is located close to, but not exactly in the plane. It may be distinguished from the Galactic equator, which is the plane of a coordinate system defined for convenience to pass through the Sun, tied only approximately to the true distribution of matter in the disc.

Galactic spheroid A structural component of the Milky Way, with the shape of a spheroid, consisting of the halo and nuclear bulge. It extends several tens of kiloparsecs from the Galactic centre. The disc lies within the spheroid, but is not considered to be part of the spheroid.

galaxies Collections of luminous stars, non-luminous dark matter, and in the case of spiral and irregular galaxies some amount of gas and dust, that are gravitationally bound to one another and separated from other similar structures usually by distances of tens of kiloparsecs or more. Various categories of galaxies may be defined based on their appearance, such as spiral galaxies (barred or normal), elliptical galaxies, lenticular galaxies and irregular galaxies.

gaseous corona The body of very hot tenuous gas in the halo of a spiral galaxy.

general relativity A theory of gravity, proposed by Albert Einstein in 1916, according to which gravitational phenomena are a consequence of the geometric distortion of space and time (described mathematically by the curvature of space–time). Formally, the theory is based on the Einstein field equations, but it is often summarized by the somewhat overly simple statement 'matter tells space how to curve; space tells matter how to move'.

geometrical methods (of distance measurement) Any method of distance measurement based on measuring the angular diameter of a feature of known linear diameter. In practice, geometrical methods of distance measurement are not commonly used because there are few astronomical bodies with known linear diameters.

geometry The branch of mathematics concerned with the study of points, lines, surfaces and volumes in space or space–time and the relationships between them.

globular clusters Clusters of 10^5 to 10^6 very old stars tightly bound by gravity into a spherical region of space less than about 50 pc in diameter. The 150 or so globular clusters associated with the Milky Way are found in a spherical distribution about the centre of our Galaxy. Similar distributions are seen in other galaxies.

grand unified theory (GUT) A physical theory which, it is supposed, should describe the strong, weak and electromagnetic interactions as different manifestations of a single type of interaction. Several candidate grand unified theories exist, but all are speculative and difficult to test experimentally.

gravitational instability The process by which a region of enhanced density becomes more pronounced as a result of its own enhanced gravitational attraction.

gravitational lens An object that, by virtue of its gravitational field, forms an image (or images) of a background source of electromagnetic radiation.

gravitational microlensing The term used to describe gravitational lensing effects that are produced by relatively low mass objects such as stellar remnants, brown dwarfs or planets.

gravitationally bound (system) A system of bodies whose gravitational field and distribution of velocities is such that members of the system cannot escape from the system (except by the relatively slow process of evaporation).

group A collection of galaxies that contains fewer than about 50 members. They are believed to be gravitationally bound systems.

Gunn–Peterson effect The effect, expected to be seen in the spectra of sufficiently distant quasars, whereby electromagnetic radiation at wavelengths shorter than the Lyman α line (121 nm) should be absorbed by smoothly distributed neutral hydrogen in the intergalactic medium. This effect has not been unambiguously observed and is certainly not seen in the spectra of quasars with redshifts up to about 5, indicating that the reionization of the intergalactic medium occurred when the Universe was less than about 10% of its present age.

hadron An elementary particle that consists of a cluster of three quarks (or three antiquarks) or of a quark–antiquark pair.

halo A major component of spiral galaxies, spheroidal in shape, and extending several tens of kiloparsecs from the centre of the galaxy. The disc lies within the halo, but is not considered part of the halo. The halo contains mainly Population II stars, with some tenuous gas (see gaseous corona). The halo is sometimes referred to as the 'stellar halo' in order to distinguish it from the dark matter halo.

Heisenberg's uncertainty principle A fundamental principle of quantum physics which, in one form, states that it is not possible to determine to an arbitrarily high precision both the energy of a system and the time at which the measurement is made. Mathematically, the relationship between the uncertainties in the energy of the system (ΔE) and in the time of measurement (Δt) can be expressed as $(\Delta E \times \Delta t) > h/2\pi$ (where h is the Planck constant).

Hertzsprung–Russell diagram A diagram showing the luminosity and temperature of stars, which is useful for comparing large numbers of stars and for tracking their evolution. Photospheric temperature is shown along the horizontal axis (increasing to the left), and luminosity is shown along the vertical axis. A star appears as a point on the diagram, corresponding to its observed temperature and luminosity.

hierarchical scenario A proposed process for the formation of structure in the Universe which proceeds by the merging of relatively low-mass structures to form more massive structures. It is also referred to as the bottom-up scenario.

high-velocity clouds Clouds of atomic hydrogen well away from the Galactic disc, that are moving rapidly relative to the Sun. Their distances are almost impossible to judge, and there is uncertainty whether they are located within or beyond the Galactic halo.

high-velocity stars Stars, typical of Population II but seen as their orbits carry them through the Galactic disc, whose velocities consequently are abnormally high relative to the disc stars that surround them.

HII regions Hot, luminous region of the interstellar medium, comprising ionized hydrogen gas that is made visible by the presence of a hot, young star or stars. Strong ultraviolet radiation from hot stars ionizes the hydrogen, and the occasional recombination of an electron and proton to form a neutral hydrogen atom results in the emission of light, before the hydrogen is reionized.

homogeneous A term meaning 'the same everywhere'.

horizon distance At any instant in the history of the Universe, the maximum distance that a physical signal could have travelled in the time that had elapsed up to that instant.

horizon mass The mass contained within a sphere with a radius equal to the horizon distance.

horizontal branch A region on the Hertzsprung–Russell diagram occupied by stars of low mass and low metallicity after they have left the red giant branch during helium core burning. It is often seen in H–R diagrams of globular clusters, where many stars have similar luminosity, but a wide range of surface temperatures and hence lie in an approximately horizontal strip.

host galaxy (of an AGN) The galaxy in which an AGN is found.

hot big bang A theory of cosmic evolution, according to which the current state of the Universe results from the expansion and cooling of a hot, dense and highly uniform initial state.

hot dark matter (HDM) Dark matter which is comprised of particles that are moving at speeds close to the speed of light.

H–R diagram *See* Hertzsprung–Russell diagram.

Hubble classes The four major classes of galaxy: elliptical (E), irregular (Irr), lenticular (S0) and spiral (S). The lenticular and spiral galaxies can be further classified as barred or non-barred.

Hubble classification scheme A classification scheme for galaxies based on their observed shape and structure. *See* Hubble classes; Hubble types.

Hubble constant *See* Hubble's law.

Hubble diagram A plot of redshift against distance for a sample of distant objects such as galaxies or clusters of galaxies. Such a plot may employ linear or logarithmic axes; if linear axes are used, then the gradient (i.e. slope) of the straight line drawn through the plotted data should equal the Hubble constant divided by the speed of light in a vacuum.

Hubble flow A term used to describe the smooth overall expansion of the Universe that is described by Hubble's law. Distant galaxies provide observable tracers of this expansion, but only imperfectly since each individual galaxy will have its own 'peculiar motion' relative to the Hubble flow.

Hubble parameter The time-dependent quantity $H(t) = \dot{R}(t)/R(t)$ that arises in any Friedmann–Robertson–Walker model in which the scale factor at time t is $R(t)$ and the rate of change of the scale factor at that time is $\dot{R}(t)$. To the extent that such a model represents the real Universe, the current value of the Hubble parameter, $H(t_0)$, should equal the observed Hubble constant H_0.

Hubble time The time $t = 1/H_0$, where H_0 is the Hubble constant, that provides a useful reference value in discussions of cosmic age.

Hubble types The subdivisions of the Hubble classes in the Hubble classification scheme for galaxies. The galaxies belonging to the elliptical class may be typed as E0, E1, E2 … E7, according to their observed shape. Spiral (and barred spiral) galaxies can be typed as Sa, Sb, Sc (and SBa, SBb, SBc), according to the openness of the spiral arms and the size of the galactic nucleus relative to the disc of the galaxy.

Hubble's law The observationally based law, discovered by Edwin Hubble, according to which the distance (d) and redshift (z) of (moderately) distant galaxies are approximately related by

$$z = \frac{H_0}{c} d$$

where H_0 is the Hubble constant and c is the speed of light in a vacuum.

ICM *See* intracluster medium.

inflation An episode of rapid and accelerating expansion in the early Universe. Such a process would have occurred if the effective value of the cosmological constant temporarily became very large. It is speculated that this may have happened immediately before the end of grand unification, as a result of the development of a 'false vacuum' with a high density of vacuum energy. However, there is no accepted theoretical explanation of why such conditions might have occurred. Despite the lack of a mechanism for inflation, it is an attractive hypothesis because it provides a natural solution to the horizon and flatness problems, as well as offering an explanation of the origin of cosmic structure.

initial singularity The state, in some cosmological models, in which some physical quantities (such as density) have implied values that are infinite at the time $t = 0$.

instability strip A roughly vertical region on the Hertzsprung–Russell diagram where the structure of stars is unstable. Any star in this region pulsates and therefore shows variability. Amongst the stars found in this region are classical Cepheids and RR Lyrae variables.

integrated spectrum The overall spectrum of electromagnetic radiation from an entire galaxy, or from a large region of a galaxy, made up from the spectra of stars and other luminous matter.

interacting galaxies Two (or more) galaxies, interacting with each other in a manner that wreaks profound internal changes in both.

interaction energy The typical amount of energy available in a particle interaction. In a system that is in thermal equilibrium at a temperature T, the interaction energy has a value of approximately kT (where k is the Boltzmann constant).

intercloud medium A component of the interstellar medium characterized by very low density, within which the other components of the interstellar medium, such as dense clouds and HII regions, are embedded.

Intermediate Population The name given to stars having ages, metallicities and motions intermediate between those of Population I and Population II stars. It is synonymous with the thick disc.

interstellar medium (ISM) The matter that thinly fills interstellar space in the Galaxy. It consists of gas (mainly hydrogen), with a trace of dust, and occurs as many, highly varied types of region, such as dense clouds, HII regions and the intercloud medium.

intracluster medium (ICM) The gas that lies between the galaxies within a cluster of galaxies. Typically such gas is very hot and ionized, and has a very low density.

ionized hydrogen Hydrogen in a state where the single proton and single electron that form atomic hydrogen have acquired sufficient energy (13.6 eV or more) that they are no longer bound to one another. The energy may come from collisions with other fast-moving particles, or from electromagnetic radiation of sufficiently high energy/short wavelength.

irregular (galaxy) Any member of the Hubble class of galaxies characterized by having no overall symmetry or regularity. Membership of this class is denoted by the symbol Irr.

ISM *See* interstellar medium.

isochrone A curve in the Hertzsprung–Russell diagram showing the theoretically expected locations of stars of different masses, temperatures and luminosities but the same age (and the same initial metallicity).

isophote A curve linking points of equal apparent surface brightness.

isotropic A term meaning 'the same in all directions'.

Jeans mass The minimum mass that a uniform, spherical, non-rotating cloud must have if it is to collapse under its own gravitation. In the context of evolutionary cosmology, the Jeans mass at any time (based on the mean cosmic density and temperature at that time) determines which of two evolutionary pathways an over-dense region will follow. A region that exceeds the Jeans mass will contract under the influence of gravity. A region that has a mass lower than the Jeans mass will be supported by its internal pressure and will be stable against gravitational collapse.

Keplerian orbit An orbit arising when the mass of a gravitating system is dominated by a single body. This applies in the case of the Solar System where the Sun dominates, but not in the case of the disc of a galaxy where large fractions of the mass lie away from the centre.

kiloparsec A unit of distance, equal to one thousand parsecs and usually denoted 1 kpc, that is convenient for measuring distances on the scale of a galaxy. $1\,\text{kpc} = 1000\,\text{pc} = 3.09 \times 10^{19}\,\text{m}$.

$\boldsymbol{\lambda F_\lambda}$ (lambda-eff-lambda) The product of multiplying the spectral flux density F_λ at a wavelength λ by that wavelength. When plotted against wavelength (to form a spectral energy distribution) this quantity provides a measure of the contribution to the total luminosity of a source that arises from different parts of the electromagnetic spectrum.

large-scale structure A generic term for the distribution of matter in the Universe on or exceeding the scales of superclusters, i.e. on linear scales exceeding tens of megaparsecs.

last-scattering surface The surface defined by the locations at which photons in the cosmic microwave background last underwent significant interaction with matter (with the exception of gravitational effects). This interaction was due primarily to electron scattering, and so last-scattering occurred at about the time of recombination.

Lemaître model A cosmological model, belonging to the class of Friedmann–Robertson–Walker models, which starts with a big bang and which expands perpetually, but in such a way that there is a 'coasting' or 'pseudo-static' phase at intermediate times during which the rate of change of the scale factor approaches zero so that the model behaves like the Einstein model. The Lemaître model is characterized by a positive cosmological constant ($\Lambda > 4\pi G\rho/c^2$) and a positive curvature parameter ($k = +1$).

lenticular (galaxy) Any member of the Hubble class of galaxies characterized by having a disc but no spiral arms, possibly related to spiral galaxies. Membership of this class is denoted by the symbol S0, or SB0 in the case of a barred lenticular galaxy.

lepton One of a family of six elementary particles that includes the electron and the three types of neutrino.

lepton number A quantity that is conserved in all particle interactions (with the exception of some speculative interactions predicted by grand unified theories). The lepton number of any lepton is +1 and that of any antilepton is −1 respectively. The lepton number of any other particle is zero.

light curve A diagram showing the variation of brightness (e.g. magnitude, flux density or luminosity) with time, for a celestial object such as a variable star or supernova.

light-year The distance travelled by light (or any other form of electromagnetic radiation) through a vacuum in one (tropical) year. $1\,\text{ly} \approx 9.46 \times 10^{15}\,\text{m}$.

Local Group A sparse cluster of over 30 galaxies within about 1 Mpc of the Milky Way, and including the Milky Way.

Local Supercluster The supercluster of clusters of galaxies to which the Local Group belongs. It is 25–50 Mpc across, and contains 1000 or so bright galaxies.

luminosity A quantity describing the rate at which energy is carried away from a luminous object by electromagnetic radiation. The SI unit of luminosity is the watt (W), where $1\,\text{W} = 1\,\text{J}\,\text{s}^{-1}$.

Lyman α (line) The spectral line that arises from the electronic transitions in the hydrogen atom from $n = 1$ to $n = 2$ (absorption) or from $n = 2$ to $n = 1$ (emission).

Lyman α forest A set of absorption lines (which are predominantly due to Lyman α absorption) appearing in the spectrum of a quasar. The absorption lines are due to clouds of neutral intergalactic gas that lie along the line of sight to that quasar.

Lyman series The series of electronic transitions in the hydrogen atom that involve a change to or from the $n = 1$ state.

MACHO (massive astrophysical compact halo object) A hypothetical astronomical body with a moderate mass but a low luminosity (such as a stellar remnant or a body of substellar mass) that might exist undetected in the halo of a galaxy. A large population of such objects might account for a significant amount of (baryonic) dark matter.

main sequence turn-off The point on the main sequence of the Hertzsprung–Russell diagram of a star cluster above which no stars are present. It corresponds to stars that are just reaching the end of their time on the main sequence, and is therefore an indication of the age of the cluster.

mass accretion rate The rate at which material is transferred to an astronomical body.

mass-to-light ratio The value obtained by dividing the mass M of a system by its luminosity L.

mathematical model A mathematical representation of some process or system that captures certain essential features of its subject but does not attempt to recreate every detail. A mathematical model is usually based on one or more equations and many involve one or more parameters that might have to be determined by observation.

merger tree A schematic representation of the history of a galaxy in terms of the merger events that have led to the formation of that galaxy.

metallicity (Z) A numerical measure of the proportion of heavy elements in a sample of material, obtained by dividing the mass of heavy elements (i.e. ‘metals’ to an astronomer) in the sample by the total (baryonic) mass of the sample. In the Sun, $Z \approx 0.02$.

metals To an astronomer, all elements except hydrogen and helium.

Milky Way The name given to the Galaxy of which the Sun is a member. Also the name given to the diffuse band of light seen when an observer on the Earth looks in a direction near the plane of the Galaxy, where uncountable numbers of unresolved stars produce a background glow.

molecular clouds Any cloud-like region in the interstellar medium in which hydrogen is predominantly in the form of molecular hydrogen. Dense clouds are found in this type of region.

molecular hydrogen Hydrogen in a state where many pairs of hydrogen atoms have become bound to one another to form hydrogen molecules (H_2). This is only possible in cold, dense clouds where neither collisions with fast-moving particles, nor ultraviolet radiation is likely to break apart (dissociate) the molecules.

momentum A property of systems (such as arrangements of particles of matter or distributions of radiation) that measures their ability to impart an impulse. According to general relativity, the distribution of momentum throughout a region of space–time is one of the factors that plays a role in determining the curvature of that region of space–time. The SI unit of momentum is the kilogram metre per second ($\mathrm{kg\,m\,s^{-1}}$).

monolithic collapse A scenario for galaxy formation in which the gravitational collapse of a single over-dense region gives rise to a single galaxy.

morphology (of a galaxy) The observed shape and large-scale structure of a galaxy, used as the basis of the Hubble classification.

M-theory A speculative physical theory that unifies gravitation with the strong, weak and electromagnetic interactions. One feature of M-theory is that it requires 11 dimensions, rather than the four dimensions of space–time with which we are familiar.

multipole number The numerical quantity, usually denoted l, that is plotted on the horizontal axis of an angular power spectrum, and which indicates an angular scale (on an anisotropy map or elsewhere) of $\theta = 180°/l$.

narrow-line region (NLR) The body of gas responsible for emitting the narrow emission lines in an AGN. The width of narrow emission lines corresponds to radial velocity variations in the range 200 to 900 $\mathrm{km\,s^{-1}}$.

neutralino An uncharged elementary particle that is predicted by some supersymmetric extensions to the standard model. The existence of such particles has not been established. The neutralino is a candidate weakly interacting massive particle (WIMP).

neutrino decoupling A process in which changing physical conditions prevent the frequent interaction between neutrinos and other types of elementary particles. The term neutrino decoupling is often used to refer to the postulated episode in cosmic history in which the declining density and temperature of matter caused cosmic neutrinos to cease their frequent interactions with every other kind of particle (except for the effects of gravity). Neutrino decoupling is believed to have occurred when the age of the Universe was about 0.7 s.

non-baryonic dark matter A component of dark matter which can be shown not to be made of baryons.

normal galaxy A galaxy which has an approximately constant luminosity that can largely be accounted for in terms of the stars and gas that the galaxy contains.

number density The quantity used to describe the number per unit volume of particles or bodies of some specified type (e.g. electrons or stars). The SI unit of number density is the per cubic metre (m^{-3}).

OB association A group of young stars containing several stars of spectral types O and B.

oblate spheroid An ellipsoid having the shape of a flattened sphere, i.e. with two principal axes of equal length and a shorter third axis.

observational cosmology The branch of science concerned with measuring the parameters that characterize the Universe. These parameters include the Hubble constant, the current value of the deceleration parameter and the current values of the density parameter for matter and the density parameter for the cosmological constant.

open cluster A cluster of up to a few hundred stars, formed from a cloudlet that has fragmented from a larger dense cloud. The stars are only loosely bound together by gravity, hence the name 'open', in contrast to the much stronger binding of stars in a globular cluster.

open model A cosmological model, belonging to the class of Friedman–Robertston–Walker models, that starts with a big bang and expands continuously without limit, so the rate of change of the scale factor is always positive (i.e. $\dot{R} > 0$ at all times). The open model is characterized by a zero cosmological constant ($\Lambda = 0$) and a negative curvature parameter ($k = -1$). In such a model the cosmic density is always less than the critical density.

optically violent variables (OVV) A subclass of blazar. In contrast to BL Lac objects, some broad emission lines are often observed in the spectra of OVVs.

Orion–Cygnus Arm *See* Orion Spur.

Orion Spur Also called the Orion–Cygnus arm. A strip-shaped region of the Galaxy near the Sun occupied by astronomically young objects, either a spur of a spiral arm, or an arm in its own right. The Sun is located in the Orion Spur.

pair-creation The physical process in which, given sufficient energy, a particle and its antiparticle can spontaneously form. This is the opposite process to annihilation.

parallax The quantity that describes the change in direction to a celestial body (relative to a background of far more distant bodies) resulting from a given change in position of the observer perpendicular to the direction of the body. The term parallax is often used to refer specifically to stellar parallax, p, where the change in position of the observer is one astronomical unit. This quantity is important in the determination of the distance of nearby stars.

parsec The distance to a celestial body that has a parallax of one arc second. $1\,\text{pc} \approx 3.26$ light-years $\approx 3.09 \times 10^{16}\,\text{m}$.

peculiar galaxy A galaxy of more-or-less readily apparent Hubble type, but with some abnormal feature (such as a jet); denoted by 'p' after the Hubble type.

peculiar motion (of a galaxy) The component of motion of a galaxy as a whole that is additional to that arising from its participation in the Hubble flow.

period–luminosity relationship A correlation between period and luminosity; in particular the relationship between period and luminosity of Cepheid variables that enables these stars to be used as standard candles. (Absolute visual magnitude, M_V, is generally used in place of luminosity when displaying this relationship.)

Perseus Arm A strip-shaped region of the Galaxy, slightly further from the Galactic centre than the Sun, occupied by astronomically young objects. It is one of the local spiral arms of the Galaxy.

photodisintegration The process in which a nucleus is split apart by the absorption of a gamma-ray photon. This type of reaction plays an important role in the later stages of stellar nucleosynthesis.

photon The particle of electromagnetic radiation in the photon model of light. The photon energy ε is proportional to the frequency f of the associated radiation; $\varepsilon = hf$ where h is the Planck constant.

photon–baryon fluid The fluid-like system in the early Universe, formed by the incessant interaction of radiation and charged baryons, that is characterized in any sufficiently localized region by a specific temperature and pressure. The photon–baryon fluid is subject to the gravitational influence of the dark matter that is also present in the early Universe.

photon energy distribution function A quantity that describes the relative numbers of photons at different energies. Specifically, at some specified energy, the photon energy distribution function is the proportion of photons whose energies lie in a narrow energy range around that energy.

Planck era The period in the history of the Universe prior to the Planck time.

Planck time A time determined by a combination of physical constants ($(Gh/2\pi c^5)^{1/2} = 5.38 \times 10^{-44}$) that represents the earliest time in cosmic history at which currently established physical theory might be used to study the nature and evolution of the Universe. Prior to the Planck time, gravity might have played a significant role in particle interactions.

Population I Stars found in the discs of spiral galaxies, generally less than 10^{10} yr old, and have a metallicity similar to that of the Sun ($Z \sim 0.01$ to 0.04).

Population II Stars found in the Galactic spheroid of spiral galaxies and in elliptical galaxies, generally more than 10^{10} yr old. Population II stars in the halo have metallicities $Z < 0.002$, but Population II stars in the bulge have metallicities similar to Population I stars ($Z \sim 0.01$ to 0.04).

population synthesis A method of investigating the stellar content of galaxies, in which the relative abundance of various types of star is assumed, and their integrated spectrum calculated and compared with that observed from the galaxy in question. On the basis of this comparison, the relative abundances of different stellar types are modified until the best fit between the model and actual spectrum is determined.

precision cosmology A term used to describe recent developments in cosmology whereby the values of a range of key cosmological parameters have been determined with high precision (and possibly good accuracy).

primordial nucleosynthesis The nuclear processes that were responsible for the initial formation of the nuclei of light elements (such as helium and lithium) in the early Universe. It is generally believed that primordial nucleosynthesis began when the age of the Universe was about 3 minutes, and that it continued for about thirty minutes.

prolate spheroid An ellipsoid with the shape of an elongated sphere, i.e. with two principal axes of equal length and a longer third axis.

Pythagoras's theorem A theorem of geometry according to which the square of the length of the longest side of a right-angled triangle is equal to the sum of the squares of the lengths of the other two sides ($c^2 = a^2 + b^2$).

quantum fluctuations Variations in energy density of the vacuum that occur on a microscopic scale due to the presence of virtual particles.

quantum theory A wide-ranging theory that describes, amongst other things, the structure and behaviour of atoms and their interaction with electromagnetic radiation. It accounts for the phenomena that are embraced by the photon model of light, and implies the existence of energy levels in atoms.

quark–hadron phase transition A process in which changing conditions cause a 'gas' of free quarks and antiquarks to transform itself into a gas of hadrons and antihadrons, The term is also used to describe the episode in cosmic history in which this process is believed to have affected the baryonic matter in the Universe. It is believed that the quark–hadron phase transition occurred when the age of the Universe was about 10^{-5} s.

quasar/QSO A kind of active galaxy, typically characterized by a point-like appearance and a very large redshift. Quasars provide very distant and very bright examples of the effect of an AGN in a galaxy where the rest of the galaxy is so faint that it can only be discerned with difficulty, if at all.

quintessence A hypothetical and exotic form of matter, probably better thought of as a field filling the Universe, that would exert a negative pressure. The energy associated with this kind of matter (or field) would constitute the dark energy. In contrast to some of the other proposed explanations of dark energy, the energy density of quintessence might vary with time and spatial position.

radiation-dominated era The period of the history of the Universe when the energy density of radiation exceeded that of matter.

radiation pressure A pressure exerted by photons on any object that absorbs or scatters them.

radio galaxy A kind of active elliptical galaxy which shows (usually) two regions of diffuse radio emission from either side of the galaxy – radio lobes. An AGN is needed to power the radio lobes, and can be seen in the centre of the parent galaxy.

random uncertainties Uncertainties in the measured value of a quantity that cause repeated measurements of that quantity to vary about some mean value.

recombination A process in which an electron and an ion combine, i.e. the opposite of ionization. The electron is typically captured into a high-energy orbit and then cascades downward through the atom's energy levels emitting photons as it does so. The term recombination is also used to refer to the postulated episode in cosmic history in which the baryonic matter of the Universe made the transition from being predominantly plasma to predominantly neutral atoms. Recombination is believed to have occurred when the age of the Universe was between about 3 and 4×10^5 years.

redshift The numerical quantity used to measure the shift in wavelength of a spectral line. If a spectral line is emitted at a wavelength λ_{em} and observed at a wavelength λ_{obs}, the redshift is defined by

$$z = \frac{\lambda_{\mathrm{obs}} - \lambda_{\mathrm{em}}}{\lambda_{\mathrm{em}}}$$

reionization A process in which a formerly ionized medium that had undergone recombination to become neutral is again ionized. The term reionization is often used to refer to the postulated episode in cosmic history in which much of the neutral hydrogen became ionized, perhaps due to an increase in the intensity ultraviolet light from hot stars or from AGN. Reionization is believed to have occurred when the age of the Universe was less than 10% of its current value.

relative density fluctuation The numerical quantity used to describe the extent to which the density of a given region of the Universe departs from the mean density of the Universe by expressing the difference between the density of the region and the mean density as a fraction of the mean density.

retrograde Motion around the Galaxy in the opposite direction to that of disc stars.

richness A quantity used in the classification of clusters of galaxies that describes the number of galaxies (above a certain threshold luminosity) present within a cluster. Rich clusters contain relatively high numbers of galaxies.

rigid body rotation A pattern of rotation in which all parts of the rotating system have the same period of rotation, irrespective of their distance from the centre of rotation. This is the kind of rotation exhibited by a solid planet and should be contrasted with the differential rotation that characterizes objects such as the Sun and the Milky Way.

Robertson–Walker metric An expression, applying to any space–time that is homogenous and isotropic, that relates the physical separation ds of two narrowly separated events to the coordinate differences (typically dx, dy, dz and dt) that may be used to describe the relative locations of those events. The Robertson–Walker metric involves a curvature parameter k and a scale factor $R(t)$ that respectively characterize the curvature of space and its expansion (or contraction) with time.

rotation curve A plot of rotation speed against radial distance for a rotating system.

RR Lyrae stars A type of regular variable star. RR Lyrae stars are found on the horizontal branch of the H–R diagram, and within the instability strip and hence their envelopes pulsate. Pulsation periods are around 12 hours. As all horizontal branch stars have very similar absolute magnitudes, RR Lyraes are good standard candles for measuring distances within the Galaxy. They are Population II stars.

Sachs–Wolfe effect The dominant source of angular power in the angular power spectrum of the cosmic microwave background for multipole numbers of 50 or less (i.e. on angular scales of a few degrees or more). The effect is largely due to the gravitational redshift of radiation coming from the denser parts of the last-scattering surface.

Sagittarius A* A very compact, strong radio source that lies at the very centre of the Galaxy. The motions of stars around Sgr A* suggest it is a black hole with a mass about 2.6×10^6 greater than the mass of the Sun.

Sagittarius–Carina arm A strip-shaped region of the Galaxy, slightly closer to the Galactic centre than the Sun, occupied by astronomically young objects. It is one of the local spiral arms of the Galaxy.

Sagittarius dwarf galaxy A dwarf galaxy (discovered in 1995) that is in the process of merging with the Milky Way.

scale factor A time-dependent quantity, usually denoted $R(t)$, that appears in the Robertson–Walker metric where it describes the expansion or contraction of space in a homogeneous and isotropic Universe. The scale factor plays a crucial role in relating the coordinates of points to the physical distance between these points. In an expanding Universe, two points that have a fixed co-moving coordinate separation r will be separated by a growing physical distance l that is proportional to $R(t)$, and which may be, for example, $l = R(t) \times r$.

scale height The distance, measured from the Galactic plane, over which the number density of disc stars decreases to 1/e times the density in the Galactic plane. (The value e ≈ 2.718 is the basis of the exponential function.)

Schwarzschild radius The radial distance from the centre of a black hole at which the escape speed equals the speed of light.

SED *See* spectral energy distribution.

semimajor axis Half the longest diameter of an ellipse.

semiminor axis Half the shortest diameter of an ellipse.

Seyfert galaxy A kind of active spiral galaxy which has an AGN that appears as a central, point-like source in optical images.

SFR *See* star formation rate.

Silk damping The dominant source of angular power in the angular power spectrum of the cosmic background radiation for multipole numbers in excess of $l = 1000$ (or angular scales of less than 0.1 degree or so). The effect arises from the suppression of acoustic waves of very short wavelength due to the free movement of photons between encounters with charged particles.

space The aspect of space–time that consists of all the possible positions that a particle might occupy according to some observer. Space is three-dimensional and possesses a range of geometrical properties.

space–time The four-dimensional entity that unites space and time. It consists of all the possible events at which a particle might be present, and is characterized by geometrical properties such as curvature. When making measurements, any observer will divide space–time into space and time, but the way in which that division is made by two different observers will generally be different and depends on the relative motion of those two observers.

spectral energy distribution (SED) A form of the broadband spectrum of an astronomical source that shows the quantity λF_λ against wavelength λ. It shows the relative contributions to the total luminosity that are emitted in different wavelength ranges.

spectral excess The feature in the spectrum of a galaxy that represents the excess of emission in a certain wavelength band over that which would be expected due to emission from stars alone. Spectral excesses in the infrared are characteristics of starburst and active galaxies.

spheroid A three-dimensional shape that may be pictured as a sphere that has been flattened or stretched in one direction. This is the *shape* of both the (stellar) halo and the dark-matter halo of the Galaxy, and it is the *name* given to the region of the Galaxy associated with the halo and sometimes also the bulge.

spiral arms The regions of a spiral galaxy traced out by bright stars, HII regions, and other astronomically young objects. These mark out a fragmented, roughly spiral pattern within the disc of the galaxy, extending outwards from near its centre.

spiral-arm tracers Those young, short-lived astronomical objects associated with recent star formation that map out the spiral arms of a spiral galaxy. They include HII regions, O and B stars, classical Cepheid variable stars, and T Tauri stars.

spiral density wave A long-lived, self-consistent pattern of density enhancement that may arise in a disc of stars and gas, thought possibly to account for the pattern of star formation that gives rise to spiral arms in spiral galaxies.

spiral galaxy Any member of the Hubble class of galaxies characterized by having a disc and spiral arms. Membership of this class is indicated by the letter S, or SB in the case of a barred spiral galaxy.

standard candle Any type of object whose luminosity is directly indicated by its observable properties, thus allowing its distance to be inferred from the difference between its apparent brightness and its true brightness.

standard candle methods Any method of distance determination based on the use of a standard candle, such as a Cepheid variable of known period, or a Type Ia supernova with a known rate of decline in brightness.

standard model (of elementary particles) A theory which describes all known elementary particles and their interactions. No discrepancy between the predictions of the standard model and experimental results has yet been discovered.

star formation rate (SFR) The rate at which stars are forming, usually quoted as the number of solar masses per year, in some specified volume.

starburst galaxy A galaxy in which a recent episode of star formation is believed to have occurred, leading to optical emission lines and infrared radiation being emitted from an extended region of the galaxy.

static A property of certain cosmological models (or more specifically of certain space–times) implying that space is neither expanding nor contracting.

stellar halo A tern sometimes used to distinguish the halo from the dark-matter halo. *See* halo.

stellar parallax *See* parallax.

stellar population A grouping of stars characterized by their age, composition and location or motion. *See* Intermediate Population; Population I; Population II.

sublimate The process in which a solid material (e.g. dust) is transformed, on heating, into the gas phase without going through a liquid phase.

sublimation radius The distance from the engine of an AGN at which the temperature is just sufficient to cause dust particles to sublimate.

superbubble A hot, bubble-like region of the interstellar medium where the gas has been heated greatly by large numbers of supernova explosions from stars in that region.

supercluster An association of galaxies of order 25 to 50 Mpc across.

supermassive black hole A black hole with a mass in excess of about $10^7 M_\odot$.

supersymmetry A type of symmetry which has been suggested, but not proven, to apply to particle interactions. Supersymmetric theories predict the existence of particles that have not been observed in nature. Some of these particles (such as the neutralino) are of cosmological significance because they are candidates for WIMPs.

surface brightness profile A plot of the apparent surface brightness of a galaxy as a function of radial distance from its centre.

systematic uncertainties Uncertainties in the measured value of a quantity that cause repeated measurements of that quantity to always differ from the true value in the same way.

T Tauri stars Newly formed, low-mass, star-like bodies that have not yet reached the main sequence.

temperature fluctuation Variations in average temperature, on a given size or angular scale, within a temperature distribution, such as that of the cosmic microwave background.

thermal bremsstrahlung A process by which X-rays are generated in a plasma. Electrons pass close to ions, but without being captured. In doing so their paths are deflected and X-ray photons are emitted.

thermal equilibrium A state in which there is a high level of interaction between matter and radiation which leads to the radiation having a black-body spectrum with a characteristic temperature that is the same as that of the matter.

thick disc A component of the disc of the Galaxy, a few times thicker than the thin disc – the scale height of the thick disc is around 1000 parsecs – and containing fewer stars. Thick-disc stars belong to the Intermediate Population.

thin disc The main component of the disc of the Galaxy, with a scale height around 300 parsecs. Thin-disc stars belong to Population I.

time The aspect of space–time that consists of all the possible instants at which a particle might exist according to some observer. Time is one-dimensional.

top-down scenario A proposed process for the formation of structure in the Universe which proceeds by the fragmentation of relatively high-mass structures to form less massive structures.

triaxial ellipsoid An ellipsoid with three unequal principal axes.

Tully–Fisher relation The relationship between the luminosity of a spiral galaxy and the width of its 21 cm hydrogen emission line. This relation is used to determine the luminosities and hence distances of spiral galaxies.

Type Ia supernovae A class of supernova, used as a standard candle.

unbarred galaxy *See* barred (spiral) galaxy.

unbounded A property of certain cosmological models (or more specifically of certain space–times) implying that any 'straight' line may be extended infinitely without ever encountering any boundary or edge. Note, however, that in an unbounded space–time there is no guarantee that a straight line may not close back upon itself, as shown by the finite but unbounded space of the Einstein model.

vacuum energy The energy possessed by a region of space that contains no radiation or real particles. This energy is not zero because of the existence of virtual particle–antiparticle pairs, which are continuously being created and annihilated in the vacuum. Vacuum energy provides a possible explanation of the nature of dark energy, though attempts to provide a quantitative basis for such an explanation have so far been unsuccessful.

velocity dispersion A quantity that describes the range of velocities found within a collection of moving objects (*see* virial theorem). The SI unit of velocity dispersion is the metre per second ($m\,s^{-1}$).

virial theorem A theorem relating the total kinetic energy to the total gravitational potential energy for a system of gravitationally interacting particles that has settled into a state of equilibrium. A statistical treatment of such systems, leads to the result that the kinetic energy of the system is equal to $-1/2$ times the gravitational potential energy of the system. A consequence of this is that the velocity dispersion of the components of the system is expected to depend on the size of the region they occupy and on their total mass. This result is used to determine the masses of elliptical galaxies and of clusters of galaxies.

virialized The equilibrium state of a gravitationally bound system. The virial theorem applies only to systems in this state.

virtual particles Particle–antiparticle pairs that have a fleeting existence in the vacuum. The rest energy required for particle–antiparticle pair creation is related to the lifetime of the pair by the Heisenberg uncertainty relation.

voids Large (~60 Mpc) regions of the Universe in which the number density of galaxies is very low.

weakly interacting massive particle *See* WIMP.

WIMP (weakly interacting massive particle) A hypothetical elementary particle that has a relatively high mass and which only interacts by the weak interaction and gravity. A large population of such particles might account for a significant amount of (non-baryonic) dark matter.

winding dilemma The observation that if a galaxy's spiral arms consisted of an unchanging population of stars then differential rotation would cause the arms to smear out within a time that is short compared with the age of that galaxy.

zone of avoidance A zone on the sky, close to the Galactic plane, where dust in the interstellar medium obscures our view of more distant objects.

zone of obscuration *See* zone of avoidance.

FURTHER READING

General works at a level comparable to, or somewhat below this book

Seeds, M.A. (2001) *Foundations of Astronomy*, Brooks/Cole, Pacific Grove.

Zeilik, M. (2002) *Astronomy: The Evolving Universe*, Cambridge University Press, Cambridge.

Fraknoi, A., Morrison, D. and Wolff, S. (2000) *Voyages to the Stars and Galaxies*, Harcourt Inc., Orlando.

More specialized works at a level comparable to this book

Green, S.F. and Jones, M.H. (2004) *An Introduction to the Sun and Stars*, Cambridge University Press, Cambridge.

Guth, A.H. (1997) *The Inflationary Universe*, Jonathan Cape, London.

Henbest, N. and Couper, H. (1994) *The Guide to the Galaxy*, Cambridge University Press, Cambridge.

Livio, M. (2000) *The Accelerating Universe*, John Wiley & Sons Inc, Chichester.

Silk, J. (1994) *A Short History of the Universe*, Scientific American Library, New York.

Tayler, R.J. (1993) *Galaxies: Structure and Evolution*, Cambridge University Press, Cambridge.

Works at a more advanced level

Binney, J. and Merrifield, M. (1998) *Galactic Astronomy*, Princeton University Press, Princeton.

Liddle, A.R. (1999) *An Introduction to Modern Cosmology*, John Wiley & Sons Inc, Chichester.

Peterson, B.M. (1997) *An Introduction to Active Galactic Nuclei*, Cambridge University Press, Cambridge.

Rees, M. (2000) *New Perspectives in Astrophysical Cosmology*, Cambridge University Press, Cambridge.

Roos, M. (2003) *Introduction to Cosmology*, John Wiley & Sons Inc, Chichester.

Rowan-Robinson, M. (2003) *Cosmology*, Oxford University Press, Oxford.

Sparke, L.S. and Gallagher, J.S. (2000) *Galaxies in the Universe: An Introduction*, Cambridge University Press, Cambridge.

ACKNOWLEDGEMENTS

The production of this book involved a number of Open University staff, to whom we owe a considerable debt of thanks for their commitment and the high professional standards of their contributions. The production of the Open University course of which this book forms a part was managed by Christopher Edwards, assisted by Valerie Cliff. The text was copy-edited by Rebecca Graham, who also played an invaluable role in steering the project through the production process. The graphic artwork was prepared by Pam Owen with considerable skill and the design and layout was undertaken in an exemplary fashion by Debbie Crouch. The index was prepared by Jane Henley. We are also grateful to Giles Clark (Open University) and Susan Francis (Cambridge University Press) for their support and help with co-publication.

In addition, we wish to thank the following people who commented on earlier versions of the text: Malcolm Longair (University of Cambridge) and Michael Merrifield (University of Nottingham) together with anonymous referees appointed by Cambridge University Press. We should also like to acknowledge the contribution made by the following members of the Open University in commenting on early drafts of the text: Carole Haswell, Anthony W. Jones and Fiona Vincent. Many other individuals and organizations furnished and/or granted permission for us to use their diagrams or photographs and to them we also express our gratitude.

Grateful acknowledgement is made to the following sources for permission to reproduce material in this book.

Cover

Background image T.A. Rector (NRAO/AUI/NSF and NOAO/AURA/NSF) and M. Hanna (NOAO/AURA/NSF); *Thumbnail images* NASA, Andrew Fruchter and the ERO Team (Sylvia Baggett (STScI), Richard Hook ST-ECF), Zoltan Levay (STScI); NASA, H. Ford (JHU), G. Illingworth (USCS/LO), M. Clampin (STScI), G. Hartig (STScI) the ACS Science Team, and ESA; NASA/SAO/R.Kraft *et al*; The BOOMERanG Collaboration;

Figures

Figure 1.1 Dennis di Cicco, Sky Publishing Corp.; *Figure 1.2* 1980–2002, Anglo-Australian Observatory, photograph by David Malin; *Figure 1.4a* J. C. Barentine and G. A. Esquerdo (PSI), Kitt Peak, NOAO; *Figure 1.4b* 1999–2002, Anglo-Australian Observatory, Photograph by S. Lee, C. Tinney and D. Malin; *Figure 1.6* Astronomical Society of Australia 1999; *Figure 1.8* NASA; *Figure 1.9* NASA/ESA. Image courtesy of Space Telescope Science Institution, Baltimore; *Figure 1.10* Copyright © 1965 by the University of Chicago; *Figure 1.11* Courtesy Mt. Wilson Observatory; *Figure 1.13c* © 1991 by Annual Reviews Inc; *Figure 1.14a* Courtesy of Axel Mellinger, University of Potsdam, Germany; *Figure 1.14b* © Ned Wright; *Figure 1.14c* NASA Goddard Space Flight Center; *Figure 1.14d* Glyn Haslam *et al*., Max-Planck-Institut für Radioastronomie, Bonn; *Figure 1.15* Royal Observatory Edinburgh/Anglo-Australian Telescope Board/David Malin; *Figure 1.16* Photo courtesy of Dennis di Cicco; *Figure 1.20* Anglo-Australian Telescope Board; *Figure 1.26 Astrophysical Journal*, 1985 Volume 293, p. 424, © University of Chicago Press; *Figure 1.27* Courtesy of Bachrach Portrait Studios;

Figure 1.28 Publications of the Astronomical Society of the Pacific, Volume 99, 1987, Hesser, Harris and Vandenberg. The Astronomical Society of the Pacific; *Figure 1.30* D. Mihalas and J. Binney (1981), *Galactic Astronomy*, copyright © 1981 W. H. Freeman and Co.; *Figure 1.32* © 2002 Nature Publishing Group; *Figure 1.33 Publications of the Astronomical Society of the Pacific*, The Astronomical Society of the Pacific; *Figure 1.34* © 2002 Nature Publishing Group; *Figure 1.36* Klaas de Boer and Blair Savage (1982), The Coronas of Galaxies, Scientific American Inc. illustration by Walken Graphics; *Figure 1.37* R. Ibata (UBC), R Wyse (JHU), R. Sword (IoA)/NASA;

Figure 2.1 © Copyright California Institute of Technology; *Figure 2.4a, 2.4b and 2.4 c* National Optical Astronomy Observatory; *Figure 2.5* © 2000–2002, Malin/Caltech, Photograph by Bill Miller; *Figure 2.6a and 2.6c* A. Sandage and J. Bedke, *The Carnegie Atlas of Galaxies*, Volume I, 1994, Carnegie Institution of Washington; *Figure 2.6b* Sloan Digital Sky Survey; *Figure 2.6d, 2.6e, 2.6f and 2.6g* NOAO/AURA/NSF; *Figure 2.6h* David and Christine Smith/Adam Block/NOAO/AURA/NSF; *Figure 2.7a, 2.7b and 2.7c* © 1982–2002, Anglo-Australian Observatory, photograph by David Malin; *Figure 2.8* © 1987–2002, Anglo-Australian Observatory, photograph by David Malin; *Figure 2.10a* NASA and John Biretta (STScI/JHU); *Figure 2.10b* NASA and Hubble Heritage Team (STScI); *Figure 2.10c* NASA and S. Gallagher (Pennsylvania State University); *Figure 2.10d* European Southern Observatory; *Figure 2.10e* NASA, H. Ford (JHU); *Figure 2.11* The compressed files of the 'Palomar Observatory - Space Telescope Science Institute Digital Sky Survey' of the northern sky, based on scans of the Second Palomar Sky Survey are copyright © 1993–2000 by the California Institute of Technology and are distributed herein by agreement. All Rights Reserved; *Figure 2.13* The compressed files of the 'Palomar Observatory - Space Telescope Science Institute Digital Sky Survey' of the northern sky, based on scans of the Second Palomar Sky Survey are copyright © 1993–2000 by the California Institute of Technology and are distributed herein by agreement. All Rights Reserved; *Figure 2.16* Westerbork Synthesis Radio Telescope, Netherlands; *Figure 2.17* D. Mihalas and J. Binney (1981), *Galactic Astronomy*, copyright © 1981 W. H. Freeman and Co.; *Figure 2.18* from Astrophysics and Space Research Group, The University of Birmingham, www.sr.bham.ac.uk; *Figure 2.19* A. J. Pickles, *Astrophysical Journal*, Volume 296, p. 340, © 1985. The American Astronomical Society; *Figure 2.20a and 2.20b* Anglo-Australian Observatory/David Malin Images; *Figure 2.21* NASA and ESA; *Figure 2.24* Bart J. Bok and Priscilla F. Bok (1974), reprinted by permission of the publishers from *The Milky Way*, Cambridge, Mas., Harvard University Press, copyright © 1941, 1945, 1957, 1974 by the President and Fellows of Harvard College; *Figure 2.26* R.Berendzen, R. Hart and D. Seeley (1976) *Man Discovers the Galaxies*, New York, Science History Publications; *Figure 2.27* Nick Suntzeff (CTIO)/NAOA/AURA/NSF; *Figure 2.31* © Virgo Consortium, University of Durham UK; *Figure 2.32* Michael Merrifield; *Figure 2.33* Kennicutt, Jr, R. C. (1998) Star formation in galaxies along the Hubble sequence. *Annual Review of Astronomy and Astrophysics* 1998, vol 36, Annual Reviews; *Figure 2.34a* Royal Observatory Edinburgh/Anglo Australian Telescope Board. Photograph by David Malin; *Figure 2.34b* from Alar Toomre (MIT) and Juri Toomre (University of Colorado); *Figure 2.38* The Sauron Project; *Figure 2.40* R. Williams and the HDF Team (STScI) and NASA; *Figure 2.41* Ferguson, H. C., Dickinson, M. and Williams, R. (2000) The Hubble deep fields, *Annual Review of Astronomy and Astrophysics* 2000, vol 38, Annual Reviews; *Figure 2.42a, 2.42b and 2.42c* NOAO;

Figure 3.4 R. C. Kennicutt, *Astrophysical Journal*, Volume 388, p. 310, © 1992 The American Astronomical Society; *Figure 3.10* NASA/IPAC Extragalactic Database NED; *Figure 3.11* NASA/IPAC Extragalactic Database NED; *Figure 3.12* NASA/IPAC Extragalactic Database (NED), Jet Propulsion Laboratory, California Institute of Technology, the National Aeronautics and Space Administration; *Figure 3.13* Netzer, H. (1990) AGN emission lines, in Blandford, R.D., Netzer, H. and Woltjer, L. (eds.) *Active Galactic Nuclei*, Springer-Verlag, Berlin; *Figure 3.14* Courtesy of Barry Poteete 2000 ©; *Figure 3.15* Kaufmann III, W. J. *Galaxies and Quasars*, 1979. W. H. Freeman and Company Publishers; *Figure 3.16 and 3.17* Peterson, B. *An Introduction to Active Galactic Nuclei*, Cambridge University Press; *Figure 3.18a and 3.18b* NASA/STScI; *Figure 3.18c* MERLIN; *Figure 3.18d* NASA/CXC/SAO/H. Marshall *et al.*; *Figure 3.19* John Bahcall (Institute for Advanced Study, Princeton), Mike Disney (University of Wales), and NASA; *Figure 3.20a* NASA/IPAC Extragalactic Database NED; *Figure 3.20b* Bob Fosbury/European Southern Observatory; *Figure 3.21* Copyright © NRAO/AUI 1998/1999; *Figure 3.22* © 1976 The American Astronomical Society; *Figure 3.23a* From Peculiar Galaxies, Chapter 5 in *Foundations of Astronomy* by Michael A. Seeds, Wadsworth Publishing Co. Inc., 1988 (2nd edn.); *Figure 3.23b* © 1987–2002, Anglo-Australian Observatory, photograph by David Malin; *Figure 3.23c* NASA/SAO/R. Kraft *et al.*; *Figure 3.24a* NASA and J. Biretta (STScI/JHU); *Figure 3.24b* NASA, NRAO and J. Biretta (STScI); *Figure 3.25* © 2000 The American Astronomical Society; *Figure 3.27* J. C. Lee *et al.*, *Astrophysical Journal* Volume 570, © 2002 The American Astronomical Society; *Figure 3.34a (radio data)* NASA/IPAC Extragalactic Database NED; *Figure 3.34a (optical data) and 3.35 (isophotal data)* The Digitized Sky Survey was produced at the Space Telescope Science Institute under US Government grant NAG W-2166. The images of these surveys are based on photographic data obtained using the Oschin Schmidt Telescope on Palomar Mountain and the UK Schmidt Telescope. The plates were processed into the present compressed digital form with the permission of these institutions. The Second Palomar Observatory Sky Survey (POSS-II) was made by the California Institute of Technology with funds from the National Science Foundation, the National Aeronautics and Space Administration, the National Geographic Society, the Sloan Foundation, the Samuel Oschin Foundation, and the Eastman Kodak Corporation. The Oschin Schmidt Telescope is operated by the California Institute of Technology and Palomar Observatory. Supplemental funding for sky-survey work at the STScI is provided by the European Southern Observatory; *Figure 3.34b* L. Ferrarese (Johns Hopkins University) and NASA; *Figure 3.35 (image)* © 1998 The American Astronomical Society;

Figure 4.1 from Le Grand Atlas de l'Astronomie (1983), by permission of Encyclopaedia Universalis; *Figure 4.2* © 1991–2002, Malin/IAC/RGO. Photograph from Isaac Newton Telescope plates by David Malin; *Figure 4.3a and 4.3b* Based on photographic data obtained using Oschin Schmidt Telescope on Palomar Mountain. The Palomar Observatory Sky Survey was funded by the National Geographic Society. The Oschin Schmidt Telescope is operated by the California Institute of Technology and Palomar Observatory. The plates were processed into the present compressed digital format with their permission. The Digitized Sky Survey was produced at the Space Telescope Science Institute (STScI) under US Government grant NAG W-2166; *Figure 4.4 and 4.6* © Copyright California Institute of Technology; *Figure 4.7a* NASA; *Figure 4.7b* Based on photographic data obtained using The UK Schmidt Telescope. The UK Schmidt Telescope was operated by the Royal Observatory Edinburgh, with funding from the UK Science and Engineering

Research Council, until 1988 June, and thereafter by the Anglo-Australian Observatory. Original plate material is copyright © the Royal Observatory Edinburgh and the Anglo-Australian Observatory. The plates were processed into the present compressed digital form with their permission. The Digitized Sky Survey was produced at the Space Telescope Science Institute under US Government grant NAG W-2166; *Figure 4.12* W. N. Colley and E. Turner (Princeton University), J. A. Tyson (Bell Labs, Lucent Technologies) and NASA; *Figure 4.13* NASA, A. Fruchter and the ERO Team (STScI and ST-ECF); *Figure 4.15* L. J. King (U. Manchester), NICMOS, HST, NASA; *Figure 4.16* © 2000. The American Astronomical Society; *Figure 4.17* Courtesy of R. Brent Tully/Sky & Telescope; *Figure 4.18* Image by Luis Teodoro, University of Durham, taken from www-astro.physics.ox.ac.uk.; *Figure 4.19* © Copyright Maddox, S. et al.; *Figure 4.21* Credit NASA, N. Benitez (JHU), T. Broadhurst (The Hebrew University), H. Ford (JHU), M. Clampin (STScI), G. Hartig (STScI), G. Illingworth (UCO/Lick Observatory), the ACS Science Team and ESA; *Figure 4.22a* Margaret, J. Geller and John, P. Huchra, Smithsonian Astrophysical Observatory; *Figure 4.22b* Courtesy of Professor Richard Ellis, Institute of Astronomy, University of Cambridge; *Figure 4.23* Sloan Digital Sky Survey; *Fig*ure 4.24 adapted from data supplied by M. Colless; *Figure 4.26* Mount Stromlo Observatory; *Figure 4.28* © 2000. The American Astronomical Society; *Figure 4.29* © 1993. The American Astronomical Society; *Figure 4.31a, 4.31b and 4.31c* Images sourced from http//www.astro.princeton.edu/~refreg/weak_lensing/pictures.html, Alexandre Refregier, University of Cambridge.

Figure 5.1 AURA/STScI/NASA; *Figure 5.2* Sparke, L. S. and Gallagher, J. S. *Galaxies in the Universe: An Introduction* (2000) Cambridge University Press; *Figure 5.3* Steve Maddox, APM Galaxy Survey; *Figure 5.4* Douglas Scott; *Figure 5.5* Robert Smith, The 2df Quasar Redshift Survey; *Figure 5.7, 5.17, 5.20 and 5.24* Science Photo Library; *Figure 5.14* Kittel, C., Knight, W. D. and Ruderman, M. A. Mechanics-Berkeley Physics Course – Volume 1 1965. Education Development Center, Inc; *Figure 5.15* Raine, D. J. *The Isotropic Universe*. 1981 Adam Hilger Ltd; *Figure 5.21* © Howard Percy Robertson; *Figure 5.22* © Arthur Geoffrey Walker; *Figure 5.23* Adapted from P.T. Landsberg and D.A Evans, *Mathematical Cosmology*, Oxford University Press, 1977; *Figure 5.25* The Royal Astronomical Society Library; *Figure 5.26 and 5.32* Sky Publishing Corp.; *Figure 5.33* © 1992 Annual Reviews;

Figure 6.13 T.P. Walker, *et al.* 'Primordial Nucleosynthesis Redux', *Astrophysical Journal* (1991) Volume 376, p. 51 © American Astronomical Society; *Figure 6.16* Image courtesy of Bell Laboratories, AT & T; *Figure 6.18* Astronomical Society of the Pacific; *Figure 6.20* The VSA Collaboration; *Figure 6.21* Longair, M. S. *Galaxy Formation* 1998. Springer-Verlag, Berlin/London; *Figure 6.22* Kolb, E. W. and Turner, M.S. *The Early Universe*. (1990). Addison Wesley Publishing Company; *Figure 6.23a and 6.23b* Dr Adrian Jenkins and The Virgo Consortium. © American Astronomical Society;

Figure 7.1 Courtesy of National Academy of Sciences; *Figure 7.2* Sky Publishing Corporation; *Figure 7.4* Image courtesy of NRAO/AUI; *Figure 7.5* Henbest, N. and Marten, M. *The New Astronomy* (1983) Cambridge University Press; *Figure 7.7* Caltech Archives; *Figure 7.8* Courtesy Adam Reiss and the Supernova Cosmology Project; *Figure 7.9* © WY'east Consulting, 2002; *Figures 7.10 and 7.11* Schwarzschild, B. Very Distant Supernovae Suggest that the Cosmic Expansion is Speeding Up, *Physics Today* (June 1998), pp. 17–19; *Figure 7.14* NASA;

Figure 7.15 © 1998–2000 Edward L. Wright; *Figure 7.16* Courtesy of Ted Bunn; *Figure 7.17, 7.18 and 7.19* Image courtesy of The BOOMERanG Collaboration; *Figure 7.20* NASA; *Figure 7.21, 7.22 and 7.27* Bennett, C.L. *et al*. First Year Wilkinson Microwave Anisotropy Probe (WMAP) Observations: Preliminary Maps and Basic Results, *Astrophysical Journal* (submitted); *Figure 7.23* Professor Edward Wright; *Figure 7.24* Hinshaw, G. *et al*. First Year Wilkinson Anisotropy Probe (WMAP) Observations: The Angular Power Spectrum, *Astrophysical Journal* (submitted);

Figure 8.2 Charles Roger Alcock *et al. Nature* Volume 365, p.621 (1993); *Figure 8.3* © CERN photo; *Figure 8.4* Adapted from an image supplied by CCLRC Rutherford Appleton Laboratory.

Every effort has been made to locate all copyright holders, but if any have been overlooked the publishers will make the necessary arrangements at the first opportunity.

FIGURE REFERENCES

Abell, G.O., Corwin, H.G. and Olowin, R.P. (1989) A catalog of rich clusters of galaxies, *Astrophysical Journal Supplement Series*, **70**, p.1.

Alcock, C. *et al*. (1993) Possible Gravitational Microlensing of a Star in the Large Magellanic Cloud, *Nature*, **365**, p.621.

Arp, H.C. (1958) *Handbook of Physics*, Vol. 51, p.75, Springer-Verlag, Berlin.

Bennett, C.L. *et al*. (2003) First-Year Wilkinson Microwave Anisotropy Probe (WMAP) Observations: Preliminary Maps and Basic Results, *Astrophysical Journal Supplement Series*, **148** (1), pp.1–27.

Berendzen, R., Hart, R. and Seeley, D. (1976) *Man Discovers the Galaxies*, Science History Publications, New York.

Binney, J. and Merrifield, M. (1998) *Galactic Astronomy*, Princeton University Press, Princeton.

Blaauw, A. and Schmidt, M. (eds) (1965) *Galactic Structure*, University of Chicago Press, Chicago.

Blitz, L. and Spergel, D.N. (1991) Direct evidence for a bar at the Galactic center, *Astrophysical Journal*, **379**, p.631.

Bok, B.J. and Bok, P.F. (1974) *The Milky Way*, Harvard University Press, Cambridge, Massachusetts.

Broadhurst, T.J., Ellis, R.S., Koo, D.C. and Szalay, A.S. (1990) Large-scale distribution of galaxies at the Galactic poles, *Nature*, **343**, p.726.

Burton,W.B. (1985) Leiden-Green Bank survey of atomic hydrogen in the galactic disk. I. *l*, *v* and *b*, *v* maps, *Astronomy and Astrophysics Supplement Series*, **62**, p.365.

Carroll, S.M., Press, W.H. and Turner, E.L. (1992) The cosmological constant, *Annual Review of Astronomy and Astrophysics*, **30**, p.499.

Combes, F. (1991) Distribution of CO in the Milky Way, *Annual Review of Astronomy and Astrophysics*, **29**, pp.195–237.

Condon, J.J. and Broderick, J.J. (1988) Radio identifications of UGC galaxies – Starbursts and monsters, *Astronomical Journal*, **96**, p.30.

Condon, J.J., Helou, G., Sanders, D.B. and Soifer, B.T. (1996) A 1.425 GHz Atlas of the IRAS Bright Galaxy Sample, Part II, *Astrophysical Journal Supplement Series*, **103**, p.81.

Davies, R.L., Kuntschner, H., Emsellem, E., Bacon, R., Bureau, M., Carollo, C.M., Copin, Y., Miller, B.W., Monnet, G., Peletier, R.F., Verolme, E.K. and de Zeeuw, P.T. (2001) Galaxy Mapping with the SAURON Integral-Field Spectrograph: The Star Formation History of NGC 4365, *Astrophysical Journal*, **548**, L33.

de Boer, K. and Savage, B. (1982) The Coronas of Galaxies, *Scientific American*, **247**, p.54.

Elvis, M., Wilkes, B.J., McDowell, J.C., Green, R.F., Bechtold, J., Willner, S.P., Oey, M.S., Polomski, E. and Cutri, R. (1994) Atlas of quasar energy distributions, *Astrophysical Journal Supplement Series*, **95**, p.1.

Ferguson, H.C., Dickinson, M. and Williams, R. (2000) The Hubble Deep Fields, *Annual Review of Astronomy and Astrophysics*, **38**, p.667.

Finkbeiner, A.K. (1998) Cosmic yardsticks: supernovae and the fate of the Universe, *Sky and Telescope*, September, p.43.

Francis, P.J., Hewett, P.C., Foltz, C.B., Chaffee, F.H., Weymann, R.J. and Morris, S.L. (1991) A high signal-to-noise ratio composite quasar spectrum, *Astrophysical Journal*, **373**, p.465.

Freedman, W.L. et al. (2001) Final Results from the Hubble Space Telescope Key Project to Measure the Hubble Constant, *Astrophysical Journal*, **553**, p.47.

Genzel, R. and Cesarsky, C. (2000) Extragalactic Results from the Infrared Space Observatory, *Annual Review of Astronomy and Astrophysics*, **38**, p.761.

Georgelin, Y.M. and Georgelin, Y.P. (1976) The spiral structure of our Galaxy determined from H II regions, *Astronomy and Astrophysics*, **49**, p.57.

Georgelin, Y.P. and Georgelin, Y.M. (1971) Spiral Structure of our Galaxy from H II Regions, *Astronomy and Astrophysics*, **12**, p.482.

Ghez, A.M., Morris, M. and Becklin, E.E. (1999) High Proper Motion Stars in the Vicinity of Sgr A*: Evidence for a supermassive black hole, The Central Parsecs of the Galaxy: Galactic Centre Workshop, H. Flacke *et al.* (eds), *Astronomical Society of the Pacific Conference Series*, **186**, p.21.

Grabelsky, D.A., Cohen, R.S., Bronfman, L. and Thaddeus, P. (1988) Molecular clouds in the Carina arm – The largest objects, associated regions of star formation, and the Carina arm in the Galaxy, *Astrophysical Journal*, **331**, p.181.

Hartmann, D. and Burton, W.B. (1997) *Atlas of Galactic Neutral Hydrogen*, Cambridge University Press, Cambridge.

Henbest, N. and Marten, M. (1983) *The New Astronomy*, Cambridge University Press, Cambridge.

Hesser, J., Harris, W. and VandenBerg, D. (1987) Inferences from a color-magnitude diagram for 47-Tucanae, *Publications of the Astronomical Society of the Pacific*, **99**, p.1148.

Hibbard, J.E., Guhathakurta, P., van Gorkom, J.H. and Schweizer, F. (1994) Cold, warm, and hot gas in the late-stage merger NGC 7252, *Astronomical Journal*, **107**, p.67.

Hinshaw, G. *et al*. (2003) First-Year Wilkinson Anisotropy Probe (WMAP) Observations: The Angular Power Spectrum, *Astrophysical Journal Supplement Series*, **148** (1), pp.135–59.

Jenkins, A., Frenk, C.S., Pearce, F.R., Thomas, P.A., Colberg, J.M., White, S.D.M., Couchman, H.M.P, Peacock, J.A., Efstathiou, G. and Nelson, A.H. (The Virgo Consortium) (1998) *Evolution of Structure in Cold Dark Matter Universes, Astrophysical Journal*, **499**, pp.20–40.

Kaufmann III, W.J. (1979) *Galaxies and Quasars*, W.H. Freeman and Company Publishers, San Francisco.

Kennicutt, R.C. (1992) The integrated spectra of nearby galaxies – General properties and emission-line spectra, *Astrophysical Journal*, **388**, p.310.

Kennicutt, R.C., (1998) Star Formation in Galaxies along the Hubble Sequence, *Annual Review of Astronomy and Astrophysics*, **36**, p.189.

Kerr, F.J., Bowers, P.F., Jackson, P.D. and Kerr, M. (1986) Fully sampled neutral hydrogen survey of the southern Milky Way, *Astronomy and Astrophysics Supplement Series*, **66**, p.373.

Kittel, C., Knight, W.D. and Ruderman, M.A. (1965) Mechanics-Berkeley Physics Course – Volume 1, Education Development Center, Inc.

Kolb, E.W. and Turner, M.S. (1990) *The Early Universe*, Addison-Wesley, Reading, Massachusetts.

Landsberg, P.T. and Evans, D.A. (1977) *Mathematical Cosmology*, Oxford University Press, Oxford.

Lee, J.C., Iwasawa, K., Houck, J.C., Fabian, A.C., Marshall, H.L. and Canizares, C.R. (2002) The shape of the relativistic iron Kα line from MCG – 6–30–15 measured with the Chandra High Energy Transmission Grating Spectrometer and the Rossi X-ray Timing Explorer, *Astrophysical Journal*, **570**, L47.

Li, A. and Draine, B.T. (2001) Infrared Emission from Interstellar Dust. II. The Diffuse Interstellar Medium, *Astrophysical Journal*, **554**, p.778.

Longair, M.S. (1998) *Galaxy Formation*, Springer, Berlin/ London.

Markevitch M., *et al*. (2000) Chandra Observations of Abell 2142: Survival of dense subcluster cores in a merger, *Astrophysical Journal*, **541**, p.542.

Mihalas, D. and Binney, J. (1981) *Galactic Astronomy*, Freeman and Co., Oxford.

Mirabel, I.F., *et al*. (1998) The dark side of star formation in the Antennae galaxies, *Astronomy and Astrophysics*, **333**, L1–L4.

Morse, J.A., Cecil, G., Wilson, A.S. and Tsvetanov, Z.I. (1998) Inclined gas disks in the lenticular Seyfert Galaxy NGC 5252, *Astrophysical Journal*, **505**, p.159.

Netzer, H. (1990) AGN emission lines, in Blandford, R.D., Netzer, H. and Woltjer, L. (eds) *Active Galactic Nuclei*, Springer-Verlag, Berlin.

Nicolson, I. (1982) *The Sun*, Mitchell Beazley, London.

Nikolaev, S. and Weinberg, M.D. (1997) A rigorous reanalysis of the IRAS variable populations: scale lengths, asymmetries and microlensing, *Astrophysical Journal*, **487**, p.885.

Oliver, S.J., Rowan-Robinson, M., Broadhurst, T.J., McMahon, R.G., Saunders, W., Taylor, A., Lawrence, A., Lonsdale, C.J., Hacking, P. and Conrow, T. (1996) Large-scale structure in a new deep IRAS galaxy redshift survey, *Monthly Notices of the Royal Astronomical Society*, **280**, p.673.

Osterbrock, D.E., Koski, A.T. and Phillips, M.M. (1976) The optical spectra of 3C 227 and other broad-line radio galaxies, *Astrophysical Journal*, **206**, p.898.

Perley, R.A., Dreher, J.W. and Cowan, J.J. (1984) The jet and filaments in Cygnus A, *Astrophysical Journal*, **285**, L35.

Peterson, B.M. (1997) *An Introduction to Active Galactic Nuclei*, Cambridge University Press, Cambridge.

Pickles, A.J. (1985) Differential population synthesis of early-type galaxies. III – Synthesis results, *Astrophysical Journal*, **296**, p.340.

Raine, D.J. (1981) *The Isotropic Universe*, Adam Hilger Ltd., Bristol.

Roth, J. (1997) Dating the cosmos: a progress report, *Sky and Telescope*, October, p.46.

Ryder, S.D., Walsh, W. and Malin, D., (1999) HI study of the NGC 6744 system, *Publications of the Astronomical Society of Australia*, **16**, p.84.

Sandage A., and Bedke, J. (1994) *The Carnegie Atlas of Galaxies*, Volume I, Carnegie Institution of Washington.

Saunders, W., Sutherland, W.J., Maddox, S.J., Keeble, O., Oliver, S.J., Rowan-Robinson, M., McMahon, R.G., Efstathiou, G.P., Tadros, H., White, S.D.M., Frenk, C.S., Carramiñana, A. and Hawkins, M.R.S. (2000) The PSCz catalogue, *Monthly Notices of the Royal Astronomical Society*, **317**, p.55.

Scarpa, R., Urry, C.M., Falomo, R., Pesce, J.E. and Treves, A. (2000) The Hubble Space Telescope Survey of BL Lacertae Objects. I. Surface Brightness Profiles, Magnitudes, and Radii of Host Galaxies, *Astrophysical Journal*, **532**, p.740.

Schild, R. and Thomson, D. (1997) The Q0957+561 time delay from optical data, *Astronomical Journal*, **113**, p.130.

Schödel, R. et al. (2002) A star in a 15.2-year orbit around the supermassive black hole at the centre of the Milky Way, *Nature*, **419**, p.694.

Schwarzschild, B. (1998) Very distant supernovae suggest that the cosmic expansion is speeding up, *Physics Today*, June, pp.17–19.

Seeds, M.A. (1988) *Foundations of Astronomy*, (2nd edn) Wadsworth Publishing, Belmont, California.

Silva, D.R. and Cornell, M.E. (1992) A new library of stellar optical spectra, *Astrophysical Journal Supplement Series*, **81**, p.865.

Sparke, L.S. and Gallagher, J.S. (2000) *Galaxies in the Universe: An Introduction*, Cambridge University Press, Cambridge.

Stern, D., Spinrad, H., Eisenhardt, P., Bunker, A.J., Dawson, S., Stanford, S.A. and Elston, R. (2000) Discovery of a Color-selected Quasar at z = 5.50, *Astrophysical Journal*, **533**, L75.

Tully, R.B., Verheijen, M.A.W., Pierce, M.J., Huang, Jia-Sheng and Wainscoat, R.J. (1996) The Ursa Major Cluster of Galaxies. I. Cluster Definition and Photometric Data, *Astronomical Journal*, **112**, p.2471.

Walker, T.P., Steigman, G., Kang, Ho-Shik, Schramm, D.M. and Olive, K.A. (1991) Primordial nucleosynthesis redux, *Astrophysical Journal*, **376**, pp.51–69.

Weinberg, M.D. (1992) Detection of a large-scale stellar bar in the Milky Way, *Astrophysical Journal*, **384**, p.81.

Wolfe, A.M., Turnshek, D.A., Lanzetta, K.M. and Lu, L. (1993) Damped Lyman-alpha absorption by disk galaxies with large redshifts. IV – More intermediate-resolution spectroscopy, *Astrophysical Journal*, **404**, p.480.

Zinn, R. (1985) The globular-cluster system of the Galaxy .4. The halo and disk subsystems, *Astrophysical Journal*, **293**, p. 424.

INDEX

Entries and page numbers in **bold type** refer to key words which are printed in **bold** in the text. Italics indicate items mainly, or wholly, in a figure or table.

D

N

O

P

Q

R